DEVELOPMENT OF MICRO-SAMPLING TECHNIQUES UTILIZING INDUCTIVELY COUPLED PLASMA-MASS SPECTROMETRY (ICP-MS) AND THEIR APPLICATION TO GEOCHEMICAL STUDIES OF PRECIOUS METAL-RICH NICKEL-COPPER ORES AT SUDBURY

ZHONGXING CHEN

DEVELOPMENT OF MICRO-SAMPLING TECHNIQUES UTILIZING INDUCTIVELY COUPLED PLASMA-MASS SPECTROMETRY (ICP-MS) AND THEIR APPLICATION TO GEOCHEMICAL STUDIES OF PRECIOUS METAL-RICH NICKEL-COPPER ORES AT SUDBURY

BY

© ZHONGXING CHEN, B.Sc., M.Sc.

A thesis submitted to the School of Graduate Studies in partial fulfilment of the requirements for the degree of Doctor of Philosophy

Department of Earth Sciences
Memorial University of Newfoundland

August 1993

St. John's Newfoundland

ISBN 0-612-06110-8

Canada

ABSTRACT

Three micro-sampling techniques for inductively coupled plasma-mass spectrometry (ICP-MS) have been developed for geochemical studies of trace elements: (1) a solution recycling nebulization system with a disposable spray chamber, (2) determination of precious metals in milligram samples of sulphides and magnetite after cation exchange separation using an automated 2 speed peristaltic pump speed controller, and (3) in-situ determination of precious metals in sulphides using sample introduction by laser ablation of solids.

With the recycling nebulization system, 0.5 g of sample solution is sufficient for 8 minutes of data acquisition. The sensitivity of the recycling nebulization system is similar to that of a conventional Scott spray chamber system. Twenty six trace elements were determined by ICP-MS using four internal standards (Ge, In, Re, and Bi) to correct for matrix, instrumental drift, and enrichment of the sample solution by evaporation. The ability to analyze mineral separates weighing less than 0.1 mg with detection limits similar to conventional procedures is demonstrated. Analyses of the geological reference materials SY-2, BCR-1, W-1, and BR indicate good limits of detection, good accuracy and precision, negligible memory, and low consumption of sample solution. Results compare well with data reported using conventional ICP-MS analysis. Analyses of the geological reference materials; PCC-1, AL-1, FK-N, NBS70a and NBS99a, for 15 Rare Earth Elements (REE), at ultra-trace

concentration levels, using cation exchange preconcentration are demonstrated, with solid limits of detection from 0.01 to 1 ng g^{-1} (ppb), and relative standard deviations of less than 15% for homogenous samples.

The Memorial laser ablation microprobe-inductively coupled plasma-mass spectrometry (LAM-ICP-MS) is described and applied to the determination of precious metals in minerals, though its use in this study is very preliminary. Solid limits of detection range from 30 ppb to 240 ppb for the precious metals, and it provides a useful technique to examine the distributions of precious metals, particularly the heavy PGE (Ir, Pt) and Au in sulphides. However, serious interferences from base metal-argon polyatomic ions on Ru, Rh, and Pd were observed.

A method for the quantitative separation of the precious metals from the associated base metals using a cation exchange resin was established. The method has been applied to the determination of precious metals in small quantities (2-20 mg) of high purity sulphide and magnetite mineral separates using an automated 2 speed peristaltic pump speed controller and ICP-MS. Solid limits of detection for a 20 mg sample were less than 4 ppb for Ru, Rh, Re, Ir, Pt, and Au, and 29 ppb for Pd, due to significant memory. Analyses of nickel sulphide fire assay beads of the reference material, SARM-7, show good agreement with certified values, with relative standard deviations (RSD) of less than 8% for platinum-group elements (PGE).

Two Ni-Cu-(PGE) mines - Strathcona and Thayer Lindsley at Sudbury were studied for their PGE and rare earth element (REE) geochemistry using the micro-sampling techniques.

The distribution of precious metals in the principle ore minerals, and platinum-group minerals (PGM) in the two mines was documented. The distribution of Ru, Rh, and Ir indicates that these element are or were dominantly in solid solution in the sulphides and magnetite. The remarkable variations of Pd, Pt, and Au contents in these minerals suggest the presence of discrete precious metal phases later confirmed by electron microprobe analyses. Mass balance calculations also indicate that considerable amounts of Ru, Rh, Pd and Ir are in solid solution in the major ore minerals, whereas the rest of precious metals are dominantly in separate discrete phases either as minor inclusions in the ore minerals or as precious metal minerals which were found at the boundaries of these minerals. Study of the Thayer Lindsley Mine indicate that there are no apparent systematic spatial variations of precious metals in the same ore minerals from different parts of the ore zones although bulk NiS sulphide fire analyses show that the ores from the orebody margin are more enriched in Pd, Pt and Au.

Partition coefficients (K_d values) at ppb to ppm levels of precious metals among the major ore minerals at the Thayer Lindsley Mine have been investigated. Partitioning of Ru, Rh, and Ir between these minerals follows one

sequence (with decreasing order): pyrrhotite > pentlandite > chalcopyrite > magnetite. Partitioning of Pd, Re, Pt, and Au does not follow this sequence; and each is different from the other. Fractional crystallization and subsequent exsolution are mainly responsible for the distribution and fractionation of precious metals in sulphides and magnetite. A fractionation model is proposed for the explanation of precious metal ore genesis.

Trace element analyses of the Thayer Lindsley Mine indicate that sulphide ores in the footwall granite and in the Sublayer were depleted in lithophile trace elements during magmatic sulphide segregation. In comparison with analyses of the South Range norites which represent the parent magma, the Sublayer rocks are enriched in light rare earth elements (LREE) and exhibit slightly Eu negative anomalies, whereas sulphide ores in the Sublayer and in the footwall Murray granite are depleted in LREE and have a strongly Eu negative anomaly. The original REE composition of the Sublayer magma can be modeled from 35% Sublayer rocks and 65% Sublayer sulphide ores. Chondrite normalized REE distribution patterns indicate that the massive ores in the footwall granite are parts of a highly fractionated sulphide liquid which was expelled from the original sulphide magma along structural weakness into the footwall granite. A distinctive REE distribution pattern indicates a hydrothermal fluid was involved in the development of the orebody margin.

ACKNOWLEDGEMENTS

I would like to express my deep thanks to my supervisors Dr. B.J. Fryer, Dr. H.P. Longerich, and Dr. M.R. Wilson for their guidance, assistance and patience throughout the various phases of this thesis. Dr. Fryer and Dr. Longerich are particularly appreciated for supporting my research activities and providing financial support for this work through their NSERC operating grants. Dr. S.E. Jackson is grateful for his useful suggestions and comments related to ICP-MS.

The assistance of P. King, W. Gosse, L. Hewa and P. Horan in sample preparation; B. Chapman in ICP-MS instrument operation; D. Clarke in computer assistance; M. Piranian in electron microprobe analysis; and C. Emerson in scanning electron microscope analysis, is greatly appreciated. T. Perks and D. Bolger of the Technical Service Department are thanked for their technical assistance. Members of the General Office in the Department of Earth Sciences were always helpful and accommodating.

Falconbridge Ltd. at Sudbury is gratefully acknowledge for access to the mine and permission to collect underground and drill core samples. I am grateful to geological staff at Falconbridge, particularly to Mr. E. S. Barnett, and Mr. G. Miller for their help with underground observations and sample collection.

I would also like to thank my fellow graduate students, G.-W. Sung, and

A. Frimpong for their advice, assistance and friendship.

Most importantly I thank my wife, Yuqing Lu, for her encouragement, understanding and companionship.

Finally, I wish to acknowledge receipt of a Graduate Student Fellowship from the School of Graduate Studies and the additional financial support from the Department of Earth Sciences, Memorial University of Newfoundland.

TABLE OF CONTENTS

APPENDICES

LIST OF TABLES

LIST OF FIGURES

LIST OF ABBREVIATIONS AND SYMBOLS

AMS	Accelerator mass spectrometry
Cpy	Chalcopyrite
ETV	Electrothermal volatilization
FIA	Flow injection analysis
HREE	Heavy rare earth elements
ICP	Inductively coupled plasma
ICP-AES	Inductively coupled plasma-atomic emission spectrometry
ICP-MS	Inductively coupled plasma-mass spectrometry
INAA	Instrumental neutron activation analysis
IPGE	Ir group of platinum-group elements (Ru, Rh, Os, and Ir)
K_d	Partition coefficient
LAM	Laser ablation microprobe
LREE	Light rare earth elements
mg	Milligram
ml	Millilitre
μg	Microgram
μl	Microlitre
Mss	Monosulphide solid solution
Mt	Magnetite
MUN	Memorial University of Newfoundland
PGE	Platinum-group elements
PGM	Platinum-group minerals
PIXE	Proton-induced X-ray emission
ppb	parts per billion (ng/g)
PPGE	Pd group of platinum-group elements (Pd, Pt, and Au)
ppm	parts per million (μg/g)
Pn	Pentlandite
Po	Pyrrhotite
RD	Relative difference
REE	Rare earth elements
RSD	Relative standard deviation
SIC	Sudbury Igneous Complex
XRD	X-ray diffraction
XRF	X-ray fluorescence spectrometry
SEM	Scanning electron microscope
SIMS	Secondary ion mass spectrometry
Wt%	Weight percent

CHAPTER 1

SCOPE AND PURPOSE OF THE STUDY

1.1 INTRODUCTION

Scientific revolutions and developments are more and more dependent on modern technology. Contemporary analytical techniques are vital tools that geochemists frequently use for studying the chemistry of the Earth and the Universe. Analytical methods developed by pure analytical chemists do not always meet the requirements of geochemists who intend to solve very specific problems. It is the purpose of this thesis to develop micro-sampling inductively coupled plasma-mass spectrometry (ICP-MS) techniques to study a specific geochemical problem - the distribution and fractionation of precious metals in ore zones and between constituent minerals.

Since the first commercial inductively coupled plasma-mass spectrometry (ICP-MS) became available in 1983, the instrument has gained rapid and wide acceptance in many analytical laboratories. ICP-MS has been proven to be a promising analytical technique, with the potential to be an excellent analytical tool in earth sciences (Date and Gray, 1985; Houk, 1986; Longerich *et al.*, 1990; Jenner *et al.*, 1990; Jackson *et al.*, 1990; Longerich, *et al.*, 1993; and

Fryer *et al.*, 1993). For geochemical analysis, ICP-MS offers several advantages over conventional analytical methods. These include: (1) multi-element capability, sensitivity and speed; (2) simple spectra, even for complex matrices; (3) superior detection limits, particularly for heavy elements; (4) wide linear dynamic range; and (5) rapid isotope ratio capability. For example, it is possible to routinely determine 33 elements, spanning the range of geochemical behaviour, with solid detection limits ranging between 0.006 and 0.5 ppm (Jenner *et al.*, 1990), in a 0.1 g sample. Once instrumental procedures are established, it takes only 3-5 days to obtain analyses on 17 samples, from sample preparation to final data reduction.

However, as has been stated by G.E.F. Lundell in 1933: "There is no dearth of methods that are entirely satisfactory for the determination of elements when they occur alone. The rub comes in because elements never occur alone, for nature and man both frown on celibacy". Despite extensive research indicated by the large number of publications, as has been pointed out by Montaser (1992), significant challenges exist in five areas (Table 1.1). Among them, the introduction of samples into plasmas continues to be the limiting factor of analytical plasma spectrometry.

Table 1.1 Challenges in ICP-MS

1.	The introduction of samples into plasmas.
2.	Spectral interferences including isobaric, double-charged ions and polyatomic ions.
3.	Matrix effects.
4.	Insufficient short- and long-term precision.
5.	Equipment and operating costs.

Modified from Montaser (1992)

The most common method used for sample introduction into an ICP-MS system is solution nebulization, *viz*, a spray chamber combined with a pneumatic nebuliser. However, this conventional method of sample introduction has several limitations, including low nebulization efficiency, and problems inherent in dissolving mineral or rock samples (*i.e.*, incomplete dissolution of some samples, time-consuming dissolution procedures, significant dilution, loss of analyte by volatilization and possible contamination). A study of the standard solution nebulization system consisting of a Meinhard concentric nebulizer in conjunction with a Scott spray chamber has shown that the efficiency of sample introduction to the plasma is less than 5%, hence more than 95% of the sample is discarded to waste (Isoyama *et al.*, 1990a). Because of this poor efficiency, large samples are required for routine ICP-MS

analysis.

When the amount of sample solution available is not limited, poor efficiency in sample transfer to the plasma is normally of little importance. There are occasions, however, when the volume is limited by the amount of sample available or the amount that can be dissolved. In some geological applications, such as zoned minerals or fine-grained intergrowths, separation of a specific phase may be very difficult or even impossible. Painstaking careful manual separation is required to minimize the inclusion of minor mineral phases with high trace element concentrations.

Two possible ways to meet the requirement of micro-sampling are: 1) a recycling nebulization system, and 2) direct introduction of solid samples. For solution introduction, a recycling nebulization system provides a considerable gain in the efficiency of sample solution used so that sample size can be greatly reduced by recovering the bulk of the solution that normally drains to waste and recycling it to the nebuliser (Novak *et al.*,1980; Hulmston, 1983; Zhuang and Barnes, 1985; Vieira *et al.*, 1986; Zicai *et al.*, 1986 and Kato and Takashima, 1989; Isoyama *et al.*, 1990a).

Previous studies of direct introduction of solid samples have utilized electrothermal vaporization (Date and Cheung, 1987; Park and Hall, 1988; and Gregoire, 1988), graphite rod direct sample insertion (Williams *et al.*, 1987) and laser ablation systems (Gray, 1985; Arrowsmith, 1987; Hager, 1989; Darke *et*

al., 1989a; Darke *et al* 1989b; Pearce *et al.*, 1992; Longerich *et al.*, 1993; and Jackson *et al.*, 1993). Of these, laser ablation seems to be the most promising. Many samples, particularly in geochemistry, are initially in solid form, and there are many advantages to sample introduction without the necessity of an intermediate dissolution step.

1.2 REVIEW OF MICRO-SAMPLING ICP-MS TECHNIQUES

1.2.1 RECYCLING NEBULIZATION SYSTEMS

The first recycling nebulization system was designed for inductively coupled plasma-atomic emission spectrometry (ICP-AES) and used a purpose-built cross-flow nebulizer with impact bead and sample cup (Novak *et al.*,1980). Subsequently, more sophisticated designs for ICP-AES have been reported (Hulmston, 1983; Zhuang and Barnes, 1985; Virira *et al.*, 1986; Zicai *et al.*, 1986 and Kato *et al.*, 1989). In the system reported by Hulmston (1983), a normal concentric all-glass nebulizer was operated in a vertical position inside a conical aerosol chamber. The large droplets that were retained in the spray chamber were fed back to the nebulizer and nebulized again. The system works for 10 min on a 1 ml sample. The chamber is flushed with water between samples. The sensitivity, detection limits, and short-term precision of

measurements obtained with the system are comparable to those of a normal concentric nebulizer system. Zhuang and Barnes (1985) modified the recycling nebulizer system described by Hulmston. Their system consists of a concentric nebulizer mounted vertically inside a streamlined conical aerosol chamber. Vieira *et al.* (1986) used a cyclone aerosol chamber in a recycling nebulizer system. Signal-to-background ratios and detection limits were equal to or better than those provided by a dual concentric aerosol chamber. All these recycling systems permit continuous nebulization with small volumes for long periods of time and the measurement of many elements with a sequential ICP-AES system. However, recycling systems inherently have two major problems, *viz.*, enrichment of the sample concentration with time, and memory effects. The enrichment could be improved by humidifying the nebuliser gas to a certain extent (Zicai and Barnes, 1986), but the latter is more severe and less easily avoided (Isoyama *et al.*, 1990a). For practical measurements, the spray chamber and nebulizer has to be washed thoroughly by the repeated nebulization of a blank and/or the next sample on exchange of each sample. More recently Isoyama *et al.* (1990a) have reported a new recycling configuration which permitted exchangeable spray chambers for ICP-AES. These workers discussed the problem of concentration of the sample by evaporation. However, they did not apply methods to correct for sample evaporation. The application of a recycling solution nebulizing system to ICP-

MS has been reported recently (Chen *et al.*, 1992a)

1.2.2 LASER ABLATION

As early as 1965, Ready studied laser vaporization processes. The history and recent developments of laser ablation introduction systems have been extensively reviewed by Moenke-Blankenburg (1989). Thompson *et al.* (1981) combined a commercially available laser microprobe with an ICP source atomic emission spectrometer together with a sample chamber and a light-activated switch. The system was tested with a series of standard steel samples, which produced linear calibrations for several elements. The precision was good for elements that were homogeneously distributed through the sample. Dittrich and Wennrich (1990) have reviewed in detail laser vaporization in atomic spectrometry. Adriain and Watson (1984) have discussed the physical characteristics of laser-produced plasmas. Thompson *et al.* (1990) recently discussed the nature of particulate matter produced by laser ablation.

Gray (1985) first reported solid sample introduction by laser ablation for ICP-MS. A laser ablation microprobe (LAM) sample-introduction system, designed for in-situ microsampling of minerals in petrographic sections, has been interfaced to an ICP-MS at Memorial University of Newfoundland (MUN) (Longerich *et al.*, 1993a; Jackson *et al.*, 1993; and Fryer *et al.*, 1993). This system has been successfully applied to in-situ trace element analyses and (U)-

Pb geochronology (Jackson *et al.*, 1993; and Fryer *et al.*, 1993).

1.2.3 TWO SPEED PERISTALTIC PUMP SPEED CONTROLLER

Longerich (1993a) reported an automated 2 speed peristaltic pump speed controller for ICP-MS and its applications to reduce sample wash out time and to decrease analytical sample volumes. Such a device allows automatic selection of the "high speed purge" or "rabbit" mode of the commonly used Gilson Minipuls 2 peristaltic pump. The pump controller also allows efficient automated data acquisition using reduced liquid sample uptake rates (0.1 g/min) reducing the minimum quantity of solution required for an automated solution analysis to less than 3 g of solution.

1.2.4 DIRECT SAMPLE INSERTION

Direct sample insertion offers another micro-sampling technique. The first such device for ICP spectrometry was reported by Salin and Horlick (1979), with later publications by Abdullah and Haraguchi (1985), Shao and Horlick (1986), Williams *et al.* (1987), and Chan and Horlick (1990). It has been successfully applied to geological samples (Pettit and Horlick, 1986; Brenner *et al.*, 1987). The technique of direct sample insertion allows determinations at or below the micrograms-per-gram levels in the solid (McLeod *et al.*, 1992). The benefit of attaining rapid and complete vaporization of the analyte into the ICP is favoured

for volatile elements which yield a high ratio of signal to background. However, the technique is susceptible to interference effects, and the transient nature of signals and selective volatilization behaviour makes assessment and implementation of corrective measures difficult. Precision, generally, is inferior to that of solution nebulization techniques, with a typical working precision of 7% to 10% RSD (McLeod *et al.*, 1992).

1.2.5 ELECTROTHERMAL VAPORIZATION

Electrothermal volatilization (ETV) from a graphite rod or furnace, or from a refractory wire or tape is a very convenient method of introducing small solution samples of a few μl to the plasma (Date and Gray, 1983; Gray, 1986; Date and Cheung, 1987; Park and Hall, 1988; and Gregoire, 1988; Shen *et al.*, 1990). The function of the electrothermal vaporization device is to electrically heat the sample into "vapour". The vapour is then introduced into the plasma. It usually produces a transient signal lasting a few seconds while the burst of vapour from the heated surface traverses the plasma. Some benefits of this sample introduction method to the plasma are minimization of matrix effects and superior detection limits versus conventional solution nebulization.

1.2.6 FLOW INJECTION ANALYSIS

Flow injection analysis (FIA) techniques have been used for sample introduction

by Olivares and Houk (1985), Date (1984), Thompson and Houk (1986), Dean *et al.* (1988), and Viczian *et al.* (1990). The typical sample size for FIA is on the order of 100 μL. In FIA, the detector signal is a sharp transient peak rather than a steady-state response. It provides high sample throughput and the possibilities for sample dilution, matrix separation, and analyte concentration. It offers a number of advantages for analysis of samples with a high matrix concentration.

1.3 REVIEW OF METHODS FOR DETERMINATION OF THE PRECIOUS METALS AND THEIR DISTRIBUTION AND PARTITIONING AMONG COEXISTING MINERALS

1.3.1 DETERMINATION OF THE PRECIOUS METALS IN MINERAL SEPARATES

Analysis of rocks and ores for the precious metals - platinum group elements (PGE: Ru, Rh, Pd, Os, Ir and Pt) and gold is now commonly performed using a NiS fire assay collection (Robert *et al.*, 1971; Hoffman *et al.*, 1978; Jackson *et al.*, 1990), with quantification by one of a number of techniques; *e.g.*, atomic absorption spectroscopy (AAS) (Robert *et al.*, 1971), neutron activation analysis (NAA) (Hoffman *et al.*, 1978), graphite furnace-atomic absorption spectroscopy (GF-AAS) (Sen Gupta, 1989), inductively coupled plasma-optical

emission spectrometry (ICP-OES) (Wemyss and Scott, 1978; and Chung and Barnes, 1988), or ICP-MS (Date *et al.*, 1987; Gregoire, 1988; and Jackson *et al.*, 1990).

Data on the precious metal concentrations of common ore sulphides are essential for precious metal geochemistry and exploration, and for determining the mineralogical distribution of precious metals in samples from processing circuits. However, analyses of precious metals in mineral separates presents considerable difficulties, with most methods designed for sulphide-rich rocks, *e.g.* fire assay not being practical for milligram size samples. Keays and Crocket (1970) first reported precious metal concentrations in major sulphide ore minerals at the Strathcona Mine using a neutron activation method. However, Rh, Ir, and Pt were not reported in their study and the sample size they used (25 to 100 mg) is not pratical for high purity mineral separate studies. Subsequently, Chyi and Crocket (1976) presented Pt, Pd, Ir, and Au data at Strathcona Mine, but Ru, Rh, and Os were not reported.

Cabri *et al.* (1984) analyzed major sulphide ore minerals from mineral deposits in the Sudbury area, Ontario, using the Heidelberg proton microprobe in a search for trace quantities of the platinum-group elements (PGE). They did not detect any PGE because of high limits of detection (1.2 to 3 ppm for Pd and Rh, and 50-60 ppm for Pt).

Chryssoulis *et al.* (1989) described a method of quantitative trace

precious metal analyses of ore minerals by secondary ion mass spectrometry (SIMS). They claimed that detection limits below one part per million (ppm) for Ag, Au, Pt, Pd, Ir, and Rh could be achieved. However, no analytical data were presented in their study. Wilson *et al.* (1991) and Chai *et al.* (1993) reported "in-situ" analysis of precious metals in polished mineral samples using accelerator mass spectrometry (AMS). Their measurements showed extremely low backgrounds and low detection limits for the precious metals. However, the beam diameter of AMS (0.5 mm) is not normally considered to be microsampling. Furthermore, they did not apply internal standards to correct for instrumental drift and matrix effects. Time and analytical cost are also drawbacks for both SIMS and AMS.

1.3.2 DISTRIBUTION AND PARTITIONING OF PRECIOUS METALS AMONG COEXISTING MINERALS

In recent years, the precise and accurate determination of the precious metals (Ru, Rh, Pd, Ir, Pt and Au) in a range of rock and ore types has become increasingly important. Interpretation of the precious metal geochemistry of igneous rocks, ores, and minerals is important for the understanding of igneous petrogenesis and ore genesis. The precious metals were formerly considered to be geochemically coherent with strong siderophile affinity (Fleet and Stone, 1991). Barnes *et al.* (1985) and Naldrett *et al.* (1982) indicated that if these

elements are chondrite normalized and plotted in order of descending melting points of the metals, the patterns show the fractionation of these element during crystallization. Interest in PGE behaviour has stimulated numerous investigators of their partitioning behaviour (*e.g.* Stone *et al.*1990, Fleet *et al.*, 1991, and Frimpong *et al.*, 1993). Bethke and Barton (1971) raised the hope that if clean mineral separates of contemporaneous phases could be accurately analyzed, the distribution of minor elements among the phases could allow estimation of the temperature of ore formation. However, current research on partitioning of these elements is limited to experiments between sulphide and silicate liquids. Furthermore, only limited empirical data is available on precious metal distributions and their partitioning among the coexisting ore minerals due to considerable analytical difficulties in analyzing small samples.

1.4 SUBJECT AND SCOPE OF THE THESIS

This thesis combines geoanalytical chemistry and geochemistry. The purpose of this study was to develop specific analytical methods with the aim of studying some unsolved geochemical problems.

In geoanalytical chemistry, this study further develops three micro-sampling introduction techniques for ICP-MS:

(1) a solution recycling nebulization system with a disposable spray chamber,

(2) determination of precious metals in milligram samples of sulphides and magnetite using an automated 2 speed peristaltic pump speed controller for ICP-MS, after cation exchange separation, and

(3) in-situ determinations of precious metals in sulphide minerals using solid sample introduction by laser ablation.

With the advantage of the above analytical techniques, this study also systematically examines two Ni-Cu-(PGE) deposits - Strathcona and Thayer Lindsley at Sudbury, Ontario, and investigates the following geochemical problems:

(1) the distribution of the precious metals in the ores and minerals in the two deposits,

(2) the partitioning of the precious metals between the major ore minerals,

(3) the fractionation of the precious metals during crystallization and development of the orebodies, and

(4) trace element geochemistry of the Thayer Lindsley Mine and its implications for ore genesis.

1.5 ORGANIZATION OF THE THESIS

The following nine chapters of the thesis are organized into two parts:

(1) Part I (Chapters 2, 3, 4, and 5) deals with analytical developments for micro-sampling with inductively coupled plasma-mass spectrometry (ICP-MS). Chapters 2 and 3 establish the first micro-sampling technique: a recycling nebulization system with a disposable spray chamber for ICP-MS and describe its application to the determination of trace elements in geological samples. Chapter 2 describes the recycling nebulization system with a disposable spray chamber and its performance. Chapter 3 demonstrates two geoanalytical applications of the recycling nebulization system: trace element analyses of sub-milligram samples and the determination of the rare-earth elements at ultra-trace concentration levels after preconcentration. Chapter 4 describes the second micro-sampling analytical technique: laser ablation microprobe (LAM) ICP-MS and its preliminary applications to the in-situ determination of precious metals in sulphides and magnetite. Chapter 5 establishes the third micro-sampling technique: determination of precious metals in milligram samples of sulphides and magnetite using an automated 2 speed peristaltic pump speed controller for ICP-MS after separation of the precious metals from the associated base metals by

cation exchange.

(2) Part II, consisting of Chapters 6, 7, 8, 9 and 10, investigates geological applications of the micro-sampling ICP-MS techniques developed in Part I to the study of precious metal-rich Ni-Cu sulphide ores at Sudbury. The advantages of micro-sampling techniques are demonstrated in the study of specific geological problems - distributions of precious metals and their partitioning among coexisting minerals, which are difficult to accomplish using earlier routine analytical techniques. Chapter 6 summarizes the geology of the Sudbury basin and the geological setting of the precious metal-rich Ni-Cu sulphide mineralization. The geology and geochemistry of the Sudbury Igneous Complex (SIC), and general features of the mineral deposits are described. The mineralogy, and metal zonation of the deposits are also presented. Chapters 7 and 8 present case studies of precious metal distributions of two of the mineral deposits. Chapter 7 describes the precious metal distribution in the well-studied Strathcona Mine in the North Range with emphasis on the Deep Copper Zone. Chapter 8 reports the study of the geochemistry and distributions of precious metals between and within sulphide minerals in a new deposit in the South Range - the Thayer Lindsley Mine, with emphasis on the 4B Ore Zone which is similar to the Deep Copper Zone. Chapter 9 summarizes the precious metal studies at Sudbury, particularly

the partitioning of precious metals between the principle ore minerals, and the mobility and fractionation of the precious metals in the footwall ores related to segregation and crystallization. Chapter 10 discusses the trace element geochemistry of the Sudbury ores and its implications for ore genesis.

Figures are located at the end of the respective chapters. Tables are included within the text.

Appendix I describes modifications to the nickel sulphide fire-assay collection and tellurium coprecipitation procedure for the determination of the precious metals, originally described by Jackson *et al.* (1990). Appendix II presents the locations and gives descriptions of the samples from the Sudbury Igneous Complex (SIC). Appendix III describes the analysis of pressed pellets of geological samples using wavelength dispersive X-Ray fluorescence spectrometry. Appendix IV presents Na_2O_2 sinter data acquisition and reduction procedures for the analyses of the rare earth elements (REE). Appendix V presents a publication related to this thesis.

CHAPTER 2

RECYCLING NEBULIZATION SYSTEM WITH A DISPOSABLE SPRAY CHAMBER FOR INDUCTIVELY COUPLED PLASMA-MASS SPECTROMETRY

2.1 INTRODUCTION

The usual method for sample introduction into an ICP-MS is solution nebulization, *viz.* a Meinhard concentric nebulizer with a Scott spray chamber. However, with this technique, the efficiency of transport of sample into the plasma is low with more than 95% of the sample discarded to waste (Isoyama *et al.*, 1990). Although poor sample transfer efficiency to the plasma is not generally important, there are analyses where the sample volume is limited by the weight of sample available or by the difficulty of dissolving large weights of sample. As well, in some geological materials, such as zoned minerals or fine-grained intergrowths, separation of large amounts of specific homogeneous phases may be very difficult or even impossible. In these cases painstaking manual separation is required to minimize the inclusion of minor phases.

Several designs of recycling nebulization systems have been reported which recycle the waste solution to the nebulizer (Novak *et al.*, 1980; Hulmston, 1983; Zhuang and Barnes, 1985; Vieira *et al.*, 1986; Zicai and

Barnes, 1986; and Kato and Takashima 1989). These systems demonstrated continuous nebulization with small volumes for long periods and the measurement of multiple elements with optical emission spectrometers. However, these systems have two major problems, *viz.* enrichment of the concentration of the sample solution by evaporation during analysis and memory effects which are signal enhancements caused by previous sample material remaining in the tubing, nebulizer, spray chamber and torch, and by the material deposited on and later eroded off the sample interference and skimmer. Evaporation of the sample solution can be reduced by humidifying the nebulizer gas, but the memory effect is a more severe problem (Isoyama *et al.*, 1990a). The dilution and contamination of samples by the liquid remaining in the spray chamber from previous samples and wash solutions, has not been addressed by previous workers. Recently Isoyama *et al.* (1990a) have reported a recycling configuration which used a replaceable spray chamber for ICP-AES. These workers discussed the problem of concentration of the sample by evaporation, however, they did not apply internal standards to correct for sample evaporation.

Alternative small sample introduction techniques are electrothermal volatilization (ETV) (Date and Cheung, 1987; Park and Hall, 1988; and Gregoire, 1988), flow injection analysis (FIA) (Thompson and Houk, 1986; Dean *et al.*, 1988; and Viczian *et al.* 1990), laser ablation microprobe (LAM)

(Gray, 1985; Arrowsrnith, 1987; Hager, 1989; Darke *et al.*, 1989a and 1989b; Longerich *et al.*, 1993; and Jackson *et al.*, 1993), direct insertion nebulizer (DIN) (Williams *et al.*, 1987), and ultrasonic nebulizer (USN) (Fassel and Bear, 1986; and Jin *et al.*, 1990). However, a recycling nebulization system has following advantages compared to these methods: 1) homogeneous solutions, 2) long data acquisition time (5 min) with a "stable" signal, and 3) the ability to reduce the weight of samples without the accompanying analytical difficulties of transient signal acquisition and data reduction.

In this chapter, a recycling nebulization system with a disposable spray chamber for ICP-MS is described. The performance of the system, in terms of precision, accuracy, sensitivity and the memory effect, is evaluated.

2.2 SCOPE AND PURPOSE

The design of the recycling nebulizing system was based on the following objectives:

(1) Reduce the consumption of sample solutions and enhance the efficiency of nebulization to allow the analysis of small sample volumes. Sample solution trapped in the spray chamber during the nebulization process is collected and recycled by mounting a concentric nebulizer inside a spray

chamber. When the chamber containing the sample is mounted, a closed nebulizing process ensues until all liquid forms an aerosol and is transported to the plasma.

(2) Produce a uniform aerosol droplet distribution and reduce pressure variation. The spray chamber is positioned vertically. This configuration ensures that generally the finest droplets are introduced into the ICP. Gravitational precipitation and inertial impaction of big droplets on the chamber wall are smooth.

(3) Eliminate memory effect. Earlier recycling systems have exhibited a larger memory effect than conventional nebulizer systems. With a disposable spray chamber, signal enhancements caused by previous sample material remaining in the spray chamber are avoided, and the memory effect can be eliminated.

With this new recycling nebulization system, 0.5 g of sample solution is sufficient for 8 min of data acquisition. The sensitivity of the recycling nebulization system is similar to a conventional Scott spray chamber system. Twenty six trace elements can be determined by ICP-MS using four internal standards (Ge, In, Re, and Bi) to correct for matrix, instrumental drift, and enrichment of the sample solution by evaporation. The ability to analyze mineral separates weighing less than 0.1 mg is demonstrated with detection

limits similar to conventional procedures. Analyses of selected geological reference materials SY-2, BCR-1, and W-1 indicate good limits of detection, good accuracy and precision, negligible memory, and low consumption of sample solution. Results compare well with data reported using conventional ICP-MS analysis.

2.3 EXPERIMENTAL

2.3.1 INSTRUMENTATION

The instrument used in these studies was a modified SCIEX (now Perkin-Elmer SCIEX) ELAN model 250 ICP-MS (Longerich *et al.*, 1986; Longerich *et al.*, 1987; and Longerich, 1989). The sampler and skimmer are slightly modified and made in-house (Jackson, *et al.*, 1990). The instrument has been upgraded to the model 5000 computer system using Perkin-Elmer supplied hardware and software for model 250 and 500 instruments (Chen *et al.*, 1992a). All of the old printed circuit boards in the computer rack were removed and replaced with 2 new boards. One of these boards is connected to an IBM PS/2 Model 70, 386/387 computer using IEEE-488 interface hardware. New ELAN 5000 software, from Perkin-Elmer, version 1.04-ICPS (a modification of version 1.04 which incorporates an ICP Shut-off enhancement) was used. For automated

analysis, a Gilson 212B autosampler was used which replaced the ISCO ISIS autosampler. The Gilson supplied sipper was replaced by a piece of quartz tubing (3 mm o.d. and 1 mm i.d.) installed in a teflon holder, fabricated in-house.

No on-line concentration calculations were made. Only count rates were collected using the ELAN software. The ELAN software was used to create "report" files, which contain the count rate data in an ASCII format. These files are translated using a complied, in-house written, Microsoft Basic program which translates the data into a Lotus formatted spread sheet file, and saves the file to floppy disc. This translate program is executed under the SCIEX recommended DOS shell, vpix. All subsequent data manipulations were done off-line using commercial spread sheet software on personal computers. For each analytical run (4-12 hours), the nebulizer gas flow was adjusted to 0.9-1.1 l min^{-1}, using a solution containing 100 ng g^{-1} of Cs and Th (Jenner *et al.*, 1990), so that: (1) $ThO^+/Th^+ < 0.1$; (2) sensitivity of Cs > 1000 (counts sec^{-1})/(ng g^{-1}), and (3) sensitivity of Bi > 500 (counts sec^{-1})/(ng g^{-1}). These conditions represent a compromise between maximum sensitivity and minimum polyatomic ion formation. Other operating conditions are given in Table 2.1.

Table 2.1 ICP-MS operating conditions	
Inductively coupled plasma:	
Plasma gas	Argon
Forward power	1200 W
Reflected power	< 5 W
Gas flow:	
Plasma (outer) gas flow-rate	13.0 l min^{-1}
Auxiliary (intermediate) gas flow-rate	1.0 l min^{-1}
Nebulizer (inner) gas flow-rate	see text
Interface:	
Sampling distance (load coil to sample aperture)	21 mm
Sampling aperture	Nickel, 1.1 mm diameter
Skimmer aperture	Nickel, 0.9 mm diameter
Ion lens settings:	
B lens	7.0 V
P lens	-9.0 V
E-1 lens	-19.8 V
S-2 lens	0 V
Data acquisition parameters:	
measurement mode	multichannel
Replicate time	10 s
Dwell time	50 ms
Sweeps/replicate	200
Number of replicates	1
Points across peak	1
Resolution	Normal

2.3.2 RECYCLING NEBULIZATION SYSTEM

Two recycling nebulization systems, referred to here as "cyclone" and "parallel", (Figure 2.1) were evaluated. It is recognized that the dimensions of the "cyclone" spray chamber are not large enough for true cyclone gas flow dynamics, the term "cyclone" being used only to describe the configuration. Both systems consisted of a nebulizer, disposable spray chamber, glass transport tube, and holder. A concentric nebulizer (either Meinhard, model SB-30-C1 or TR-30-C1) was used with a PTFE capillary tubing for sample recycling (25 mm long, 0.3 mm i.d. or 0.5 mm i.d.). The design of the disposable spray chamber was constrained by the availability of low cost and instrumental dimension considerations. The disposable spray chamber was a screw-top plastic centrifuge tube (25 mm o.d., 107 mm high, 30 ml capacity, Sarstedt). The 8 mm o.d. Pyrex transport tube, with the end expanded to 12 mm o.d. to reduce blockage, was connected to the ICP torch with 0.75 m of 8 mm o.d. tygon tubing. The holder was constructed of teflon and used O-ring seals for the nebulizer and the glass transport tube, and a press fit for the teflon solution transport tubing. In the "parallel" recycling nebulization system, the concentric nebulizer was positioned vertically and parallel to the transport tube (Figure 2.1a), while in the "cyclone" system (Figure 2.1b), the nebulizer was positioned perpendicular to the transport tube. Initial experiments demonstrated that the "parallel" recycling system yielded sensitivities higher

than the "cyclone" recycling system. Further investigations were restricted to the "parallel" recycling system.

2.3.3 SAMPLE PREPARATION AND REAGENTS

Certified American Chemical Society (A.C.S.) acids were distilled in nonboiling quartz or teflon stills and diluted with Barnstead Nano-pure deionized-distilled water. Standard and spike solutions for each element were prepared by dissolving ultra-pure metals (AMES Laboratory, Ames, Iowa, U.S.A.), or Plasma Grade powders (SPEX Industries, Metuchen, New Jersey, U.S.A.) using HNO_3 and deionized-distilled water. A 0.05% solution of the surfactant, Triton X-100, in water was used in all experiments. Preparations of sample and standard solutions were carried out in a Class 100 clean laboratory facility. All solutions were prepared and dispensed by weight.

Geological reference materials and their distributers are listed in Table 2.2

The sample preparation procedure was modified from Jenner *et al.* (1990) as follows:

1) 100 mg of powdered samples (10 mg for apatite and amphibole samples) were dissolved in 15 ml covered screw-top teflon jars (Savillex) using 1 ml of HF and 2 ml of 8 M HNO_3 on a hot plate at 150^{0}C for a day.

2) Sample solutions were evaporated to dryness in the opened jars

at 75-100°C. Silicon was thereby removed as SiF_4 after the evaporation.

3) Steps (1) and (2) were repeated.

4) Approximately 2 ml of 8 M HNO_3 was added to each sample solution, and then sample solutions were evaporated to dryness in the opened jars at 75-100°C.

5) step (4) was repeated.

6) The samples were diluted with 0.2 N HNO_3 by weight to a final weight of 90 g (20 g for apatite and amphibole samples) to a final acid concentration of approximately 0.2 M HNO_3, in 125 ml polyethylene bottles (Nalgene).

Table 2.2 Description of the geochemical reference materials used in this study and their suppliers

Samples	Suppliers	Materials
SY-2	Canada Centre for Energy and Mineral Technology (CANMET)	Syenite
BCR-1	U.S.G.S. (United State Geological Survey, U.S.A.)	Basalt
W-1	U.S.G.S. (United State Geological Survey, U.S.A.)	Diabase
Apatite	Dr. B.J. Fryer	Apatite from Gaultois granite, Newfoundland
Amphibole	Dr. B.J. Fryer	Amphibole from Preissac-Lacorne batholith, Abitibi Greenstone Belt

2.3.4 SAMPLING CHANGING PROCEDURE

While Isoyama *et al.* (1990a) used a stop valve on the tubing which led to the ICP torch for sample exchange, it was observed that the argon back pressure of the plasma gas is sufficient to flush the spray chamber and further that the torch will not be extinguished when the nebulizer line to the torch is opened to the atmosphere. If the spray chamber is slowly attached, argon from the torch will flush air from the spray chamber, and the need for a valve, which must act to some extent as an obstruction and hence as a cause of memory, is removed.

Sample changes, without extinguishing the plasma, were achieved using the following procedure:

(1) The R.F. power trip was disabled.

(2) The capillary tubing was withdrawn from the solution. After the solution remaining in the tubing was completed aspirated, the nebulizer gas flow was turned off.

(3) The spray chamber was removed.

(4) Liquid which remained on the inside surface of the chamber holder, the nebulizer, and the transport tube was removed with a Kimwipe tissue paper.

(5) The inside surfaces of the holder, the nebulizer, and the transport tube were rinsed using 0.2 M HNO_3 from a wash bottle.

(6) As in step (4), adhering liquid was removed.

(7) A new spray chamber containing 10 g of 1 M HNO_3 wash solution was slowly attached.

(8) The nebulizer gas flow-rate was slowly increased to approximately 1 l min^{-1}, while maintaining the R.F. reflected power < 50 W. The capillary tubing was then inserted into the solution.

(9) The wash solution was nebulized for 1 min to wash the nebulizer and capillary tubing.

(10) Steps (2), (3), (4), (5), and (6) were repeated.

(11) A new spray chamber, containing the next sample, was attached as in step (7) and (8).

(12) The R.F. power trip was enabled. Total time for changing samples was 15 minutes., including wash.

2.3.5 DATA ACQUISITION AND CALIBRATION

Mass selection and interferences are as in Jenner *et al* (1990). The sensitivities of all but two of the analyte elements were measured in one of the two external standard solutions (STDA or STDB, Table 2.3). The sensitivities for Nb and Ta were determined by surrogate calibration because of potential solution instability and memory effects (Jenner *et al.*, 1990). The sensitivity ratios were: $^{93}Nb/^{90}Zr = 1.504$ and $^{181}Ta/^{177}Hf = 4.81$. The elements Ge, In, Re, and Bi (Table 2.3) were used as internal standards. An accurately weighed

Table 2.3 Elements and concentrations for STDA, STDB, and internal Standard.

Element	STDA (ng g^{-1})	STDB (ng g^{-1})	Internal Standard (ng g^{-1})
Ge			46180
Rb	157.9	198.7	
Sr	658.9		
Y	104.2		
Zr	205.5		
In			3930
Cs	112.2	99.5	
Ba	993.9		
La	110.7		
Ce	88.9	107.4	
Pr	105.2		
Nd		204.5	
Sm		194.3	
Eu		206.6	
Gd		197.9	
Tb	94.5		
Dy	243.0		
Ho	105.5		
Er	186.8		
Tm	92.9		
Yb	109.9		
Lu		108.3	
Hf		79.1	
Re			9690
Bi			3450
Pb	251.7		
Th	89.0	107.7	
U	93.5		

aliquot of approximately 20 mg spike was added to each 2 g of sample solution. To decrease the liquid adhering to the inside surfaces of the nebulizer system, 1 drop of the Triton X-100 surfactant solution was added to each sample (Isoyama *et al.*, 1990). For samples in which Th was known to be low, 0.05 g of a 3 μg g^{-1} solution of Th was added to monitor oxide formation, precluding the determination of Th. Samples were run in the following sequence: acid calibration blank (0.2 M HNO_3), STDA, flush (1 M HNO_3), STDB, flush, acid calibration blank, sample 1, flush, ..., sample 4, flush, acid calibration blank, STDA, *etc.* After the data was collected, the background was calculated as the mean of 6 determinations of the acid blank. The most significant interferences in the suite of elements determined in this study are those of Ba and the light REE oxides on the heavy REE, Hf, and Ta (Jenner *et al.*, 1990; Jarvis, 1989). For each sample, all oxide interference factors are normalized to the $^{232}ThO^+/^{232}Th^+$ ratio measured in the standard solutions (Jenner *et al.*, 1990). After instrument drift and matrix effects were corrected, sample solution concentrations were calculated by external calibration using the mean sensitivity of the 2 closest calibration standards. Solid sample concentrations were then calculated from sample and solution weights.

2.4 RESULTS AND DISCUSSION

2.4.1 COMPARISON BETWEEN THE RECYCLING NEBULIZATION SPRAY CHAMBER AND THE SCOTT SPRAY CHAMBER SYSTEM

In order to evaluate the sensitivity of the recycling nebulizer spray chamber system with that of the Scott system under similar conditions, the Scott spray chamber was mounted outside the match box and connected to the ICP torch using approximately 0.75 m of 8 mm o.d. tygon. Solutions containing 100 ng g^{-1} of Y, Tm, and Bi were nebulized using nebulizer gas flow rates of 0.7 to 1.3 l min^{-1} for both systems. The 2 systems were alternated to correct for instrument drift. Figure 2.2 demonstrates that the analytical sensitivity of the recycling nebulization system is similar to those obtained with the Scott spray chamber system in this configuration.

2.4.2 MINIMUM SAMPLE SOLUTION REQUIRED FOR DATA ACQUISITION

One of the aims of this study was the reduction of solution consumption, to make possible the analysis of small quantities of, or low concentrations in, geological materials. Note that in all work reported in this study, all solution are prepared and dispensed by weight and hence are reported in weight units. The use of weight rather than volume allows accurate measurements to be made quickly over a large dynamic range, thus the "volumes" reported in this section

are measured in g of solution. In initial work, a standard concentric nebulizer (Meinhard, model TR-30-C1) with a PTFE capillary tubing for sample recycling (25 cm length, 0.5 mm i.d.) was used and the dead volume was found to be 0.29 g (Figure 2.3). Using this configuration, 0.5 g of solution was sufficient for 5.4 min of data acquisition. In order to further reduce the minimum volume, a "Small Bore", SB-30-C1 Meinhard nebulizer was used, with a smaller i.d. (0.3 mm) PTFE capillary tubing. A "TR" nebulizer has a glass solution input tube which is 4 mm o.d. with an i.d. of 2 mm. A "SB" nebulizer is identical to a "TR" nebulizer except for a modified solution input tube which has a reduced o.d. of 3 mm and an i.d. of 1 mm. This nebulizer was connected to the tubing using a two-way OMNIFIT (Atlantic Beach, New York) connector. These modifications reduced the dead volume from 0.29 g to 0.25 g, and increased data acquisition time for a 0.5 g sample from 5.4 minutes to 8 minutes.

To determine the fraction of the dead volume contained in the nebulizer and capillary tubing, water was nebulized for 2 min, and the nebulizer and capillary tubing weighed. Then the nebulizer and capillary tubing were dried in an oven at 60°C for 1 hour and their dry weight again recorded. This determined that of the total 0.25 g dead volume, 0.08 g was contained in the nebulizer and capillary tubing, while 0.17 g was in the spray chamber, holder, and transport tube.

2.4.3 DRIFT AND MATRIX EFFECTS

Drift and matrix effects can not be separated chemometrically and in this study are both corrected using internal standards. In a long ICP-MS run sensitivity typically drifts. In an analysis using a recycling nebulization system, the gradual enrichment of samples with time (Figure 2.4), due to evaporation, is a more serious cause of signal change (Isoyama, *et al.*, 1990; Zicai and Barnes, 1986; and Kato and Takashima, 1989). Matrix effects also cause signal enhancement or depression in sample solutions relative to calibration standards. Matrix effects are mass dependent, with the light elements more significantly affected by the matrix than heavy elements (Doherty, 1989; and Longerich *et al.*, 1990). In this study, the drift-matrix corrections were made using a mass interpolation of the correction factor determined from the intensities of the internal standards; Ge, In, Re, and Bi in the calibration standards and samples.

2.4.4 MEMORY EFFECTS

Signal enhancements can also be caused by the previous sample remaining in the tubing, nebulizer, spray chamber, and torch; or being deposited on the ICP-MS sampler and skimmer interface cones (Longerich *et al.*, 1990). A major difficulty in the use of poorly designed spray chambers is memory caused by inadequate washing of the previous sample from the chamber, caused in part by poor gas flow dynamics. Systems, such as those used in this study, which

use replaceable spray chambers and manual washing, reduce spray chamber memory to insignificant levels. In this study, calibration blanks immediately following standards showed no observable contamination.

2.4.5 LIMITS OF DETECTION (LOD's)

Limits of detection (LOD's) are a measure of instrument performance, defined here as 3 times the standard deviation of the difference between the count rate of a sample and n replicate determinations of the count rate of the calibration blank. The limit of detection is calculated as $[3*\sigma*\sqrt{(1/n+1)}]$, where σ is expressed in concentration units. Solid limits of detection, for a 100 mg sample dissolved in 200 g solution (0.5 g solid/kg solution), and with 6 determinations of the calibration blank ($n=6$), are given in Table 2.4. For samples prepared at lower concentrations, the limits of detection increase proportionally.

2.4.6 PRECISION AND ACCURACY

Results obtained in this study for the 3 geological reference materials, SY-2, BCR-1, and W-1 are presented in Table 2.4 and Figures 2.5-2.7. Relative standard deviations for most elements are less than 5% (Table 2.5 and

Table 2.4 Concentrations (g g^{-1}) obtained in this work (recycling nebulizer), the same solutions analyzed using the method of Longerich *et al.* (1990), and literature values, for the geological reference materials; SY-2, BCR-1 and W-1. Solid limits of detection are calculated for samples prepared at 0.5 g solid per kg solution.

	Recycling Nebulizer			ICP-MS Standard Addition Procedure		Literature Values			Solid Limits of detection
	SY-2 n=1	BCR-1 n=2	W-1 n=2	SY-2 n=5	BCR-1 n=5	SY-2*	BCR-1**	W-1**	(g g^{-1})
Rb	226	49.7	19.9	221	47.1	226	47.2	21.4	0.028
Sr	286	358	198	275	338	270	330	186	0.06
Y	128	35.5	20.6	120	33.1	129	38	26	0.009
Zr	300	199	90.9	294	186	306	190	99	0.06
Nb	36.1	13.2	8.50	33.6	13.8	30	14	9.9	0.0007
Cs	2.70	0.97	0.89	2.59	0.87	2.7	0.96	0.96	0.015
Ba	452	684	155	459	696	445	681	162	0.19
La	73.1	26.1	11.1	70.7	25.8	67	24.9	11	0.008
Ce	168	54.9	23.4	167	55.2	159	53.7	23.5	0.015
Pr	20.0	6.82	2.93	20.3	6.95	19.5	6.8	3.2	0.008
Nd	76.3	28.3	12.6	77.7	29.1	73.7	28.8	14.6	0.013
Sm	15.8	6.54	3.17	16.3	6.65	15.7	6.59	3.68	0.016
Eu	2.40	1.92	1.06	2.55	1.98	2.5	1.95	1.12	0.016
Gd	17.5	7.05	3.69	17.9	7.45	16.8	6.68	4.01	0.016
Tb	2.89	1.02	0.59	2.97	1.05	3.1	1.05	0.63	0.008
Dy	19.9	6.19	3.65	20.5	6.41	21.3	6.34	3.39	0.019
Ho	4.57	1.24	0.74	4.67	1.28	5.1	1.26	0.81	0.007
Er	15.1	3.55	2.12	15.3	3.68	15.2	3.63	2.3	0.015
Tm	2.41	0.50	0.32	2.51	0.53	2.4	0.56	0.34	0.009
Yb	17.2	3.28	1.94	18.1	3.39	18.1	3.38	2.03	0.005
Lu	2.91	0.50	0.31	2.99	0.51	2.9	0.51	0.317	0.009
Hf	8.07	4.96	2.38	8.69	5.00	8.4	4.95	2.5	0.010
Ta	1.77	0.63	0.54	1.82	0.77	1.9	0.81	0.48	0.0011
Pb	82.1	12.4	6.34	95.5	14.0	96	13.6	7.5	0.08
Th	392	6.20	2.31	385	5.94	389	5.98	2.4	0.05
U	275	1.73	0.61	298	1.74	297	1.75	0.57	0.004

*Longerich *et al.* (1990) **Govindaraju (1989)

Figures 2.5-2.7). Accuracy, calculated as the relative difference between this work and literature values is given in Table 2.5 and Figure 2.7. The relative difference for most of elements is less than 15%; and is less than 10% for the more abundant elements.

Analytical data of two mineral separates; apatite and amphibole, obtained using the recycling nebulization system and a modified standard addition procedure using conventional nebulization and Scott spray chamber at MUN are presented in Table 2.6 and Figures 2.8-2.9. Results acquired using these two technique are quite comparable. Relative standard deviations for most elements using the recycling system are less than those using conventional and Scott spray chamber.

2.5 CONCLUSIONS

A recycling nebulization system with a disposable spray chamber is demonstrated for ICP-MS. The system described operated successfully to provide 8 min of data acquisition using 0.5 ml of sample solution. The memory of preceding samples was reduced to insignificant levels by the use of a removable, disposable spray chamber with manual washing. The performance of the system, in terms of precision, accuracy, and sensitivity, is similar to, or better than, that of the conventional Scott spray chamber system using 10 ml sample volumes.

Table 2.5 Relative standard deviations (RSD) and relative differences (RD) (compared with literature values) in this work (recycling nebulizer), for geological reference materials; SY-2, BCR-1, and W-1.

	Relative Standard Deviations		Relative Differences		
	BCR-1 n=2 (%)	W-1 n=2 (%)	SY-2 (%)	BCR-1 (%)	W-1 (%)
Rb	1	1	-0.2	5.3	-7.0
Sr	1	2	5.7	8.5	6.2
Y	0.4	2	-0.7	-6.5	-20
Zr	0.6	2	-1.7	4.9	-8.2
Nb	1	0.03	16	-5.6	-14
Cs	0.9	0.6	-0.06	1.0	-7.5
Ba	3	3	1.6	0.4	-4.6
La	4	4	9.0	4.8	1.1
Ce	4	4	5.7	2.3	-0.6
Pr	4	3	2.4	0.3	-8.5
Nd	3	3	3.5	-1.7	-14
Sm	3	4	0.9	-0.8	-14
Eu	2	4	-4.2	-1.5	-4.9
Gd	0.4	2	4.1	5.5	-8.0
Tb	5	0.2	-6.7	-2.5	-6.4
Dy	7	2.8	-6.5	-2.3	7.6
Ho	6	0.3	-10.4	-1.3	-8.1
Er	5	0.8	-0.5	-2.2	-8.0
Tm	5	8	0.6	-10	-5.5
Yb	1	1	-4.9	-3.0	-4.5
Lu	3	2	0.5	-1.9	-2.2
Hf	0.1	4	-3.9	0.2	-4.8
Ta	0.2	5	-1.5	-22.5	12
Pb	65	0.9	-14.5	71.9	-15
Th	0.5	0.9	0.9	3.7	-3.8
U	5	4	-7.4	-1.0	6.9

Table 2.6 Comparison of the concentrations ($\mu g\ g^{-1}$) and relative standard deviations (RSD) obtained in this work (recycling nebulizer) and those for the same solutions analyzed using the method of Longerich *et al.*[13], for geological materials: apatite and amphibole.

	Recycling Nebulizer				ICP-MS Standard Addition Procedure			
	Apatite (n=3)		Amphibole (n=3)		Apatite (n=3)		Amphibole (n=3)	
	Mean	RSD(%)	Mean	RSD(%)	Mean	RSD(%)	Mean	RSD(%)
Rb	2.69	25	35.3	6	2.58	25	36.7	7
Sr	183		20.0	4	173	1	20.2	2
Y	1473	1	106	5	1367	1	106	8
Zr	0.95	28	356	7	0.35	50	355	9
Nb	1.66	18	4.53	56	1.41	13	4.38	60
Cs	0.27	21	0.10	4	0.26	19	0.09	5
Ba	5.02	26	5.94	2	5.39	20	6.10	6
La	155	0.7	105	3	156	4	109	8
Ce	467	0.4	96.3	2	482	3	101	7
Pr	77.4	0.7	22.0	4	76.9	3	22.8	8
Nd	394	0.6	82.2	6	391	8	86.9	8
Sm	175	0.8	17.0	6	173	4	17.5	9
Eu	23.4	1	2.22	4	23.4	4	2.27	10
Gd	255	3	20.0	9	258	5	20.1	11
Tb	43.1	3	3.43	3	42.1	5	3.30	10
Dy	238	2	19.9	2	231	5	19.6	9
Ho	39.6	2	3.89	3	38.2	6	3.81	9
Er	92.8	2	10.7	3	89.5	6	10.5	10
Tm	10.8	2	1.58	3	10.5	3	1.58	7
Yb	53.0	3	12.0	3	53.1	4	12.1	8
Lu	5.97	3	2.18	2	6.07	5	2.25	6
Hf	0		7.50	5	0.36	13	7.60	8
Ta	1.41	37	0.33	73	0.82	20	0.32	74
Pb	6.34	7	8.65	4	7.25	4	9.93	8
Th	1.49	29	0.75	14	1.39	24	0.82	5
U	1.07	8	0.18	43	1.01	10	0.19	21

Figure 2.1 Two recycling nebulization systems (a) "parallel" and (b) "cyclone", consist of a holder, concentric nebulizer, PTFE capillary tubing for sample recycling, a disposable screw top spray chamber and a Pyrex transport tube

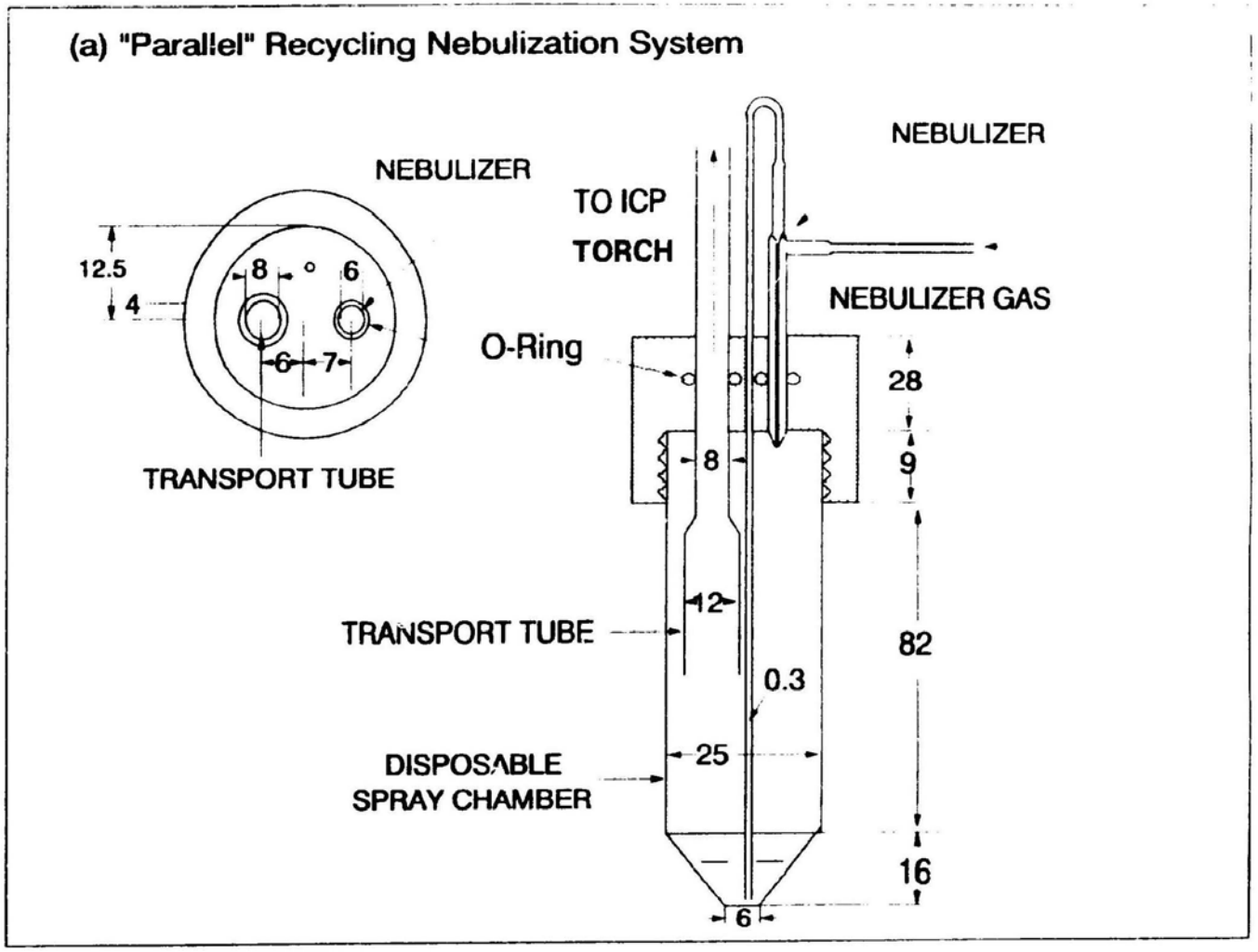
(a) "Parallel" Recycling Nebulization System
NEBULIZER
12.5
4
8
6
6
7
TRANSPORT TUBE
NEBULIZER
TO ICP
TORCH
NEBULIZER GAS
O-Ring
28
9
8
12
TRANSPORT TUBE
82
0.3
25
DISPOSABLE
SPRAY CHAMBER
16
6

(b) "Cyclone" Recycling Nebulization System

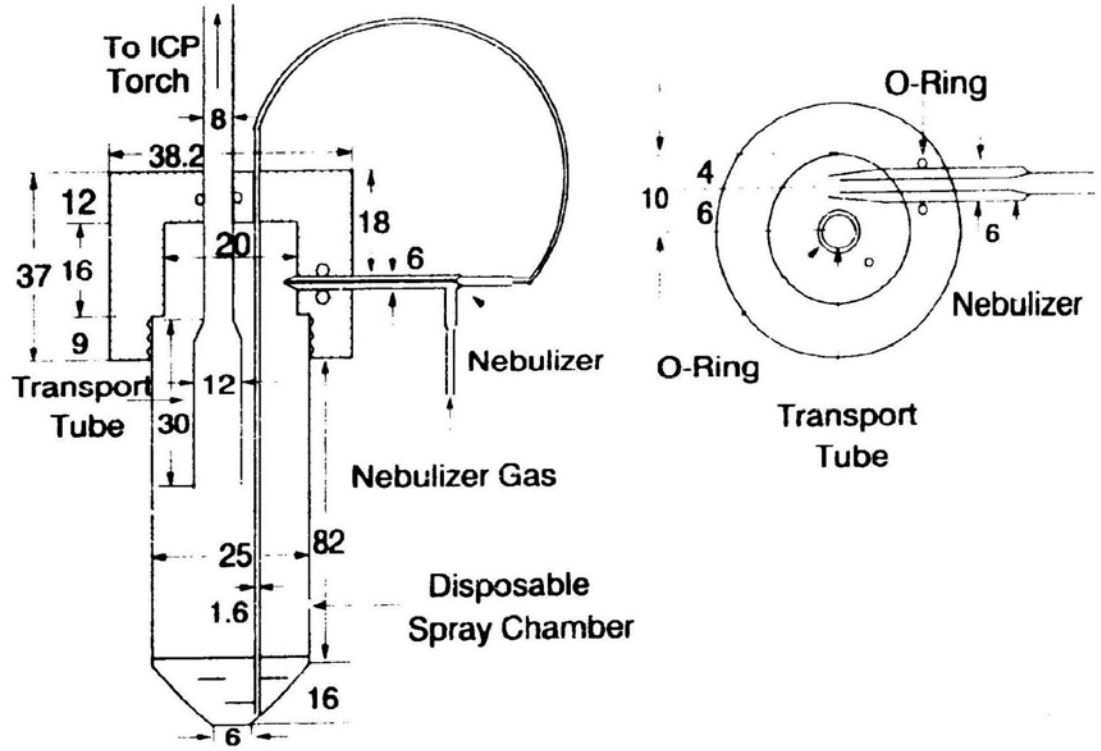

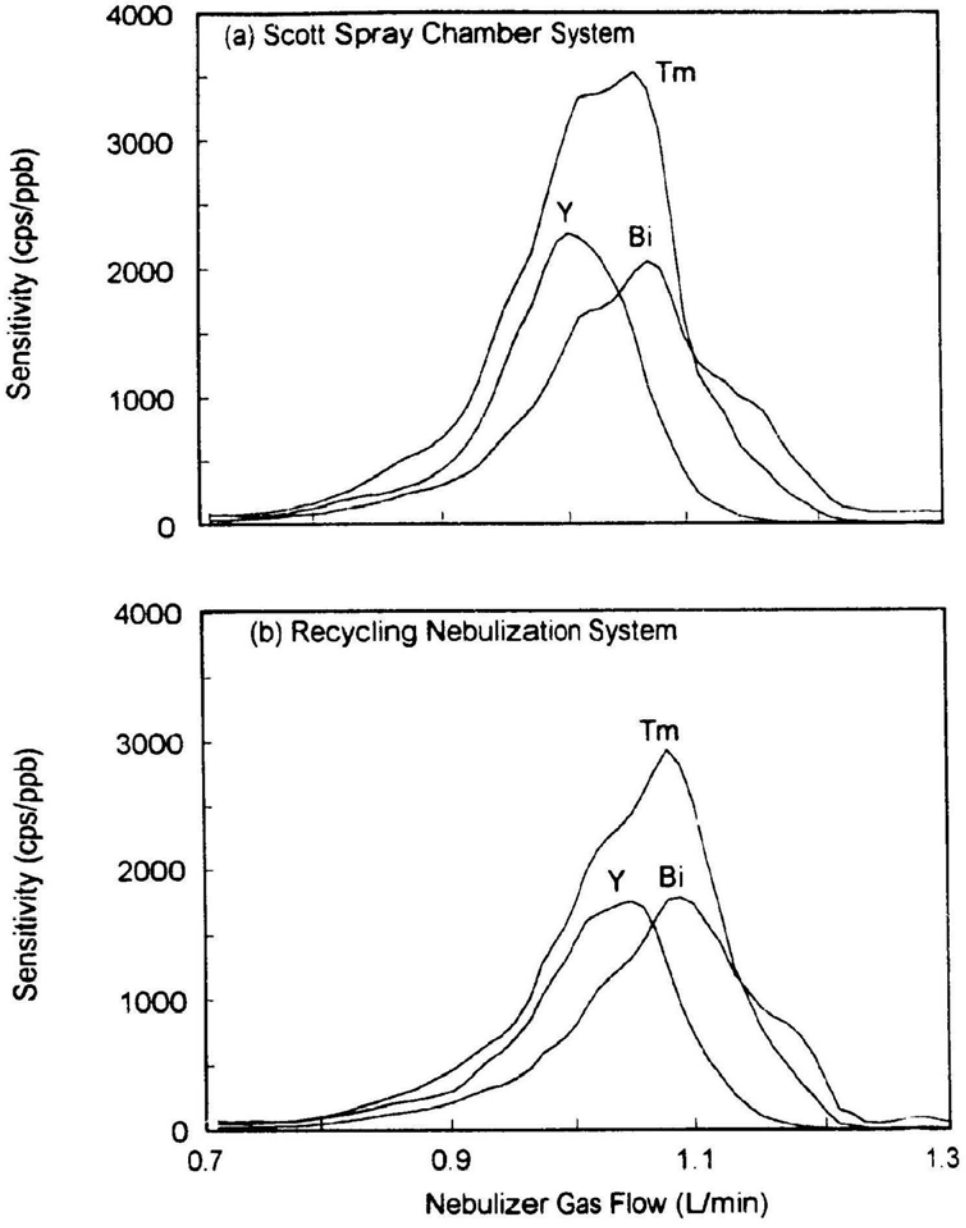

Figure 2.2 Sensitivity as a function of nebulizer gas flow rate for a solution containing 100 ppb of Y, Tm, and Bi. (a) The Scott spray chamber and (b) the recycling nebulization system

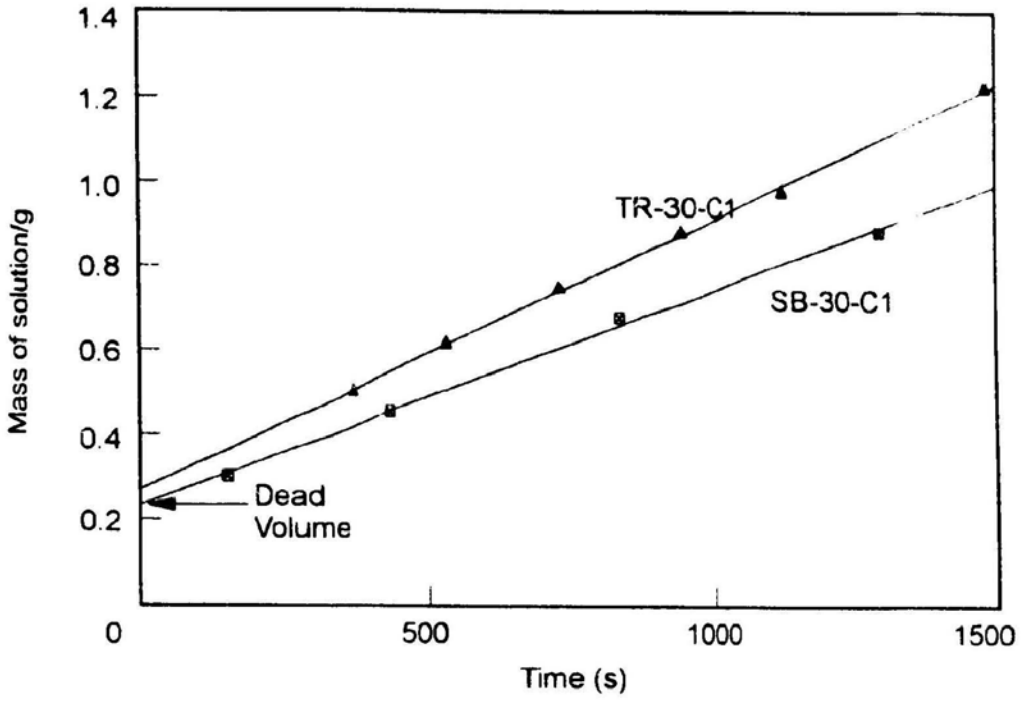

Figure 2.3 Mass of sample solution versus total nebulization time. Total nebulization time is taken as the time when the count rate reaches a maximum, as observed in Figure 2.4. Using the Meinhard SB-30-C1 nebulizer, 0.5 g of solution is sufficient for 8 min of data acquisition (dead volume = 0.25 g), while the TR-30-C1 nebulizer provides 5.4 min of data acquisition (dead volume = 0.29 g).

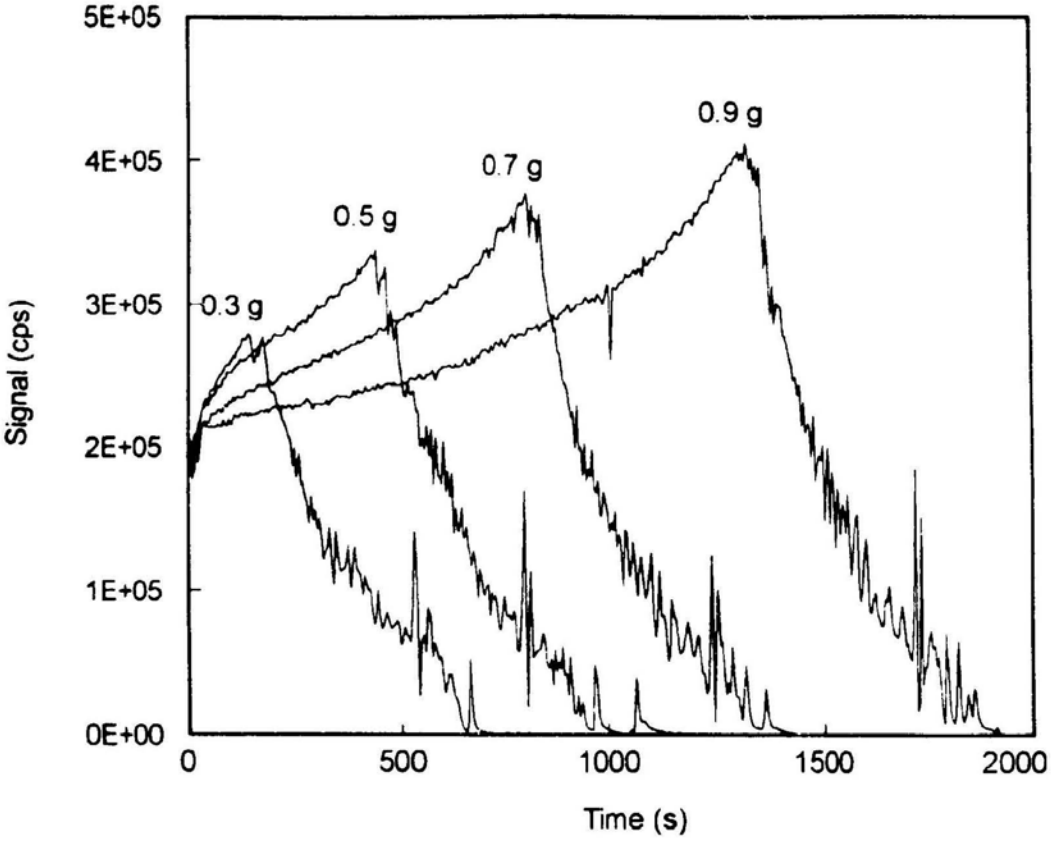

Figure 2.4 Signal versus time for various masses of sample solution: 0.3, 0.5, 0.7, and 0.9 g. Each solution initially contained 100 ng/g of Cs. Following the maximum count rate, the sipper is not continuously immersed in the solution, causing the sharp decrease in signal, while gas bubbles are periodically aspirated causing the large spikes in the intensity data.

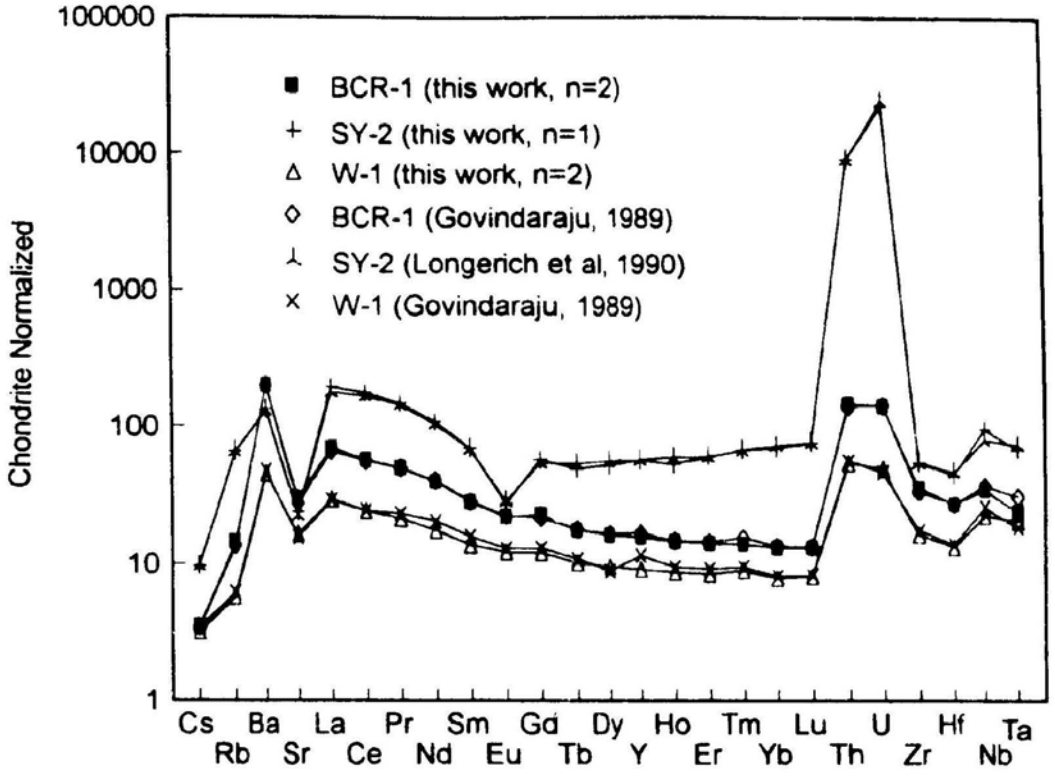

Figure 2.5 Mean chondrite-normalized data for geological reference materials SY-2, BCR-1, and W-1 Solutions were prepared using 100 mg sample dissolved in 100 g solution

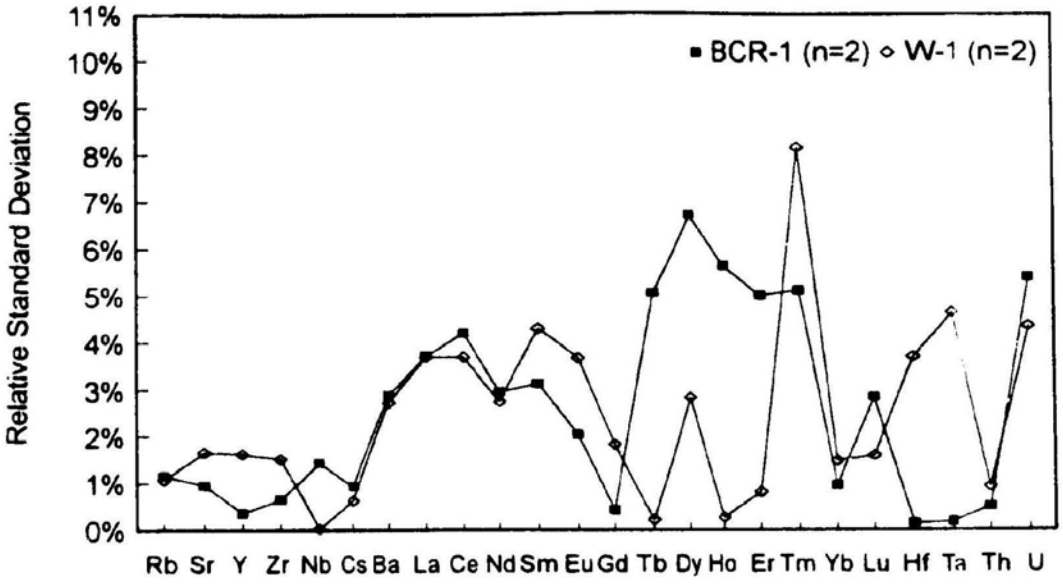

Figure 2.6 Precision expressed as relative standard deviation (RSD) obtained in the analysis of BCR-1 and W-1 using the recycling nebulizer system

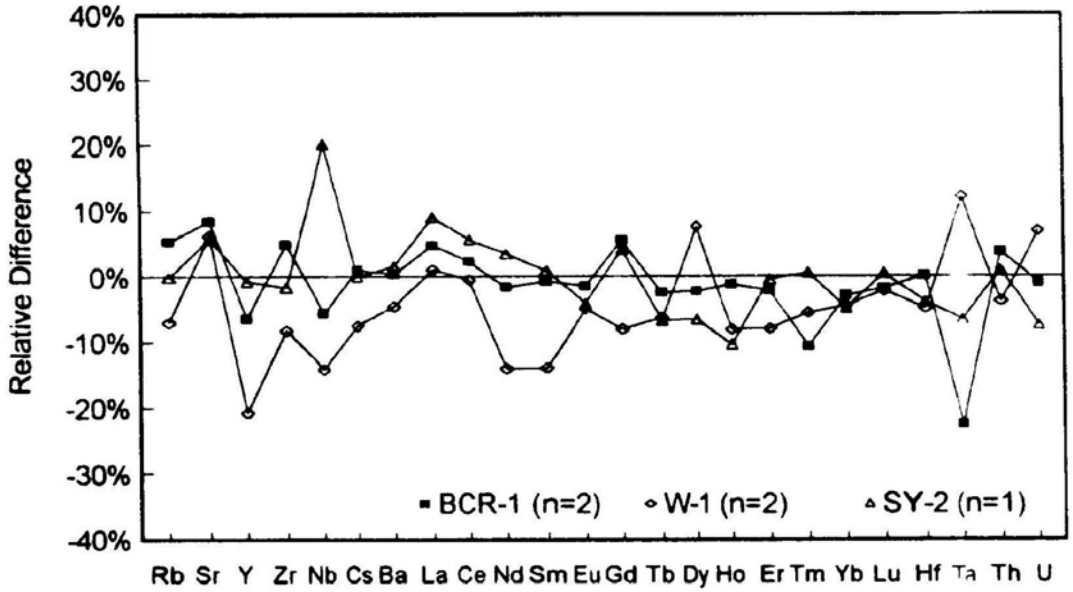

Figure 2.7 Accuracy expressed as relative difference between results obtained in this work, using the recycling nebulization system, and literature values for BCR-1 (n=2), W-1 (n=2), and SY-2 (n=1)

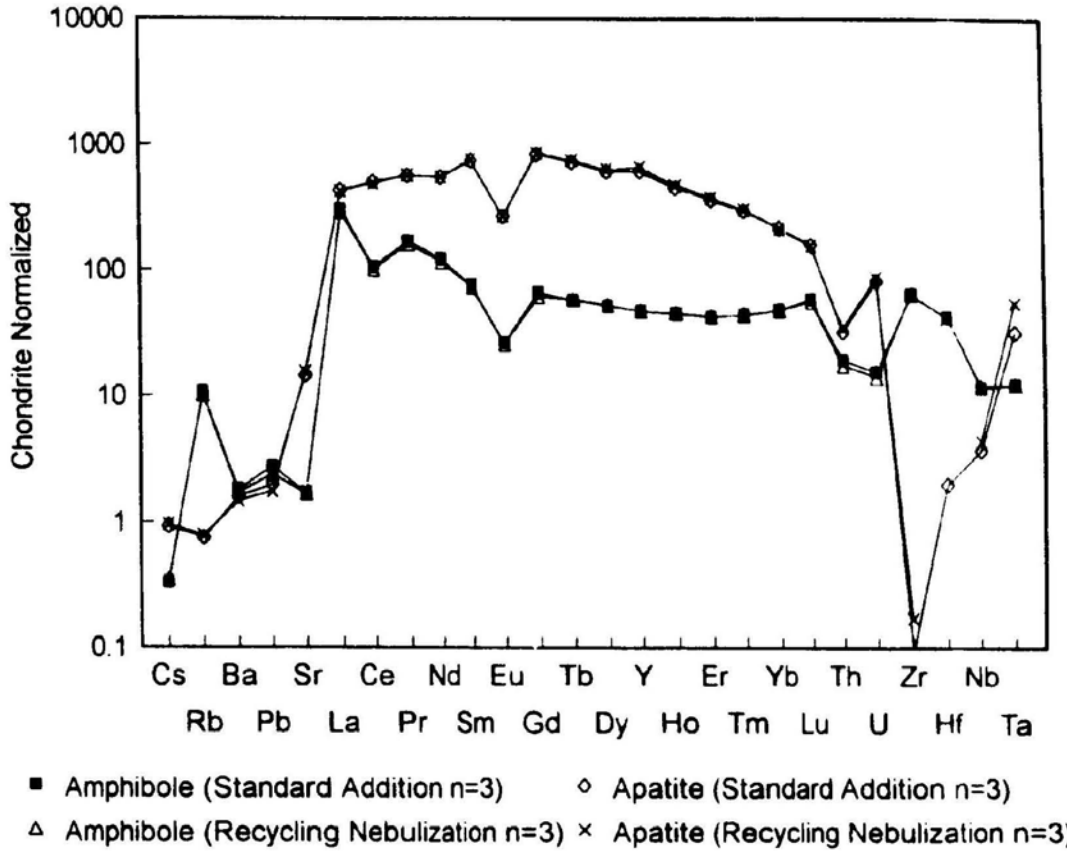

Figure 2.8 Mean chondrite-normalized data for geological samples: amphibole and apatite, using the recycling nebulization system and the standard addition procedure. Solutions were prepared using 10 mg sample dissolved in 20 g solution

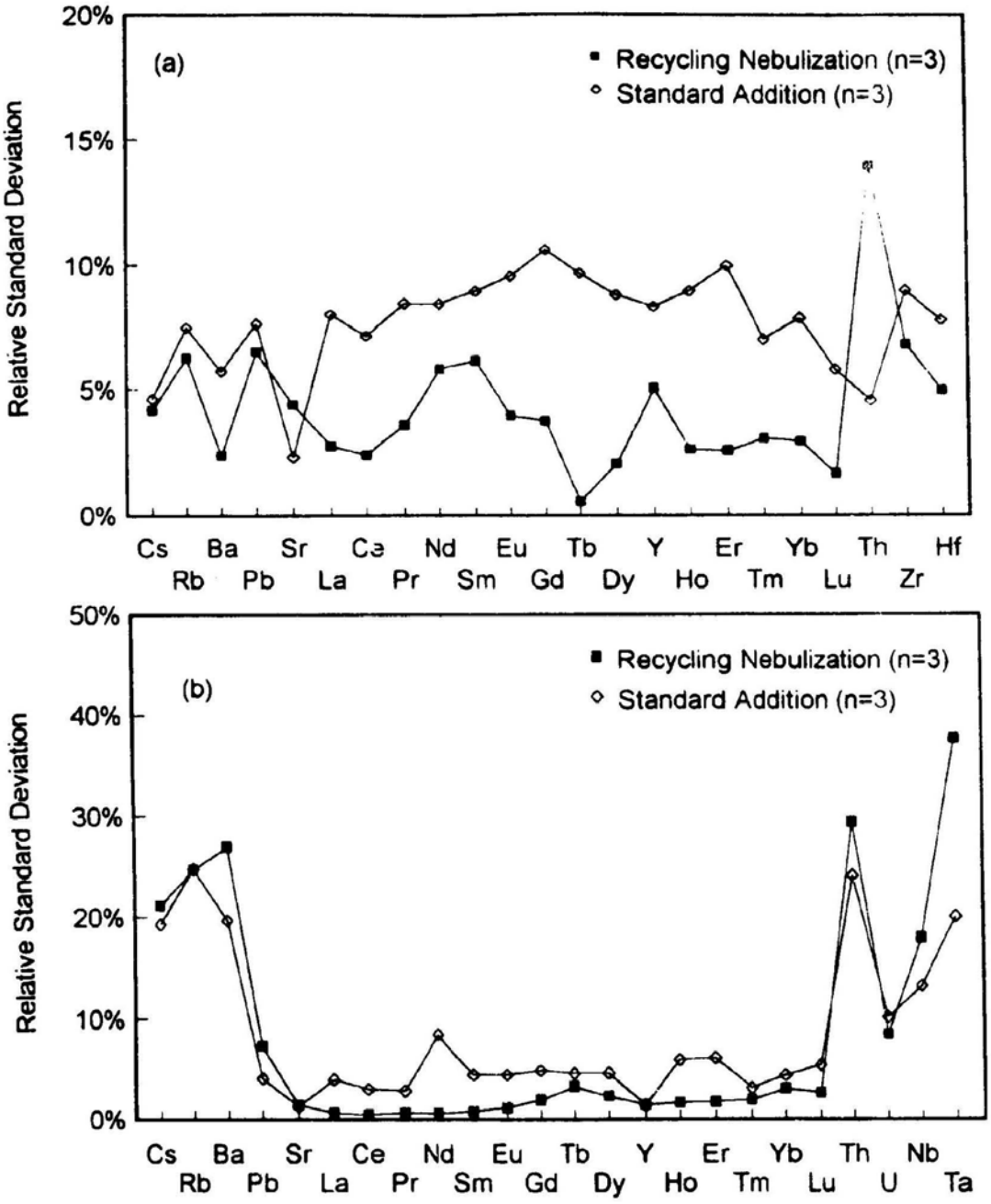

Figure 2.9 Precision expressed as relative standard deviation (RSD) obtained in the analysis of (a)amphibole and (b)apatite, using the recycling nebulization and the standard addition procedure

CHAPTER 3

TWO GEOANALYTICAL APPLICATIONS OF THE RECYCLING NEBULIZATION SYSTEM WITH A DISPOSABLE SPRAY CHAMBER FOR INDUCTIVELY COUPLED PLASMA-MASS SPECTROMETRY

3.1 INTRODUCTION

In this chapter, two geoanalytical applications which are difficult to accomplish by routine ICP-MS analysis are demonstrated using the recycling nebulization with a disposable chamber described in Chapter 2. Multielement trace element analyses of sub-milligram samples provide earth scientists a new technique to study the trace element geochemistry of very small samples and to investigate sample heterogeneity. The determination of the rare-earth elements (REE) at ultra-trace concentration levels after preconcentration is also demonstrated which has considerable applications to REE studies of ultramafic rocks.

3.2 TRACE ELEMENT ANALYSES OF SUB-MILLIGRAM SAMPLES

3.2.1 INTRODUCTION

Due to the poor efficiency of the standard solution nebulization system, the

standard trace element analysis package at Memorial University of Newfoundland (MUN) requires either 10 ml (internal standardization) or 20 ml (standard addition) of sample solution for analysis (Longerich, 1990). Although the poor efficiency in sample transfer to the plasma is normally of little importance where the amount of sample solution available is not limited, there are occasions when the volume is limited by the amount of sample available, or the amount that can be dissolved. In some geological applications, such as studies of zoned minerals or fine-grained mineral intergrowths, tens of mg of mineral separates of a specific phase may be very difficult or even impossible to obtain. Painstaking manual separation is required for accurate work to minimize the inclusion of minor mineral phases with potentially high trace element concentrations. To circumvent this problem it is advantageous to determine various elements by micro-sampling techniques. There are growing requirements to analyze very small samples in geological studies. To demonstrate the capability of the recycling nebulizer system, replicate small samples of Centre de Recherches Petrographiques et Geochimiques (CRPG) reference material BR were analyzed.

3.2.2 EXPERIMENTAL

3.2.2.1 INSTRUMENT

The instrument, operating conditions, data acquisition, and calibration used in this study were the same as those discussed in Chapter 2.

3.2.2.2 SAMPLE PREPARATION AND REAGENTS

Reagents used were the same as those of Chapter 2. Preparations of sample and standard solutions were carried out in a Class 100 clean laboratory facility.

Sample preparation, similar to that described in Chapter 2 was done, as follows:

(1) Sample weights varying from 0.01 to 1 mg were dissolved in triplicate in 5 or 2 ml screw-top teflon jars (Savillex) using 1 ml of HF and 1 ml of 8 M HNO_3.

2) Sample solutions were evaporated to dryness in the opened jars at 75-100°C. Silicon was removed as SiF_4 by the evaporations.

3) Steps (1) and (2) were repeated.

4) Approximately 1 ml of 8 M HNO_3 was added to each sample and the sample solutions were evaporated to dryness in the opened jars at 75-100°C.

5) Step (4) was repeated.

6) Each sample was diluted to a final weight of 2 g in a disposable spray chamber (30 ml screw-top plastic centrifuge tube, Sarstedt).

3.2.3 RESULTS AND DISCUSSION

Results of the replicate analyses are presented in Table 3.1. Accuracy for samples larger than 0.1 mg are shown in Table 3.2 and Figure 3.1. The agreement with data from X-ray fluorescence analysis (this work; determined at MUN using the procedure of Longerich, 1993) and literature values (Govindaraju, 1989) is acceptable, except for Ho, which is difficult to accurately determine using neutron activation or isotope dilution methods. The anomaly in the chondrite normalized diagram for Ho (Figure 3.1) suggests that the literature value is in error. For the 0.01 mg sample, there is also a significant disagreement for Ce, possibly due to partitioning of Ce^{3+} and Ce^{4+} in different minerals, which may suggest sample heterogeneity, and for elements like Lu, which are near the limit of detection. For comparison, limits of detection are presented in Table 3.3 and Figure 3.4, for various sample weights.

Relative standard deviations, for replicates (n = 3) of samples weighing more than 0.10 mg, are less than 10% for most elements (Table 3.4 and Figure 3.2). The RSD's for samples weighing 0.01 mg are from 30-60 % (Figure 3.2), suggesting that the large standard deviation of the data for the smallest sample

Table 3.1 Mean concentrations determined in this study ($\mu g\ g^{-1}$) and literature values for the geological reference material, BR, using various sample weights.

	1.00 mg n=3	0.50 mg n=3	0.20 mg n=3	0.10 mg n=3	0.01 mg n=3	100 mg (diluted to 0.01 mg level)	Standard Addition	XRF n=4	Literature Values
Rb	47.8	48.3	46.1	47.9	44.3	47.3	49.8	48.8	47
Sr	1424	1412	1328	1340	1070	1365	1368	1364	1320
Y	27.8	27.8	27.2	27.5	26.8	29.1	25.3	26.9	30
Zr	276	271	254	269	347	288	270	261	250
Nb	115	105	80.4	89.6	116	117	134	115	98
Cs	0.79	0.91	0.79	0.92	2.06	0.76	0.81	-	1
Ba	1068	1115	1068	1071	867	1095	1062	1161	1050
La	81.6	82.7	80.9	81.6	68.7	88.4	82.6	-	82
Ce	152	153	150	156	336	161	158	180	151
Pr	17.3	17.4	17.0	17.5	15.8	17.1	17.4	-	-
Nd	65.3	65.0	63.7	65.7	57.6	66.0	65.3	-	65
Sm	11.9	11.9	11.8	12.6	11.8	12.4	11.8	-	12
Eu	3.60	3.67	3.65	3.69	4.02	3.72	3.78	-	3.7
Gd	10.2	10.6	10.4	10.9	12.2	8.57	12.0	-	9.5
Tb	1.26	1.31	1.31	1.32	1.44	1.08	1.25	-	1.25
Dy	6.18	6.24	6.38	6.62	5.66	6.02	6.45	-	6.2
Ho	1.04	1.07	1.07	1.12	1.08	1.09	1.07	-	0.2
Er	2.53	2.55	2.51	3.04	3.05	2.08	2.53	-	2.4
Tm	0.30	0.35	0.31	0.43	0.46	0.31	0.33	-	-
Yb	1.67	1.69	1.76	1.76	1.77	0.32	1.79	-	1.9
Lu	0.23	0.29	0.25	0.27	0.70	0.19	0.25	-	0.25
Hf	5.62	5.56	5.31	5.69	8.33	7.19	5.76	-	5.4
Ta	4.30	4.71	4.56	4.52	10.8	4.64	5.24	-	6.2
Pb	5.74	7.83	11.6	12.4	67.7	9.62	5.78	6.3	8
Th	9.75	9.44	7.96	7.88	7.94	10.5	11.1	11.7	11
U	2.40	2.17	1.92	2.03	1.65	0	2.42	-	2.5

XRF: X-Ray Fluoresces Spectrometry Analysis.
Literature Values of BR are from Govindaraju (1989).

Table 3.2 Relative Difference (%) compared to literature values for the geological reference material, BR, for various sample weights.

	1.00 mg	0.50 mg	0.20 mg	0.10 mg	0.01 mg	100 mg (diluted)*
Rb	1.8	2.8	-2.0	1.9	-6	0.7
Sr	8	7	0.6	1.5	-19	3
Y	-7	-7	-9	-8	-11	-3
Zr	10	8	1.6	8	39	15
Nb	17	7	-18	-9	18	19
Cs	-21	-9	-21	-8	106	-24
Ba	1.7	5	1.7	2.0	-18	4
La	-0.4	0.8	-1.3	-0.5	-16	8
Ce	0.8	1.2	-0.5	3	122	6
Nd	0.4	0.05	-1.9	1.1	-11	1.5
Sm	-0.8	-0.6	-1.4	5	-1.9	4
Eu	-2.6	-0.7	-1.3	-0.04	9	-0.7
Gd	8	11	10	14	29	-10
Tb	0.8	5	5	6	15	-13
Dy	-0.22	0.7	3	7	-9	-3
Ho	422	437	433	464	438	445
Er	5	6	5	27	27	-14
Yb	-12	-11	-8	-7	-7	-83
Lu	-6	14	0.11	8	181	-22
Hf	4	2.9	-1.7	6	54	33
Ta	-31	-24	-26	-27	74	-25
Pb	-28	-2.1	46	54	746	20
Th	-11	-14	-28	-28	-28	-5
U	-4	-13	-23	-19	-34	-119

* 100 mg of a sample is dissolved, and then diluted to a solid concentration of 0.01 mg/2 g as per other.

Table 3.3 Solid limits of detection (ppm) for the geological reference standard BR with various sample weights.

	1.00 mg	0.50 mg	0.20 mg	0.10 mg	0.01 mg	100 mg (diluted)*
Rb	0.027	0.05	0.10	0.21	1.9	4
Sr	0.08	0.14	0.30	0.63	6	4
Y	0.016	0.029	0.06	0.13	1.2	0.4
Zr	0.11	0.20	0.4	0.9	8	1.9
Nb	0.008	0.015	0.03	0.07	0.6	0.26
Cs	0.020	0.04	0.08	0.16	1.4	2.4
Ba	0.18	0.3	0.7	1.4	2.8	18
La	0.018	0.03	0.07	0.14	1.3	0.5
Ce	0.023	0.04	0.09	0.18	1.6	1.3
Pr	0.007	0.013	0.028	0.06	0.5	0.4
Nd	0.026	0.05	0.10	0.20	1.8	3.4
Sm	0.025	0.04	0.09	0.20	1.8	1.9
Eu	0.029	0.05	0.11	0.23	2.1	1.2
Gd	0.030	0.05	0.12	0.24	2.2	2.0
Tb	0.008	0.015	0.03	0.07	0.6	0.4
Dy	0.014	0.024	0.05	0.11	1.0	0.8
Ho	0.010	0.017	0.04	0.08	0.7	0.4
Er	0.022	0.04	0.08	0.17	1.5	0.7
Tm	0.006	0.010	0.021	0.04	0.4	0.4
Yb	0.009	0.016	0.04	0.07	0.7	1.3
Lu	0.018	0.03	0.07	0.14	1.2	0.7
Hf	0.020	0.04	0.07	0.15	1.4	17
Ta	0.003	0.006	0.012	0.024	0.22	0.4
Pb	0.017	0.03	0.07	0.14	1.2	7
Th	0.06	0.102	0.22	0.5	4.1	17
U	0.019	0.03	0.07	0.15	1.3	42

* 100 mg of a sample is dissolved, and then diluted to a solid concentration of 0.01 mg/2 g as per other.

Table 3.4 Relative Standard Deviations (%) for geological reference standard, BR, using various weights of sample.

	1.00 mg	0.50 mg	0.20 mg	0.10 mg	0.01 mg	100 mg (diluted)*
	n=3	n=3	n=3	n=3	n=3	n=4
Rb	1.5	1.7	2.7	8	41	2.1
Sr	2.1	0.9	2.9	4	48	0.38
Y	2.1	1.1	2.8	7	34	3
Zr	2.4	0.8	2.8	6	34	1.6
Nb	11	6	17	15	79	2.4
Cs	2.7	14	8	11	51	52
Ba	3	2.4	5	1.2	46	1.2
La	4	1.3	2.3	6	57	2.1
Ce	4	1.7	2.3	1.9	44	2.4
Pr	3	1.3	2.4	7	43	0.9
Nd	4	2.5	4	5	45	2.4
Sm	5	4	4	11	38	4
Eu	4	5	3	6	40	7
Gd	1.9	6	6	14	35	23
Tb	1.4	4	4	11	33	13
Dy	1.8	1.7	4	8	44	6
Ho	1.3	2.8	2.8	8	36	11
Er	4	3.3	1.5	22	38	22
Tm	1.4	19	11	37	31	37
Yb	4	5	9	13	41	236
Lu	4	20	12	20	110	93
Hf	2.3	2.3	2.4	5	16	26
Ta	20	13	56	25	43	4
Pb	1.3	14	32	40	28	114
Th	4	4	8	4	61	53
U	9	6	2.5	38	38	-22

* 100 mg of the sample is dissolved, and then diluted to a solid concentration of 0.01 mg/2 g.

is due to sample heterogeneity. To demonstrate that the analytical error of the procedure for this size of sample is also generally less than 10%, a 100 mg sample was also prepared, and diluted to contain the same amount of sample as the 0.01 mg sample preparations. The result of these analyses, which measure analytical reproducibility on the same solution, is shown in Figure 3.3, where the RSD's are typically less than 10% for most elements. These results (Table 3.4 and Figure 3.3) show that the higher error for the determination of most elements in a 0.01 mg sample may be attributed in part to sampling heterogeneity. Based on these results for BR, analyses of samples of less than 0.1 mg are not reliable for establishing meaningful average composition.

3.2.4 CONCLUSIONS

A recycling Nebulization ICP-MS micro-sampling technique has been demonstrated to successfully analyze sub-milligram samples of geological materials.

3.3 DETERMINATION OF THE REE AT ULTRA-TRACE CONCENTRATION LEVELS AFTER PRECONCENTRATION

3.3.1 INTRODUCTION

In recent years, the precise and accurate determination of the REE in a range of rock types has become increasingly important. Interpretation of the REE geochemistry of igneous and metamorphic rocks and minerals is required for the development of many petrogenetic models. Inductively coupled plasma-mass spectrometry (ICP-MS) is a multi-element analytical method having detection limits across the whole mass range which are superior to most conventional techniques, particularly for heavy elements. However, there are samples in which the REE concentrations are below the detection limits (0.01-0.1 ppm) of whole rock procedures (Doherty, 1989) where samples are prepared at working dilutions of 0.5 g rock per kg solution (0.1 g per 200 g solution). Preliminary attempts to analyze these types of samples using standard techniques at MUN were unsuccessful due to high blanks. It is not possible to improve analytical sensitivity by increasing the sample size, since the ICP-MS is intolerant of high total dissolved solids (TDS) and matrix effects would increase (Longerich *et al.*, 1990). A procedure, such as ion exchange, which increases the concentration of the REE's while maintaining the total

dissolved solids at less then 0.1% is required.

In this study, the recycling nebulization system described in chapter 2 was used to analyze geochemical reference materials at ultra-trace levels, after preconcentrating the REE's from a standard 100 mg sample using cation exchange. Fifteen ultra-trace rare earth elements (REEs) have been determined in 5 international geochemical reference samples: PCC-1 (USGS), AL-1 (GIT-IWG), FK-N (ANRT), 70a and 99a (NBS). Solid limits of detection are 0.01-1 ppb. Sample heterogeneity was found.

3.3.1 EXPERIMENTAL

3.3.2.1 INSTRUMENT

The instrument used, operating conditions, data acquisition, and calibration were the same as those of Chapter 2.

3.3.2.2 SAMPLE PREPARATION AND REAGENTS

Reagents used were as detailed in Chapter 2. The geochemical reference materials and their suppliers are listed in Table 3.5 (Govindaraju, 1989; and Jarvis, 1988). Sample preparations and chromatography were carried out in a Class 100 clean laboratory facility. Sample preparation was similar to that described in Chapter 2 except for Step 6: samples were dissolved in 2 g of

mixed acid (1.13 M HNO_3-0.63 M HCL), and transferred onto cation exchange columns for separation instead of being diluted to a final concentration of approximately 0.2 M HNO_3 in 125 ml polyethylene bottles.

The procedure for quantitative separation of rare earth elements from the silicate matrix by cation exchange is as follows:

1) The cation exchange resin (Amberlite, CG-120) was transformed into the chloride form with 6 M HCl in a 600 ml teflon beaker for one week.

2) 10 ml of the resin slurry was placed into a 60 ml clean quartz column.

3) The resin was washed with 50 ml of 8 M HNO_3 followed by 50 ml of mixed acid (1.13 M HNO_3-0.63 M HCl).

4) The sample solution (in 2 g of the mixed acid) was transferred onto the cation exchange column.

5) 50 ml of mixed acid was added to the column; and major elements were eluted, and discarded.

(6) The REE were collected using 25 ml of 8 M HNO_3.

(7) The solution containing the REE's was evaporated to dryness in a 30 ml teflon beaker.

(8) The residue was dissolved in 0.5 g of 8 M HNO_3, and diluted to a weight of 2 g using 0.2 M HNO_3 in a disposable spray chamber.

(9) The sample solution was spiked with internal standards as described in Chapter 2.

(10) 0.05 g of a 3 ppm solution of Th was added to monitor oxide formation. A drop of 0.05% solution of the surfactant, Triton X-100, in water was added.

Table 3.5 Description of the geochemical reference materials used in this study, and their suppliers

Sample	Supplier	Material
PCC-1	U.S.G.S. (United State Geological Survey, U.S.A.)	peridotite
AL-1	GIT-IWG (Group International de Travail-International Working Group)	albite
FK-N	A.N.R.T. (Association National de la Recherche Technique), France	potash feldspar
NBS70a	N.B.S. (National Bureau of Standards), U.S.A., now NIST (National Institute of Standards and Technology)	potash feldspar
NBS99a	N.B.S. (National Bureau of Standards), U.S.A., now NIST (National Institute of Standards and Technology)	soda feldspar

3.3.3 RESULTS AND DISCUSSION

Limits of detection, defined here as 3 times the standard deviation of the difference between the count rate of a sample and n replicates of the

calibration blank, is calculated as $[3*\sigma*\sqrt{(1/n+1)}]$. Solid limits of detection, for sample weights of 100 mg dissolved in 2 g solution, based on 6 determinations of the calibration blank ($n=6$), are 0.01-0.1 ppb (Table 3.6 and Figure 3.5).

The results for the REE in the 5 international reference materials analyzed by recycling nebulization ICP-MS are presented in Table 3.7 and Figures 3.6-3.8 along with literature data (Govindaraju, 1989; and Jarvis, 1988). For the USGS reference material PCC-1, the agreement between this data and literature values (Govindaraju, 1989) for most elements, except Gd, is good (Table 3.7 and Figure 3.6). The anomaly at Gd in the chondrite normalized diagram (Figure 3.6) indicates that the literature value is suspect. Relative standard deviations for duplicates are less than 15% (Figure 3.7). Reference materials FK-N, AL-1, NBS70a and NBS99a are alkali feldspars. Analytical results are close to the literature values (Table 3.7), and show similar chondrite normalized patterns (Table 3.7 and Figure 3.8). Further work, such as isotope dilution and conventional ICP-MS analyses, are required to establish whether the differences are due to losses in sample preparation, inaccurate literature values, or sample heterogeneity. Sample heterogeneity has been observed in Pb concentration in alkai feldspars (Housh and Bowring, 1991)

Table 3.6 Solid limits of detection by recycling nebulization ICP-MS after preconcentration.

Element	La	Ce	Pr	Nd	Sm	Eu	Gd	Tb	Dy	Ho	Er	Tm	Yb	Lu	Y
LD(ppb)	0.3	0.7	0.2	0.8	0.7	0.8	0.7	0.09	0.5	0.1	0.6	0.1	0.5	0.4	0.1

3.3.4 CONCLUSIONS

A recycling nebulization ICP-MS micro-sampling technique has been demonstrated to determined ultra-trace REE concentrations in 5 selected geochemical reference materials. For homogenous samples (*e.g.*, PCC-1), very good results are obtained. There are significant problems with sample heterogeneities in using small samples to determine ultra trace concentrations. For these types of sample, a certain minimum number of determinations (or increasing sample size) are required to obtain representative values.

Table 3.7 Concentrations (ppm) in geochemical reference samples determined by recycling nebulization ICP-MS. The data are compared to the literature values of Govindaraju (a) and Jarvis (b).

PCC-1 (Peridotite)

	No.1*	No.2	Average	Literature values (a)
Ce	0.066	0.072	0.069	0.1
Pr	0.0076	0.0087	0.0081	0.013
Nd	0.031	0.033	0.032	0.042
Sm	0.0091	0.0073	0.0082	0.0066
Eu	0.0018	0.0015	0.0016	0 0018
Gd	0.0071	0.0082	0.0076	0.014
Tb	0.0013	0.0014	0.0013	0.0015
Dy	0.0091	0.010	0.0096	0.01
Ho	0.0026	0.0031	0.0028	0.0025
Er	0.011	0.011	0.011	0.012
Tm	0.0024	0.0021	0.0023	0.0027
Yb	0.021	0.023	0.022	0.024
Lu	0.0045	0.0048	0.0046	0.0057
Y	0.077	0.083	0.080	0.1

La is not reported here due to PCC-1 sample powder being contaminated during previous laboratory use.

AL-1 (Albite)

	No.1	No.2	Average	Literature values (a)
La	5.7	7.4	6.6	9.9
Ce	15.0	18.5	16.7	21.0
Pr	2.0	2.4	2.2	
Nd	7.5	8.7	8.1	10
Sm	2.2	2.4	2.3	2.7
Eu	0.13	0.15	0.14	0.19
Gd	1.23	1.45	1.3	1.9
Tb	0.14	0.19	0.16	0.30
Dy	0.61	0.98	0.79	1.4
Ho	0.095	0.16	0.13	0.20
Er	0.25	0.45	0.35	0.59
Tm	0.039	0.070	0.054	
Yb	0.27	0.47	0.37	0.78
Lu	0.043	0.076	0.060	0.11
Y	2.2	3.8	3.0	7.0

FK-N (Potash Feldspar)

	No.1	No.2	Average	Literature values (a)	(b)
La	0.16	0.14	0.15	1.0	1.000
Ce	0.22	0.23	0.23	1.0	0.691
Pr	0.017	0.019	0.018		0.072
Nd	0.054	0.065	0.060	0.3	0.231
Sm	0.012	0.024	0.018	0.06	0.058
Eu	0.10	0.12	0.11	0.42	0.302
Gd	0.016	0.017	0.017	0.05	0.047
Tb	0.0024	0.0026	0.0025	0.01	0.009
Dy	0.015	0.018	0.016	0.06	0.046
Ho	0.0032	0.004	0.0036		0.011
Er	0.010	0.013	0.012	0.04	0.032
Tm	0.0017	0.0021	0.0019		0.007
Yb	0.014	0.0167	0.015	0.04	0.034
Lu	0.0022	0.0028	0.0025	0.01	0.006
Y	0.10	0.10	0.10	0.3	0.310

NBS70a (Potash feldspar)

	No.1	No.2	Average	Literature Values (b)
La	0.091	0.060	0.075	0.161
Ce	0.12	0.093	0.10	0.402
Pr	0.016	0.013	0.014	0.059
Nd	0.062	0.063	0.062	0.229
Sm	0.020	0.027	0.023	0.074
Eu	0.14	0.12	0.13	0.397
Gd	0.029	0.029	0.029	0.081
Tb	0.0052	0.0056	0.0054	0.020
Dy	0.039	0.044	0.042	0.117
Ho	0.0092	0.010	0.0097	0.027
Er	0.029	0.032	0.031	0.081
Tm	0.0049	0.0057	0.0053	0.014
Yb	0.049	0.036	0.042	0.081
Lu	0.0094	0.014	0.012	0.012
Y	0.23	0.20	0.215	0.630

NBS99a (Soda Feldspar)

	No.1	No.2	Average	Literature Values(b)
La	1.1	0.75	0.94	1.00
Ce	2.2	1.6	1.9	2.44
Pr	0.28	0.21	0.24	0.326
Nd	1.2	0.86	1.0	1.25
Sm	0.29	0.21	0.25	0.323
Eu	0.41	0.36	0.38	0.575
Gd	0.26	0.20	0.23	0.292
Tb	0.032	0.025	0.029	0.042
Dy	0.15	0.12	0.14	0.180
Ho	0.023	0.018	0.021	0.031
Er	0.053	0.042	0.048	0.068
Tm	0.0070	0.0053	0.0061	0.009
Yb	0.037	0.031	0.034	0.055
Lu	0.0052	0.0048	0.0050	0.008
Y	0.54	0.39	0.465	0.718

* No.1 and No. 2 are two determinations of replicates

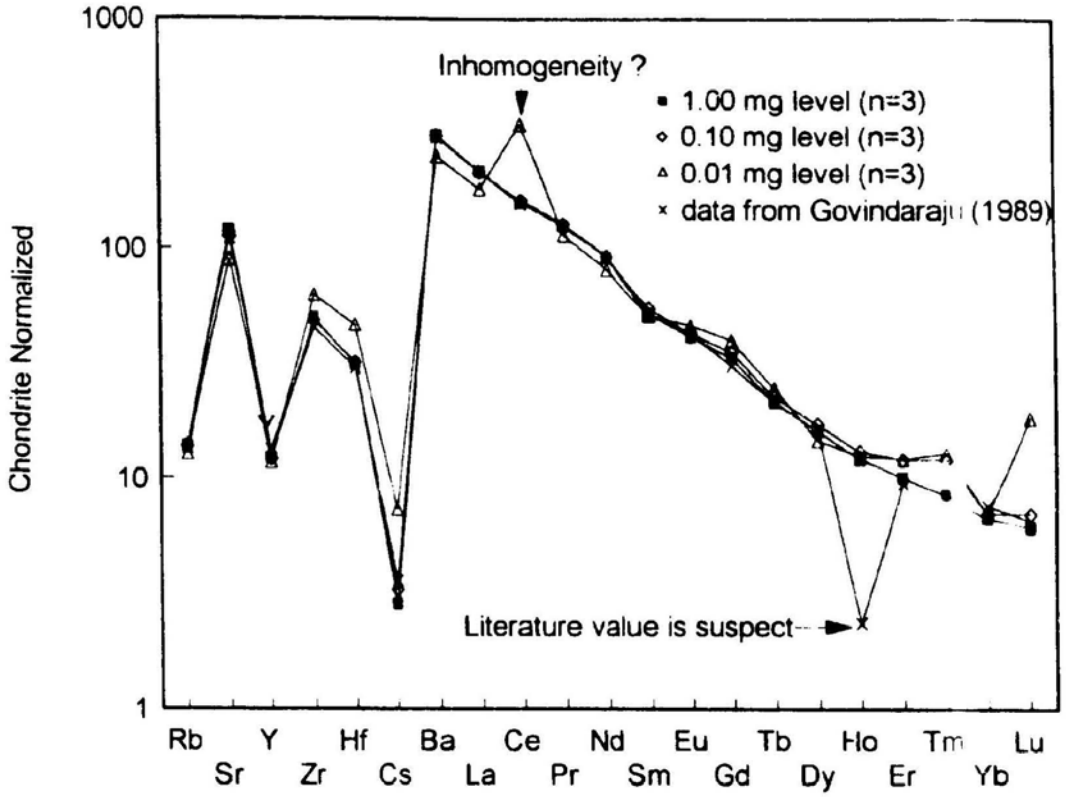

Figure 3.1 Mean chondrite-normalized data for the geological reference material, BR, for different masses of sample: (a) 1.00 mg level (n=3), (b) 0.10 mg level (n=3), (c) 0.01 mg level (n=3), and (d) data from Govindaraju (1989) The literature value for Ho, indicated by an arrow is suspect. The value for Ce at the 0.01 mg level may indicate sample inhomogeneity

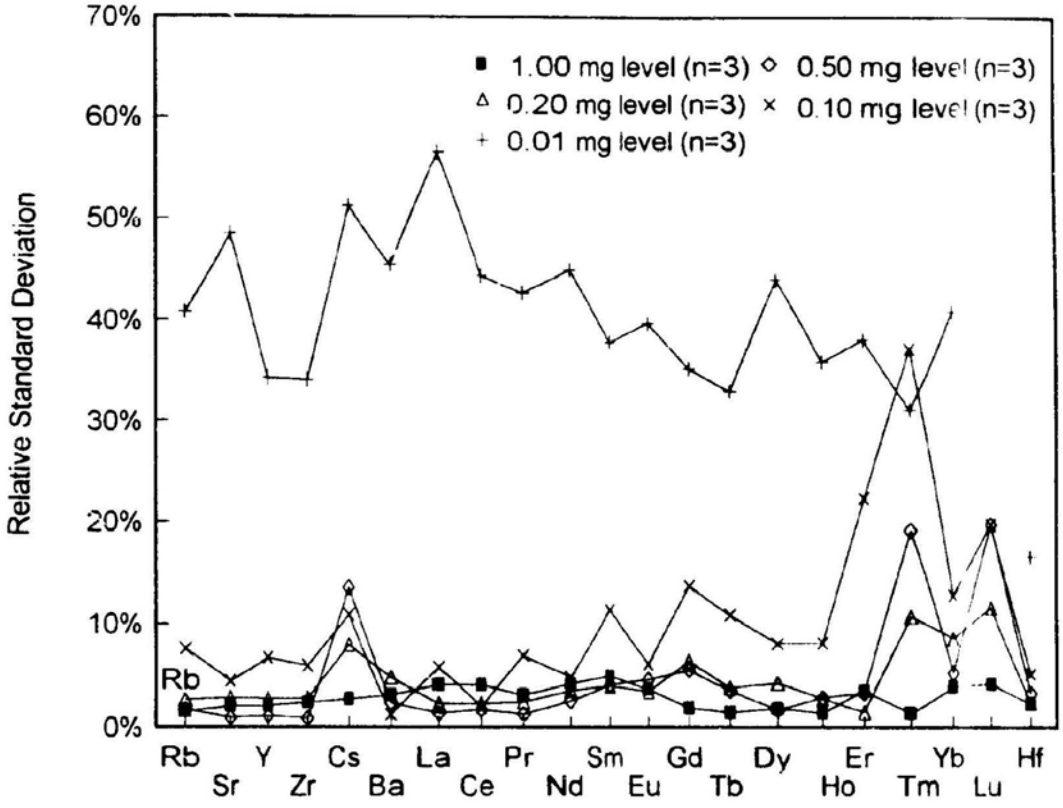

Figure 3.2 Relative standard deviation for different sampled masses of the geological reference material, BR: 1.00, 0.50, 0.20, 0.10, and 0.01 mg n=3 in each instance

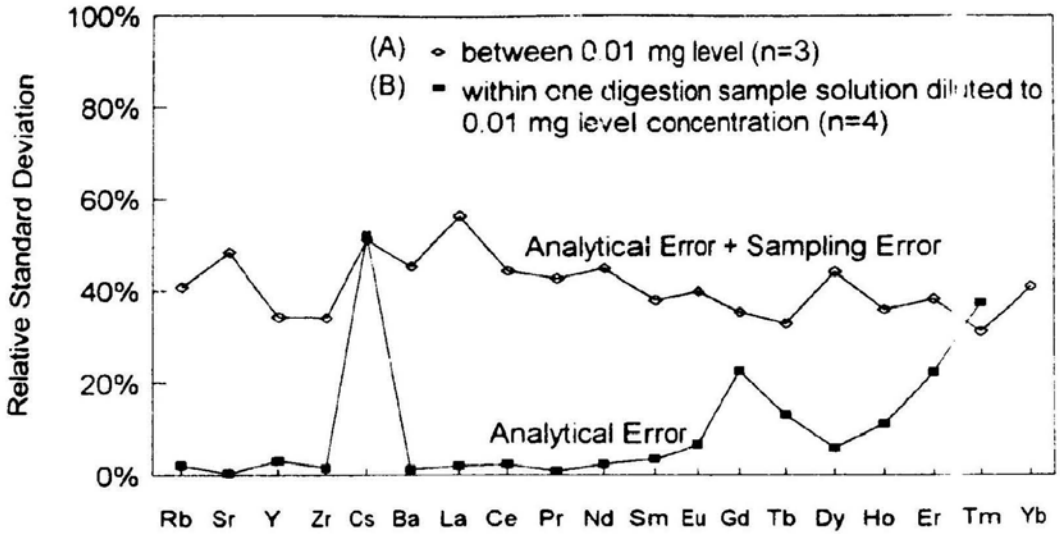

Figure 3.3 Relative standard deviation for analyses of the geological reference material, BR. Results are given for A, the analysis of three separate digestions of 0.01 mg weight in 2 g of solution, and B, the analysis (n=4) of a single sample digestion of 100 mg weight diluted to the same concentration (equivalent to a dilution to 20 kg of solution)

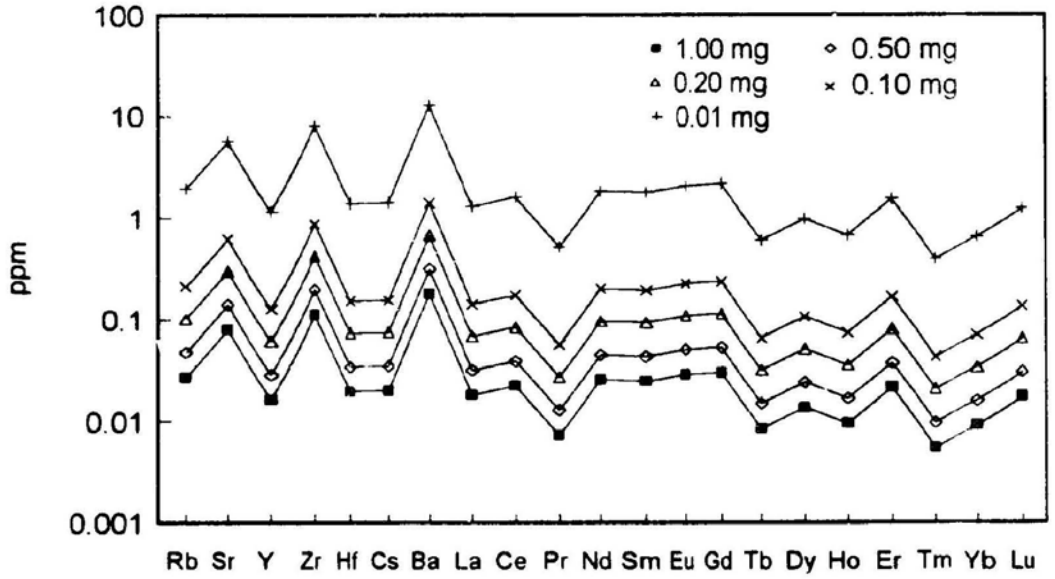

Figure 3.4 Solid limits of detection for various sample weights: 1.0, 0.5, 0.2, 0.1, and 0.01 mg dissolved in 2 g of solution

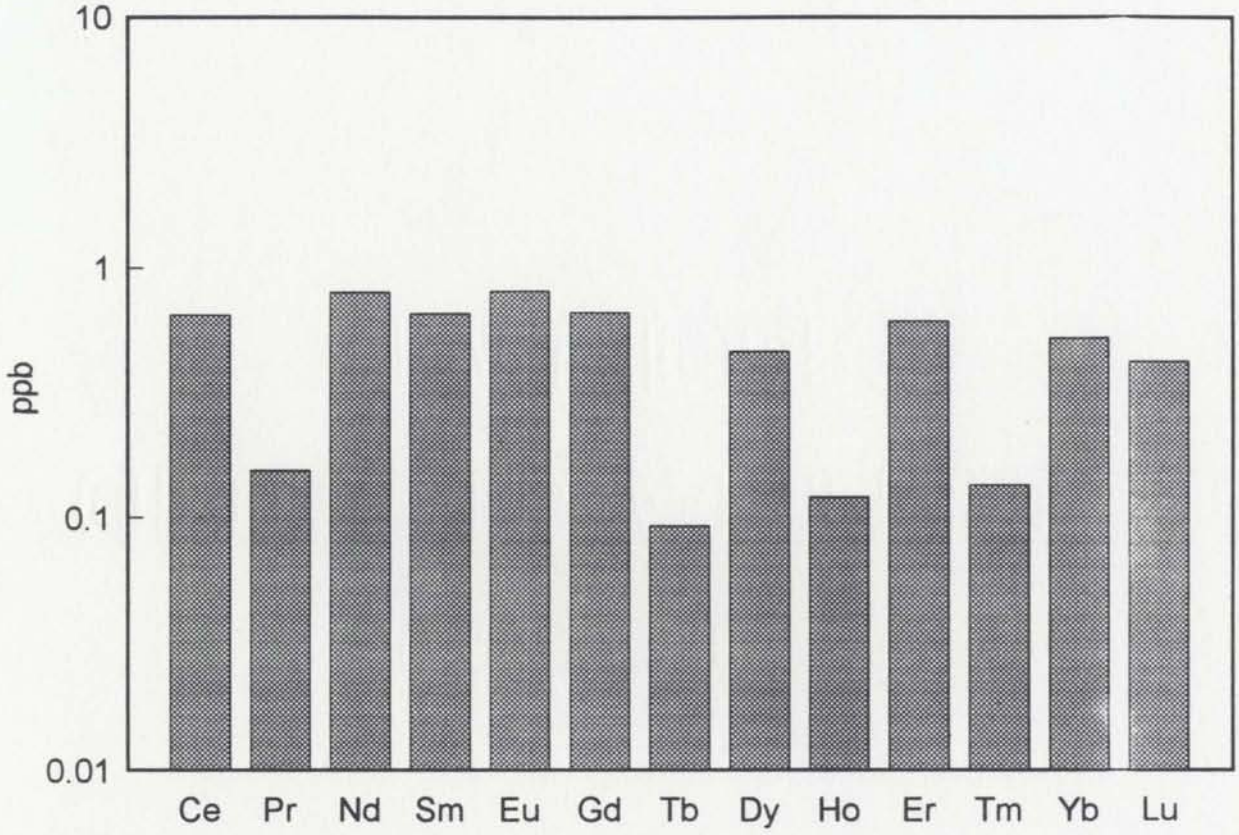

Figure 3.5 Limits of detection for a solid sample of 100 mg taken to a final volume of 2 g. A REE ion-exchange separation procedure is required

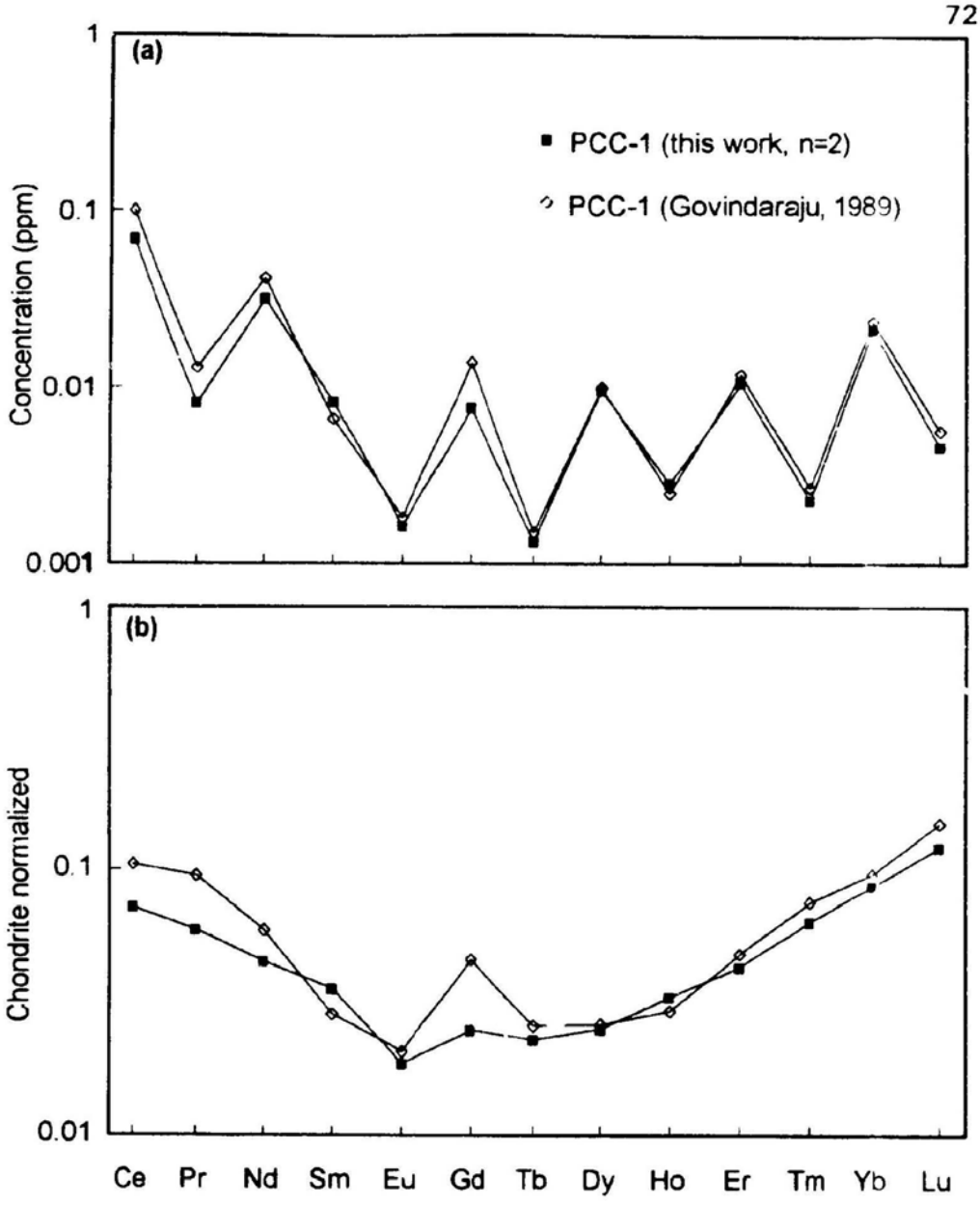

Figure 3.6 (a) Concentrations (ppm) and (b) mean chondrite-normalized data for the geological material, PCC-1 in this work and literature values (Govindaraju, 1989). The REE in 100 mg samples were separated using ion exchange and taken to a final solution mass of 2 g. Literature values from Govindaraju (1989).

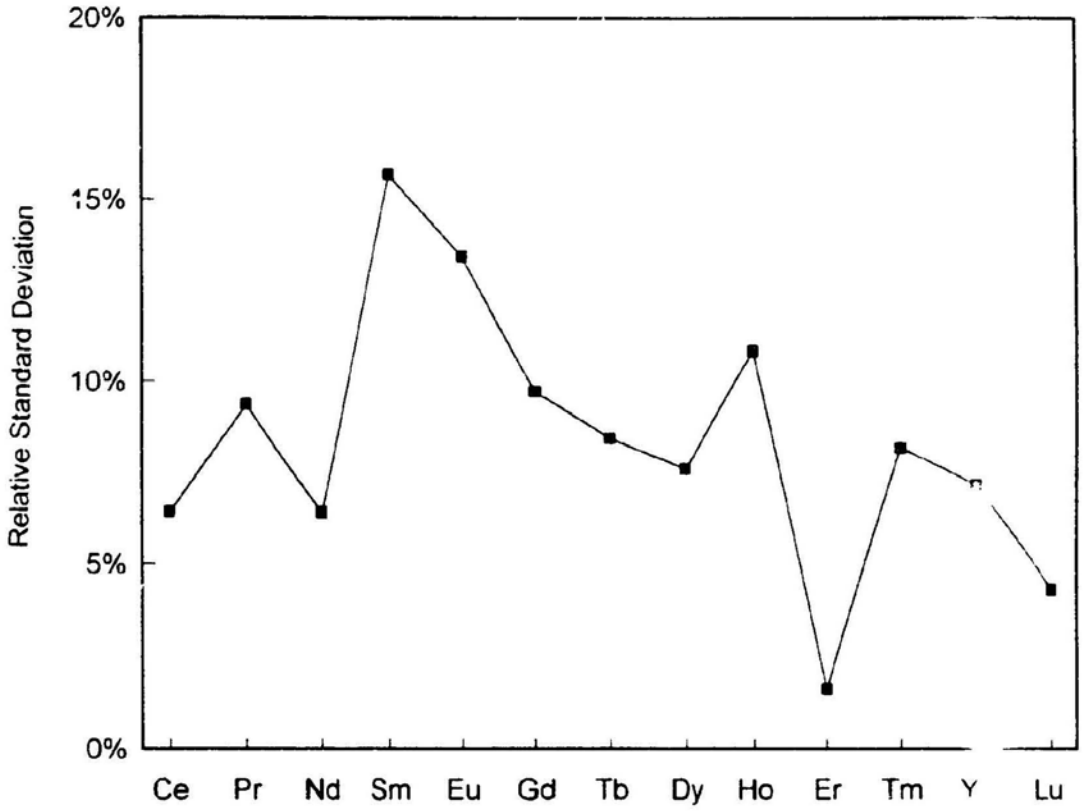

Figure 3.7 Relative standard deviation for analyses (n=2) of the geological reference material, PCC-1, following an ion-exchange concentration of the REE.

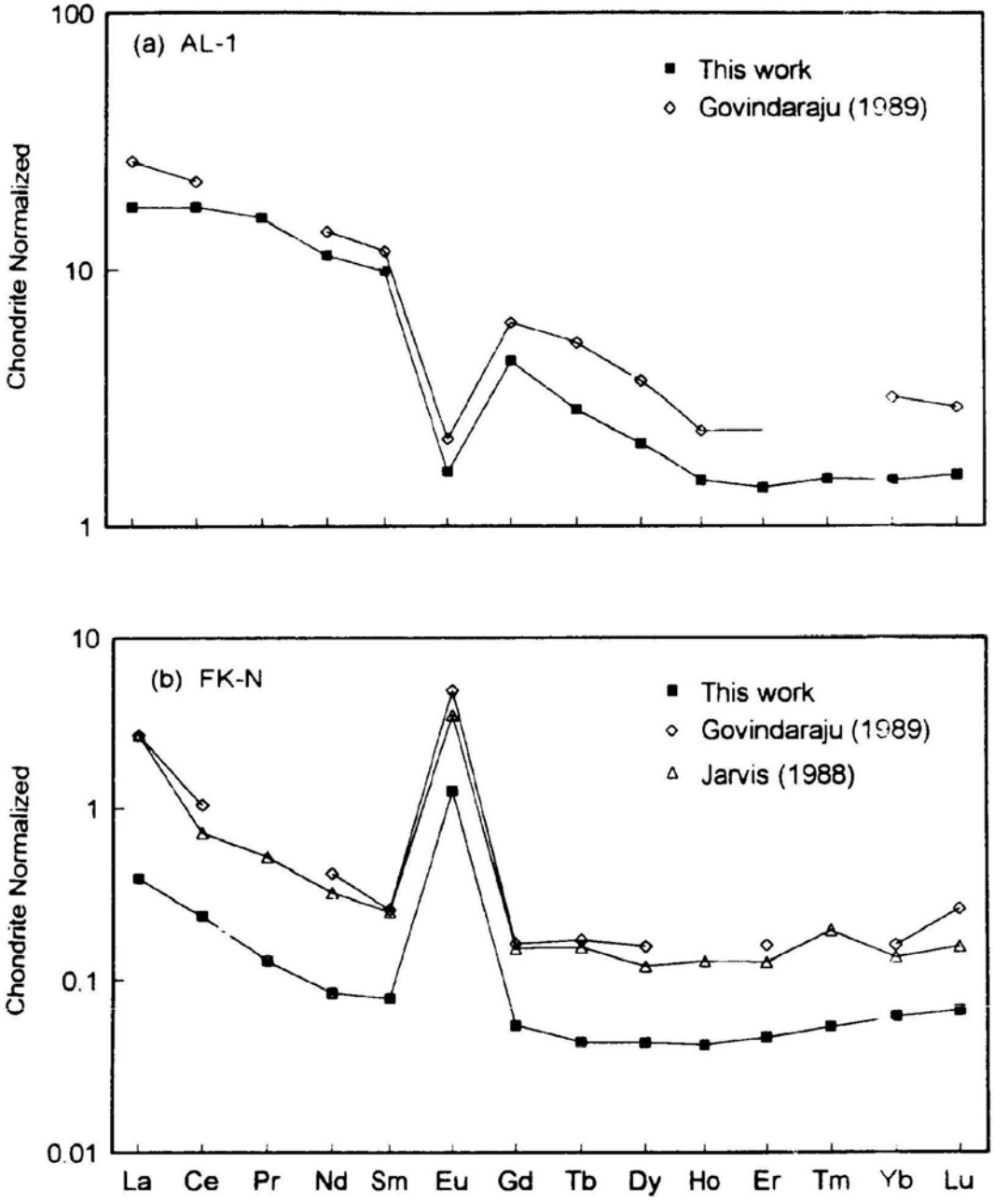
(a) AL-1
This work
Govindaraju (1989)
Chondrite Normalized
100
10
1
(b) FK-N
This work
Govindaraju (1989)
Jarvis (1988)
Chondrite Normalized
10
1
0.1
0.01
La
Ce
Pr
Nd
Sm
Eu
Gd
Tb
Dy
Ho
Er
Tm
Yb
Lu

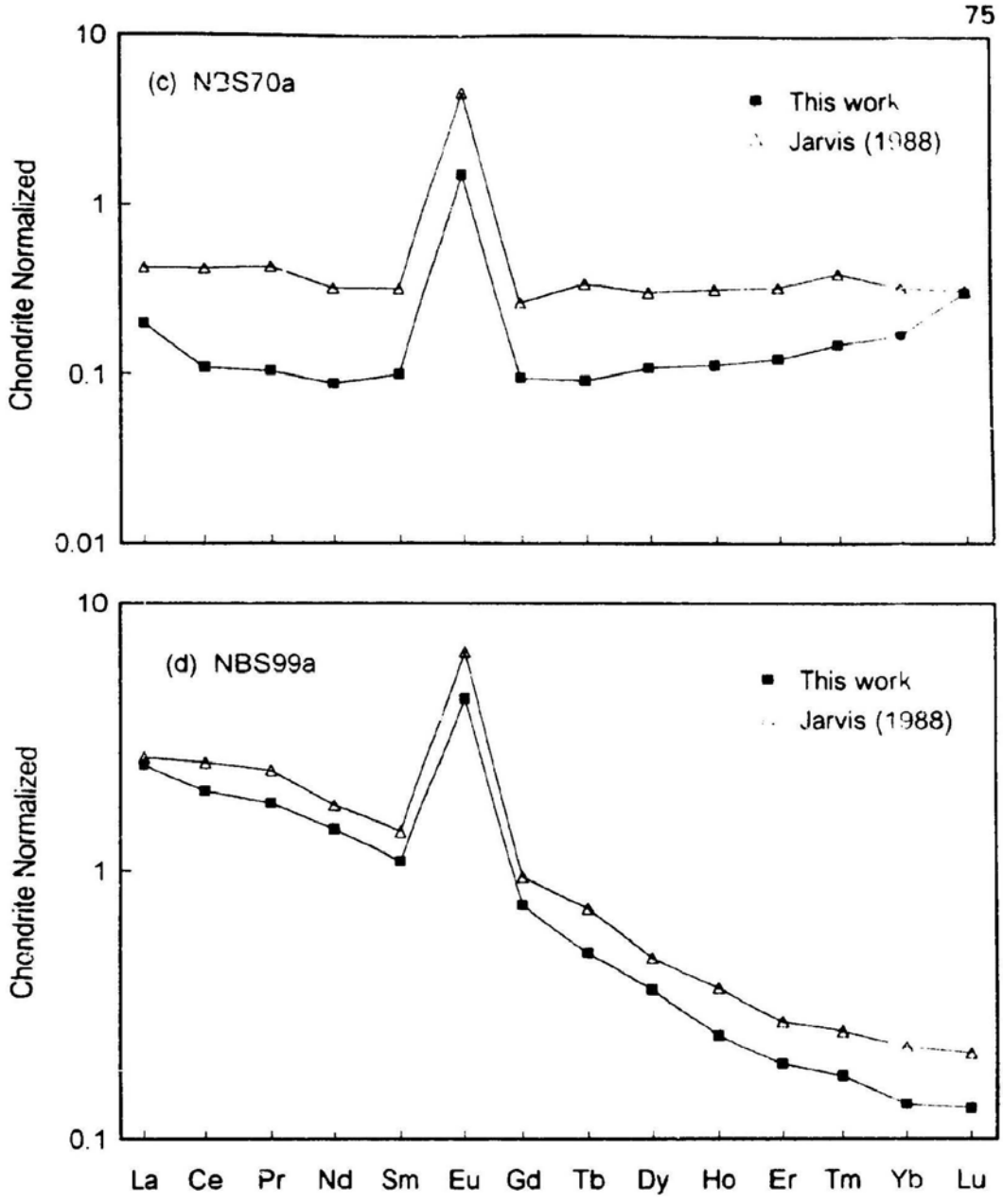

Figure 3.8 Mean chondrite-normalized data for the geological reference materials: (a) AI-1, (b) FK-N, (c) NBS70a, and (d) NBS99a in this work (n=2) and literature values (Govindaraju, 1989; and Jarvis, 1988). The REE in 100 mg samples were separated using ion-exchange and taken to a final solution weight of 2 g

CHAPTER 4

LASER ABLATION MICROPROBE-INDUCTIVELY COUPLED PLASMA-MASS SPECTROMETRY (LAM-ICP-MS) AND ITS APPLICATIONS TO THE IN-SITU DETERMINATION OF THE PRECIOUS METALS IN MINERALS

4.1 INTRODUCTION

Copper-nickel sulphide deposits commonly contain economically important concentrations of the platinum-group elements (PGE). Detailed mineralogical studies in the last two decades have provided a good understanding of the distribution of the PGE in platinum-group minerals (PGM), but the acquisition of data on the distribution of trace PGE concentrations in sulphide minerals in Cu-Ni deposits has not progressed as rapidly (Cabri *et al.*, 1984). The determination of the concentrations of the precious metals in individual mineral phases has been the goal of many investigations. It is always possible that the bulk analysis of a mineral separate for these trace metals runs the risk that a few highly enriched precious metal phases are included in the analyzed mineral separates. The development of in-situ microanalytical techniques at trace levels has long been a dream of earth scientists. The electron probe is restricted by its high detection limits; 1000 ppm is typical (Cabri *et al.*, 1984). Micro

proton-induced X-ray emission (PIXE) which uses a proton probe (beam size 5-20 μm), yields a sensitivity only 3 to 30 times better than the electron probe (Remond *et al.*, 1987). Secondary ion mass spectrometry (SIMS), an ion microprobe, also has been used with reported detection limits near the ppm level (Chryssoulis *et al.*, 1989). Accelerator mass spectrometry (AMS) has also been used to analyzed these elements (Wilson *et al.*, 1991; Rucklidge *et al.*, 1992; and Chai *et al.*, 1993). Typically, however, the beam diameter is 0.5 mm which is normally far too large to be focused on individual grains (Rucklidge *et al.*, 1992). Because of the expense in running an AMS machine, and the difficulties of reproducible preparation of samples, Rucklidge et al. (1992) did not consider this a viable method of analyzing sulphide concentrates for trace elements (Rucklidge *et al.*, 1992). Also, the ion probe, PIXE and AMS are too costly for most earth scientists.

Interaction of laser radiation with a solid has been reviewed thoroughly by Darke and Tyson (1993). This interaction may cause ablation including vaporization by processes that depend upon both the characteristics of laser beam and the physical properties of the solid. The ability of focused laser radiation to volatilize virtually any material has provided the analytical chemist with a versatile method of direct solid sampling for subsequent analysis. The history and recent developments of laser ablation introduction systems have been extensively reviewed by Moenke-Blankenburg (1989). Sample

introduction by the laser ablation offers several advantages over conventional pneumatic nebulization. These include: reduced reagent and labour costs; elimination of dilution errors; minimization of reagent contamination; avoiding sample transfer losses arising from sample-handling steps; application to dissolution-resistant minerals (*e.g.*, tourmaline, wolframite, beryl, rutile, zircon, chromite, and cassiterite); avoiding volatile element loss (*e.g.*, As, Se and B); avoiding some interferences; and providing spatial information by allowing analysis of small selected areas.

Within the last several years laser sampling of solids has been combined with various analytical techniques such as atomic absorption (Dittrich and Wennrich, 1984), microwave-induced plasma atomic emission (Ishizuka and Uwamino, 1980), DCP atomic emission (Mitchell, 1987), ICP-AES (Darke *et al.*, 1989a; Thompson *et al.*, 1989; Su and Lin, 1988); ICP-MS (Gray, 1985; Arrowsmith, 1987: Hager, 1989; Darke *et al.*, 1989b; Williams and Jarvis, 1993; Jarvis and Williams, 1993; Fedorowich *et al.*, 1993; Longerich *et al.*, 1993; and Jackson *et al.*, 1993) with varying degrees of success. Direct laser sampling of powdered materials of rock for ICP-AES was studied using a carbon dioxide laser (Lin and Peng, 1990). There are, however, potential difficulties associated with laser ablation techniques. Previous investigators have shown that the sensitivity of laser sampling with ICP-MS detection is dependent on the mode of the operation of laser (long or short pulse duration), physical properties

of the solid and calibration strategy.

In this chapter, a laser ablation microprobe-inductively coupled plasma spectrometry-mass spectrometry (LAM-ICP-MS) is described and its application to the in-situ analysis of precious metals in minerals is demonstrated.

4.2 PRINCIPLES OF THE LASER ABLATION MICROPROBE IN ATOMIC SPECTROMETRY

Analytical atomic spectrometry consists of four types: atomic absorption, atomic emission, atomic fluorescence, and atomic mass spectra. In all these cases, free atoms or ions are required for the interaction with light energy. The sampling-generation of free atoms or ions by dissociation and ionization can be achieved either in one step (*e.g.*, arcs, sparks, and discharge) or in two steps (*e.g.*, combination of an arc with an inductively coupled plasma). The potential use of laser light as a vaporization, dissociation and excitation source for spectrometric analysis was known soon after the first report of laser action in ruby (Maiman, 1960). A laser beam focused by the optics of a microscope on the surface of a solid can lead to the evaporation of a microamount of the sample.

The role of lasers in atomic spectrometry can be divided into two distinctive categories. In the first, the laser is used both to ablate and ionize

the samples (one-step analytical processes), while, in the second, laser energy is used only to introduced materials into an ionizing device (two-step analytical processes) (Williams and Jarvis, 1993). There are some differences between these two versions of operation. In one-step techniques, the laser energy affects the sampling, the atomization, and the excitation. Since the ablated material is not fully vaporized, the measured signal is not a direct function of the measured crater volume (Dittrich and Wennrich, 1990).

Two-step procedures have two nearly independent steps. The laser ablation (first process) deals only with sampling. After this first process, the microamount of laser ablated material is transported by a carrier gas to the second excitation process (*e.g.*, ICP). In the second process, the ablated material is evaporated, atomized, and excited by the second energy source. An advantage of this two-step operation is the potential of increased efficiencies during the evaporation, atomization, and excitation steps. In this study, two-step procedures that combined a laser ablation microprobe with an ICP-MS were used.

4.3 EXPERIMENTAL

4.3.1 INSTRUMENTATION

The laser ablation microprobe-inductively coupled plasma-mass spectrometry

(LAM-ICP-MS) system described by Jackson *et al.* (1993a), Longerich *et al.* (1993) and Jackson *et al.* (1993b) was used for this study. The LAM system consists of a laser, steering optics, a petrographic microscope, a TV viewing system, and a sample cell (Figure 4.1). A Q-switched YG 660 - 10 Nd:YAG laser (Santa Clara, California), with maximum 320-mJ pulse energy at 1064 nm wavelength in the near infrared, with a maximum repetition rate of 10 Hz, was used to ablate the solid samples in this study. The basic laser has been upgraded with temperature-stabilized frequency doubling and quadrupling optics which produce second and fourth harmonics of the fundamental output (1064 nm) at 532 nm in the visible green, and at 266 nm in the ultra violet. The wavelength separation optics allow the operator to select one of the three possible beams. The steering optics consist of dielectric mirrors, with a diameter of 25 mm, coated for a 45° incident angle of the laser beam. The microscope is a Nikon Optiphot (Tokyo, Japan) with transmitted and reflected polarized light sources, and a trinocular viewing eyepiece. The sample cell used for ablation (Figure 4.2) has top and bottom quartz windows (ESCO Products, Inc., New Jersey, 12-IR quartz disc, P210215, 25.4 mm diameter, 3.18 mm thick) mounted in a cylindrical brass body, 100 mm in internal diameter and 50 mm high, with tangential arms for gas inlet and outlet. The sample to be ablated can be: 1) mineral mounts, 2) thin sections, 3) opaque sections, or 4) polished slabs. The sample was placed on a circular PTFE base, which is

sealed with an O-ring. The base can easily be removed for sample changeover. The whole assembly can be mounted on the microscope stage. After each re-sealing, a 3-4 second period was allowed to elapse before reconnecting the argon carrier gas flow, to flush the air out of the cell. The ablated material was carried along 1.5 m of 3 mm i.d. connecting Tygon tube to the ICP plasma torch by an argon gas flow of 1.3 l min^{-1} via a sheath gas junction (Beauchemin and Craig, 1990) inserted between the spray chamber and the torch, which is used without a solution nebulization spray chamber. Sample changing is straightforward, and similar to that used with the recycling nebulization system (see Chapter 2 of this thesis, and Chen *et al.*, 1992b). Laser operating conditions are presented in Table 4.1.

Table 4.1 Laser operating conditions

Laser mode	Q-switch Nd:YAG laser
Laser energy	1-320 mJ/pulse
Pulse width	10 ns
Repetition rate	2, 5, or 10 Hz
Wavelength	266, 532, or 1064 nm
Pit diameter	20-50 μm
Aerosol transportation tube	3 mm i.d. x 2 m
Carrier gas flow	1.3 l/min

The ICP-MS instrument used in this study was the modified SCIEX (now Perkin-Elmer SCIEX) ELAN model 250 ICP-MS described in Chapter 2. The instrument has been upgraded to the model 5000 computer system using Perkin-Elmer supplied hardware and software for model 250 and 500 instruments (Chen *et al*, 1992b). New ELAN 5000 software, from Perkin-Elmer, version 2.0-ICPS (a modification of version 2.0 which incorporates an ICP Shut off enhancement) was used. As described by Jackson *et al*. (1993), initial alignment of the instrument was usually performed using solution nebulization, and optimisation for LAM was performed using selected elements in the spiked silicate glass NBS (now NIST) standard reference material 612 by ablation at 5 Hz to obtain a steady signal. For each analytical run, the nebulizer gas flow was adjusted, using the NBS 612 glass, so that maximum sensitivity was obtained. Other ICP-MS operating conditions are given in Table 4.2.

4.3.2 STANDARD AND SAMPLE PREPARATIONS

Since there are no sulphide standard reference materials available for precious metals, synthetic fire assay NiS beads were used as reference materials in this study. The collection procedures and reagents for a nickel sulphide fire assay has been described by Jackson *et al*. (1990) (Appendix I). The bead (used as a standard) was cut, polished, and mounted in epoxy for analysis.

Table 4.2 ICP-MS operating conditions	
Inductively coupled plasma:	
Plasma gas	Argon
Forward power	1200 W
Reflected power	<5 W
Gas flow:	
Plasma (outer) gas flow-rate	13.0 l min^{-1}
Auxiliary (intermediate) gas flow-rate	1.3 l min^{-1}
Nebulizer (inner) gas flow-rate	1.03 l min^{-1}
Interface:	
Sampling distance (load coil to sample aperture)	21 mm
Sampling aperture	Nickel, 1.1 mm diameter
Skimmer aperture	Nickel, 0.9 mm diameter
Ion lens settings:	
B lens	7.0 V
P lens	-9.0 V
E-1 lens	-19.8 V
S-2 lens	0 V
Data acquisition parameters:	
measurement mode	multichannel
Replicate time	200 ms
Dwell time	10 ms
Sweeps/replicate	20
Number of replicates	60
Points across peak	1
Resolution	Normal

Sample chips to be analyzed were mounted in epoxy, and then polished.

4.3.3 DATA ACQUISITION AND CALIBRATION

Mass selection and molecular interferences are listed in Table 4.3. The sensitivities were measured by external standardization (SARM-7 NiS bead). Background was established by acquiring data for approximately 60 s prior to ablation (Jackson *et al.*, 1993). Ablation of samples was performed at 10 Hz, and the laser was fired for 40 seconds. Samples were run in the following sequence: standard (SARM-7 NiS bead), standard, sample 1, ..., sample 7, standard, standard, etc. As described by Jackson *et al.* (1993), data was transmitted to a PC and processed off-line using spreadsheet software. A mean background intensity was calculated from count rates for each element during the preablation data acquisition period. The mean sample elemental intensities were then calculated as the mean count rate during the ablation signal. The net background corrected intensities were then calculated. The signal from ^{34}S was used as the internal standard to correct for drift, ablation efficiency, and matrix effects. The most significant interferences in the suit of elements determined in this study are the argon polyatomic ions of Co, Ni, Cu, and Zn on Ru, Rh, and Pd. After instrumental drift, matrix effects, ablation efficiency, and polyatomic interferences were corrected, sample concentrations were calculated by external calibration using the mean sensitivity of the 4

temporally closest calibration standards.

Table 4.3 Analytical masses, isotope abundance, and molecular interferences for determination of precious metals by LAM-ICP-MS

Element	Mass	Isotopic abundance	Interference
S	34	4.2%	
Co	59	100%	
Ni	61	1.16%	
Cu	65	30.9%	
Zn	67	4.1%	
Ru	99	12.7%	$^{59}Co^{40}Ar^+$
Rh	103	100	$^{63}Cu^{40}Ar^+$
Pd	104	11.0%	$^{64}Zn^{40}Ar^+$ $^{64}Ni^{40}Ar^+$, $^{104}Ru^+$
Pd	105	22.2%	$^{65}Cu^{40}Ar^+$
Pd	108	26.7%	$^{68}Zn^{40}Ar^+$, $^{108}Cd^+$
Cd	111	12.8%	
Ir	193	62.6%	
Pt	195	33.8%	
Au	197	100%	

4.4 RESULTS AND DISCUSSION

One of the fundamental advantages of the LAM-ICP-MS system is the almost complete separation of the ablation process from the excitation process. The

ablation process produces vapour phase products, some of which are excited. The sample material, regardless of its physical state, is efficiently transmitted to the ICP where the high temperature ($>6000^0$C) dominantly produces singly charged ions with very high efficiencies for most elements (Longerich *et al.*, 1993a). There is a reduction of oxygen content of the sample by a factor of over 1000 when the solid mineral is introduced compared to the introduction of an aqueous whole rock solution prepared at a dilution of 1 g rock/Kg (Longerich *et al.*, 1993a). This reduction of oxygen in the plasma reduces oxide polyatomic ion interferences by a factor of 10. Solution nebulization studies indicated that the ratios $CuAr^+/Cu^+$, $NiAr^+/Ni^+$, and $NiCl^+/Ni^+$ each vary approximately proportionally to ThO^+/Th^+ (Jackson *et al.*, 1990). However, this relationship for the dry sampling of laser ablation is unknown. It is possible that the reduction of oxide polyatomic ions may coincide with a decline of argon polyatomic ions.

Major sulphide ore minerals from mineral deposits in the Sudbury area, Ontario, have been analyzed with the Heidelberg proton microprobe by Cabri *et al.* (1984) in a search for trace quantities of the platinum-group elements (PGE). They reported no detectable PGE because of high limits of detection (1.2 to 3 ppm for Pd and Rh, and 50-60 ppm for Pt). Using LAM-ICP-MS to determine the precious metals, greatly improves solid limits of detection which range from 30 to 240 ppb (Table 4.4). This increased sensitivity might allow

the study of the distribution and partitioning of precious metals in the ore sulphides at ppb concentrations.

The strong absorption of Nd:YAG radiation (1064 nm) in sulphides, allowed ablation at low power and hence attenuation of the transmitted energy rapidly below the mineral surface avoiding catastrophic absorption within the minerals (Jackson *et al.*, 1993a). Ablation produced cylindrical laser pits from 30 to 50 μm in diameter for most sulphide minerals (Figure 4.3). However, small eject melt droplets were observed.

Limits of detection, defined here as 3 times the standard deviation of the difference between the count rate of a sample and n replicates of the background, is calculated as $[3*\sigma*\sqrt{(1/n+1)}]$. Limits of detection are presented in Table 4.4 and Figure 4.4.

To demonstrate the capability of LAM-ICP-MS to determine in-situ precious metal concentrations, and to examine the distributions of the elements in sulphides, the major sulphide minerals from the Deep Copper Zone of the Strathcona Cu-Ni sulphide deposit were analyzed, and the analytical results are presented in Table 4.4. The concentrations of the precious metals in the sulphides are generally below the limits of detection (Table 4.3). One of the chalcopyrite ablation events showed an extremely high concentration of Pt indicating the presence of a tiny Pt-rich inclusion in the mineral. A 10 second transient Pt signal was observed during 35 seconds of ablation (Figure 4.5).

Serious interferences from the base metal-argon polyatomic ions (Table 4.3) hampered the accurate determination of the light precious metals. Further investigations are required to overcome these problems. The following suggestions are proposed for further study: (1) use of neon gas (more expensive) instead of argon; (2) use of a mixed nitrogen-argon gas to minimize argon polyatomic ion formation; or (3) using a high resolution mass spectrometer (Morita *et al.*, 1989; Walder and Freedman, 1992) to resolve the molecular interferences, but with the loss of some sensitivity.

Table 4.4 Analytical results (ppb) of sulphide minerals from the Strathcona Cu-Ni sulphide ores using the laser ablation microprobe ICP-MS

Sample	Mineral	Ru	Rh	Pd	Ir	Pt	Au
91ZC15c	Po	670	<43	<180	1900	177000	350
91ZC15c	Po	<240	<43	<180	<26	<88	<88
91ZC15c	Po	<240	<43	<180	<26	<88	<88
91ZC15c	Cpy	<240	<43	1600	95	<88	<88
91ZC15c	Cpy	570	<43	<180	<26	<88	<88
91ZC15c	Ga	2100	<43	<180	<26	<88	<88
91ZC15d	Po	890	360	<180	<26	<88	150
91ZC15d	Po	270	<43	<180	<26	<88	<88
91ZC15d	Po	<240	<43	360	<26	<88	<88
91ZC15d	Po	310	<43	<180	<26	210	<88
91ZC15d	Cpy	<240	<43	2100	30	<88	<88
91ZC15d	Cpy	<240	<43	830	<26	320	<88
91ZC16	Pn	380	<43	600	<26	<88	<88
91ZC16	Pn	<240	<43	510	<26	<88	100
Limits of detection		240	43	180	26	88	88

Po: pyrrhotite Cpy: chalcopyrite
Pn: pentlandite Ga: galena <: below limits of detection

4.5 CONCLUSIONS

Although LAM-ICP-MS has been demonstrated as a promising new technique for the determination of in-situ trace and ultra-trace elements in minerals (Longerich *et al.*, 1993a; Jackson *et al.*, 1993; and Fryer *et al.*, 1993), analysis of precious metals in sulphides by LAM-ICP-MS in this study was not very successful. Solid limits of detection range from 30 ppb to 240 ppb. It provides a useful technique to examine the distributions of precious metals, particularly the heavy PGE (Ir, Pt) and Au in sulphide minerals. However, serious interferences of base metal-argon polyatomic ions on Ru, Rh, and Pd were observed. Further developments are required to minimized these interference to improve Ru, Rh, and Pd analytical results. The analytical results of sulphide minerals from the Deep Copper Zone of the Strathcona Mine indicate very low precious metals contents in solid solution. Therefore, analytical techniques using mineral separates will be utilized in further work in this thesis.

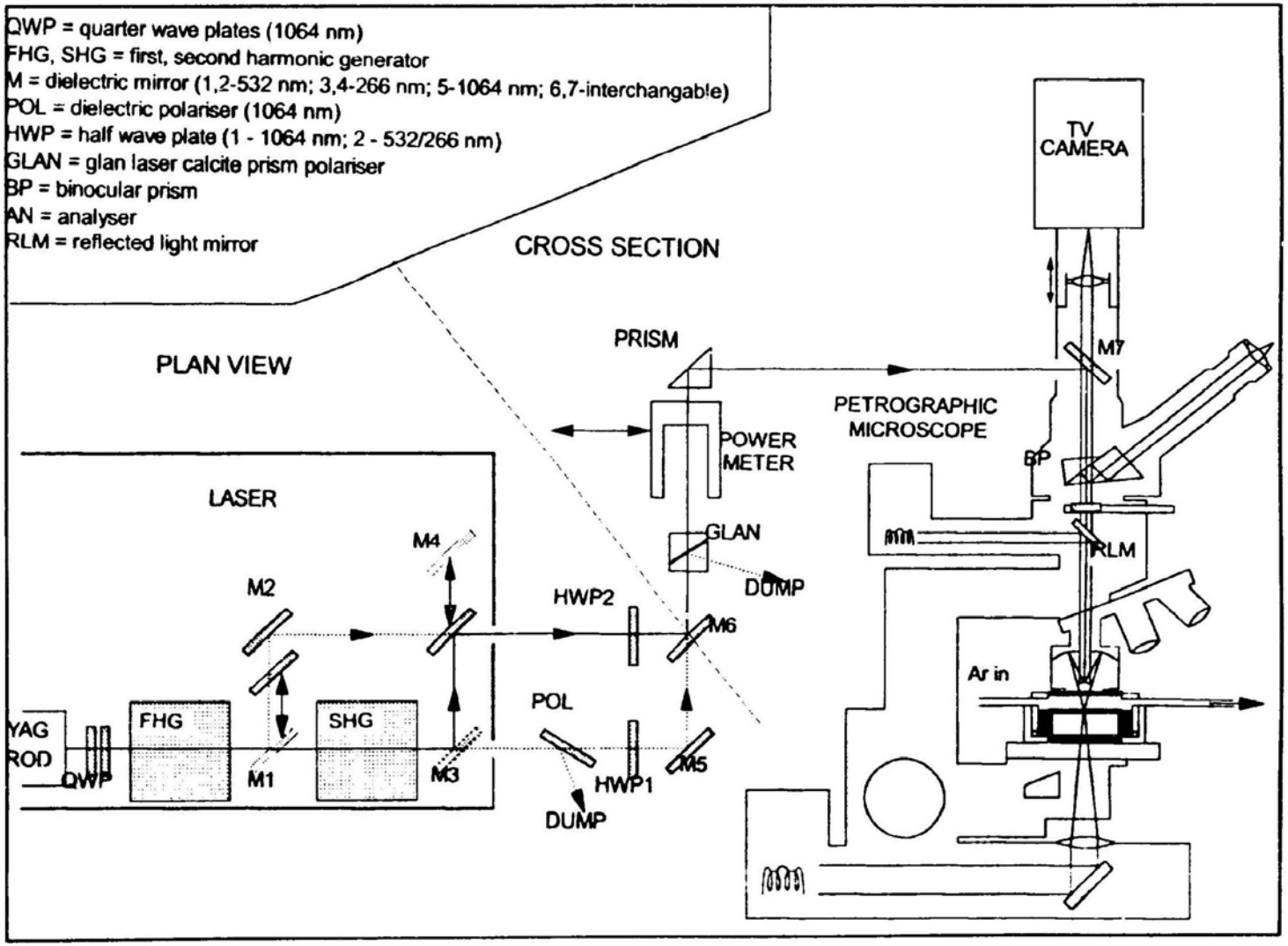

Figure 4.1 Schematic drawing of the laser ablation microprobe system (Jackson et al., 1992, V.G. Goldschmidt Conference Abstract) used for the in-situ precious metal analysis of sulphide minerals in this study

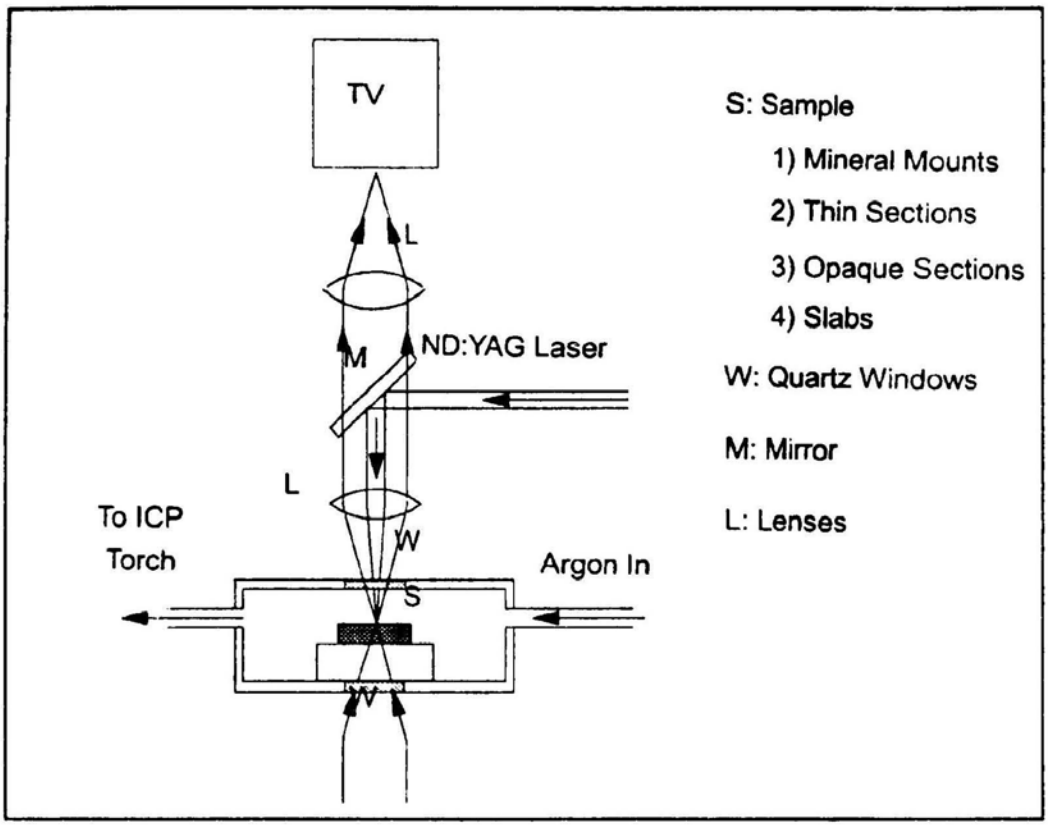

Figure 4.2 Schematic drawing of sample cell for laser ablation microprobe-inductive coupled plasma-mass spectrometry (LAM-ICP-MS)

Figure 4.3 Scanning electron micrographs of laser ablation pits in pyrrhotite (a, b, c, and d), chalcopyrite (e, f, g, and h), magnetite (i), and galena (j); showing ejected melt droplets

a

b

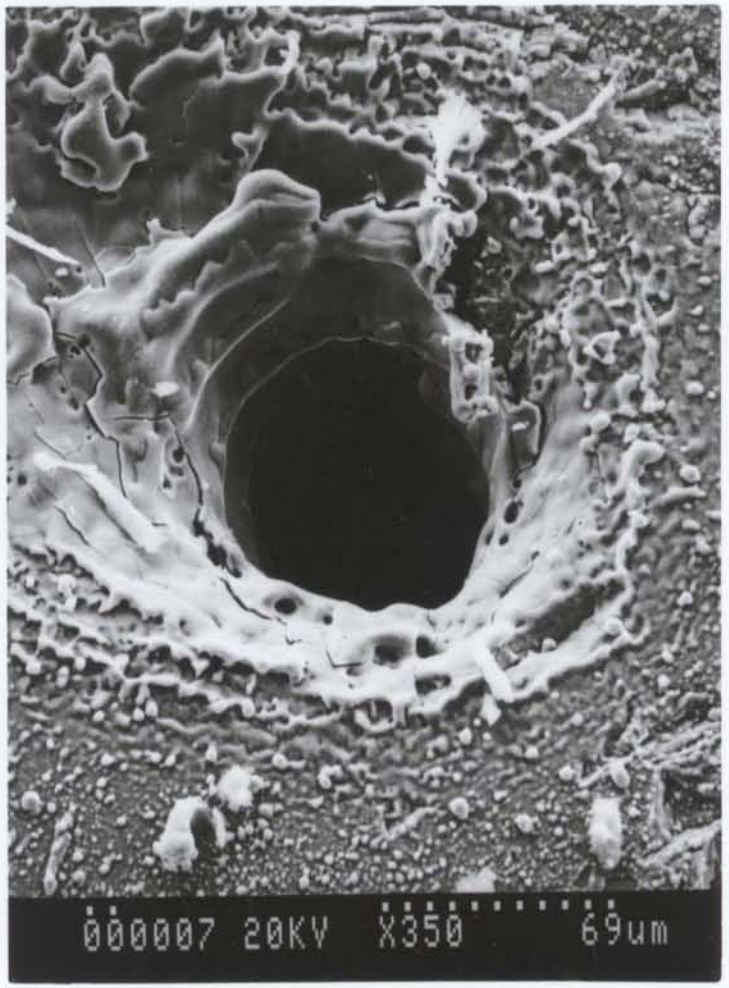

c

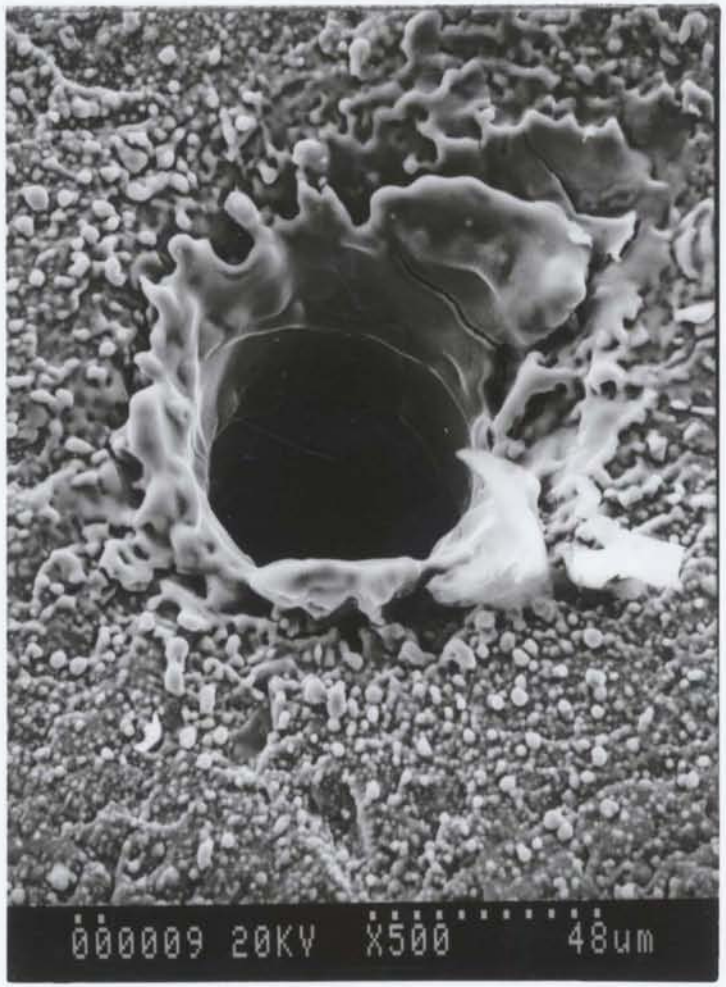

d

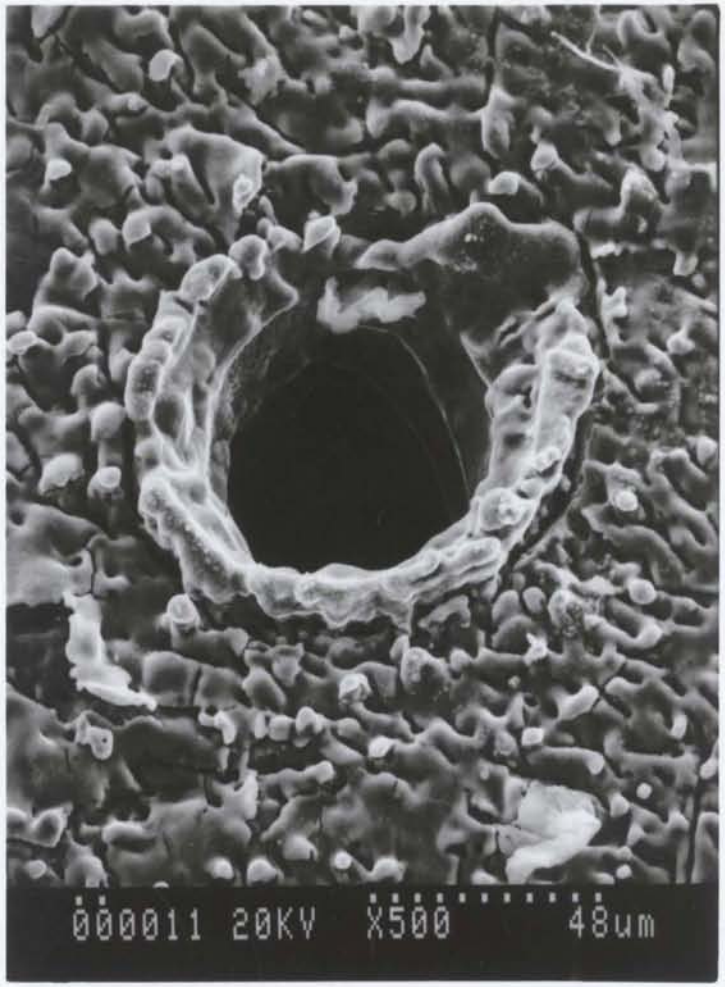

f

e

g

h

i

j

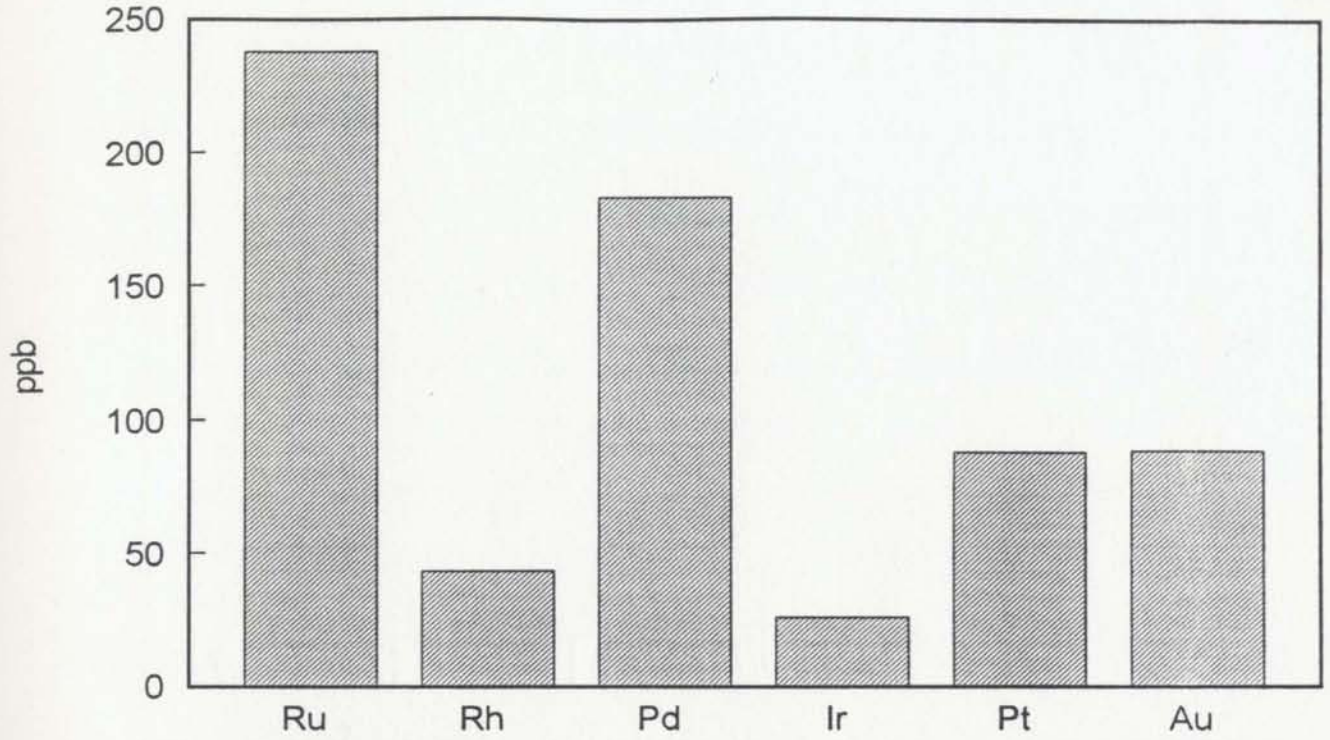

Figure 4.4 Solid limits of detection for the precious metals using LAM-ICP-MS

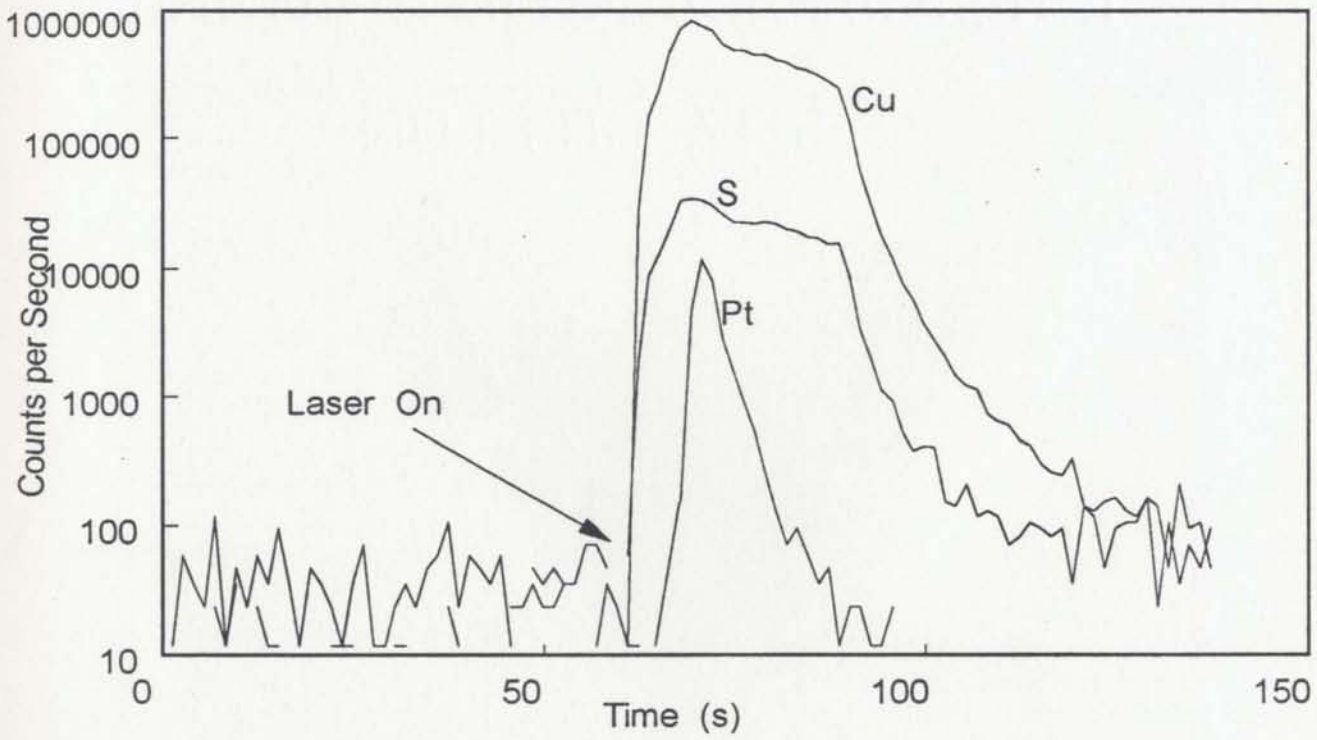

Figure 4.5 Analytical signal from one of the in-situ laser ablation analysis of chalcopyrite using LAM-ICP-MS showing the presence of micro-platinum rich inclusions in chalcopyrite

CHAPTER 5

DETERMINATION OF THE PRECIOUS METALS IN MILLIGRAM SAMPLES OF SULPHIDES AND MAGNETITE AFTER PRECONCENTRATION USING ION EXCHANGE WITH AN AUTOMATED 2 SPEED PERISTALTIC PUMP SPEED CONTROLLER AND INDUCTIVELY COUPLED PLASMA-MASS SPECTROMETRY

5.1 INTRODUCTION

The determination of the natural concentrations of precious metals must take into consideration their occurrence in rare, discrete, and inhomogeneously distributed minerals. The analysis of rocks and ores for these elements is often performed on large (10-60 g) samples using fire-assay collection to obtain representative bulk concentrations. To examine the distribution of these elements within and between minerals requires analytical techniques using a more specific microsampling technique. This study utilizes the high sensitivity of ICP-MS to determine Ru, Rh, Pd, Re, Ir, Pt, and Au concentrations to study the distribution and partitioning of these elements among coexisting chalcopyrite, pyrrhotite, pentlandite, and magnetite.

Serious interference of base metal-argon polyatomic ions and matrix

effects hamper the accurate determination of precious metals, and require quantitative separations of precious metals from base metals (Jackson *et al.*, 1990 and Chapter 4). Solvent extraction (Shrendrikar and Berg, 1969; Hahn-Weinheimer, 1958) or Te precipitation (Sandell, 1959; Fryer and Kerrich, 1978) have been used for the separation of precious metals from the matrix elements in samples. Cation exchange has also been used for separation of Pd and Pt (Plummer and Beamish, 1959), Rh (Saint and Beamish, 1961), Ir (Tertipis and Beamish, 1962) and Ru (Zachariasen and Beamish, 1962). However, separation of the seven precious metals in a single step using cation exchange is a more difficult procedure.

In this chapter, a method for the quantitative separation of seven precious metals (Ru, Rh, Pd, Re, Ir, Pt, and Au) from large amounts of associated base metals in dilute hydrochloric acid solutions using a strongly acidic cation exchange resin, Amberlite CG-120, is described. The method has been applied to the determination of precious metals in small quantities (2-20 mg) of high purity sulphide and magnetite mineral separates using a high sensitivity inductively coupled plasma-mass spectrometry (ICP-MS). Solid limits of detection for a 20 mg sample are less than 4 ppb for Ru, Rh, Re, Ir, Pt, and Au, and 29 ppb for Pd due to the high memory in the calibration blank from sample solutions. Analyses of nickel sulphide fire assay beads of the reference material, SARM-7, show good agreement with certified values, with relative

standard deviations (RSD) of less than 8%. Poor accuracy for Au is due to sample heterogeneity of the nickel sulphide bead used for analysis.

Data from the analysis of sulphide and magnetite minerals from the Sudbury copper-nickel sulphide ores demonstrate the ability of the method to make useful determinations of precious metals for the study of ore genesis.

5.2 INSTRUMENTATION

The instrument used in this study was described in Chapter 2. New ELAN 5000 software, from Perkin-Elmer, version 2.0-ICPS, was used. An automated 2 speed peristaltic pump speed controller was used to control the sample solution uptake rate for analysis of small sample volumes (Longerich, 1993). With this pump controller, it is possible to reduce solution uptake during data acquisition to low rates (*e.g.*, 0.4 g min^{-1} in this study), allowing the automated analysis of reduced amounts of sample solutions at slightly reduced analyte count rate (Longerich, 1993). Compared with the recycling nebulization micro-sampling technique described in Chapter 2, an automated 2 speed peristaltic pump speed controller required a little more sample solution (about 3 g), but it was fully automated. For each analytical run, the nebulizer gas flow was adjusted, using a solution containing 100 ppb of Rh, Cs, Bi, and U, so that: (1)

$UO^+/U^+ < 0.25$; (2) sensitivity (count sec^{-1}/ppb) of $Rh > 1000$, and (3) sensitivity of $Bi > 500$. These conditions represent a compromise between maximum sensitivity and minimum polyatomic ion formation. Other ICP-MS operating conditions are given in Table 5.1.

5.3 REAGENTS AND SAMPLE PREPARATION

Certified American Chemical Society (A.C.S.) acids were distilled in nonboiling quartz or teflon stills and diluted with Barnstead Nano-pure deionized-distilled water. A strongly acidic cation exchange resin Amberlite, CG-120 (Sigma Chemical Co., St. Louis, Missouri) was used.

Since there are no sulphide and magnetite mineral separate reference materials available for the precious metals, synthetic NiS fire assay beads were used as reference materials in this study. The collection procedures and reagents for a nickel sulphide fire assay have been described by Jackson *et al.* (1990) (Appendix I). Standard and spike solutions for each element were prepared from Plasma Grade powders (SPEX Industries, Metuchen, New Jersey, U.S.A.) using HNO_3, HCl and deionized-distilled water. All sample and standard preparations were carried out in a Class 100 clean laboratory facility except for the NiS fire assay collection.

Table 5.1 ICP-MS operating conditions	
Inductively coupled plasma:	
Plasma gas	Argon
Forward power	1200 W
Reflected power	<5 W
Gas flow:	
Plasma (outer) gas flow-rate	13.0 l min^{-1}
Auxiliary (intermediate) gas flow-rate	1.0 l min^{-1}
Sample solution flow rate	0.4 ml/min^{-1}
Nebulizer (inner) gas flow-rate	1.12 l min^{-1} (see text)
Interface:	
Sampling distance (load coil to sample aperture)	21 mm
Sampling aperture	Nickel, 1.1 mm diameter
Skimmer aperture	Nickel, 0.9 mm diameter
Ion lens settings:	
B lens	7.5 V
P lens	-9.2 V
E-1 lens	-9.6 V
S-2 lens	0 V
Data acquisition parameters:	
measurement mode	multichannel
Replicate time	6 s
Dwell time	10 ms
Sweeps/replicate	600
Number of replicates	1
Points across peak	1
Resolution	Normal
Autosampler setting:	
Sample delay	70 s
Wash delay	210 s
Rabbit delay	60 s

All the sulphide and magnetite minerals are from Strathcona Ni-Cu ores, Sudbury, Ontario. Ten samples of approximately 1 Kg of ore were first crushed and sieved. All the mineral separates were hand-picked from the 60 mesh fraction under a binocular microscope. Their purities were checked by X-ray diffraction (XRD).

Sample dissolution was as follows:

1) 2-20 mg of sample grains (NiS bead, sulphide minerals or magnetite) was dissolved in a 15 ml covered screw-top teflon jar at 150°C (Savillex) using 1 ml 6 M HCl overnight. The jar was opened and the sample was evaporated to dryness at 75-100°C.
2) The residue was dissolved in 1 ml of aqua regia (3 parts of concentrated HCl and 1 part of concentrated HNO_3 in a covered teflon jar overnight. After all the sample was dissolved, the jar was opened and the sample solution was evaporated to dryness.
3) The residue was then dissolved in 1 ml of 6 M HCl in covered teflon jars, and then evaporated to dryness in open teflon jars at 75-100°C.
4) Step (3) was repeated twice.
5) The sample residue was finally dissolved in 1 ml of 0.2 M HCl for subsequent cation exchange separation.

5.4 SEPARATION OF PRECIOUS METALS FROM ASSOCIATED BASE METALS BY ION EXCHANGE

All experiments for the separation of precious metals from associated base metals by ion exchange were carried out in a Class 100 clean laboratory facility.

5.4.1 SEPARATIONS BY ANION EXCHANGE

An anion exchange resin Dowex 1 has been used to separate ruthenium from tellurium, cesium, and rare elements (Suvic, 1957). A procedure for the separation of rhodium and iridium by an anion exchanger (Amberlite IRA-400) has been reported by Berman and McBryde (1958), and Marks and Beamish (1958). None of these methods reported a complete separation for all PGE and Au from the matrix elements in a single column. In this study, the following experiment was conducted to establish the quantitative separation of the precious metals from the base metals in a single column by anion exchange.

5.4.1.1 EXPERIMENT PROCEDURE:

1) A synthetic precious and base metal solution (26.6 ppm Cu, 19.7 ppm Ni, 37.4 ppb Ru, 21.1 ppb Rh, 36.7 ppb Pd, 19.4 ppb Re, 19.0 ppb Ir, 37.5 ppb Pt, and 12.8 ppb Au) was prepared from stock

solutions.

2) 2.5 g above solution was evaporated to dryness in a open teflon jar.

3) 1 ml of aqua regia was added, and the sample solution was evaporated to dryness.

4) 1 ml of 6 N HCl was added, and the sample solution was evaporated to dryness.

5) Step 4 was repeated twice.

6) The residue was dissolved in 1 ml of 0.1 M HCl.

7) The anion exchange resin was transformed into the chloride form using 6 M HCl in 600 ml teflon beaker for one week.

8) 3 ml of resin slurry was placed into a clean 10 ml quartz column.

9) The resin column was washed with 20 ml of 6 M HCl, followed by 15 ml of 0.1 M HCl.

10) The sample solution was transferred to the column and eluted with six 5 g aliquots of 0.1 M HCl, which were collected in 10 ml test tubes.

11) The column was then eluted with ten 5 g aliquots of (a) 8 M HNO_3, and (b) aqua regia; which were collected in 10 ml test tubes.

12) The eluted solutions were analyzed by ICP-MS.

5.4.1.2 RECOVERY OF THE PRECIOUS METALS USING ANION EXCHANGE

In an initial experiment, base metals were eluted using 30 g of 0.1 M HCl, and the precious metals were collected using 50 g of 8 M HNO_3. Recoveries are presented in Table 5.2a, and elution curves shown in Figure 5.1a. Recoveries of Ru, Rh, and Ir are good, but those of Pd, Pt, and Au are poor. Poor recoveries of Pt, Pd, and Au are due to significant retention of these elements on the resin since these elements probably were reduced. To avoid the problem of retention of Pt, Pd, and Au on the resin, 50 g of aqua regia was used as a elutant. Recoveries are presented in Table 5.2b and Figure 5.1b. The recoveries for Pd, Pt, and Au were improved, but are still variable due to the aqua regia reacting with the resin. It is impractical to use aqua regia oxidizing agents to release Pd, Pt, and Au as aqua regia destroyed the resin. This experiment has showed that an anion exchange is not practical for the separation of all the precious metals from the base metals.

5.4.2 SEPARATIONS BY CATION EXCHANGE

Since the precious metals were not efficiently recovered by anion exchange, a strongly acidic cation exchange was used as the alternative. The cation exchange separation of precious metals from base metals has been described (Beamish and Van Loon, 1977; Chung and Barnes, 1988; Sen Gupta, 1989). None of these methods reported a complete separation for all PGE and Au from

Table 5.2 Cumulate recoveries (%) of the precious metals by anion exchange using two different elutants: (a) 8 M HNO_3, and (b) aqua regia

(a)

8 M HNO_3	Ni (%)	Cu (%)	Ru (%)	Rh (%)	Pd (%)	Ir (%)	Pt (%)	Au (%)
5 g	0.18	2.85	4.93	86.6	14.8	64.4	1.85	10.7
10 g	0.23	2.91	36.7	88.6	46.9	86.0	6.90	18.0
15 g	0.27	2.92	62.7	89.0	69.0	92.8	11.4	22.8
20 g	0.31	2.99	90.1	89.2	74.2	95.3	18.5	26.6
25 g	0.36	3.00	95.9	89.4	76.6	96.4	25.6	31.5
30 g	0.40	3.03	96.7	89.5	79.1	97.2	34.1	38.4
35 g	0.45	3.07	97.0	89.7	83.5	97.8	47.3	43.6
40 g	0.48	3.08	97.3	89.8	87.0	98.3	60.0	48.4
45 g	0.54	3.10	97.5	89.8	89.9	98.7	76.1	52.6
50 g	0.60	3.13	97.7	90.0	93.2	99.1	93.9	54.7

(b)

Aqua Regia	Ni (%)	Cu (%)	Ru (%)	Rh (%)	Pd (%)	Ir (%)	Pt (%)	Au (%)
5 g	0.19	0.59	0.73	84.9	7.95	82.3	1.94	1.43
10 g	0.47	2.02	23.5	88.0	34.5	85.4	9.54	22.4
15 g	0.70	2.70	37.2	88.7	46.5	87.2	19.6	35.0
20 g	0.90	2.77	53.6	89.2	55.1	90.2	28.6	45.5
25 g	1.12	2.82	79.3	89.8	62.2	92.8	39.9	55.2
30 g	1.34	2.89	89.8	90.2	66.7	93.5	50.2	61.0
35 g	1.57	2.94	94.9	90.7	73.9	94.5	62.0	71.3
40 g	1.94	2.99	96.2	91.1	81.2	95.6	72.4	80.3
45 g	2.23	3.04	[illegible]	91.3	85.6	97.0	80.9	86.3
50 g	2.45	3.08	96.[illegible]	91.5	90.4	97.8	92.1	90.8

the matrix elements in a single column. In this study, 3 ml of a strongly acidic cation exchange resin Amberlite, CG-120, contained in a 10 ml quartz column, was used. The following experiment was conducted to establish the quantitative separation of the precious metals from the base metals by cation exchange.

5.4.2.1 EXPERIMENT PROCEDURE

1) 5 g of the synthetic solution used for anion exchange separation and 20 mg of a synthetic SARM-7 NiS bead (solid) were placed in a 30 ml teflon beaker.

2)-6) Steps 2-6 of the experiment procedure used for the anion exchange separation were followed to dissolved the NiS bead.

7) The cation exchange resin was transformed into the chloride form using 6 M HCl in a 600 ml teflon beaker for one week.

8) 3 ml of the resin slurry was placed into a 10 ml clean quartz column.

9) The resin was washed with 20 ml of 6 M HCl, followed by 15 ml of (a) 0.03 M HCl, (b) 0.1 M HCl, and (c) and (d) 0.2 M HCl.

10) The sample solution was transferred to the column and eluted with (a) 0.03 M HCl, (b) 0.1 M, and (c) 0.2 M HCl in six 3 g aliquots which were collected in six 10 ml test tubes; and (d) 0.2 M HCl in five 1 g aliquots, which were collected in five 10 ml test tubes

11) For (a) and (b), the column was then eluted with five aliquots of 3 g of 2.5 M HCl and collected in five 10 ml test tubes.

12) The collected solutions were analyzed by ICP-MS.

5.4.2.2 RECOVERY OF THE PRECIOUS METALS

Recoveries of the precious metals are presented in Tables 5.3. The cumulate elution curves using different concentrations of HCl are illustrated in Figure 5.2. In the initial experiment, precious metals were collected using 18 g of 0.03 M HCl and results are presented in Table 5.3a and Figure 5.2a. The recoveries of precious metals are 66-97%. To improved the recoveries, precious metals were collected using 18 g of 0.1 M HCl and results are presented in Table 5.3b and Figure 5.2b. Except for Pd, all the precious metals show over 95% recovery. Results of recoveries using 18 g of 0.2 M HCl as elutant are presented Table 5.3c and Figure 5.2c. Recoveries for Ru, Rh, Pd, Re, Ir, Pt, and Au are all over 99%. Finally the elution mass of 0.2 M HCl was reduced to 10 g, and over 99% recovery was achieved. In fact, the concentrations of precious metals in the first 1 g fraction are insignificant, and the cumulate recoveries of the 2 g through 5 g fractions are over 97% (Table 5.3d and Figure 5.3d).

Table 5.3 Cumulate recoveries (%) of the precious metals by cation exchange using different weights and concentrations of HCl as elutant: (a) 18 g of 0.03 M HCl, (b) 18 g of 0.1 M HCl, (c) 18 g of 0.2 M HCl, and (d) 10 g of 0.2 M HCl

(a)

0.03 M HCl	Ni (%)	Cu (%)	Ru (%)	Rh (%)	Pd (%)	Ir (%)	Pt (%)	Au (%)
3 g	0.05	0.02	63.3	52.1	59.6	93.4	86.2	53.4
6 g	0.07	0.04	68.4	58.0	65.7	95.7	88.5	67.5
9 g	0.09	0.05	69.3	60.8	67.4	96.1	90.0	71.7
12 g	0.10	0.06	69.9	62.6	68.7	96.6	91.1	73.3
15 g	0.12	0.07	70.5	63.8	69.2	96.8	91.8	74.8
18 g	0.14	0.08	71.8	66.3	69.8	97.2	92.6	75.8

(b)

0.1 M HCl	Ni (%)	Cu (%)	Ru (%)	Rh (%)	Pd (%)	Ir (%)	Pt (%)	Au (%)
3 g	0.14	0.02	93.5	95.0	83.2	94.9	92.9	78.2
6 g	0.19	0.04	95.9	97.2	85.1	96.8	94.7	90.8
9 g	0.23	0.06	96.5	97.9	85.8	97.2	95.0	92.8
12 g	0.26	0.08	97.0	98.3	86.1	97.6	95.2	93.9
15 g	0.28	0.10	97.3	98.6	86.4	97.9	95.4	94.7
18 g	0.30	0.12	97.5	98.7	86.6	98.0	95.6	95.5

(c)

0.2 M HCl	Ni (%)	Cu (%)	Ru (%)	Rh (%)	Pd (%)	Re (%)	Ir (%)	Pt (%)	Au (%)
3 g	0	0	97.7	98.5	96.8	96.6	98.5	97.6	88.3
6 g	0	0	99.2	99.4	98.0	99.0	99.6	98.8	97.7
9 g	0	0	99.4	99.5	99.3	99.5	99.7	99.2	99.6
12 g	0	0	99.6	99.5	99.8	99.6	99.8	99.4	99.4
15 g	0	0	99.7	99.6	99.8	99.7	99.9	99.6	99.6
18 g	0	0	99.8	99.7	99.8	99.8	99.9	99.6	99.7

(d)

0.2 M HCl	Ni (%)	Cu (%)	Ru (%)	Rh (%)	Pd (%)	Re (%)	Ir (%)	Pt (%)	Au (%)
1 g	0	0	0	0	0	0	0	0	0
2 g	0	0	72.8	73.1	74.3	39.6	75.7	73.3	0.1
3 g	0	0	99.8	99.9	99.6	99.7	99.8	99.7	62.4
4 g	0	0	100	100	99.9	99.9	99.9	99.9	86.5
5 g	0	0	100	100	100	99.9	100	100	97.1
10 g	0	0	100	100	100	100	100	100	100

5.5 PROCEDURE FOR THE QUANTITATIVE SEPARATION OF PRECIOUS METALS FROM BASE METALS BY CATION EXCHANGE

Based on the previously described experiments, the procedure for the quantitative separation of precious metals from associated base metals in 2-20 mg of sulphide and magnetite mineral separates is as follows:

1) The cation exchange resin was transformed into the chloride form using 6 M HCl for one week.
2) 3 ml of the resin slurry was placed into a 10 ml clean quartz column.
3) The resin was then washed with 20 ml of 6 M HCl, followed by 15 ml of 0.2 M HCl.
4) The 1 ml sample solution in 0.2 M HCl was transferred to the column, and the displaced solution discarded.
5) 1 ml 0.2 M HCl was added to the column, and the eluted solution was collected in a 15 ml screw top centrifuge tube (Sarstedt).
6) After the 1 ml of 0.2 M HCl was eluted and collected, a further 3 ml of 0.2 M HCl was added, and collected in the same container.
7) After each separation, the resin was discarded, the column was cleaned, and new resin was added for the next separation.

5.6 DATA ACQUISITION AND REDUCTION

The analytical masses and interferences are modified from Jackson *et al.* (1990) (Table 5.4). Since precious metals were quantitatively separated from base metals, base metal-argon polyatomic ion interferences on Ru, Rh and Pd were not significant. Os was not determined because of its loss as volatile OsO_4 during the evaporation in open teflon jars. The sensitivities of all the analyte elements were measured in one of the external standard solutions (STDA, Table 5.5). The elements Cd and Tl were used as internal standards because of their close mass proximity (Cd for Ru, Rh, and Pd; Tl for Re, Ir, Pt, and Au) (Jackson *et al.*, 1990). Samples were run in the following sequence: acid calibration blank (0.2 M HCl), STDA, flush (0.3 M HCl and 0.4 HNO_3), STDB, acid calibration blank, sample 1, sample 2, ..., acid calibration blank, STDA, etc. After the data were collected, the backgrounds of elements Ru, Rh, Re, Ir,and Pt were calculated as the mean of two determinations of acid calibration blank closest to the samples. The backgrounds for Pd and Au were interpolated from the two determinations of the acid calibration blank closest to the samples, because of memory effect. Any Ta oxide interference on Au (from instrument memory) was calculated from count rates of STDB and samples. Matrix effects and drift were corrected with the two internal standards. After background, oxide interference, instrument drift and matrix

Table 5.4 Analytical ions and corrected interference

Determined ion	isotopic abundance	corrected interference
$^{101}Ru^+$	17.1%	
$^{103}Rh^+$	100%	
$^{105}Pd^+$	22.2%	
$^{111}Cd^+$	12.8%	
$^{181}Ta^+$	99.9%	
$^{185}Re^+$	37.4%	
$^{193}Ir^+$	62.6%	
$^{195}Pt^+$	33.8%	
$^{197}Au^+$	100%	$^{181}Ta^{16}O^+$
$^{203}Tl^+$	29.5%	

Table 5.5 Elements and concentrations for STDA, STDB, and internal Standard

Element	STDA (ppb)	STDB (ppb)	Internal Standard (ppb)
Ni		52894	
Cu		5062	
Ru	94.02		
Rh	52.97		
Pd	73.81		
Cd			4031
Ta		61.35	
Re	48.84		
Ir	47.62		
Pt	94.31		
Au	32.04		
Tl			2045

were corrected, sample solution concentrations were calculated by external

calibration using the mean sensitivity of the two closest calibration standards. Solid sample concentrations were then calculated from sample and solution weights.

5.7 RESULTS AND DISCUSSION

5.7.1 SOLID LIMITS OF DETECTION

Since the mean of all calibration blanks in a run was used as a background to correct all data, limits of detection, defined here as 3 times the standard deviation of the difference between the count rate of a sample and n replicates of the calibration blank, is calculated as $[3*\sigma*\sqrt{(1/n+1)}]$, where n is the number of calibration blanks used. Solid limits of detection, for a 20 mg sample dissolved in 4 g solution, and with 16 determinations of the calibration blank ($n = 16$) are less than 4 ppb for Ru, Rh, Pt, Ir, and Au; and 29 ppb for Pd (Figure 5.3). The high solid limit of detection for Pd is due to the large memory effect of this element in the ICP-MS.

5.7.2 PRECISION AND ACCURACY

Results for 10 replicate analyses of fragments or powder of one nickel sulphide bead of the geological reference material, SARM-7, are presented in Table 5.6.

Table 5.6 Analytical results vs. literature values (ppb) for a single SARM-7 nickel sulphide bead

a. 2 mg nickel sulphide bead fragments from the same bead

	Ru	Rh	Pd	Ir	Pt	Au
(1)	440	282	1213	95	4201	246
(2)	434	304	1383	94	3088	186
(3)	463	285	1216	72	4570	283
(4)	407	299	1181	98	4064	159
(5)	465	279	1309	101	4337	77
(6)	453	277	1263	104	4462	308
(7)	356	291	1315	86	4200	578
(8)	446	280	1308	97	3324	170
(9)	408	289	1182	92	4479	170
(10)	386	281	1255	86	4550	239
Average	426	287	1262	92	4328	241
RSD	8%	3%	5%	9%	4%	51%
LOD	2.15	0.67	6.2	1.37	4.14	15.8

b. 20 mg of nickel sulphide bead powder from the same bead

(1)	428	240	1457	82	3254	176
(2)	436	246	1525	84	3386	200
(3)	431	240	1480	82	4348	153
(4)	441	249	1505	84	3334	189
(5)	444	250	1524	85	3356	184
(6)	452	257	1548	85	3239	174
(7)	432	246	1476	84	3441	187
(8)	401	242	1277	83	3019	153
(9)	410	237	1379	83	3193	178
(10)	420	236	1473	83	3394	193
Average	430	244	1464	84	3297	179
RSD	3%	2%	5%	1%	3%	8%
LOD	2.45	0.34	29	0.51	2.04	3.72
Ref (1)	430	240	1530	74	3740	310
Ref (2)	397	212	1353	71	3395	253

Ref (1): from Steel *et al.* (1975) Ref (2): from Jackson *et al.* (1990)

Re data are not reported here because Re is not quantitatively collected by the nickel sulphide fire assay bead (Frimpong, 1992). For 2 mg size fragments, relative standard deviations (RSD) for the 10 determinations are less than 10% except for Au (Figure 5.4a), and data show good agreement with certified and literature values (Steele *et al*, 1978; and Jackson *et al.*, 1990) (Figure 5.5a). Poor accuracy and precision for Au are considered to be due to its heterogenous distribution in the NiS bead and possibly inefficient collection by the NiS (Jackson *et al.*, 1990). For 20 mg samples of the NiS bead, the RSDs are less than 8% (Figure 5.4b). Results (except for Au) are in a good agreement with certified and literature values (Figure 5.5b)

5.8 DETERMINATION OF PRECIOUS METALS IN SULPHIDE AND MAGNETITE MINERALS FROM STRATHCONA DEEP COPPER ZONE CU-NI SULPHIDE ORES.

The distribution and fractionation of the precious metals among coexisting sulphides and magnetite are important for the understanding of the ore-forming processes. However, progress has been hampered by the large quantities of high purity mineral separates required for conventional analytical techniques.

Preliminary studies of PGE and Au distributions and fractionation among coexisting sulphides and magnetite from the Strathcona Deep Cooper Zone ores

demonstrates the ability of this technique to determine the precious metals in milligram weights of samples (Figure 5.6). The geological significance and discussion of these results will be presented in Chapter 7. High concentrations of Pt and Pd in the magnetite may explain the poor metallurgical recovery of these elements from the same ores.

5.9 CONCLUSIONS

A new procedure combining aqua regia sample dissolution and cation exchange separation, with final quantification using ICP-MS, for sulphide and magnetite minerals has been developed for the simultaneous determination of 7 of the precious metals. The procedure can analyze mineral separates of 20 mg with solid limits of detection less than 4 ppb for Ru, Rh, Re, Ir, Pt, and Au, and Pd for 29 ppb. Larger samples may reduce solid limits of detection proportionally. The cation exchange procedure provides quantitative recoveries (> 99%) for the PGE and acceptable recoveries of Au, and the separation of all the precious metals from the base metals.

The low detection limits, very small required sample size and the multi-element capability of this procedure provides a major advance that will allow the examination of precious metal distributions and fractionation within and between the minerals.

(a)

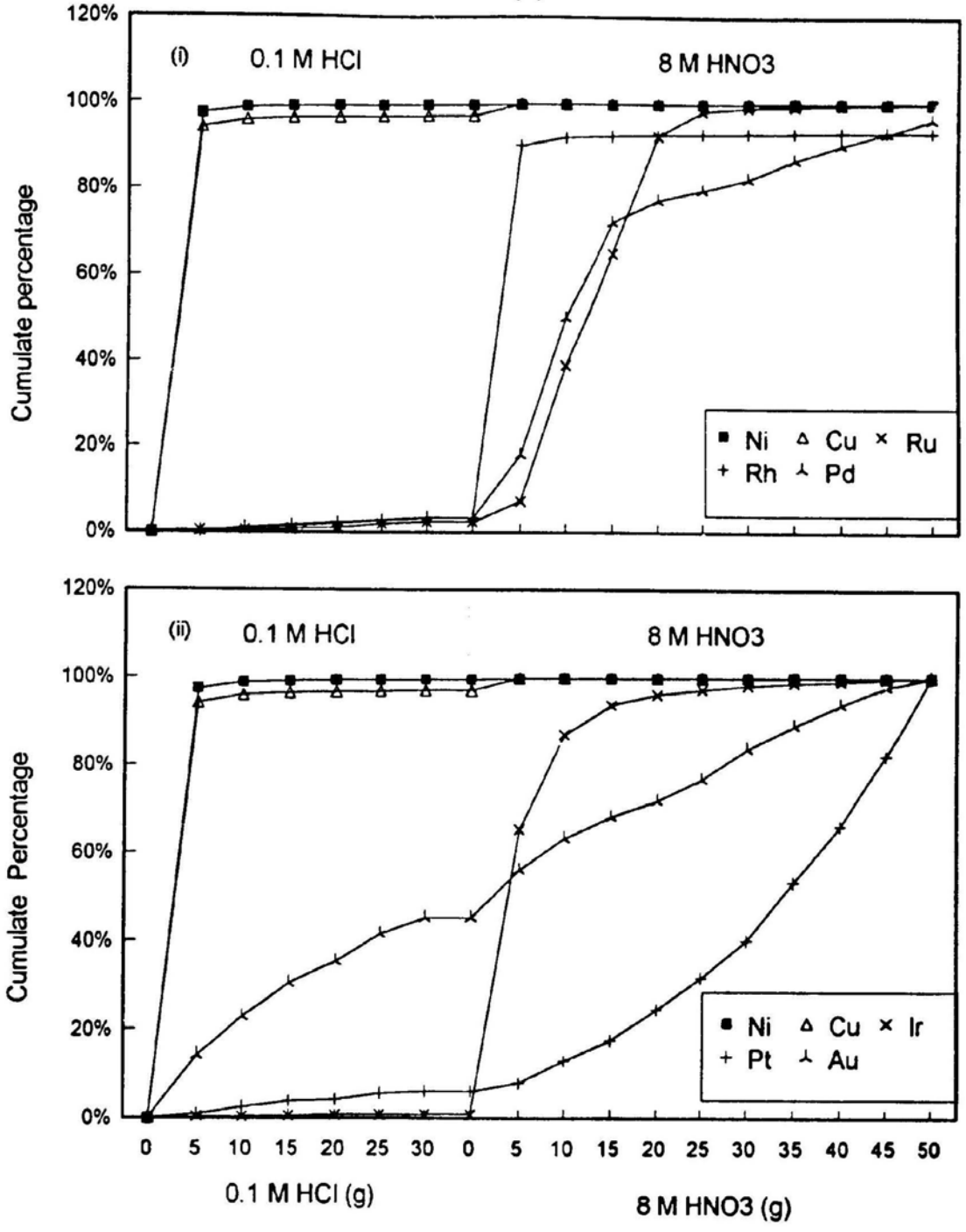
(i)
0.1 M HCl
8 M HNO3
Cumulate percentage
120%
100%
80%
60%
40%
20%
0%
Ni
Cu
Ru
Rh
Pd
(ii)
0.1 M HCl
8 M HNO3
Cumulate Percentage
Ni
Cu
Ir
Pt
Au
0 5 10 15 20 25 30 0 5 10 15 20 25 30 35 40 45 50
0.1 M HCl (g)
8 M HNO3 (g)

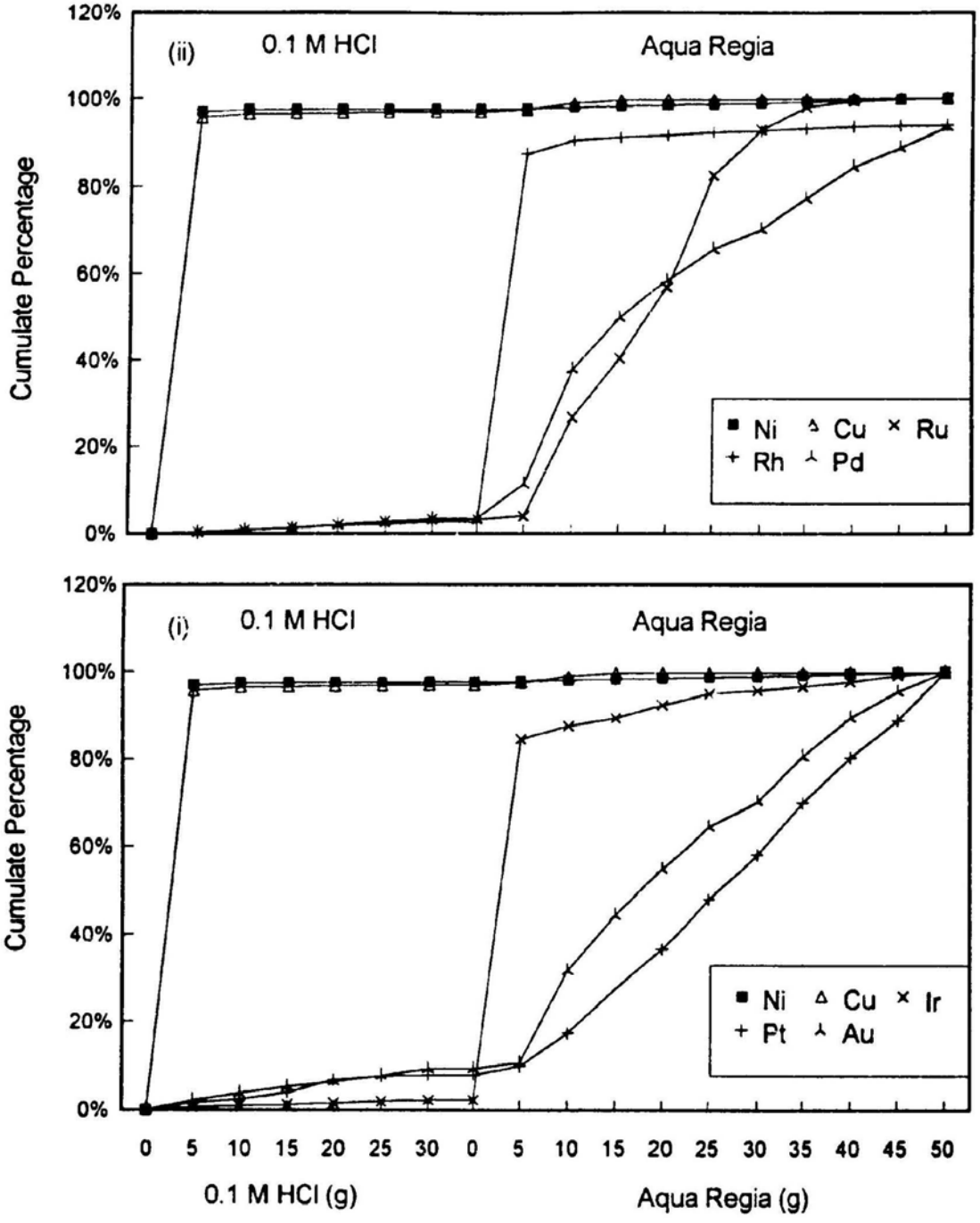

Figure 5.1 Cumulate elution curves of the precious metals and base metals by anion exchange using 30 g of 0.1 M HCl; followed by 50 g of (a) 8 N HNO3, and (b) aqua regia.

(a)

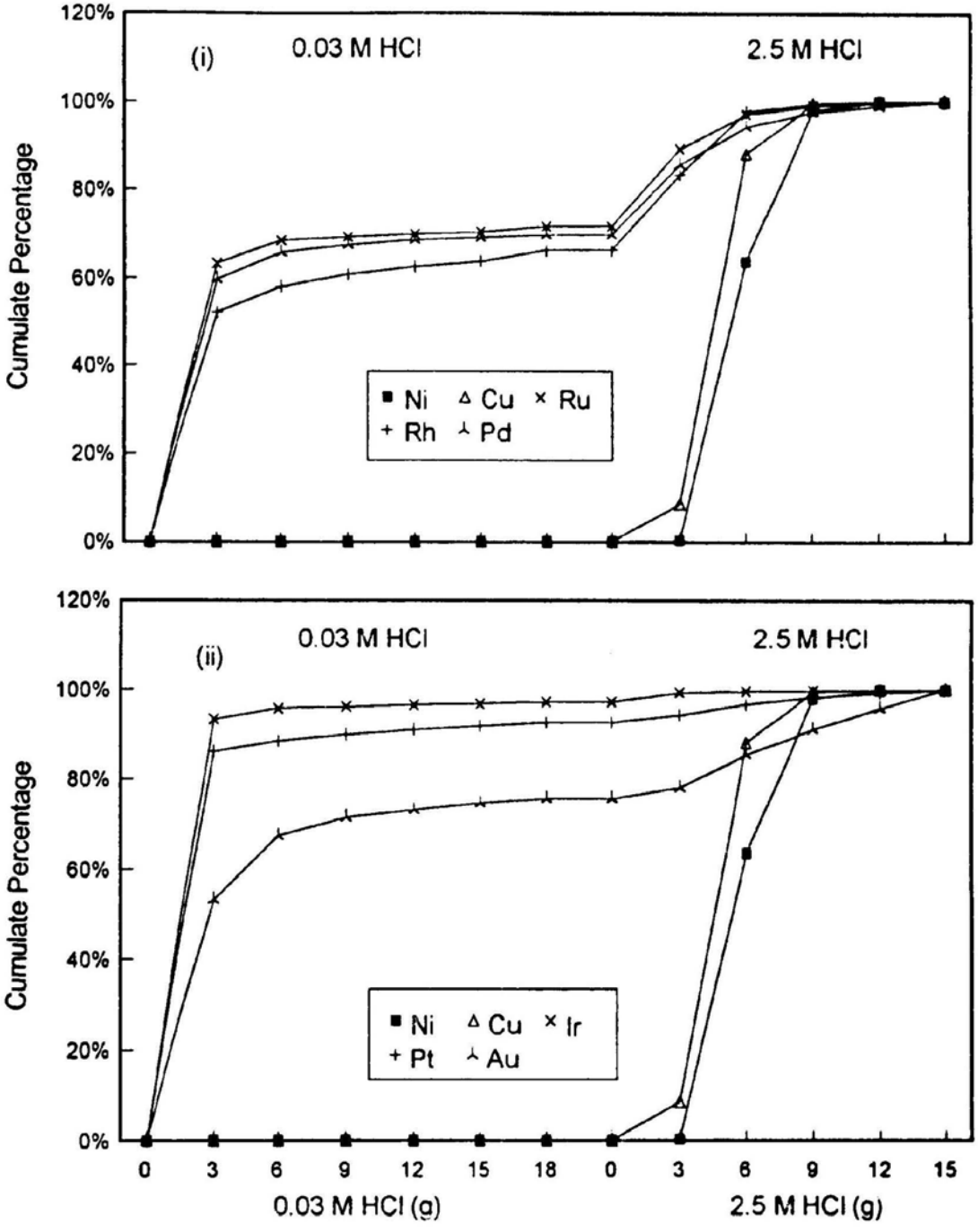
(i)
0.03 M HCl
2.5 M HCl
Cumulate Percentage
120%
100%
80%
60%
40%
20%
0%
Ni
Cu
Ru
Rh
Pd
(ii)
0.03 M HCl
2.5 M HCl
Cumulate Percentage
Ni
Cu
Ir
Pt
Au
0
3
6
9
12
15
18
0.03 M HCl (g)
2.5 M HCl (g)

(b)

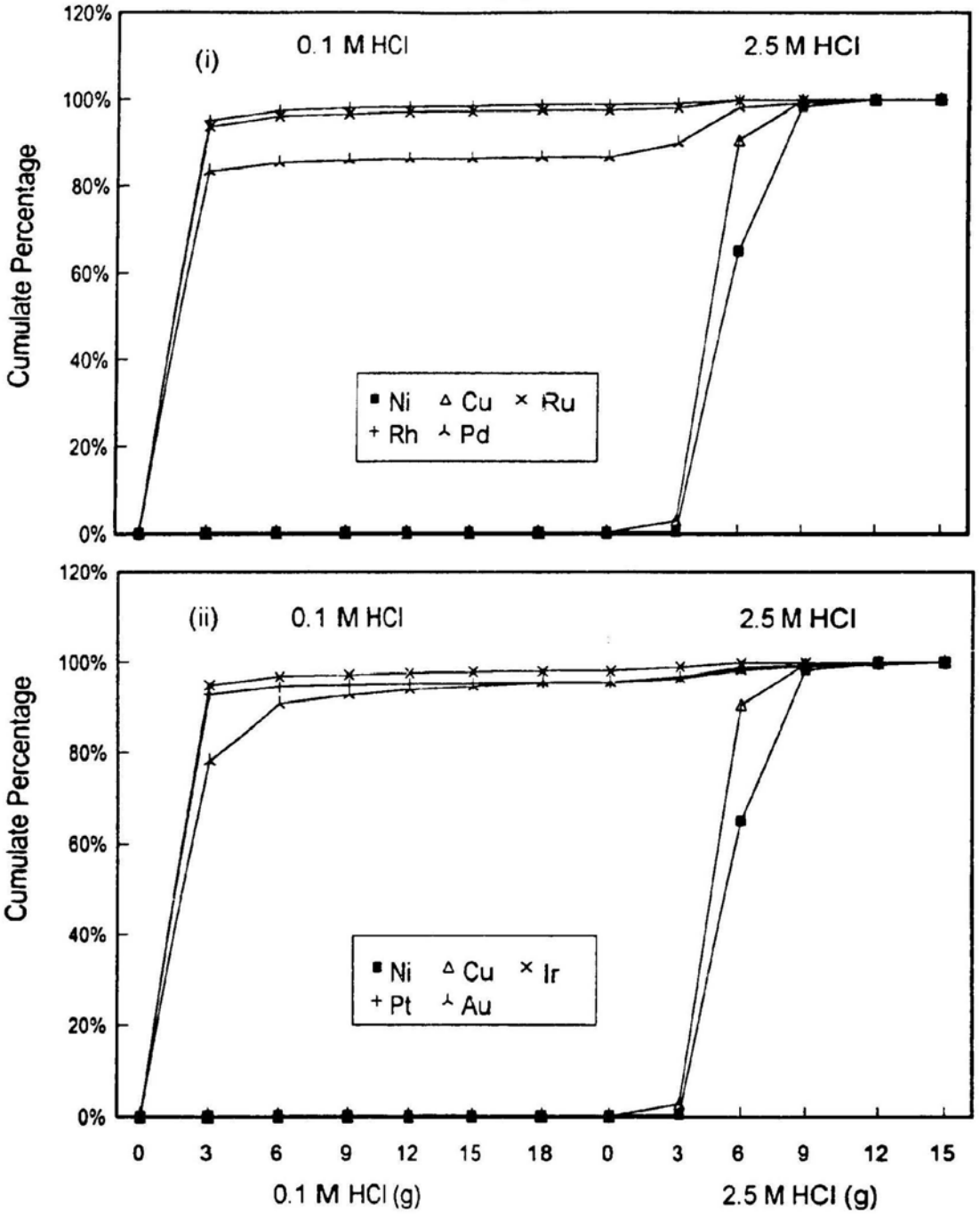
(i)
0.1 M HCl
2.5 M HCl
Cumulate Percentage
120%
100%
80%
60%
40%
20%
0%
Ni
Cu
Ru
Rh
Pd
(ii)
0.1 M HCl
2.5 M HCl
Cumulate Percentage
Ni
Cu
Ir
Pt
Au
0
3
6
9
12
15
18
0.1 M HCl (g)
2.5 M HCl (g)

(c)

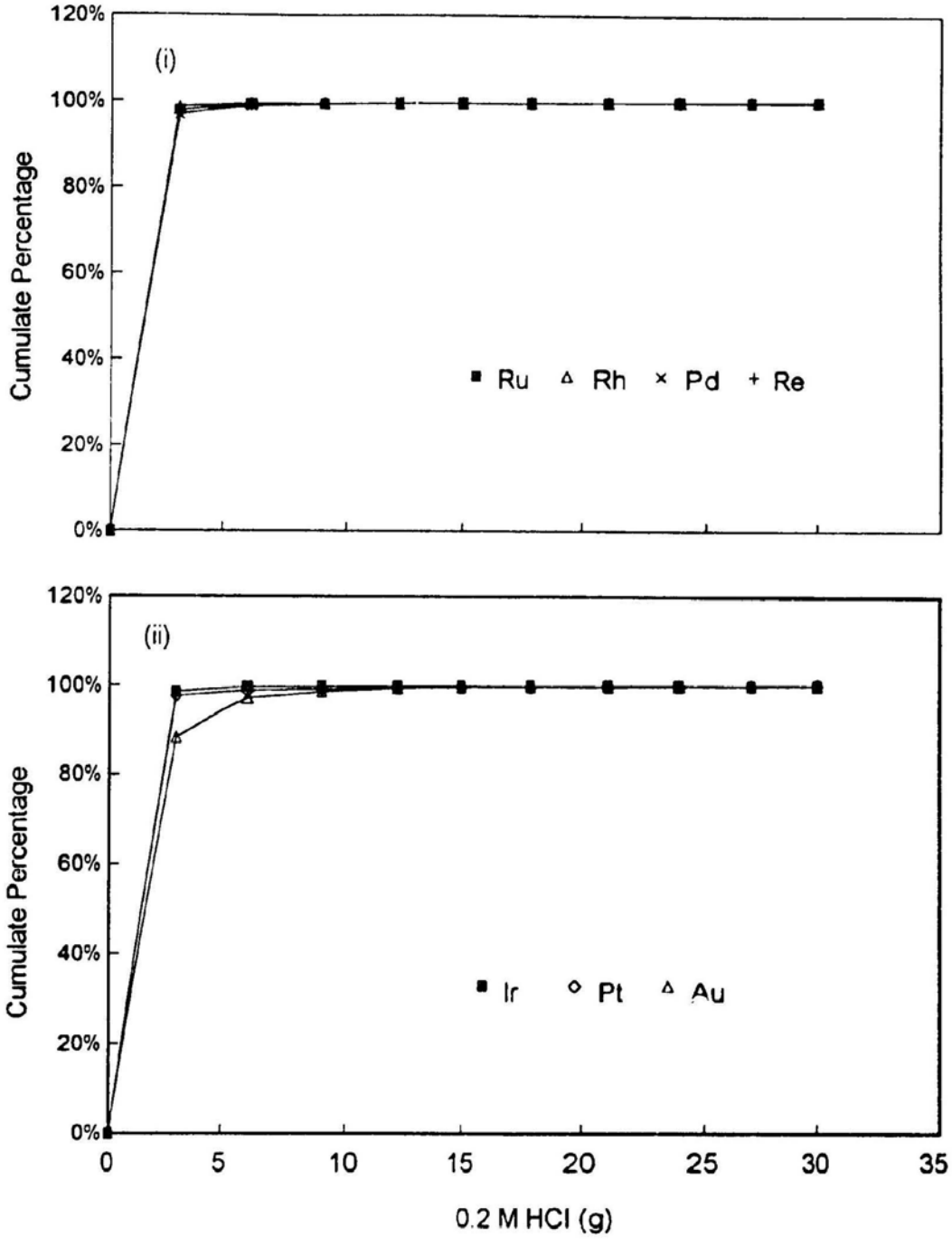
(i)
120%
100%
80%
60%
40%
20%
0%
Cumulate Percentage
Ru
Rh
Pd
Re
(ii)
120%
100%
80%
60%
40%
20%
0%
Cumulate Percentage
Ir
Pt
Au
0
5
10
15
20
25
30
35
0.2 M HCl (g)

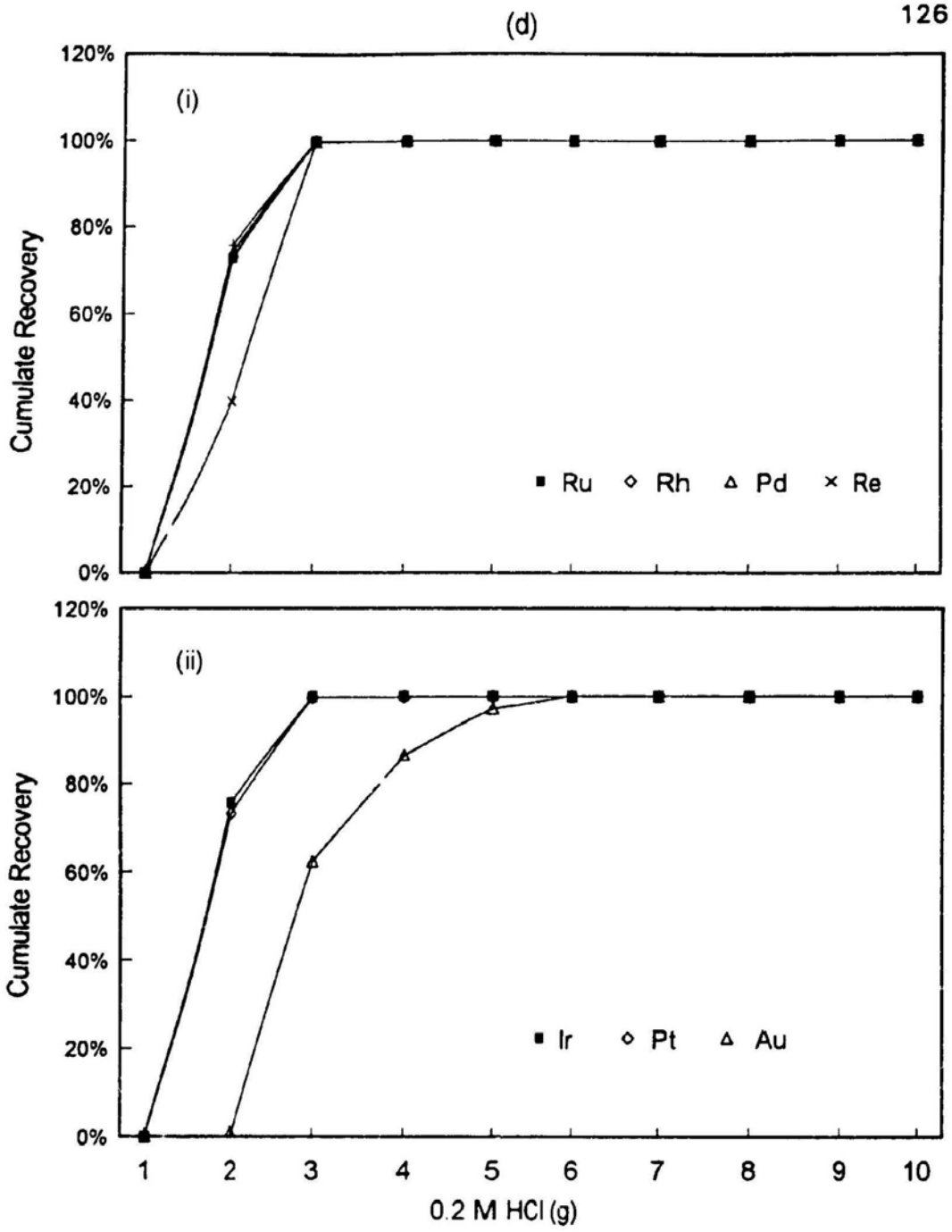

Figure 5.2 Cumulate elution curves of the precious metals by cation exchange using (a) 18 g of 0.03 M HCl, (b) 18 g of 0.1 M HCl, (c) 18 g of 0.2 M HCl, and 10 g of 0.2 M HCl; followed by 15 g of 2.5 M HCl for (a) and (b).

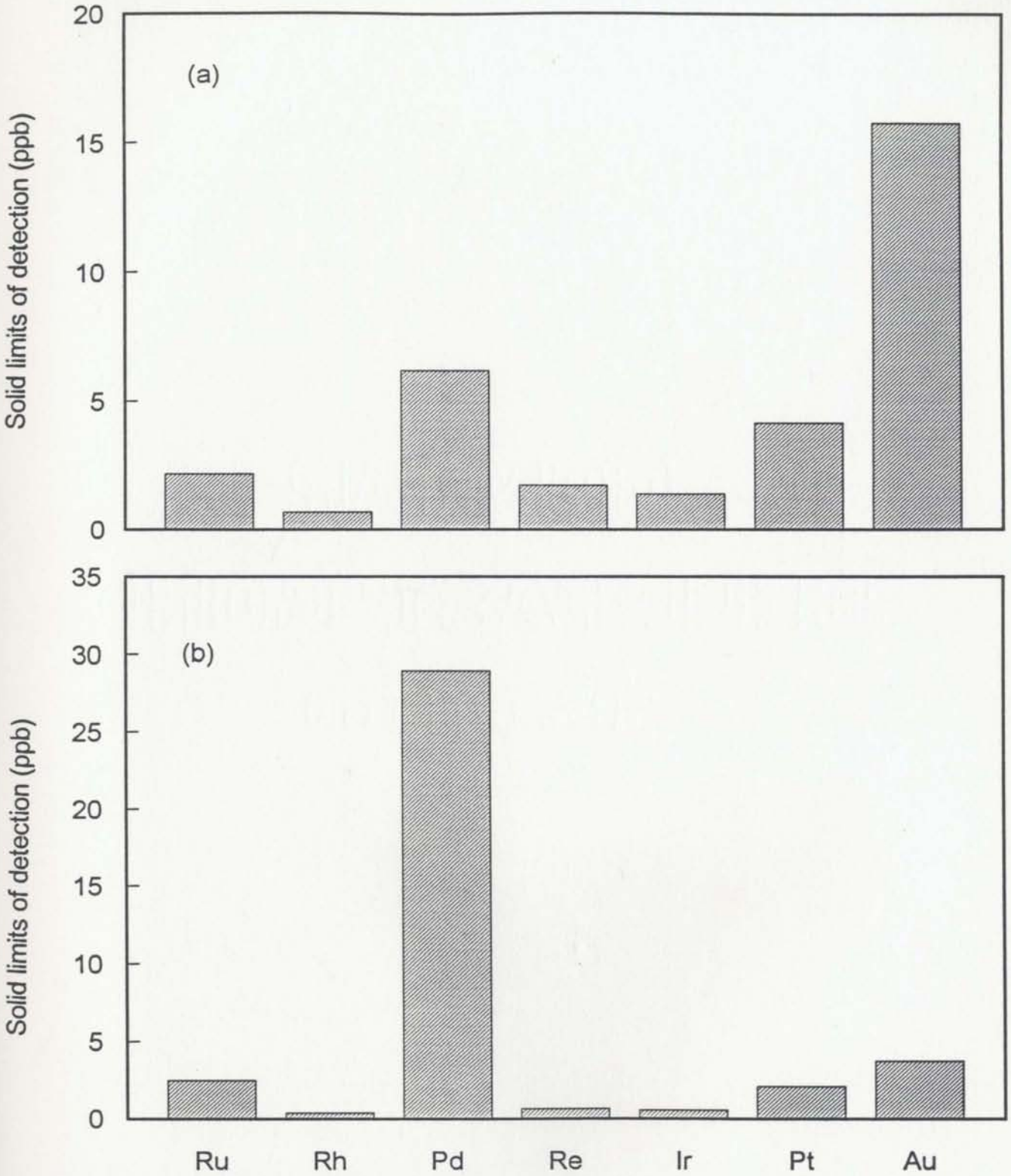

Figure 5.3 Limits of detection for solid sample masses of 20 mg taken to a final volume of 4 g. (a) nickel sulphide bead fragments and (b) nickel sulphide bead powder

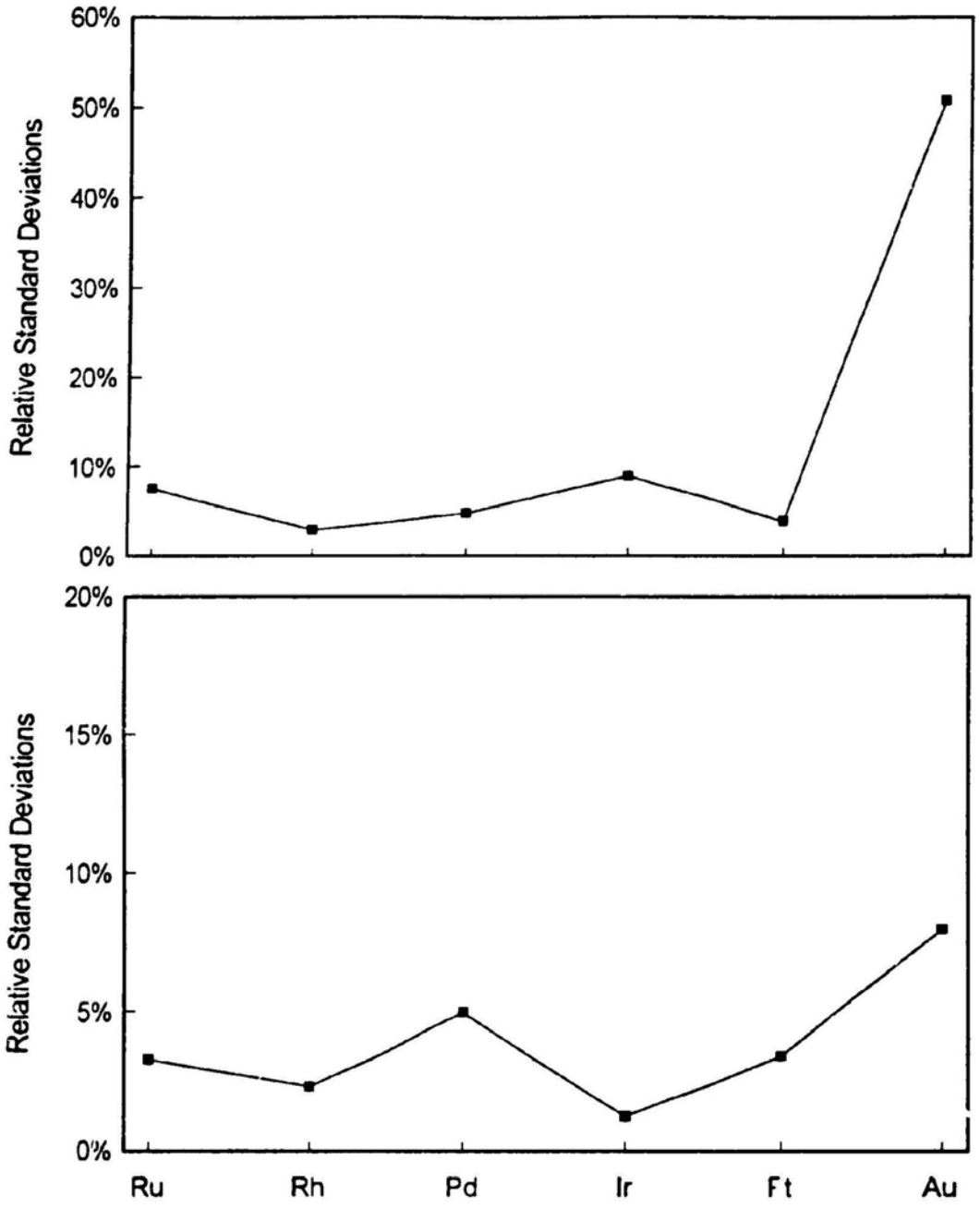

Figure 5.4 Relative standard deviations for the analyses (n=10) of precious metals in the certified geological reference material, SARM-7, by ICP-MS after cation exchange separation. (a) 2 mg replicates of nickel sulphide fragments, and (b) 20 mg replicates of nickel sulphide bead powder

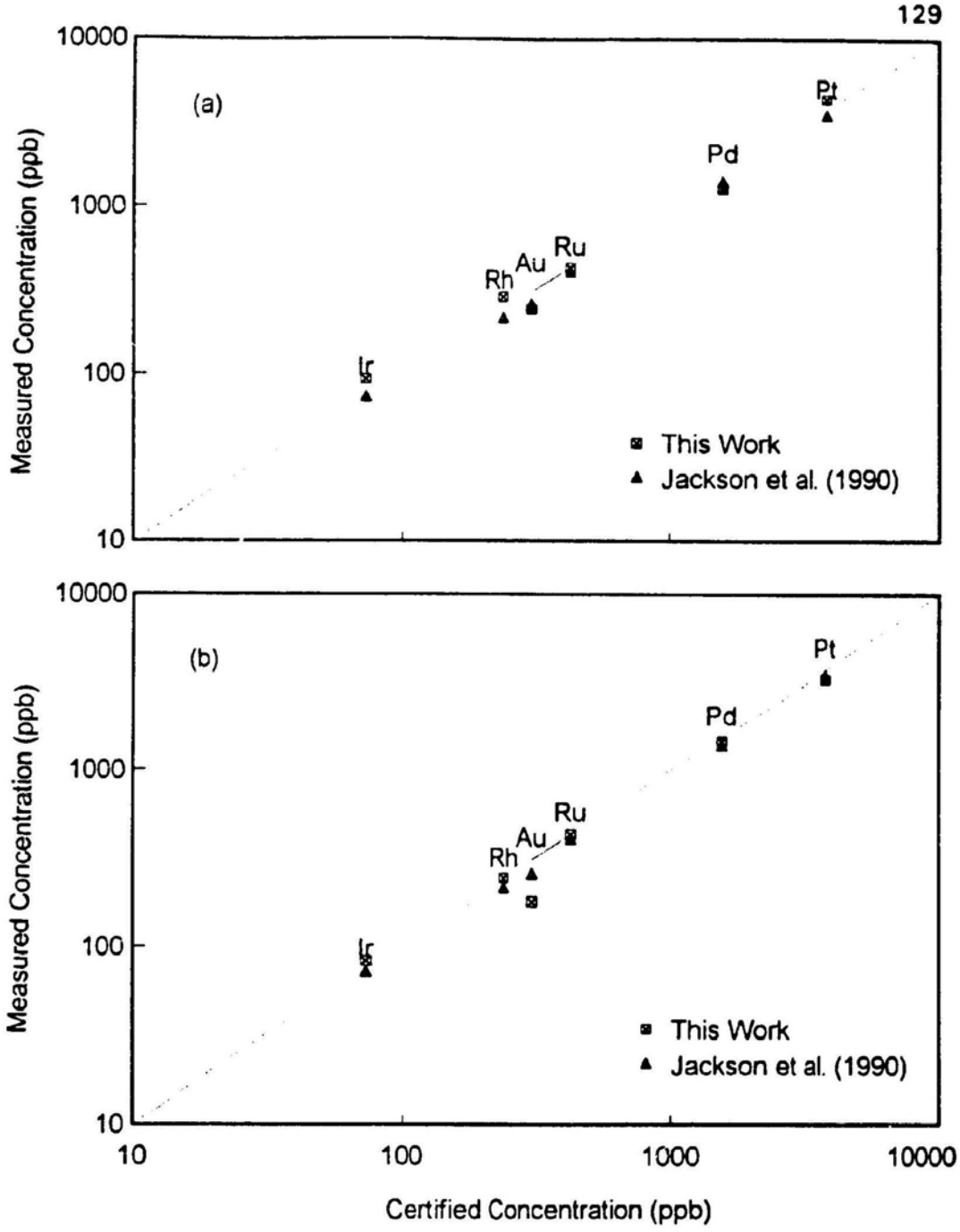

Figure 5.5 Concentrations of precious metals obtained in this study compared to the literature values for the certified geological reference material, SARM-7. (a) 2 mg nickel sulphide bead fragments, and (b) 20 mg nickel sulphide bead powder

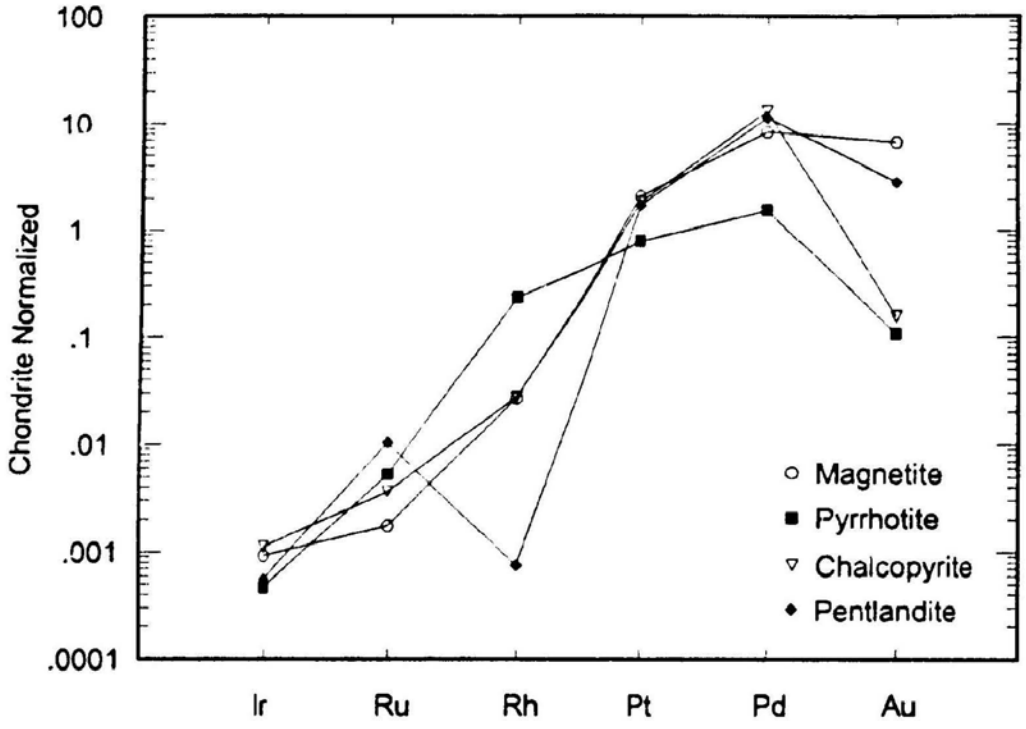

Figure 5.6 Mean chondrite-normalized data of sulphides and magnetite (sample weight: 20 mg) from Strathcona Ni-Cu sulphide ores, showing the distribution and fractionation of precious metals between these minerals

CHAPTER 6

THE GEOLOGY OF THE SUDBURY AREA AND THE SETTING OF THE NI-CU-(PGE) SULPHIDE MINERALIZATION

6.1 INTRODUCTION

The objectives of this chapter are to: 1) summarize the geological setting of the Sudbury area; 2) describe the geology and geochemistry of the Sudbury Igneous Complex (SIC), and present new trace element geochemical data relating to the SIC; and 3) describe the Ni-Cu-(PGE) ore deposit types, and summarize the characteristics of these ore deposits (their setting, mineralogy and chemical compositions).

The objectives of this chapter is to provide the geological background for the study of the precious metal distributions and partitioning in Sudbury ores which will be discussed in subsequent chapters.

6.2 GEOLOGICAL SETTING OF THE SUDBURY AREA

The Sudbury area is one of the world's largest Ni-Cu-PGE mining districts, and has long attracted geologists because of its ore deposits and intriguing

geological history. The geological setting, ores, and igneous rocks have been the subject of extensive research indicated by the large number of publications.

The Sudbury structure is located near the conjunction of three structural provinces of the Canadian Shield; the Superior, Southern and Grenville Provinces. The Sudbury structure consists of three major components (Figure 6.1) (Naldrett *et al,* 1982):

(1) Sudbury breccia in the Archean basement and Proterozoic cover peripheral to the Sudbury Igneous Complex (SIC).

(2) Sudbury Igneous Complex, a noritic and granophyric, basin-shaped body emplaced approximately coincident with the base of the Sudbury Basin. The Ni-Cu-(PGE) sulphide ore deposits are spatially close to the base of this Complex.

(3) Sudbury Basin containing the Whitewater Group comprised of the Onaping, Onwatin, and Chelmsford Formations.

The Sudbury structure, as defined by the outer limits of the Sudbury breccia, is roughly an oval-shaped area with a long:short axis ratio of 2.2:1 (Grieve *et al.*, 1991) and a long axis of about 190 km in diameter (Peredery and Morrison, 1984). On the northern and eastern sides the Sudbury structure is in contact with Archean migmatized high grade gneisses (2711 Ma), and quartz

monzonite plutons (2500-2700 Ma) of the Superior Province that contains remnant greenstone belts (2700 Ma) (Krogh *et al.*, 1984). On the southern side, the Sudbury structure is in contact with the Proterozoic metavolcanic and metasedimentary rocks of the Huronian Supergroup (2550-2110 Ma, Krogh *et al.*, 1984) which are part of the Southern Province. The granitic Creighton and Murray plutons (2388 Ma, Krough *et al.*, 1984) intrude the Huronian sequence south of the SIC. Nipissing gabbroic dykes and sills (2110 Ma, Card *et al.*, 1984) are widespread in the Sudbury area intruding in the Archean and Huronian units.

Despite being controversial (Muir, 1984), the proposal suggested by Dietz (1964) that the Sudbury structure is an astrobleme, produced by the impact of a large meteorite, is widely accepted. This is supported by the presence of shock metamorphic features in the Archean basement, Huronian cover, and in the Onaping Formation. The impact could have caused fracturing in the crust and generated magma in the deep crust which then filled the impact-crater to produce the rocks of the SIC. The age of the Sudbury structure is approximated by the intrusion of the SIC (1850 Ma, Krogh *et al.*, 1984) which is consider to have been intruded shortly after the Sudbury catastrophic event.

6.3 GEOLOGY AND GEOCHEMISTRY OF THE SUDBURY IGNEOUS COMPLEX

6.3.1 INTRODUCTION

The Ni-Cu-(PGE) mineral deposits of the Sudbury district are closely related to the Sudbury Igneous Complex (SIC), a layered intrusion ranging from quartz norite at the base, through gabbro to a granophyric cap (Naldrett *et al.*, 1985). The study of the SIC is important for understanding the genesis of the ore deposits. The main mass of the SIC is an elliptically-shaped body intruded into Archean rocks of the Superior Province to the north and east, and Huronian rocks of the Southern Province to the south (Figure 6.1). The units of the main mass of the SIC consist of: a basal discontinuous ore-bearing Sublayer or offset dykes (Pattision, 1979); mafic norite, quartz-rich norite, South Range norite, and felsic norite constituting the lower zone; quartz gabbro constituting the middle zone; and granophyre in the upper zone (Figure 6.2) (Naldrett and Hewins, 1984).

The rare-earth element geochemistry of the SIC has been studied by Kuo and Crocket (1979). Their data showed that norite and granophyre are characterized by positive and negative Eu anomalies, respectively, whereas border norites and oxide-rich gabbro lack prominent Eu anomalous. Naldrett and Evensen (1985) have studied the major and trace element geochemistry of

the SIC. They indicated that all rocks of the complex are usually sialic and rich in incompatible elements, and that the major and trace element contents can be modelled in terms of a continental flood basalt magma assimilating typical Archean tonalite and quartz monzonite.

Detailed U-Pb geochronology (Krogh *et al.*,1984) showed that zircons from the North Range felsic norite, the North Range mafic norite, and South Range black norite of the SIC yield precise overlapping ages of 1848.9 + 4.0/-2.7 Ma, 1850.0 + 3.4/-2.4 Ma, and 1850.5 ± 1.3 Ma; and that baddeleyite from the granophyre has an age of 1851 ± 3 Ma, indicating it is essentially coeval with the norite.

Sm-Nd isotopic data for whole rock samples and minerals of the SIC has been reported by Faggart *et al.* (1985). Their data gave an igneous crystallization age of 1840 ± 21. They also reported that initial epsilon neodymium values (ϵNd) for 15 whole rocks, which range from -6.84 to -8.83, are similar to those for average upper continental crust, falling on the crustal trend of neodymium isotopic evolution as defined by shales.

Oxygen isotopic results have been reported by Ding and Schwarcz (1984). Their data showed that the norite has an average whole-rock oxygen isotopic composition ($\delta^{18}O$) of 6.7‰, about 0.7‰ greater than that of fresh oceanic basalts, and similar to that of some continental basalts. The granophyre is slightly richer in ^{18}O with a $\delta^{18}O$ value of 7.3‰.

Since only 9 out of the 15 REE have been reported before (Kuo and Crocket, 1979), this chapter presents a complete set of the trace- and rare earth- element data for 14 samples collected from the norite, gabbro, and granophyre units on both south and North Range. Petrographic information about the samples is reviewed.

6.3.2 PETROGRAPHY

6.3.2.1 SUBLAYER AND OFFSET DYKES

The Sublayer is a mafic to intermediate rock occurring at the base of the SIC and is host to much of nickel-copper sulphide ore of the Sudbury structure (Yates, 1948). The Sublayer is a discontinuous unit below the norite (Figures 6.10-6.11). Pattison (1979) recognized two varieties of Sublayer: igneous-textured gabbro-norites and metamorphic-textured leucocratic breccia. Both are characterized by the presence of sulphide and abundant xenoliths. Offset dykes are a series of ore-bearing dykes stemming from the contact Sublayer and penetrating deep into the footwall terrain (Grant and Bite, 1984). The dykes have a quartz diorite composition (Naldrett, *et al.*, 1985).

6.3.2.2 LOWER ZONE

The lower zone of the SIC overlies the Sublayer or footwall Archean and

Huronian rocks (Figures 6.1-6.2). The petrographic characteristics of this unit vary in different parts of the basin. On the north and east ranges, it is a coarse-grained, hypidiomorphic norite with a typical modal mineral composition of 55% plagioclase, 25% orthopyroxene, 10% amphibole, 5% clinopyroxene, 5% biotite, and less than 3% apatite; whereas on the South Range the unit is a quartz-rich norite with a typical modal mineral composition of 50% plagioclase, 25% orthopyroxene, 5-10% biotite, 5-10% quartz, 5% amphibole, and less than 3% apatite (Figure 6.3a-b). Orthopyroxene in the norite from the South Range is replaced by amphibole around its edge, showing a reaction rim texture (Figure 6.3c). In some areas, pyroxenes in the norite are entirely replaced by amphibole and biotite (Figure 6.3d-e).

6.3.2.3 MIDDLE ZONE

The South Range norite grades into the quartz gabbro of the middle zone with decreasing modal abundances of hypersthene and increasing abundance of augite, quartz, magnetite, ilmenite, and apatite content (Figures 6.1-6.2) (Naldrett and Hewins, 1984). The quartz gabbro of the North Range middle zone is very similar to the quartz gabbro of the South Range. In the North Range, it contains more opaque oxide minerals, apatite and titanite than in the South Range. Figures 6.3f-g show micrographs of quartz gabbro from the South Range, having a modal mineralogy that includes 30% plagioclase, 35%

amphibole, 20% orthopyroxene and clinopyroxene, 10% quartz, and 5% opaque minerals.

6.3.2.4 UPPER ZONE

The granophyre, making up the upper zone of the SIC (Figures 6.1-6.2), is commonly coarse grained and consists of plagioclase (10-20%), granophyric intergrowths of quartz (15-30%) and alkali-feldspar (45-60%), and minor amounts of biotite, augite, hornblende, epidote, chlorite, and opaque oxide minerals. Granophyre in the SIC shows typical myrmekitic texture (Figure 6.3h-i).

6.3.3 MAJOR- AND TRACE-ELEMENT RESULTS FOR THE SUDBURY IGNEOUS COMPLEX

6.3.3.1 SAMPLING AND ANALYTICAL METHODS

Fourteen representative samples were collected from two traverses through the south and North Ranges of the SIC and the Onaping Formation (Appendix II) (Figures 6.4 and 6.5). Samples for bulk analysis were crushed to a minus 200-mesh powder using a tungsten carbide pulverizer. Quartz sand was pulverized between sample runs to minimize cross contamination between samples.

Major elements together with Cr, Ni, Cu, Zn, and V were analyzed by X-ray fluorescence spectrometry methods using pressed powder pellets

(Longerich, 1993). Rubidium, Sr, Ba, Li, Cs, Y, Tl, Zr, Nb, Hf, Ta, Pb, Th, and U and the rare-earth elements (REE) were determined on the same powders by inductively coupled plasma-mass spectrometry (ICP-MS) as described in Chapter 2, following the procedure of Jenner *et al.* (1990). Nb and Ta may be slightly contaminated from the crushing in the tungsten carbide pulverizer. Analytical results for the USGS reference material DNC-1 and the CCRMP reference material MRG-1 are also listed in Table 6.1. The results for these two reference materials compare well with literature values (Table 6.1).

6.3.3.2 MAJOR-ELEMENT RESULTS

The major element chemical composition of 13 samples of the SIC are plotted on Harker diagrams (Figure 6.6, and Table 6.1). Samples range from 48% SiO_2 in norite to 67% in granophyre.

Two chemical trends are evident in Figure 6.6. Norite and gabbro rocks have high MgO (4-10%) and CaO (5-8.5%) contents; and low SiO_2 (48-55%), Na_2O (less than 2.5%), and K_2O (less than 1.5%) contents. Most major elements show negative correlation with SiO_2, with the exception of Al_2O_3, K_2O, and Na_2O, which display a positive trend. Granophyric rocks unlike the norites and gabbros, have high SiO_2 (62-67%), Na_2O (3-4%), and K_2O (3-4%) contents; and low MgO (0.5-1.5%) and CaO (1.5-3%) contents.

Table 6.1 Major and trace element compositions of Sudbury Igneous Complex+

Elements	91ZC01	91ZC06	91ZC02	91ZC03	91ZC04	91ZC05	91ZC07	91ZC08	91ZC09
SiO2	55.1	49.7	51.2	51.4	50.9	66.3	53.1	52.9	48.4
TiO2	0.29	0.67	0.38	0.49	1.16	0.76	0.39	0.39	1.84
Al2O3	16.2	10.3	14.8	14.4	13.5	12.4	14.4	14.9	10.7
FeO	5.9	11.8	8.1	8.7	10.1	6.4	7.3	6.8	13.5
MnO	0.10	0.15	0.12	0.12	0.14	0.09	0.11	0.12	0.15
MgO	8.7	9.8	10.3	8.58	7.01	1.54	6.29	4.61	4.54
CaO	7.8	5.2	7.2	7.6	8.6	2.07	6.5	8.0	8.3
Na2O	2.06	2.04	2.02	2.33	2.37	3.68	2.71	2.83	2.31
K2O	1.50	1.73	1.14	1.28	1.66	3.76	1.42	1.28	1.10
P2O5	0.13	0.15	0.09	0.05	0.39	0.23	0.10	0.10	1.68
Trace elements (ppm)									
Rb	55.9	56.3	35.6	32.2	51.5	97.1	41.9	37.0	40.4
Cs	1.49	1.96	1.10	1.40	1.63	0.84	1.02	0.79	0.55
Li	15.7	32.3	21.6	18.4	14.9	11.3	9.0	6.25	10.9
Sr	361	280	430	501	457	218	490	500	407
Ba	401	490	349	326	376	964	435	411	526
U	1.73	0.95	0.78	0.66	0.91	3.09	1.26	0.97	1.32
Th	7.16	6.17	4.22	3.40	4.50	17.0	5.77	4.33	6.11
Zr	52.6	96.1	51.0	56.6	92.5	267	161	84.7	122
Nb	4.79	8.45	5.06	4.09	9.88	16.5	5.33	5.38	7.50
Ta	1.94	1.01	1.28	1.22	1.55	2.46	1.17	1.3	1.00
Hf	1.66	2.69	1.39	1.53	2.28	6.93	4.08	2.28	3.05
Y	13.2	16.3	10.1	8.74	16.8	31.4	11.6	13.1	25.6
Tl	0.34	0.39	0.22	0.22	0.31	0.39	0.24	0.21	0.21
La	27.2	27.1	18.5	14.5	28.0	61.3	22.1	20.1	38.7
Ce	53.7	56.1	37.0	28.5	58.8	122	44.4	40.6	84.6
Pr	5.93	6.48	4.11	3.15	6.95	14.0	4.90	4.61	10.4
Nd	21.9	24.3	15.2	12.0	28.0	51.5	18.1	18.0	42.7
Sm	3.69	4.62	2.80	2.25	5.15	9.18	3.30	3.38	8.16
Eu	1.08	1.11	0.98	0.97	1.25	1.84	1.15	1.22	2.11
Tb	0.40	0.51	0.32	0.27	0.53	0.99	0.34	0.43	0.89
Dy	2.63	3.12	1.87	1.64	3.26	6.02	2.26	2.53	5.18
Ho	0.53	0.65	0.39	0.33	0.64	1.18	0.45	0.49	1.01
Er	1.53	1.85	1.23	1.06	1.73	3.39	1.28	1.43	2.59
Tm	0.21	0.27	0.16	0.15	0.24	0.49	0.19	0.20	0.36
Yb	1.45	1.81	1.12	0.99	1.49	3.21	1.37	1.51	2.13
Lu	0.22	0.27	0.18	0.15	0.22	0.48	0.22	0.23	0.32
V	72	201	100	262	477	38	90	135	668
Cr	388	4078	394	211	157	0	32	9	0
Ni	53	744	73	39	23	0	0	0	0
Cu	44	663	50	40	47	9	14	14	24
Zn	52	127	67	49	62	62	59	54	81
Pb	11.8	11.2	10.8	6.1	5.47	10.3	7.7	7.9	6.3
Sc	16	21	19	22	12	13	18	18	29
Ga	21	16	19	20	20	17	22	21	23
Bi	0.16	0.30	0.082	0.032	0.061	0.097	0.018	0.028	0.02
Element ratios									
(La/Lu)n	12.9	10.6	10.5	10.2	13	13.2	10.5	9.3	12.4
Eu*	0.96	0.79	1.14	1.39	0.80	0.66	1.15	1.15	0.85

Eu* Chondrite normalized Eu value/mean of chondrite normalized Sm and Gd values.
Chondrite normalized Gd value is interpolated from chondrite normalized Sm and Tb values.

Table 6.1 Major and trace element compositions of Sudbury Igneous Complex (continued)

Elements	91ZC10	91ZC11	91ZC12	91ZC13	91ZC14	DNC-1a	MRG-1a	DNC-1b	MRG-1b
SiO2	64.7	66.8	62.1	64.3	54.3	44.3		47.0	
TiO2	0.48	0.59	0.67	0.74	0.46	0.43		0.48	
Al2O3	11.2	12.4	12.8	11.9	8.93	18.1		18.3	
FeO	7.0	6.3	7.8	7.2	10.8	10.0		9.9	
MnO	0.11	0.09	0.09	0.09	0.28	0.15		0.15	
MgO	0.80	1.32	2.39	1.64	6.9	10.1		10.1	
CaO	1.77	1.78	3.10	2.73	4.45	11.2		11.3	
Na2O	3.5	3.46	3.7	3.25	2.68	2.18		1.87	
K2O	3.86	3.78	3.36	3.71	2.05	0.27		0.23	
P2O5	0.11	0.16	0.28	0.38	0.13	0.08		0.08	
Trace elements (ppm)									
Rb	108	113	121	129	64.6	3.8	7.7	4.5	8.5
Cs	0.56	0.49	0.52	0.45	0.25	0.21	0.59	0.34	0.57
Li	6.7	8.5	12.1	7.5	8.5	4.29	3.32	0.51	4.2
Sr	161	171	232	209	90.6	143	271	145	268
Ba	1085	1126	908	707	675	102	49.5	114	61
U	3.48	3.44	2.66	2.91	4.12	0.047	0.25	0.10	0.24
Th	17.7	15.9	12.4	13.4	7.6	0.24	0.83	0.20	0.93
Zr	328	292	243	256	127	34.2	93	41	108
Nb	15.3	15.0	13.0	16.1	9.2	1.67	21.6	3.0	19.2
Ta	2.39	2.66	2.11	2.42	1.15	0.14	0.84	0.10	0.8
Hf	8.32	8.13	6.33	6.83	3.45	0.97	3.81	1.0	3.86
Y	35.1	29.6	27.4	31.4	14.8	15.3	11.5	18	14.0
Tl	0.48	0.56	0.55	0.58	0.40	0.029	0.053	0.026	0.055
La	66.6	55.6	50.9	57.6	13.8	3.59	9.19	3.8	9.8
Ce	134	113	103	119	28.6	8.3	26.1	10.6	26
Pr	15.2	12.8	11.6	13.5	3.32	1.08	3.81	1.3	3.4
Nd	56.2	47.1	43.2	51.5	13.5	5.12	18.9	4.9	19.2
Sm	10.1	8.5	7.68	8.9	3.33	1.45	4.66	1.38	4.5
Eu	1.79	1.94	1.83	1.96	0.99	0.62	1.44	0.59	1.39
Tb	1.09	1.13	0.99	1.18	0.51	0.39	0.62	0.41	0.51
Dy	6.80	5.81	5.63	6.02	2.87	2.72	3.13	2.7	2.9
Ho	1.32	1.15	1.05	1.18	0.57	0.59	0.52	0.62	0.49
Er	3.88	3.55	2.99	3.37	1.62	1.91	1.27	2	1.12
Tm	0.55	0.48	0.42	0.48	0.24	0.28	0.15	0.1	0.11
Yb	3.61	3.35	2.88	3.32	1.56	1.97	0.91	2	0.6
Lu	0.54	0.50	0.45	0.49	0.24	0.32	0.14	0.32	0.12
V	0	11	149	94	154	143		148	
Cr	0	0	0	0	106	293		285	
Ni	0	79	0	0	51	256		247	
Cu	5	20	9	14	40	87.4		96	
Zn	62	79	41	28	45	69.2		66	
Pb	7.5	29.7	10.8	8.3	28.5	5.94	6.0	5.9	10
Sc	15	8	19	18	14				
Ga	16	16	17	17	14				
Bi	0.065	0.14	0.033	0.053	0.12	0.014	0.14	0.014	0
Element ratios									
(La/Lu)n	12.9	11.5	11.8	12.2	6.05	1.16	6.81	1.23	8.48
Eu*	0.58	0.72	0.76	0.69	0.91	1.06	0.91	1.08	0.98

+ These samples were analyzed in 1991, and the BaF interference on Gd was not corrected at that time, so Gd is not reported here.

DNC-1: USGS reference material MRG-1:CCRMP reference material

a: this work b: literature values (Govindaraju, 1989)

6.3.3.3 TRACE-ELEMENT RESULTS

The variation of selected trace elements are presented in Harker diagrams in Figure 6.7. The norite and granophyre samples plot as end members for most of the trace elements in the diagrams, whereas gabbro samples lie between the two end members, though closer to the norite end member.

Chondrite normalized REE patterns for the norite, gabbro, and granophyre are shown in Figure 6.8. All of the igneous rocks of the Complex are characterized by light REE-enriched patterns with $(La/Lu)_N$ (chondrite normalized La/chondrite normalized Lu) ratios in the range of 9.3 to 13, and by flat heavy REE patterns. The Eu anomalies are distinctively different among the norite, gabbro, and granophyre samples. The border norite samples show negligible Eu anomalies (Figure 6.8a), whereas the other norite samples show positive Eu anomalies (Figure 6.8b). The gabbro samples show insignificant Eu anomalies (Figure 6.8c), whereas the granophyres show negative anomalies. Kuo and Crocket (1979) reported similar results in their study (Figure 6.8d). One sample from the Onaping Formation shows a slight light REE enrichment with no Eu anomaly (Figure 6.8e).

6.3.4 PETROGENESIS OF SUDBURY IGNEOUS COMPLEX

Kuo and Crocket (1979) concluded that the igneous units of the SIC are genetically related to each other by crystallization processes based on rare earth

element data. Their data showed that norite and granophyre are characterized by positive and negative Eu anomalies, respectively, whereas border norites and oxide-rich gabbro lack prominent Eu anomalies. They considered the border norites of the SIC to have crystallized as a relatively closed system and their REE fractionation patterns are regarded as representative of the parental magma. They concluded that the norite and granophyre are comagmatic, and related by gravitational fractionation due to the mirror-image Eu anomaly characteristics of the two. Compared to other continental basic rocks, the SIC has more fractionated REE patterns and generally higher total rare earth element contents. They suggested that mixing of a silicic component with a high La/Lu ratio with a normal basaltic melt may be responsible for the distinctive REE characteristics of the SIC magma.

Naldrett *et al.* (1985) studied the major trace element, and isotopic composition of the SIC rocks; and concluded that the main mass of the SIC was contaminated largely by typical upper crust rocks. They further suggested that extensive assimilation of silicic material was responsible for the segregation of major quantities of sulphide.

Data in this study generally supports the conclusion that the SIC was strongly contaminated by upper crustal rocks (Naldrett *et al.*, 1984) and that granophyre, gabbro, and norite are related to each other by fractional crystallization processes (Kuo and Crocket, 1979). The SIC has high SiO_2

contents and is rich in incompatible elements indicative of extensive contamination. The data is broadly consistent with binary mixing, but there are only 13 analyses for a very large igneous complex, and therefore the data by itself does not uniquely characterized the complex. Major- and trace- element Harker diagrams (Figure 6.7) generally suggest a mixing relationship between two end members. One of the end members is characterized by low SiO_2, such as a basaltic component, and the other by high SiO_2, such as continent crust. On primitive mantle normalized diagrams of trace elements, except for Sr, Eu, and Ti, the norite, gabbro, and granophyre have similar patterns with a strong depletion of Nb (Figure 6.9). Strongly negative Nb anomalies can be explained either as a magma generated by subduction processes (Nakamura *et al.*, 1985) or a magma contaminated by continent crust (Naldrett *et al.* 1984). The latter seems more favourable for the SIC due to its tectonic setting. Initial epsilon neodymium values (ϵNd) for 15 whole rocks, ranging from -6.84 to -8.83 (Faggart *et al.*, 1985), which are similar to those for average upper continental crust, falling on the crustal trend of neodymium isotopic evolution as defined by shales, also support a contamination model with continental crust. Strong depletions in Sr, Eu and Ti in granophyre samples (Figure 6.9c) could be the result of fractional crystallization processes with removal of Sr and Eu in plagioclase and Ti in magnetite.

6.4 CU-NI-(PGE) MINERAL DEPOSITS AT SUDBURY

6.4.1 MINERAL DEPOSIT TYPES

The Ni-Cu-(PGE) ores of the Sudbury district are divided by Naldrett (1981) into three categories: typical South Range deposits, typical North Range deposits, and offset deposits. The North Range deposits occur not only within the Sublayer norite but also within brecciated country rocks and fractures in country rock underlying the breccia, whereas South Range deposits occur only within the Sublayer. However, as mining exploration developed deeper levels, new deposits in the South Range, *i.e.*, Thayer Lindsley mine, show similar features to those in the North Range (Binney *et al.*, 1992). Therefore the classification by Naldrett (1981) has only limited geographic meaning. Detailed descriptions of many of the deposits have been documented by Souch *et al.* (1969), Naldrett and Kullerud (1967), Cowan (1968), Pattison (1979), and Binney *et al.* (1992). Only very brief descriptions are presented here.

6.4.1.1 NORTH RANGE DEPOSITS

The Strathcona Mine, is considered to be typical of the North Range deposits (Naldrett, 1981), and as such, was part of this study. The mine is the most studied of the North Range deposits. Detailed descriptions of the deposit are given in Chapter 7. The deposit is divided into five principal mineralization

zones: the Hanging Wall Ore Zone, the Main Ore Zone, the Deep Ore Zone, the Copper Ore Zone, and the Deep Copper Zone (Figure 6.10). The Hanging Wall Ore Zone is mainly pyrrhotite and pentlandite, which occupy interstitial volumes between silicates. Most of the Strathcona mineralization is present in the Main Ore Zone, which occurs in the footwall breccia between the norite and the underlying gneiss complex. The Deep Ore Zone was emplaced in fractures in the footwall gneiss as much as 90 m below the base of the SIC. The Copper-Zone ores occur as a complex system of fracture filling veins up to 6 m wide in footwall rocks 200-300 m beneath the base of the SIC. The chalcopyrite veins are hosted completely by the footwall gneiss complex. The Deep Copper Zone occurs in footwall rocks 450-600 m beneath the norite contact where the predominant hosting rocks are gneissic units of the footwall complex. The Deep Copper Zone ores are composed of highly irregular massive sulphide veins.

6.4.1.2 SOUTH RANGE DEPOSITS

The Little Stobie 1, Thayer Lindsley, and Murray mines are typical examples of South Range deposits. The Thayer Linsley Mine, part of this study, is discussed in more detail in Chapter 8. The South Range deposits are generally zoned from massive ore at the footwall to disseminated sulphide ore toward the Hanging Wall. The massive ore rests directly on the foot-wall rocks and

contains inclusions of the footwall material as well as fragments of gabbro and peridotite (Figure 6.11). The disseminated ores are hosted by the Sublayer norite which is in sharp contact with the overlying quartz norite.

6.4.1.3 OFFSET DEPOSITS

The offset deposits occur in dike-like offsets of the Sublayer norite and gabbro that extend several kilometres away from the SIC into the footwall. In many cases the sulphides form lens-like pods of massive and interstitial disseminated ore associated with high proportions of inclusions in the offset dikes.

6.4.2 CHEMICAL COMPOSITIONS AND MINERALOGY OF THE SUDBURY ORES

6.4.2.1 CHEMICAL COMPOSITION OF THE ORES

Early work on the composition of the Sudbury ore was summarized by Hawley (1962). This was followed by Naldrett and Kullerud (1967), Cowan (1968), and Naldrett (1984). The concentrations and distributions of precious metals were studied by Keays and Crocket (1970), Chyi and Crocket (1976), Hoffman *et al.* (1979), and Naldrett (1984).

Iron, S, Cu, and Ni are the major elements of the ores. Naldrett (1969)

noted, considering Fe, S, and O alone, that the composition of most magmatic sulphides fall in the pyrrhotite field of the Fe-S-O system. Most Ni is present in the ores as pentlandite, although up to 1 wt% remains in solid solution in pyrrhotite (Naldrett, 1984). Bulk Ni content varies from a low of 3.63 wt% at the Strathcona Mine to a high of 5.73 wt% at the Levack West Mine (Naldrett, 1984). Copper is present largely as chalcopyrite. Bulk copper ranges from a low of 1.23 wt% to a high of 2.8 wt%.

Cobalt, Zn, Pb, As, Sb, and Se are some of the more abundant trace constituents of the Sudbury ores. Pentlandite is the host for the bulk of the cobalt in the Sudbury ores. Cobalt content varies from a low of 0.065% to a high of 0.22 wt% in the ores. Zinc is mostly present in sphalerite. Zinc concentrations range from a mean of about 100 ppm in the South Range to a mean of about 230 ppm in the North Range. Lead concentrations in the ores range from a mean of 15 ppm in the South Range to a mean 30 ppm in the North Range. Galena is the major discrete phase of Pb. Arsenic and Sb contents vary from deposit to deposit. Selenium concentrations are about 90 ppm in the ore.

Data from the Strathcona and Levack West deposits show strong zoning of platinum-group elements, Au, and base metals (Naldrett, 1982). Copper, Ni, Zn, Pt, Pd, and Au increase away from the SIC hanging wall into the footwall and Co, Rh, Ru, Ir, and Os increase in the reverse direction. At Strathcona, this

zoning results in a decrease of the (Pt + Pd)/(Ru + Ir + Os) ratio from 132 in the footwall to 2.2 in the Hanging Wall Ore Zone (Naldrett, 1982).

6.4.2.2 ORE MINERALOGY

The mineralogy of the Sudbury ores has been documented by Hawley and Stanton (1962), and subsequently by Naldrett (1984). Hawley and Stanton (1962) reported 32 metallic minerals. The most detailed studies of the platinum-group minerals were reported by Cabri and Laflamme (1976). Later Li and Naldrett (1993) confirmed some of the findings from the Deep Copper Zone at the Strathcona Mine.

The minerals pyrrhotite ($Fe_{1-x}S$), pentlandite $(Fe,Ni)_9S_8$, chalcopyrite $(Cu,Fe)S_2$, cubanite ($CuFe_2S_3$), and magnetite (Fe_3O_4) account for most of the metallic phases in the Sudbury ores. Pyrrhotite is the principal host for the other sulphide minerals in the contact deposits. Pentlandite occurs as exsolution rims around pyrrhotite grains or as exsolution flame-like lamellae within pyrrhotite grains. Chalcopyrite is ubiquitous and accounts for the major part of the Cu in the Sudbury area. Cubanite occurs in many deposits associated with chalcopyrite, but is particularly concentrated in the Copper Zone and Deep Copper Zone at the Strathcona deposit. Magnetite is a very common mineral, usually present as euhedral or semi-euhedral crystals, and it accounts for about 5 to 10% of the bulk ores.

Pyrite (FeS_2), galena (PbS), sphalerite (ZnS), millerite (NiS), niccolite (NiAs), gersdorffite (NiAsS), cobaltite (CoAsS), marcasite (FeS_2), stannite (SnS_2), bornite (Cu_5FeS_4), and violarite ($FeNi_2S_4$) occur as minor ore minerals.

Michenerite (PdBiTe), moncheite ($PtTe_2$), sperrylite ($PtAs_2$), insizwaite ($PtBi_2$), sudburite (PtSb), froodite ($PdBi_2$), kotulskite (PdTe), niggliite (PtSn), merenskeyite ($PdTe_2$), mertieite [$Pd_8(Sb,As)_3$], palladian melonite [$(Ni,Pd)(Te,Bi)_2$] and gold (Au) are the major precious metal minerals found in Sudbury ores.

6.5 RELATIONSHIP OF ORE DEPOSITS TO THE SUDBURY IGNEOUS COMPLEX

Although there is considerable variation in the characteristics of different ore deposits (Pye *et al.*, 1984), as has been summarized by Naldrett *et al.*, 1985), there are a number of features in common:

(1) There are embayments or other irregularities of ore bodies at the base of SIC or penetrating into the footwall (Figures 6.10 and 6.11). An increase in sulphide content is usually observed at the lower contact throughout the SIC.

(2) The presence of Sublayer rocks. The sulphides constituting the ore bodies appear to have settled out of bodies of Sublayer. Minor amounts

(up to 5%) of sulphide also occur within border norite of the SIC. The ore deposits are invariably associated with Sublayer.

(3) Ultramafic inclusions within Sublayer. Scribbins *et al.* (1984) concluded these inclusions were derived from one or more hidden layered intrusions.

All of these characteristics indicate that ore deposits at Sudbury are genetically related to the SIC. Osmium isotope results, (Walker *et al.*, 1991; and Dickin *et al.*, 1992) from the sulphide ores of several mines at Sudbury, strongly overlap the initial ratios, suggesting a narrow range of isotope ratios in the original ore, within the range of estimated osmium isotope compositions in the country rock of the SIC at 1.85 Ga. Naldrett and Evensen (1985) suggest that the extensive assimilation of sialic material is believed to be responsible for the segregation of major quantities of sulphide, since assimilation of SiO_2-rich material by a mafic magma could lower the solubility of sulphur within it (Irvine, 1975).

6.6 SUMMARY

In this chapter, the general geological setting of the Sudbury area was documented; the geology and geochemistry of the Sudbury Igneous Complex (SIC) were briefly discussed, and the types of Cu-Ni-(PGE) deposits and their

setting, mineralogy, and metal distributions were summarized. Data in this study generally supports suggestions that the SIC was strongly contaminated by upper crustal rocks (Naldrett *et al.*, 1984); and that granophyre, gabbro, and norite are related to each other by fractional crystallization processes (Kuo and Crocket, 1979). The ore deposits at Sudbury are spatially and genetically related to the SIC. The extensive assimilation of sialic material is believed to be responsible for the segregation of major quantities of sulphide (Naldrett and Evensen, 1985). This information provides an important background for the studies of distributions and partitioning of precious metals to be discussed in Chapters 7, 8, and 9, and REE geochemistry of the sulphide ores to be discussed in Chapter 10.

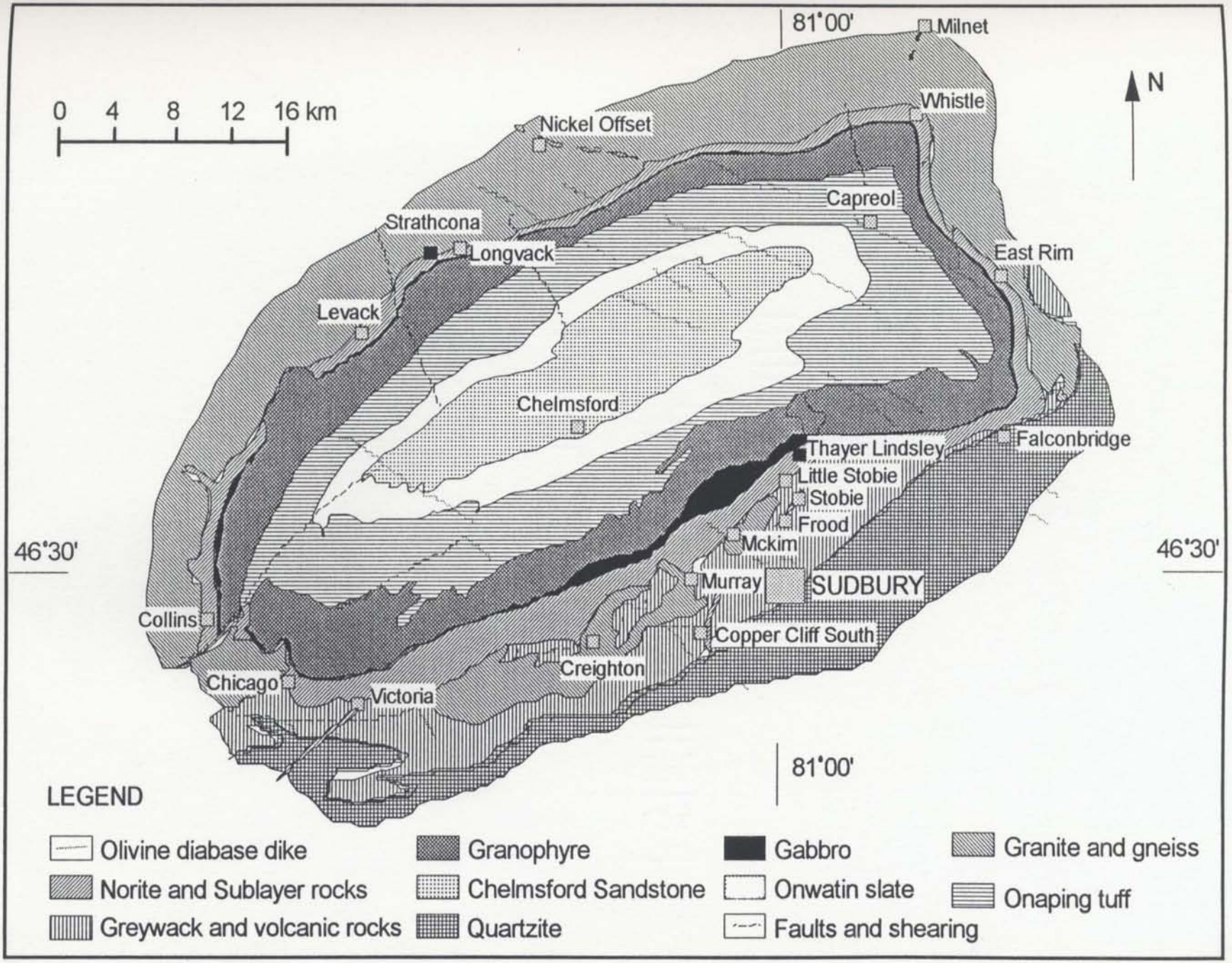

Figure 6.1 Geological map of the Sudbury area (drawn after Naldrett et al., 1982). The locations of various mine sites, including the Strathcona and Thayer Lindsley, are shown for reference.

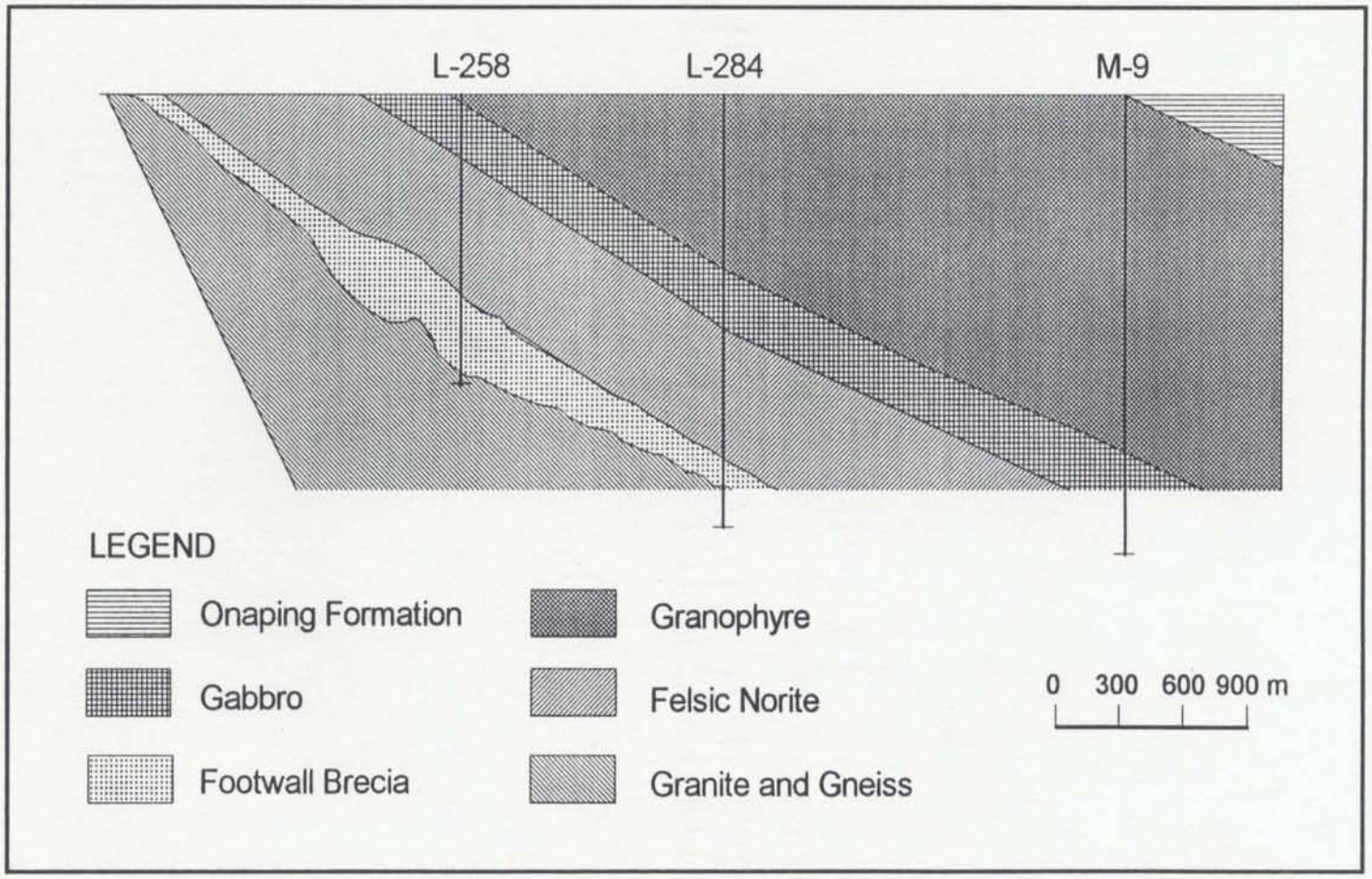

Figure 6.2 Vertical cross-section through the Sudbury Igneous Complex at Strathcona Mine (drawn after Naldrett and Hewins, 1984). The stratigraphy was constrained by drill cores.

Figure 6.3 Photomicrographs illustrating petrographic textures in the Sudbury Igneous Complex (SIC).

(a) South Range norite (PPL). Orthopyroxene grains are euhedral or semi-euhedral (91-ZC-01).

(b) Sample a in XPL.

(c) Amphibole reaction rims (PPL) (91-ZC-01). Orthopyroxene in the South Range norite is replaced by amphibole around the edges.

(d) Altered norite (PPL). Orthopyroxene grains in the South Range norite are entirely replaced by amphibole, biotite and chlorite (91-ZC-09).

(e) Sample d in XPL.

(f) Quartz gabbro (PPL) (91-ZC-09).

(g) Sample f in XPL.

(h) and (i) Granophyres in the north range showing myrmekitic texture (91-ZC-10 and 91-ZC-13)

a

1 mm

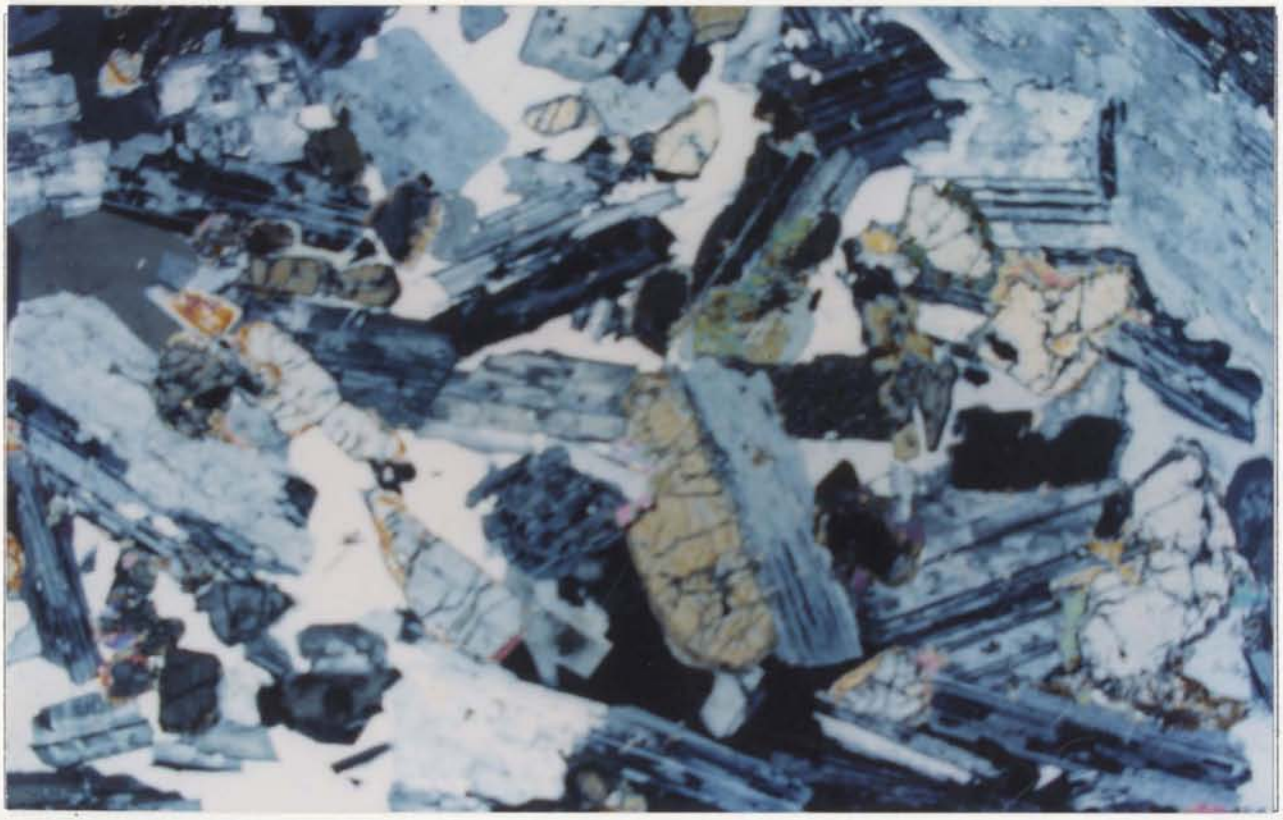

b

1 mm

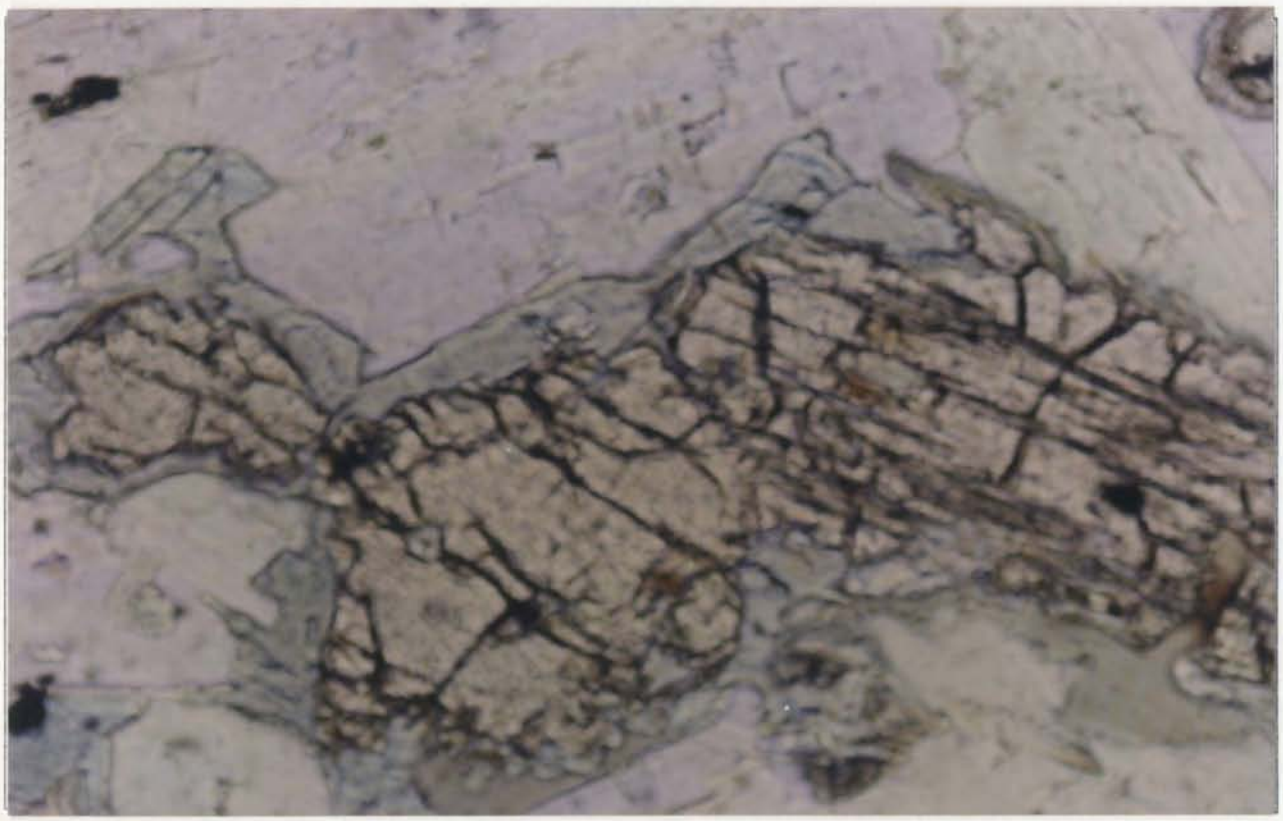

c

0.25 mm

d

1.67 mm

e

1.67 mm

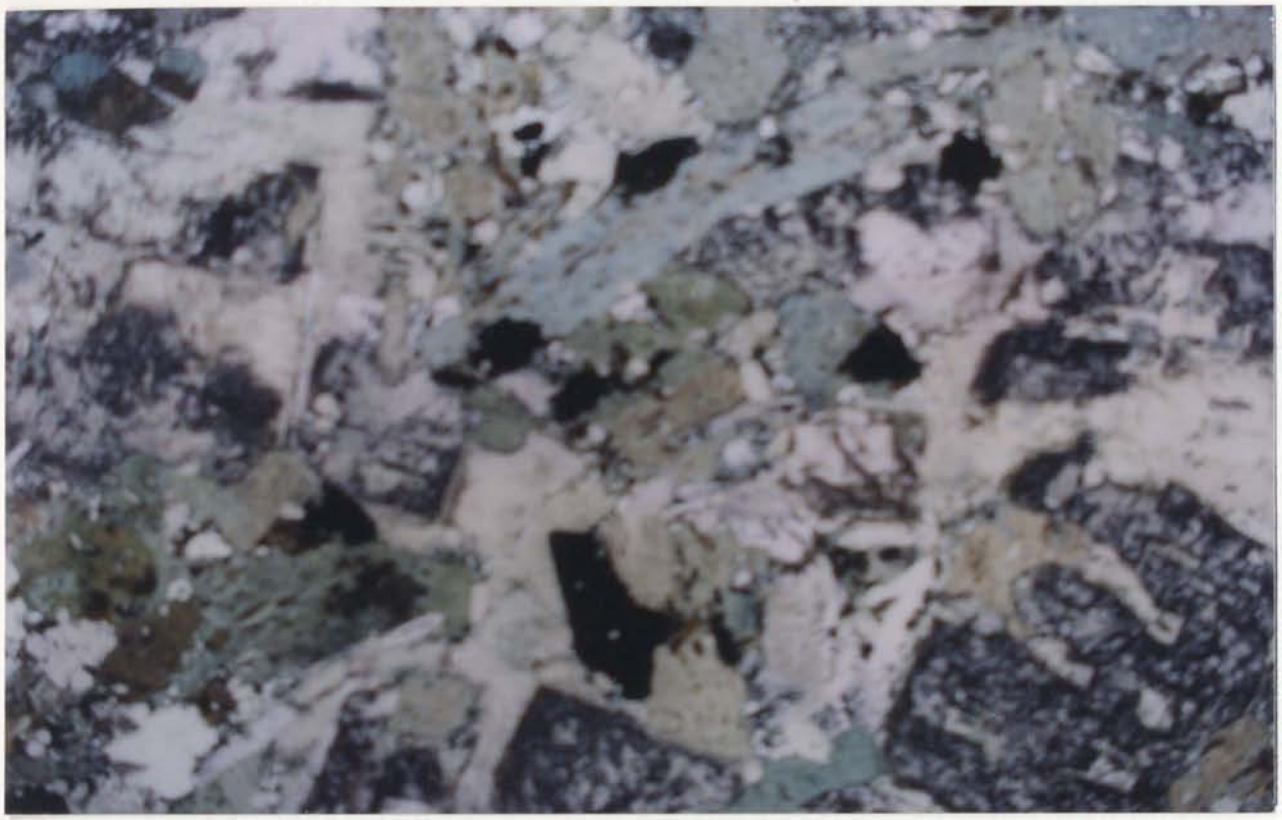

f

1 mm

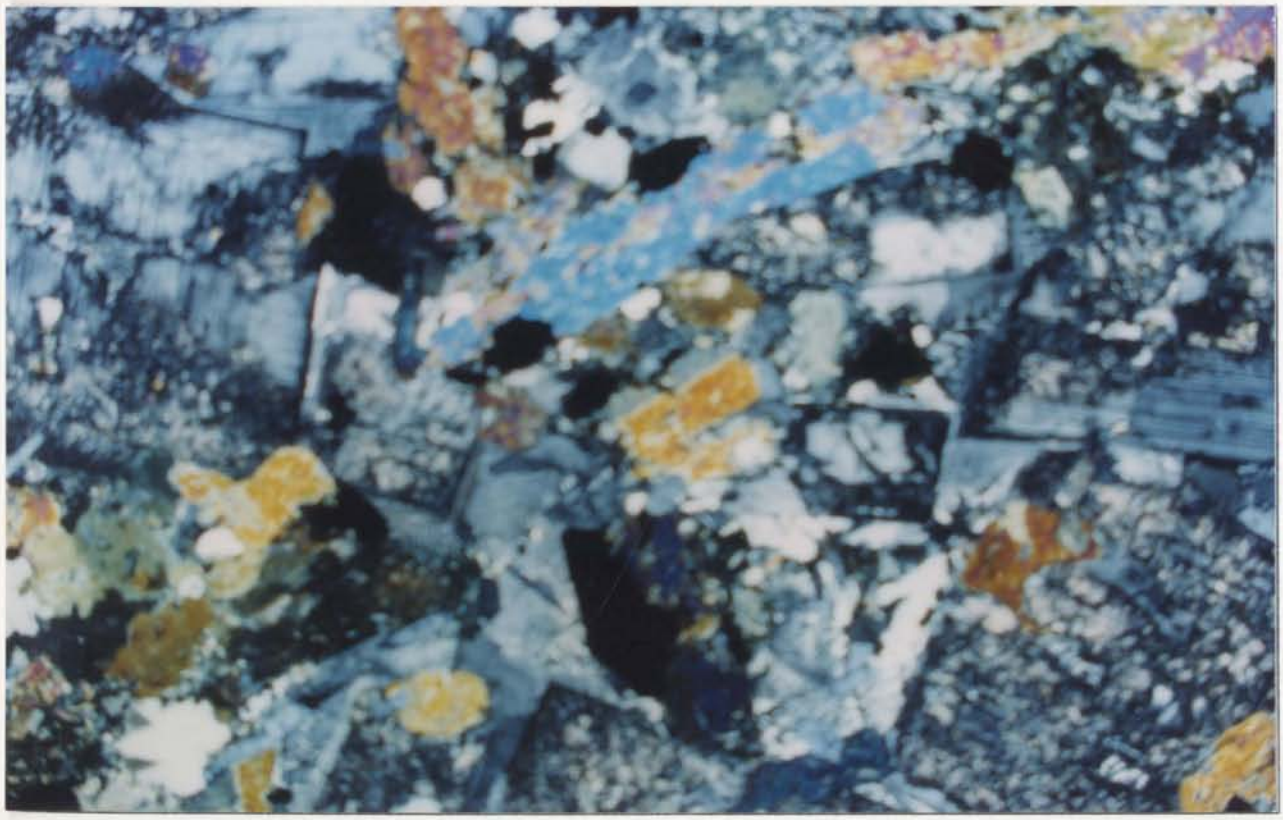

g

1 mm

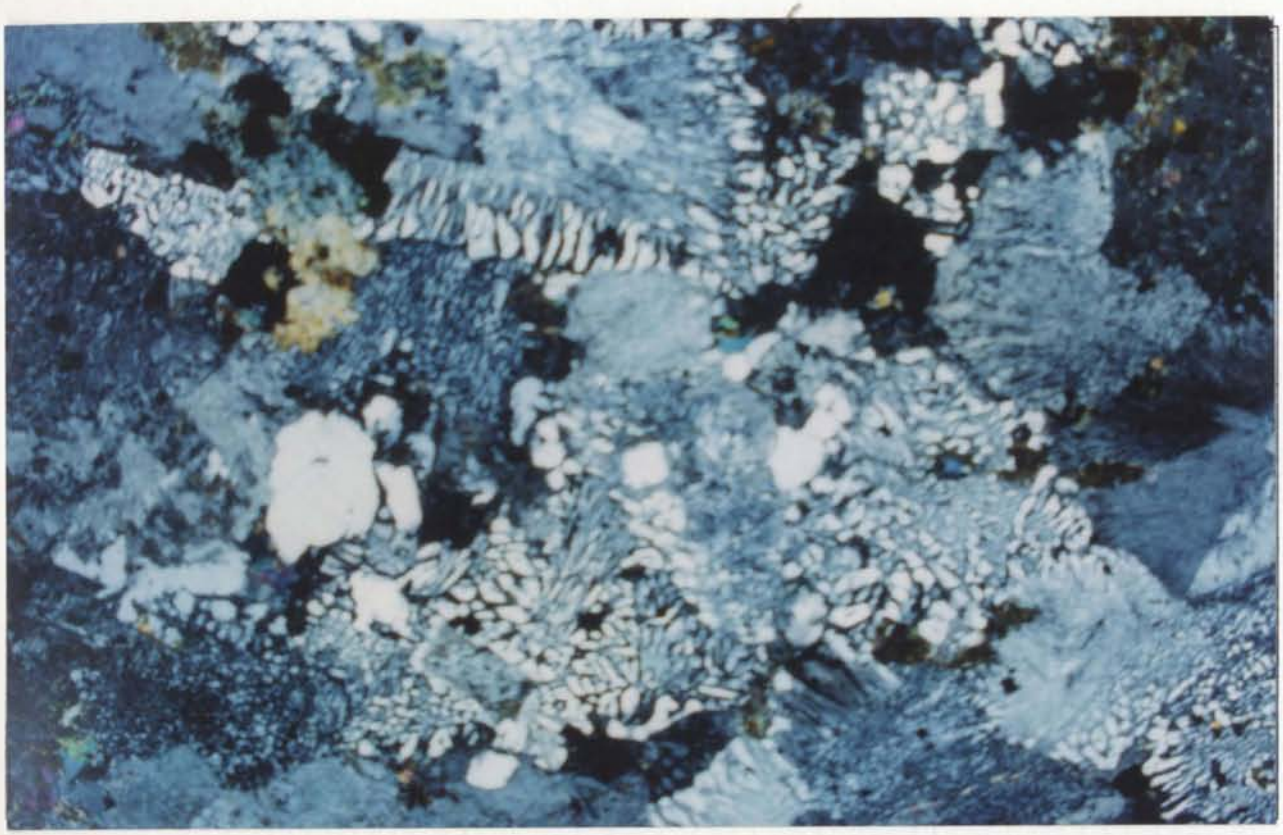

160

h

1 mm

i

1 mm

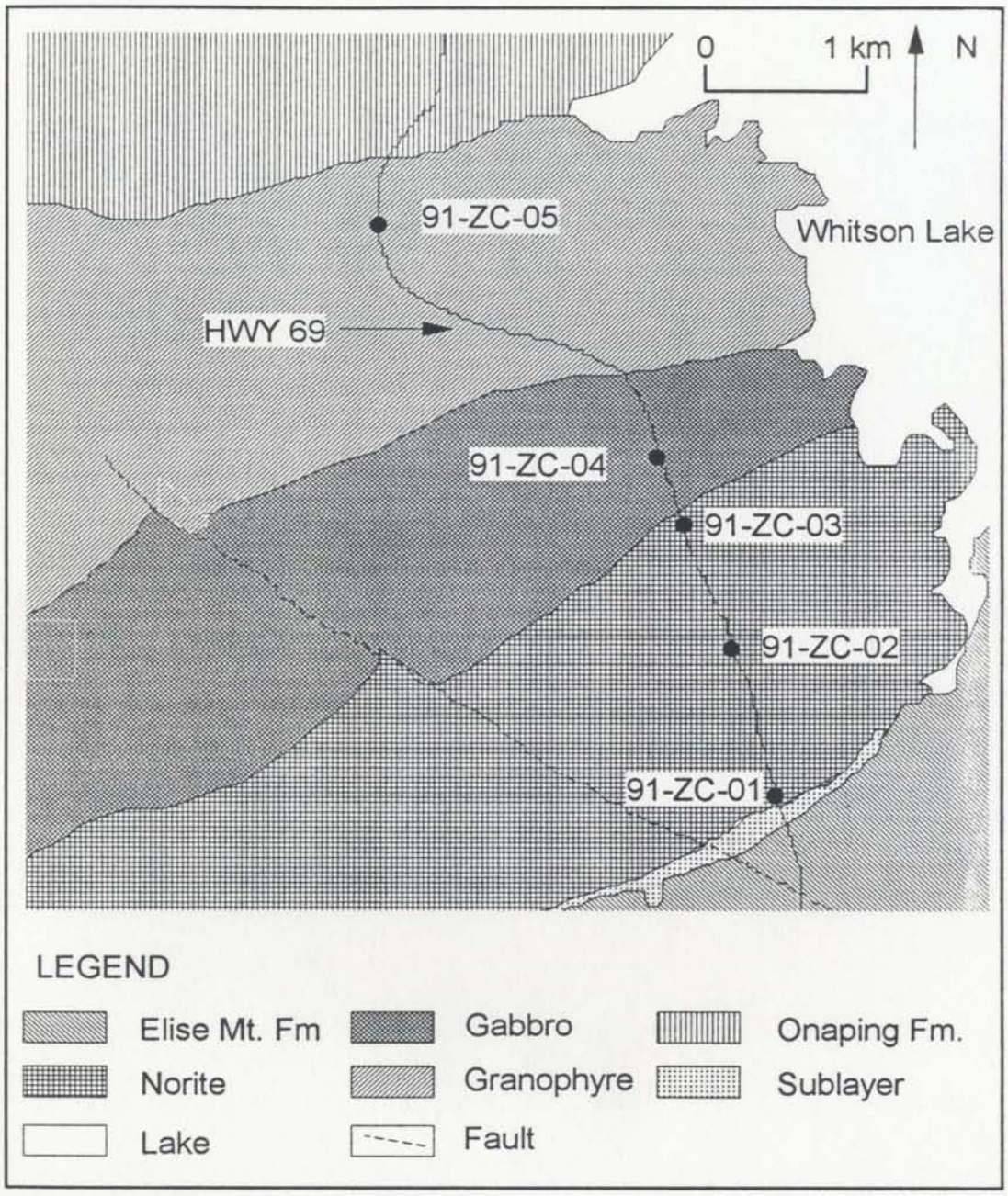

Figure 6.4 Locations of samples from the Sudbury Igneous Complex collected from the South Range along Highway 69 (drawn after Pye et al., 1984)

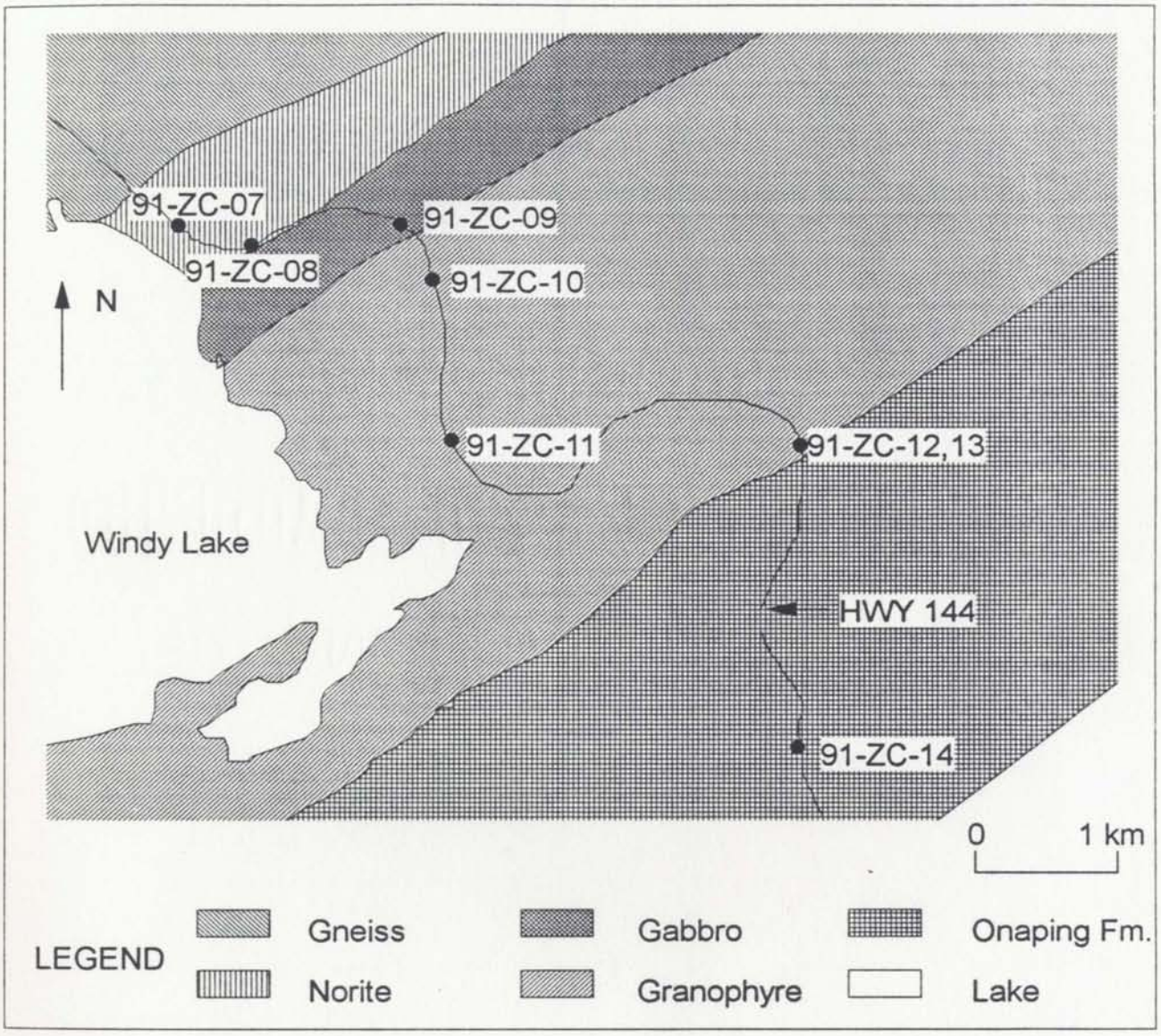

Figure 6.5 Locations of Samples from the Sudbury Igneous Complex collected from the North Range along Highway 144 (drawn after Pye et al., 1984)

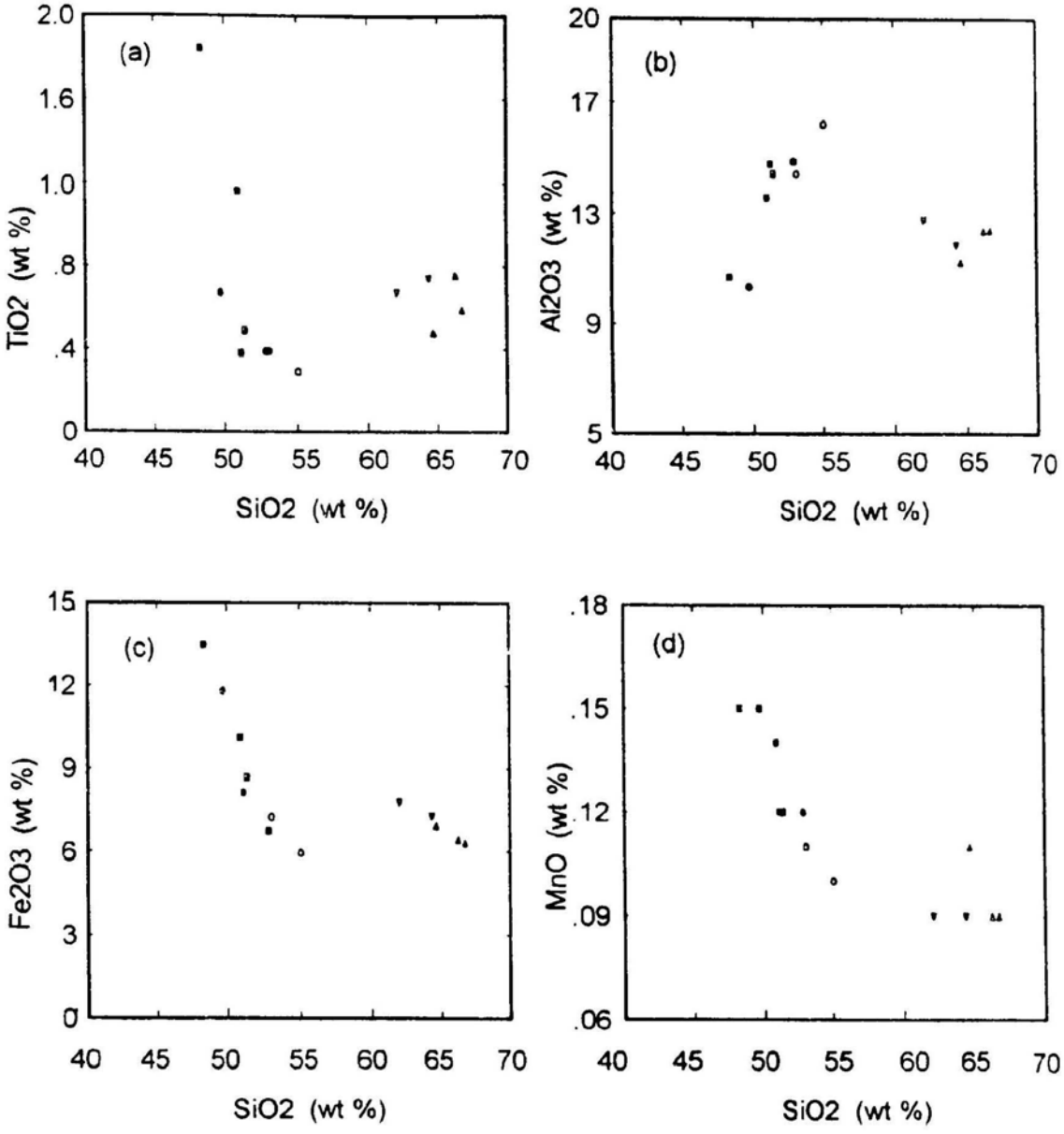
(a)
TiO2 (wt %)
2.0
1.6
1.0
.8
.4
0
40 45 50 55 60 65 70
SiO2 (wt %)
(b)
Al2O3 (wt %)
20
17
13
9
5
40 45 50 55 60 65 70
SiO2 (wt %)
(c)
Fe2O3 (wt %)
15
12
9
6
3
0
40 45 50 55 60 65 70
SiO2 (wt %)
(d)
MnO (wt %)
.18
.15
.12
.09
.06
40 45 50 55 60 65 70
SiO2 (wt %)

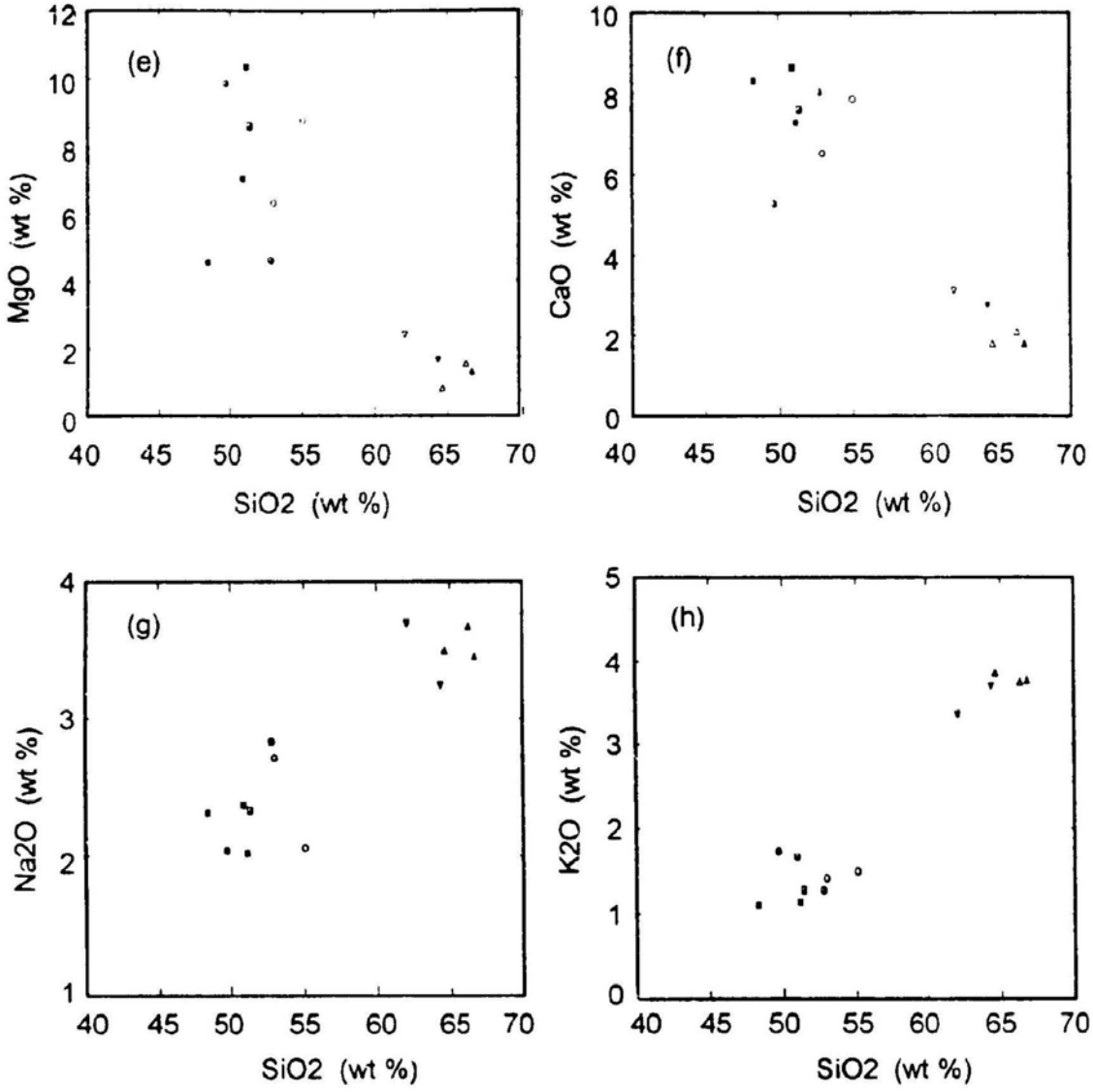

Figure 6.6 Major element Harker variation diagrams: (a) TiO2, (b) Al2O3, (c) Fe2O3, (d) MnO, (e) MgO, (f) CaO, (g) Na2O, and (h) K2O ▪ & • Norite, ◦ & • Gabbro, and • & ▲ Granophyre. Whether patterns are filled or not is insignificant

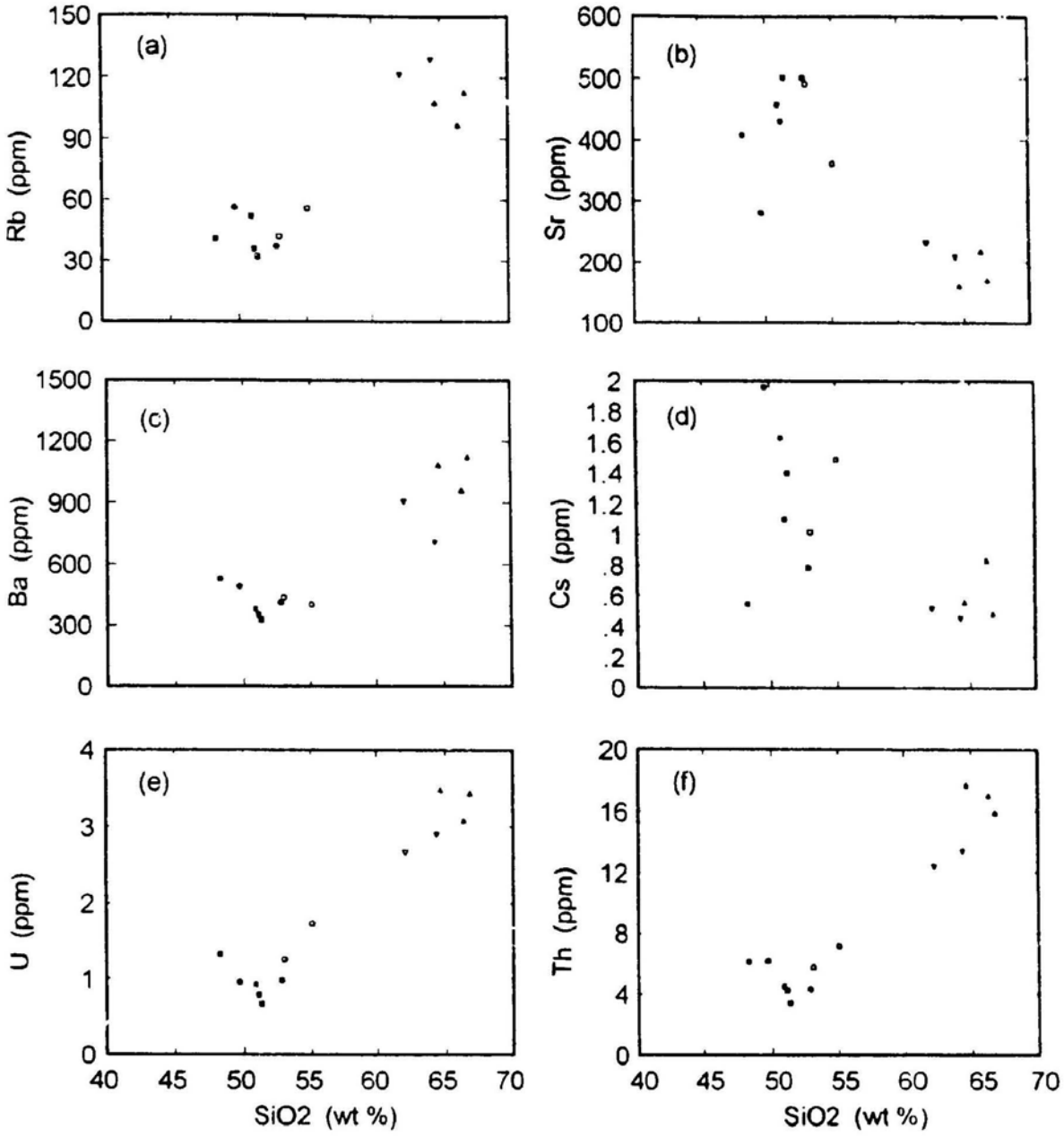
(a)
Rb (ppm)
150
120
90
60
30
0
(b)
Sr (ppm)
600
500
400
300
200
100
(c)
Ba (ppm)
1500
1200
900
600
300
0
(d)
Cs (ppm)
2
1.8
1.6
1.4
1.2
1
.8
.6
.4
.2
0
(e)
U (ppm)
4
3
2
1
0
40 45 50 55 60 65 70
SiO2 (wt %)
(f)
Th (ppm)
20
16
12
8
4
0
40 45 50 55 60 65 70
SiO2 (wt %)

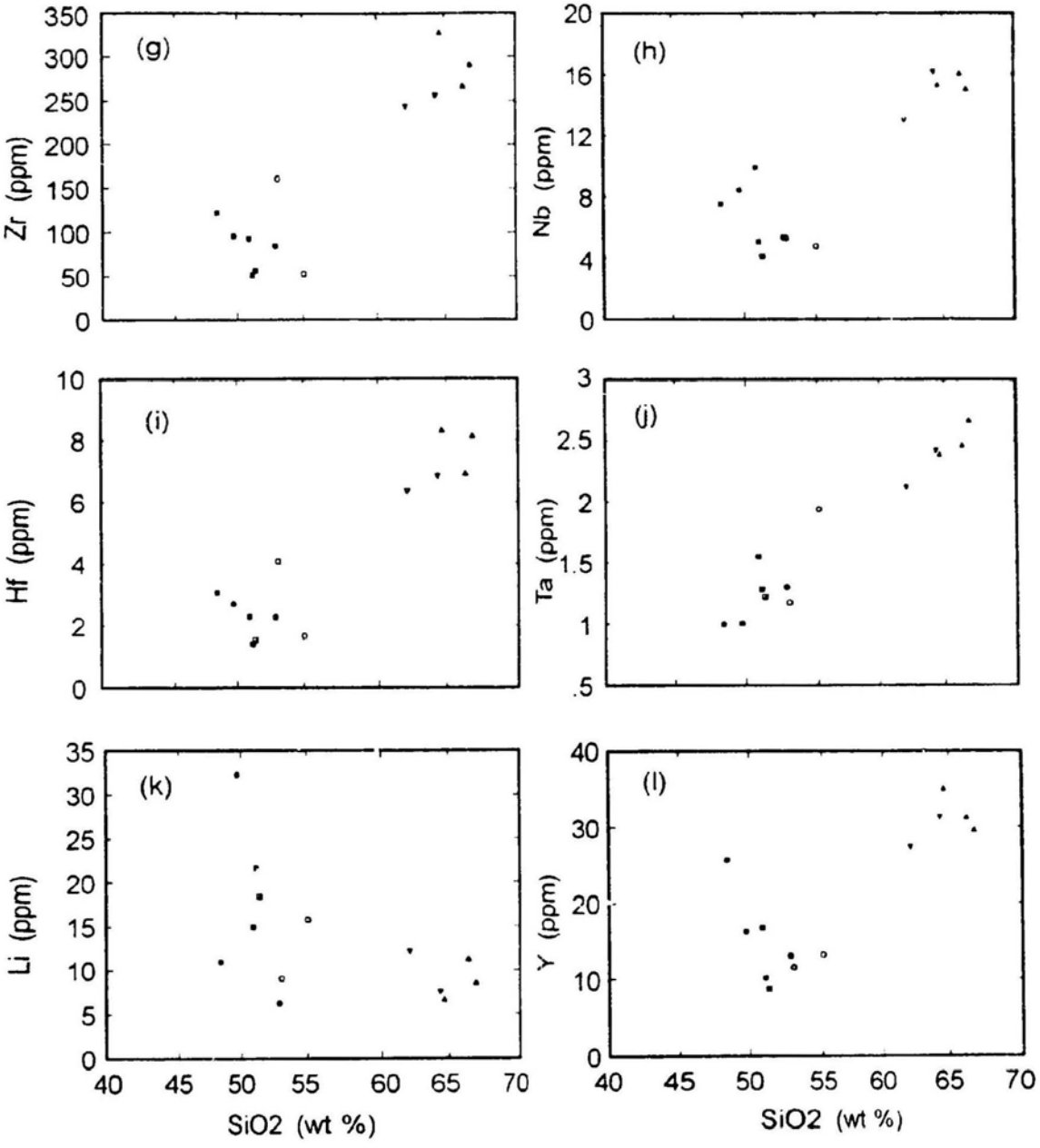
(g)
Zr (ppm)
350
300
250
200
150
100
50
0
(h)
Nb (ppm)
20
16
12
8
4
0
(i)
Hf (ppm)
10
8
6
4
2
0
(j)
Ta (ppm)
3
2.5
2
1.5
1
.5
(k)
Li (ppm)
35
30
25
20
15
10
5
0
(l)
Y (ppm)
40
30
20
10
0
40 45 50 55 60 65 70
SiO2 (wt %)
40 45 50 55 60 65 70
SiO2 (wt %)

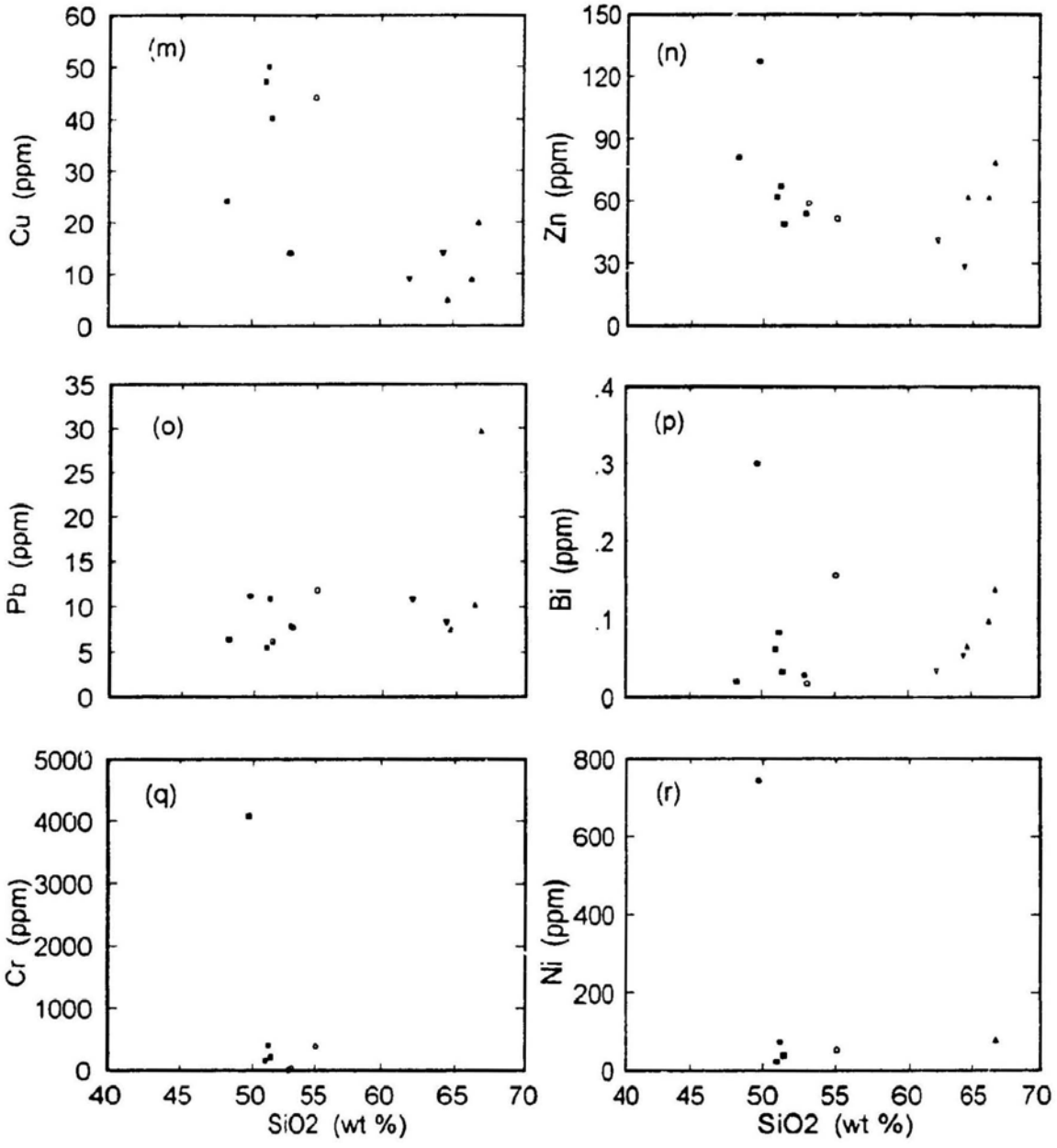
(m)
Cu (ppm)
(n)
Zn (ppm)
(o)
Pb (ppm)
(p)
Bi (ppm)
(q)
Cr (ppm)
(r)
Ni (ppm)
SiO2 (wt %)
SiO2 (wt %)

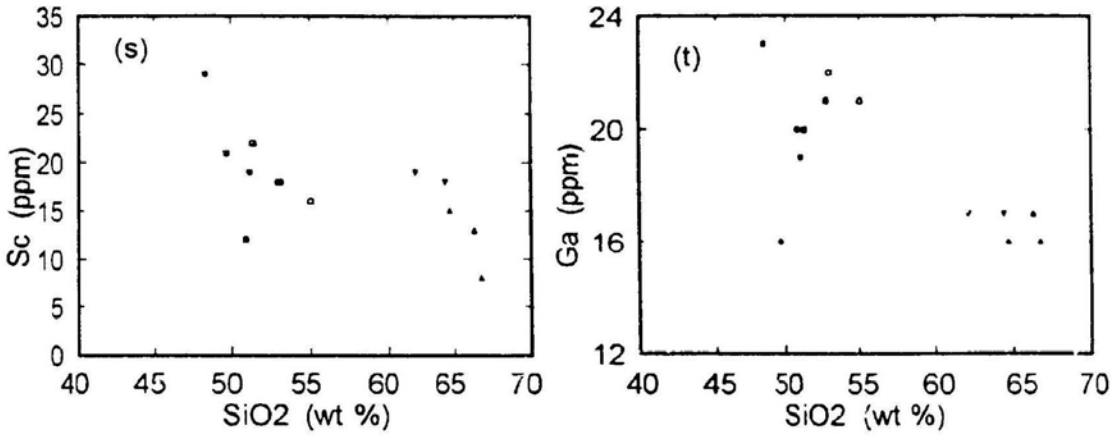

Figure 6.7 Trace element Harker variation diagrams: (a) Rb, (b) Sr, (c) Ba, (d) Cs, (e) U, (f) Th, (g) Zr, (h) Nb, (i) Hf, (j) Ta, (k) Li, (l) Y, (m) Cu, (n) Zn, (O) Pb, (p) Bi, (q) Cr, (r) Ni, (s) Sc, and (t) Ga. Symbols as in Figure 6.5

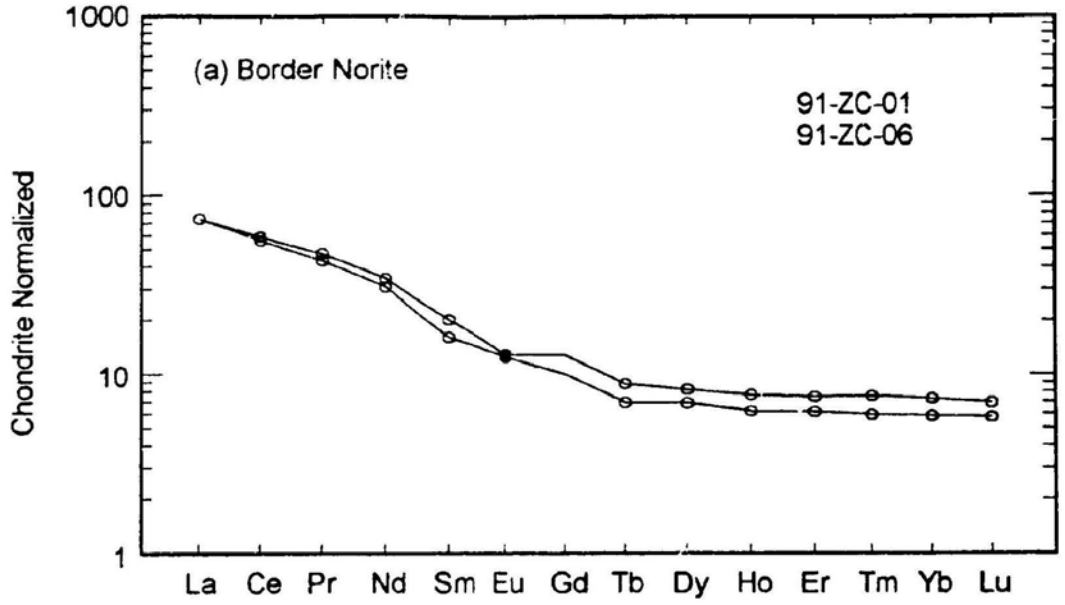
(a) Border Norite
91-ZC-01
91-ZC-06
Chondrite Normalized
1000
100
10
1
La Ce Pr Nd Sm Eu Gd Tb Dy Ho Er Tm Yb Lu

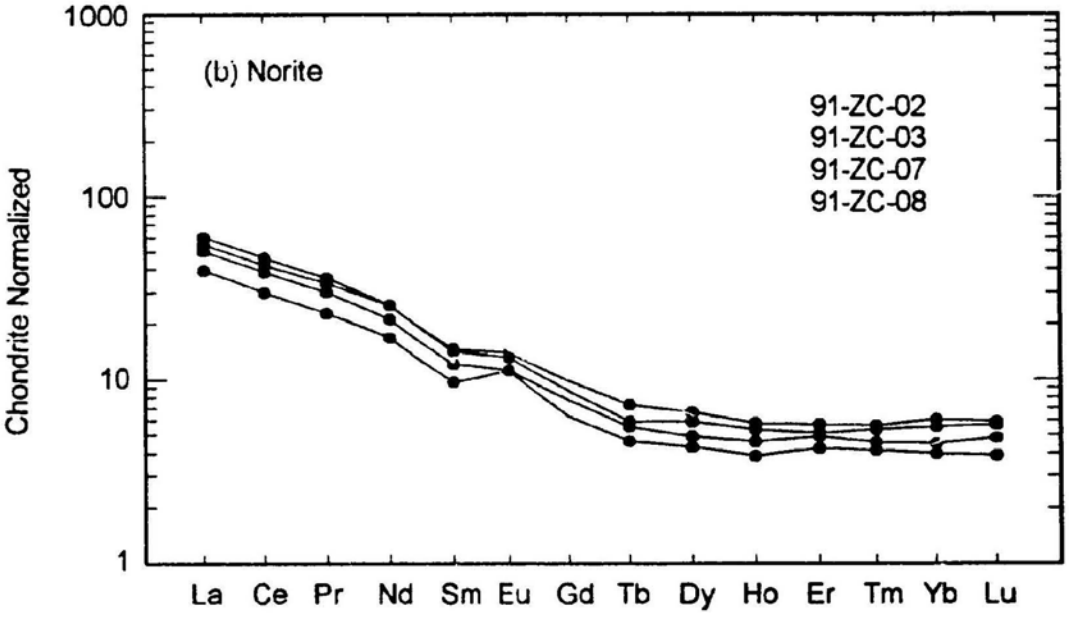
(b) Norite
91-ZC-02
91-ZC-03
91-ZC-07
91-ZC-08
Chondrite Normalized
1000
100
10
1
La Ce Pr Nd Sm Eu Gd Tb Dy Ho Er Tm Yb Lu

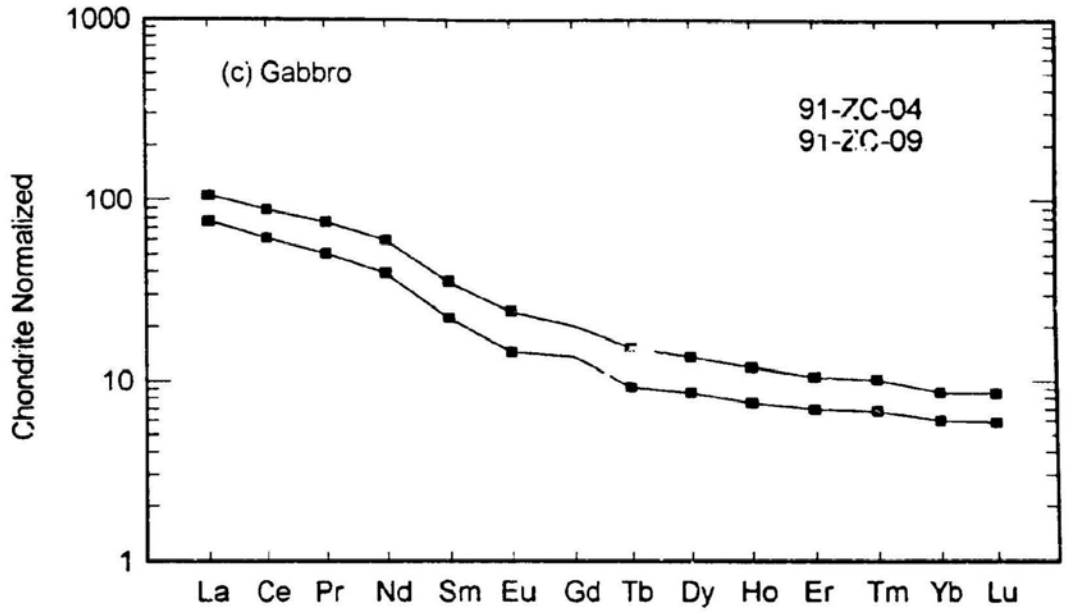
(c) Gabbro
91-ZC-04
91-ZC-09
Chondrite Normalized
1000
100
10
1
La Ce Pr Nd Sm Eu Gd Tb Dy Ho Er Tm Yb Lu

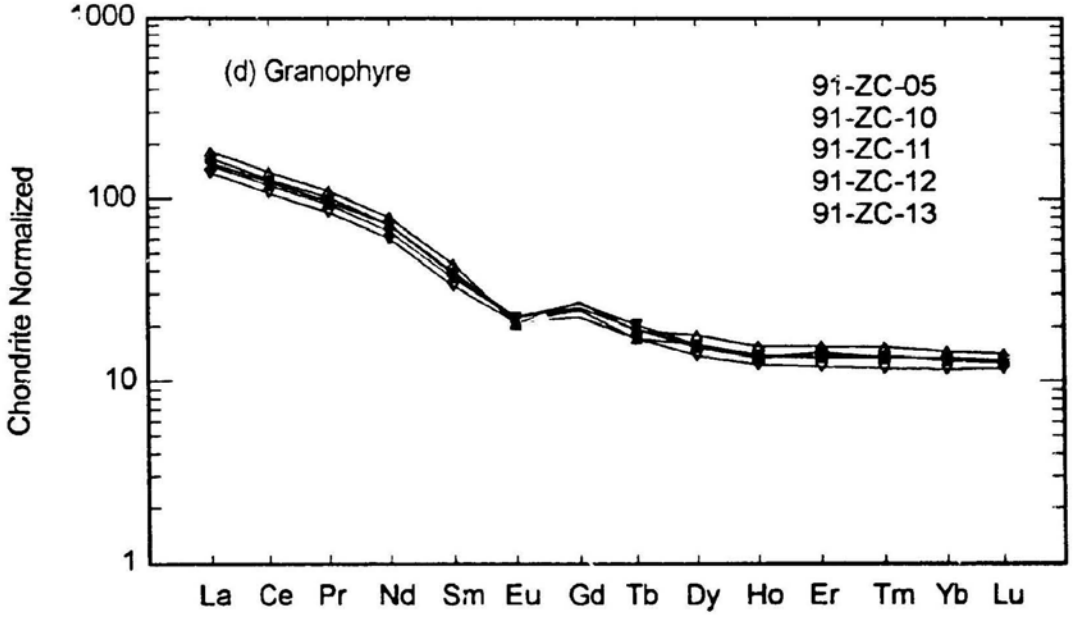
(d) Granophyre
91-ZC-05
91-ZC-10
91-ZC-11
91-ZC-12
91-ZC-13
Chondrite Normalized
1000
100
10
1
La Ce Pr Nd Sm Eu Gd Tb Dy Ho Er Tm Yb Lu

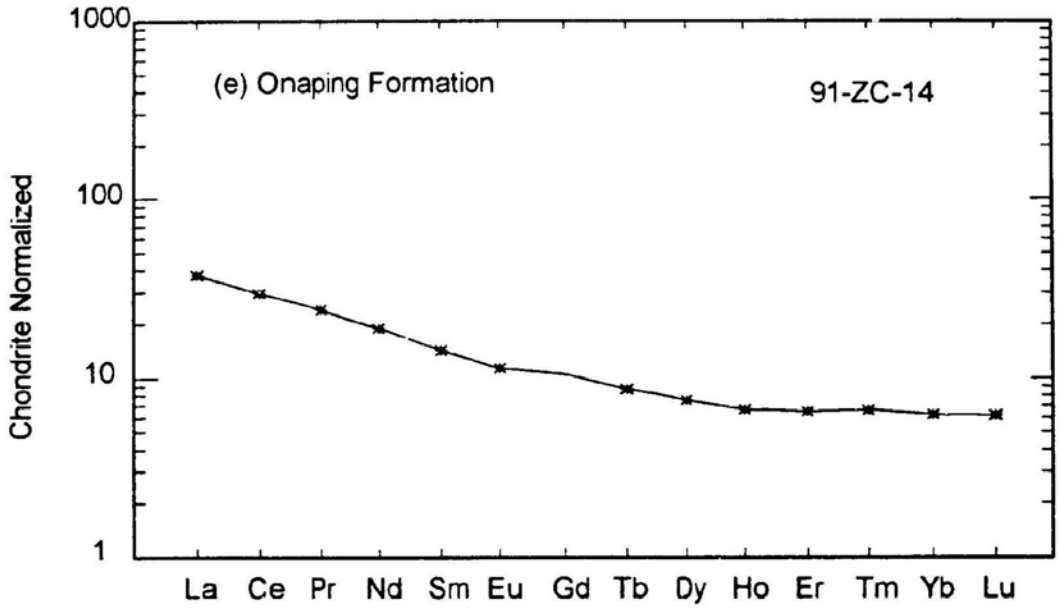

Figure 6.8 Chondrite normalized REE patterns of the Sudbury Igneous Complex: (a) Border Norite, (b) Norite, (c) Gabbro, (d) Granophyre, (e) Onaping Formation

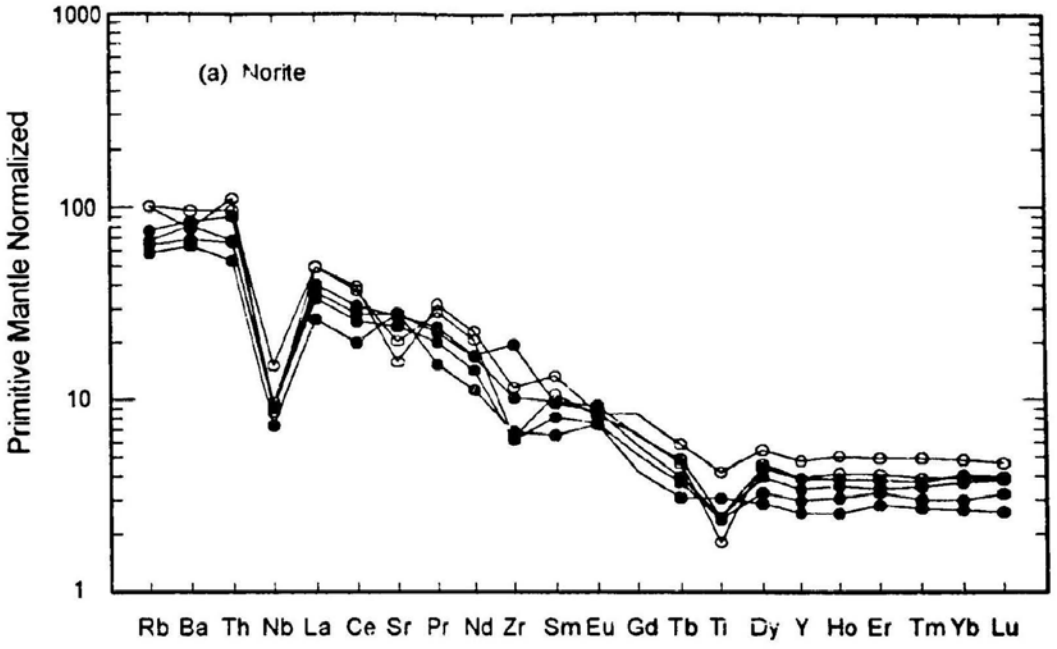
(a) Norite
Primitive Mantle Normalized
1000
100
10
1
Rb Ba Th Nb La Ce Sr Pr Nd Zr Sm Eu Gd Tb Ti Dy Y Ho Er Tm Yb Lu

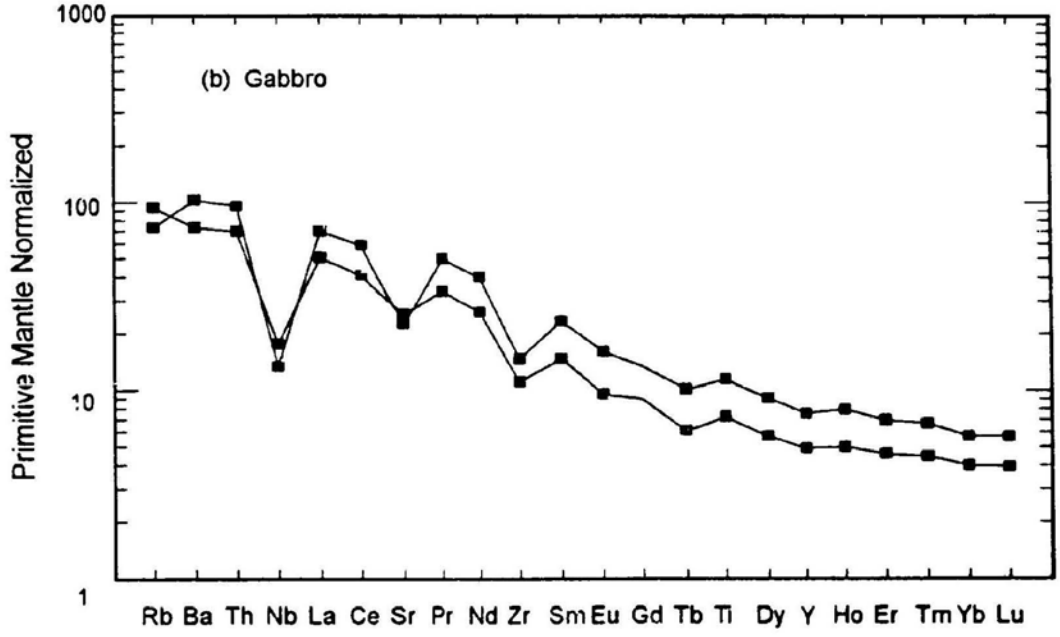
(b) Gabbro
Primitive Mantle Normalized
1000
100
10
1
Rb Ba Th Nb La Ce Sr Pr Nd Zr Sm Eu Gd Tb Ti Dy Y Ho Er Tm Yb Lu

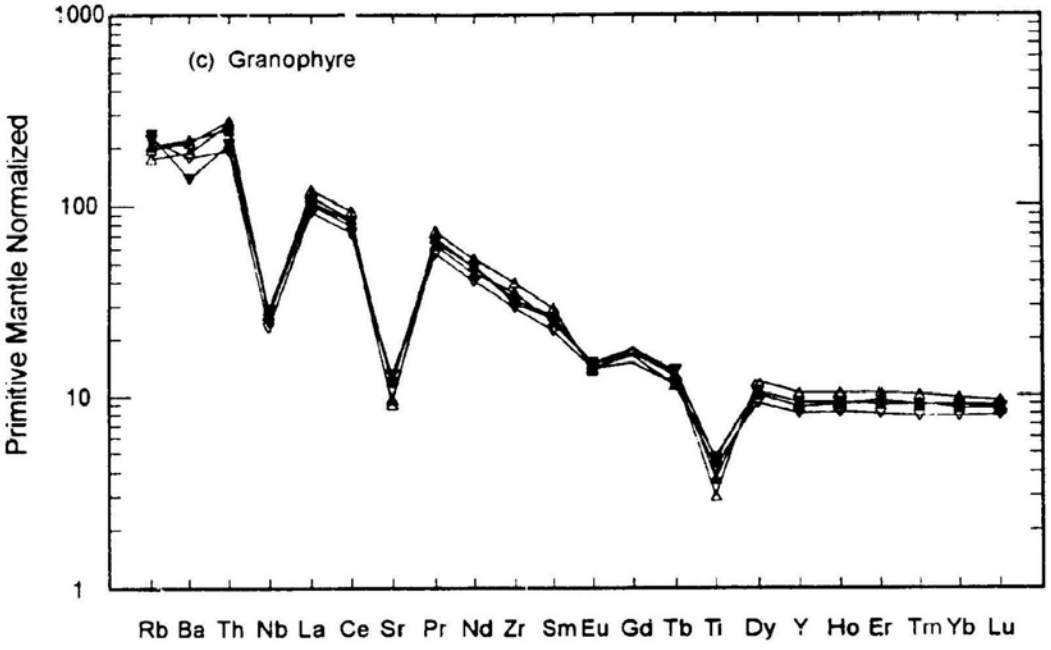

Figure 6.9 Primitive Mantle Normalized trace element diagrams; (a) Norite, (b) Gabbro, and (c) Granophyre. Normalization values for primitive mantle are from Talyor and Mclennan (1985)

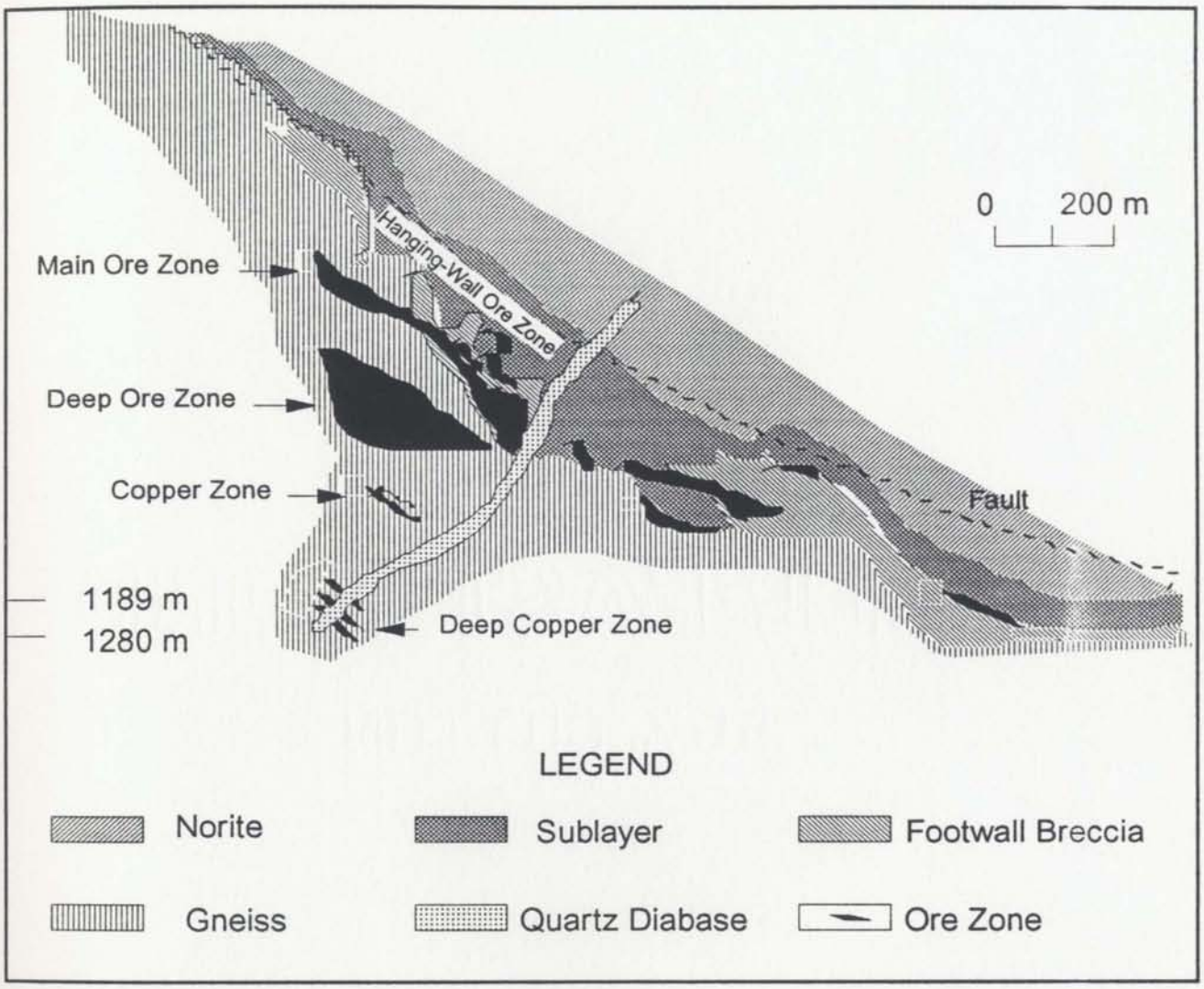

Figure 6.10 Geological vertical cross section through the Strathcona Mine (6280 E level, looking east) (drawn after Li et al., 1992)

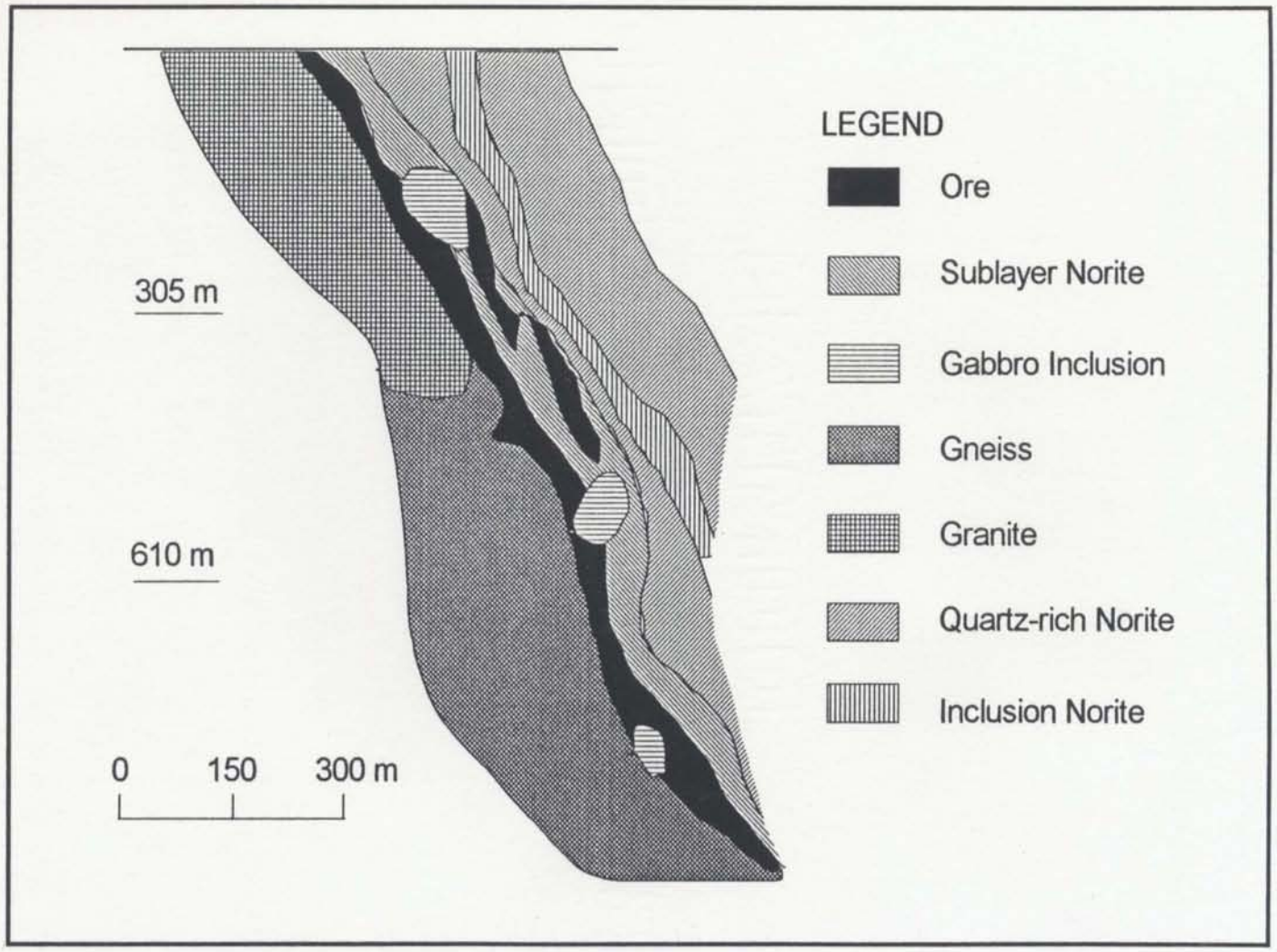

Figure 6.11 Geological vertical cross section through Little Stobie 1 orebody (looking west) (drawn after Davis, 1984)

CHAPTER 7

DISTRIBUTIONS OF THE PRECIOUS METALS IN COEXISTING ORE MINERALS FROM THE DEEP COPPER ZONE AT THE STRATHCONA MINE

7.1 INTRODUCTION

The Strathcona Mine (Falconbridge Limited) is located on the north rim of the Sudbury Igneous Complex (SIC) (Figure 6.1). The geology, petrography, and ore mineralogy of the Strathcona Mine have been discussed by Naldrett and Kullerud (1967) and Cowan (1968). The petrogenesis of the important footwall breccias and mafic norite was investigated by Naldrett *et al.* (1972) and outlined in Chapter 6. A geological cross section of the Strathcona Mine, modified from Li *et al.* (1992), shows five principal mineralization zones: the Hanging Wall Ore Zone, the Main Ore Zone, the Deep Ore Zone, the Copper Ore Zone and the Deep Copper Zone (Figure 6.10).

In a study of precious metals in the bulk ores of the Strathcona Ni-Cu sulphide mine, Naldrett *et al.* (1982) found that their distribution is zoned. Pt, Pd, Au, and Cu contents increase progressively with depth from the Hanging Wall Ore Zone through the Main Zone into the Deep Ore Zone; Rh, Ru, Ir, and

Os show a reverse trend. From this zonation, several questions arise regarding the distribution and partitioning of the precious metals:

(1) How are the precious metals distributed in each individual mineral phase, as discrete inclusions or in solid solution?

(2) If precious metals are in solid solution in these minerals, what is the partitioning of these elements between the major ore minerals?

(3) What controls the partitioning and mobility of precious metals between the minerals?

The objective of this chapter is to document and describe in detail the distribution of precious metals in the principle ore minerals (sulphides and magnetite), and platinum-group minerals (PGM), mainly in the Deep Copper Zone, but also between zones using the analytical techniques described in Chapters 4 and 5. In Chapter 9, the partitioning of precious metals between major ore minerals and the mobility of these element during segregation and crystallization will be discussed.

7.2 BRIEF DESCRIPTION OF THE ORE GEOLOGY OF THE STRATHCONA MINE

The Strathcona Mine is divided into five principal mineralized zones (Figure 6.10). The Hanging Wall Ore Zone is composed of mainly pyrrhotite and

pentlandite, which occupy interstitial areas between silicates; it occurs in hanging wall breccia and to a lesser extent in xenolithic and mafic norite. There is little or no replacement of silicates by sulphides.

Most of the Strathcona mineralization is present in the Main Ore Zone, which occurs in the Footwall Breccia between the norite and the underlying gneiss complex. This breccia varies from 10-60 m in thickness and is composed of fragments derived from the footwall gneiss complex (Cowan, 1968; and Coats and Snajdr, 1984). The mineralization of the Main Ore Zone consists of massive sulphide stringers or fine disseminated sulphides in the matrix of the footwall breccia and forms the bulk of the Strathcona ore. Small scale replacement of silicates by sulphides occurs in these ores.

The Deep Ore Zone was emplaced in fractures in the footwall gneiss as much as 90 m below the base of the SIC. Sulphide-granite gneiss contacts are sharp with no evidence of alteration or melting of the silicates by sulphides. The Deep Ore Zone is characterized by high Cu and Ni contents compared to the Hanging Wall Ore Zone and the Main Ore Zone.

The Copper Zone occurs as a complex system of, up to 6 m wide, fracture filling veins. The chalcopyrite veins are hosted completely by the footwall gneiss complex, and are located 200-300 m beneath the norite contact approximately 150 m NW of the Deep Ore Zone.

The Deep Copper Zone occurs in footwall rocks 450-600 m beneath the

norite contact where the predominant hosting rocks are gneissic units of the Footwall Complex. The ore zone is composed of highly irregular massive sulphide veins ranging in thickness from a few millimetres up to 2-3 meters. The sulphide veins are predominantly composed of chalcopyrite, cubanite, and pentlandite, in order of abundance, with lesser amounts of pyrrhotite, millerite, bornite, and magnetite. Magnetite, which is euhedral, is sometimes replaced by chalcopyrite and pentlandite (Figure 7.1a, e). Pentlandite is replaced along its cleavages by chalcopyrite (Figure 7.1c). Cubanite occurs as exsolution laminae in chalcopyrite (Figure 7.1d).

A distinct zoning of Ni over the mine as a whole was demonstrated by Cowan (1968) on the basis of 3000 analyses. The Ni content of the sulphide varies between 2.5 and 3 percent in the Hanging Wall Ore Zone but increases regularly from about 3 to about 5 percent from hanging wall to footwall across the Main Ore Zone. In general, Ni contours parallel the base of the SIC. The variation of Cu contents is more irregular but a general increase from 1 percent in the Hanging Wall Ore Zone to about 3-4 percent in the footwall and Deep Ore Zone. Further, the Cu:Ni ratio progressively increases from hanging wall to footwall in the Main Ore Zone. The distributions of the precious metals are also zoned (Naldrett *et al.*, 1982).

The focus of this study is on the distributions of the precious metals among coexisting sulphides and magnetite and is mainly concentrated on the

Deep Copper Zone, though differences among the zones are also discussed.

7.3 SAMPLING AND ANALYTICAL TECHNIQUES

Ten representative samples were collected from the Deep Copper Zone at the Strathcona Mine during the summer of 1991. Sample locations and brief descriptions are listed in Table 7.1.

Samples for mineral separates were first selected using a petrographic microscope to minimize exsolution lamellae or flames of pentlandite in pyrrhotite grains, and then approximately 1 kilogram of each sample was crushed and sieved to obtain a 60 mesh fraction. Mineral separation was carried out mainly by magnetic methods. Finally 30-40 mg of high purity mineral separates were selected by hand picking under a binocular microscope. All mineral separates for precious metal analysis were checked by X-Ray Diffraction (XRD) to ensure their purity.

Precious metal analysis of mineral separates was carried out by the methods described in Chapter 5, with quantification by ICP-MS. Samples of 20 mg were first dissolved with HCl and evaporated to dryness, then redissolved with aqua regia. Solutions were then transformed to the Cl form by three evaporations with 6 M HCl, and precious metals were separated from base metals by cation exchange.

Table 7.1 Location and brief description of the samples from the Deep Copper Zone at the Strathcona Mine

Sample	Location	Ore Type
91-ZC-15	Strathcona Deep Copper Zone, Level 39 B-46	Massive sulphide ore (55% Cpy, 25% Cub, 10% Mt, 5% Po, and 5% Pn)
91-ZC-16	Strathcona Deep Copper Zone, Level 39 B-45	Massive sulphide ore vein (75% Cpy, 10% Pn, and 15% xenolith inclusions)
91-ZC-17	Strathcona Deep Copper Zone, Level 39 B-45	Massive sulphide ore vein (80% Cpy and 15% Po)
91-ZC-18	Strathcona Deep Copper Zone, Level 39 B-45	Massive sulphide ore (60% Cpy, 20% Cub, 15% Pn, and 5% Po) in contact with a diabase dyke
91-ZC-20	Strathcona Deep Copper Zone, Level 42 D-7	Quartz-carbonate-chalcopyrite vein
91-ZC-21	Strathcona Deep Copper Zone, Level 42 D-7	Massive sulphide ore vein in contact with the Sudbury Breccia
91-ZC-22	Strathcona Deep Copper Zone, Level 42 D-13	Massive sulphide ore vein (75% Cpy, 10% Cub, 10% Pn, and 5% Mt)
91-ZC-23	Strathcona Deep Copper Zone, Level 42 D-13	The same vein above in contact with the footwall Sudbury Breccia.
91-ZC-24	Strathcona Deep Copper Zone, Level 42 D-13	Massive sulphide ore in contact with Sudbury Breccia
91-ZC-25	Strathcona Deep Copper Zone, Level 42 B-5	Massive coarse-grained millerite (85% Mi and 15% Pn)

Cpy: chalcopyrite Po: pyrrhotite Pn: pentlandite Mt: Magnetite
Cub: cubanite Mi: millerite

Platinum-group minerals were analyzed using a laser ablation microprobe ICP-MS (Jackson *et al.*, 1993) and a CAMECA SX-50 electron microprobe (EMP) at Memorial University of Newfoundland (MUN). In electron microprobe analyses, the following X-ray lines were used: PtMα, PdLα, AuMα, BiMα, SKα, NiKα, TeLα, SbLα, AsKα, SnLα, FeKα, CuKα, CdLα, ZnKα, AgLα, and CoKα. Pure precious metals, or their arsenides and bismuthides were used as calibration standards. Since the standards were not accurately determined, data in these analyses should only be considered as semi-quantitative. For minerals with dimension less than 10 μm, there was also a problem of electron excitation volume. Solid limits of detection are 240 ppb (Ru), 43 ppb (Rh), 180 ppb (Pd), 26 ppb (Ir), 88 ppb (Pt), and 88 ppb (Au) by LAM-ICP-MS; and 0.1-1.0% by energy dispersive EMP.

7.4 ANALYTICAL RESULTS

The analytical data for 7 precious metals (Ru, Rh, Pd, Re, Ir, Pt, and Au) in different minerals are presented in Table 7.2 and shown on Figure 7.2. The mean concentrations of Ru, Rh, Pd, Re, Ir, Pt, and Au are 2.5 ppb, 5.5 ppb, 2650 ppb, 1.1 ppb, 0.6 ppb, 1870 ppb, and 23.6 ppb, respectively, in chalcopyrite; less than 2.4 ppb, 5.3 ppb, 1670 ppb, 1.6 ppb, 0.5 ppb, 2120 ppb, and 1024 ppb, respectively in magnetite ; 7.1 ppb, less than 0.3 ppb,

Table 7.2 Concentrations (ppb) of precious metals in sulphides and magnetite from the Strathcona Deep–Copper Zone. Samples are described in Table 7.1

Sample	Mineral	Sample Size	Ru	Rh	Pd	Re	Ir	Pt	Au
91ZC15	Cpy	20 mg	<2.4	10.2	4600	<0.6	<0.5	2510	31.9
91ZC18	Cpy	20 mg	2.8	5.2	<29	1.2	<0.5	76	<3.7
91ZC20	Cpy	20 mg	<2.4	5.0	1920	2.3	1.0	1050	53.3
91ZC21	Cpy	20 mg	2.8	3.0	91	0.6	1.9	285	<3.7
91ZC22	Cpy	20 mg	<2.4	6.3	9140	1.7	<0.5	6440	14.1
91ZC23	Cpy	20 mg	5.6	3.2	125	<0.6	<0.5	845	38.7
Mean*	Cpy		2.5	5.5	2650	1.1	0.6	1870	23.6
91ZC15	Mt	20 mg	<2.4	6.5	2190	0.9	<0.5	4990	52.9
91ZC15	Mt	20 mg	4.6	5.7	116	<0.6	0.5	139	<3.7
91ZC15	Mt	20 mg	<2.4	6.5	1520	<0.6	0.9	2120	3.9
91ZC15	Mt	20 mg	<2.4	6.1	3030	0.6	0.5	3010	17.1
91ZC15	Mt	20 mg	<2.4	2.3	2280	<0.6	<0.5	5520	102
91ZC21	Mt	20 mg	<2.4	6.3	152	<0.6	1.0	606	8.3
91ZC22	Mt	20 mg	<2.4	8.5	667	9.6	<0.5	78	<3.7
91ZC23	Mt	20 mg	<2.4	<0.3	3390	<0.6	<0.5	480	8010
Mean*	Mt		<2.4	5.3	1670	1.6	0.5	2120	1020
91ZC20	Pn	20 mg	7.1	<0.3	2260	<0.6	<0.5	1760	429
91ZC15	Po	20 mg	3.6	46.1	307	<0.6	<0.5	805	<3.7
LOD			2.4	0.3	29	0.6	0.5	2.0	3.7

* for the data less than detection limits, 1/2 detection limit was used for mean calculation
Cpy--Chalcopyrite Mt--Magnetite Pn--Pentlandite Po--pyrrhotite
LOD--Limit of detection

2260 ppb, less than 0.6 ppb, less than 0.5 ppb, 1760 ppb, and 429 ppb, respectively in pentlandite; and 3.6 ppb, 46 ppb, 307 ppb, less than 0.6 ppb, less than 0.5 ppb, 805 ppb, and less than 3.7 ppb, respectively in pyrrhotite.

Although the precious metal contents among these minerals are variable, some general features can be drawn from these data:

(1) Analytical data for Ru, Rh, Re, and Ir are more consistent than those of Pt, Pd, and Au, suggesting that these elements may be, or originally were, in solid solution in the sulphides and magnetite. The remarkable variation of Pd, Pt, and Au contents suggest the presence of discrete precious metal phases containing these elements, which manifest themselves in the analyses by producing a heterogeneous "nugget-effect".

(2) Ru, Rh, and Ir broadly show the same distribution and partitioning. An apparent preferential association of these elements with specific minerals follows the sequence: sulphide > magnetite.

(3) Pd, Pt, and Au concentrations, are two to three orders of magnitude higher than the other precious metals, and they show no preferential partitioning among the minerals.

(4) Magnetite, usually regarded as a poor host for precious metals, is remarkably enriched in Pt and Pd in the Deep Copper Zone.

7.5 PRECIOUS METALS IN THE MINERALS FROM THE DEEP COPPER ZONE

7.5.1 MAJOR ORE MINERALS

There was considerable variation in the measured precious metal contents for some elements (*i.e.*, Pt, Pd, and Au) in replicates of magnetite in Sample 91-ZC-15 (Table 7.2). Replicate analyses of the precious metals in the magnetite (Figure 7.2) indicate that these elements are very heterogeneously distributed in 20 mg samples even within the same handspecimen, particularly Pd, Pt and Au. One reason for such variation is that some minor precious metal-enriched inclusions are included in these ore minerals. Electron microprobe and LAM-ICP-MS analyses have confirmed the presence of some of these inclusions (see Chapter 4 and later in this Chapter).

Within the Deep Copper Zone, there was also considerable variation in precious metal contents of the same mineral between the different samples (Table 7.2) and between minerals. In magnetite, Ru ranges from less than 2.4 ppb to 4.6 ppb, Rh from less than 0.3 ppb to 8.5 ppb, Pd from 116 ppb to 3390 ppb, Re from less than 0.6 ppb to 9.6 ppb, Ir from less than 0.5 ppb to 1.0 ppb, Pt from 78 ppb to 5520 ppb, and Au from less than 3.7 ppb to 8010 ppb. In chalcopyrite, Ru ranges from less than 2.4 ppb to 5.6 ppb, Rh from 3.0 ppb to 10.2 ppb, Pd from less than 29 ppb to 9140 ppb, Re from less than 0.6 ppb to 2.3 ppb, Ir from less than 0.5 ppb to 1.9 ppb, Pt from 76 ppb to

6440 ppb, and Au from less than 3.7 ppb to 38.7 ppb. In pyrrhotite, Ru, Rh, Pd, Re, Ir, Pt, and Au are 3.6 ppb, 46 ppb, 307 ppb, less than 0.6 ppb, less than 0.5, 805 ppb, and less than 3.7 ppb, respectively. In pentlandite, Ru, Rh, Pd, Re, Ir, Pt, and Au are 7.1 ppb, less than ppb, 2260 ppb, less than 0.6 ppb, less than 0.5, 1760 ppb, and less than 429 ppb, respectively.

7.5.2 PRECIOUS METAL MINERALS

Since large variations in Pd, Pt and Au concentrations are shown in individual ore minerals, they probably occur, in part, as inclusions of precious metal-enriched phases in the Deep Copper Zone ores. Some electron microprobe analyses of precious metal minerals are presented in Table 7.3. Table 7.3 shows that froodite ($PdBi_2$) is a common Pd-rich mineral. Most of these oval froodites occur at the grain boundaries between the major ore minerals or in microfractures in the ores. A few occur as isolated tiny inclusions which were probably included in the major ore mineral separates (Figure 7.3b). Electron microprobe analyses have also indicated some unidentified Pt-rich phases (Bi-As-S, Bi-Fe-As-S, Bi-Te-Bi-As-S and Cu-Fe-Bi-As-S) which contain 1-4% Pt (Table 7.3). Most of these Pt-rich phases were located at the grain boundaries of the major ore minerals, but some were included in these ore minerals. Gold occurs as discrete native Au alloys or as a component of the Pt enriched phase (Phase 1, Table 7.3) in the main ore minerals or as isolated discrete phases at

Table 7.3 Semi-quantitative electron microprobe analyses (wt %) of the precious metal-bearing phases in the sulphide ore (91-ZC-15) from the Strathcona Deep-Copper Zone

Phase	S	As	Te	Bi	Fe	Cu	Ni	Co	Zn	Cd	Sn	Sb	Pt	Pd	Au	Ag
Phase 1	27.60	18.83	0.32	36.98	2.06	1.02	0.30	0.12	7.26	0.00	0.66	0.49	3.41	0.00	0.95	0.00
Phase 1	27.87	19.77	0.53	38.65	2.97	4.02	0.04	0.05	0.03	0.00	0.62	0.47	3.80	0.00	1.19	0.00
Phase 1	26.98	19.34	0.41	39.10	6.78	0.41	0.00	0.00	0.00	0.00	0.82	0.58	4.15	0.00	1.43	0.00
Phase 2	13.05	14.68	28.71	31.71	2.28	3.40	0.12	0.01	0.34	0.00	0.63	0.59	3.98	0.00	0.51	0.00
Phase 3	32.23	14.66	0.35	25.86	14.66	8.13	0.00	0.00	0.06	0.00	0.54	0.46	2.27	0.00	0.79	0.00
Phase 3	30.17	13.82	0.60	20.31	20.66	10.94	0.00	0.00	0.00	0.00	0.53	0.53	1.69	0.00	0.75	0.00
Phase 4	4.61	1.01	0.03	8.29	84.03	0.15	0.17	0.00	0.05	0.00	0.05	0.00	1.34	0.00	0.27	0.00
Phase 5	19.98	0.40	0.05	0.00	5.81	53.30	0.00	0.00	0.18	0.23	0.00	0.00	0.00	0.06	0.00	20.00
Phase 5	22.96	0.58	0.09	0.00	12.59	48.75	0.02	0.00	0.32	0.34	0.00	0.00	0.00	0.00	0.00	14.35
Phase 5	20.56	0.63	0.30	0.00	4.00	55.01	0.10	0.00	0.04	0.68	0.01	0.00	0.00	0.00	0.00	18.68
Phase 5	25.07	0.81	0.15	0.60	12.36	46.80	0.00	0.00	0.14	0.00	0.24	0.00	0.00	0.00	0.00	13.83
Froodite	0.22	0.00	0.00	81.70	0.00	0.00	0.00	0.00	0.00	0.00	0.00	0.00	1.47	16.60	0.00	0.00
Froodite	0.58	0.00	0.00	80.18	1.09	0.00	0.00	0.00	0.00	0.00	0.09	0.17	1.55	16.34	0.00	0.00
Gold	5.00	0.00	0.01	0.00	18.07	0.32	0.11	0.00	0.00	0.59	0.00	0.00	0.00	0.44	74.17	1.29

Phase 1-5 – unidentified precious metal-bearing minerals

the grain boundaries. Electron microprobe analysis has identified one such alloy (Au-Fe-Ag) which was found at a grain boundary between chalcopyrite and magnetite (Figure 7.3b) (Table 7.3). Although sliver was not included in this study, the electron microprobe analyses indicate that the majority of the Ag is present in chalcopyrite as micro exsolutions of other phases (*i.e.* concentrated during exsolution) (Table 7.3) and as native Ag (Figure 7.3c). Li and Naldrett (1993) have reported some other platinum-group minerals: insizwaite [$Pt(Bi,Sb)_2$], niggliite (PtSn), sichenerite [(Pd,Pt)BiTe], sperrylite ($PtAs_2$), sobolevskite (PdBi), paolovite (Pd_2Sn), Pd-Bi chloride and Cl-bearing Pd-Bi sulphide from the Deep Copper Zone at the Strathcona Mine.

7.6 VARIATIONS OF THE PRECIOUS METALS IN THE MAJOR ORE MINERALS IN THE DIFFERENT ORE ZONES

The mean concentrations of the precious metals in the major sulphides and magnetite in different ore zones (compiled from Keays and Crocket, 1970, Chyi and Crocket, 1976, and this study) are presented in Table 7.4. Comparisons of precious metal concentrations in ore minerals from different ore zones are difficult, due to: (1) lack of analytical data in the literature for Ru, Rh, Re, and Pt in mineral separates from the Hanging Wall Ore Zone, the Main Ore Zone,

Table 7.4 Average concentrations (ppb) of the precious metals in sulphides and magnetite in different ore zone of Strathcona mine*

Mineral	Ore Zone	Ru	Rh	Pd	Re	Ir	Pt	Au
Chalcopyrite	MOZ	11.6		555		0.78		26.4
Chalcopyrite	DOZ	15.2		608		6.74	792	22.2
Chalcopyrite	DCZ	2.5	5.5	2650	1.10	0.60	1867	23.6
Magnetite	HWO			11.4		1.20		0.70
Magnetite	MOZ			7.05		0.27		2.24
Magnetite	DOZ			14.4		1.41	446	4.31
Magnetite	DCZ	<2.4	5.3	1670	1.60	0.50	2117	1020
Pentlandite	MOZ	22.1		101		1.95		74.5
Pentlandite	DOZ			2070		2.02	875	118
Pentlandite	DCZ	7.1	<0.3	2260	0.20	<0.5	1758	429
Pyrrhotite	HWO	25.4		69.1		44.1		7.50
Pyrrhotite	MOZ	6.0		177		4.93		18.8
Pyrrhotite	DOZ	50.5		179		1.45	735	10.6
Pyrrhotite	DCZ	3.6	46.1	307	<0.6	<0.5	805	<3.7

DCZ – Deep Copper Zone
DOZ – Deep Ore Zone
MOZ – Main Ore Zone
HWO – Hanging–Wall Ore
* data of DOZ, MOZ, and HWO are compiled from Keay and Crocket (1970). and Chyi and Crocket (1976), DCZ data from this study

the Deep Ore Zone, and the Copper Ore Zone; and (2) different analytical methods (INAA vs. ICP-MS) were used, particularly for low concentrations of Ru and Ir which show some difference between the two techniques. However, available data (Table 7.4) shows variation trends of precious metals in co-existing ore minerals from different ore zones. The precious metal concentrations in the four minerals in the different ore zones normalized to the those in the Deep Copper Zone are presented in Figure 7.4.

Magnetite

The concentrations of Pd and Au in magnetite increase substantially with depth from 11.4 ppb and 0.70 ppb respectively in the Hanging Wall Ore Zone to a high of 1670 ppb and 1020 ppb respectively in the Deep Copper Zone (Figure 7.4b). Platinum contents increase from 446 ppb in the Deep Ore Zone to 1610 ppb in the Deep Copper Zone (Figure 7.4b). The concentrations of Ir in magnetite change erratically from 1.2 ppb in the Hanging Wall Ore Zone to 0.5 ppb in the Deep Copper Zone (Figure 7.4b).

Chalcopyrite

Similar to magnetite, the concentrations of Pd in chalcopyrite increase from 555 ppb in the Main Ore Zone to 2650 ppb in the Deep Copper Zone (Figure 7.4d). Platinum contents increase from 792 ppb in the Deep Ore Zone to 1870

ppb in the Deep Copper Zone (Figure 7.4d). The concentrations of Ru, Ir and Au in chalcopyrite change erratically from 11.6 ppb, 0.78 ppb, and 26.4 ppb respectively in the Main Ore Zone to 2.5 ppb, 0.6 ppb and 23.6 respectively in the Deep Copper Zone (Figure 7.4d).

Pyrrhotite

Similar to magnetite and chalcopyrite, the concentrations of Pd in pyrrhotite increase from 69 ppb in the Hanging Wall Ore Zone to 307 ppb in the Deep Copper Zone (Figure 7.4a). The concentrations of gold change erratically from 7.5 ppb in the Hanging Wall Ore Zone to less than 3.7 ppb in the Deep Copper Zone. Platinum contents increase from 735 ppb in the Deep Ore Zone to 805 ppb in the Deep Copper Zone (Figure 7.4a). The concentrations of Ru and Ir in pyrrhotite change erratically from 25 ppb and 44 ppb respectively in the Hanging Wall Ore Zone to 3.6 ppb and less than 0.5 ppb respectively in the Deep Copper Zone.

Pentlandite

The concentrations of Pd and Au in pentlandite increase from 101 ppb and 74.5 ppb respectively; to 2260 ppb and 429 ppb respectively in the Deep Copper Zone (Figure 7.4c). Platinum contents increase from 875 ppb in the Deep Ore Zone to 1940 ppb in the Deep Copper Zone (Figure 7.4c). The

concentrations of Ru and Ir in pentlandite decrease from 22 ppb and 1.95 ppb, respectively in the Main Ore Zone to 7.1 ppb and less than 0.5 ppb, respectively in the Deep Copper Zone (Figure 7.4c).

7.7 DISCUSSION

7.7.1 DISTRIBUTION OF THE PRECIOUS METALS IN THE MAJOR ORE MINERALS FROM THE DEEP COPPER ZONE

Chalcopyrite, pentlandite, pyrrhotite, and magnetite are the major ore minerals in the Deep Copper Zone. The contents of the Ru, Rh, and Ir in these minerals in the replicate analyses are more consistent than those of Pt, Pd, and Au, indicating that these elements may be, or have been, in solid solution in these minerals. The remarkable variation of Pd, Pt, and Au contents suggest the presence of discrete precious metal phases in these minerals, which has been confirmed by electron microprobe data (Table 7.3). Micrographic studies show that most of these precious metal minerals occur at the grain boundaries between the major ore minerals or in microfractures in the ores, but a few such minerals are included in the major ore minerals as tiny inclusions. Precious metal analysis of the mineral separates in this study probably includes some of these inclusions. However, reasonable correlation between Pt and Pd was observed (Figure 7.5a), which may indicate that the "nugget-effect" for these

elements is somewhat reproducible. No linear correlations between the concentrations of Ru, Rh, and Ir; and those of Pt, Pd, and Au were observed (Figure 7.5b).

The distributions of the precious metals impact on the metallurgical extraction of the metals. High contents of Pt and Pd in the form of Pt- and Pd-rich trace phases included in the magnetite may explain the poor metallurgical recovery of these elements from some ores.

Chyi and Crocket (1976) have shown that individual PGEs and gold are strongly associated with specific sulphide minerals. Pd and Au are concentrated in pentlandite, and Pt and Ir are associated with chalcopyrite. Relative to the most abundant sulphide, pyrrhotite, Pd and Au are concentrated in pentlandite by a factor of approximately 14, and Pt and Ir are concentrated in chalcopyrite by a factor of approximately 6. However, data in this study shows these trends are not applicable to the Deep Copper Zone. Ruthenium, Rh, and Ir have essentially the same distribution and partitioning between the major ore minerals. An apparent preferential association of Ru, Ir, and Rh with specific minerals follows the sequence: sulphide > magnetite (Table 7.2 and Figure 7.6). However, Pd, Pt, and Au concentrations that are two to three orders of magnitude higher than the rest of the precious metals, show no pronounced preferential partitioning among these minerals (Table 7.2 and Figure 7.6).

Mean chondrite normalized data of precious metals between coexisting ore minerals in the Deep Copper Zone at the Strathcona Mine (Figure 7.6) indicate that these major ore minerals are all depleted in the Ir group of platinum-group elements (Ru, Rh, Os, and Ir) (IPGE), and enriched in the Pd group of platinum group elements (Pd, Pt, and Au) (PPGE).

7.7.2 FRACTIONATION OF THE PRECIOUS METALS IN MAJOR ORE MINERALS IN THE DIFFERENT ORE ZONES

Naldrett *et al.* (1982) have shown that mean chondrite normalized concentrations of PGE and Au from bulk ores exhibit a pronounced zoning within the Strathcona deposit (Figure 7.7a). The Hanging Wall Ore Zone has an unusually shallow slope with a (Pt + Pd)/(Ru + Ir + Os) ratio of 2.2. The ore from the Main Ore Zone shows a strongly sloping profile [(Pt + Pd)/(Ru + Ir + Os) = 34]. The ore from the Deep Ore Zone shows an even steeper profile with a (Pt + Pd)/(Ru + Ir + Os) ratio of greater than 134.

Available data (Keays and Crocket, 1970, Chyi and Crocket, 1976, and this study) shows that the PGE fractionation patterns in the co-existing major ore mineral separates from the four mineralization zones are quite different (Figure 7.7b-e). In general, the concentrations of Pt, Pd, and Au in the major ore minerals increase progressively from the Hanging Wall Ore Zone through the Main Ore Zone and the Deep Ore Zone into the Deep Copper Zone; and Ru, Rh,

and Ir show the reverse trend. These trends are consistent with results for bulk precious metal analyses (Figure 7.7a) (Naldrett *et al.*, 1982). However, each individual mineral shows different degrees of fractionation between the different ore zones. From the Hanging Wall Ore Zone into the Deep Copper Zone, magnetite and pyrrhotite display strong precious metal fractionation (Figure 7.7b-c). Pyrrhotite and magnetite in the Hanging Wall Ore Zone show almost flat chondrite normalized PGE patterns, and increasingly steeper patterns from the Main Ore Zone to the Deep Copper Zone (Figure 7.7b-c). Both Pt and Pd reach their maximum in the Deep Copper Zone. However chalcopyrite and pentlandite show little fractionation of the precious metals between the different ore zones. Analytical data for chalcopyrite and pentlandite from the Hanging Wall Ore Zone are not available. Chalcopyrite exhibits similar steep patterns from the Main Ore Zone to the Deep Copper Zone (Figure 7.7d). The PGE patterns for pentlandite are increasingly steep from the Main Ore Zone to the Deep Copper Zone ore (Figure 7.7e).

The marked fractionation of precious metals between Footwall and Hanging Wall Ore Zones suggests strong partitioning of these metals between pyrrhotite solid solution and a sulphide melt phase (Keays and Crocket, 1970). Naldrett and Kullerud (1968) studied the Strathcona ore mineral paragenesis on the basis of textural observations and inferences from experimental data. They concluded that the hanging wall sulphides resulted from crystallization of a high

temperature pyrrhotite solid solution at around 1100°C from an immiscible sulphide-oxide liquid emplaced at approximately 1200°C, together with the Sublayer magma. Subsolidus exsolution of pyrite occurred below 700°C, chalcopyrite below 450°C, and pentlandite below 300°C. The footwall sulphides represent that portion of the immiscible sulphide-oxide liquid which settled out of the Sublayer magma and collected at the base of the SIC or in fissures in the footwall rocks.

The results of an experimental study of the behaviour of the light PGE's in nickel-iron melts showed that during crystallization these elements are distributed differently between the early crystalline phase [an iron-nickel mono-sulphide solid solution (Mss)] and the residual melt (Distler *et al.*, 1977 and Malevskiy *et al.*, 1977). The Mss is enriched in Rh and Ru, and the residual melt in Pd. Thus during crystal fractionation of the sulphide melt, early forming Mss could crystallize and settle out to the base of the sulphide pile, thereby depleting the remaining sulphide melt in the IPGE and Fe and Ni, and enriching the remaining melt in the PPGE and Cu. The distributions of the precious metals in coexisting ore minerals from the different ore zones at the Strathcona Mine are consistent with the above experiment results.

7.8 CONCLUSIONS

(1) Analytical data for Ru, Rh, Re, and Ir are less variable than those

for Pt, Pd, and Au. The low variability in concentrations of Ru, Rh, and Ir suggests that these element are probably in, or were originally in, solid solution in the sulphides and magnetite. The remarkable variation of Pd, Pt, and Au contents suggest the presence of discrete precious metal phases in the ore minerals, which was confirmed by electron microprobe data.

(2) Ru, Rh, and Ir partition in a coherent fashion. An apparent preferential association of these elements with specific minerals follows the sequence: sulphide > magnetite.

(3) Pd, Pt, and Au concentrations are two to three orders of magnitude higher than the rest of the precious metals and do not exhibit preferential partitioning among these minerals. Most of these metals were found as tiny discrete phases either located at the grain boundaries of the major ore minerals and in microfractures, or included in these ore minerals.

(4) Magnetite, usually regarded as poor in precious metals, included significant Pt- and Pd-rich phases in the Deep Copper Zone.

The distribution of the precious metals in coexisting ore minerals provide clues to understanding the petrogenesis, such as the behaviour of these element during crystallization and exolution (see Chapter 9). Precious metal analyses of mineral separates also provide an important technique in evaluating the ore body, *i.e.*, precious metal extraction in metallurgical processes.

198

a

1 mm

b

1 mm

c

0.13 mm

d

0.25 mm

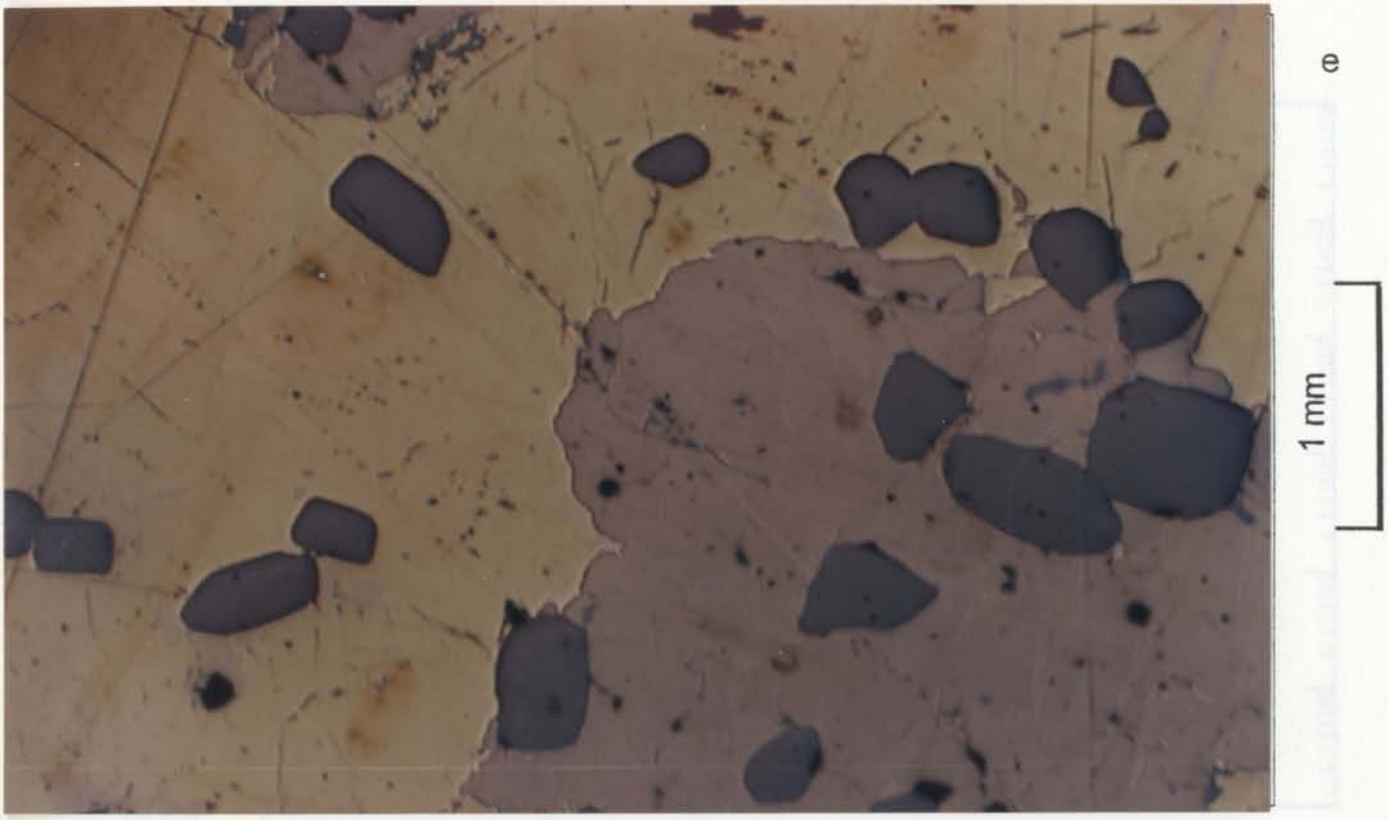

Figure 7.1 Photomicrographs illustrating textural relations of ore minerals. (a) Magnetite replaced by chalcopyrite and pentlandite (91-ZC-15). (b) Intergrowth between pentlandite and chalcopyrite (91-ZC-16). (c) Pentlandite replaced along its cleavages by chalcopyrite (91-ZC-20). (d) Cubanite exsolution laminae in chalcopyrite (91-ZC-23). (e) Euhedral or subeuhedral magnetite in massive sulphide ore (91-ZC-23)

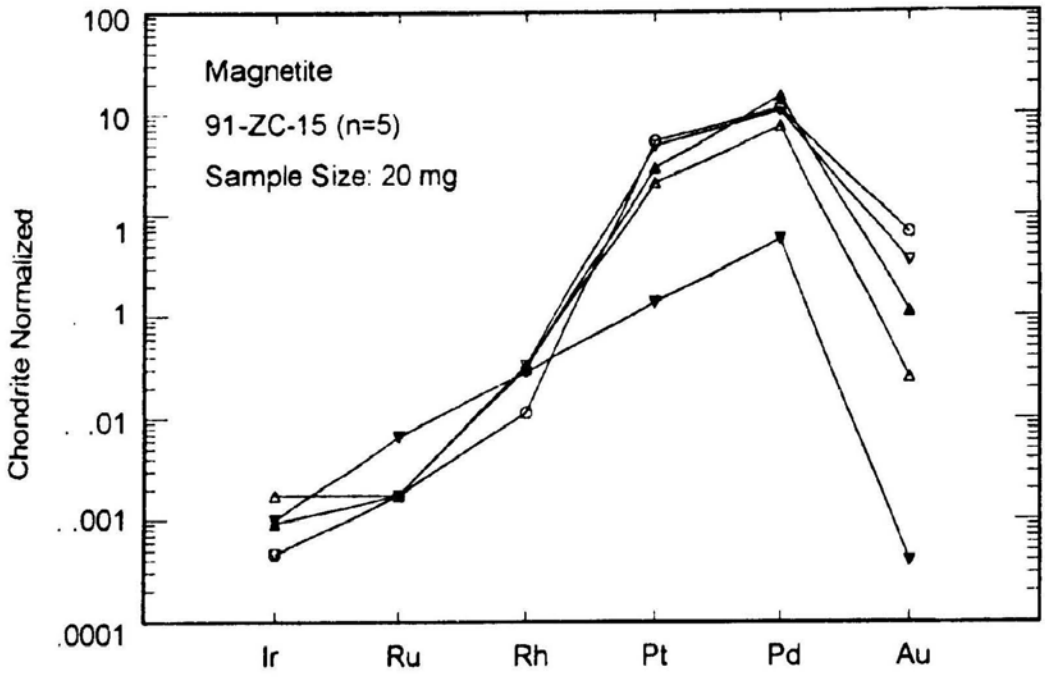

Figure 7.2 Variation of precious metal contents in magnetite (91-ZC-15) from the Deep Copper Zone of the Strathcona Mine normalized to chondrite values. Five individual replicate analyses are presented for one sample. Sample weights are 20 mg .

a

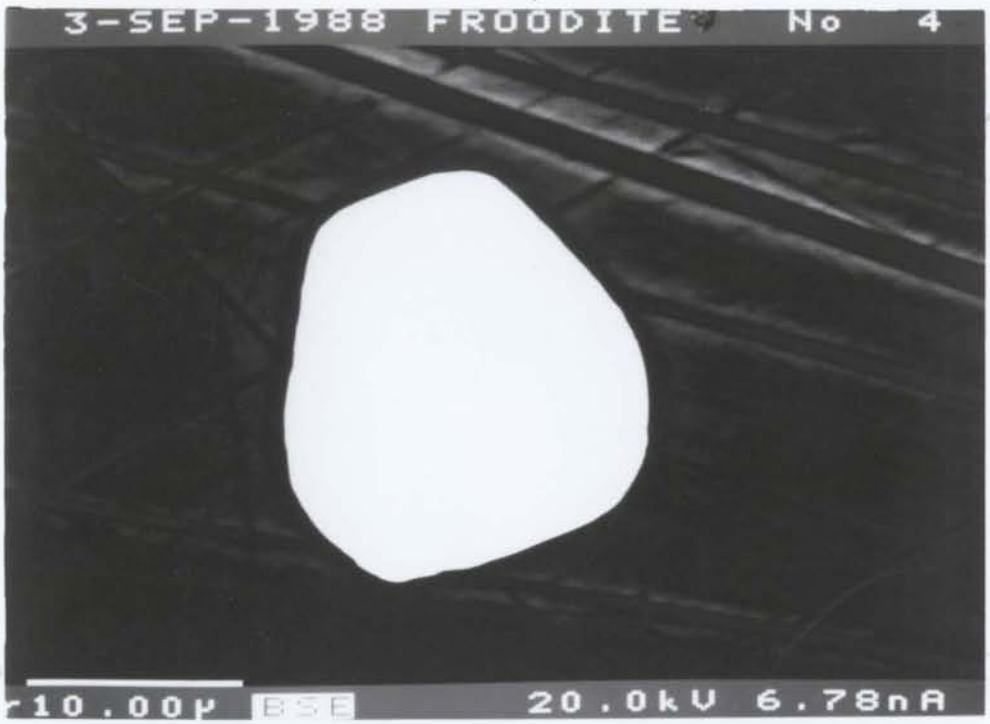
3-SEP-1988 FROODITE No 4
10.00µ BSE 20.0kV 6.78nA

b

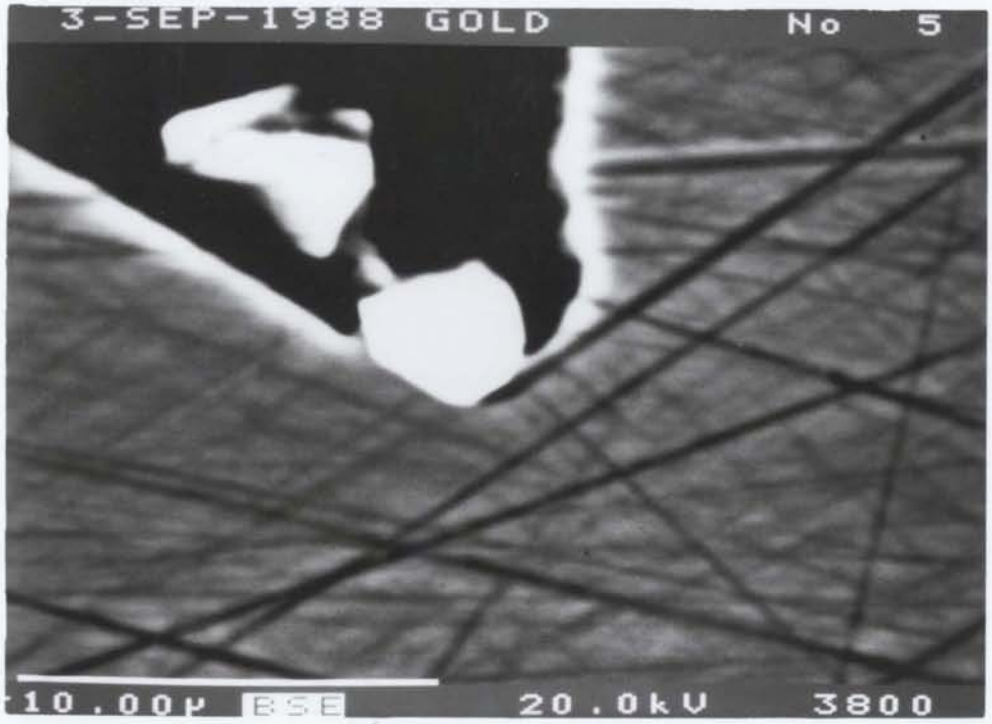
3-SEP-1988 GOLD No 5
10.00µ BSE 20.0kV 3800

c

Figure 7.3 Scanning electron photomicrograph of the precious metal minerals and their host minerals in Sample 91-ZC-15. (a) froodite, (b) gold, and (c) silver

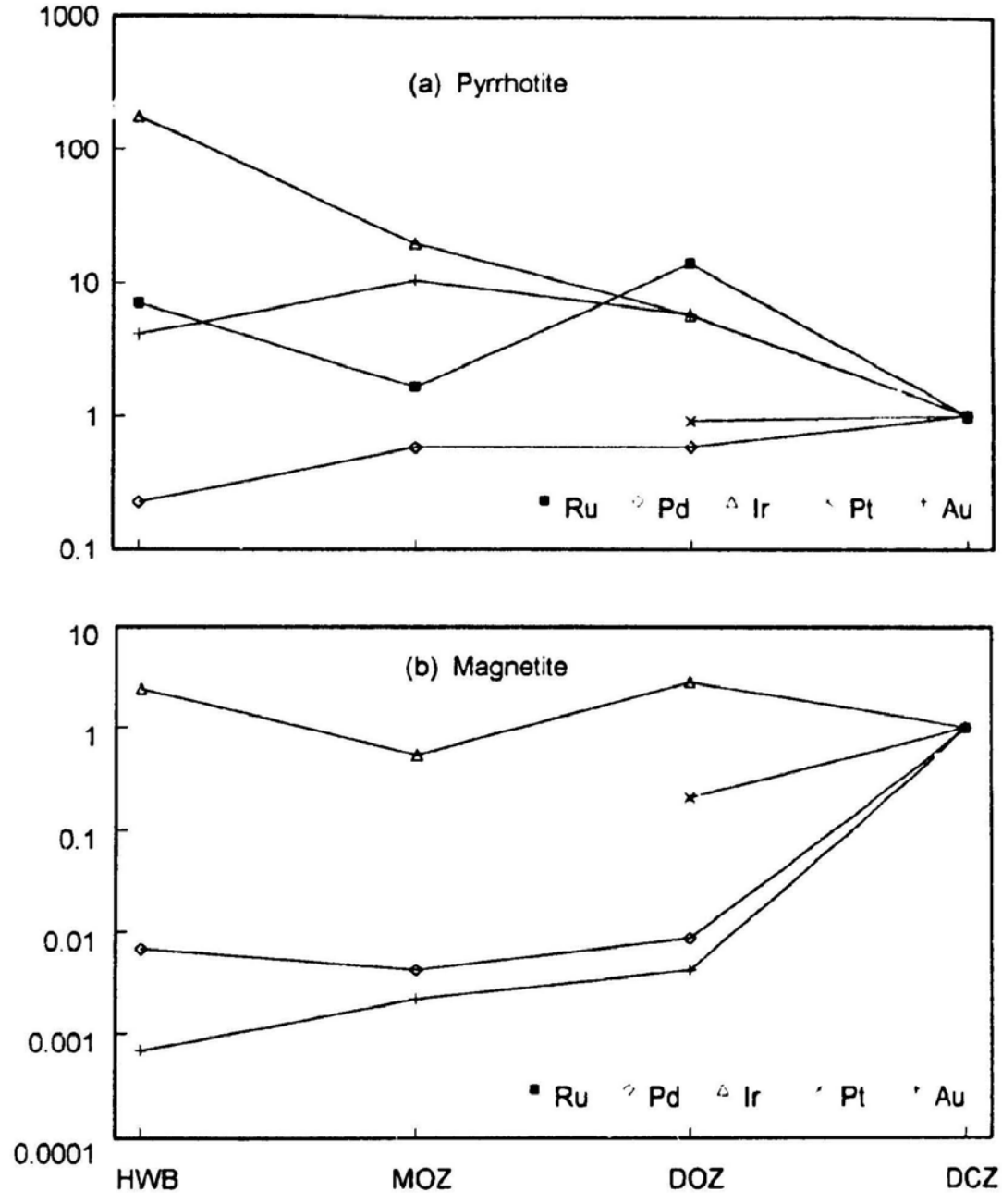
(a) Pyrrhotite
1000
100
10
1
0.1
Ru
Pd
Ir
Pt
Au
(b) Magnetite
10
1
0.1
0.01
0.001
0.0001
Ru
Pd
Ir
Pt
Au
HWB
MOZ
DOZ
DCZ

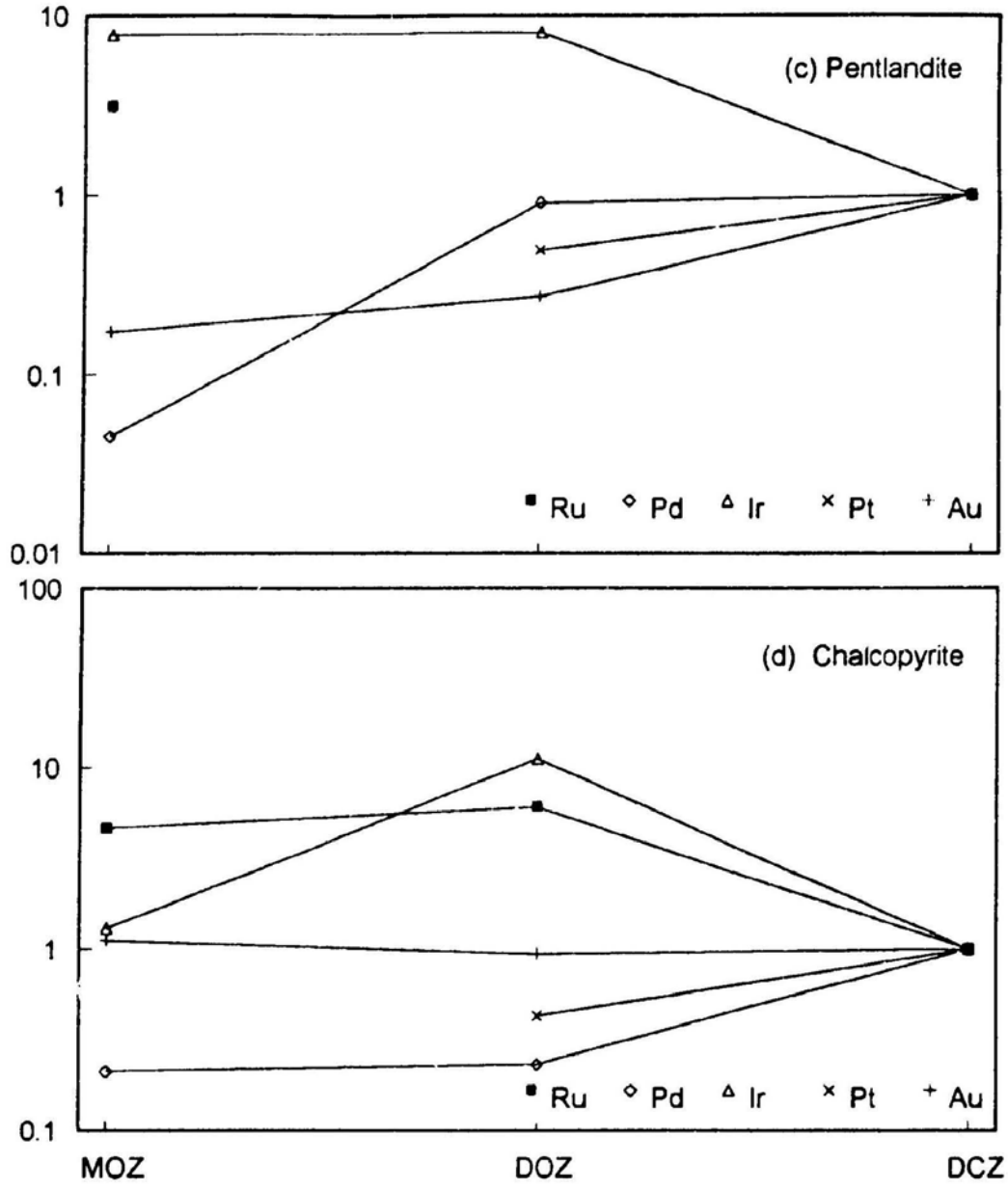

Figure 7.4 Variations of precious metal contents in the major minerals from the different ore zones (data from Keays and Crocket, 1970; and Chyi and Crocket, 1976) normalized to those in the Deep Copper Zone (data from this study): (a) pyrrhotite, (b) magnetite, (c) pentlandite, and (d) chalcopyrite. HWO: Hanging Wall Ore , MOZ: Main Ore Zone, DOZ: Deep Ore Zone, and DCZ: Deep Copper Zone. Data summarized in Table 7.4.

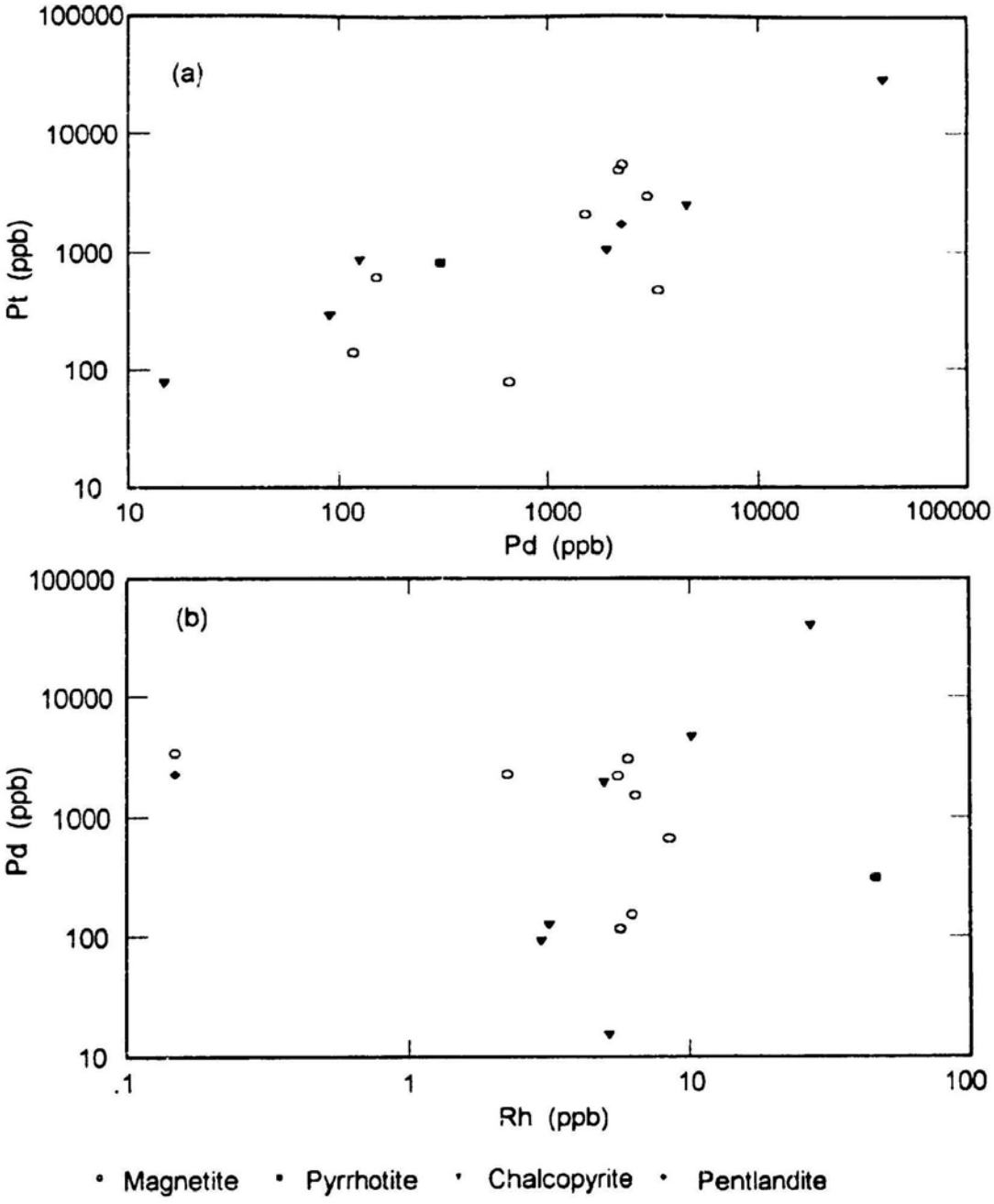

Figure 7.5 Correlations of the precious metal concentrations in the major ore minerals (magnetite, pyrrhotite, pentlandite, and chalcopyrite) from the Strathcona mine: (a) Pt and Pd, and (b) Rh and Pd.

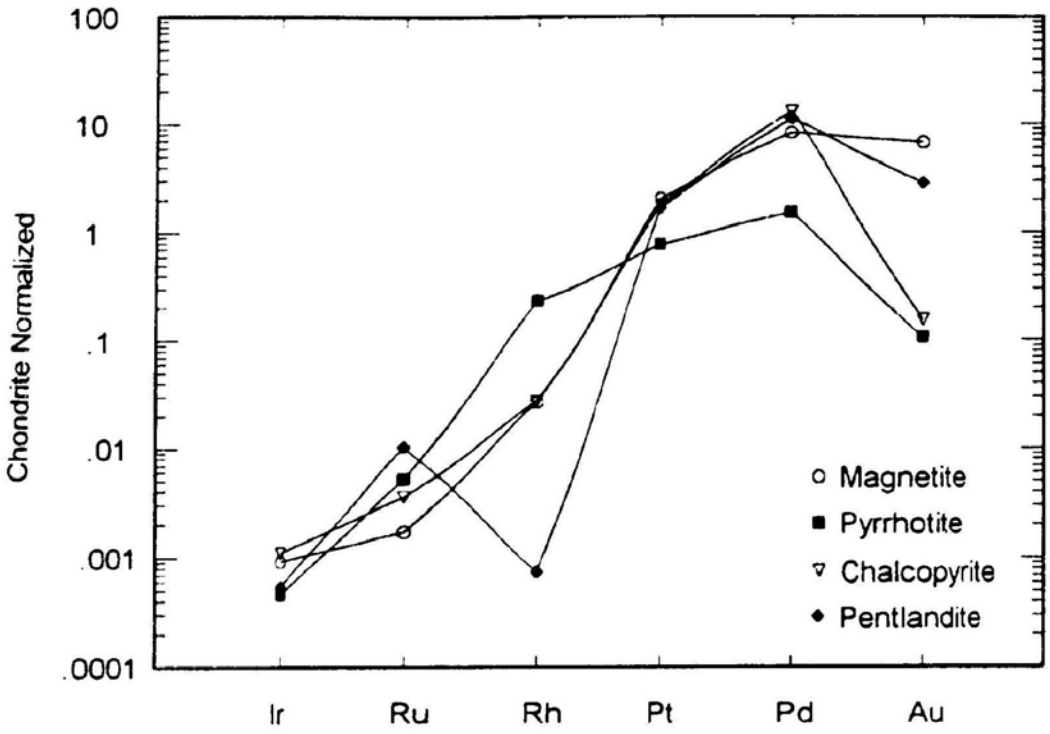

Figure 7.6 Mean chondrite-normalized data for the precious metals in the coexisting ore minerals from the Deep Copper Zone at the Strathcona Mine.

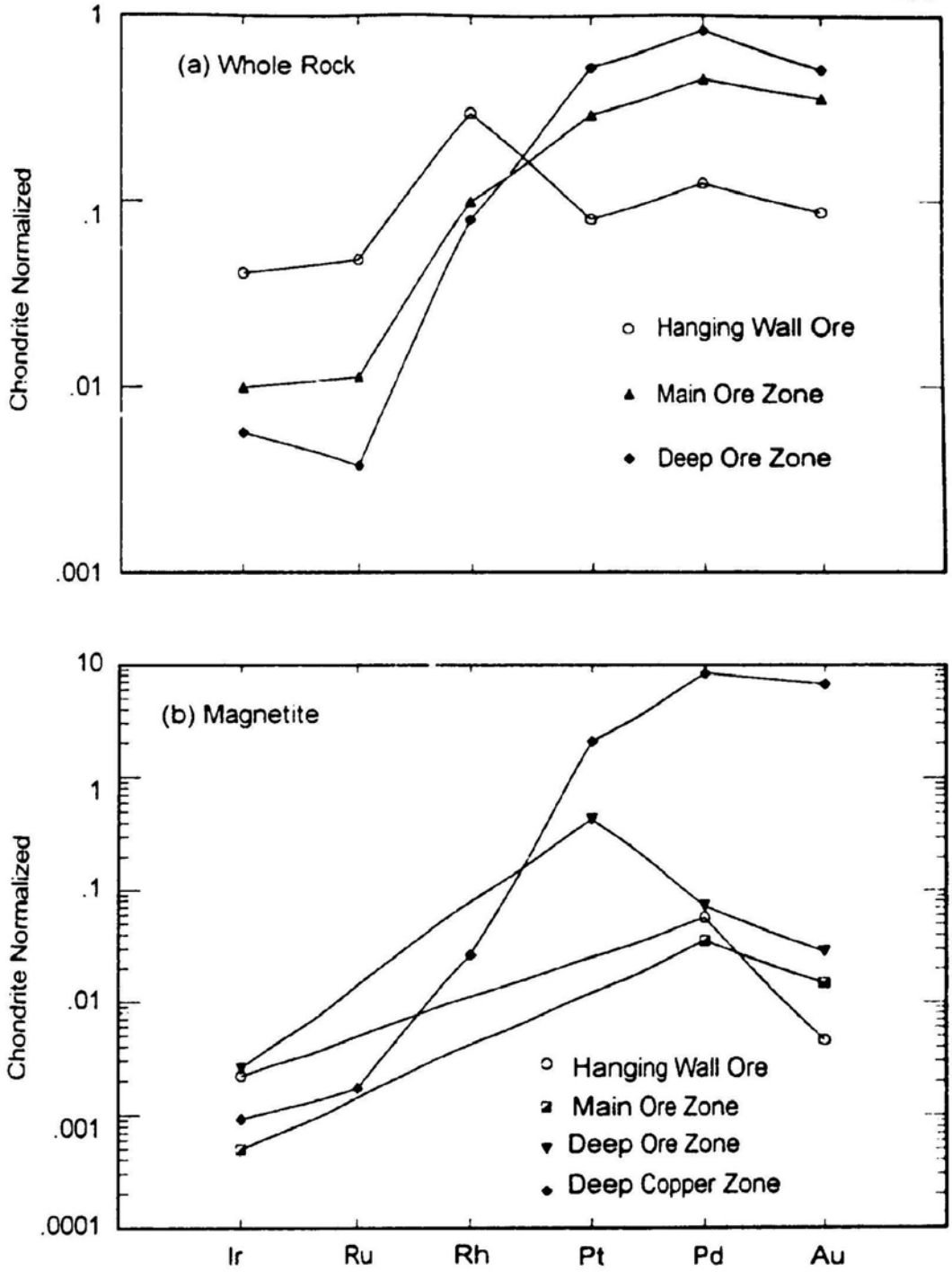
(a) Whole Rock
Chondrite Normalized
1
.1
.01
.001
Hanging Wall Ore
Main Ore Zone
Deep Ore Zone
(b) Magnetite
Chondrite Normalized
10
1
.1
.01
.001
.0001
Hanging Wall Ore
Main Ore Zone
Deep Ore Zone
Deep Copper Zone
Ir
Ru
Rh
Pt
Pd
Au

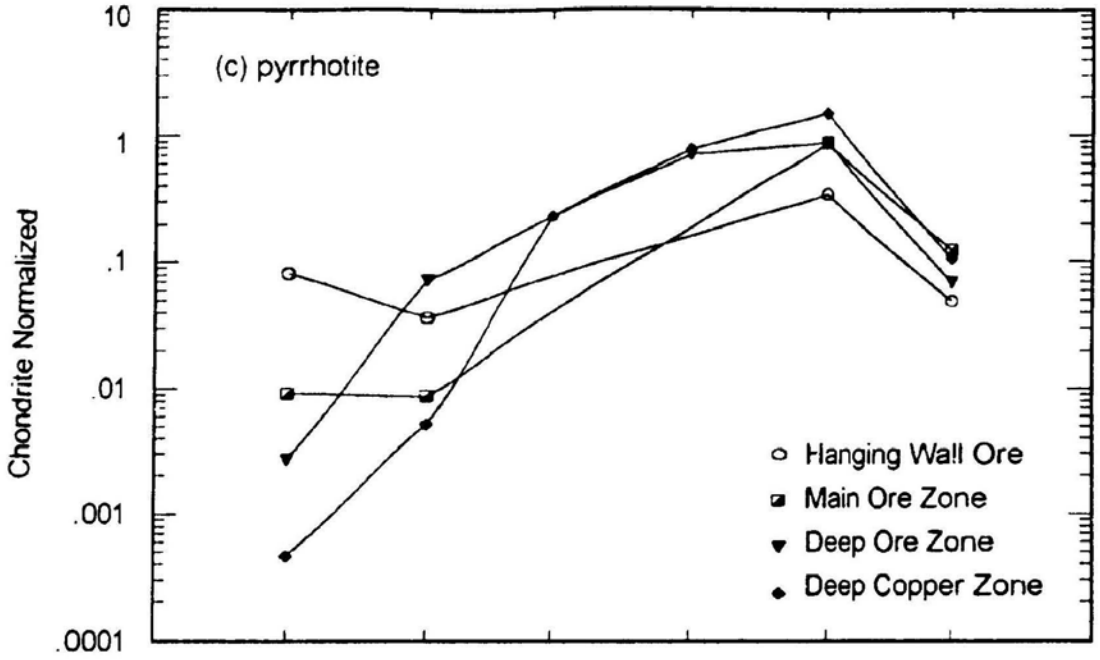
(c) pyrrhotite
Chondrite Normalized
10
1
.1
.01
.001
.0001
Hanging Wall Ore
Main Ore Zone
Deep Ore Zone
Deep Copper Zone

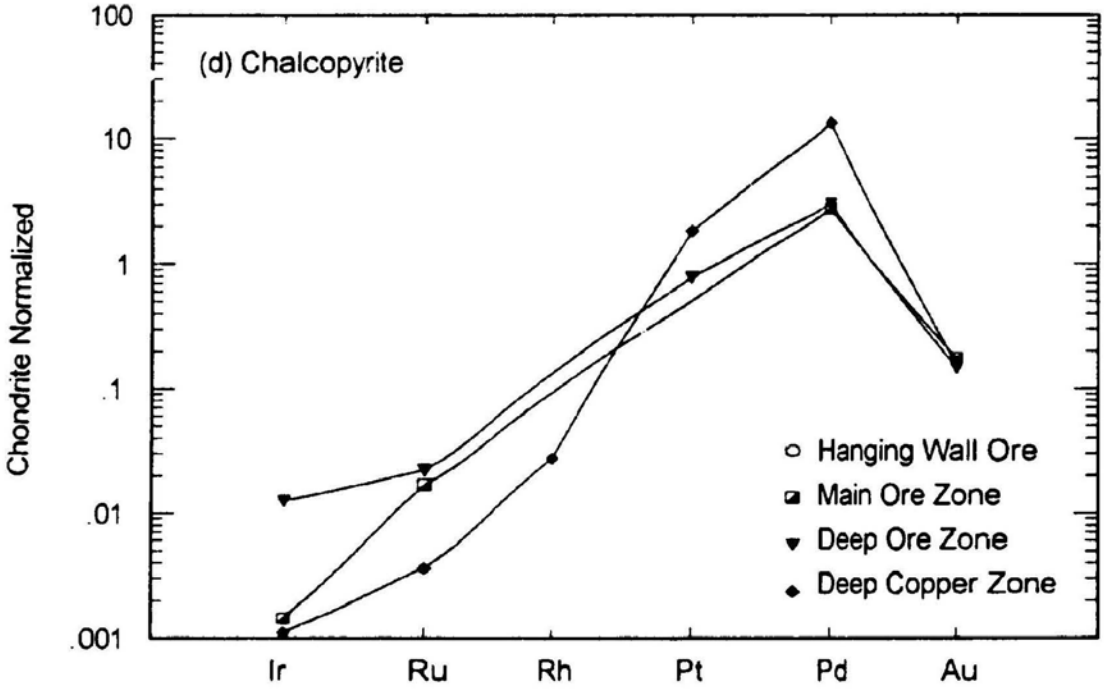
(d) Chalcopyrite
Chondrite Normalized
100
10
1
.1
.01
.001
Ir
Ru
Rh
Pt
Pd
Au
Hanging Wall Ore
Main Ore Zone
Deep Ore Zone
Deep Copper Zone

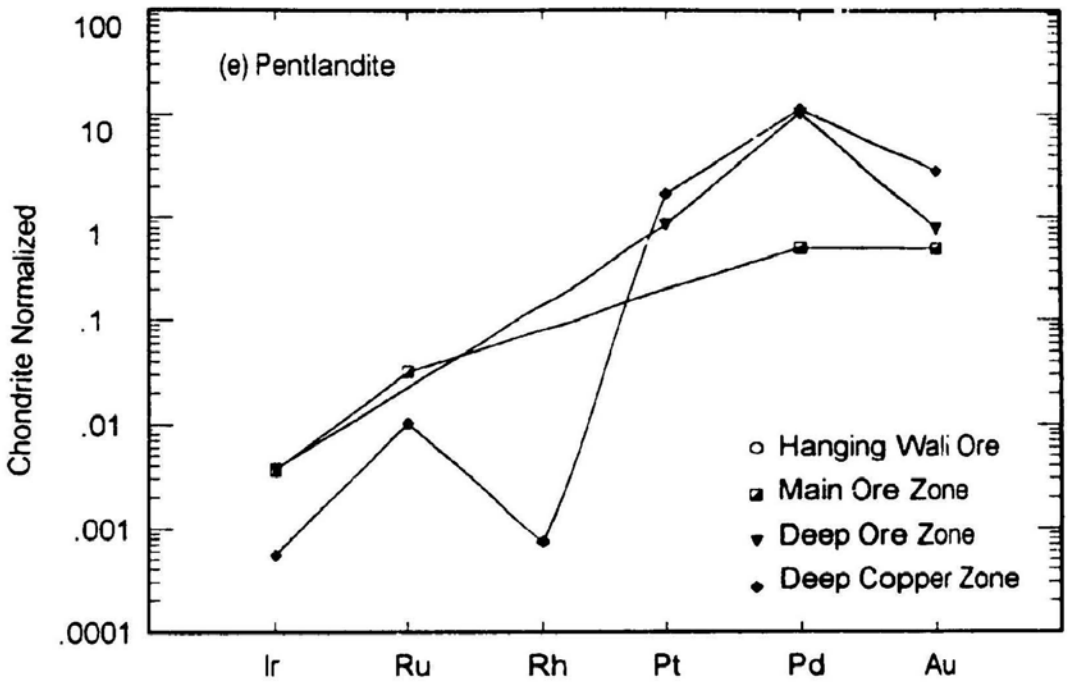

Figure 7.7 Chondrite normalized patterns of the precious metals in (a) whole rock (data from Naldrett, 1984), (b) magnetite, (c) pyrrhotite, (d) pentlandite, and (e) chalcopyrite in the different ore zones. Data for (b), (c), (d), and (e) from Keays and Crocket (1970), Chyi and Crocket (1976), and this study (Table 7.4)

CHAPTER 8

GEOLOGY AND PRECIOUS METAL DISTRIBUTIONS OF THAYER LINDSLEY MINE, SUDBURY

8.1 INTRODUCTION

The Thayer Lindsley Mine (Falconbridge Limited), located in the South Range of the Sudbury Igneous Complex (SIC) (Figure 6.1), is one of many Ni-Cu-PGE orebodies hosted in the Sublayer and the footwall Sudbury Breccia to the SIC. It is a recently developed Ni-Cu-PGE deposit with preliminary underground diamond drilling only completed in June, 1992. A report by Binney *et al.* (1992) indicated that progressive depletion of Ni, Co, Ir, and Ru is accompanied by enrichment of Pt, Pd, Au, and Cu in a sequence from the Cu-poor Sublayer through to the extreme margins of the footwall 4B Ore Zone. However, no detailed study of the geology and precious metal geochemistry has been reported.

The objectives of this chapter are to:

1) document the geology (geological setting, mineralogy, texture, and fabric) of the ore deposit based on megascopic observations and ore petrographic studies;

2) determine the concentrations of the precious metals (Ru, Rh, Pd, Re, Ir, Pt, and Au) in bulk sulphide ores, and in high purity sulphide (pyrrhotite, chalcopyrite, pentlandite, pyrite, and marcasite) and magnetite separates using the analytical techniques described in chapters 4 and 5;

3) determine the distribution of the precious metals among coexisting sulphides and magnetite;

4) investigate the platinum-group minerals (PGM) using a scanning electron microscope and an electron microprobe;

5) estimate the relative proportions of the precious metals in solid solution in the major ore minerals and in discrete independent precious metal phases in the sulphide ores; and

6) investigate the spatial distributions and variations of the precious metals within the 4B Ore Zone (Figure 8.2);

8.2 GEOLOGY OF THE THAYER LINDSLEY MINE

8.2.1 GENERAL GEOLOGY

The Thayer Lindsley Mine is located on the South Range of the SIC (Figure 6.1). Binney *et al.*(1992) described the general geology of the deposit. The footwall rocks to the SIC at the Thayer Lindsley Mine consist of Huronian volcanic and intrusive rocks of the Elsie Mountain Formation, intruded by the

Murray Granite (Figure 8.1). The hanging wall rocks are South Range norite and gabbro of the SIC. The sheet-like Sublayer appears continuous along the contact between the SIC and the footwall Huronian volcanic rocks and granite.

South Range Norite and Quartz Gabbro

South Range norite that overlies either Sublayer or footwall rocks at the Thayer Lindsley Mine is approximately 1800 m thick (Binney *et al.*, 1992). The mean modal mineralogical composition for the norite is 40-50% plagioclase (An 45-50), 25-30% amphibole, 5-10% biotite, and 5% quartz. Most amphiboles were derived from alteration of ortho-pyroxenes. Minor constituents include apatite, zircon, magnetite, disseminated sulphides, and altered chlorite. Quartz gabbro overlies the South Range norite to the north. It is a medium- to coarse-grained light coloured rock with a modal mineral composition of 40% plagioclase, 40% amphibole (after pyroxene), 10% quartz, with trace apatite and magnetite.

Sublayer

The Sublayer, which is an important ore host at the Thayer Lindsley Mine, forms an irregular, discontinuous sheet up to 60 m in thickness at the base of the SIC (Binney *et al.*, 1992). The Sublayer comprises subrounded fragments (up to 10 m across) of norite, gabbro, ultramafic rock, meta-basalt, and granite. Sulphides are ubiquitous in the matrix of breccia.

Elsie Mountain Formation

Elsie Mountain Formation which underlies the SIC includes meta-basalt, and an irregular sill of meta-gabbro (Figure 8.1). The modal mineral composition of the altered basalt is 55-60% amphibole, 20-30% feldspar, 2-10% quartz, with lesser amounts of sericite, epidote, carbonate, and magnetite. Trace amounts of pyrrhotite and chalcopyrite are present. Gabbro sills, from fine to medium grained, consist of 70% amphibole, 25-30% feldspar, and 2% quartz.

Murray Granite

The Murray Granite, which intruded the Huronian rocks in the footwall, is a pink biotite granite (2388 +20/-13 Ma, Krogh *et al.*, 1984). The mean modal mineral composition of this fine grained and equigranular rock is 55-60% feldspar (microcline, albite, and cryptoperthite), 25-30% quartz, 5% biotite, 1% muscovite, 2% epidote, and minor carbonate, sphene, zircon, and magnetite. The granite contains numerous 1-2 m size basaltic xenoliths and less common gabbro xenoliths near its contacts with Huronian rocks. In close proximity to the ore zones, the granite is sheared, silicified, cut by quartz or chalcopyrite veins, or impregnated with disseminated chalcopyrite (Binney *et al.*, 1992).

8.2.2 GEOLOGY OF THE DEPOSIT

Most of the Thayer Lindsley mineralization occurs in the Sublayer breccia

located at the base of the SIC. There are four ore zones at depths between 660 m and 1700 m below the surface (Binney *et al.*, 1992) (Figure 8.1). Zone 1 and Zone 2 are hosted by Sublayer breccia and plunge steeply to the north. They are located from 660 m to 1300 m below surface, between the SIC and the Huronian basalts. Zone 3 is hosted by Sublayer breccia but plunges at depths of 1350 m to 1700 m to the south below the granite. Zone 4, which consists of massive sulphide ore bodies, lies approximately 40-60 m south of the base of the SIC at depths between 1250 m and 1370 m. It is hosted by the Murray Granite (Figure 8.2). Pyrrhotite, chalcopyrite, pentlandite, magnetite, pyrite, and marcasite are the main ore minerals in each of these ore zones. The distributions of the precious metals among coexisting sulphides and magnetite in Zone 4 are the focus of this study.

8.2.3 ORE PETROLOGY

There are two main types of ore in the 4 ore zones, disseminated and massive sulphide ores. The disseminated type mostly occurs in rocks of the Sublayer, particularly the Sublayer Breccia (Figures 8.3i-j). Disseminated ore contains 5-50% sulphides and magnetite, and sometimes the sulphide ore occurs as discrete patches in the silicate rocks (Figure 8.3j). The contact between the ores and the host rocks are diffuse. The modal mineralogy includes chalcopyrite (10-30%), pyrrhotite (10-15%), pyrite (5-10%), marcasite

(5-10%), magnetite (0-5%), and minor pentlandite. Pyrite is replaced by marcasite. Pentlandite occurs dominantly as exsolution lamellae or flames in pyrrhotite grains or as rims surrounding pyrrhotite grains (Figures 8.4d and 8.4h).

The massive sulphides in the 4B Ore Zone were collected for this study. The massive sulphide ores are the predominant ore type in this zone, and the contacts between ore and the sheared granite are sharp. Pyrrhotite (30-90%), chalcopyrite (5-40%), magnetite (5-10%), and pentlandite (0-10%) are the main metallic minerals (Figures 8.3a-b). Sphalerite, galena, and precious metal alloys are minor components. Magnetite typically occurs as discrete euhedral crystals (Figure 8.4i). Pentlandite almost always occurs as exsolution lamellae or flames in, or surrounding, pyrrhotite grains (Figures 8.4e and Figure 8.4g). Pentlandite sometimes fills the sharp contact between massive pyrrhotite and chalcopyrite (Figures 8.4a-b). Some streaky monomineralic chalcopyrite veinlets which cut massive pyrrhotite-pentlandite-chalcopyrite-magnetite mineral assemblages can be observed (Figure 8.3e-f). Adjacent to silicate xenoliths in this ore zone, mineral zoning is displayed wherein massive chalcopyrite grades into pentlandite-pyrrhotite to pyrrhotite-chalcopyrite-magnetite-pentlandite away from the xenoliths towards massive sulphides (Figures 8.3g-h and Figure 8.4j). Close to the granite contacts, there are massive chalcopyrite veins or highly disseminated ores. Sometimes the

massive sulphide veins extend from the orebodies into the granite.

8.3 SAMPLING STRATEGY AND ANALYTICAL TECHNIQUES

8.3.1 SAMPLING STRATEGY

Three categories of samples were selected to study the spatial distribution of precious metals within the 4B Ore Zone: (1) systematic samples from a drill core (TL13-32) through the 4B Ore Zone (Table 8.1 and Figure 8.5); (2) systematic samples from several drill cores on a strike along a transect through the 4B Ore Zone (Table 8.1 and Figure 8.6); (3) samples from Sublayer ores. In all, twenty samples were carefully selected from drill cores. The selected samples had uniform mineral assemblages and avoided obvious cases of two generations, such as monomineralic chalcopyrite veinlets cutting massive ore. Each drill core sample, weighing 0.5 to 1 kilogram, was cut along its length into three parts: the middle part was used for petrographic work, the two side parts were used for bulk ore analysis and mineral separate analysis.

Table 8.1 Location and description of the samples from the Thayer Lindsley Mine

(a) Samples from a drill core (TL13-32) through the 4B Ore Zone (Figure 8.5)

Sample	Location	Ore Type
TL13-34B	Drill core TL13-34, 9.47 m	Massive sulphide ore near the orebody margin. Po (70%), Cpy (20), Mt (5%), and Pn (5%)
TL13-32A	Drill core TL13-32, 19.5 m	Massive sulphide ore near the orebody margin. Po (85%), Cpy (5%), Mt (5%), and Pn (5%)
TL13-32F	Drill core TL13-32, 27.6 m	Massive sulphide ore. Po (65%), Cpy (20%), Mt (10%), and Pn (5%)
TL13-32J	Drill core TL13-32, 34.3 m	Massive sulphide ore. Po (85%), Cpy (5%), Mt (5%), and Po (5%)
TL13-32N	Drill core TL13-32, 40.65 m	Massive sulphide ore. Po (70%), Cpy (15%), Mt (10%), and Pn (10%)
TL13-32R	Drill core TL13-32, 48.55 m	Quartz-chalcopyrite-pyrrhotite ore in contact with the Murray Granite. Po (60%), Cpy (30%), Mt (5%), and Pn (5%)

Cpy: chalcopyrite Po: pyrrhotite Pn: pentlandite Mt: Magnetite

(b) Samples from a transect along strike through the 4B Ore Zone (Figure 8.6)

Sample	Location	Ore Type
TL13-61A	Drill core TL13-61, 56.9 m	Disseminated sulphide ore. Po (10%) and Cpy (5%)
TL13-35C	Drill core TL13-35, 36.8 m	Massive sulphide ore. Po (70%), Cpy (15%), Mt (10%), and Pn (5%)
TL13-32J	Drill core TL13-32, 34.3 m	Massive sulphide ore. Po (85%), Cpy (5%), Mt (5%), and Po (5%)
TL13-63A	Drill core TL13-63, 33.1 m	Massive sulphide ore. Po (75%), Cpy (10%), Mt (10%), and Pn (<5%)
TL13-98A	Drill core TL13-98, 76.7 m	Massive sulphide ore. Po (70%), Cpy (10%), Mt (10%), and Pn (10%)
TL13-96A	Drill core TL13-96, 82.5 m	Massive sulphide ore. Po (40%), Cpy (20%), Mt (10%), and Pn (5%)
TL13-97A	Drill core TL13-97, 95.7 m	Disseminated sulphide ore. Po (35%) and Cpy (15%)
TL13-109A	Drill core TL13-109, 80.27 m	Massive sulphide ore. Po (65%), Cpy (20%), Mt (10%), and Pn (5%)
TL13-162B	Drill core TL13-162, 98.6 m	Massive sulphide ore. Po (80%), Cpy (10%), Mt (5%), and Pn (5%)
TL13-161F	Drill core TL13-161, 116.4 m	Massive sulphide ore. Po (85%), Cpy (5%), Mt (5%), and Pn (<5%)
TL15-01A	Drill core TL15-01, 158.3 m	Massive sulphide ore. Po (75%), Cpy (5%), Mt (5%), and Pn (10%)

(c) Samples from the Sublayer ores

Sample	Location	Ore Type
TL13-64A	Drill core TL13-64, 126.8 m	Sublayer massive sulphide ore. Po (70%), Cpy 15%), and Pn (5%)
TL13-97B	Drill core TL13-97, 102.1 m	Sublayer disseminated sulphide ore. Po (35%) and Cpy (15%)
TL13-98B	Drill core TL13-98, 93.8 m	Sublayer disseminate sulphide ore. Po (15%) and Cpy (10%)

Samples for bulk analysis were crushed to less than 200 mesh powder using a tungsten carbide pulverizer. Quartz sand was pulverized between samples to minimize cross contamination between samples. Samples for mineral separates were selected petrographically to minimize problems with exsolution lamellae or flames of pentlandite in pyrrhotite grains, and then crushed and sieved, retaining the 60 mesh size fraction. Initial mineral separation was carried out using magnetic methods. Finally 30-40 mg of each mineral separate was hand picked using a binocular microscope. All mineral separates for precious metal analysis, were checked by X-Ray Diffraction Spectrometry (XRD) to ensure their purity.

8.3.2 ANALYTICAL TECHNIQUES

Bulk ore precious metal analyses were carried out using a nickel sulphide fire collection procedure modified from Jackson *et al.* (1990) (Appendix I), and with quantification by inductively coupled plasma-mass spectrometry (ICP-MS) at

Memorial University of Newfoundland. The procedure used for collecting the PGE and Au combined the standard NiS fire assay technique (Hoffman *et al.*, 1978), accompanied by Te precipitation (Fryer and Kerrich, 1978), which significantly improve the recovery of the PGE and Au. A NiS button was prepared by fusing 10.0 g of powdered samples with a mixture of Ni, S, sodium carbonate, borax, and silica. The button was then dissolved in 6 M HCl, and the PGE and Au were coprecipitated with Te metal. Concentrated HNO_3 was used to dissolve the Te precipitate for ICP-MS analysis. Solid limits of detection were 0.55 ppb for Ru, 0.76 ppb for Rh, 5.1 ppb for Pd, 0.20 ppb for Re, 0.29 ppb for Os, 0.14 ppb for Ir, 1.6 ppb for Pt, and 0.93 ppb for Au.

Precious metal analyses of the mineral separates were carried out by the methods described in Chapter 5. Twenty milligram samples were dissolved in 6 M HCl, evaporated to dryness, and then redissolved by aqua regia. Sample solutions were then transformed to Cl form by three evaporations with 6 M HCl, and the precious metals separated from the base metals by cation exchange. The cation exchange procedure provides recoveries of greater than 95% of the precious metals (>99% for the PGE) and separates them from base metals (Table 5.3d). Solid limits of detection are 1.1 ppb for Ru, 0.78 ppb for Rh, 23 ppb for Pd, 0.65 ppb for Re, 0.42 ppb for Ir, 2.0 ppb for Pt, and 10 ppb for Au. Os was not determined because of its loss due to the volatility of OsO_4. Analysis of NiS fire assay beads of the reference material, SARM-7,

show good agreement with certified values with relative standard deviations of less than 8% (Table 5.6).

Platinum-group minerals in polished thin sections were analyzed by a CAMECA SX-50 electron microprobe operated at 15 kV, with beam current 10.07 nA at Memorial University of Newfoundland. In the electron microprobe analyses, the following X-ray lines were used: PtMα, PdLα, AuMα, BiMα, SKα, NiKα, TeLα, SbLα, AsKα, SnLα, FeKα, CuKα, CdLα, ZnKα, AgLα, and CoKα. Solid limits of detection are 0.1-1.0% by energy dispersive EMP.

8.4 RESULTS

8.4.1 CHEMICAL COMPOSITION OF THE ORES

XRF analyses for the major and trace element components of the bulk sulphide ores are presented in Table 8.2. SiO_2 contents reflect the proportion of silicate minerals in the ores, and are usually very low (1-5%). However, samples from disseminated ores (*i.e.*, Sublayer ore) contain significant amounts of SiO_2. Copper contents in the ores vary greatly from 0.5% to 20%, with the majority from 1% to 4%. Nickel contents in the ores, which are more consistent than Cu contents, range from 0.26% to 3.8% with the majority from 1% to 3.8%. There are no correlations between Cu and Ni contents in the ores.

Table 8.2 Chemical composition of the bulk sulphide ores at Thayer Lindsley mine by XRF analysis of pressed powder pellets. Sample locations and descriptions in Table 8.1

Sample	SiO2	TiO2	Al2O3	MgO	Fe	MnO	CaO	K2O	Na2O	P2O5	S	Cu	Ni	Cl	Cr	Sc
TL13-34B	2.03%	0.03%	0.26%	0.42%	43.8%	0.01%	0.10%	0.09%	0.00%	0.00%	48.00%	0.59%	3.21%	75	186	1
TL13-32A	2.40%	0.10%	0.35%	0.34%	44.6%	0.02%	0.27%	0.17%	0.00%	0.00%	47.02%	1.01%	2.97%	125	59	4
TL13-32F	3.04%	0.09%	0.39%	0.03%	41.5%	0.03%	0.13%	0.22%	0.00%	0.01%	44.72%	8.65%	2.66%	44	180	3
TL13-32J	1.13%	0.03%	0.14%	0.06%	42.4%	0.03%	0.05%	0.05%	0.30%	0.00%	44.75%	0.60%	3.76%	53	120	0
TL13-32N	1.79%	0.05%	0.22%	0.07%	43.9%	0.03%	0.12%	0.09%	0.00%	0.01%	47.78%	2.26%	3.10%	27	130	0
TL13-32R	8.65%	0.03%	0.15%	0.32%	34.7%	0.05%	2.81%	0.07%	0.00%	0.01%	40.42%	19.73%	1.45%	96	104	6
TL13-61A	55.67%	0.19%	7.48%	0.53%	13.0%	0.03%	2.76%	2.77%	0.00%	0.02%	15.78%	4.19%	0.26%	434	10	2
TL13-35C	0.54%	0.01%	0.00%	0.04%	45.6%	0.02%	0.05%	0.00%	0.00%	0.00%	46.60%	1.11%	3.26%	58	7	7
TL13-63A	1.07%	0.08%	0.15%	0.00%	44.0%	0.02%	0.09%	0.07%	0.00%	0.00%	47.28%	1.20%	3.41%	60	208	2
TL13-98A	2.39%	0.06%	0.19%	1.22%	40.9%	0.01%	0.64%	0.04%	0.00%	0.01%	48.10%	3.13%	3.20%	598	95	6
TL13-96A	2.41%	0.05%	0.28%	0.99%	39.4%	0.01%	0.73%	0.05%	0.00%	0.01%	44.28%	12.11%	2.80%	196	93	6
TL13-97A	48.38%	0.65%	8.71%	4.81%	17.5%	0.10%	2.92%	2.94%	0.89%	0.08%	8.23%	0.94%	0.38%	1469	116	13
TL13-109A	2.39%	0.15%	0.29%	0.38%	46.8%	0.02%	0.37%	0.14%	0.00%	0.01%	41.05%	3.67%	3.17%	102	220	3
TL13-162B	3.68%	0.09%	0.46%	0.49%	42.6%	0.01%	0.12%	0.23%	0.00%	0.01%	45.10%	2.62%	3.69%	116	90	7
TL13-161F	1.34%	0.06%	0.17%	0.09%	43.9%	0.01%	0.06%	0.09%	0.00%	0.00%	46.84%	1.43%	3.78%	68	99	1
TL13-161L	1.75%	0.05%	0.26%	0.46%	43.6%	0.01%	0.19%	0.05%	0.00%	0.00%	47.54%	1.42%	3.60%	222	101	3
TL15-01A	9.38%	0.10%	1.30%	1.84%	39.6%	0.02%	2.59%	0.17%	0.00%	0.01%	41.79%	0.53%	3.46%	293	85	7
TL13-64A	20.15%	0.25%	3.79%	4.06%	28.9%	0.08%	4.74%	0.44%	0.00%	0.03%	27.59%	8.40%	1.65%	290	416	13
TL13-97B	17.81%	0.44%	3.68%	8.56%	27.5%	0.04%	2.48%	0.31%	0.00%	0.03%	30.69%	4.88%	2.45%	1740	222	27
TL13-98B	42.37%	0.46%	7.01%	6.12%	19.8%	0.08%	5.84%	0.81%	0.70%	0.04%	14.46%	1.18%	0.86%	539	465	20

Sample	V	Zn	Ga	As	Rb	Sr	Y	Zr	Nb	Ba	Ce	Pb	Th	U	total	Wt% Sulphide
TL13-34B	44	108	0.00	2.69	4.1	2.13	3.0	22.2	2.12	5.1	0.0	34	<6	<7	98.6%	97.0%
TL13-32A	134	66	0.38	0.00	6.4	4.10	3.7	17.5	3.20	4.8	0.0	55	9.24	<7	99.4%	96.3%
TL13-32F	112	668	0.00	0.00	7.8	2.81	4.8	29.6	3.56	7.7	0.0	131	<6	<7	101.6%	96.1%
TL13-32J	35	22	0.00	17.29	2.7	0.00	0.4	6.5	2.07	3.3	0.9	84	<6	<7	93.1%	98.4%
TL13-32N	66	74	0.00	1.31	4.2	1.55	3.2	8.3	1.68	1.2	0.0	85	7.88	<7	99.5%	97.6%
TL13-32R	57	1874	0.00	17.01	5.5	11.79	7.6	8.5	3.13	0.0	2.6	35	16.4	<7	108.6%	88.9%
TL13-61A	0	529	15.68	20.12	60.6	153	61.6	363	26.3	429	123	146	81.7	<7	102.9%	32.5%
TL13-35C	28	35	0.00	18.28	1.0	0.51	0.0	3.3	3.69	0.0	0.1	28	<6	<7	97.3%	99.3%
TL13-63A	62	42	0.33	0.00	3.3	0.00	2.8	9.2	3.31	1.9	0.0	29	<6	<7	97.4%	98.5%
TL13-98A	79	571	0.00	10.10	2.6	9.41	3.4	18.5	3.09	2.6	0.3	232	<6	<7	100.0%	95.5%
TL13-96A	72	1231	0.00	0.00	3.8	10.34	3.6	9.9	3.60	5.0	0.0	116	7.28	<7	103.2%	95.6%
TL13-97A	102	292	13.50	0.00	162	206	37.7	353	16.5	612	77.6	125	12.7	<7	96.9%	28.3%
TL13-109A	213	276	0.00	0.00	6.7	0.54	5.4	26.6	6.10	9.0	1.4	20	10.0	<7	98.6%	96.2%
TL13-162B	117	179	0.00	7.52	7.3	4.07	4.1	18.0	2.59	14.5	0.0	40	6.60	<7	99.2%	94.9%
TL13-161F	80	49	0.00	0.00	3.0	0.60	0.8	18.5	2.39	2.3	0.4	24	8.59	<7	97.8%	98.1%
TL13-161L	78	66	0.00	5.95	1.5	5.80	2.8	9.7	2.89	2.7	0.0	73	5.38	<7	99.0%	97.2%
TL15-01A	84	3	4.00	10.24	9.6	30.79	10.1	47.3	5.52	13.3	1.8	40	6.57	<7	100.9%	84.7%
TL13-64A	97	732	0.00	17.97	20.4	119	17.7	63.2	6.35	58.1	14.8	10	7.27	<7	100.3%	66.6%
TL13-97B	212	295	13.55	0.00	22.5	58.27	17.1	61.1	8.22	19.7	0.0	1739	0.98	<7	99.3%	66.4%
TL13-98B	142	154	11.30	0.39	37.4	229	23.3	244	7.31	101	78.7	47	12.0	<7	100.0%	36.5%

% – Weight percentage, all other – ppm

8.4.2 PRECIOUS METAL CONCENTRATIONS OF THE ORES IN THE 4B ORE ZONE

Precious metal analytical results of the bulk ores using the NiS sulphide fire assay method, results of four sample duplicates, solid limits of detection, and results for the geological reference material SARM-7 are presented in Table 8.3. The concentrations of these metals recalculated to 100 percent sulphides (Naldrett, 1984) are shown in Table 8.4. Compared to the highly variable Pt, and Au contents, the concentrations of Ru, Rh, Pd, Os, and Ir are less variable. The ruthenium content in bulk ores varies from 8.5 ppb to 239 ppb with an mean of 109 ppb. Two of the samples (TL13-35C and TI13-61A) show extremely low concentrations of Ru. Rhodium contents range from 80 ppb to 1,120 ppb with the majority of samples having concentrations between 200 to 350 ppb with an mean of 319 ppb. One sample (TL13-61A) has an extremely high concentration of Rh (1,120 ppb). Palladium contents are very high, ranging from 928 ppb to 20,900 ppb with the majority of samples having concentrations from 3000 ppb to 6000 ppb. Two of the samples (TL13-61A and TL13-32R) have extremely high Pd (20,900 ppb and 15,600 ppb). Osmium and iridium contents are usually low, osmium ranging from 1 ppb to 37 ppb and iridium from 1 ppb to 90 ppb. Both platinum and gold contents vary greatly, Pt ranging from 181 ppb to 13,300 ppb and Au from 7 ppb to 1283 ppb.

Table 8.3 Precious metal concentrations (ppb) of the bulk sulphide ores at the Thayer Lindsley Mine

sample	Ru	Rh	Pd	Os	Ir	Pt	Au
TL13-34b (1)**	201	265	6619	19.7	75.4	988	6.6
TL13-34b (2)**	201	281	5169	21.6	77.4	1017	8.4
TL13-34B	201	273	5894	20.7	76.4	1002	7.5
TL13-32A (1)**	54.2	177	5408	9.1	30.5	334	16.6
TL13-32A (2)**	61.3	218	6329	8.9	34.5	524	26.0
TL13-32A	57.8	197	5868	9.0	32.5	429	21.3
TL13-32F (1)**	83.0	313	4942	14.6	45.5	197	176
TL13-32F (2)**	90.1	303	5034	14.7	46.2	151	129
TL13-32F	86.5	308	4988	14.6	45.9	174	153
TL13-32J (1)**	178	348	1688	28.0	75.5	2091	32.7
TL13-32J (2)**	184	358	1580	25.7	77.7	1562	13.8
TL13-32J	181	353	1634	26.8	76.6	1826	23.3
TL13-32N	156	324	4785	26.1	73.3	5079	1008
TL13-32R	44.4	327	13836	9.1	45.3	11817	693
TL13-61A	5.0	365	6800	0.6	0.4	96	418
TL13-35C	8.5	80	7338	1.1	5.2	360	18.7
TL13-63A	97.3	290	4251	12.5	5[illegible]2	3806	19.1
TL13-98A	117	237	9472	15.1	56.9	1706	112
TL13-96A	57.2	241	6059	6.6	43.5	1356	226
TL13-97A	16.2	27	1497	5.0	14.7	1793	49.0
TL13-109A	37.9	138	3052	8.4	25.8	2025	130
TL13-162B	107	293	3772	20.8	68.1	1290	129
TL13-161F	160	326	2538	20.7	76.9	1142	118
TL13-161L	135	275	5062	22.2	63.2	1338	84.6
TL15-01A	74.1	178	4304	10.5	39.3	472	53.0
TL13-64A	137	297	3126	27.1	64.8	374	115
TL13-97A	56.3	278	1164	12.6	23.6	2995	97.5
TL13-98B	87.6	106	339	13.5	29.5	2165	42.3
SARM-7(this run)	3[illegible]8	207	1346	48.3	70.6	3620	251
SARM-7(certified)	430	240	1530	63	74	3740	310
SARM-7(Jackson et al)	397	212	1353	53	71	3395	253
LOD*	0.55	0.76	5.2	0.29	0.14	1.63	0.93

* LOD: Limits of detection

** (1) and (2): Duplicates

Table 8.4 Precious metal concentrations (ppb) of the bulk sulphide ores reculculated to 100 percent sulphides at the Thayer Lindsley Mine

sample	Ru	Rh	Pd	Os	Ir	Pt	Au	Wt% Sulphide
TL13-34B	207	282	6077	21.3	78.8	1033	8	97.0%
TL13-32A	60	205	6092	9.4	33.7	445	22	96.3%
TL13-32F	90	320	5189	15.2	47.7	181	159	96.1%
TL13-32J	184	359	1661	27.3	77.8	1856	24	98.4%
TL13-32N	159	332	4902	26.8	75.1	5203	1032	97.6%
TL13-32R	50	368	15569	10.2	50.9	13297	780	88.9%
TL13-61A	15	1120	20898	2.0	1.2	296	1284	32.5%
TL13-35C	9	81	7389	1.1	5.2	362	19	99.3%
TL13-63A	99	294	4317	12.7	57.0	3865	19	98.5%
TL13-98A	122	248	9923	15.9	59.6	1788	117	95.5%
TL13-96A	60	252	6337	6.9	45.5	1419	236	95.6%
TL13-97A	57	96	5298	17.8	52.0	6343	173	28.3%
TL13-109A	39	143	3173	8.8	26.8	2105	135	96.2%
TL13-162B	113	309	3976	21.9	71.8	1359	136	94.9%
TL13-161F	163	332	2586	21.0	78.4	1164	120	98.1%
TL13-161L	139	283	5207	22.9	65.1	1376	87	97.2%
TL15-01A	87	211	5080	12.4	46.4	557	63	84.7%
TL13-64A	206	446	4695	40.8	97.3	561	173	66.6%
TL13-97A	85	419	1753	19.0	35.5	4510	147	66.4%
TL13-98B	240	291	928	36.9	80.8	5924	116	36.5%
Average	109	319	6052	17.5	54.3	2682	242	

8.4.3 PRECIOUS METAL CONCENTRATION OF MAJOR ORE MINERALS

Analytical results for the precious metals in the major ore minerals using the cation separation method described in Chapter 5 are presented in Table 8.5.

Magnetite

The concentrations of precious metals in magnetite are usually very low; Ru ranges from 0.6 ppb to 24 ppb; Rh from 4.2 ppb to 20.9 ppb; Pd from less than 1 ppb to 141 ppb (with the exception of two samples which have extremely high Pd concentrations of 245,000 ppb and 4,800 ppb); Re from 3.87 ppb to 147 ppb (with the exception of three samples which have high Re concentrations from 147 ppb to 1710 ppb); Ir from less than 0.42 ppb to 2.93 ppb; Pt from 34 ppb to 98 ppb (with the exception of one sample which has 1610 ppb); and Au from less than 1 ppb to 843 ppb with the majority of the samples from 1 ppb to 32 ppb. Some of magnetite samples with anomalously high concentrations of one or two precious metals probably contained minor precious metal-enriched phases (see later in this chapter). Chapter 7 in this thesis and Li *et al.* (1993) reported an oval inclusion of froodite in magnetite in the Deep Copper Zone of the Strathcona Mine.

Table 8.5 Precious metal concentrations (ppb) of the major ore minerals in the Thayer Lindsley mine

	Ru	Rh	Pd	Re	Ir	Pt	Au
Magnetite (20 mg)							
TL13-34B	1.72	4.2	39	32	<0.42	38	2
TL13-32A	2.14	5.8	142	75	<0.42	44	844
TL13-32F	23.7	5.0	54	21	<0.42	36	4
TL13-32J	4.74	49.2	244700	64	2.4	1610	13
TL13-32N	6.80	9.1	43	37	0.6	37	12
TL13-32R	2.92	5.1	77	81	0.5	51	9
TL13-35C	2.62	4.6	<23.5	4	<0.42	34	1
TL13-63A	19.0	4.2	<23.5	1710	<0.42	54	2
TL13-98A	<1.1	8.2	<23.5	207	0.7	44	32
TL13-96A	4.11	20.8	<23.5	60	2.9	92	23
TL13-109A	<1.1	10.0	<23.5	21	1.4	40	10
TL13-162B	2.34	7.5	26	39	<0.42	47	6
TL13-161F	<1.1	9.3	4800	148	<0.42	38	221
TL13-161L	1.51	7.6	<23.5	90	<0.42	46	478
TL15-01A	2.66	19.4	<23.5	23	2.9	98	129
Chalcopyrite (20 mg)							
TL13-34B	12.9	86.2	1370	525	5.3	45	143
TL13-32A	12.3	69.9	649	75	4.1	40	14
TL13-32F	12.8	8.5	1170	5	<0.42	31	80
TL13-32J	22.2	17.5	863	360	2.0	32	14
TL13-32N	11.4	6.0	369	1	<0.42	32	235
TL13-32R	12.0	4.4	439	113	<0.42	37	9
TL13-35C	6.0	4.0	499	90	<0.42	38	10
TL13-63A	10.4	5.4	245	19	0.7	32	414
TL13-98A	16.0	67.9	1280	67	1.1	266	27
TL13-96A	78	179	332	99	9.0	77	3060
TL13-97A	87	9.8	801	17	0.5	40	103
TL13-109A	8.6	50.0	324	56	1.3	37	195
TL13-162B	8.6	14.5	27	34	<0.42	36	17
TL13-161F	9.0	6.6	49	253	1.1	49	108
TL13-161L	7.2	5.8	151	1	<0.42	35	556
TL13-64A	6.6	7.2	<23.5	<0.65	<0.42	45	17
TL13-97A	58.3	65.6	63	45	1.6	323	375
TL13-98B	29.9	128	168	78	2.2	121	31
LOD*	1.1	0.78	23.5	0.65	0.42	2.0	10.5

LOD: Limits of detection

Table 8.5 Precious metal concentrations (ppb) of the major ore minerals in the Thayer Lindsley mine (continued)

	Ru	Rh	Pd	Re	Ir	Pt	Au
Pyrrhotite (20 mg)							
TL13-34B	239	33	350	30	23.2	4	<10.5
TL13-32A	75	107	332	37	19.3	46	<10.5
TL13-32F	148	288	693	31	31.5	34	17
TL13-32J	217	330	127	184	48.6	33	<10.5
TL13-32N	210	309	267	10	38.0	4	<10.5
TL13-32R	292	120	579	126	10.6	2	<10.5
TL13-35C	15	98	355	44	7.1	34	<10.5
TL13-63A	86	73	258	66	1.4	16	17
TL13-98A	176	81	436	23	2.5	24	21
TL13-96A	141	175	242	104	6.0	129	20
TL13-109A	88	102	10300	216	8.0	23	11
TL13-162B	145	76	64	229	0.4	18	<10.5
TL13-161F	126	98	315	13	24.2	8	<10.5
TL15-01A	200	59	79	670	12.3	2	<10.5
Pentlandite (20 mg)							
TL13-34B	189	83	12000	51	18.7	40	21
TL13-32A	68	54	16100	112	12.6	4	31
TL13-32F	83	157	11800	5	9.6	<2.0	998
TL13-32J	176	277	4620	85	36.0	<2.0	59
TL13-32N	155	221	12800	208	17.5	2	1110
TL13-35C	12	60	16700	381	3.6	8	217
TL13-63A	96	76	14100	60	19.7	<2.0	49
TL13-98A	71	43	6360	14	2.0	112	61
TL13-96A	162	62	9390	81	1.8	9	753
TL13-109A	60	30	4490	22	1.5	<2.0	498
TL13-162B	81	38	1250	181	<0.42	<2.0	842
TL13-161F	117	48	1450	406	5.5	<2.0	5920
TL13-161L	125	25	2120	5	1.1	3	855
TL15-01A	88	94	3660	23	2.0	14	<10.5
TL13-64A	111	72	1600	45	1.4	12	64
Marcasite (20 mg)							
TL13-161A	10	<0.78	<23.5	1	<0.42	<2.0	<10.5
97bma	203	114	32.1	43	1.6	8	<10.5
Pyrite (20 mg)							
161apy	12	<0.78	<23.5	<0.65	0.0	3	231
63apy	11	<0.78	233	1	0.0	7	201
Limits of Detection (20 mg)							
LOD*	1.1	0.78	23.5	0.65	0.42	2.0	10.5

Chalcopyrite

The concentration of precious metals in chalcopyrite is usually higher than in magnetite (Table 8.5): Ru ranges from 6.0 ppb to 87 ppb, Rh from 4.0 ppb to 178 ppb, Pd from 12 ppb to 1280 ppb, Re from less than 0.65 ppb to 525 ppb, Ir from less than 0.42 ppb to 9.0 ppb, Pt from 31.1 ppb to 265 ppb, and Au from 10.2 ppb to 3060 ppb. Like magnetite, some of the chalcopyrite samples have anomalously high concentrations of one or two of the precious metals suggesting that they contained a minor precious metal-enriched phase.

Pyrrhotite

Pyrrhotite is more enriched in Ru, Rh, Re, and Ir than magnetite and chalcopyrite (Table 8.5). The contents of precious metals in pyrrhotite are: Ru ranges from 15.4 ppb to 292 ppb; Rh from 33.2 ppb to 329 ppb; Pd from 63.8 ppb to 692 ppb (with exception of one sample with 10,300 ppb); Re from 9.9 ppb to 229 ppb; Ir from 0.43 ppb to 48.6 ppb; Pt from 1.66 ppb to 129 ppb; and Au from less than 10.5 ppb to 20 ppb. Compared to the other major ore minerals, the concentrations in pyrrhotite are generally more consistent.

Pentlandite

Pentlandite contains more precious metals than the other major ore minerals, and is particularly enriched in Pd and Au (Table 8.5). The contents of precious

metals in pyrrhotite are: Ru ranges from 12.0 ppb to 189 ppb; Rh from 24.8 ppb to 277 ppb; Pd from 1,250 ppb to 16,700 ppb; Re from 4.98 ppb to 406 ppb; Ir from less than 0.42 ppb to 36.0 ppb; Pt from 2.0 ppb to 112 ppb; and Au from 8.92 to 5,900 ppb.

Pyrite

The two pyrite samples show very low contents of PGE, but contain about 200 ppb Au.

Marcasite

The two marcasite samples are very low in Pd, Re, Ir, Pt, and Au, but one sample (TI13-97B) contains 203 ppb Ru and 114 ppb Rh.

8.5 DISCUSSION

8.5.1 MASS BALANCES

In order to calculate what proportions of precious metals are present in the major ore minerals, all drill cores were vertically cut into three parts: one for bulk analyses, one part for mineral separates, and one for petrographic thin sections, so that sample similarity was maintained. The bulk concentrations of the precious metals are shown in Table 8.3, and the modal abundances of the

major ore minerals are presented in Table 8.6. Since pyrrhotite, pentlandite, chalcopyrite, and magnetite account for over 95% of the ore minerals, the concentrations of the precious metals and the modal abundance of these minerals are used to calculate the modal concentrations of the bulk ores. Since the purpose of this calculation is to estimate the proportion of the precious metals which are homogenously distributed in the major ore minerals versus those in trace discrete precious metal phases, data with anomalously high concentrations suggestive of precious metal-enriched inclusions are not included in the model calculation. The calculated results are presented in Table 8.6 and Figure 8.7. Based on this model concentration, the proportion of the precious metals which is homogenously distributed in the four ore minerals is: 89% (Ru), 33% (Rh), 10% (Pd), 21% (Ir), 3% (Pt), and 39% (Au) (Figure 8.7).

The low proportions of Rh, Pd, Pt, and Au found in the major ore minerals are not surprising. Electron microprobe analyses (Tables 8.7-8.10) show large amounts of Rh, Pd, Pt and Au occur in discrete precious metal-rich phases in the sulphide ores (see later in this chapter). Chapters 4 and 7 in this thesis and Li *et al.* (1993) have shown similar results from the Deep Copper Zone of the Strathcona Mine. The question of why the calculated model concentrations of Ir are less than those of bulk analysis is unknown and needs to be investigated further.

Table 8.6 Model calculations based on the precious metal concentrations in the mineral separates and modal abundance of the minerals, and percentage difference of the metals compared to the bulk fire assay analysis

	Mineral Modal Abundance (%)				Precious Metal Contents Based on Model Calculations (ppb)						Percentage Difference Compared to Bulk Fire Assay Analysis* (%)					
Sample	MT	CPY	PO	PN	Ru	Rh	Pd	Ir	Pt	Au	Ru	Rh	Pd	Ir	Pt	Au
TL13-34b	5	20	68	5	175	44	1113	18	15	30	13%	84%	81%	77%	98%	-305%
TL13-32A	5	5	85	5	68	97	1125	17	43	48	-18%	51%	81%	47%	90%	-123%
TL13-32F	10	20	65	5	105	197	1282	21	32	77	-22%	36%	74%	54%	81%	50%
TL13-32J	5	5	85	5	194	297	12617	43	110	6	-8%	16%	-672%	43%	94%	76%
TL13-32N	10	15	70	5	157	229	887	28	12	93	-1%	29%	81%	62%	100%	91%
TL13-32R	5	30	60	5	179	73	483	6	15	5	-303%	78%	97%	86%	100%	99%
TL13-61A	0	5	10	0	0	0	1	0	2	1	93%	100%	100%	100%	98%	100%
TL13-35C	10	15	70	5	13	72	1158	5	33	14	-48%	10%	84%	-1%	91%	26%
TL13-63A	10	10	75	2	69	57	501	2	20	55	29%	80%	88%	97%	99%	-187%
TL13-98A	10	10	70	10	132	69	1071	2	59	27	-13%	71%	89%	96%	97%	76%
TL13-96A	10	20	40	5	81	111	634	5	77	659	-41%	54%	90%	89%	94%	-192%
TL13-97A	0	15	35	0	13	1	120	0	6	15	20%	95%	92%	99%	100%	69%
TL13-109A	10	20	65	5	62	79	7014	6	26	72	-64%	43%	-130%	78%	99%	45%
TL13-162B	5	10	80	5	121	64	118	0	20	49	-13%	78%	97%	99%	98%	62%
TL13-161F	5	5	85	2	110	85	539	21	12	138	31%	74%	79%	73%	99%	-17%
TL13-161L	5	5	90	5	7	2	114	0	4	94	95%	99%	98%	100%	100%	-12%
TL15-01A	5	5	75	10	159	55	426	10	8	12	-114%	69%	90%	76%	98%	76%
TL13-64A	0	15	70	5	7	5	82	0	7	6	95%	98%	97%	100%	98%	95%
TL13-97A	0	15	35	0	9	10	10	0	48	56	84%	96%	99%	99%	98%	42%
TL13-98B	0	10	15	0	3	13	17	0	12	3	97%	88%	95%	99%	99%	93%

* (measured concentration - model concentration)/measured concentration x 100%

8.5.2 THE IMPORTANCE OF PRECIOUS METAL MINERALS (PGM)

Since, in the Thayer Lindsley ores, large proportions of the Rh, Pd, Pt and Au in the ore are not in solid solution in the major c . minerals, they probably predominantly occur as precious metal-enriched discrete phases. Some electron microprobe analyses of these precious metal minerals are presented in Tables 8.7-8.10.

The consistently high Pd contents in pentlandite (1.2-16.7 ppm) suggest that Pd is or was in solid solution in pentlandite (Table 8.5). Cabri *et al.* (1984) has reported 0.2-1.4% Pd in pentlandite from Stillwater ores using the electron microprobe and PIXE. Chai *et al.* (1993) detected a maximum of 2.8 ppm Pd in pentlandite from the Jinchuan deposit using accelerator mass spectrometry (AMS). The small proportion of Pd present in solid solution in the pentlandite, accounts for less than 10% of the total Pd content of the ores (Table 8.6 and Figure 8.7). Therefore, additional Pd-enriched phases are present in the ores probably as discrete precious metal phases. Figures 8.8-8.9 and Table 8.7-8.8 show that michenerite [$Pd(Te,Bi)_2$] and an unnamed mineral ($PdSb_{0.4}$) are minerals which contain high concentrations of Pd. The michenerite at the Thayer Lindsley Mine which contains 20%-25% Pd, 31%-56% Te, and 19%-50% Bi (Table 8.7), is different from that reported by Cabri and Laflamme (1976), and Li and Naldrett (1993). The unnamed mineral ($PdSb_{0.4}$) at the Thayer Lindsley Mine contains 66%-70% Pd and 30%-33% Sb (Table 8.8), and

Table 8.7 Electron microprobe analyses of the michenerite from the 4B Ore Zone

		Element weight percent					
Sample	Dimensions (μm)	Pd	Fe	Ni	Bi	Te	Total*
TL13-98A	4 x 6	24.0	2.38	2.02	19.8	51.8	100
TL13-98A	20 x 30	24.1	1.11	0.93	17.2	56.6	100
TL13-63A	5 x 7	22.9	3.95	0.16	29.7	43.3	100
TL13-63A	2 x 2	20.7	2.45	2.05	48.3	26.5	100
TL13-63A	5 x 6	21.8	4.47	0.60	45.9	27.3	100
TL13-63A	3 x 5	23.0	2.54	3.04	27.8	43.7	100
TL13-63A	15 x 32	22.6	0.48	0.78	33.7	42.4	100
TL13-63A	12 x 18	20.4	1.18	1.41	48.6	28.4	100
TL13-63A	2.5 x 3.6	24.7	3.89	1.04	16.4	53.9	100
TL13-63A	40 x 40	20.8	0.53	0.00	47.6	31.1	100
TL13-63A	30 x 36	22.8	0.45	0.41	36.6	39.7	100

	Atomic proportions						
Sample	Pd	Fe	Ni	Total	Bi	Te	Total
TL13-98A	0.75	0.14	0.11	1.00	0.31	1.34	1.65
TL13-98A	0.86	0.08	0.06	1.00	0.31	1.69	2.00
TL13-63A	0.75	0.25	0.01	1.00	0.49	1.18	1.67
TL13-63A	0.71	0.16	0.13	1.00	0.84	0.76	1.60
TL13-63A	0.69	0.27	0.03	1.00	0.74	0.73	1.47
TL13-63A	0.69	0.15	0.17	1.00	0.43	1.09	1.52
TL13-63A	0 91	0.04	0.06	1.00	0.69	1.42	2.11
TL13-63A	0.81	0.09	0.10	1.00	0.98	0.94	1.92
TL13-63A	0.73	0.22	0.06	1.00	0.25	1.32	1.57
TL13-63A	0.95	0.05	0.00	1.00	1.11	1.19	2.30
TL13-63A	0.93	0.04	0.03	1.00	0.76	1.35	2.12

* Recaculated to 100%

Table 8.8 Electron microprobe analyses of the unnamed Pd-Sb mineral from the 4B Ore Zone

		Element weight percent			Atomic proportions	
Sample	Dimensions (μm)	Pd	Sb	Total*	Pd	Sb
TL13-32R	2.5 x 3	67.2	32.8	100	1	0.43
TL13-32R	1 x 1	66.7	33.7	100	1	0.44
TL13-32N	3.5 x 7.5	70.1	29.9	100	1	0.37

* Recaculated to 100%

has not been reported before. Most of these precious metal minerals (3-40 μm) occur at the grain boundaries between the major ore minerals or in microfractures in the ores (Figures 8.9b, 8.9d, 8.9f, and 8.10a-b). A few tiny inclusions were in the major ore minerals (Figure 8.9a).

Although chalcopyrite contains a small amount of Pt (30-300 ppb), over 99% of the Pt is not in solid solution in the four principle ore minerals (pyrrhotite, pentlandite, chalcopyrite, and magnetite). It must occur predominantly in discrete Pt-rich minerals. Electron microprobe analysis has identified an euhedral unnamed Pt-Rh-As mineral which contains 10%-47% Pt, 10%-30% Rh, and 36%-48% As (Table 8.9 and Figures 8.10). Most of these minerals (4-12μm) occur at the grain boundaries between the major ore minerals or in microfractures (Figures 8.8b-f and 8.10a-b). A few occurred as tiny inclusions in the ore minerals (Figure 8.8a). The presence of other Pt minerals needs to be further investigated.

A small proportion of Au occurs in pentlandite and chalcopyrite, but over 60% of the Au occurs as discrete Au alloys or as minor inclusions in the ore minerals. Electron microprobe analysis has identified one such alloy (Au-Ag) which contains 86%-94% Au and 6%-14% Ag (Figure 8.11) (Table 8.10). Most of these alloys were found as tiny discrete phases (3-16μm) located either at grain boundaries and in microfractures of the major ore minerals, or

Table 8.9 Electron microprobe analyses of the unnamed Pt–Rh–As mineral from the 4B Ore Zone

		Element weight percent				Atomic proportions			
Sample	Dimensions (μm)	Pt	Rh	As	Total*	Pt	Rh	total	As
TL13–32R1	1.5 x 4	33.5	23.1	43.3	100	0.43	0.57	1.00	1.46
TL13–32R1	4 x 4	25.5	30.8	43.8	100	0.30	0.70	1.00	1.36
TL13–32N?	3 x 4.8	25.5	38.6	35.9	100	0.26	0.74	1.00	0.95
TL13–32N2	3.5 x 8	46.5	15.2	38.2	100	0.62	0.38	1.00	1.32
TL13–32N2	3 x 12	23.8	39.9	36.3	100	0.24	0.76	1.00	0.95
TL13–98A1	5 x 6	9.5	42.2	48.3	100	0.11	0.89	1.00	1.40
TL13–98A4	6 x 9	9.8	42.5	47.6	100	0.11	0.89	1.00	1.37
TL13–63A2	6 x 12	9.7	47.1	43.2	100	0.10	0.90	1.00	1.14

* Reculated to 100%

Table 8.10 Electron microprobe analyses of the gold alloy from the 4B Ore Zone

		Element weight percent			Atomic proportions		
Sample	Dimensions (μm)	Au	Ag	TOtal*	Au	Ag	Total
TL13–63A	2 x 3	86.3	13.7	100	0.78	0.22	1.00
TL13–98A	2 x 2	90.0	10.0	100	0.83	0.17	1.00
TL13–98A	8 x 24	93.6	6.4	100	0.89	0.11	1.00
TL13–98A		91.0	10.5	100	0.83	0.17	1.00

* Reculated to 100%

as inclusions in these ore minerals.

Although mass balance calculations indicate that considerable amounts of Ir may also form discrete precious metal phases, the limited numbers of electron microprobe analyses have not yet found any discrete minerals of these metals. More work is required to search for the Ir minerals.

8.5.3 SPATIAL DISTRIBUTION AND VARIATION OF PRECIOUS METALS IN THE ORES AND MAJOR ORE MINERALS FROM THE 4B ORE ZONE

In order to study the spatial distributions of the precious metals within the 4B Ore Zone, two horizontal transverse sections through the 4B Ore Zone were systematically sampled: (1) a horizontal transection along a drill core (TL13-32) through the 4B Ore Zone toward the norite of SIC (Figure 8.5); and (2) a horizontal transection along strike through along the 4B Ore Zone (Figure 8.6). The analytical results are shown in Table 8.3-5.

The distributions of precious metals in the bulk ore and in the individual minerals are shown in Figures 8.12-13. In a transection along the drill core (TL13-32) through the 4B Ore Zone, Pt contents in the major minerals (pyrrhotite and pentlandite) decrease toward the SIC, whereas the Pt content in the bulk ores show the reverse trend, suggesting more discrete Pt phases in the ores toward the SIC. However, except for Pt, there are no overall apparent systematic spatial variations of precious metals in the same minerals from

different parts of the 4B Ore Zone (Figures 8.12b-e and Figures 8.13b-e) although minor bulk variation in NiS sulphide fire analyses show that the ores from the margin are enriched in Pd, Pt and Au (Figure 8.12a and Figure 8.13a). There are some analyses with extremely high concentrations of Pd, Rh, Pt, and Au, probably due to minor inclusions of precious metal containing discrete phases. These results are in agreement with electron microprobe analysis (Tables 8.7-8.10) that show that Pd, Rh, Pt, and Au are dominantly in separate discrete phases either as minor inclusions in these minerals or as precious metal alloys containing S, As,Bi, Fe, Ni, Pt, and Pd located at the boundaries of these minerals.

8.6 SUMMARY AND CONCLUSIONS

Data presented in this chapter show the following:

(1) The distributions of the precious metals show that considerable amounts of the Ru, Rh, Pd, and Ir are homogenously distributed (solid solution?) in the sulphides and magnetite, whereas the remaining precious metals are dominantly in separate discrete phases either as minor inclusions in the ore minerals or as precious metal alloys at the boundaries of the ore minerals.

(2) Model mass balance calculations indicate that the proportions of

the precious metals which are homogenously distributed in these four ore minerals, are 89% (Ru), 33% (Rh), 10% (Pd), 21% (Ir), 3% (Pt), and 39% (Au).

(3) Michenerite and the unnamed ($PdSb_{0.4}$) mineral are the most Pd-enriched minerals, and the unnamed (Pt,Rh)As are the most Pt- and Rh-enriched minerals found in the 4B Ore Zone at the Thayer Lindsley Mine. The presence of other Pt minerals needs to be further investigated to account for the Pt abundance in the bulk ores.

(4) There are no overall apparent systematic spatial variations of precious metals in the same minerals from different parts of the 4B Ore Zone, although bulk NiS sulphide fire analyses show that the ore from the orebody margins are more enriched in Pd, Pt and Au.

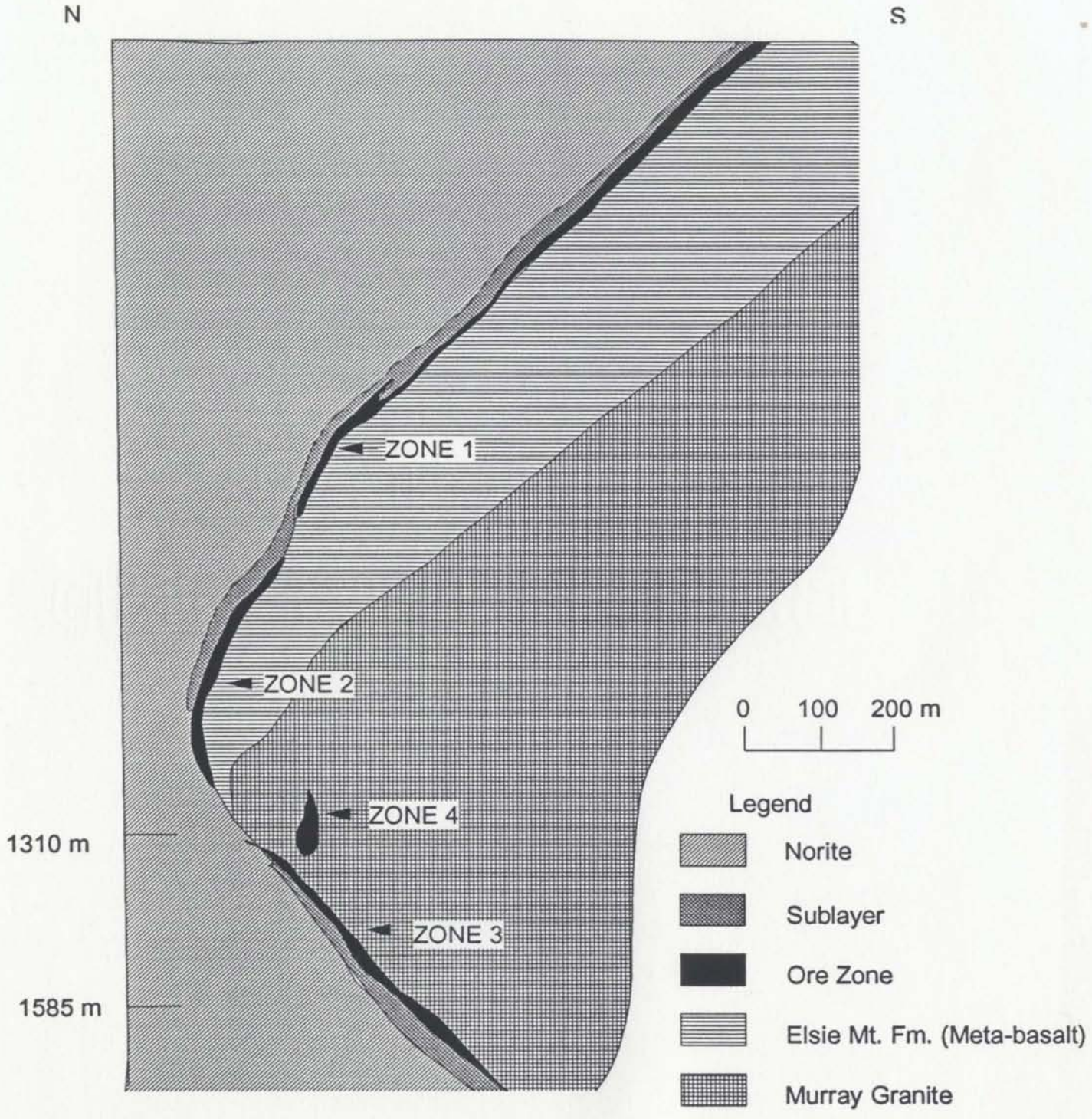

Figure 8.1 Geological vertical cross section through the Thayer Lindsley Mine showing the distribution of ore zones (drawn after Binney et al., 1992)

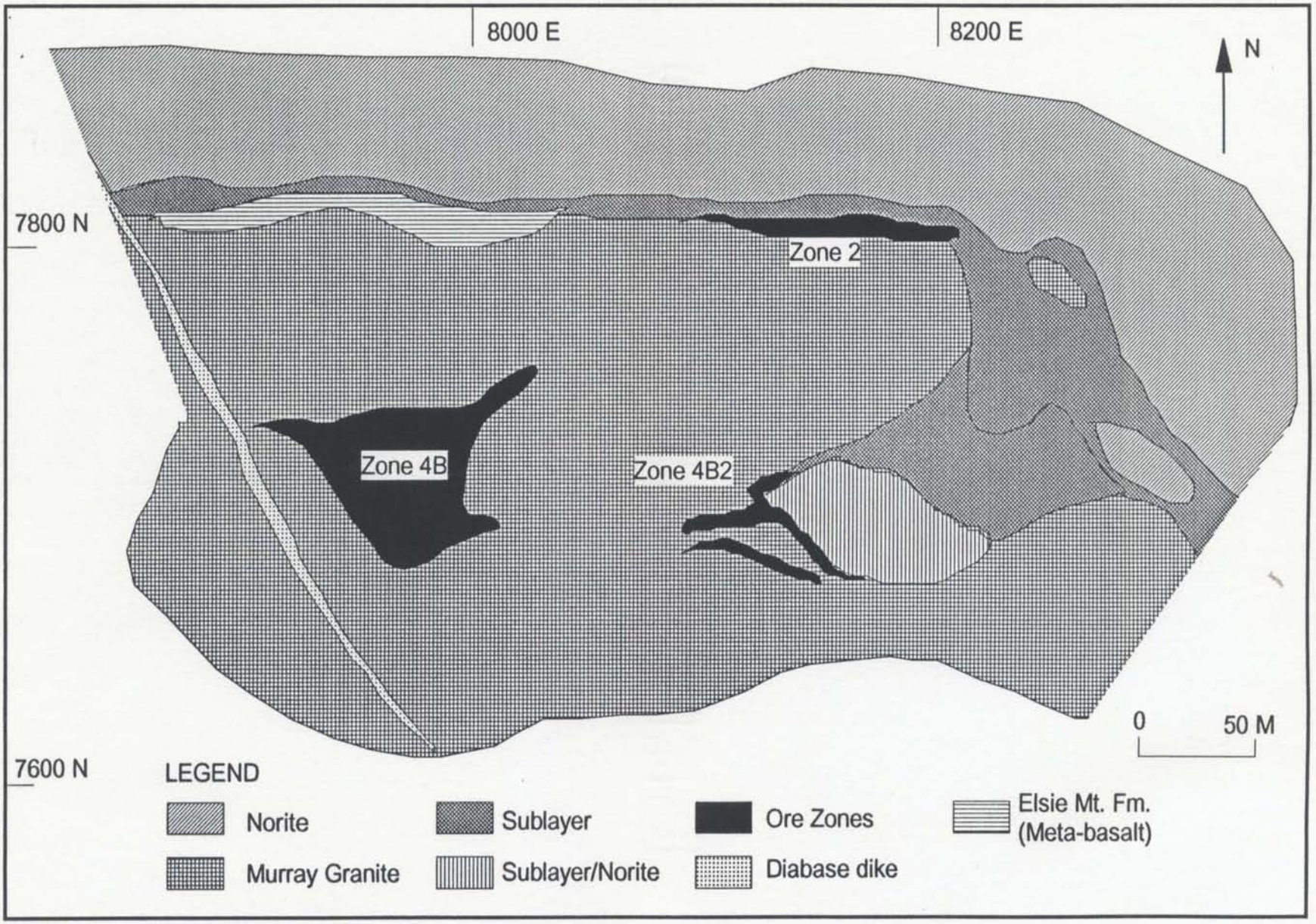

Figure 8.2 Horizontal geological cross section on the 1310 level (see also Figure 8.1) showing the geology and ore zones of the Thayer Lindsley Mine (after Binney et al., 1992)

a


po
cpy
0 1 3 5 7
CENTIMETRES
TL13-63b

b


0 1 3 5 7
CENTIMETRES
92-ZC-02
po
cpy

c

d

e


cpy
po
po
0 1 3 5 7
CENTIMETRES
TL13-162c

f


cpy
po
0 1 3 5 7
CENTIMETRES
TL13-161d

g


po
cpy
si
po
0 1 3 5 7
CENTIMETRES
TL13-161o

h


0 1 3 5 7
CENTIMETRES
92-ZC-01
po
cpy
si

i


si
sul
si
0 1 3 5 7
CENTIMETRES
TL13-98a

j


sul
si
si
sul
0 1 3 5 7
CENTIMETRES
TL13-64a

k

Figure 8.3 Photographs of the drill cores and hand specimens illustrating the ore textures at Thayer Lindsley Mine. (a) and (b): Typical Thayer Lindsley ores, massive pyrrhotite with disseminated chalcopyrite. (c): Sharp contact between massive pyrrhotite and massive chalcopyrite. (d): Melange ore. (e) and (f): Streaky chalcopyrite veins in massive pyrrhotite ores. (g) and (h): Silicate xenoliths in massive sulphide ores. Mineral zoning is displayed around the xenolith. Away from the xenoliths mineral assemblages change from massive chalcopyrite, through chalcopyrite and pentlandite, to massive pyrrhotite. (i): Typical Sublayer rocks. (j): Typical Sublayer ores. (k): Chalcopyrite and quartz vein at the orebody margin of the 4B Ore Zone

249

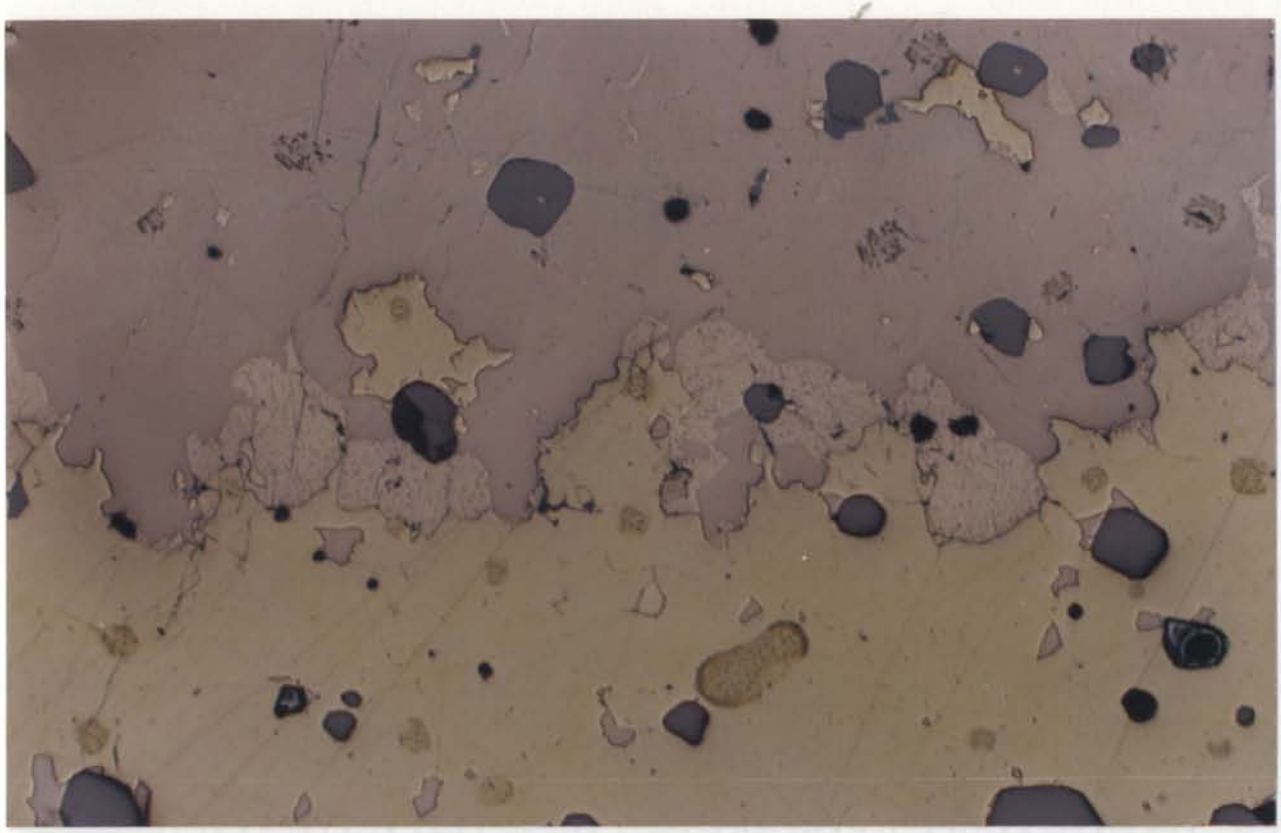

a

1 mm

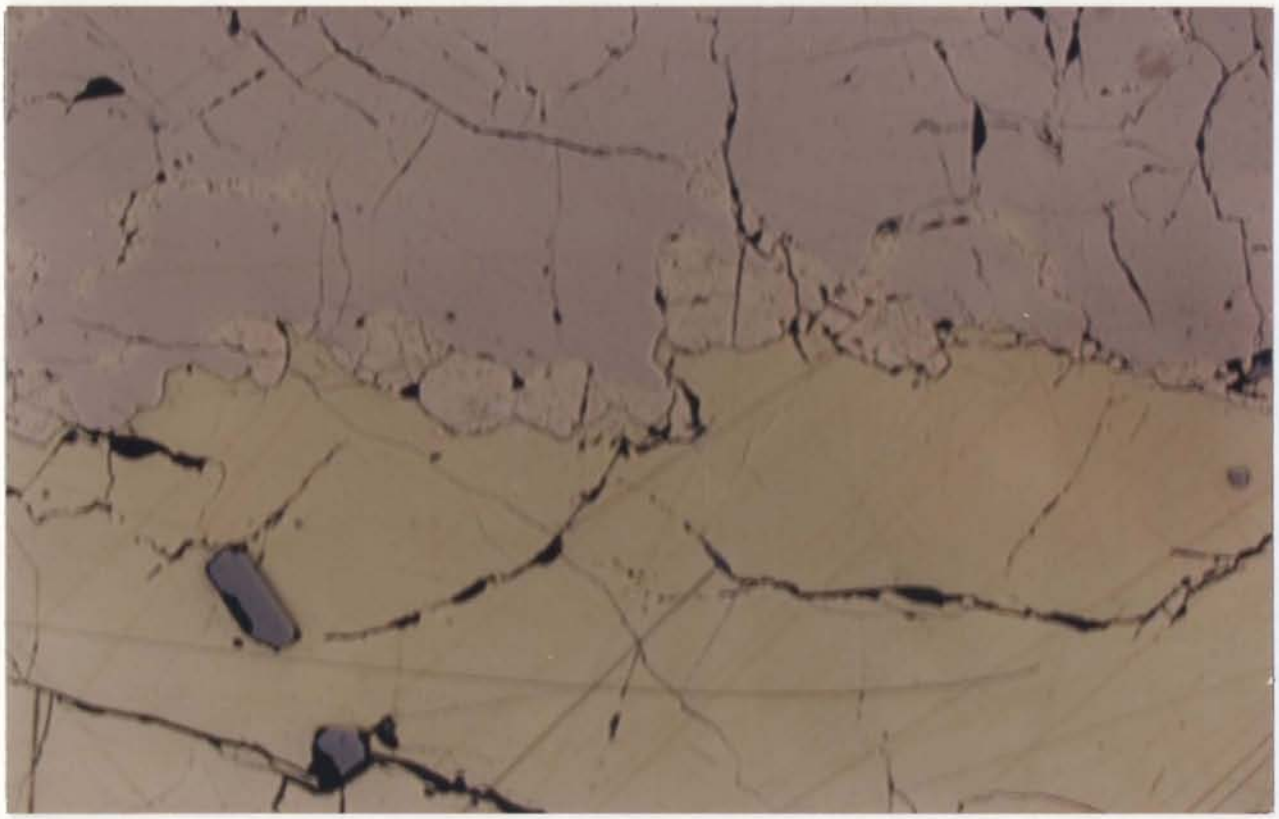

b

1 mm

250

c

1 mm

d

1 mm

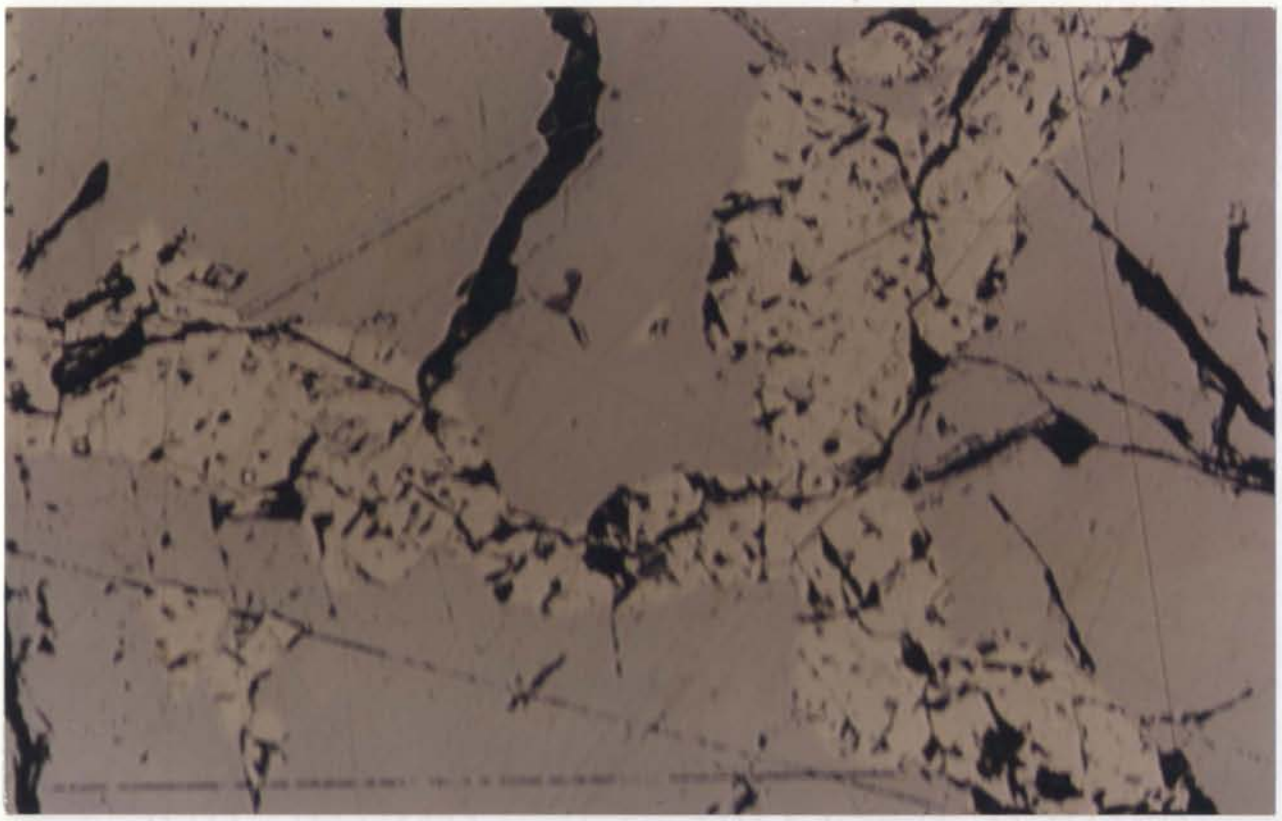

e

0.25 mm

f

1 mm

g
0.25 mm

h
0.25 mm

253

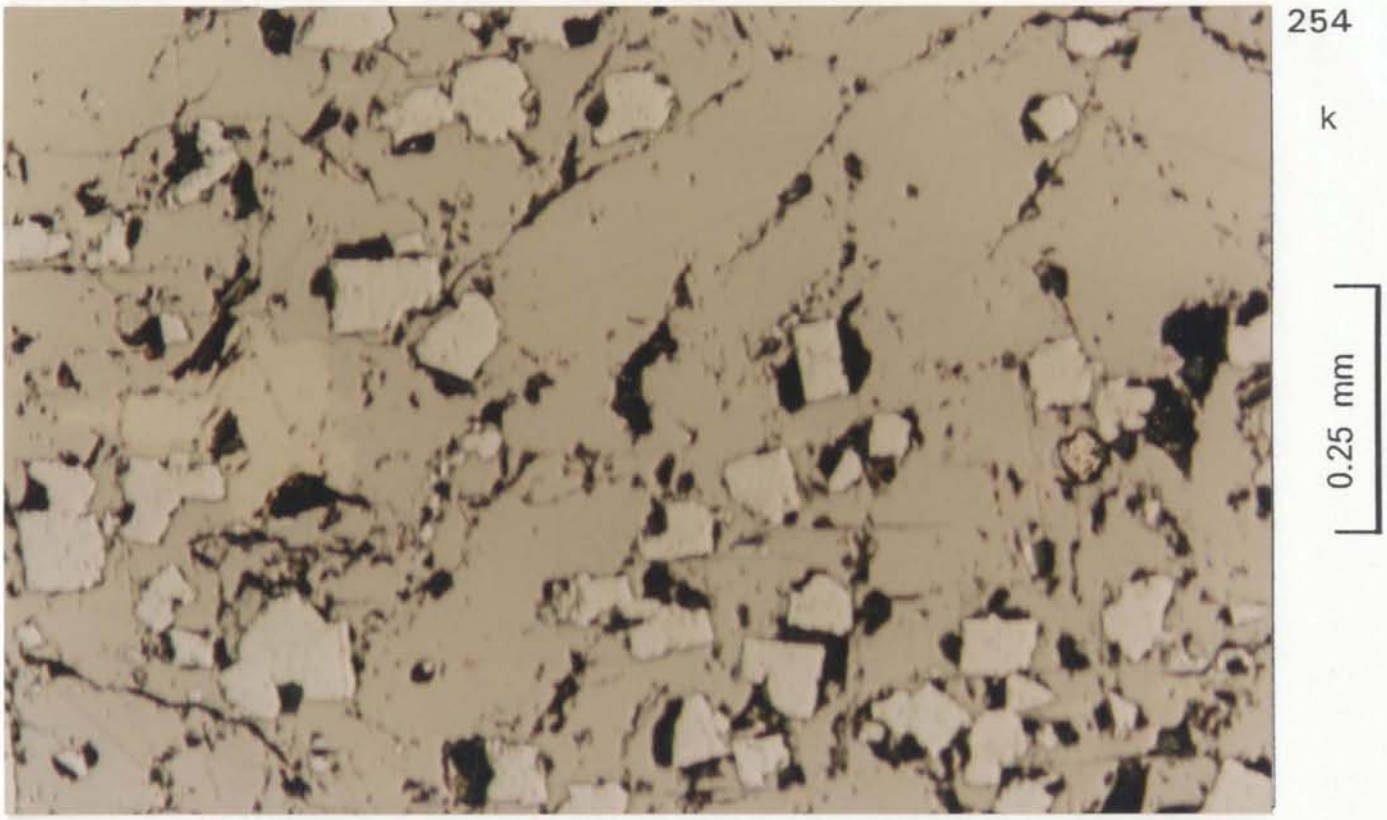

Figure 8.4 Photomicrographs illustrating textural relations of ore minerals at the Thayer Lindsley Mine. (a) and (b) Sharp contact between massive pyrrhotite and massive chalcopyrite (TL2-B and TL2-D), pentlandite fills in the contact. (c) Sharp contact between massive chalcopyrite, and massive pyrrhotite and magnetite (TL-2D). (d) and (e). Exsolved pentlandite forms rims around grains of pyrrhotite (TL2-C and TL13-32J)). (f) Fine, flame like lamellae of exsolved pentlandite in pyrrhotite with euhedral magnetite (TL13-34B). (g) Small flames of exsolved pentlandite develop on either side of fracture(TL2-C). (h) Anhedral chalcopyrite and pentlandite fill in the boundary of pyrrhotite and magnetite grains (TL2-E). (i) Euhedral magnetite replaced by pyrrhotite and pentlandite in the centre(TL2-C) . (j) Mineral zoning displayed around the silicate xenoliths (TL13-161G). Away from the xenolith, mineral assemblages change from chalcopyrite, through pentlandite, to pyrrhotite and magnetite. (k) Pyrrhotite replaced by small euhedra of pyrite (TL15-01A)

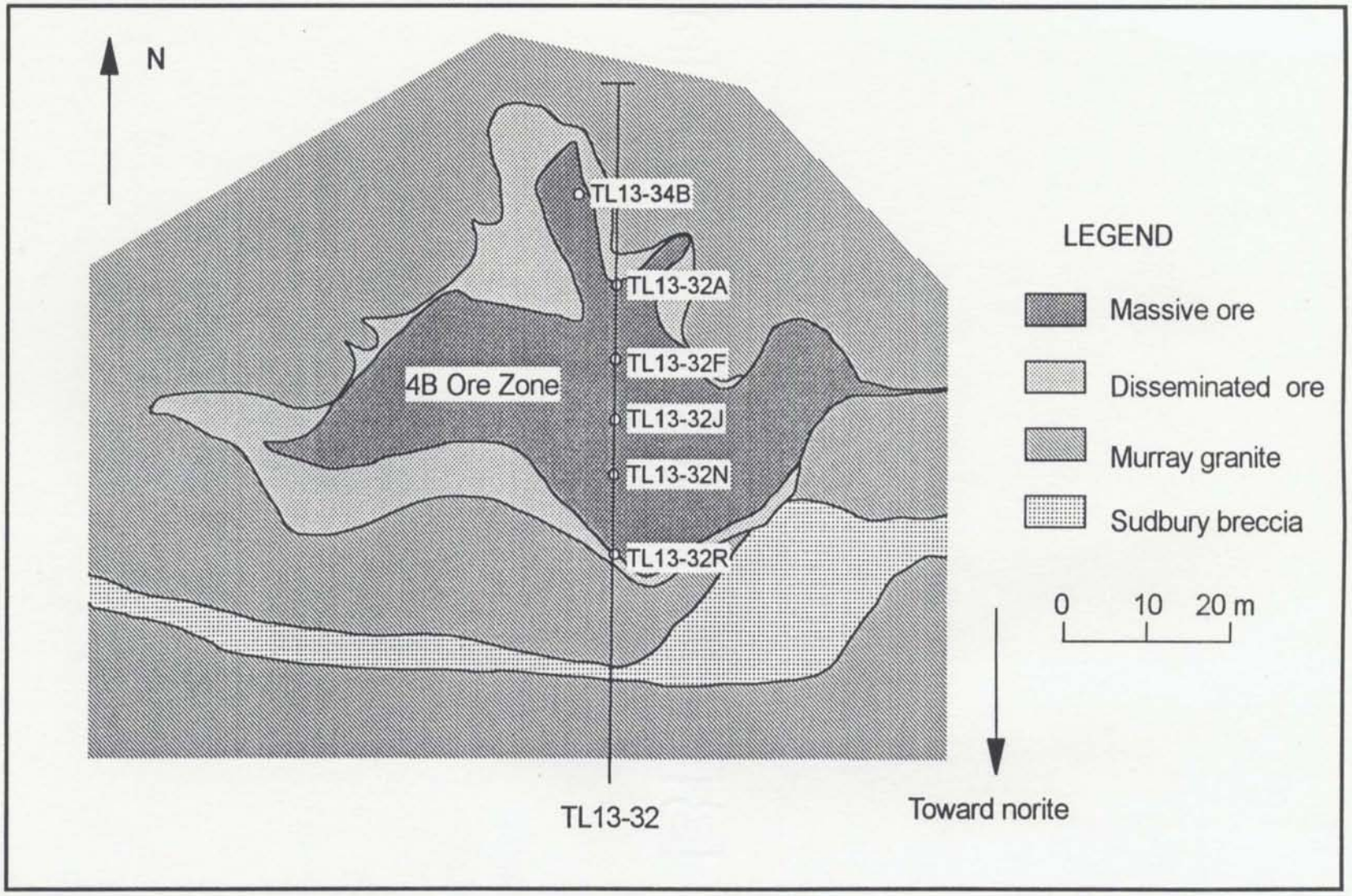

Figure 8.5 Locations of systematic samples from a drill core (TL13-32) through the 4B Ore Zone

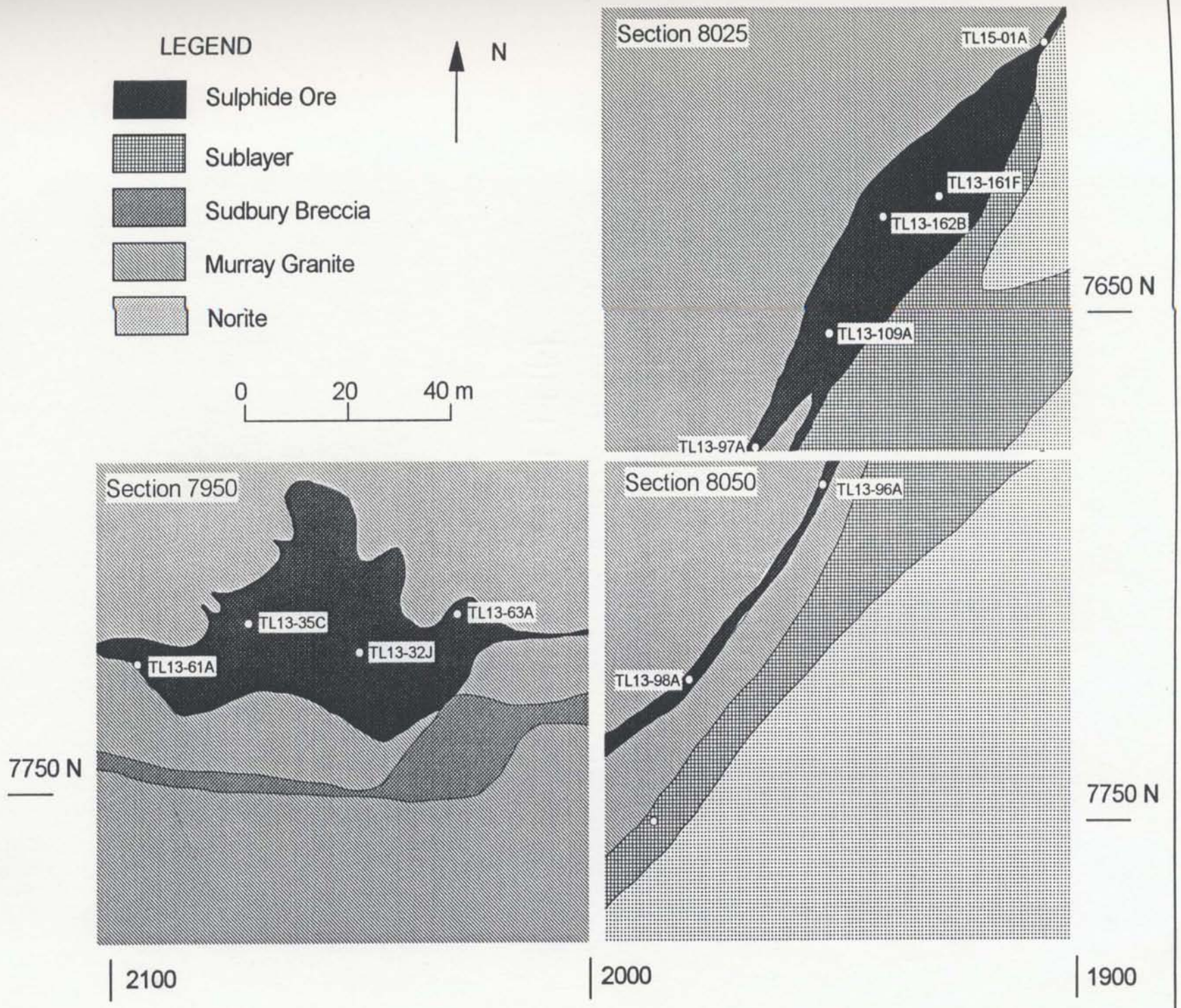

Figure 8.6 Locations of systematic samples from a transection along the orientation of the 4B Ore Zone

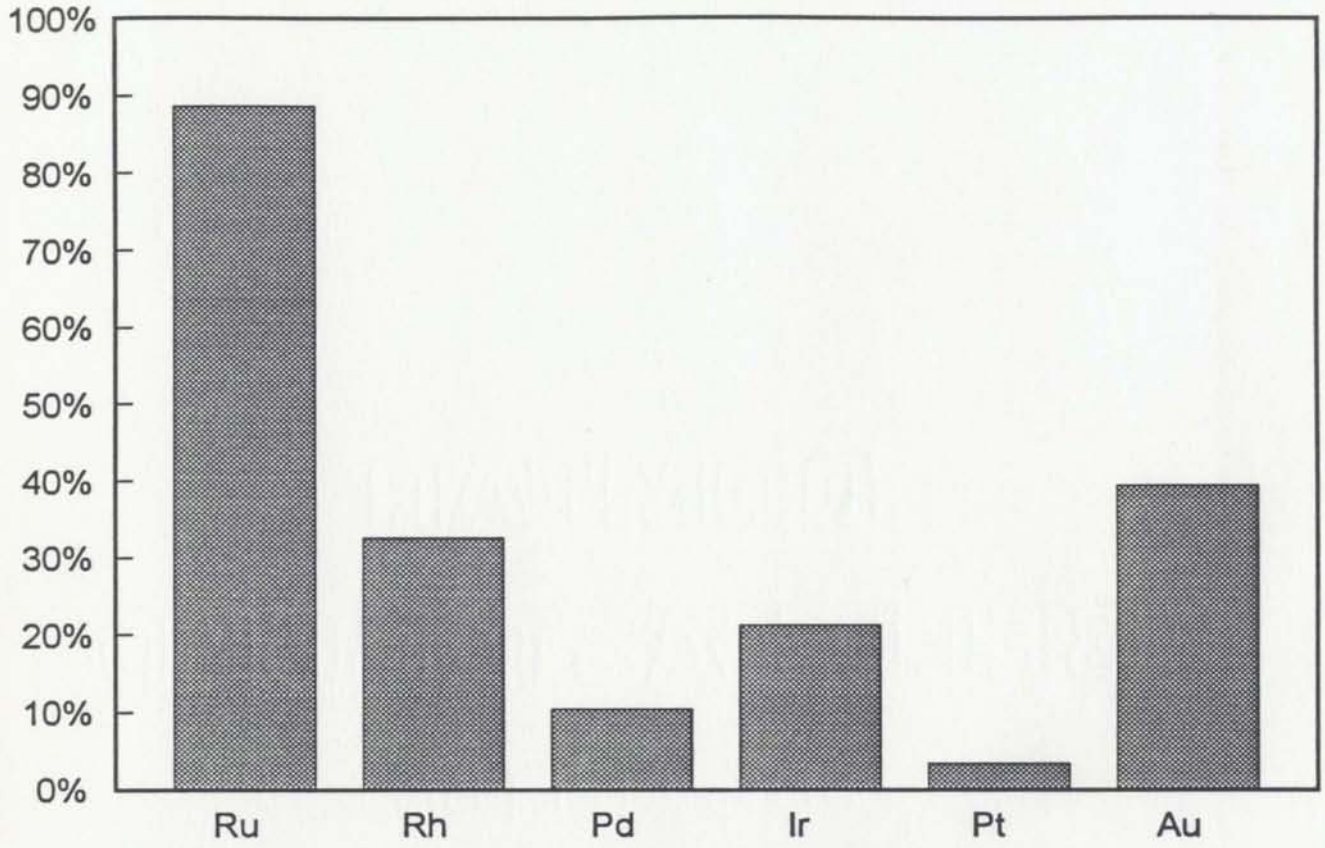

Figure 8.7 Mean percentage of the precious metals contained in the four principle ore minerals (pyrrhotite, magnetite, chalcopyrite, and pentlandite) at the Thayer Lindsley Mine. Data with anomalous concentrations are not included in the calculation (see text for explanations).

Figure 8.8 Scanning electron photomicrographs of the unnamed precious metal mineral (Pt-Rh-As) (Table 8.7) with its host minerals. (a) Euhedra of the unnamed mineral included in chalcopyrite near the microfracture (TL13-32R). (b) Euhedra of the unnamed mineral occuring in microfractures in pyrrhotite (TL13-32N). (c) Euhedra of the unnamed mineral included in pyrrhotite near a microfracture (TL13-98A). (d) The unnamed mineral associated with gersdorrffite-cobaltite occurs in a microfracture of pyrrhotite (TL13-98A). (e) The deformed unnamed mineral associated with gersdorffite-cobaltite occurs in a microfracture in pyrrhotite (TL13-98A). (f) Euhedra of the unnamed mineral occurs at the edge of a silicate xenolith (TL13-63A)

a

b

c

d

e

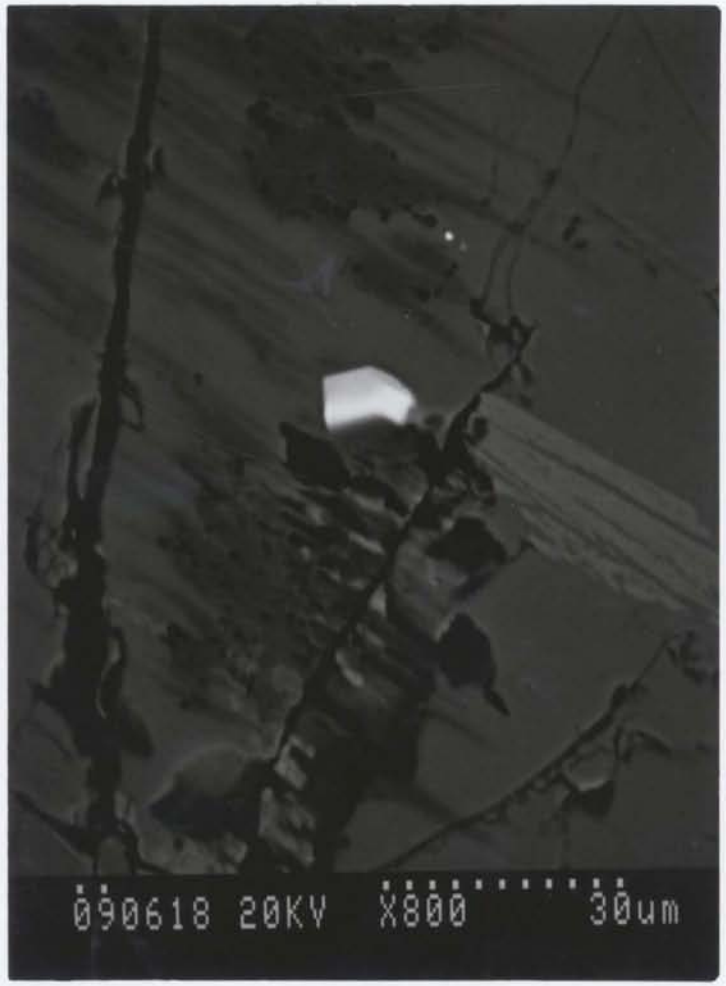

f

Figure 8.9 Scanning electron photomicrographs of michenerite [Pd(Bi,Te)2] (Table 8.7) with its host minerals. (a) Anhedral michenerite included in chalcopyrite (TL13-98A). (b) Anhedral michenerite occurs at the boundary between pyrrhotite and magnetite (TL13-63A). (c) Anhedral michenerite included in pentlandite (TL13-63A). (d) Anhedral michenerite occurs at the boundary between a silicate xenolith and sulphide minerals (TL13-63A). (e) Anhedral michenerite occurs at the boundary between chalcopyrite and magnetite (TL13-63A). (f) Anhedral michenerite occurs at a microfracture in pyrrhotite (TL13-63A).

a

b

c

d

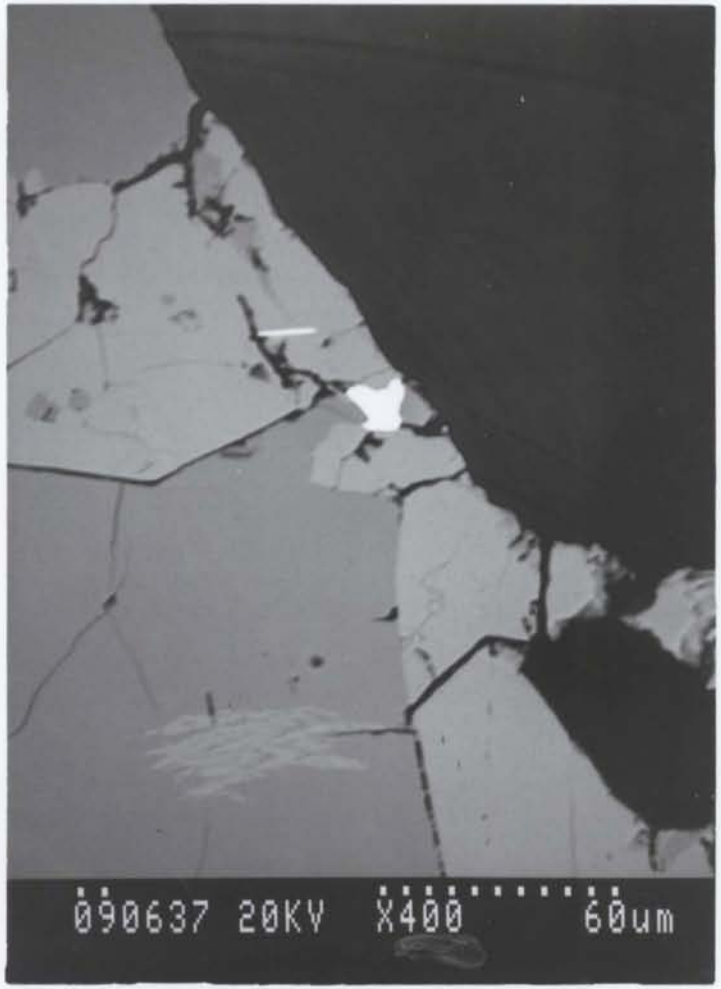

e

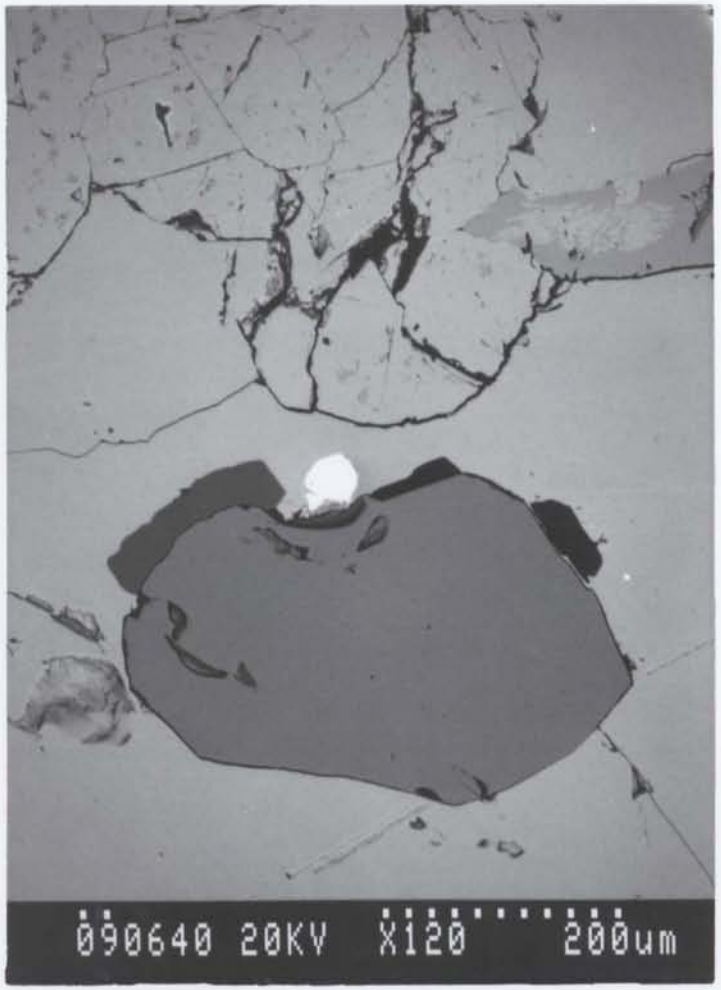

f

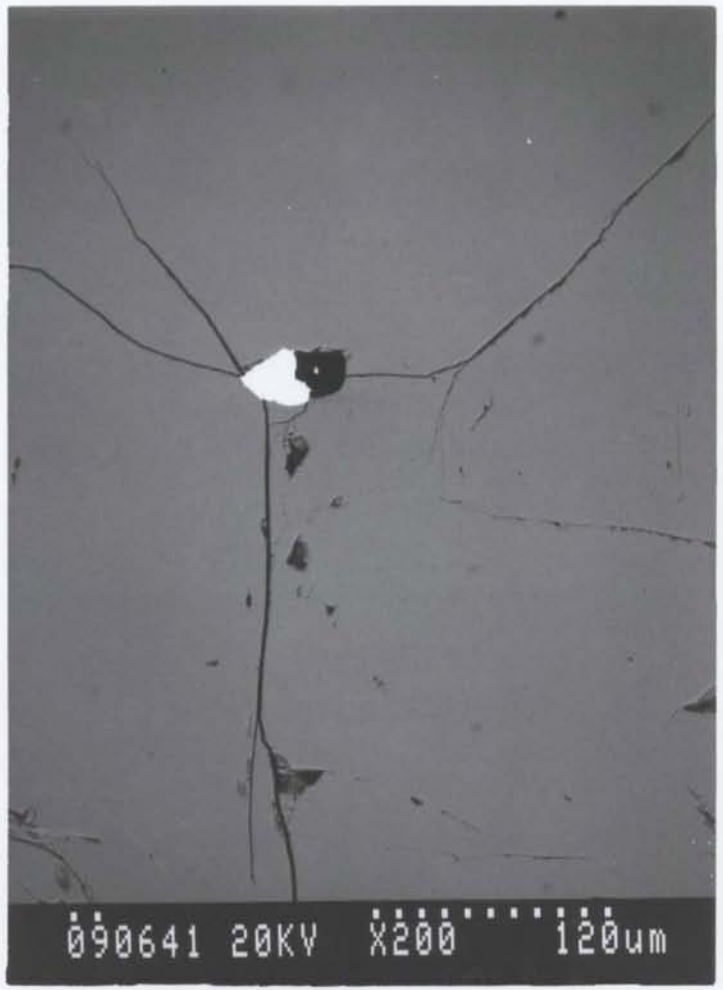

a

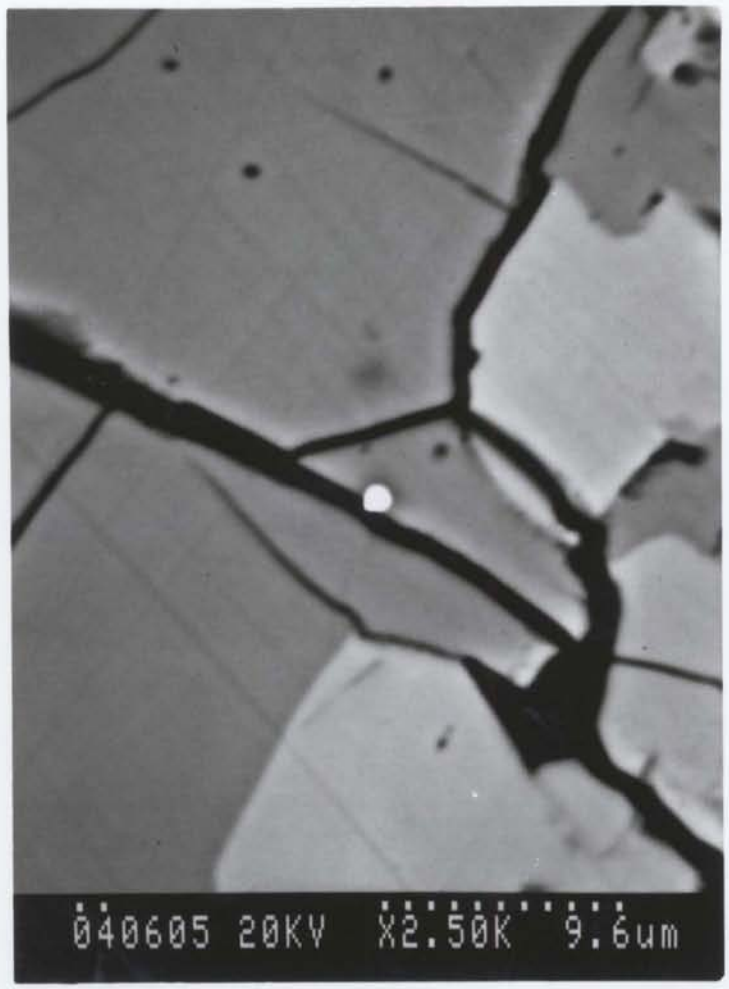

b

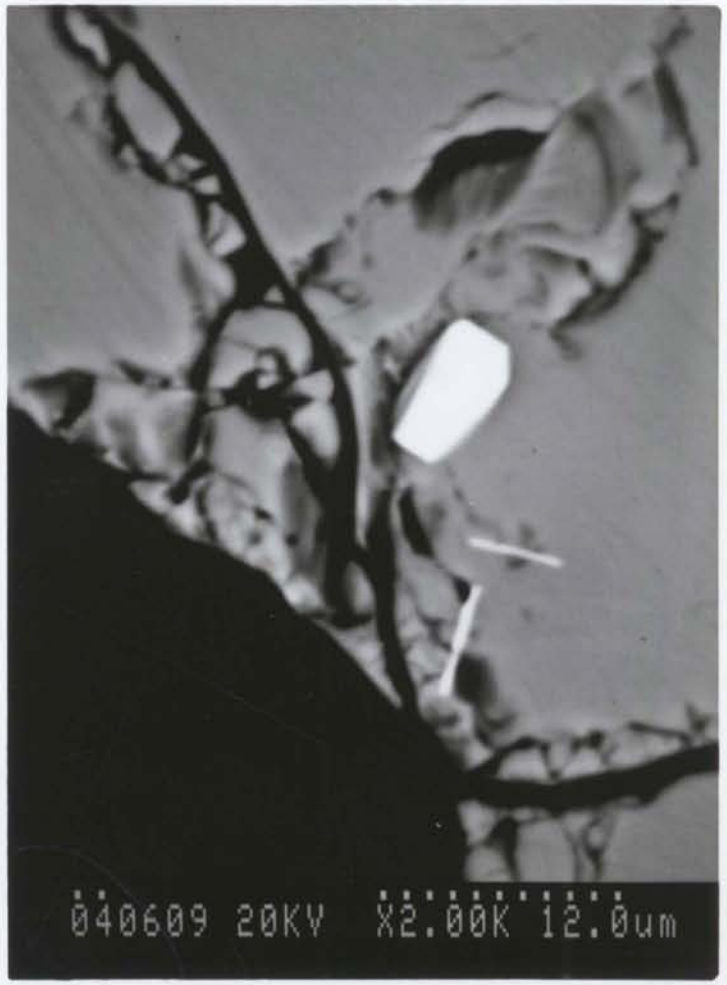

Figure 8.10 Scanning electron photomicrographs of the unnamed mineral (PdSb0.4) with its host minerals. (a) The unnamed mineral occurs in a microfracture in pyrrhotite (TL13-32R). (b) The euhedral mineral occurs in a microfracture in pyrrhotite near the boundary between a silicate xenolith and the sulphide (TL13-32N).

a

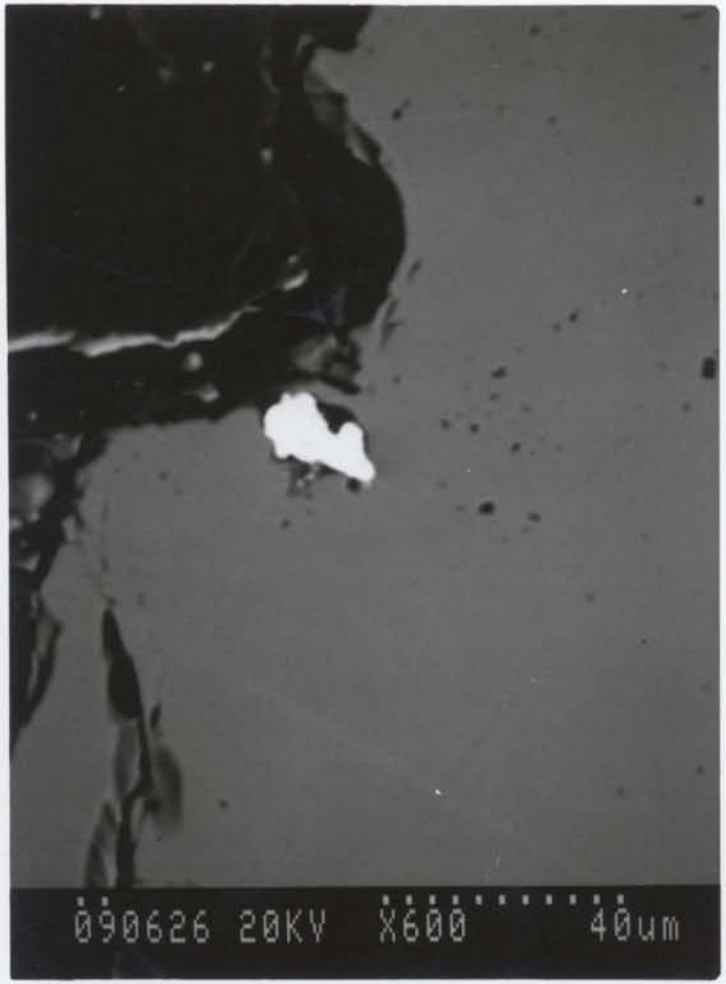

b

Figure 8.11 Scanning electron photomicrographs of gold with its host minerals. (a) Anhedral gold occurs at the boundary between a silicate xenolith and the pyrrhotite (TL13-98A). (b) An oval inclusion of gold occuring in pentlandite (TL13-63A).

Figure 8.12 Variations of the precious metal concentrations in (a) bulk sulphide ores (recalculated to 100% sulphides), (b) magnetite, (c) pyrrhotite, (d) pentlandite, and (e) chalcopyrite from one side of an orebody to the other side in the 4B Ore Zone toward the Sudbury Igneous Complex (SIC) along a drill core (TL13-32) (see Figure 8.5 for sample locations) at Thayer Lindsley Mine

(a) Bulk sulphide Ores

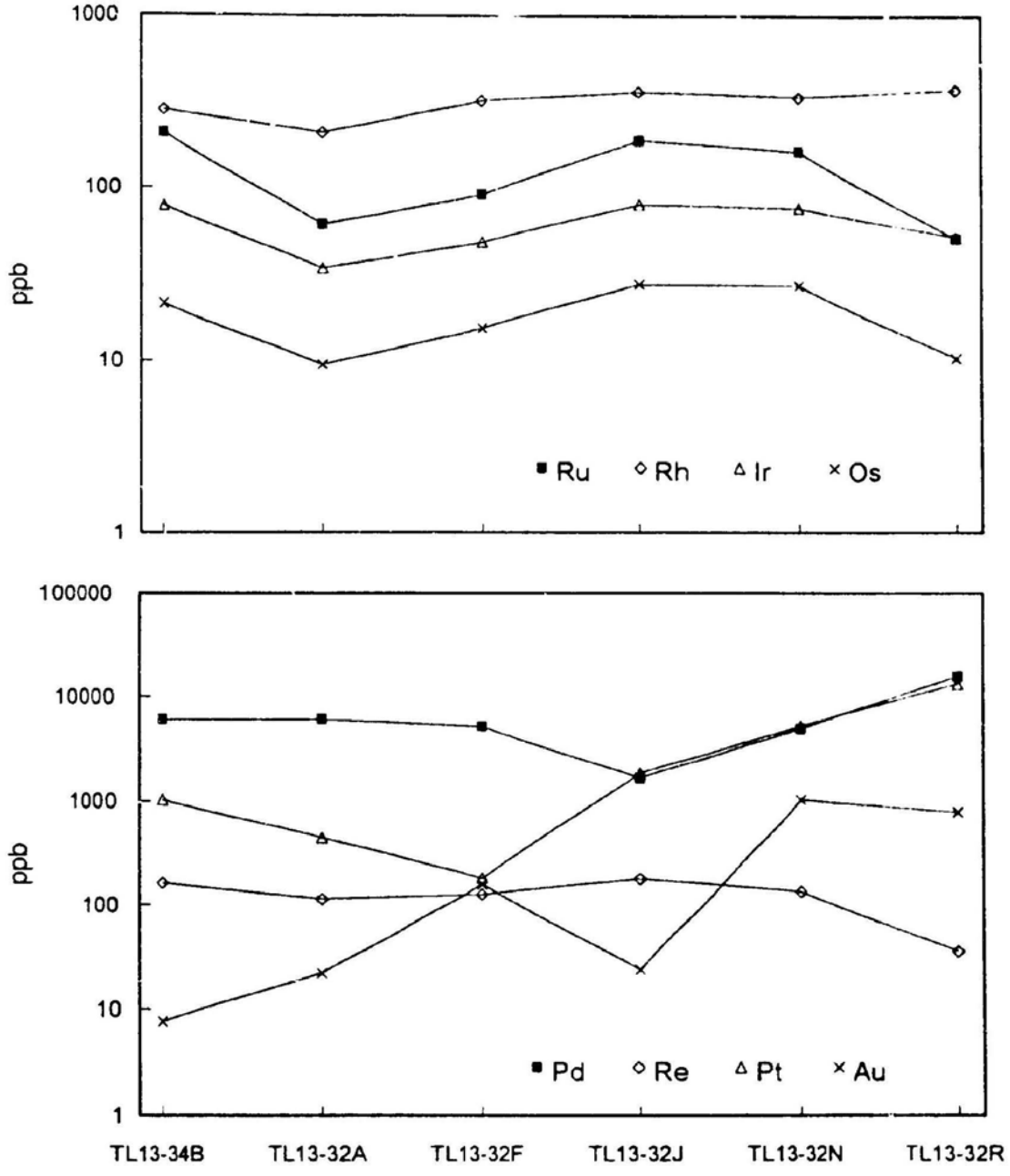

(b) Magnetite

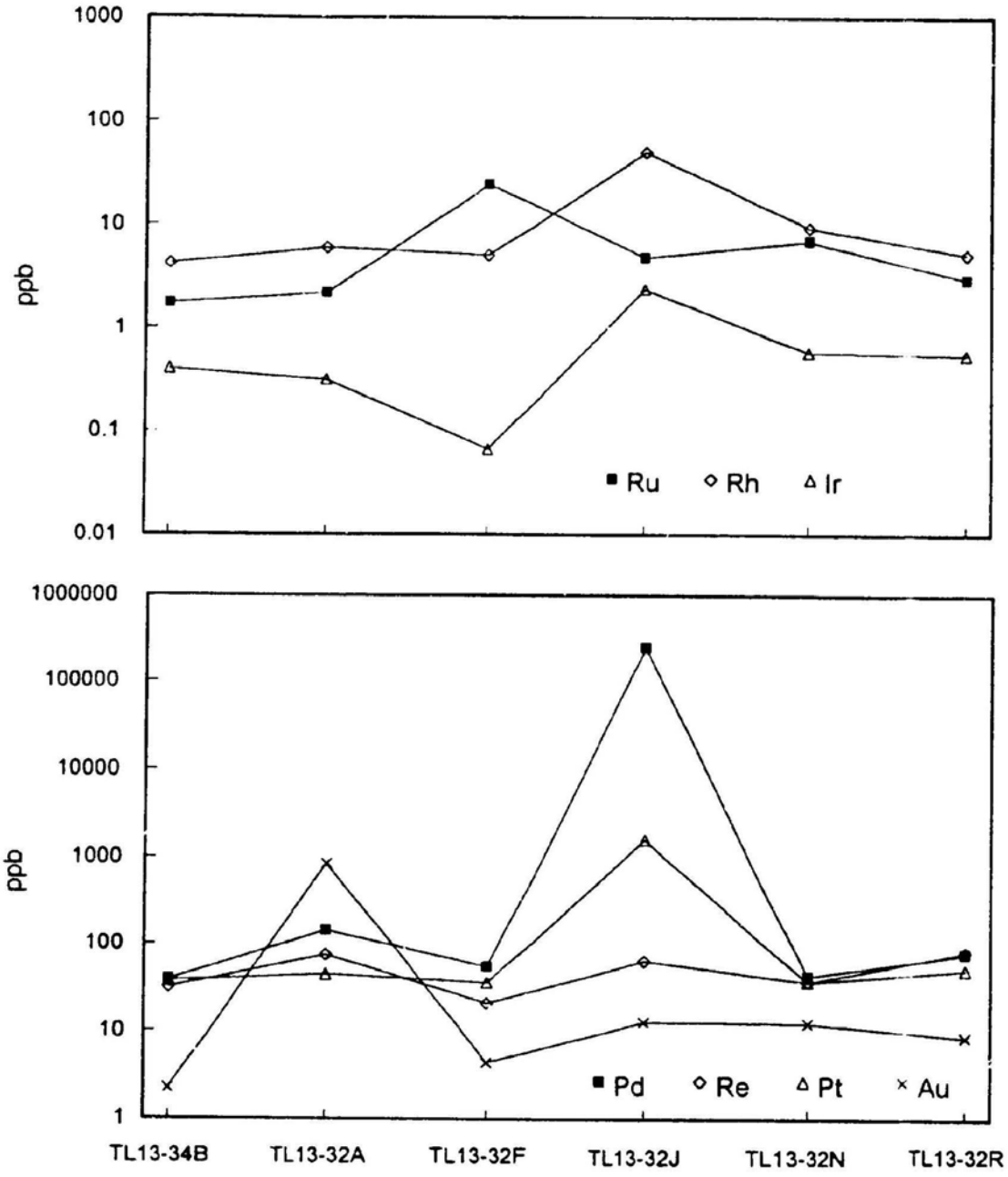
1000
100
10
1
0.1
0.01
ppb
Ru
Rh
Ir
1000000
100000
10000
1000
100
10
1
ppb
Pd
Re
Pt
Au
TL13-34B
TL13-32A
TL13-32F
TL13-32J
TL13-32N
TL13-32R

(c) Pyrrhotite

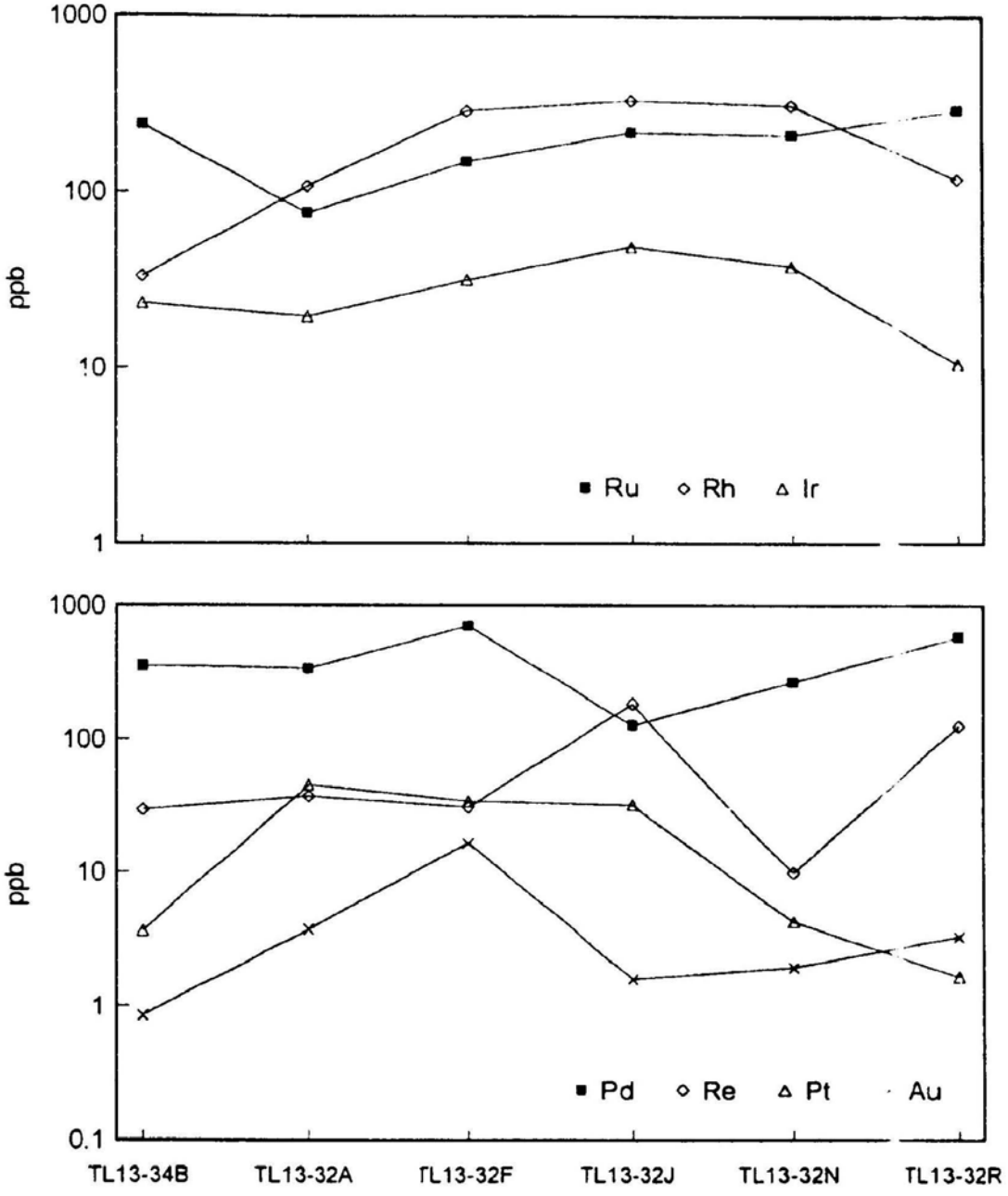

(d) Pentlandite

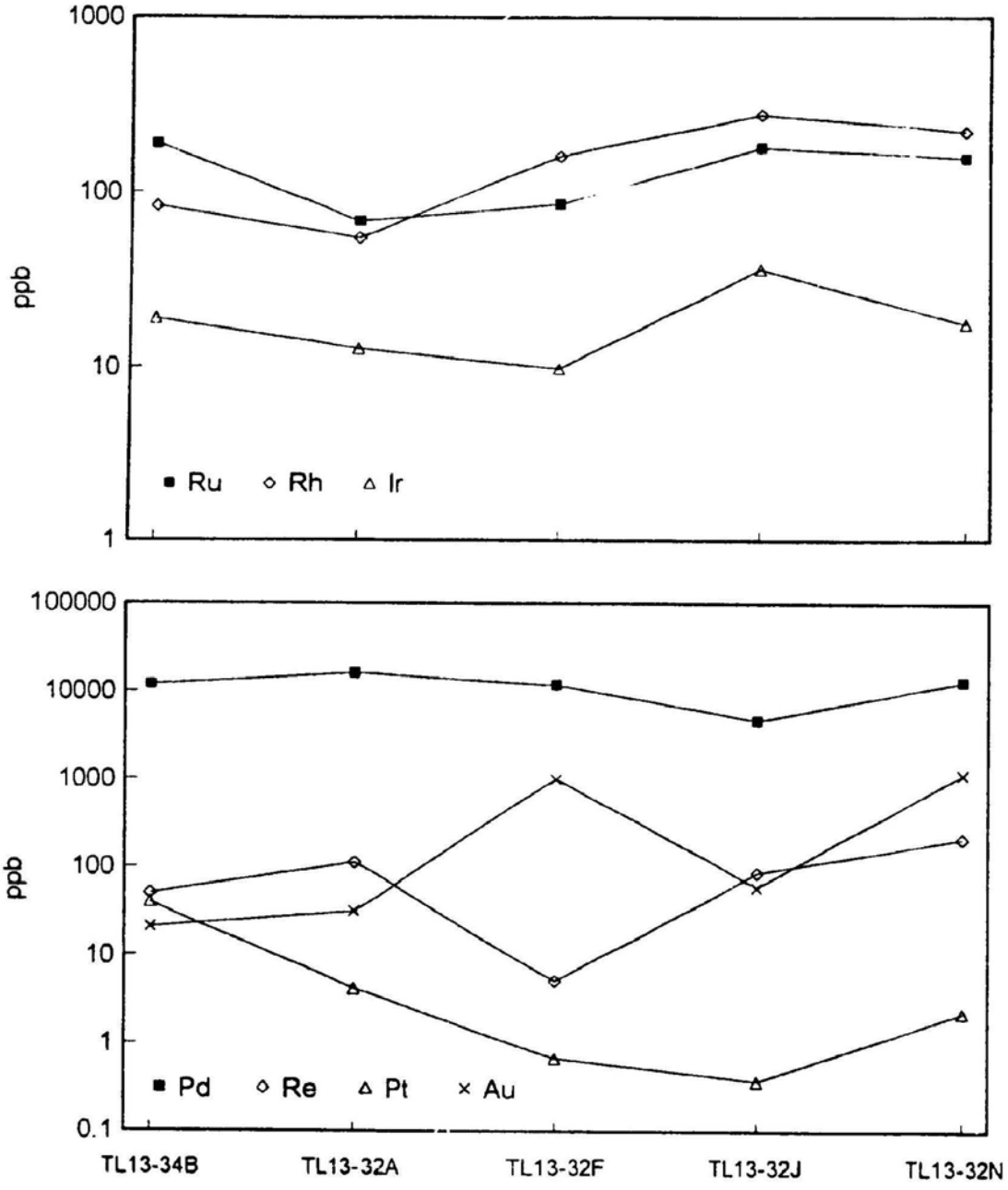

(e) Chalcopyrite

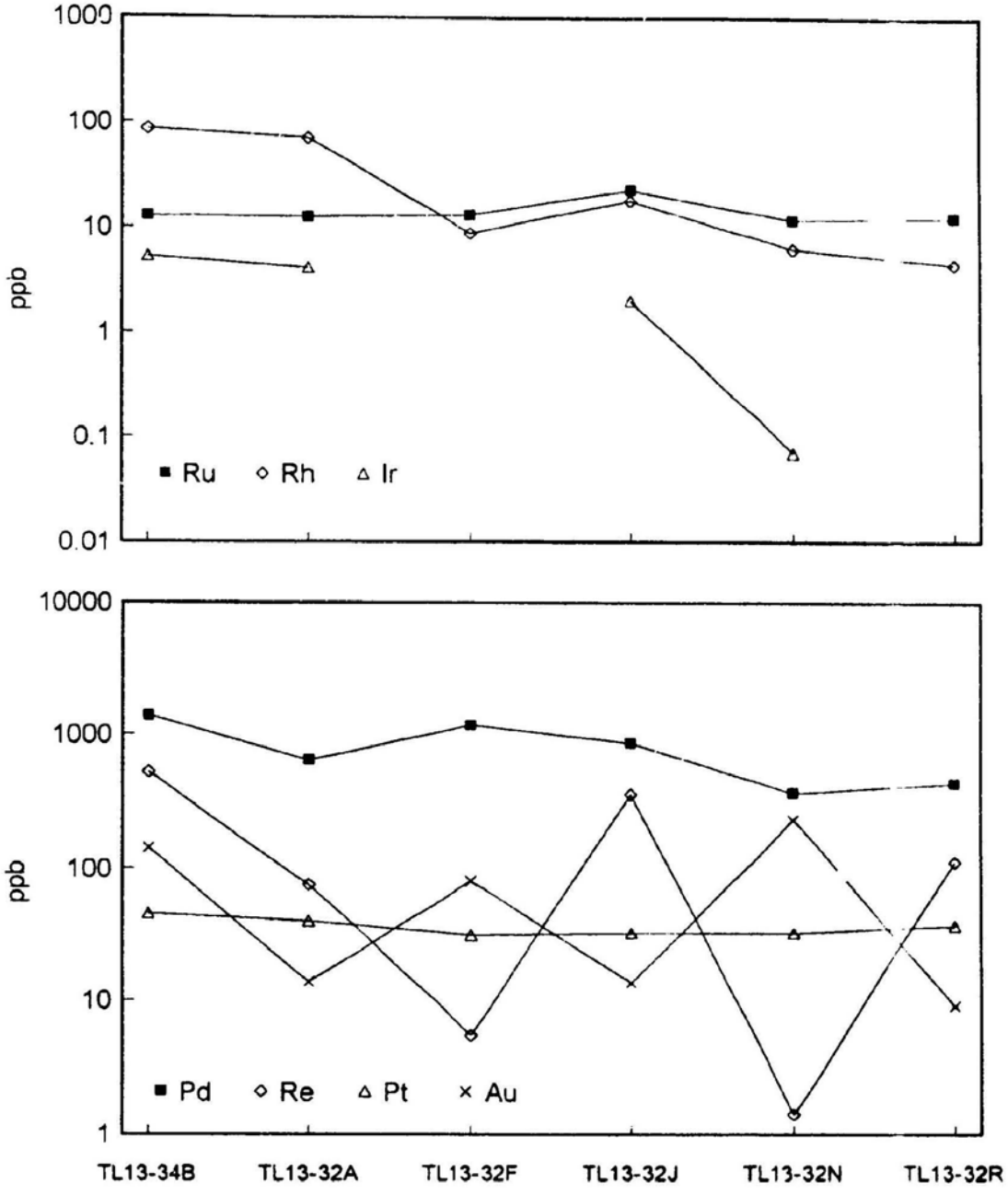

Figure 8.13 Variations of the precious metal concentrations in (a) bulk sulphide ores (recalculated to 100% sulphides), (b) magnetite, (c) pyrrhotite, (d) pentlandite, and (e) chalcopyrite in a transection along the orientation of 4B Ore Zone from east to west (see Figure 8.6 for sample locations) at the Thayer Lindsley Mine

(a) Bulk sulphide ores

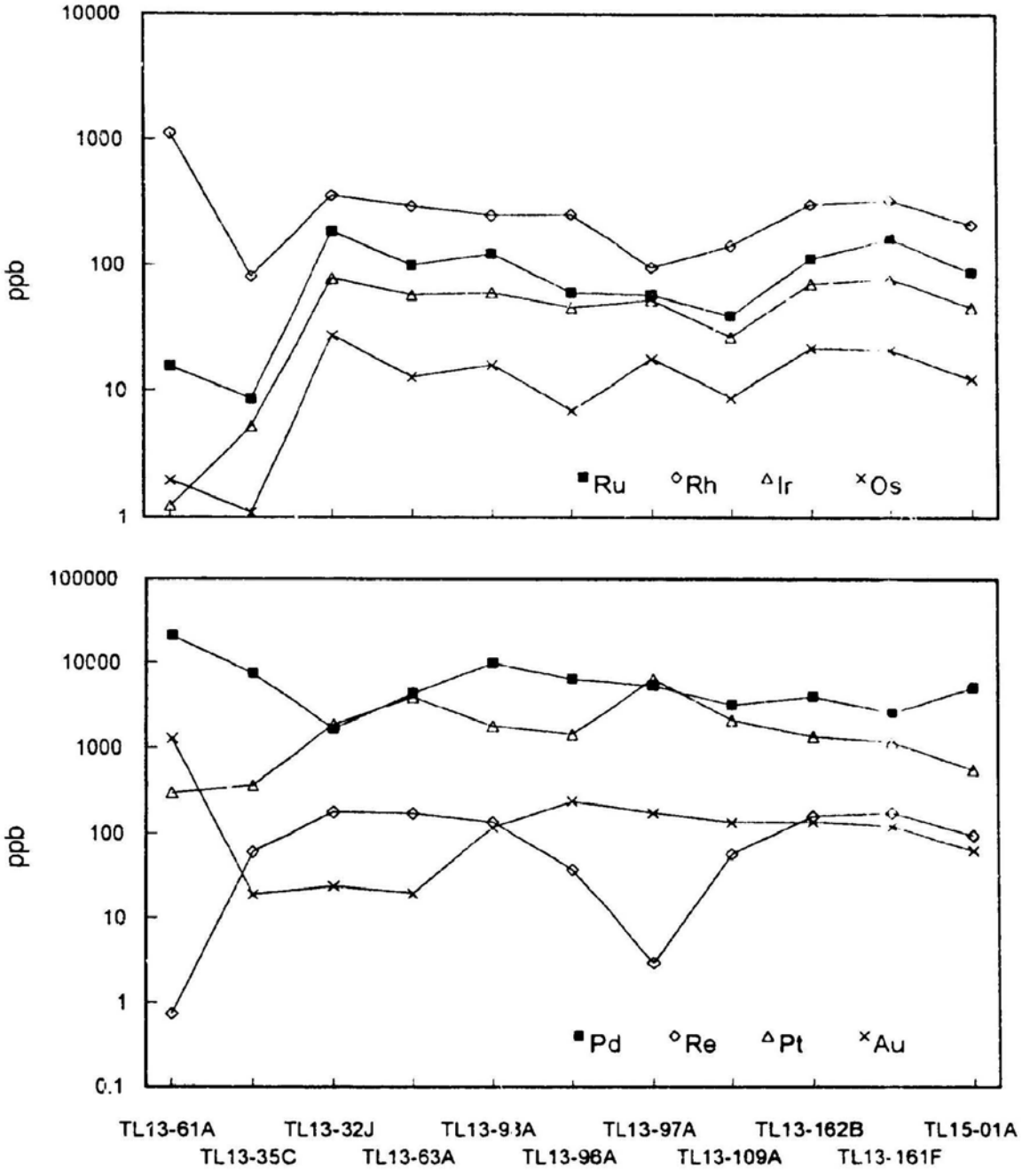

(b) Magnetite

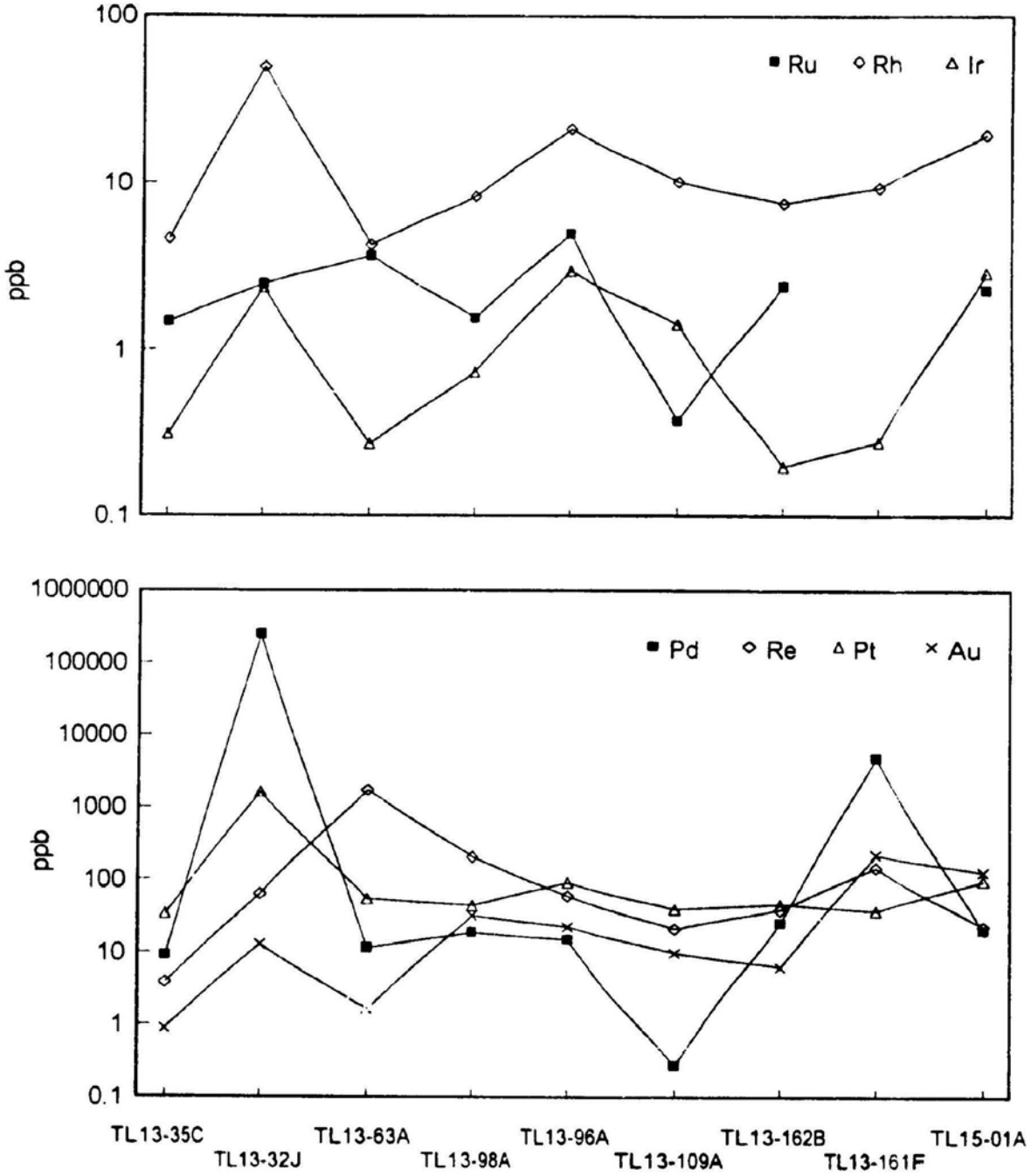
100
10
1
0.1
ppb
Ru
Rh
Ir
1000000
100000
10000
1000
100
10
1
0.1
ppb
Pd
Re
Pt
Au
TL13-35C
TL13-32J
TL13-63A
TL13-98A
TL13-96A
TL13-109A
TL13-162B
TL13-161F
TL15-01A

(c) Pyrrhotite

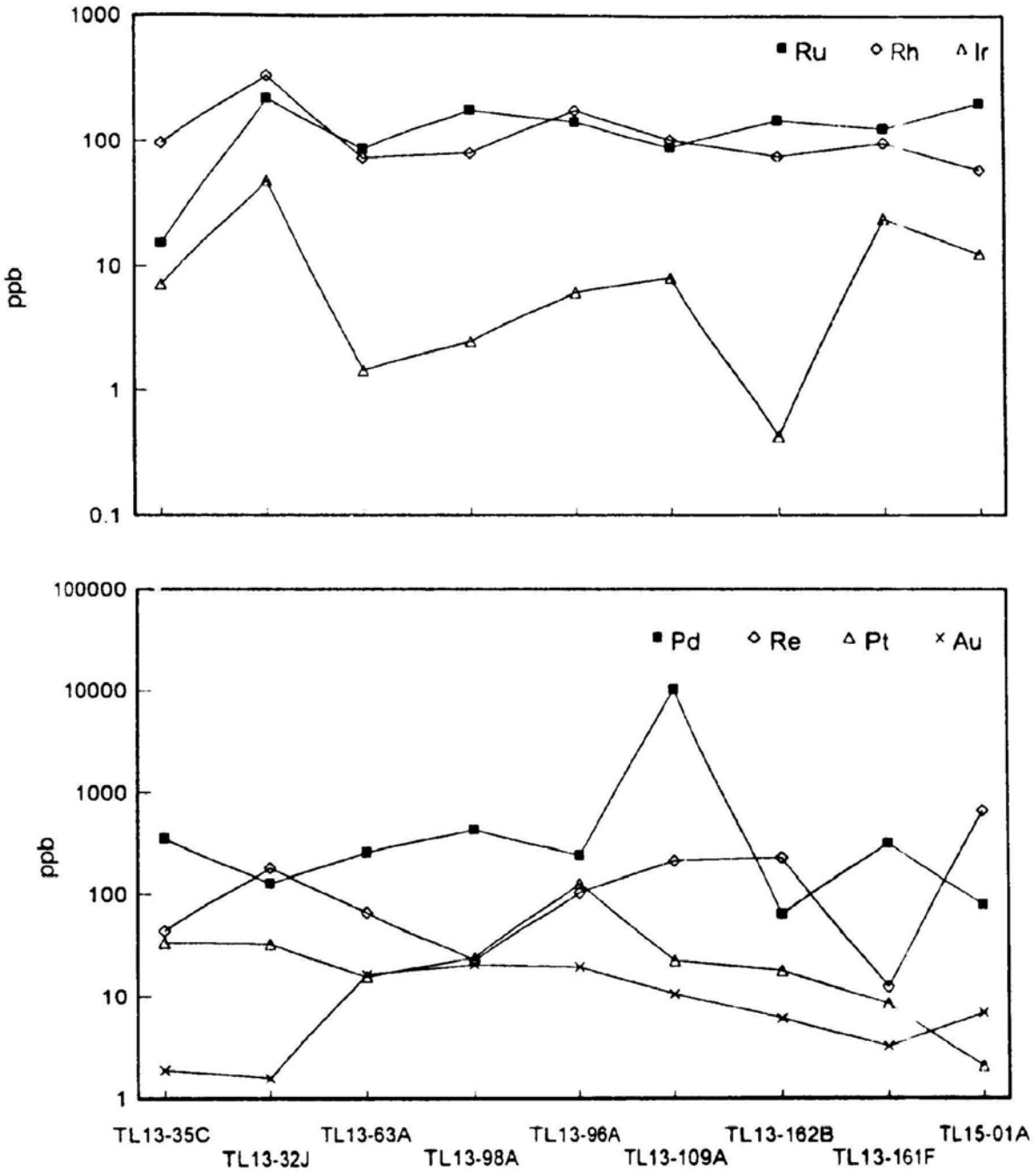

(d) Pentlandite

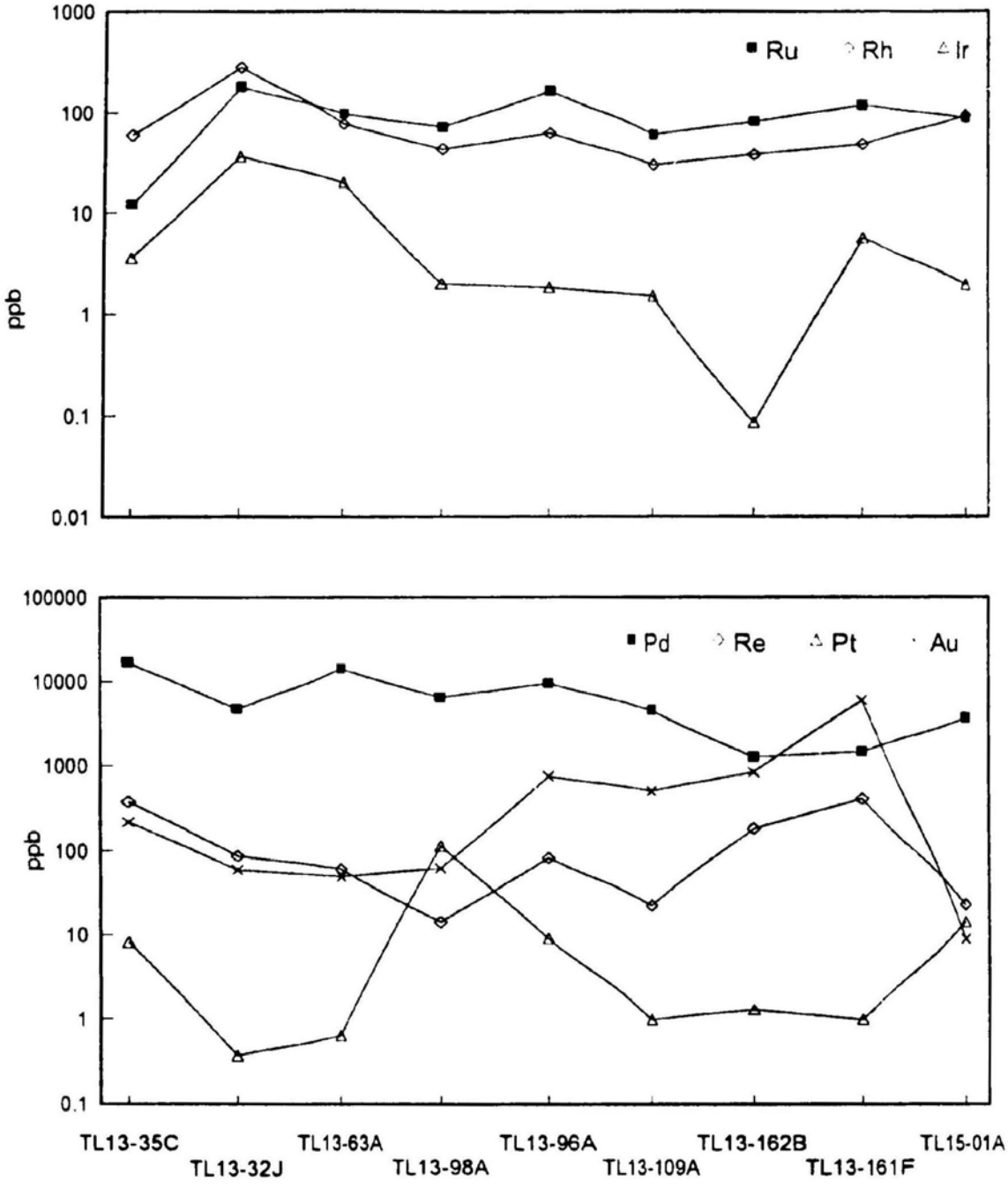

(e) Chalcopyrite

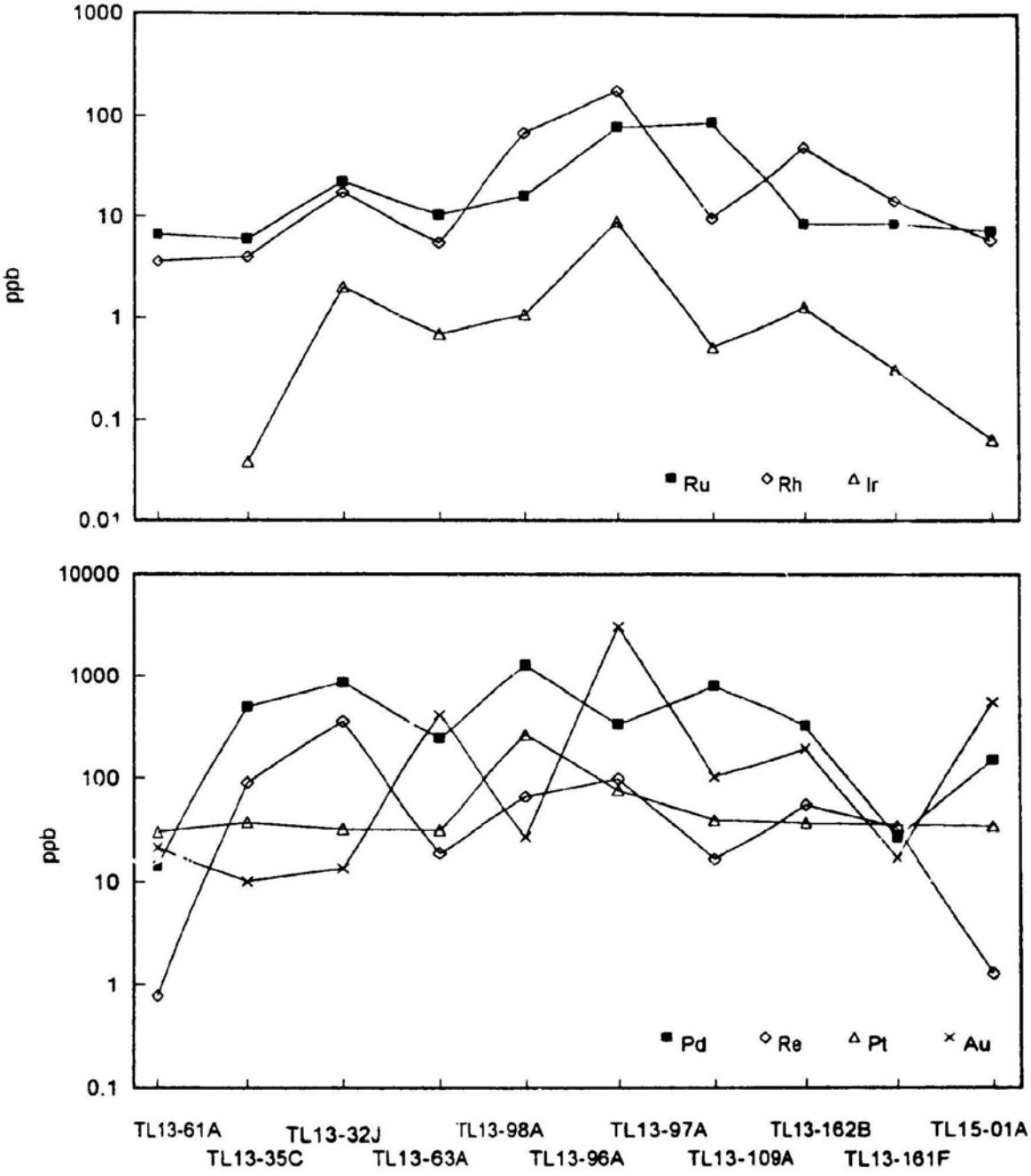

CHAPTER 9

PARTITIONING OF THE PRECIOUS METALS BETWEEN COEXISTING ORE MINERALS AND MOBILITY OF THESE ELEMENTS DURING SULPHIDE SEGREGATION AND CRYSTALLIZATION AT SUDBURY

9.1 INTRODUCTION

The precious metals (Ru, Rh, Pd, Ir, Pt, and Au) were formerly considered to be geochemically coherent with strong siderophile affinity. Barnes *et al.* (1985) and Naldrett *et al.* (1982) indicated that if these elements are chondrite normalized and plotted in order of descending melting points, their pattern shows the fractionation of these element during crystallization. Interest in these elements has produced numerous investigations of their partitioning behaviour (Stone *et al.*1990, Fleet *et al.*, 1991, and Frimpong *et al.*, 1993). Bethke and Barton (1971) raised the hope that if clean mineral separates of contemporaneous phases could be accurately analyzed, the distribution of the minor elements among the phases could allow estimation of the temperature of ore formation. However, current research on partitioning of these elements is strictly limited to experiments between sulphide liquid and basaltic silicate melt. Very few data are available on precious metal partitioning between the

coexisting ore minerals in copper-nickel sulphide ores, other than the studies of Keays and Crocket (1970) and Chyi and Crocket (1976), due to the considerable analytical difficulty of working with small samples.

In this chapter partition coefficients (K_d), at ppb to ppm levels, of precious metals between major ore minerals are evaluated based on the analytical data presented in Chapter 8. The results in this study provide further support for precious metal fractionation based on equilibrium partitioning during crystallization (Hawley, 1965; Keays and Crocket, 1970; Chyi and Crocket, 1976; Naldrett *et al.*, 1982; Barnes *et al.*, 1985 and Li *et al.*, 1992). Crystallization and subsequent exsolution are mainly responsible for the distribution and fractionation of precious metals in sulphides and magnetite. A fractionation model is proposed for the explanation of precious metal ore genesis.

9.2 PARTITIONING OF PRECIOUS METALS BETWEEN THE MAJOR ORE MINERALS

The partition coefficient $K_{d_i}^{\alpha/\beta}$ is defined here as the ratio of the concentration (ppb) of metal i in phase α to that in phase β at equilibrium. Data used for K_d calculations have been presented in the previous chapters. In spite of the very high purity of the mineral separates, some PGE and Au alloy inclusions at the

micrometer scale (Figures 8.8-8.11) within some minerals could not be eliminated. These minor PGE and Au alloy inclusions have been observed by laser ablation microprobe (LAM) ICP-MS (Chapter 4) and electron microprobe (Chapters 7 and 8), and are indicated by extremely high concentrations of precious metals in some mineral separates, and also by the high standard deviations of the replicate analyses. These anomalously high data are not included in the K_d calculations.

The calculated K_d's for the precious metals between the minerals for different individual samples are listed in Table 9.1. The K_d Values between the sulphides and magnetite for some precious metals (*i.e.,* Ru) vary significantly due to the concentrations of these metals in the magnetite close to the limits of detection. It is also possible that the minerals may still contain minor inclusions of some precious metal phases (*i.e.,* Au) which contribute to the K_d variations.

Mean K_d values between the minerals are presented in Table 9.2. Partition coefficients (K_d) between chalcopyrite and magnetite for Ru, Rh, Ir, Pd, Re, Pt, and Au are 4.5, 4.5, 1.6, 24, 1.2, 0.9 and 1.1 respectively; between pyrrhotite and magnetite 73, 17, 23, 13, 3.7, 0.47, and 1.05 respectively; between pentlandite and magnetite 50, 11, 20, 521, 1.7, 0.16, and 12 respectively; between pyrrhotite and chalcopyrite 12, 15, 3.1, 1.3, 2.4, 0.6, and 0.20 respectively; between pentlandite and chalcopyrite 8.7, 9.8, 5.7, 24,

Table 9.1 Calculated Kd Values between mineral pairs for individual sample from tne Thayer Lindsley Mine*

Pentlandite/Magnetite

Sample	Ru	Rh	Pd	Re	Ir	Pt	Au
TL13–34B	109.9	19.7	306	1.60	47.1	1.06	9.5
TL13–32A	31.6	9.4	113	1.50	40.9	0.09	
TL13–32F	3.5	31.6	220	0.25		0.02	
TL13–32J	37.2	5.6		1.34	15.3		4.6
TL13–32N	22.7	24.2	300		30.7	0.06	
TL13–35C	4.6	12.9	1849		11.6	0.24	
TL13–63A	5.0	18.2	1219		73.4	0.01	30.0
TL13–98A	104.3	5.3	335		2.7		1.9
TL13–96A	39.4	3.0	630	1.34	0.6	0.10	
TL13–109A	68.3	3.0		1.04	1.1	0.02	
TL13–162B	34.5	5.1	49	4.64	0.4	0.03	
TL13–161F	117.3	5.2		2.75	19.9	0.03	
TL13–161L	82.6	3.3				0.06	
TL15–01A	33.1	4.8	183	1.00	0.7	0.15	
Mean	50	10.8	521	1.7	20	0.16	11.5
STD**	38	8.8	546	1.2	22	0.28	11.0

Pyrrhotite/Magnetite

Sample	Ru	Rh	Pd	Re	Ir	Pt	Au
TL13–34B	139.5	7.9	9.0	0.9	58.3	0.10	0.38
TL13–32A	35.1	18.4	2.3	0.5	62.7	1.03	
TL13–32F	6.2	57.9	12.9	1.5		0.96	3.78
TL13–32J	45.8	6.7		2.9	20.7		0.12
TL13–32N	30.9	33.9	6.3	0.3	66.3	0.11	0 16
TL13–32R	100.1	23.5	7.6	1.6	19.6		0.38
TL13–35C	5.9	21.1	39.3	11.4	23.1	0.99	2.12
TL13–63A	4.5	17.6	22.4		5.3	0.29	
TL13–98A	259.5	9.9	23.0		3.3	0.54	0.64
TL13–96A	34.4	8.4	16.2	1.7	2.1		0.87
TL13–109A	100.8	10.2		10.1	5.6	0.56	1.07
TL13–162B	62.0	10.2	2.5	5.9	2.2	0.39	0.98
TL13–161F	127.0	10.6				0.23	
TL15–01A	75.2	3.1	4.0		4.3	0.02	
Mean	73	17	13	3.7	23	0.47	1.05
STD**	67	14	11	3.9	24	0.36	1.07

* Data from Table 8.5. Data with anomalous concentrations resulting from inclusions of precious metal rich phases were excluded

** Standard deviatior.

Table 9.1 Calculated Kd Values between mineral pairs for individual samples from the Thayer Lindsley Mine (continued)

Pentlandite/Chalcopyrite

Sample	Ru	Rh	Pd	Re	Ir	Pt	Au
TL13-34B	14.7	1.0	8.7	0.10	3.53		0.15
TL13-32A	5.5	0.8	24.7	1.48	3.11	0.10	2.28
TL13-32F	6.5	18.4	10.1	0.94		0.02	
TL13-32J	7.9	15.8	5.4	0.24	18.25	0.01	4.34
TL13-32N	13.6	36.6	34.7			0.07	
TL13-35C	2.0	15.0	33.4	4.22		0.22	
TL13-63A	9.3	14.0	57.4	3.13		0.02	0.12
TL13-98A	4.4	0.6	5.0	0.21	1.88		2.22
TL13-96A	2.1		28.2	0.82	0.20	0.12	
TL13-109A	7.0	0.6	13.8	0.39	1.18	0.03	2.56
TL13-162B	9.4	2.6	46.5	5.35	0.27	0.04	
TL13-161F	12.9	7.3	29.7	1.60	5.19	0.02	
TL13-161L	17.2	4.3	14.1	3.88	17.73	0.08	1.54
Mean	8.7	9.8	24.0	1.9	5.7	0.07	1.9
STD**	4.6	10.4	15.7	1.7	6.7	0.06	1.4

Pyrrhotite/Chalcopyrite

Sample	Ru	Rh	Pd	Re	Ir	Pt	Au
TL13-34B	18.6	0.4	0.25	0.06	4.37	0.08	0.01
TL13-32A	6.1	1.5	0.51	0.50	4.76	1.15	0.27
TL13-32F	11.6	33.8	0.59	5.67		1.11	0.21
TL13-32J	9.8	18.8	0.15	0.51		1.01	0.12
TL13-32N	18.5	51.2	0.72	7.03		0.13	0.01
TL13-32R	24.3	27.5	1.32	1.12		0.05	0.36
TL13-35C	2.6	24.6	0.71	0.49		0.89	0.19
TL13-63A	8.3	13.5	1.05	3.49	2.06	0.49	0.04
TL13-98A	11.0	1.2	0.34	0.34	2.31	0.09	0.75
TL13-96A	1.8	1.0	0.73	1.06	0.67	1.69	
TL13-109A	10.3	2.0		3.84	6.24	0.60	0.05
TL13-162B	16.9	5.2	2.37	6.76	1.37	0.50	0.36
TL13-161F	14.0	14.8	6.43	0.05		0.17	0.03
Mean	11.8	15.0	1.3	2.4	3.1	0.6	0.20
STD**	6.3	15.1	1.7	2.5	1.9	0.5	0.21

Table 9.1 Calculated Kd Values between mineral pairs for individual samples from the Thayer Lindsley Mine (continued)

Pentlandite/Pyrrhotite

Sample	Ru	Rh	Pd	Re	Ir	Pt	Au
TL13-34B	0.79	2.50	34.2	1.69	0.81		24.7
TL13-32A	0.90	0.51	48.4		0.65	0.09	8.5
TL13-32F	0.56	0.55	17.1	0.17	0.31	0.02	60.2
TL13-32J	0.81	0.84	36.4	0.46	0.74	0.01	37.1
TL13-32N	0.73	0.71	47.9		0.46	0.52	
TL13-35C	0.78	0.61	47.0		0.50	0.24	
TL13-63A	1.12	1.04	54.5	0.90		0.04	3.0
TL13-98A	0.40	0.53	14.6	0.62	0.81		3.0
TL13-96A	1.15	0.35	38.8	0.78	0.30	0.07	38.3
TL13-109A	0.68	0.29		0.10	0.19		46.8
TL13-162B	0.56	0.50	19.6	0.79	0.20	0.07	
TL13-161F	0.92	0.49	4.6		0.23	0.12	
TL13-01A	0.44	1.58	46.2		0.16		1.3
Mean	0.76	0.81	34	0.69	0.45	0.13	25
STD**	0.22	0.59	16	0.47	0.24	0.15	21

Chalcopyrite/Magnetite

Sample	Ru	Rh	Pd	Re	Ir	Pt	Au
TL13-34B	7.49	20.45	35.2			1.21	
TL13-32A	5.75	12.02	4.6	1.01		0.90	0.02
TL13-32F	0.54	1.71	21.8	0.26		0.86	
TL13-32J	4.68	0.36			0.84		1.05
TL13-32N	1.67	0.66	8.7	0.04	0.12	0.87	
TL13-32R	4.11	0.86	5.7	1.39		0.73	1.05
TL13-35C	2.27	0.86	55.3		0.12	1.10	
TL13-63A	0.55	1.30	21.2		2.55	0.59	
TL13-98A		8.29	67.4		1.44		0.85
TL13-96A		8.56	22.3	1.64	3.09	0.83	
TL13-109A	9.81	5.00		2.63	0.90	0.93	
TL13-162B	3.66	1.95	1.1	0.87	1.59	0.77	2.73
TL13-161F	9.08	0.71		1.72	3.84	1.32	
TL13-161L	4.79	0.76				0.75	
Mean	4.5	4.5	24.3	1.2	1.6	0.9	1.1
STD**	3.0	5.7	21.2	0.8	1.2	0.2	0.9

1.9, 0.07, and 1.9 respectively; and between pentlandite and pyrrhotite 0.76, 0.81, 0.45, 34, 0.45, 0.13, and 25 respectively.

There are very few K_d data in the literature for the precious metals between sulphides and between sulphides and magnetite. The only K_d values available are for Ru, Rh, and Pd between pentlandite and pyrrhotite from experimental results (Distler *et al.*, 1977).

Table 9.2 mean K_d values between the minerals

Ru

	Magnetite	Chalcopyrite	Pyrrhotite
Chalcopyrite	4.5* ± 3.0**		
Pyrrhotite	73 ± 67	11.8 ± 6.3	
Pentlandite	50 ± 38	8.7 ± 4.6	0.76 ± 0.22

* Concentration in chalcopyrite/concentration in magnetite, and same for the rest of table

** 1σ

Rh

	Magnetite	Chalcopyrite	Pyrrhotite
Chalcopyrite	4.5 ± 5.7		
Pyrrhotite	17 ± 14	15 ± 15	
Pentlandite	11 ± 8.8	9.8 ± 10.4	0.81 ± 0.59

Ir

	Magnetite	Chalcopyrite	Pyrrhotite
Chalcopyrite	1.6 ± 1.2		
Pyrrhotite	23 ± 24	3.1 ± 1.9	
Pentlandite	20 ± 22	5.7 ± 6.7	0.45 ± 0.24

Pd

	Magnetite	Chalcopyrite	Pyrrhotite
Chalcopyrite	24 ± 21		
Pyrrhotite	13 ± 11	1.3 ± 1.7	
Pentlandite	521 ± 546	24 ± 16	34 ± 16

Re

	Magnetite	Chalcopyrite	Pyrrhotite
Chalcopyrite	1.2 ± 0.8		
Pyrrhotite	3.7 ± 3.9	2.4 ± 2.5	
Pentlandite	1.7 ± 1.2	1.9 ± 1.7	0.69 ± 0.47

Pt

	Magnetite	Chalcopyrite	Pyrrhotite
Chalcopyrite	0.9 ± 0.2		
Pyrrhotite	0.47 ± 0.36	0.6 ± 0.5	
Pentlandite	0.16 ± 0.28	0.07 ± 0.06	0.13 ± 0.15

Au

	Magnetite	Chalcopyrite	Pyrrhotite
Chalcopyrite	1.1 ± 0.9		
Pyrrhotite	1.1 ± 1.1	0.20 ± 0.21	
Pentlandite	12 ± 11	1.9 ± 1.4	25 ± 21

The K_d values of Ru and Rh (0.76 and 0.81) between pentlandite and pyrrhotite determined in this study are very close to the experimental results (0.97 and 1.0). However, the K_d value for Pd (34) between pentlandite and pyrrhotite determined in this study for Pd is very different from the experimental results (0.97) (Distler *et al.*, 1977). One possible explanation for the difference in K_d's is that the concentrations of Ru and Rh in Distler's experimental products range from 1.1% to 1.3% for Ru and from 0.4% to 0.7% for Rh which are easily detected by electron microprobe. In contrast, the concentrations of Pd in Distler's experimental products were less than 0.1%, which are near the limit of detection for electron microprobe analysis.

The concentrations of Ru, Rh, Ir, and Pd in sulphides and magnetite are positively correlated (Figures 9.1a-d), which results in more consistent K_d values (Table 9.2). In contrast, the concentrations of Re, Pt, and Au are poorly correlated (Figure 9.1e-g) which results in variable K_d values (Table 9.2). The partitioning behaviour of Ru, Rh, Ir, and Re between these minerals produces the largest enrichment in precious metals in the sequence (with decreasing

order): pyrrhotite > pentlandite > chalcopyrite > magnetite. Partitioning of Pd, Pt, and Au among the same minerals follows a different sequence. The sequence for Pd is pentlandite > pyrrhotite ≥ chalcopyrite > magnetite; for Pt the sequence is magnetite > chalcopyrite > pyrrhotite > pentlandite; and for Au the sequence is pentlandite > chalcopyrite > pyrrhotite > magnetite. Pentlandite that exsolved from pyrrhotite solid solution scavenged almost all of the Pd from pyrrhotite. Previous studies showed that Pd and Au are concentrated with pentlandite, and Pt and Ir are associated chalcopyrite (Keays and Crocket, 1970; and Chyi and Crocket, 1976). This is not true for Ir in this study, which is associated with pyrrhotite.

9.3 PARTITIONING OF PRECIOUS METALS DURING SULPHIDE SEGREGATION

The partitioning of precious metals between immiscible (Fe, Ni)-monosulphide liquid and basalt has been investigated by Peach *et al.* (1990), Stone *et al.* (1990), Fleet *et al.* (1991), Barnes (1993), and Barnes and Picard (1993). The investigation by Peach *et al.* (1990) showed partitioning coefficients (K_d values) are in excess of 10^4 for Ir, Pt, and Au between the sulphide globule and natural silicate glass pairs. The investigation of the precious metal partitioning between sulphide liquid and basalt melt at 1200°C with $fo_2 = 10^{9.2}$ and

$fs_2 = 10^{-0.9}$ by Stone *et al.* (1990) shows that the sulphide liquid-silicate melt partitioning coefficients (K_d values) are $(9 \pm 7)\times10^4$ for Pd, $(1 \pm 0.7)\times10^5$ for Ir, $(9 \pm 6)\times10^3$ for Pt, and $(1 \pm 0.9)\times10^3$ for Au; indicating that the precious metals are strongly partitioned into sulphide liquids. Later, Fleet *et al.* (1991) studied the partitioning of Pd, Ir, and Pt between sulphide liquid and basalt melt at 1300°C and at low pressure over the concentration range 40 to 20,000 ppm PGE. Their study showed K_d values vary markedly with the composition of the sulphide liquid and the silicate melt. For 5 ppb PGE in the silicate melt and the iron-silica phase-fayalite buffer, K_d (Pd) and K_d (Pt) are about 2×10^3, and K_d (Ir) is about 3×10^3; whereas, at the maximum concentration of PGE investigated, K_d (Pd) and K_d (Pt) are about 2×10^4, and K_d (Ir) is about 3×10^4. Campbell and Barnes (1984) and Campbell *et al.* (1983) had earlier argued that sulphide liquid-silicate liquid partition coefficients for all of the PGE are very high (10^5 or greater).

Despite the great variations of K_d values for precious metals measured by different investigators, one conclusion that can be made is that K_d values are very high (10^3-10^5), at least for basaltic systems, and that the precious metals are strongly partitioned into sulphide liquids during magmatic sulphide segregation.

9.4 FRACTIONATION OF PRECIOUS METALS DURING MINERAL CRYSTALLIZATION

Some possible mechanisms for the origin of precious metal fractionation are: redistribution of the precious metals by diffusion in response to thermal gradients, hydrothermal alteration, partial melting and crystal fractionation (Naldrett *et al.*, 1982 and Barnes *et al.*, 1985). Previous investigations concluded that the fractional crystallization of monosulphide solid solution from a sulphide melt provided the best explanation for the distribution of precious metals for the zoning and origin of Sudbury Cu-Ni and precious metal ore deposits (Hawley, 1965; Keays and Crocket, 1970; Chyi and Crocket, 1976; Naldrett *et al.*, 1982; Barnes *et al.*, 1985 and Li *et al.*, 1992).

9.4.1 MINERAL CHEMISTRY OF PRECIOUS METALS IN THE PRINCIPLE ORE MINERALS

Figure 9.2 demonstrates strong linear correlations between Ru, Rh, Re and Ir in bulk ores. Figure 9.3 shows strongly linear relationships in logarithmic scale in the concentrations among the precious metals in sulphides and magnetite. These strong linear correlations suggest that these elements are or were in solid solutions in these minerals; thus they behaved as compatible elements during magnetite and sulphide crystallization. Poor linear correlations for Pd, Re, Pt,

and Au indicate that these elements are dominantly found in separate discrete phases either as minor inclusions in the ore minerals or as precious metal alloy located at the boundaries between the major ore minerals (Figures 7.3, and 8.8-8.11). This behaviour is supported by the crystallization experiments on sulphide melts (Distler *et al.*, 1977). Distler *et al.* (1977) investigated the distribution of minor amounts of Ru, Rh, and Pd between pyrrhotite and pentlandite and residual liquids. Their experiments showed that Pd is progressively concentrated in the residual sulphide liquid, and Ru and Rh in the solid solution in pyrrhotite. For the Thayer Lindsley Mine, as magnetite and sulphides crystallized, the residual liquid which was enriched in Pd, Pt and Au was expelled to the margin of orebodes. This may also explain why the ore from the margin is enriched in chalcopyrite with high concentrations of Pd, Pt and Au (Chapter 8).

The reason that Ru, Rh, and Ir are in solid solutions of sulphide, whereas the rest of precious metal are dominantly in discrete phases is a subject of debate. One possible explanations might be related to atomic radii of the precious metals. Table 9.3 shows that the atomic radii of Ru, Rh, and Ir are closer to those of Fe, Ni, and Cu than those of Pd, Re, Pt and Au. This suggests that substitutions could take place more readily between Ru, Rh, and Ir and the base metals in sulphides and magnetite.

Table 9.3 Atomic Radii of Fe, Ni, Cu, and Precious Metals (Greenwood and Earnshaw, 1984)

Element	Fe	Ni	Cu	Ru	Rh	Pd	Re	Ir	Pt	Au
Radii (pm)	126	124	128	134	134	137	137	135.5	138.5	144

9.4.2 FRACTIONATION OF PRECIOUS METALS DURING CRYSTALLIZATION

The chondrite normalized PGE pattern of the bulk ores (Figure 9.4a) shows that the precious metals are strongly fractionated, with strong enrichment in PPGE (Pt, Pd, and Au) and depletion in IPGE (Ir, Os, Ru, and Rh) in the 4B Ore Zone at the Thayer Lindsley Mine. Chondrite normalized patterns of sulphides and magnetite from the 4B Ore Zone at the Thayer Lindsley Mine are shown in Figures 9.4b-e. Since a large amount of exsolution took place after the sulphide minerals were crystallized, the only pattern that might represent crystallization fractionation is the one from the early crystallized magnetite which may not have been subjected to subsequent exsolution. Figures 9.4b shows that the chondrite normalized pattern of magnetite is very similar to the one from bulk ore analysis (Figure 9.4a). In order to compare the fractionation of the precious metals to the bulk ore, the concentrations of the precious metals in the sulphides and magnetite were normalized to the mean concentration of the whole rocks (Figure 9.5). The whole rock normalized

patterns of magnetite (Figure 9.5c) are almost flat, although they are enriched in Au. In contrast, the whole rock normalized patterns of the sulphide minerals (except for the chalcopyrite) (Figures 9.5a-b) show strong depletions of Pt, indicating that the bulk of these elements are exsolved from the sulphides as discrete Pt and Au phases. The whole rock normalized patterns of the pyrrhotite and pentlandite are characterized by depletion and enrichment of Pd, respectively, indicating Pd was strongly partitioned into the pentlandite during exsolution. These features agree well with experimental results. The solubilities of precious metal in base metal sulphides in the Fe-PGE-S and Cu-Fe-PGE-S systems have been investigated by Makovicky *et al.* (1986). Their experiments showed that Pt, Pd, Rh, and Ru solubilities in pyrrhotite decrease dramatically from 900°C to 500°C; quenching or cooling can thus cause exsolution of almost all the PGE from the pyrrhotite phase; and at 500°C, in equilibrium with a sulphide liquid containing 6 to 15 wt percent Pt, coexisting pyrrhotite dissolved small amounts of Pt (1.2%) whereas intermediate solid solution and chalcopyrite do not dissolve microprobe-detectable quantities of PGE. The results indicate that Pt will concentrate in the coexisting liquid during the crystallization of a sulphide melt. Under slow cooling, additional PGE can be rejected from the originally PGE-saturated monosulphide solid solution structure and diffuse into the coexisting liquid or form discrete phases at grain boundaries.

9.5 A MODEL OF PRECIOUS METAL FRACTIONATION DURING SULPHIDE SEGREGATION AND CRYSTALLIZATION

A model of precious metal fractionation during sulphide segregation and crystallization is shown in Figure 9.6. Sulphide melt segregating from the magma scavenges almost all of the precious metals from the silicate melt. The fractionation of the precious metals during crystallization follows two distinct trends:

(1) The bulk of the Ru, Rh, Os, Re, Ir, and small proportions of Pd, Pt, and Au are incorporated into the early crystallized monosulphide solid solution at high temperature. These metals substitute for the base metals in monosulphide solid solution. Subsequent cooling results in subsolidus exsolution of chalcopyrite, followed by pentlandite. Precious metals are partitioned between the monosulphide and the exsolution products of chalcopyrite and pentlandite. Ru, Rh, Os, and Ir are more enriched in pyrrhotite; whereas Pd, Pt, and Au are enriched in chalcopyrite and pentlandite. On further cooling, Pd, Pt, and Au are rejected from these sulphide mineral lattices which results in exsolution of precious metal-enriched phases either as inclusions within or minute grains at the boundaries between the sulphide minerals.

(2) The majority of Pd (90%), Pt (98%), Au (76%), and small proportions

of Rh and Ir are incompatible in monosulphide solid solution. These metals are enriched in the late stage sulphide liquids, and form discrete precious metal-minerals in the late stage of crystallization.

9.6 SUMMARY AND CONCLUSIONS

The major conclusions of this chapter are:

(1) Partitioning of Ru, Rh, Ir, and Re between these minerals are following one sequence (with decreasing order): pyrrhotite > pentlandite > chalcopyrite > magnetite. Partitioning of Pd, Pt, and Au are different.

(2) Ruthenium, Rh, and Ir are dominantly found in solid solutions with sulphide, whereas the rest of precious metal are dominantly in discrete phases.

(3) Precious metals are strongly partitioned into sulphide liquids during magmatic sulphide segregation.

(4) Crystallization and subsequent exsolution are mainly responsible for the distribution and fractionation of the precious metals in sulphides and magnetite for the Cu-Ni-(PGE) deposits at Sudbury.

Figure 9.1 Precious metal concentrations in pyrrhotite versus those in coexisting pentlandite from the Thayer Lindlsey mine: (a) Ru, (b) Rh, (c) Ir, (d) Pd, (e) Pt, (f) Re, and (g) Au

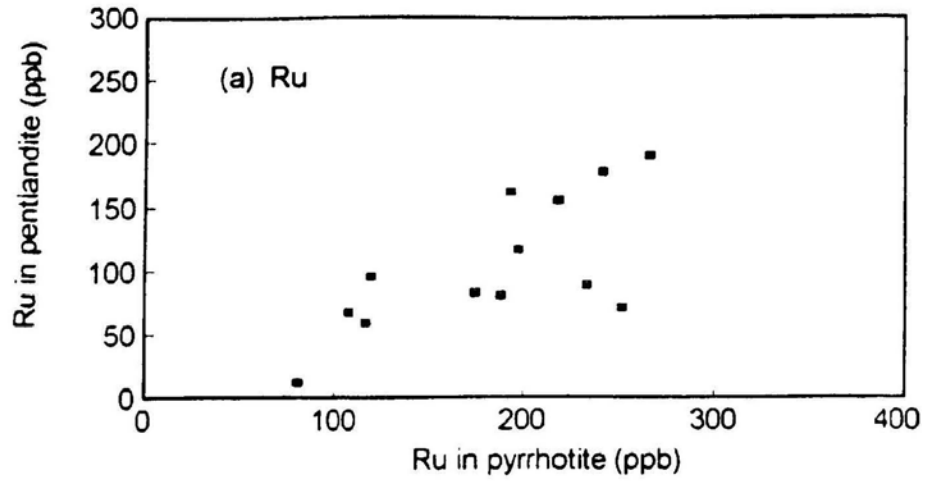
(a) Ru
Ru in pentlandite (ppb)
Ru in pyrrhotite (ppb)
0
50
100
150
200
250
300
0
100
200
300
400

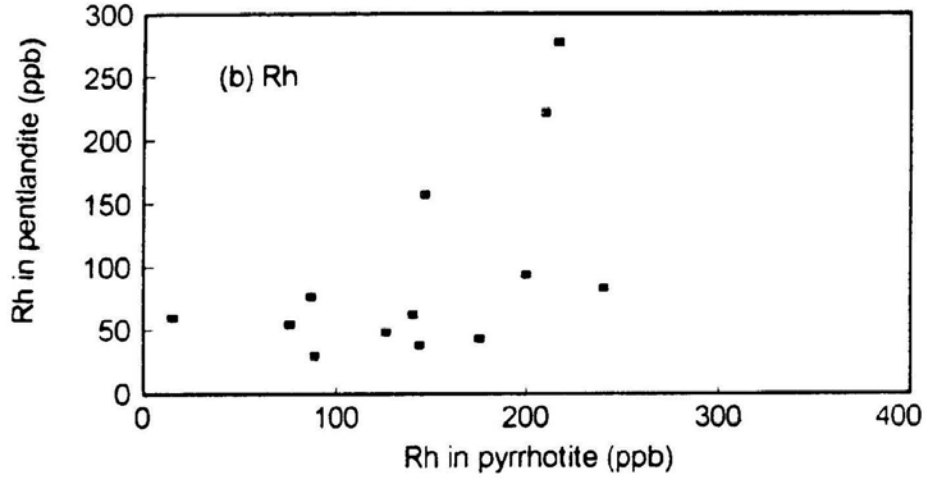
(b) Rh
Rh in pentlandite (ppb)
Rh in pyrrhotite (ppb)
0
50
100
150
200
250
300
0
100
200
300
400

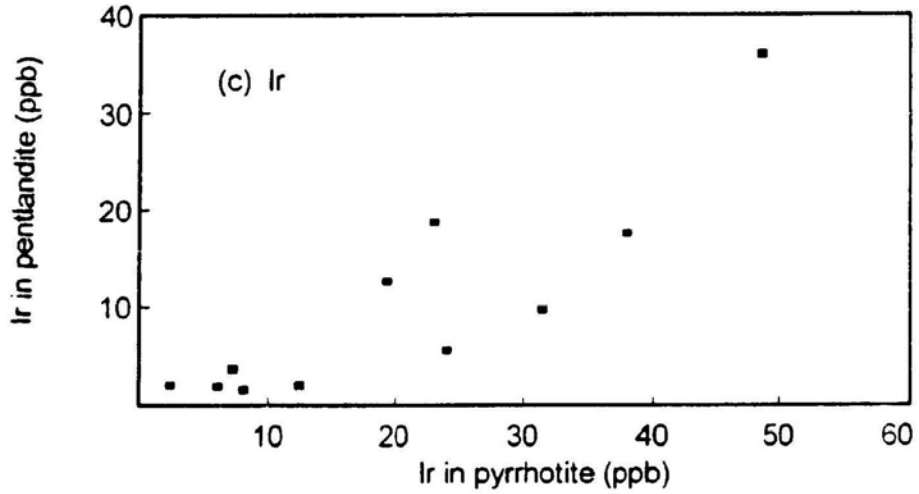
(c) Ir
Ir in pentlandite (ppb)
Ir in pyrrhotite (ppb)
10
20
30
40
10
20
30
40
50
60

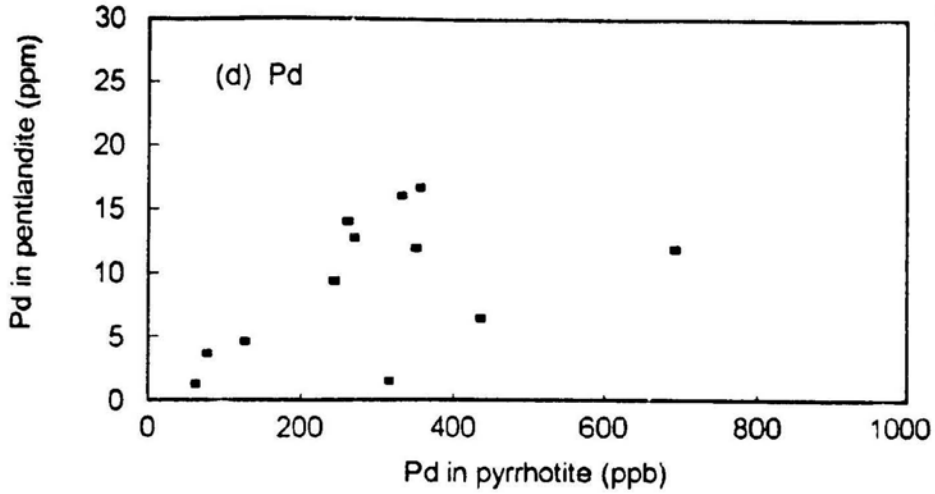
(d) Pd
Pd in pentlandite (ppm)
Pd in pyrrhotite (ppb)
0
5
10
15
20
25
30
0
200
400
600
800
1000

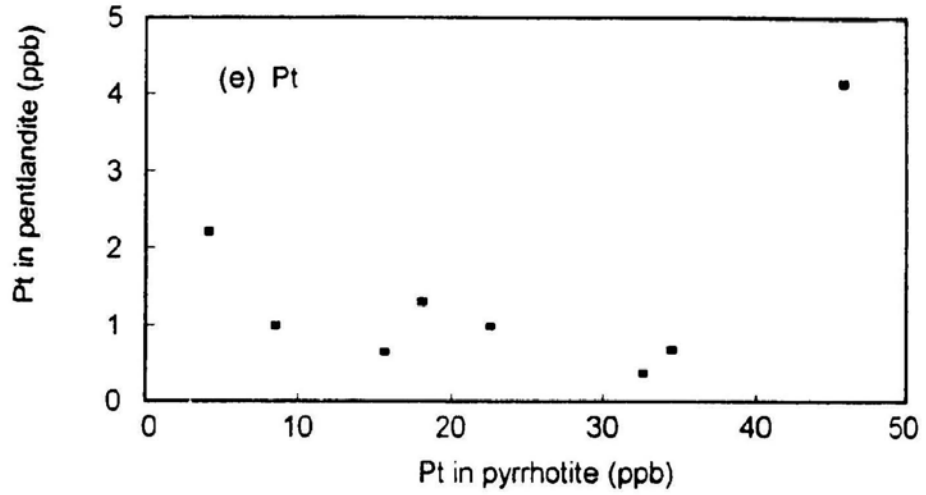
(e) Pt
Pt in pentlandite (ppb)
Pt in pyrrhotite (ppb)
0
1
2
3
4
5
0
10
20
30
40
50

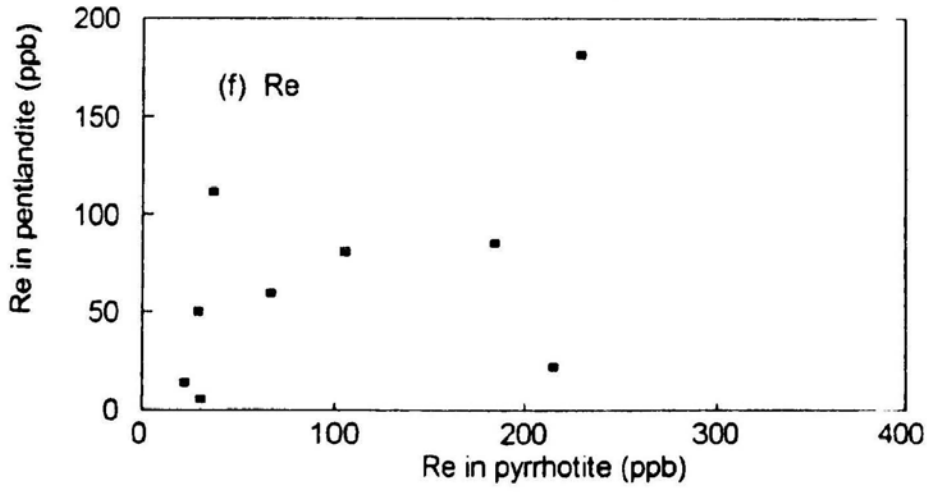
(f) Re
Re in pentlandite (ppb)
Re in pyrrhotite (ppb)
0
50
100
150
200
0
100
200
300
400

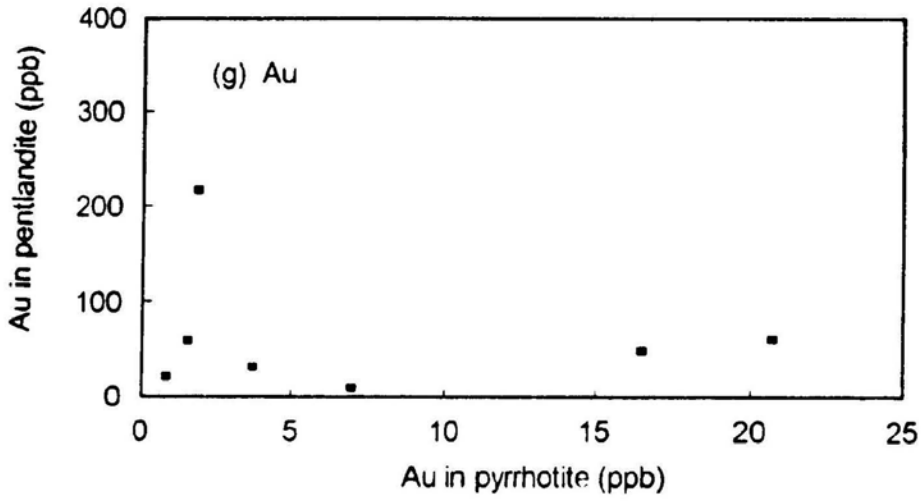
(g) Au
Au in pentlandite (ppb)
400
300
200
100
0
0
5
10
15
20
25
Au in pyrrhotite (ppb)

Figure 9.2 Correlations of precious metal concentrations in bulk sulphide ores from the Thayer Lindsley Mine, between: (a) Rh and Ru, (b) Os and Ru, (c) Ir and Ru, (d) Os and Rh, (d) Ir and Rh, (f) Ir and Os, (g) Pd and Ru, and (h) Pt and Pd

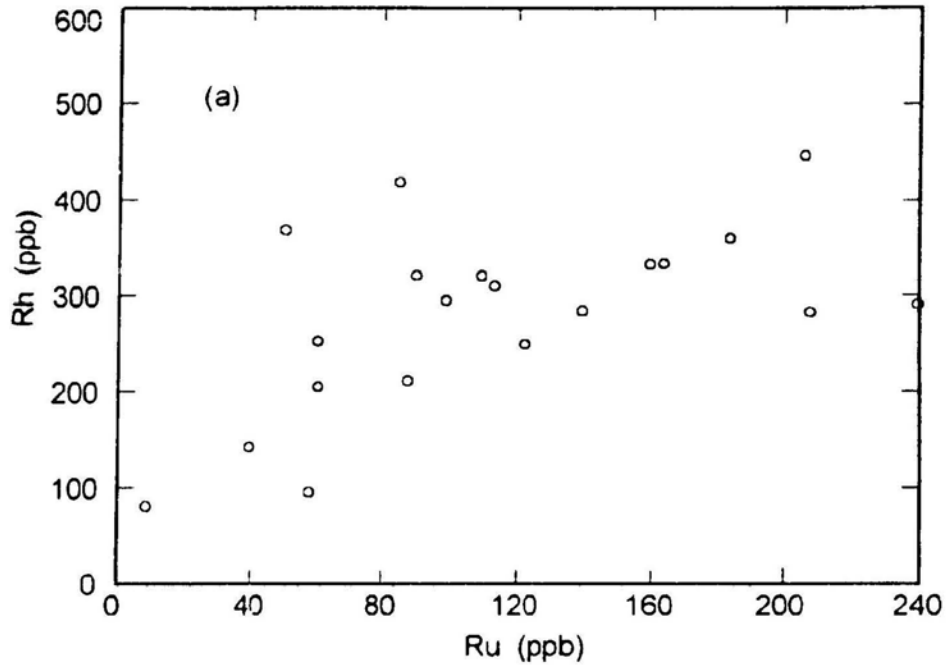
(a)
Rh (ppb)
Ru (ppb)
0
100
200
300
400
500
600
0
40
80
120
160
200
240

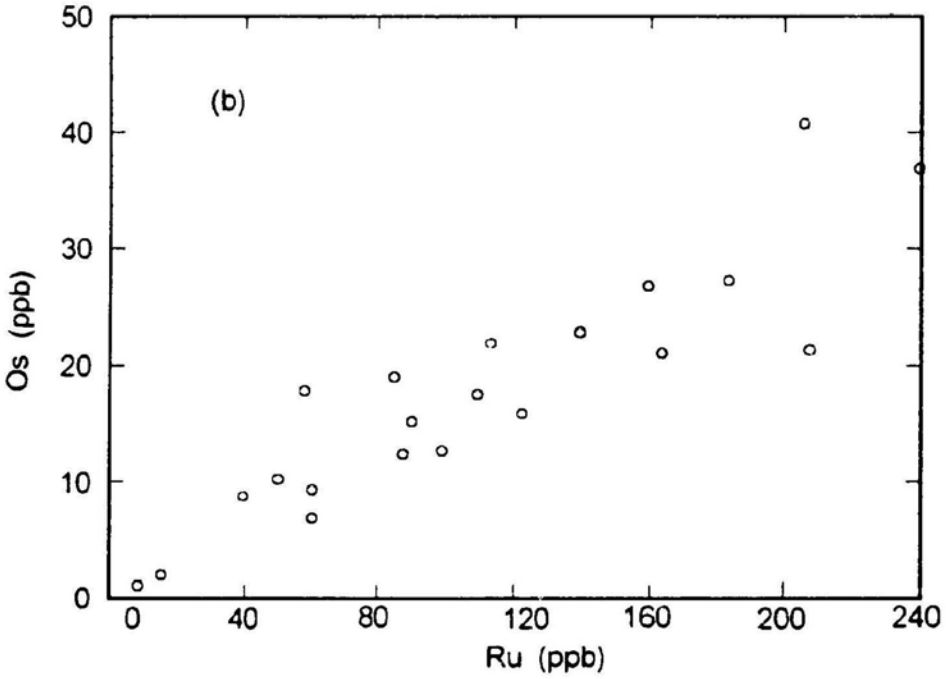
(b)
Os (ppb)
Ru (ppb)
0
10
20
30
40
50
0
40
80
120
160
200
240

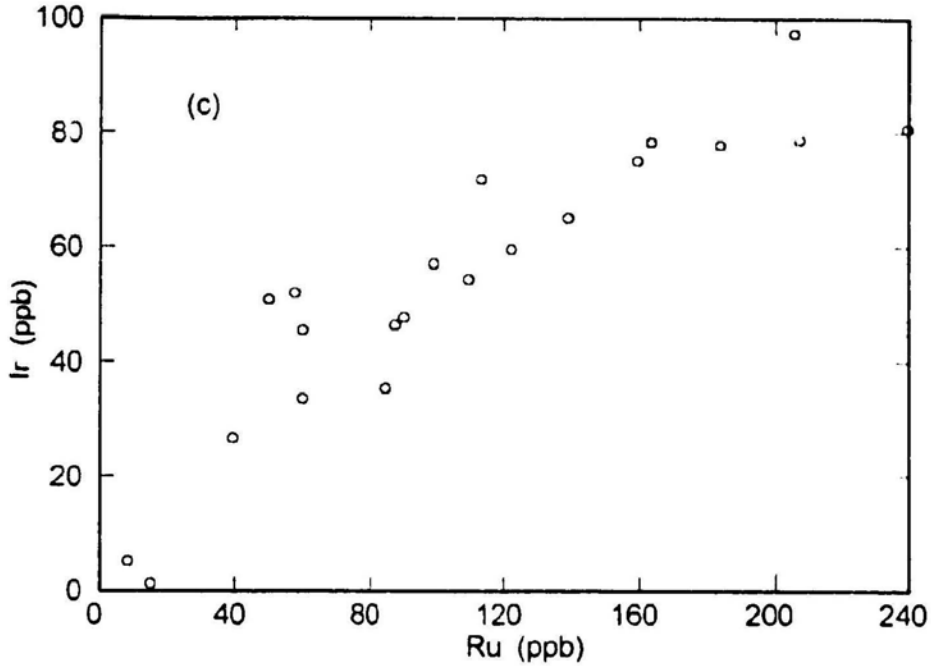
(c)
Ir (ppb)
Ru (ppb)
0
20
40
60
80
100
0
40
80
120
160
200
240

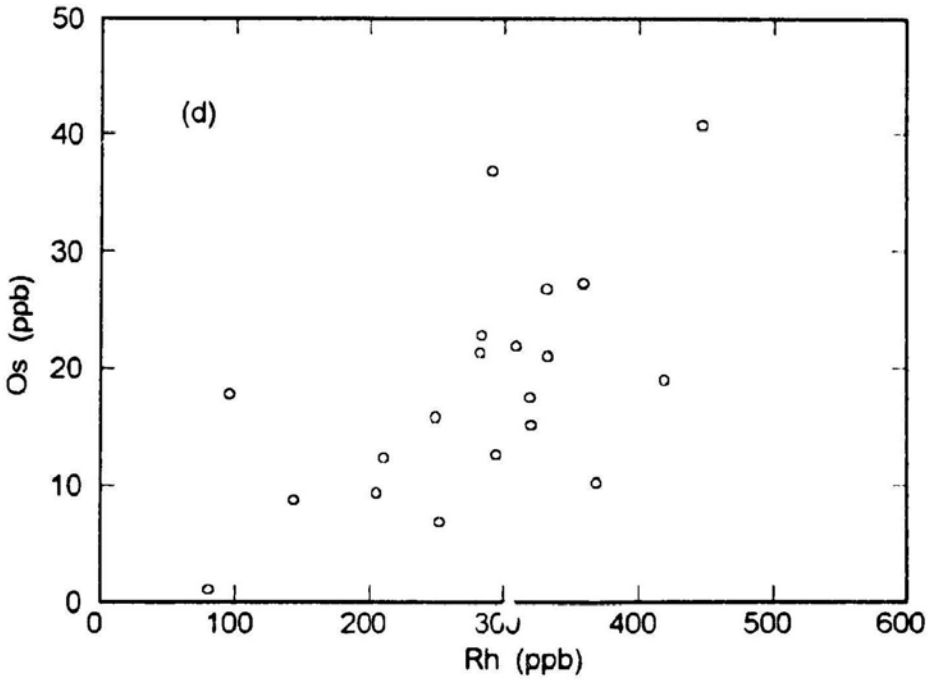
(d)
Os (ppb)
Rh (ppb)
0
10
20
30
40
50
0
100
200
300
400
500
600

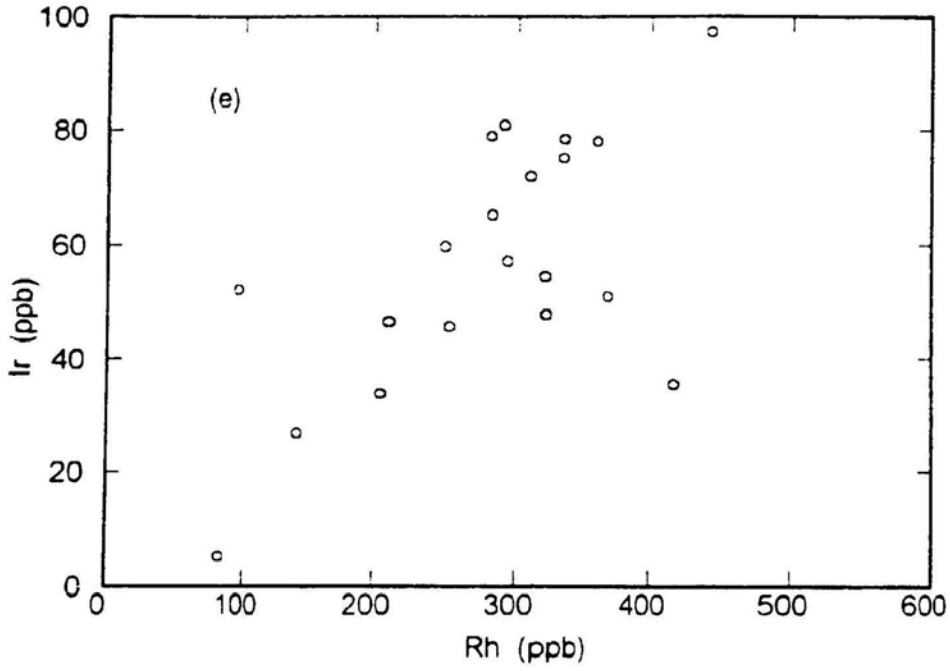
(e)
Ir (ppb)
Rh (ppb)
0
20
40
60
80
100
0
100
200
300
400
500
600

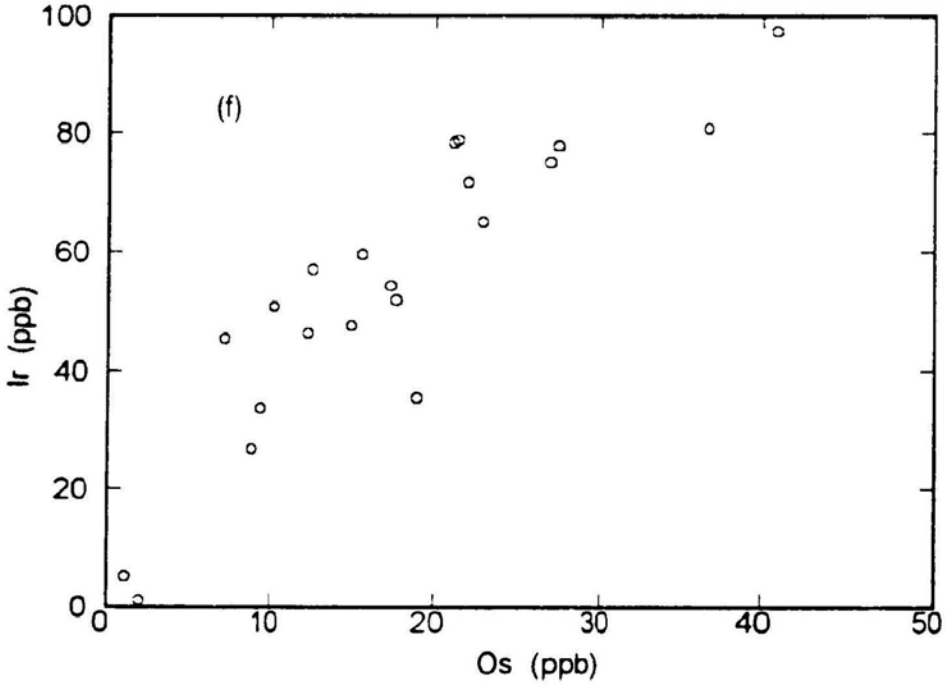
(f)
Ir (ppb)
Os (ppb)
0
20
40
60
80
100
0
10
20
30
40
50

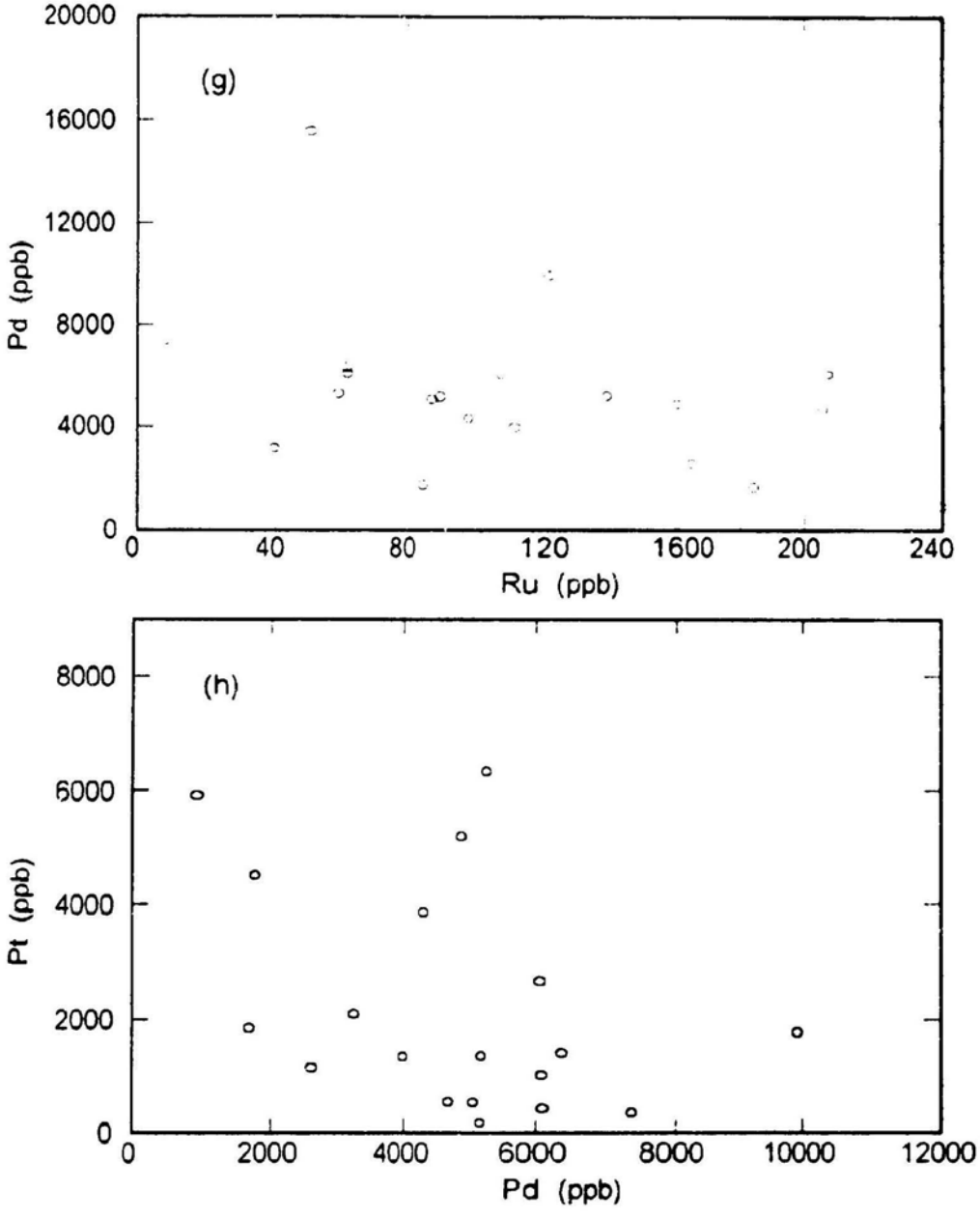
(g)
Pd (ppb)
Ru (ppb)
20000
16000
12000
8000
4000
0
0
40
80
120
1600
200
240
(h)
Pt (ppb)
Pd (ppb)
8000
6000
4000
2000
0
0
2000
4000
6000
8000
10000
12000

Figure 9.3 Correlation of precious metal concentrations in the principle ore minerals from the Thayer Lindsley Mine between: (a) Rh and Ru, (b) Ir and Ru, (c) Ir and Rh, (d) Pd and Ru, (e) Pt and Ru, (f) Pd and Pt, and (g) Au and Pt

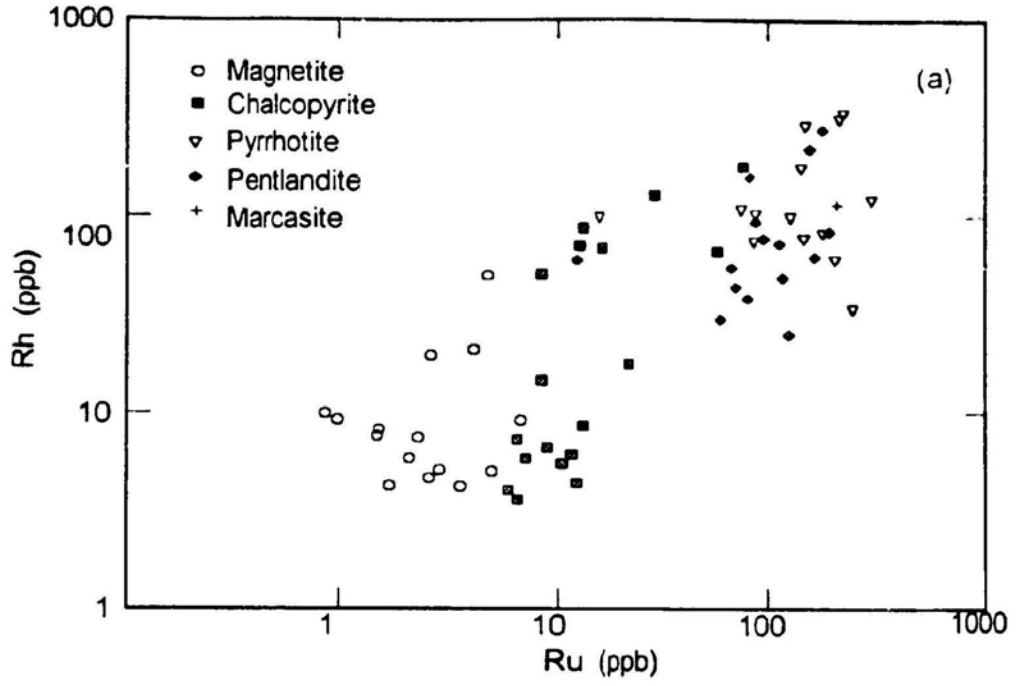
1000
100
10
1
Rh (ppb)
Magnetite
Chalcopyrite
Pyrrhotite
Pentlandite
Marcasite
(a)
1
10
100
1000
Ru (ppb)

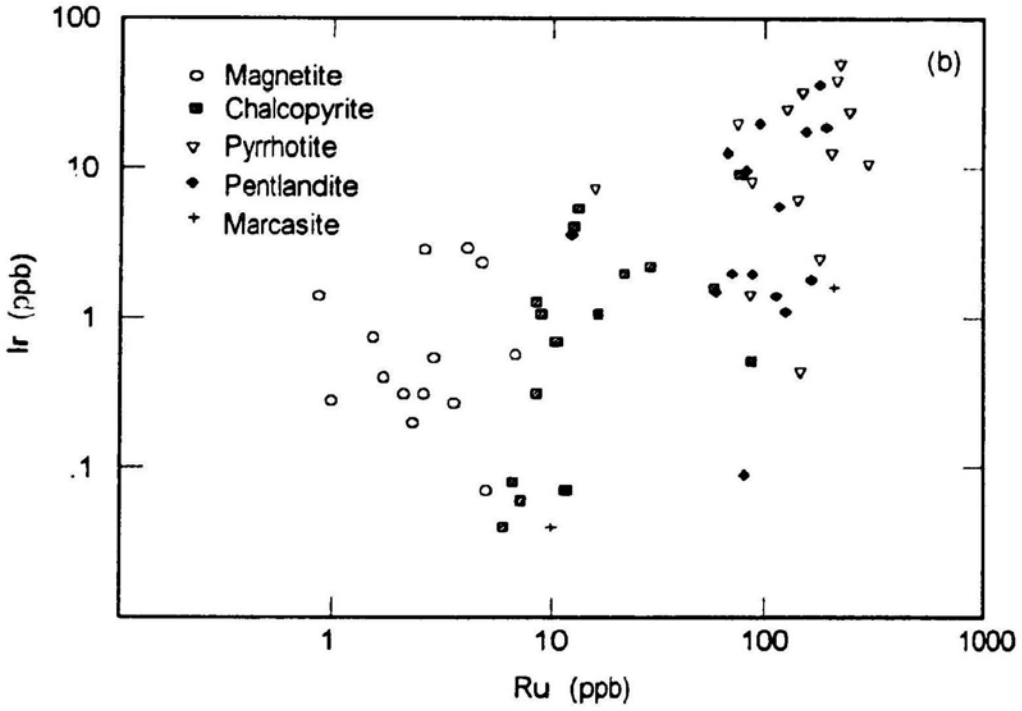
100
10
1
.1
Ir (ppb)
Magnetite
Chalcopyrite
Pyrrhotite
Pentlandite
Marcasite
(b)
1
10
100
1000
Ru (ppb)

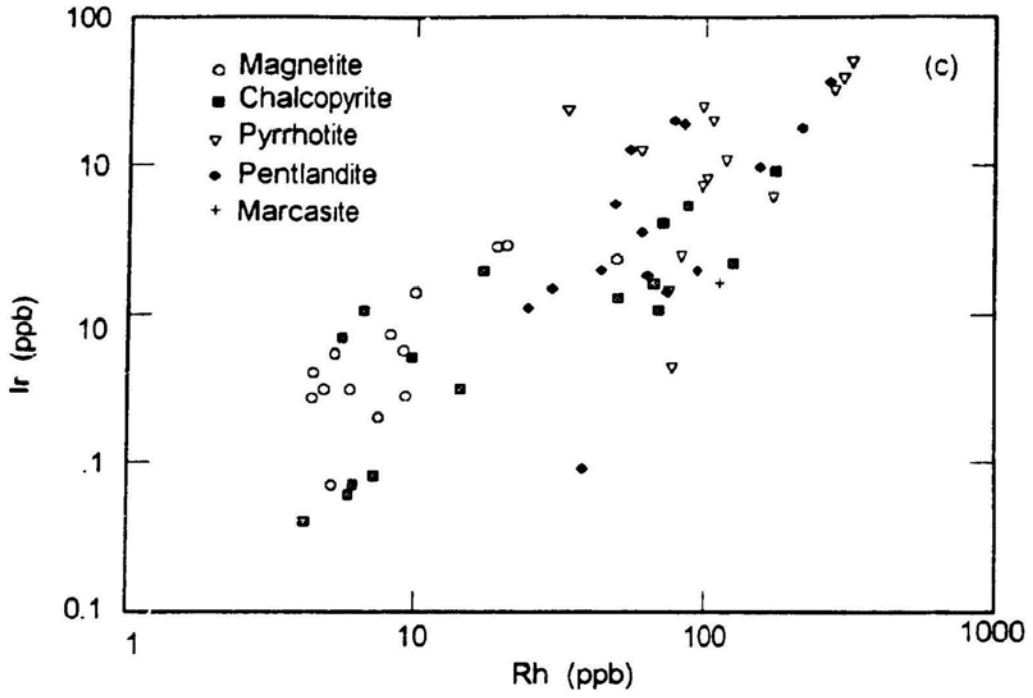
Magnetite
Chalcopyrite
Pyrrhotite
Pentlandite
Marcasite
(c)
Ir (ppb)
Rh (ppb)
100
10
10
.1
0.1
1
10
100
1000

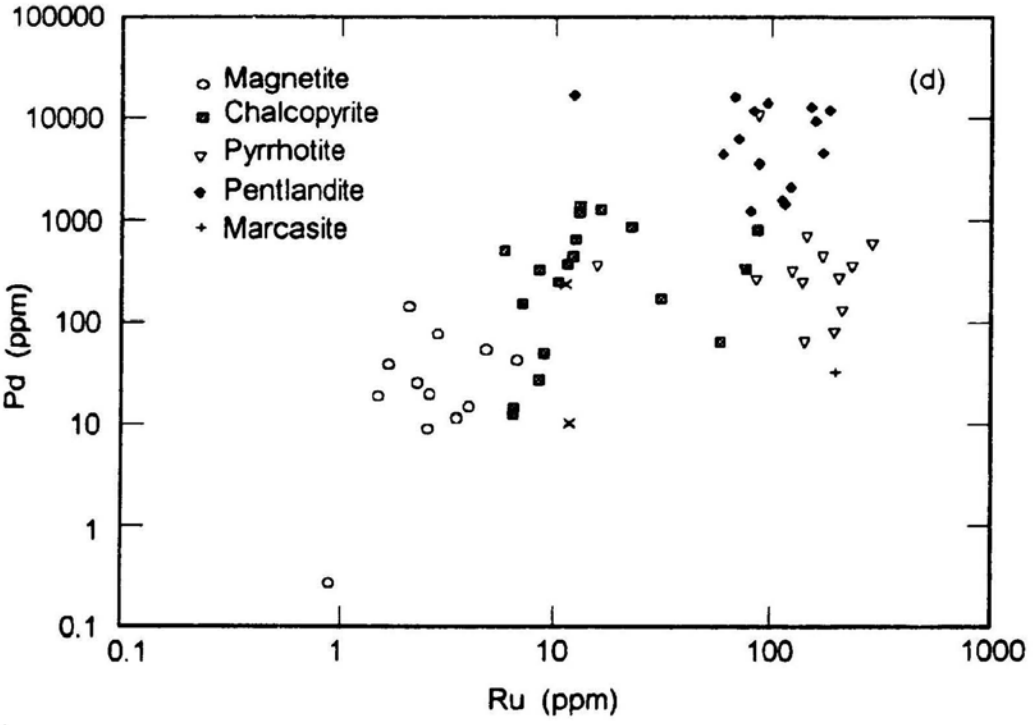
Magnetite
Chalcopyrite
Pyrrhotite
Pentlandite
Marcasite
(d)
Pd (ppm)
Ru (ppm)
100000
10000
1000
100
10
1
0.1
0.1
1
10
100
1000

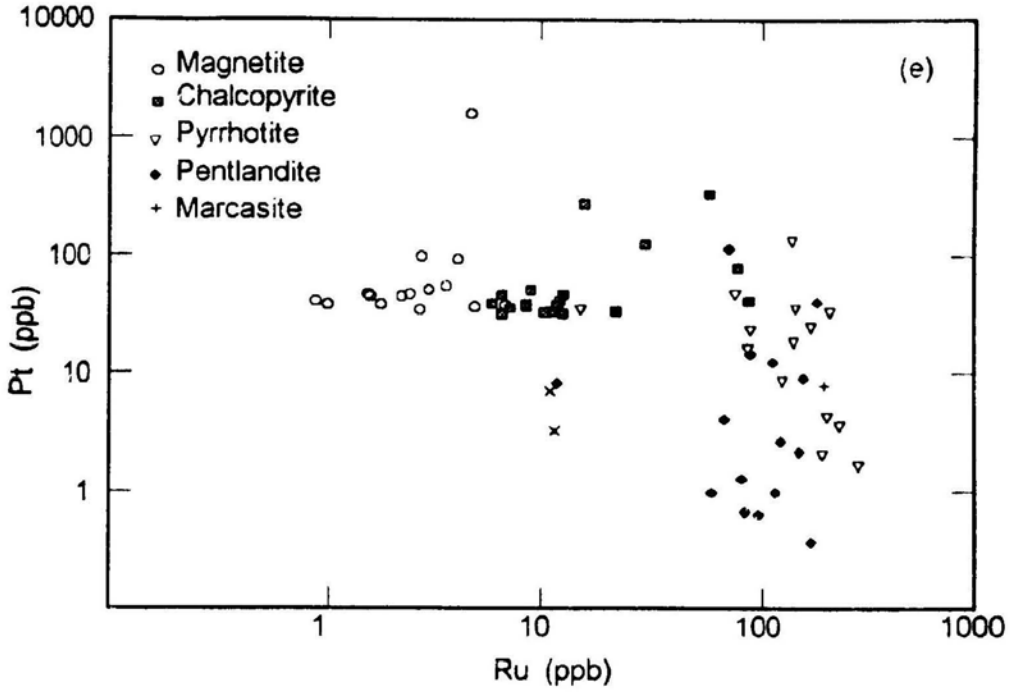
10000
1000
100
10
1
Pt (ppb)
Magnetite
Chalcopyrite
Pyrrhotite
Pentlandite
Marcasite
(e)
1
10
100
1000
Ru (ppb)

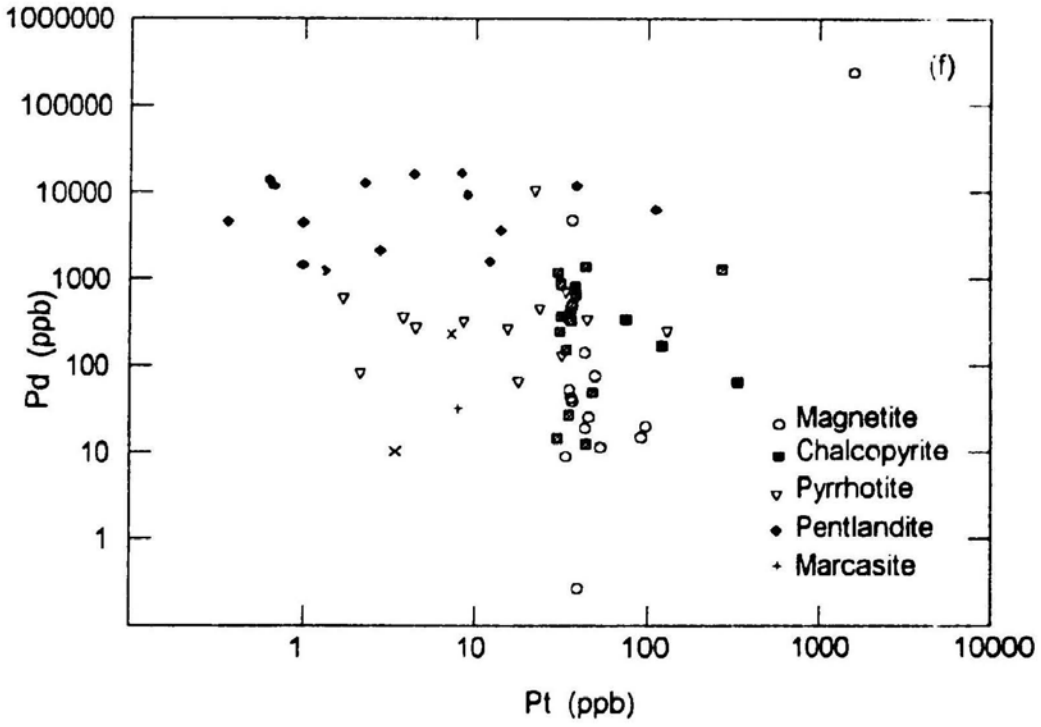
1000000
100000
10000
1000
100
10
1
Pd (ppb)
(f)
Magnetite
Chalcopyrite
Pyrrhotite
Pentlandite
Marcasite
1
10
100
1000
10000
Pt (ppb)

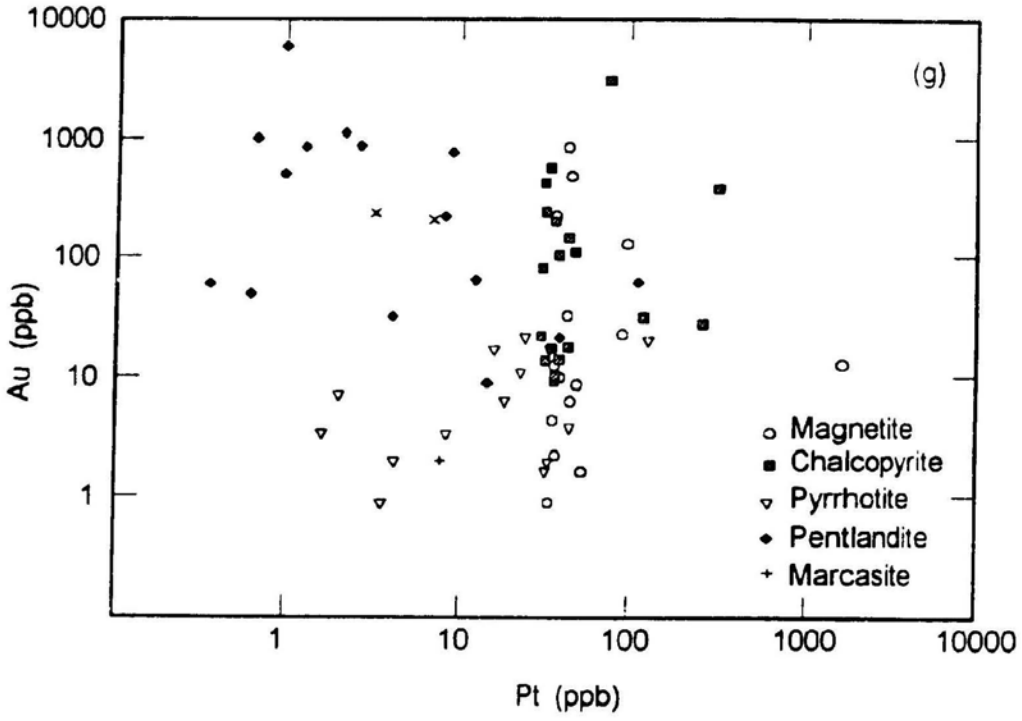
10000
1000
100
10
1
Au (ppb)
(g)
Magnetite
Chalcopyrite
Pyrrhotite
Pentlandite
Marcasite
1
10
100
1000
10000
Pt (ppb)

Figure 9.4 Chondrite normalized precious metal patterns of (a) whole rocks, (b) magnetite, (c) pyrrhotite, (d) pentlandite, (e) chalcopyrite, and (f) marcasite in sulphide ores from the Thayer Lindsley Mine

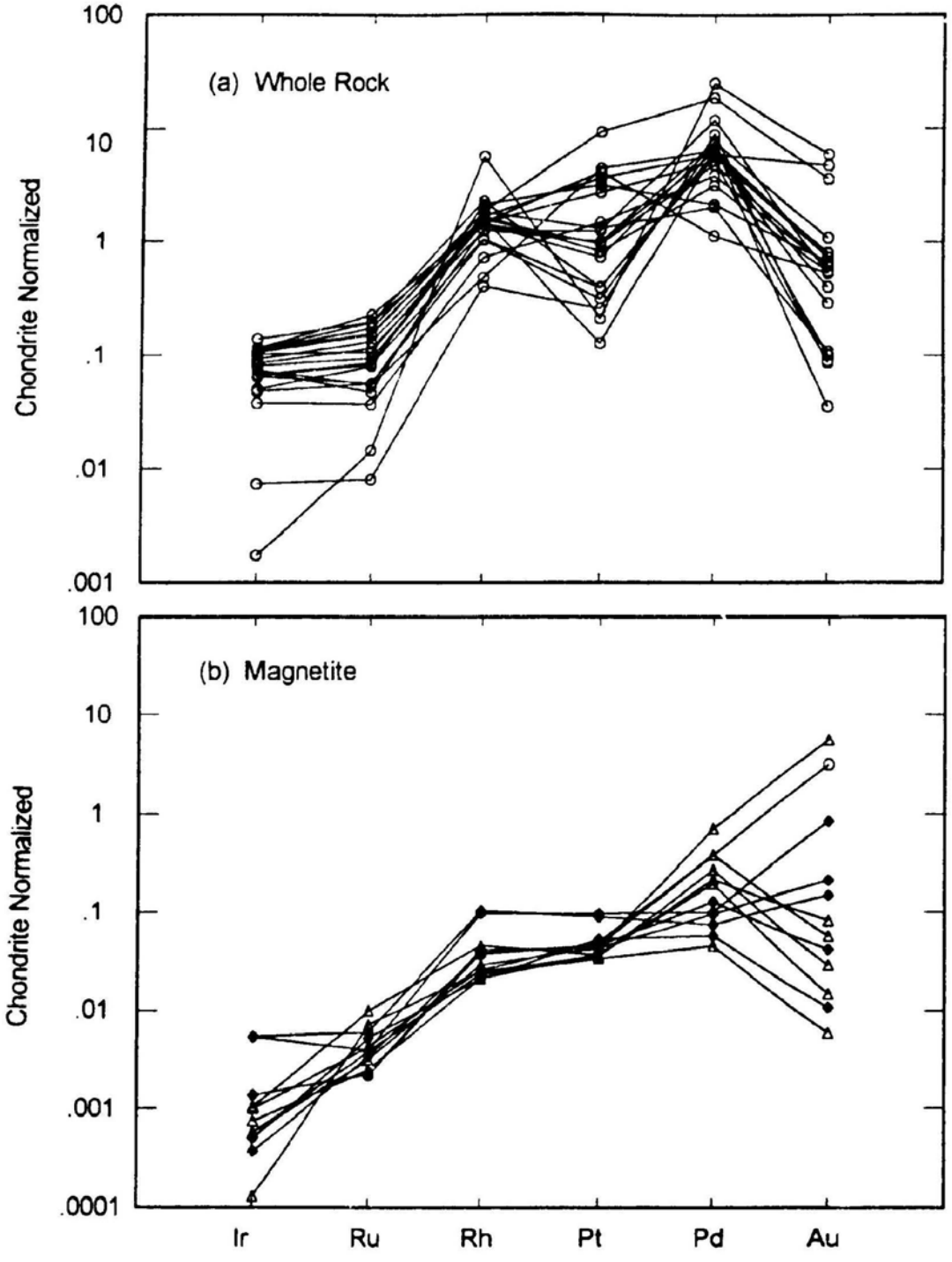
(a) Whole Rock
(b) Magnetite
Chondrite Normalized
100
10
1
.1
.01
.001
.0001
Ir
Ru
Rh
Pt
Pd
Au

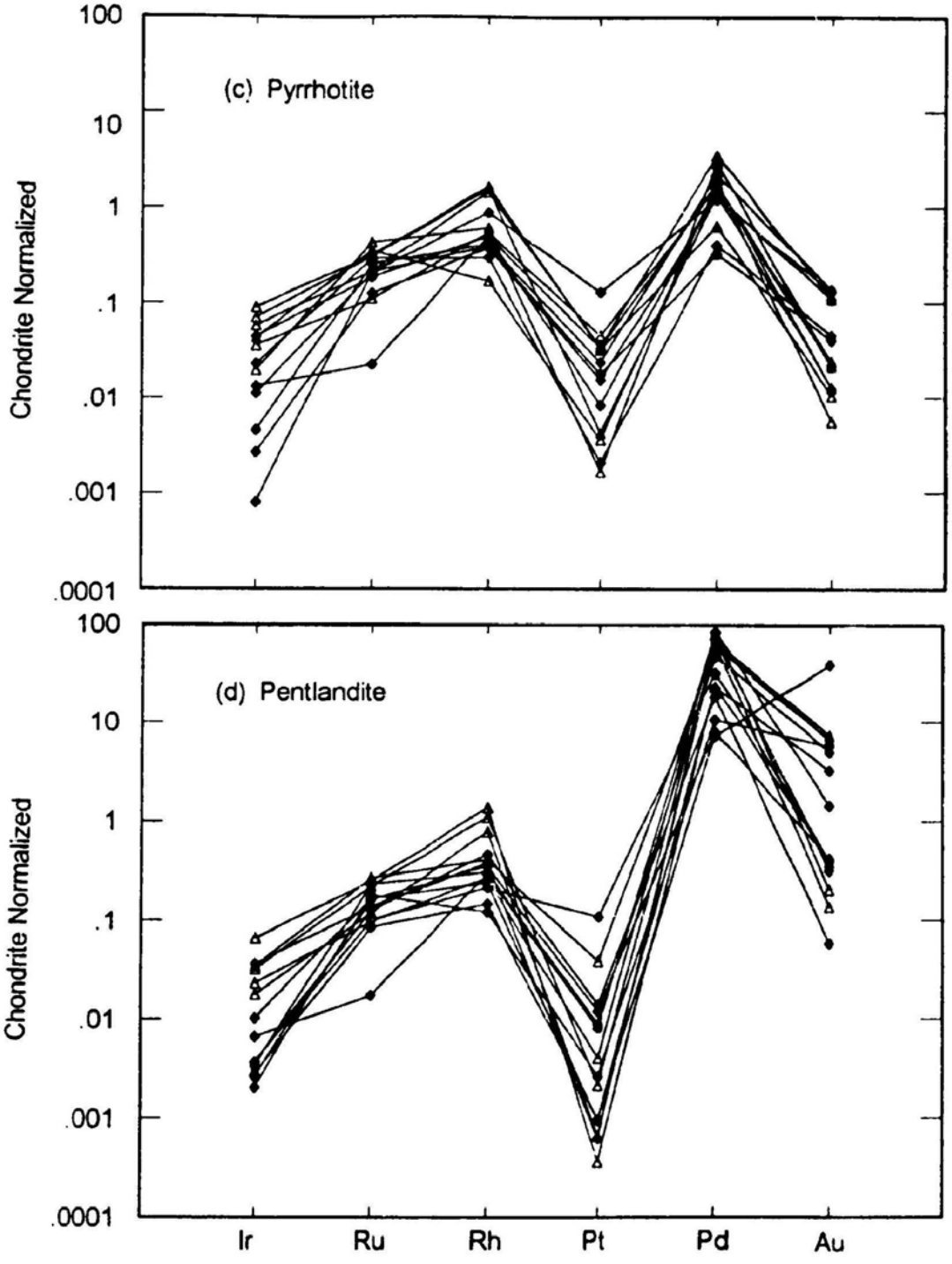
(c) Pyrrhotite
(d) Pentlandite
Chondrite Normalized
100
10
1
.1
.01
.001
.0001
Ir
Ru
Rh
Pt
Pd
Au

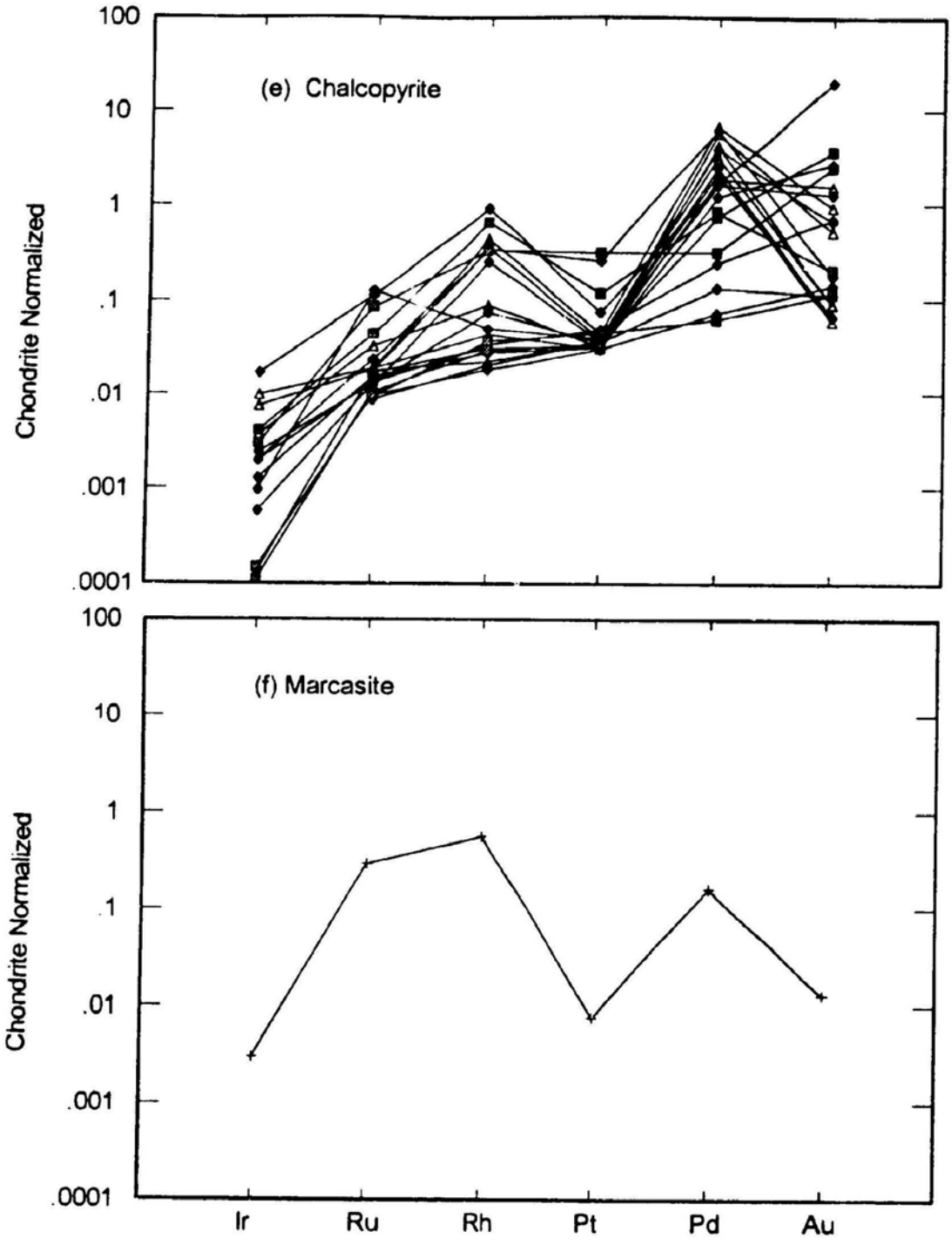
(e) Chalcopyrite
Chondrite Normalized
100
10
1
.1
.01
.001
.0001
(f) Marcasite
Chondrite Normalized
100
10
1
.1
.01
.001
.0001
Ir
Ru
Rh
Pt
Pd
Au

Figure 9.5 Whole rock normalized precious metal patterns of (a) pyrrhotite, (b) pentlandite, (c) magnetite, (d) chalcopyrite, (e) marcasite, and (f) pyrite in sulphide ores from the Thayer Lindsley Mine.

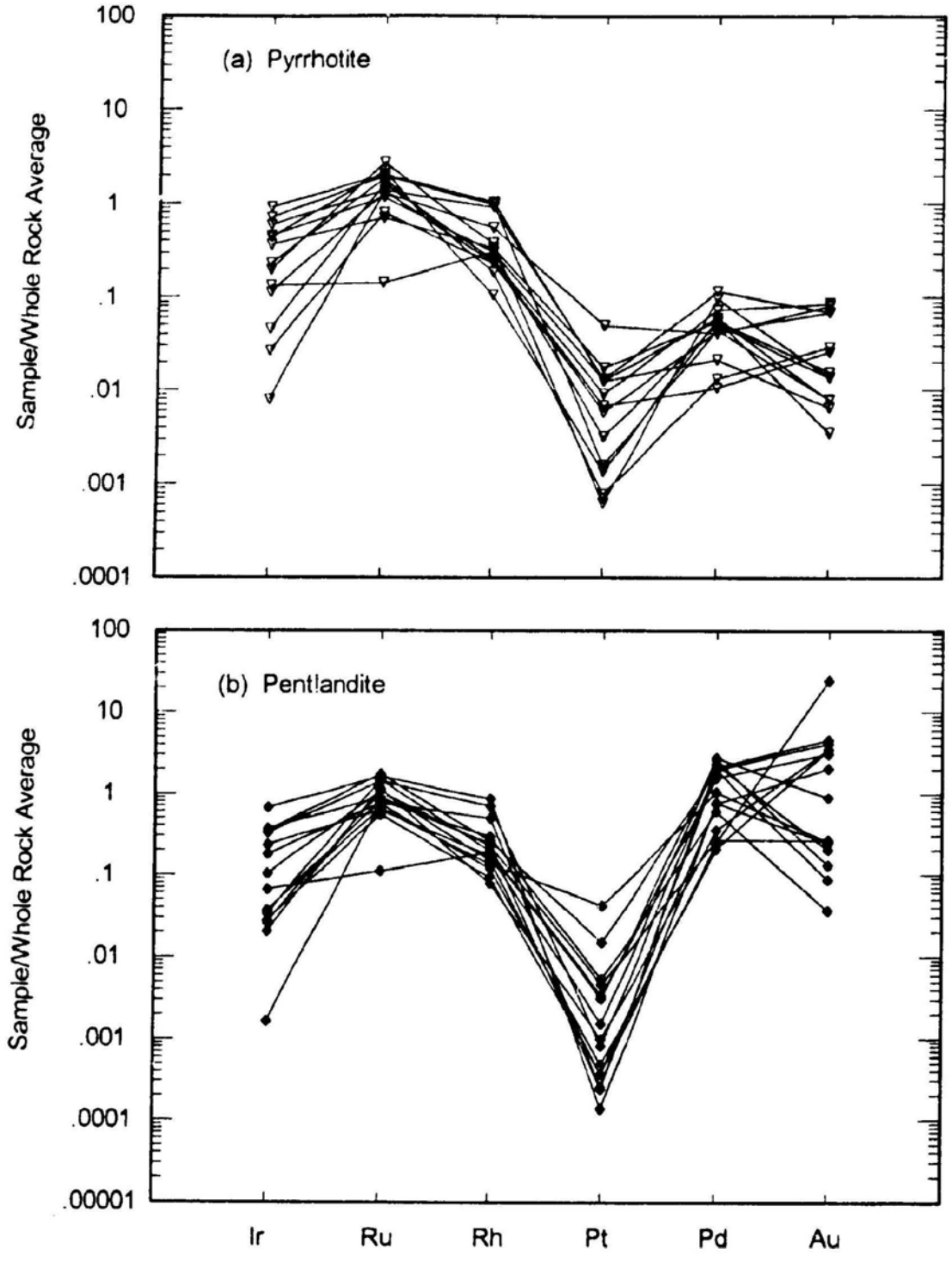
(a) Pyrrhotite
(b) Pentlandite
Sample/Whole Rock Average
100
10
1
.1
.01
.001
.0001
.00001
Ir
Ru
Rh
Pt
Pd
Au

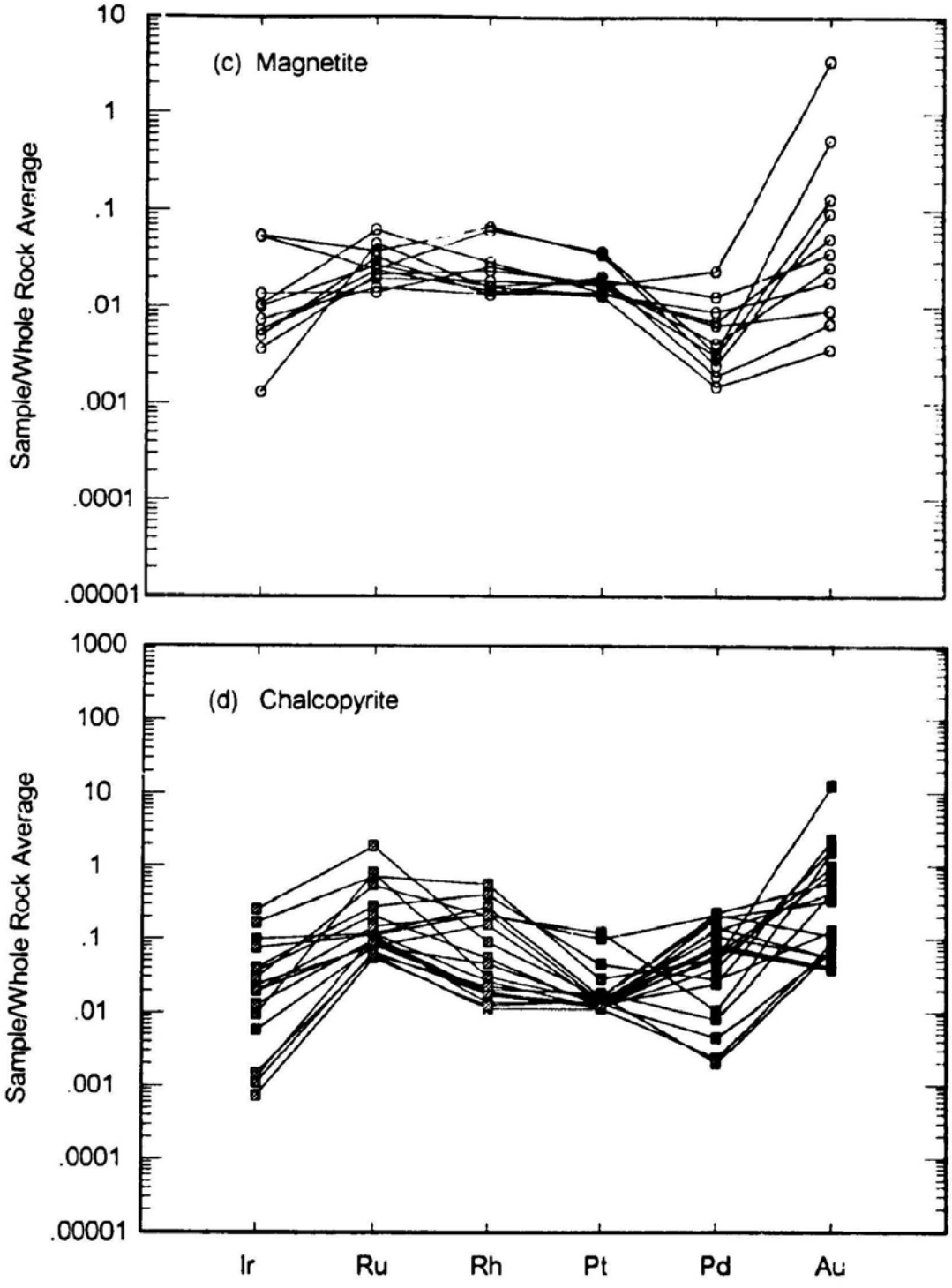
(c) Magnetite
Sample/Whole Rock Average
10
1
.1
.01
.001
.0001
.00001
(d) Chalcopyrite
Sample/Whole Rock Average
1000
100
10
1
.1
.01
.001
.0001
.00001
Ir
Ru
Rh
Pt
Pd
Au

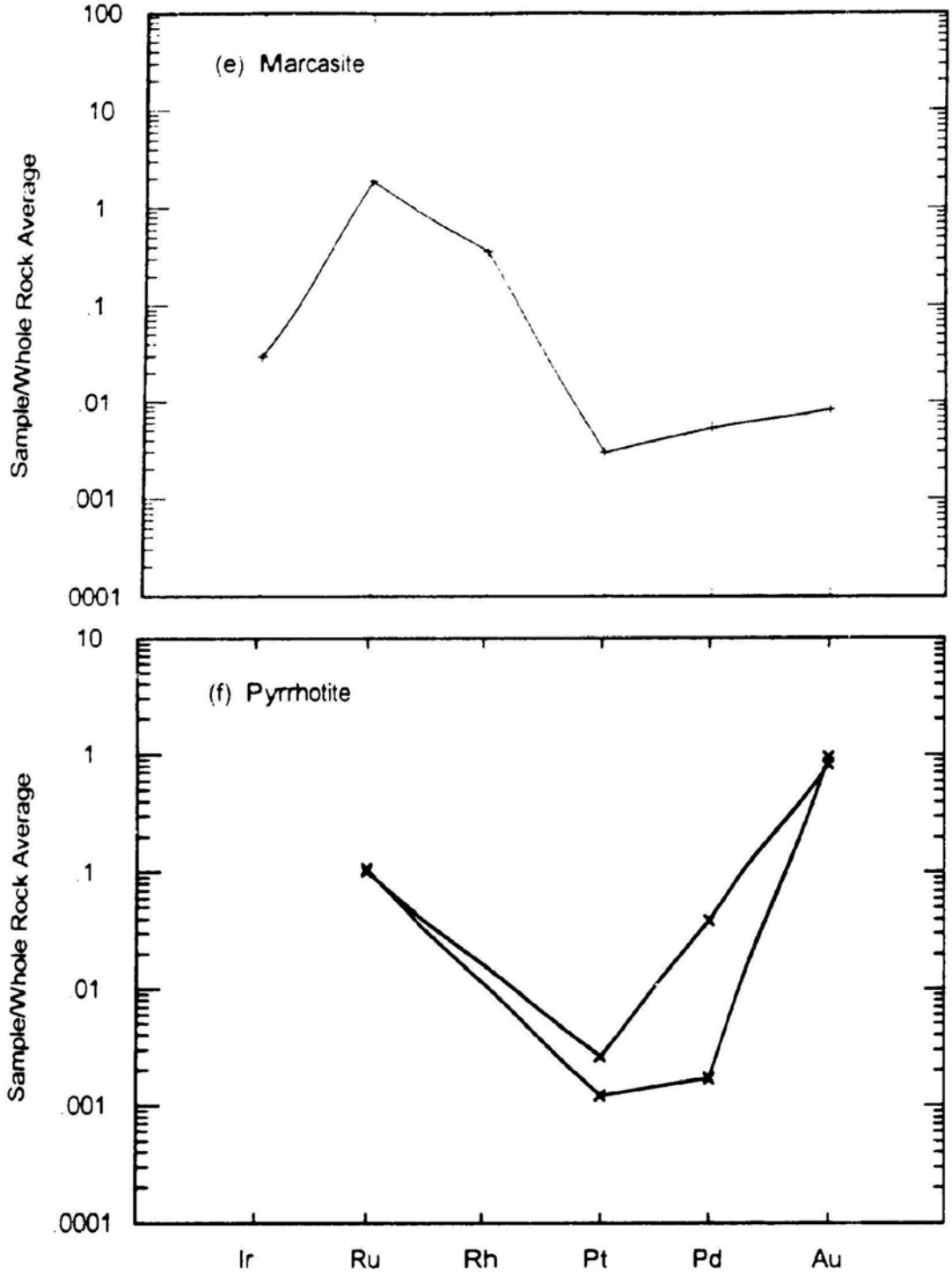
(e) Marcasite
Sample/Whole Rock Average
100
10
1
.1
.01
.001
.0001
(f) Pyrrhotite
Sample/Whole Rock Average
10
1
.1
.01
.001
.0001
Ir
Ru
Rh
Pt
Pd
Au

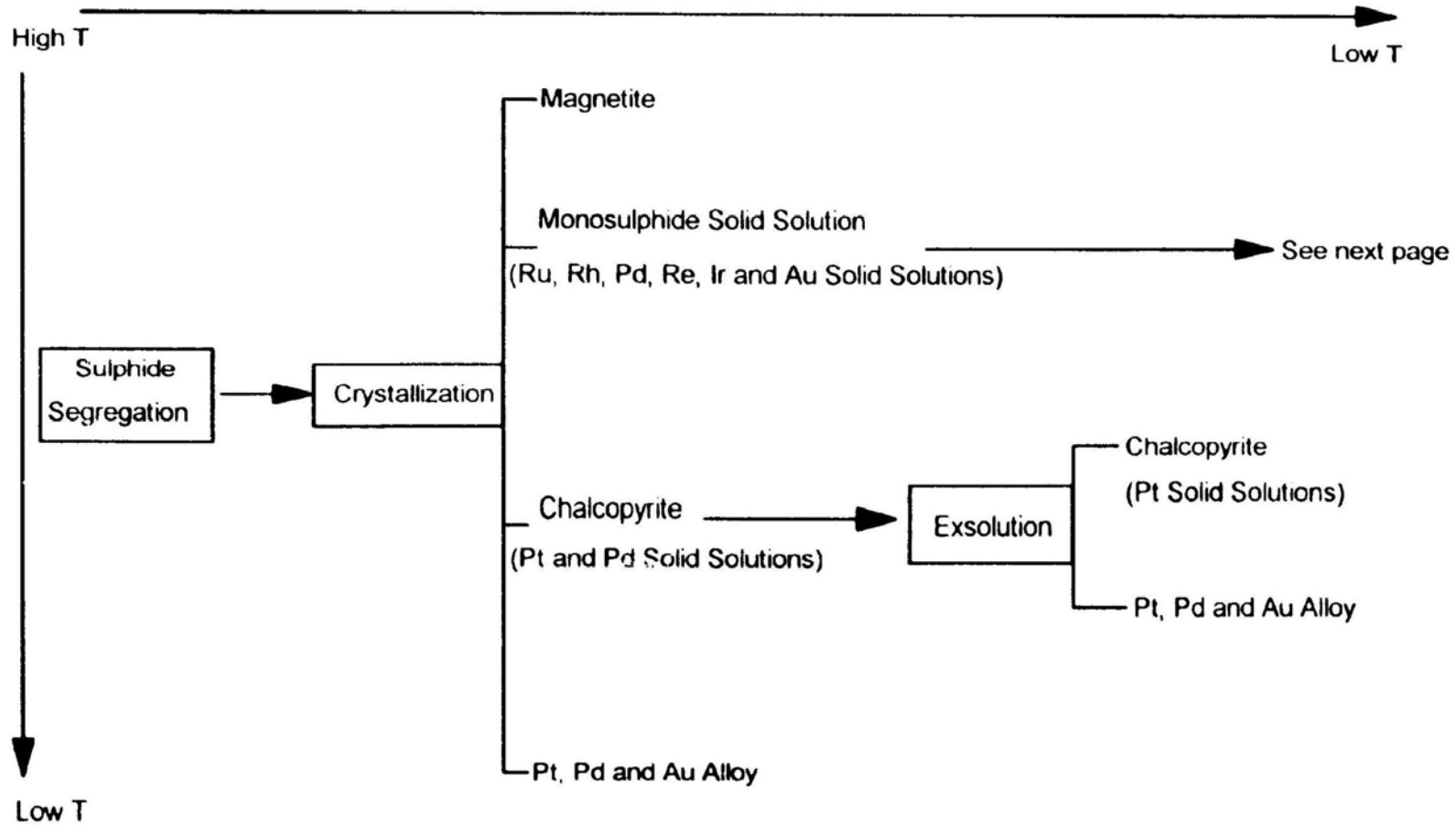
High T
Low T
Magnetite
Monosulphide Solid Solution
(Ru, Rh, Pd, Re, Ir and Au Solid Solutions)
See next page
Sulphide Segregation
Crystallization
Chalcopyrite
(Pt and Pd Solid Solutions)
Exsolution
Chalcopyrite
(Pt Solid Solutions)
Pt, Pd and Au Alloy
Pt, Pd and Au Alloy
Low T

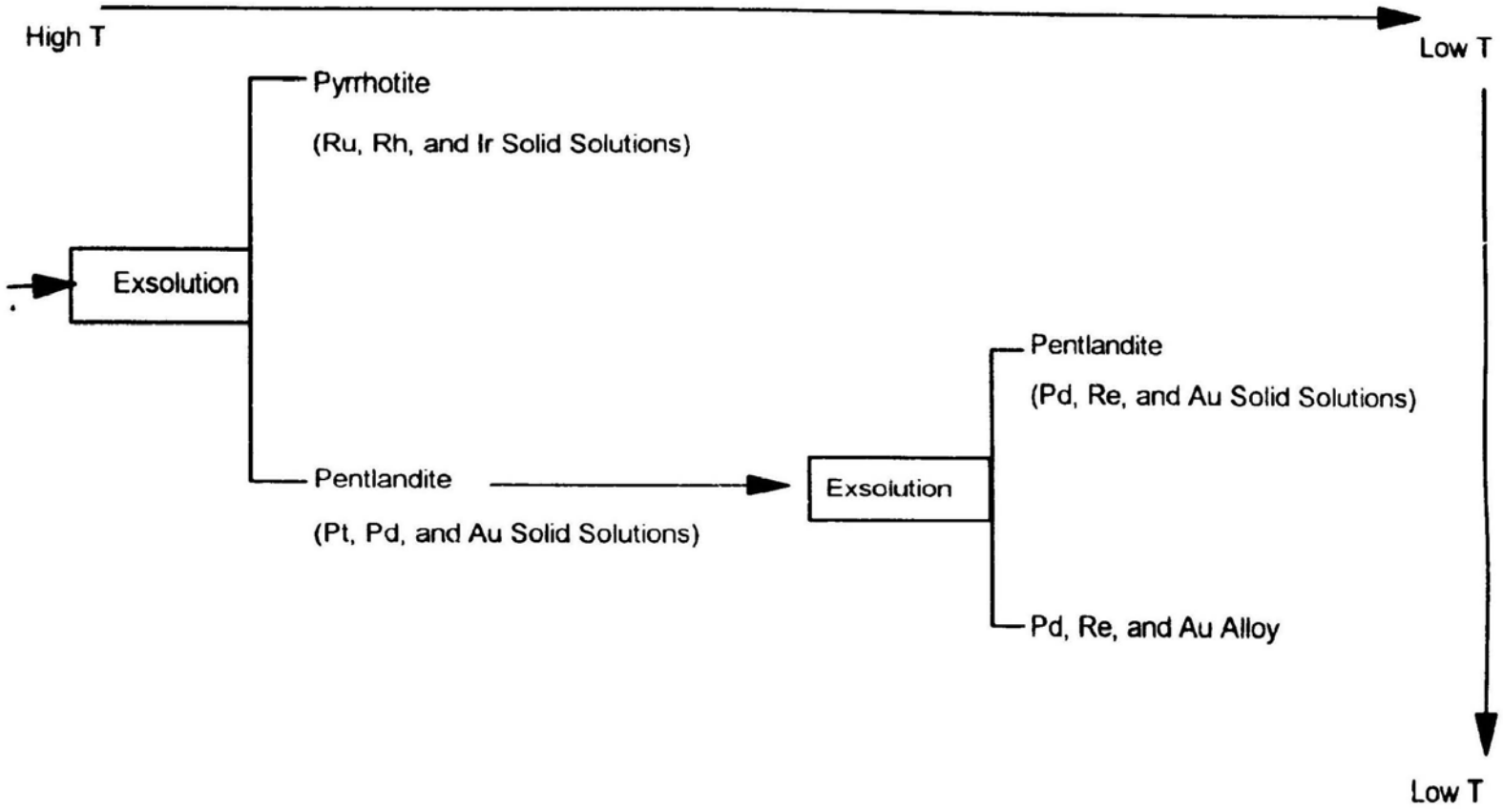

Figure 9.6 Genetic model for precious metal fractionation during sulphide segregation and mineral crystallization. See section 9.5 in the text for discussion.

CHAPTER 10

TRACE- AND RARE EARTH-ELEMENT GEOCHEMISTRY OF THE THAYER LINDSLEY MINE: IMPLICATIONS FOR ORE GENESIS

10.1 INTRODUCTION

Trace- and rare earth-element (REE) geochemistry is important to understanding petrogenesis and ore genesis. The trace- and rare earth- element contents of rocks from the Sudbury Igneous Complex (SIC) have been reported by Kuo and Crocket (1979), Naldrett (1984), and Naldrett *et al.* (1985); and in Chapter 6 of this thesis. However, no data on the trace- and rare earth- element contents of the sulphide ores have been reported due to the considerable analytical difficulty of working with the ultra-trace concentration levels of sulphide samples.

In this chapter, a preliminary set of geochemical data from Ni-Cu sulphide ores and the country rocks adjacent to the orebodies at the Thayer Lindsley Mine are presented, and their implications for ore genesis and future work are discussed.

10.2 SAMPLE PREPARATION AND ANALYTICAL METHODS

The locations of sulphide ore samples analyzed are given in Table 8.1, and samples from the host country rocks are listed in Table 10.1

Table 10.1 Location and description of the samples from the nearest country rocks at the Thayer Lindsley Mine

Sample	Location	Rock Type
TL13-34A	Drill core TL13-34, 9.47 m	Murray Granite, no sulphide or alteration
TL13-34C	Drill core TL13-34, 11.3 m	Murray Granite near the contact with the orebody, strong quartz enrichment (30%)
TL13-61A2	Drill core TL13-61, 56.9 m	Murray Granite with disseminated sulphide (15%)
TL13-64A	Drill core TL13-64, 126.8 m	Sublayer rock with disseminated sulphide (<5%)
TL13-98B2	Drill core TL13-98, 93.8 m	Sublayer rock with disseminated sulphide (5%)
TL13-32M	Drill core TL13-32, 40.0 m	Silicate xenolith

10.2.1 ICP-MS ANALYSIS

Fifteen REEs, Zr, Nb, Ba, Hf, Ta, and Th were analyzed by ICP-MS using the Na_2O_2 sinter sample dissolution technique (Longerich *et al.*, 1990; and Longerich *et al.*, 1993b). Data acquisition and reduction protocols are given in

Appendix IV. The sample dissolution procedure was modified from Longerich *et al.* (1990) and Longerich *et al.* (1993b) as follows:

1) High sulphide samples were ignited in an oven at 1100°C to oxidize the sulphide sulphur which is then lost as volatile SO_2. During this procedure the Fe was oxidized to Fe^{+3}.

2) 0.2 g of the ignited sample and 0.8 g of Na_2O_2 were weighed into a Ni crucible, mixed well, and then sintered in a muffle furnace at 480°C for 1.5 hours.

3) The crucible was removed from the furnace, covered, and allowed to cool for approximately 20 minutes. Ten ml of distilled water were carefully added, a few drops at a time, until the exothermic reaction stopped.

4) The cover was rinsed into the crucible and the mixture was quantitatively transferred to a 50 ml centrifuge tube. Distilled water was added until the total volume was 30 ml. The sample was then centrifuged for 20 minutes. The liquid was decanted and discarded.

5) The residue was rinsed with 25 ml distilled water, and then centrifuged for 20 minutes again. The liquid was decanted and discarded.

6) Step 5 was repeated.

7) The residue was dissolved in 2.5 ml of 8 N HNO_3 and 1 ml of 2% oxalic acid. The crucible was rinsed with 0.2 N HNO_3 and this wash was

added to the centrifuge tube.

8) Four ml of a 0.113 M HF/0.453 M boric acid solution were added, and the centrifuge tube and contents placed in the drying oven at 75°C for 2 hours.

9) The solution was transferred to a clean centrifuge tube and diluted with distilled water to a final volume of 50 g.

10) The solution was further diluted prior to analysis on the ICP-MS. Approximately 2 g of sample solution and 8 g of 0.2 N HNO_3 were accurately weight into a 12 ml test tube.

Solid limits of detection in ppb are 6 (Y), 5 (Zr), 10 (Nb), 1957 (Ba), 2 (La), Ce 1 (Ce), 1 (Pr), 28 (Nd), 10 (Sm), 2 (Eu), 16 (Gd), 1 (Tb), 10 (Dy), 1 (Ho), 11 (Er), 2 (Tm), 10 (Yb), 2 (Lu), 12 (Hf), 13 (Ta) and 5 (Th). These samples were run at a time of particularly high sensitivity on the ICP-MS, so the limits of detection were lower than usual.

10.2.2 XRF ANALYSIS

Major elements (>0.01 wt%) together with Cr, Zn, V Ga, As, Rb, Sr, Pb, and U were analyzed by X-Ray fluorescence spectrometry (XRF) methods for whole rock powder pellets (Longerich, 1993). The precision and accuracy are presented in Appendix III.

10.3 RESULTS

Analytical results using XRF pressed powder pellets are presented in Tables 8.2 and 10.2, and those using ICP-MS, in Table 10.3.

10.3.1 MASSIVE SULPHIDE ORES IN THE 4B ORE ZONE

Massive sulphide ores in footwall granite in the 4B Ore Zone contain 30-35% S, 1-3% Ni, 1-4% Cu; and are low in Rb (1-9 ppm), Sr (0-4 ppm), Y (1-4 ppm), Ba (5-40 ppm), Zr (2-20 ppm), Nb (1-5 ppm), Hf (0.01-0.3 ppm), Ta (0.3-0.5 ppm) and Th (0.2-0.9 ppm) (Table 8.2).

All of the massive sulphide ores in the 4B Ore Zone, except the ores from the orebody margin, show very similar rare earth element (REE) concentrations and chondrite normalized patterns (Figure 10.1). The total rare earth element ($\sum$REE), total light rare earth element ($\sum$LREE), and total heavy rare earth element ($\sum$HREE) concentrations range from 19.4 ppm, 13.3 ppm, and 2.78 ppm; to 4.9 ppm, 2.7 ppm, 0.89 ppm respectively (Table 10.3). The $\sum$REE content of an individual sample reflects the modal abundance of sulphide versus silicate present; the more abundant the silicate fraction, the higher the $\sum$REE content. Regardless of the $\sum$REE, all of the samples are characterized by weak LREE-enrichment of flat "v-shape" REE patterns (Figure 10.1) with $(La/Lu)_n$ (chondrite normalized La value/chondrite normalized Lu value) ratios in

Table 10.2 Chemical composition of the country rocks at the Thayer Lindsley Mine*

Sample	rock	SiO2	TiO2	Al2O3	Fe2O3	MnO	MgO	CaO	Na2O	K2O	P2O5	S	Sc
TL13–34A	Murray Granite	69.0%	0.15%	17.0%	2.8%	0.06%	1.07%	2.77%	6.45%	1.28%	0.01%	1837	2
TL13–34M	Silicate Inclusion	81.7%	0.00%	12.7%	1.8%	0.03%	0.87%	0.04%	2.68%	5.52%	0.00%	4339	1
TL13–34C	Murray Granite	89.3%	0.30%	4.3%	5.1%	0.10%	1.18%	0.34%	0.74%	1.18%	0.01%	5255	2
TL13–64A	Sublayer Rock	49.6%	0.35%	10.3%	13.7%	0.17%	11.07%	9.64%	1.83%	0.77%	0.05%	11802	31
TI13–98B	Sublayer Rock	75.1%	0.33%	11.9%	4.3%	0.02%	0.72%	3.45%	2.94%	0.68%	0.02%	16818	0
TL13–61A	Ore in the Granite	64.0%	0.20%	7.6%	10.9%	0.02%	0.03%	3.69%	0.00%	2.33%	0.02%	69623	4
SiO2–blank.LD		0.00%	0.00%	0.01%	0.00%	0.00%	0.02%	0.00%	0.01%	0.00%	0.00%	72	3
LOD**		0.01%	0.00%	0.01%	0.01%	0.00%	0.01%	0.00%	0.01%	0.00%	0.00%	13	6

Sample	rock	V	Cr	Ni	Cu	Zn	Ga	As	Rb	Sr	Pb	U	total
TL13–34A	Murray Granite	9	3	45	1389	6	24	17	50	287	58	6	101%
TL13–34M	Silicate Inclusion	0	27	27	3187	2	11	31	192	29	428	3	107%
TL13–34C	Murray Granite	23	111	169	3386	71	9	21	50	30	9	4	104%
TL13–64A	Sublayer Rock	179	1011	1274	855	67	12	12	36	269	2	3	101%
TI13–98B	Sublayer Rock	10	0	402	9746	94	7	18	45	569	7	4	105%
TL13–61A	Ore in the Granite	1	0	614	70669***	621	15	26	57	210	40	2	115%
SiO2–blank.LD		5	6	3	3	2	2	11	0.4	1.6	2	3	NA
LOD**						3	3	14	0.7	1.2	4	4	NA

* ppm for trace elements

** Limits of detection

*** Out of calibration range, may be in error

Table 10.3 Trace- and rare earth- element concentration (ppm) of the sulphide ores and the nearest country rocks

Name	Y	Zr	Nb	Ba	La	Ce	Pr	Nd	Sm	Eu	Gd	Tb	Dy
Massive Ore													
TL13-34B	2.10	4.33	1.56	16.9	1.38	2.88	0.33	1.22	0.29	0.04	0.29	0.04	0.35
TL13-34B1	2.06	4.55	1.51	16.9	1.25	2.75	0.31	1.23	0.29	0.03	0.30	0.05	0.40
TL13-34B(Avg)	2.08	4.44	1.53	16.9	1.31	2.81	0.32	1.22	0.29	0.03	0.29	0.05	0.37
TL13-32A	3.12	7.10	2.47	25.4	1.66	3.56	0.44	1.86	0.50	0.07	0.50	0.08	0.51
TL13-32A1	3.37	9.14	2.56	25.4	1.73	3.76	0.46	1.92	0.46	0.07	0.51	0.09	0.66
TL13-34A(Avg)	3.25	8.12	2.51	25.4	1.69	3.66	0.45	1.89	0.48	0.07	0.51	0.08	0.58
TL13-32F	3.54	19.84	2.44	36.0	2.77	6.07	0.71	2.71	0.63	0.07	0.49	0.07	0.61
TL13-32F1	3.49	15.67	2.40	35.0	2.96	6.44	0.76	2.83	0.56	0.07	0.53	0.09	0.63
TL13-32F(Avg)	3.51	17.76	2.42	35.5	2.87	6.25	0.73	2.77	0.60	0.07	0.51	0.08	0.62
TL13-32J	0.97	3.41	0.88	11.5	0.80	1.98	0.24	0.84	0.17	0.03	0.15	0.02	0.19
TL13-32N	2.02	6.43	1.55	18.4	2.01	4.50	0.52	1.82	0.41	0.05	0.32	0.06	0.37
TL13-35C	0.47	2.11	2.01	2.0	0.77	1.81	0.21	0.81	0.20	0.02	0.12	0.02	0.10
TL13-63A	1.25	6.13	1.72	11.1	0.65	1.50	0.18	0.73	0.18	0.02	0.16	0.03	0.21
TL13-98A	2.37	6.84	2.05	9.5	0.58	1.35	0.18	0.77	0.25	0.03	0.31	0.05	0.47
TL13-96A	2.70	8.71	2.32	12.2	2.17	4.70	0.54	1.85	0.43	0.08	0.37	0.07	0.49
TL13-109A	3.93	22.85	5.15	25.2	2.30	5.28	0.66	2.63	0.58	0.06	0.60	0.10	0.77
TL13-162B	2.77	10.56	1.83	39.0	1.77	3.99	0.45	1.69	0.45	0.08	0.37	0.06	0.48
TL13-161F	1.26	7.26	1.48	11.4	0.59	1.27	0.15	0.57	0.11	0.02	0.20	0.03	0.23
TL13-161L	1.80	8.38	2.03	7.7	1.04	2.58	0.32	1.19	0.31	0.03	0.29	0.04	0.31
Mean	2.42	9.14	2.13	20.1	1.59	3.53	0.42	1.61	0.38	0.05	0.36	0.06	0.44
Margin Ore													
TL13-32R	5.81	7.86	1.94	19.268	3.61	6.96	0.78	3.06	0.70	0.10	0.52	0.09	0.77
Ore in Granite													
TL13-61A	54	361	27	474	71	142	16	59	10.9	1.18	9.3	1.38	9.5
TL13-97A	35	345	18	607	45	87	10	38	6.9	1.31	6.5	0.93	6.6
TL13-61A2	70	443	33	501	76	155	18	63	12.6	1.47	11.1	1.74	12.5
Mean	53	383	26	527	64	128	15	53	10.1	1.32	9.0	1.35	9.5
Sublayer rock													
TL13-98B	38	745	12.7	174	117	218	24	86	14.1	2.9	11.6	1.6	9.4
TL13-98B2	22	261	8.0	118	39	75	8	29	5.3	1.0	4.7	0.7	4.3
Mean	30	503	10.4	146	78	147	16	58	9.7	1.9	8.1	1.1	6.9
Disseminated ore in Sublayer													
TL13-64A	20	71	6.0	181	16.6	36.2	4.3	16.5	3.5	0.6	3.1	0.6	3.9
TL13-64A2	15	65	7.2	93	10.5	22.3	2.5	10.1	2.1	0.3	2.1	0.4	2.7
Mean	18	68	6.6	137	13.5	29.2	3.4	13.3	2.8	0.5	2.6	0.5	3.3
Sublayer ore													
TL13-97B	14	48	7.0	53	5.4	13.2	1.6	6.1	1.6	0.3	1.8	0.3	2.5
TL15-01A	8	37	4.4	38	8.6	17.8	2.0	7.7	1.6	0.3	1.3	0.2	1.5
Mean	11	43	5.7	45	7.0	15.5	1.8	6.9	1.6	0.3	1.5	0.3	2.0
Murray Granite													
TL13-34A	76	486	11.3	220	108	214	24	87	16.8	2.0	15.4	2.4	15.4
TL13-34A1	76	466	14.7	223	108	215	24	87	17.0	2.0	15.1	2.4	15.5
TL13-34A (Avg)	76	476	13.0	222	108	215	24	87	16.9	2.0	15.3	2.4	15.4
TL13-34C	15	104	17.4	327	24	44	5	19	3.63	0.42	2.95	0.48	3.13
Silicate Inclusion													
TL13-32M	5.58	36.6	6.3	283	6.52	11.9	1.26	4.56	0.87	0.17	0.75	0.15	1.09
Blank 1*	0.67	1.11	0.05	-0.35	0.07	0.28	0.03	0.10	0.04	0.01	0.03	0.02	0.05
Blank 2*	1.11	0.18	0.02	-0.46	0.03	0.30	0.01	0.03	0.02	0.00	0.03	0.01	0.03
PTC-1A**	1.75	5.52	0.71	10.13	1.92	3.93	0.42	1.63	0.37	0.07	0.33	0.05	0.32
PTC-1B**	1.71	6.06	0.68	9.86	1.81	3.78	0.43	1.56	0.40	0.07	0.31	0.04	0.31
PTC-1(Avg)	1.73	5.79	0.70	10.00	1.87	3.86	0.43	1.60	0.39	0.07	0.32	0.05	0.31
DNC-1***	15.1	34.4	1.7	92.6	3.6	8.1	1.0	4.6	1.30	0.59	2.06	0.36	2.60
DNC-1(Govindaraju)	18	41	3	114	3.8	10.6	1.3	4.9	1.38	0.59	2	0.41	2.7
DNC-1 (MUN Avg)	15.1	35.1	1.65	98.3	3.57	8.06	1.05	4.73	1.38	0.56	1.94	0.34	2.66
Limit of Detection	0.006	0.005	0.010	1.957	0.002	0.001	0.001	0.028	0.010	0.002	0.013	0.001	0.010
CHONDRITE	2.25	5.54	0.375	3.41	0.367	0.957	0.137	0.711	0.231	0.087	0.306	0.058	0.381

* Blank 1 and Blank 2: two reagent blank. Y was slightly contaminated by previous high concentration samples

** PTC-1A and PTC-1B: two analyses of CAMMET sulphide reference material

*** DNC-1: USGS reference material, diabase

Table 10.3 Trace- and rare earth- element concentration (ppm) of sulphide ores and the nearest country rocks (continued)

Name	Ho	Er	Tm	Yb	Lu	Hf	Ta	Th	Tot REE	LREE	HREE	(La/Lu)n	Eu*
Massive Ore													
TL13-34B	0.07	0.23	0.036	0.24	0.040	0.06	0.35	0.41	9.5	6.1	1.3	3.6	0.37
TL13-34B1	0.08	0.22	0.031	0.20	0.033	0.08	0.35	0.64	9.2	5.9	1.3	3.9	0.36
TL13-34B(Avg)	0.07	0.22	0.033	0.22	0.036	0.07	0.35	0.52	9.4	6.0	1.3	3.7	0.36
TL13-32A	0.11	0.34	0.059	0.36	0.052	0.14	0.52	0.46	13.2	8.1	2.0	3.3	0.46
TL13-32A1	0.13	0.34	0.055	0.38	0.054	0.13	0.57	0.68	14.0	8.4	2.2	3.3	0.45
TL13-34A(Avg)	0.12	0.34	0.057	0.37	0.053	0.13	0.54	0.57	13.6	8.2	2.1	3.3	0.46
TL13-32F	0.14	0.37	0.058	0.45	0.065	0.35	0.51	0.88	18.8	13.0	2.3	4.4	0.40
TL13-32F1	0.12	0.40	0.059	0.41	0.049	0.22	0.48	0.86	19.4	13.6	2.3	6.3	0.35
TL13-32F(Avg)	0.13	0.39	0.058	0.43	0.057	0.28	0.49	0.87	19.1	13.3	2.3	5.3	0.37
TL13-32J	0.04	0.11	0.025	0.12	0.022	0.08	0.18	0.29	5.7	4.1	0.7	3.8	0.62
TL13-32N	0.07	0.22	0.036	0.24	0.035	0.12	0.48	0.52	12.7	9.3	1.3	6.0	0.37
TL13-35C	0.02	0.07	0.007	0.06	0.007	0.04	0.36	0.05	4.7	3.8	0.4	12.2	0.38
TL13-63A	0.05	0.12	0.029	0.16	0.024	0.14	0.38	0.25	5.3	3.3	0.8	2.8	0.29
TL13-98A	0.09	0.27	0.041	0.30	0.038	0.14	0.56	0.31	7.1	3.2	1.6	1.6	0.35
TL13-96A	0.10	0.35	0.055	0.37	0.055	0.14	0.36	0.66	14.3	9.8	1.9	4.1	0.55
TL13-109A	0.17	0.48	0.084	0.50	0.077	0.33	0.49	0.76	18.2	11.5	2.8	3.1	0.30
TL13-162B	0.11	0.37	0.046	0.28	0.054	0.21	0.40	0.72	13.0	8.4	1.8	3.4	0.57
TL13-161F	0.06	0.14	0.023	0.17	0.027	0.12	0.36	0.41	4.9	2.7	0.9	2.3	0.65
TL13-161L	0.06	0.23	0.031	0.21	0.022	0.15	0.45	0.52	8.5	5.5	1.2	4.8	0.34
Mean	0.09	0.27	0.043	0.29	0.042	0.15	0.43	0.55	11.6	7.6	1.6		
Margin Ore													
TL13-32R	0.19	0.73	0.148	1.466	0.417	0.17	0.989	0.438	25.358	15.211	4.336	0.898	0.45
Ore in Granite													
TL13-61A	2.06	6.62	1.09	7.79	1.14	9.13	4.16	21.6	394	301	39	6.5	0.35
TL13-97A	1.35	4.11	0.63	4.02	0.60	7.94	1.95	10.8	248	188	25	7.8	0.58
TL13-61A2	2.56	8.45	1.32	9.47	1.46	10.96	6.79	21.8	446	327	49	5.4	0.37
Mean	1.99	6.40	1.01	7.09	1.06	9.34	4.30	18.1	362	272	37		
Sublayer rock													
TL13-98B	1.54	3.59	0.46	2.59	0.41	17.3	8.4	24.0	530	461	31	14	0.59
TL13-98B2	0.80	2.22	0.31	2.06	0.30	6.6	1.5	8.8	195	158	15	30	0.66
Mean	1.17	2.90	0.39	2.33	0.35	11.9	5.0	16.4	363	310	23		
Disseminated ore in Sublayer													
TL13-64A	0.78	2.2	0.35	2.0	0.31	2.0	2.7	3.6	111	78	13.2	3.4	0.47
TL13-64A2	0.56	1.7	0.29	1.9	0.32	1.7	0.7	1.7	73	48	9.9	5.6	0.55
Mean	0.67	2.0	0.32	2.0	0.31	1.9	1.7	2.6	92	63	11.6		
Sublayer ore													
TL13-97B	0.52	1.6	0.25	1.7	0.24	1.13	0.72	2.2	51	28	6.9	2.3	0.50
TL15-01A	0.32	1.0	0.16	1.2	0.18	0.80	0.80	2.0	52	38	5.8	5.1	0.51
Mean	0.42	1.3	0.21	1.4	0.21	0.97	0.76	2.1	52	33	7.3		
Murray Granite													
TL13-34A	2.9	8.1	1.03	5.9	0.87	10.5	7.6	31.9	580	452	52	13	0.37
TL13-34A1	2.9	8.0	1.06	6.5	0.88	10.9	8.0	31.8	581	453	52	13	0.36
TL13-34A (Avg)	2.9	8.0	1.04	6.2	0.88	10.7	7.8	31.8	581	453	52	13	0.36
TL13-34C	0.6	1.5	0.19	1.2	0.17	2.6	9.0	7.1	121	96	10	14	0.36
Silicate Inclusion													
TL13-32M	0.23	0.75	0.12	0.80	0.13	1.19	9.3	3.8	35	25	4.0	5.2	0.60
Blank 1	0.003	0.026	0.006	0.086	0.002	0.044	0.019	0.018	1.4	0.5	0.23	3.2	0.66
Blank 2	0.000	-0.005	0.008	0.043	0.000	0.003	0.012	0.014	1.6	0.4	0.12	5.5	0.14
PTC-1A	0.073	0.203	0.031	0.200	0.030	0.149	0.048	1.47	11.3	8.3	1.23	6.6	0.60
PTC-1B	0.061	0.195	0.030	0.182	0.026	0.160	0.036	1.36	10.9	8.1	1.16	7.3	0.54
PTC-1(Avg)	0.067	0.199	0.030	0.191	0.028	0.155	0.042	1.41	11.1	8.2	1.19	6.9	0.57
DNC-1	0.576	1.805	0.276	1.901	0.298	0.948	0.083	0.259	44.3	19.3	9.9	1.3	1.09
DNC-1(Govindaraju)	0.62	2	0.1	2.01	0.32	1.01	0.098	0.2	50.7	22.6	10.2	1.2	1.08
DNC-1 (MUN Avg)	0.59	1.82	0.27	1.84	0.28	0.93	0.08	0.26	44.2	19.4	9.74	1.32	NA
Limit of Detection	0.001	0.011	0.002	0.010	0.002	0.012	0.013	0.005	0.104	0.045	0.052	0.085	0.58
CHONDRITE	0.085	0.249	0.036	0.248	0.038	0.179	0.026	0.043	6.141	2.490	1.401	1.000	1.00

the range of 2.3 to 5.2, and by strong negative Eu anomalies with Eu* (chondrite normalized Eu value/mean of the chondrite normalized Sm and Gd values) mostly in the range of 0.35 to 0.50.

Only one sample (TL13-32R) of the massive sulphide ores from the margin of the orebody has been analyzed for its REE concentrations. Data for this sample are entirely different from that for other massive sulphide ores. In Chapter 8, it was shown that the margin of the orebody was characterized by high concentrations of Pd, Pt, and Au. Similarly, $\sum$REE, $\sum$LREE, and $\sum$HREE are enriched at 25.4 ppm, 15.2 ppm, and 4.3 ppm respectively (Table 10.3). The sample from the margin of the orebody is characterized by strong LREE and HREE enrichment, and depletion in the middle REE, resulting in a "U-shaped" REE pattern (Figure 10.2) with a $(La/Lu)_n$ ratio of 0.90 and a negative Eu anomaly with a Eu* value of 0.45.

10.3.2 SUBLAYER ROCKS AND SUBLAYER ORES

There is no sha.p boundary between the Sublayer rocks and the Sublayer ores. If sulphide concentrations in the Sublayer are high enough, Sublayer ores are formed. Samples of Sublayer rocks contain less than 5% S, 630 ppm Ni, 1.05% Cu, 44 ppm Rb, 400 ppm Sr, 29 ppm Y, 146 ppm Ba, 503 ppm Zr, 10.4 ppm Nb, 12.0 ppm Hf, 5.0 ppm Ta, and 16.4 ppm Th (Table 10.2). Selected samples of Sublayer ores contain 20% S, 2.0 % Ni, 6.7% Cu, 21.5

ppm Rb, 89 ppm Sr, 14.5 ppm Y, 73 ppm Ba, 56.5 ppm Zr, 7.1 ppm Nb, 1.4 ppm Hf, 0.76 ppm Ta, and 1.9 ppm Th (Table 8.2).

$\sum$REE, $\sum$LREE, and $\sum$HREE range from 530 ppm, 461 ppm, and 31 ppm respectively in Sublayer rocks; to 51 ppm, 28 ppm, 8.9 ppm respectively in Sublayer ores (Table 10.3). Chondrite normalized REE patterns for the Sublayer rocks and ores are illustrated in Figure 10.3. With increasing sulphide concentrations, the shapes of REE patterns change. Sublayer rocks are characterized by LREE-enrichment with a $(La/Lu)_n$ ratio of 29.6 and a weaker negative Eu anomaly ($Eu^* = 0.66$). The sublayer ores have a weaker LREE-enrichment, generally a flat "V-shaped" REE pattern with a $(La/Lu)_n$ ratio of 2.3 and a stronger Eu anomaly ($Eu^* = 0.50$) in the Sublayer ores than the sublayer rocks.

10.3.3 DISSEMINATED SULPHIDE ORE IN THE MURRAY GRANITE

The disseminated sulphide ores in the Murray Granite have higher REE concentrations than the other sulphide ores since the granite is REE-rich. The ores have $\sum$REE from 248 to 446 ppm, $\sum$LREE from 188 to 327 ppm, and $\sum$HREE from 24.8 to 48.6 ppm (Table 10.3). The ores are characterized by strong LREE-enriched REE patterns (Figure 10.4) with $(La/Lu)_n$ ratios in the range of 5.4 to 7.8; and by a strong negative Eu anomaly with Eu^* values in the range of 0.35 to 0.58. The typical disseminated ores in the granite contain

6-11% S, 0.26-0.38 % Ni, 1-12% Cu, 57-162 ppm Rb, 152-209 ppm Sr, 35-70 ppm Y, 473-606 ppm Ba, 344-443 ppm Zr, 18-33 ppm Nb, 7-11 ppm Hf, 1.9-6.7 ppm Ta, and 10-21 ppm Th (Table 10.2).

10.3.4 MURRAY GRANITE

Two samples (one sample in duplicate) of Murray Granite were analyzed for their REE contents. One of the samples (TL13-34C) is near the contact with massive sulphide ores and is strongly enriched in quartz (30%). The more typical Murray Granite contains 0.18% S, 45 ppm Ni, 1389 ppm Cu, 50.2 ppm Rb, 287 ppm Sr, 76 ppm Y, 220 ppm Ba, 486 ppm Zr, 11.4 ppm Nb, 10.7 ppm Hf, 7.8 ppm Ta, and 31.8 ppm Th (Table 10.2).

The granite has mean $\sum$REE of 581 ppm, $\sum$LREE of 453 ppm, and $\sum$HREE of 52 ppm (Table 10.3). The quartz-enriched sample (TL13-34C) has $\sum$REE of 121 ppm, $\sum$LREE of 96 ppm, and $\sum$HREE of 10 ppm. The chondrite normalized REE patterns for both granites are shown in Figure 10.5. Both of the samples are characterized by strong LREE-enrichment REE patterns with $(La/Lu)_n$ ratios in the range of 12.8 to 14.3; and by a strong negative Eu anomaly with Eu* values in the range of 0.36 to 0.37.

10.3.5 SILICATE INCLUSION IN MASSIVE SULPHIDE ORES

One of the felsic silicate inclusions in the massive sulphide ore was analyzed

for its trace element and REE concentrations. The inclusion contained 0.43% S, 27 ppm Ni, 3^87 ppm Cu, 192 ppm Rb, 29.2 ppm Sr, 5.6 ppm Y, 283 ppm Ba, 36.6 ppm Zr, 6.3 ppm Nb, 1.19 ppm Hf, 9.32 ppm Ta, and 3.77 ppm Th (Table 10.2).

The inclusion has ∑REE, ∑LREE, and ∑HREE of 34.9 ppm, 25.3 ppm, and 4.0 ppm respectively (Table 10.3). The REE pattern of the inclusion is characterized by strong LREE enrichment and little enrichment in HREE (Figure 10.6) with a $(La/Lu)_n$ ratio of 5.3; and by a negative Eu anomaly, with a Eu* value of 0.60.

10.4 DISCUSSION

10.4.1 DISTRIBUTIONS OF RARE EARTH ELEMENTS IN DIFFERENT GEOLOGICAL UNITS FROM THE THAYER LINDSLEY MINE

In order to compare the REE mixing and the REE fractionation of different rock types, the mean concentrations of the rock types were normalized first to Lu and then to chondrite values. By normalizing to Lu, average analyses of individual units (for example 13 analyses of massive sulphides, Figure 10.1) can be represented on a REE variation diagram as a single line. This facilitates comparison and interpretation. The doubly normalized REE patterns of the different geological units from the Thayer Lindsley Mine are illustrated in Figure

10.7. The South Range border norite (see also Chapter 6) is characterized by a LREE enrichment with a negligible Eu anomaly. The Sublayer unit shows the strongest LREE enrichment with a weak negative Eu anomaly. The Murray Granite shows LREE enrichment with the strongest negative Eu anomaly. Massive sulphide ores, Sublayer ores, disseminated ores in the Murray Granite, and a silicate inclusion in the massive sulphide ores show similar normalized REE patterns which are characterized by a slight LREE enrichment and a strong negative Eu anomaly. The marginal massive sulphide ore displays a distinctive REE normalized pattern which is significantly different from other ore and rock types.

10.4.2 FRACTIONATION OF REE BETWEEN SUBLAYER ROCKS AND SUBLAYER ORES DURING SULPHIDE SEGREGATION

The strong REE fractionation (particularly for the LREE) between silicate melt and sulphide liquid during the sulphide segregation in the Sublayer is shown in the chondrite normalized REE patterns (Figure 10.3). LREE which are more compatible in the silicate melt than in the sulphide liquid are enriched in the silicate melt during the segregation. Figure 10.8 shows a negative correlation between (La/lu) (logarithmic) and S contents in the sulphide ores and the Sublayer rock. Therefore, the Sublayer rocks are characterized by LREE-enrichment with a $(La/Lu)_n$ ratio of 29.6, whereas the Sublayer ores are

characterized by weak LREE-enrichment of flat "V-shaped" REE patterns with a $(La/Lu)_n$ ratio of 2.3.

Osmium isotope initial ratios (Walker *et al.*, 1991 and Dickin *et al.*, 1992) from sulphide ores of several mines at Sudbury are very similar, suggesting a common isotopic composition for the original ore. Neither the Os model age nor the Os initial isotopic composition of the Sublayer are significantly different from the Main Mass norite, suggesting that the Sublayer and the Main Mass norite are related magma types. Naldrett *et al.* (1970), and Kuo and Crocket (1979) interpreted the border quartz-rich norite as a rapidly cooled marginal facies, and suggested that it preserved the original composition of the parent magma. If the original magma of the Sublayer, before sulphide segregation, is assumed to have a REE composition similar to that of the South Range border norite, then the relative proportions of silicate and sulphide in the magma can be calculated from REE fractionation between the Sublayer rocks and ores. Given a mixing model with 35% Sublayer rocks (less than 5% sulphide) and 65% Sublayer ores, then the calculated REE patterns of the resulting mixture is a close match to that of the border norite (Figure 10.9). The mixing model predicts there should be 65% sulphide in the Sublayer, however, there is much less sulphide ore in the Sublayer. The question of where the rest of the sulphide resides needs to be answered.

10.4.3 ORIGIN OF MASSIVE SULPHIDE ORES IN THE 4B ORE ZONE

The massive sulphide ore bodies of the 4B Ore Zone are located in the Murray Granite approximately 30 m south of the base of the SIC at depths of between 1250 and 1370 m (see Chapter 8). Some of the sulphide ore bodies can be traced into the Sublayer (Figure 8.6). The massive sulphide ores in the 4B Ore Zone have very similar chondrite normalized REE patterns to the Sublayer ores which are characterized by weak LREE-enrichment of flat "V-shaped" REE patterns (Figure 10.1 and Figure 10.3), with $(La/Lu)_n$ ratios in the range of 2.3 to 5.2, and strong Eu negative anomalies. However, the absolute REE contents of the massive sulphide ores are less than the Sublayer ores (Table 10.3). Petrographic examination shows that there is always a small proportion of silicate contained in the Sublayer ores. If the REE concentrations of the silicate are subtracted from the Sublayer ores, the Sublayer ores will have similar concentrations to the massive sulphide ores in the 4B Ore Zone. Therefore, the REE data is consistent with the model in Chapter 9, in which the massive ores in the footwall granite are parts of a highly fractionated sulphide liquid which was expelled from the original sulphide magma along a structural weakness into the footwall granite. The interpretation of the fractional crystallization of the monosulphide solid solution from a sulphide melt has been discussed in Chapter 9, and is supported by several workers including Hawley (1965), Keays and Crocket (1970), Chyi and Crocket (1976), Naldrett *et al.*(1982), and Li *et al*

(1992).

10.4.4 INVOLVEMENT OF A HYDROTHERMAL FLUID AT THE MARGIN OF OREBODY

The chondrite normalized REE pattern of the massive sulphide near the margin of the orebody is different from those of the other massive sulphide ores, suggesting a different mineralization process. The pattern is characterized by strong LREE and HREE enrichment, and depletion in the middle REE resulting in a "U-shaped" REE pattern; and a strong negative Eu anomaly (Figure 10.2). The "U-shaped" pattern is very similar to some REE patterns of Archean mesothermal gold deposits (Kerrich and Fryer, 1979). The host rocks at the margin of the orebody are altered to epidote, chlorite, and carbonate. This suggests that a hydrotherrnal fluid was locally active there. Hydrothermal alteration has also been reported at the margins of the massive veins at the Strathcona Mine (Farrow *et al.*, 1992; and Li *et al.*, 1992). Hermann (1972) concluded that transport of the REE as carbonate, fluoride, or sulphate complexes in alkaline solutions has played a dominant role in their mobility and deposition; and that the increasing stability of these complexes with increasing atomic number of the REE results in enrichment of the heaviest REE in the latest stage deposits, where the most stable complexes were the last to break down. Kosterin (1959) suggested that decreasing pressure, fixation of CO_3^{-2},

or a change in alkalinity are possible reasons for the complexes to break down and the REE to precipitate. The strong HREE enrichment of the sulphide ore at the margin of the 4B Ore Zone may indicate involvement of a hydrothermal fluid. The fluid may either be late stage magmatic volatiles or a post-mineralization hydrothermal solution which remobilized the HREE.

10.4.5 ORIGIN OF DISSEMINATED SULPHIDE ORE IN THE GRANITE

The REE contents of the disseminated sulphide ore in the footwall granite can be modeled by different proportions of two end members: massive sulphide ores and the Murray Granite. Given a mixing model of 40% massive sulphide ores and 60% Murray Granite, then the resulting mixture has a calculated REE pattern that matches the REE pattern of disseminated ores in the granite (Figure 10.10). The REE pattern of the calculated mixture is consistent with that of the disseminated ores in the granite except for Er, Tm, Yb, and Lu. One explanation for why the HREE's of the ores are higher than those from the model calculation may reflect interaction with a late magmatic stage or post-mineralization hydrothermal remobilization as has been suggested for the margin of the orebody (see Figures 10.2 and 10.10 for comparison).

10.5 CONCLUSIONS

(1) Sulphide ores in footwall granite and in the Sublayer were depleted in lithophile trace elements (Rb, Ba, REE, Zr, Hf, Nb, Ta, Th, and Sr) during magmatic sulphide segregation.

(2) In comparison with the South Range norite, which represents the parent magma, Sublayer rocks are enriched in light rare earth elements (LREE) and have a slightly more negative Eu anomaly, whereas sulphide ores in the Sublayer and in the footwall Murray Granite are depleted in LREE with more strongly negative Eu anomalies.

(3) The original REE composition of the Sublayer can be modeled as a mixture of 35% typical Sublayer rocks (less than 5%) and 65% Sublayer sulphide ores.

(4) Chondrite normalized REE patterns indicate that the massive ores in the footwall granite are parts of a highly fractionated sulphide liquid which was expelled from the original sulphide magma along a structural weakness into the footwall granite.

(5) A distinctive HREE-rich pattern indicates that a late stage magmatic or a post-mineralization hydrothermal fluid was involved along the margin of the orebody as part of the latest stage of mineralization.

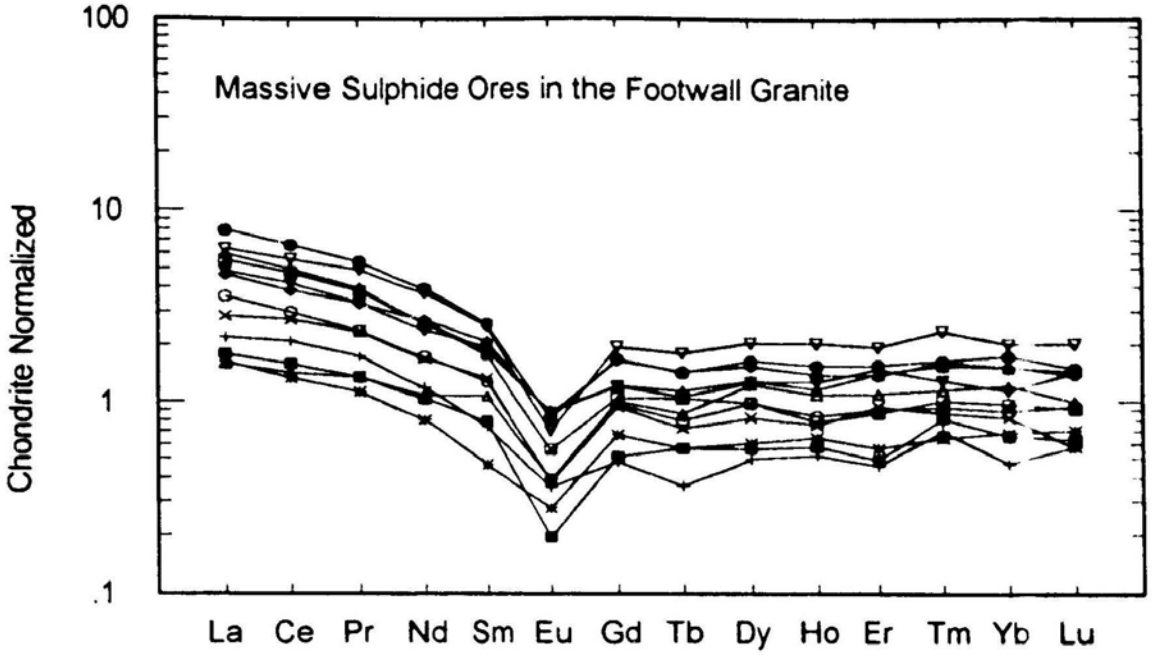

Figure 10.1 Chondrite normalized REE patterns of the massive sulphide ores in the 4B Ore Zone at the Thayer Lindsley Mine

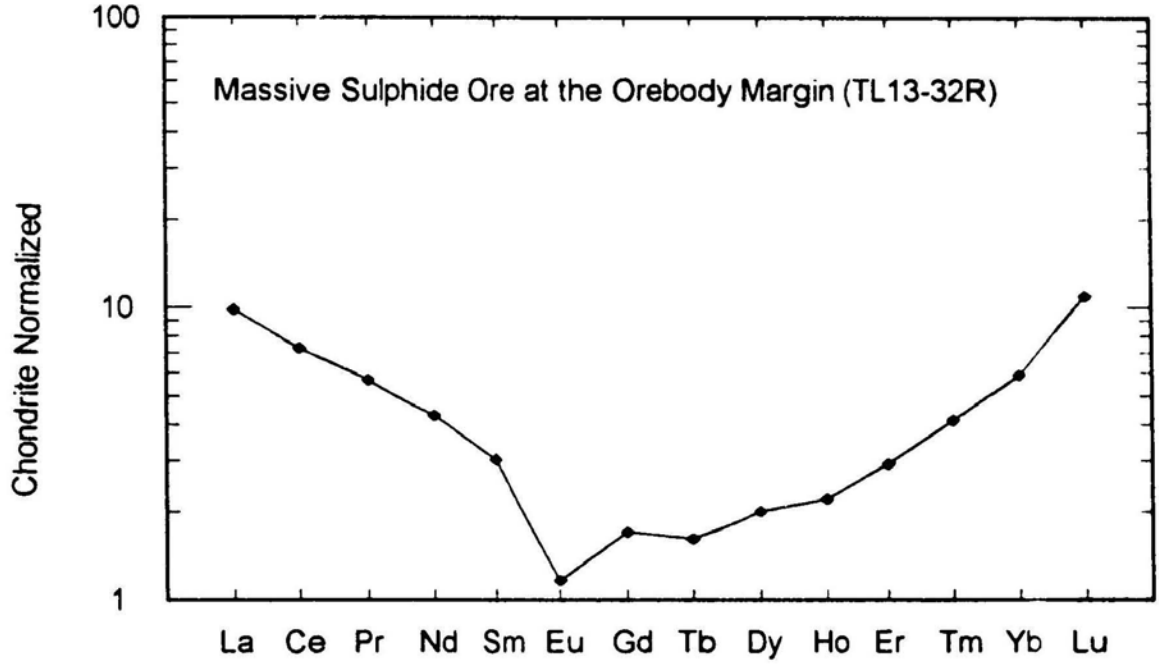

Figure 10.2 Chondrite normalized REE patterns of a massive sulphide ore (TL13-32R) at the orebody margin in the 4B Ore Zone at the Thayer Lindsley Mine

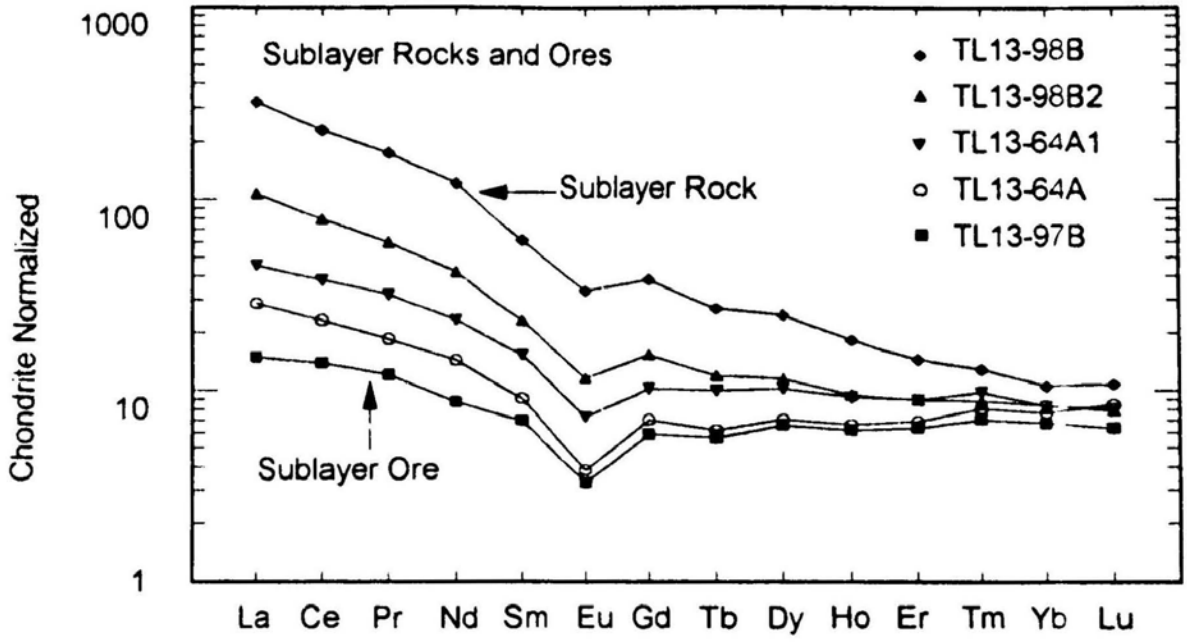

Figure 10.3 Chondrite normalized REE patterns of the Sublayer rocks and ores at the Thayer Lindsley Mine

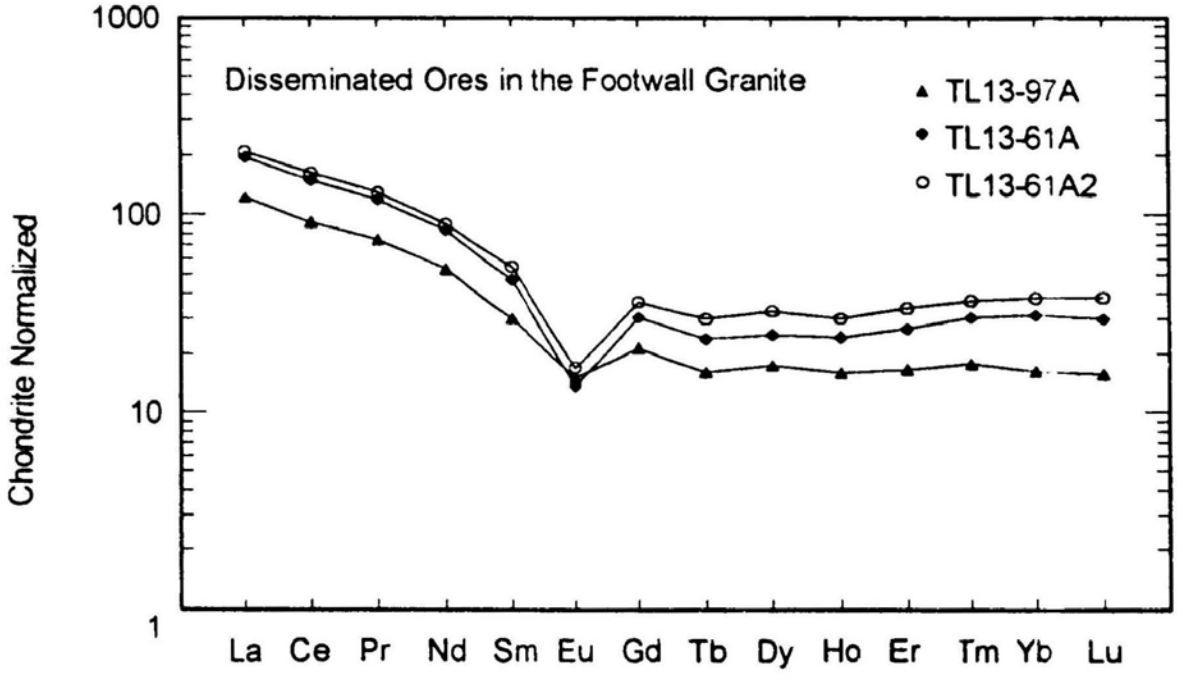

Figure 10.4 Chondrite normalized REE patterns of the disseminated ores in the Murray granite at the Thayer Lindsley Mine

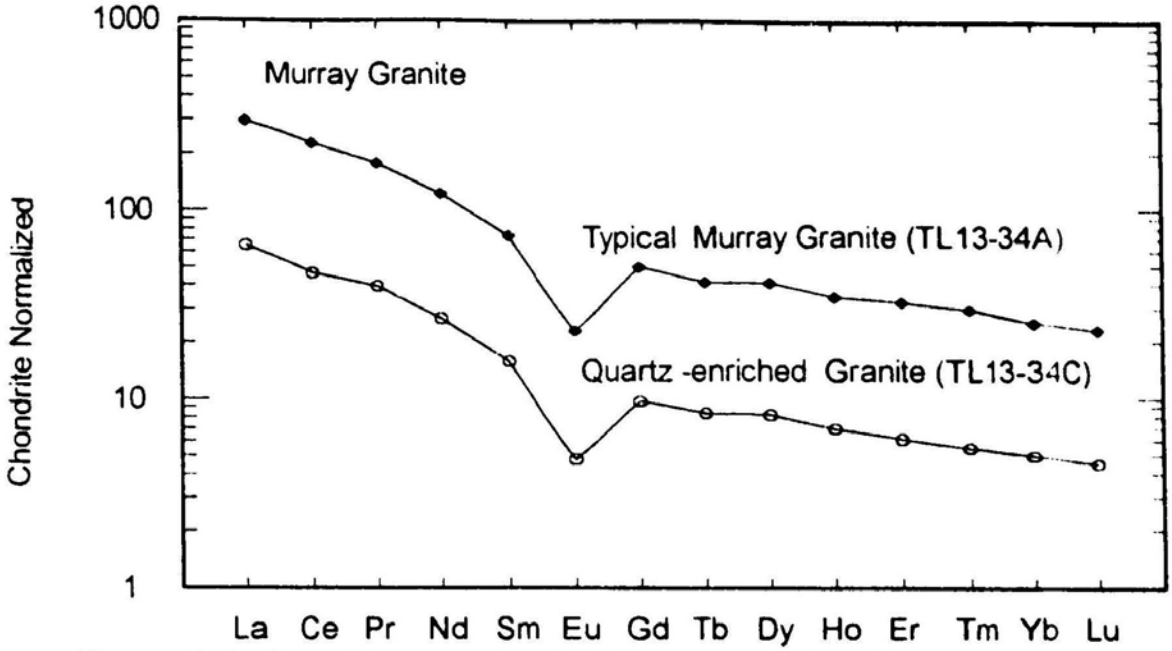

Figure 10.5 Chondrite normalized REE patterns of the Murray granite at the Thayer Lindsley Mine, including a quartz-rich sample near the contact with ores.

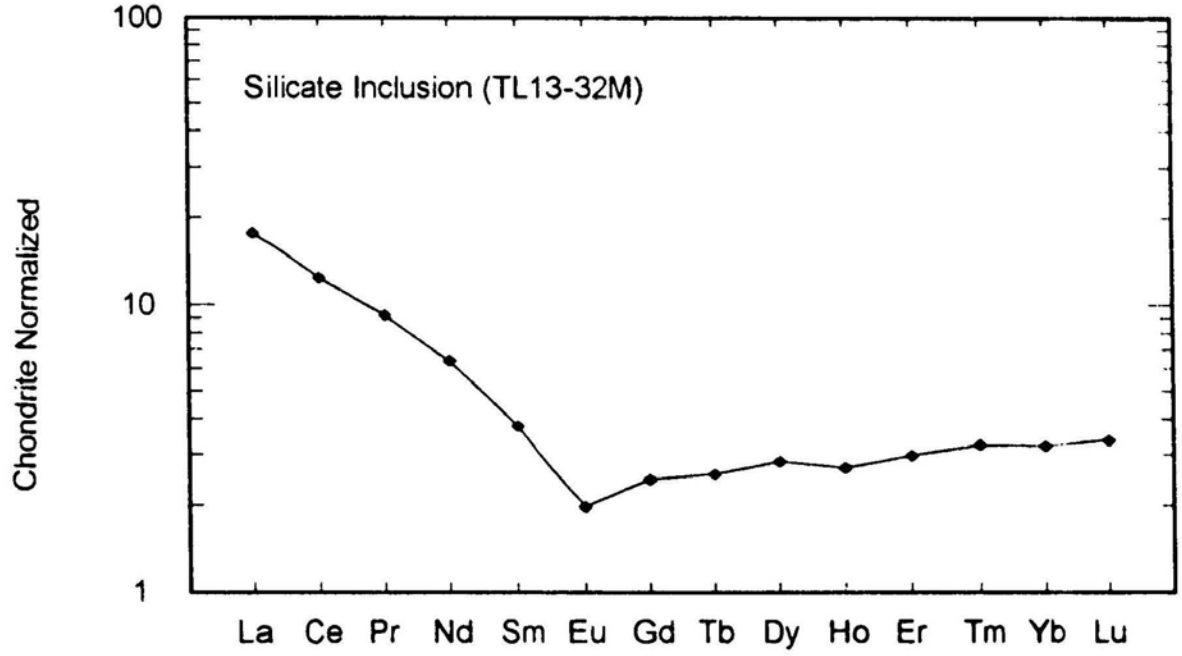

Figure 10.6 Chondrite normalized REE patterns of a felsic silicate inclusion (TL13-32M) in the massive sulphide ores at Thayer Lindsley Mine

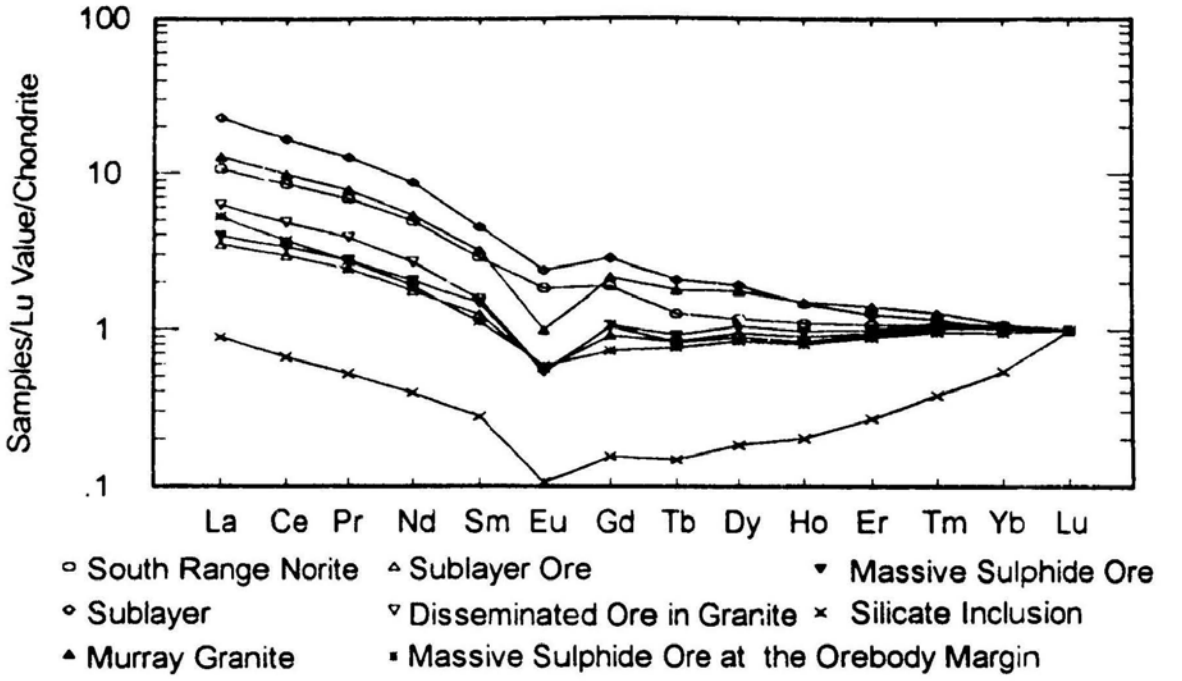

Figure 10.7 Chondrite and Lu doubly normalized REE patterns of the different rock and ore types at the Thayer Lindsley mine

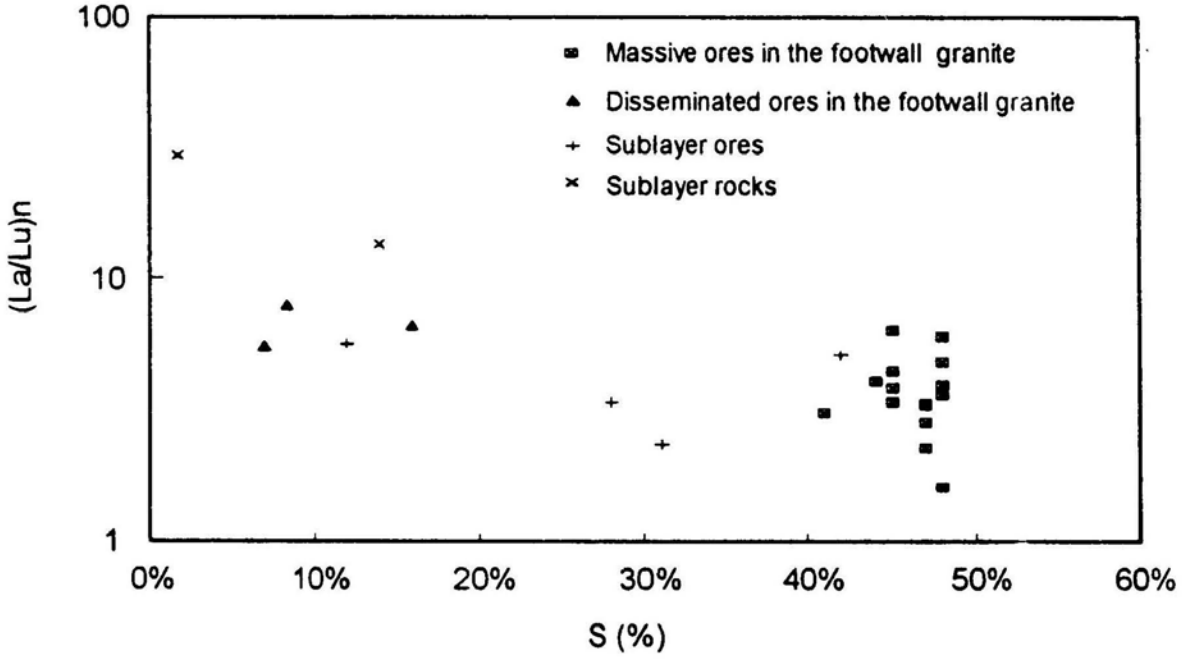

Figure 10.8 Negative correlation between logarithmic (La/Lu)n and S contents in the sulphide ores at the Thayer Lindsley mine

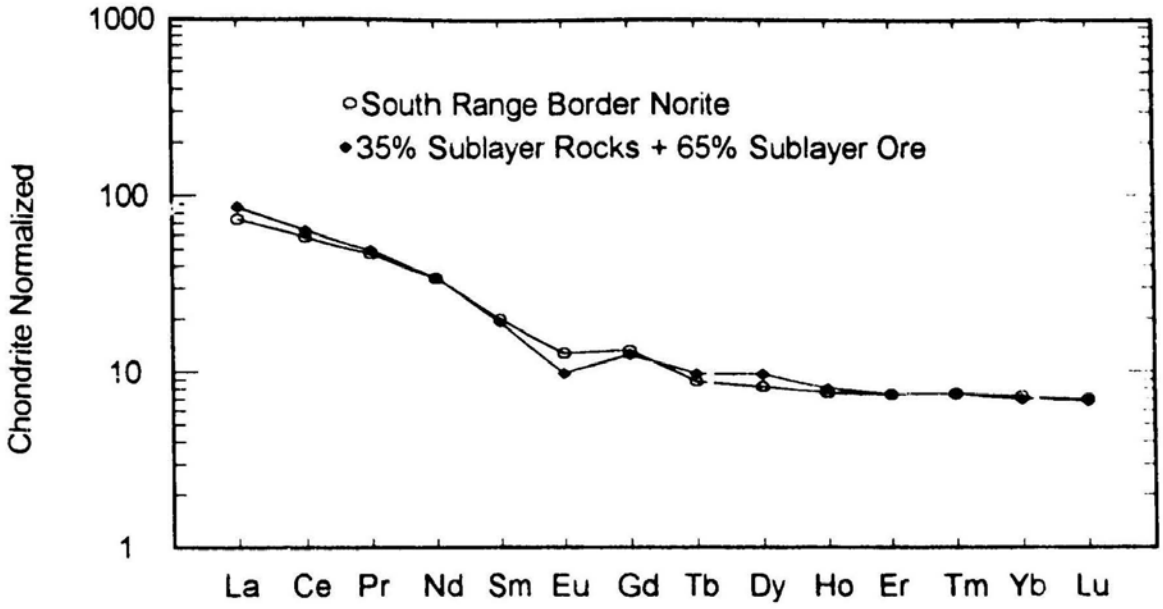

Figure 10.9 Chondrite normalized REE pattern of the calculated concentration of the original Sublayer magma (35% Sublayer rocks and 65% Sublayer ores , compared with that of the south range border norite

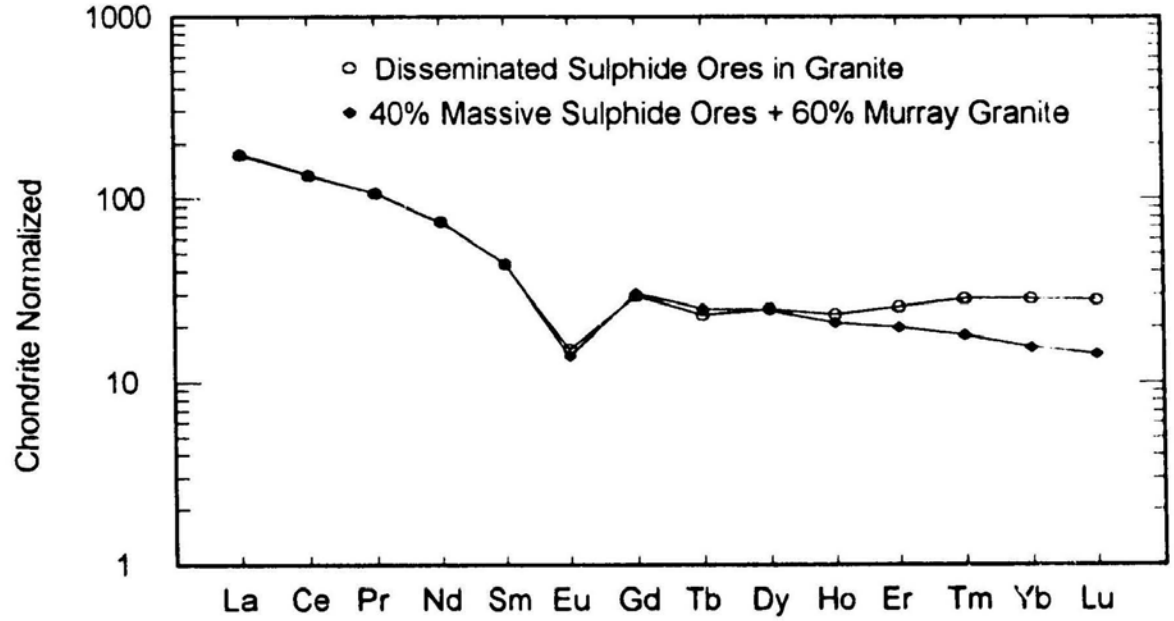

Figure 10.10 Chondrite normalized REE pattern of the calculated concentration of the disseminated ores in the granite (40% massive sulphide ore and 60% granite, compared with that of mean analyses of disseminated sulphide ores in the granite

CHAPTER 11

SUMMARY AND CONCLUDING REMARKS

11.1 THE DEVELOPMENT OF MICRO-SAMPLING TECHNIQUES USING INDUCTIVELY COUPLED PLASMA-MASS SPECTROMETRY

Three micro-sampling introduction techniques for inductively coupled plasma-mass spectrometry (ICP-MS) have been developed for application to geochemical studies of precious metal-rich nickel-copper ores at Sudbury: (1) a solution recycling nebulization system with a disposable spray chamber, (2) determination of precious metals in milligram samples of sulphides and magnetite using an automated 2 speed peristaltic pump speed controller for ICP-MS after cation exchange separation, and (3) in-situ determinations of precious metals in sulphide minerals using solid sample introduction by laser ablation.

With the recycling nebulization system, 0.5 g of sample solution is sufficient for 8 min of data acquisition. The sensitivity of the recycling nebulization system is similar to a conventional Scott spray chamber system. Twenty six trace elements were determined by ICP-MS using four internal standards (Ge, In, Re, and Bi) to correct for matrix, instrumental drift, and enrichment of the sample solution by evaporation. The ability to analyze

mineral separates weighing less than 0.1 mg was demonstrated with detection limits similar to conventional procedures. Analyses of selected geological reference materials SY-2, BCR-1, W-1, and BR indicate good limits of detection, good accuracy and precision, negligible memory, and low consumption of sample solution. Results compare well with data reported using conventional ICP-MS analysis. Analyses of the geological reference materials; PCC-1, AL-1, FK-N, NBS70a and NBS99a, for 15 Rare Earth Elements (REE), at ultra-trace concentration levels, using cation exchange preconcentration were demonstrated, with solid limits of detection from 0.01 to 1 ng g^{-1} (ppb), and relative standard deviations of less than 15% for homogenous samples.

The ability of focused laser radiation to volatilize virtually any material has provided a versatile method of direct solid sampling for subsequent analysis. A laser ablation microprobe-inductively coupled plasma-mass spectrometry (LAM-ICP-MS) was described and its applications to the determination of the precious metals in minerals was demonstrated. Although LAM-ICP-MS has been demonstrated as a promising new technique for the determination of in-situ trace and ultra-trace in minerals (Longerich *et al.*, 1993a; Jackson *et al.*, 1993a and 1993b; and Fryer *et al.*, 1993), analysis of precious metals in sulphides by LAM-ICP-MS in this study was only very preliminary because of lack of sufficient sensitivity. Solid limits of detection ranged from 26 ppb to 238 ppb. It provides a useful technique to examine the

distributions of precious metals, particularly the heavy PGE (Ir, Pt) and Au in sulphide minerals. However, serious interferences from base metal-argon polyatomic ions on Ru, Rh, and Pd were observed. Further developments are required both to minimize these interferences to improve Ru, Rh, and Pd analytical results and to provided the analytical sensitivities necessary for studies of natural sulphides.

To examine the distribution of the precious metals within and between minerals requires analytical techniques using microsampling techniques. However, serious interference of base metal-argon polyatomic ions and matrix effects hampers the accurate determination of precious metals by ICP-MS. A method for the quantitative separation of seven precious metals (Ru, Rh, Pd, Re, Ir, Pt, and Au) from large amounts of associated base metals in dilute hydrochloric acid solutions using a strongly acidic cation exchange resin, Amberlite CG-120, was established. The method has been applied to the determination of precious metals in small quantities (2-20 mg) of high purity sulphide and magnetite mineral separates using an automated 2 speed peristaltic pump speed controller and ICP-MS. Solid limits of detection for a 20 mg sample were less than 4 ppb for Ru, Rh, Re, Ir, Pt, and Au, but higher (29 ppb) for Pd due to the high memory. Analyses of nickel sulphide fire assay beads of the reference material, SARM-7, shows good agreement with certified values with relative standard deviations (RSD) of less than 8% for platinum-

group elements (PGE). Data from the analysis of sulphide and magnetite minerals from the Sudbury copper-nickel sulphide ores demonstrate the ability of the method to make useful determinations of precious metals for the study of ore genesis.

11.2 DISTRIBUTIONS AND PARTITIONING OF THE PRECIOUS METALS IN THE SULPHIDE ORES AT SUDBURY

Distributions and partitioning of the precious metals between the major sulphide ore minerals, and geochemistry of the REE in sulphides has long attracted geochemists because of their implications for petrogenesis. However, progress has been hampered due to the considerable analytical difficulty of working with small samples using conventional techniques. With the advantage of the micro-sampling analytical techniques developed in this study, two Ni-Cu-(PGE) deposits - Strathcona and Thayer Lindsley at Sudbury have been examined for their PGE and REE geochemistry.

The distribution of precious metals in principle ore minerals (sulphides and magnetite), and platinum-group minerals (PGM) at the Strathcona Mine was documented. Analytical data for Ru, Rh, Re, and Ir are more consistent than those of Pt, Pd, and Au. The distributions of Ru, Rh, and Ir indicates that these element are or were dominantly in solid solution in the sulphides and magnetite.

The remarkable variations of Pd, Pt, and Au contents in these minerals suggest the heterogeneous presence of discrete precious metal phases in these minerals which was documented using electron microprobe data. Ru, Rh, and Ir show similar distributions and partitioning. An apparent preferential association of these elements with specific minerals follows the sequence: sulphide > magnetite. Pd, Pt, and Au concentrations, are 10 to 100 times higher than the rest of precious metals and show no preferential partition among these minerals. Magnetite, usually regarded as having low concentrations of the precious metals, is remarkably enriched in Pt and Pd in the Deep Copper Ore Zone.

The geology and geochemistry of a new developed Ni-Cu-PGE deposit - Thayer Lindsley Mine were documented. Precious metals (Ru, Rh, Pd, Re, Ir, Pt and Au) were determined by ICP-MS from bulk sulphide ores and 20 mg of high purity sulphides (pyrrhotite, chalcopyrite, and pentlandite) and magnetite in the copper-nickel sulphide ores of the Thayer Lindsley Mine. The distribution of precious metals shows that considerable amounts of Ru, Rh, Pd and Ir are or were in solid solution in the sulphides and magnetite, whereas the rest of the precious metals are dominantly in separate discrete phases either as minor inclusions in the ore minerals or as precious metal minerals which are found at the boundaries of these minerals. There are no apparent systematic spatial variations of precious metals in individual ore minerals from different parts of

the 4B Ore Zone, although bulk NiS sulphide fire analyses shows that the ores from the orebody margin are more enriched in Pd, Pt and Au.

The 4B Ore Zone at the Thayer Lindsley Mine is stratigraphically equivalent to the Deep Copper Zone at the Strathcona Mine in that both ore zones are hosted by footwall rocks of the SIC. They are also similar in in that characterized by strong enrichment of the precious metals. The Deep Copper Zone is composed of highly irregular massive sulphide veins which are predominantly composed of chalcopyrite and cubanite, whereas the 4B Ore Zone consists of massive sulphide ore bodies which are predominantly composed of pyrrhotite and chalcopyrite. Precious metal analyses of mineral separates in both ore zones show considerable amounts of Ru, Rh, Pd and Ir are or were in solid solution in the sulphides and magnetite, whereas the rest of the precious metals are dominantly in separate discrete phases either as minor inclusions in the ore minerals or as precious metal minerals which are found at the boundaries of the ore minerals. However, the ore minerals in the 4B Ore Zone are much more strongly depleted in Pt and show no correlations between Pt and Pd, which is quite different from relationships in the Deep Copper Ore Zone.

Partition coefficients (K_d values) at ppb to ppm levels of precious metals among the ore minerals at the Thayer Lindsley Mine have been investigated. Partitioning of Ru, Rh, and Ir between these minerals follows the same

sequence (with decreasing order): pyrrhotite > pentlandite > chalcopyrite > magnetite. Partitioning of Pd, Re, Pt, and Au does not follow this sequence; and is different for each element. Crystallization and subsequent exsolution are mainly responsible for the distribution and fractionation of precious metals in sulphides and magnetite. A fractionation model is proposed to explain the precious metal ore genesis.

A study of the trace element geochemistry at the Thayer Lindsley deposit indicates that sulphide ores in footwall granite and in the Sublayer are depleted in lithophile trace elements (Rb, Ba, REE, Zr, Hf, Nb, Ta, Th, and Sr) during magmatic sulphide segregation. In comparison with the South Range norite which is thought to represent the parent magma, the Sublayer rocks are enriched in light rare earth elements (LREE) and have slightly negative Eu anomalies, whereas sulphide ores in the Sublayer and in the footwall Murray granite are depleted in LREE have a strongly negative Eu anomaly. The original REE composition of the Sublayer magma can be modeled from 35% Sublayer rocks and 65% Sublayer sulphide ores. Chondrite normalized REE distribution patterns indicate that the massive ores in the footwall granite are parts of a highly fractionated sulphide liquid which was expelled from the original sulphide magma along structural weakness into the footwall granite. A distinctive REE distribution pattern indicates a hydrothermal fluid was involved in the development of the orebody margin.

11.3 FUTURE WORK

A method for the determination of the precious metals in milligram samples of sulphides and magnetite after preconcentration using ion exchange with an automated 2 speed peristaltic pump speed controller and ICP-MS allows the examination of precious metals distributions and fractionation within and between the minerals. However, in spite of very small quantities of high purity mineral separates, some PGE and Au alloy inclusions at the micrometer scale within some minerals could not eliminated, which will require specific in-situ probe analytical techniques for future work. LAM-ICP-MS was preliminarily investigated for this purpose. However, serious interferences of base metal-argon polyatomic ions on Ru, Rh, and Pd were observed. Further development is required to minimize these interferences to improve analytical results, or other in-situ microprobe techniques need to be developed.

Mass balance calculation in the ore in the 4B Ore Zone at the Thayer Lindsley Mine indicates that the majority of Pt, Pd, and Au are in discrete mineral phases. Although some precious metal minerals was found in this study, further work is required to document the detailed precious metal mineralogy and its distribution within the ore zone.

REFERENCES

Abdullah, M., Fuwa, K., and Leis, F., 1984. Simultaneous multielement analysis of microliter volumes of solution samples by inductively coupled plasma atomic emission spectrometry utilizing a graphite cup direct insertion technique. Spectrochim. Acta 39B: 1129-1139.

Abdullah, M. Haraguchi, H., 1985. Computer-controlled graphite cup direct instertion device for direct analysis of plant samples by inductively coupled plasma atomic emission spectrometry. Anal. Chem., 57: 2059-2064.

Adrain, R.S. and Watson, J., 1984. Laser microspectral analysis: a review of principles and applications. J. Phys. D., 17: 1915-1940.

Arrowsmith, P., 1987. Laser ablation of solids for elemental analysis by inductively coupled plasma mass spectrometry. Anal. Chem., 59: 1437-1444.

Barnes, S-J. and Picard, C.P., 1993. The behaviour of platinum-group elements during partial melting, crystal fractionation, and sulphide segregation: An example from the Cape Smith Fold Belt, northern Quebec. Geochimica et Cosmochimica Acta, 57: 79-87.

Barnes, S-J., Naldrett. A.J. and Gorton, M.P., 1985. The origin of the fractionation of platinum-group elements in terrestrial magmas. Chem. Geol., 53: 303-321.

Barnes, S.-J., 1993. Partitioning of the platinum group elements and gold between silicate and sulphide magmas in the Munni Complex, Western Australia. Geochimica et Cosmochimica Acta, 57: 1277-1290.

Beamish, F.E. and Van Loon, J.C., 1977. Analysis of noble metals-overview and selected methods, Academic Press, Inc (London) Ltd., London, 327pp.

Beauchemin, D. and Craig, J.M., 1990. Investigation on mixed gas plasma produced using a sheathing device in ICP-MS, in Plasma Source Spectrometry, The proceeding of the Third Surrey Conference on Plasma Mass Spectrometry, edited by Jarvis, K.E., Gray, A.L., Jarvis, I. and

Williams, J., Royal Society of Chemistry, Cambridge, England, P. 25-42.

Berman, S.S., and McBryde, W.A.E., 1958. Separations of the platinum metals by ion exchange. Can.J. Chem. 36: 835-844.

Berman, S.S., McBryde, W.A.E., 1958. The separations of Rhodium and Iridium by ion exchange. Can.J. Chem. 36: 845-854.

Bethke, P.M. and Barton, P.B., Jr., 1971: Distribution of some minor elements between coexisting sulphide minerals. Econ. Geol., 66: 140-163.

Binney, W.P., Poulin, R.Y., Sweeny, J.M., and Halladay, S.H., 1992. The Lindsley Ni-Cu-PGE deposit and its geological setting. In A.J. Naldrett, P.C. Lightfoot and P. Sheahan eds., Proceedings of the Sudbury-Norilsk symposium. Special Publication, Ontario Geological Survey (in press).

Brenner, I.B., Lorber, A. and Goldbart, Z., 1987. Trace element analysis of geological materials by direct solids insertion of a graphite cup into an inductively coupled plasma, Spectrochim. Acta. 42B:219-225.

Cabri, L.J. and Laflamme, J.H.G., 1976. The mineralogy of the platinum-group elements from some copper-nickel deposits of the Sudbury area, Ontario. Econ. Geol., 71: 1159-1195.

Cabri, L.J., Blank, H., El Goresy, A., Laflamme, J.H.G., Nobiling, R., Sizgoric, M.B. and Traxel, K., 1984. Quantitative trace-element analysis of sulfides from Sudbury and Stillwater by proton-Microprobe. Can. Mineral. 22: 521-542.

Cabri, L.J., Campbell, J.L., Lamflamme, J.H.G., Leigh, R.G., Maxwell, J.A. and Scott, J.D., 1985. Proton-microprobe analysis of trace elements in sulfides from some massive-sulphide deposits. Can. Mineral., 23: 133-148.

Campbell, I.H. and Barnes, S.-J., 1984. A model for the geochemistry of the platinum group elements in magmatic sulphide deposits. Canadian Mineralogist, 22: 151-160.

Campbell, I.H., Naldrett, A.J., and Barnes, S.-J., 1983. A model for the origin of platinum-rich sulphide horizons in the Bushveld and Stillwater

Complexes. J. Petrol., 24: 133-165.

Card, K.D., Gupta, V.K., Mcgrath, P.H., and Grant, F.S., 1984. The Sudbury structure: its regional geological and geophysical setting. P. 25-43, In E.G. Pye, A.J. Naldrett, and P.E. Giblin eds., Ontario Geological Survey, special volume 1, 604pp.

Chai, G., Naldrett, A.J., Rucklidge, J.C., and Kilius, L.R., 1993. In situ quantitative analysis for PGE and Au in sulphide minerals of the Jinchuan Ni-Cu deposit by accelerator mass spectrometry. Canadian Mineralogist, 31: 19-30.

Chan, W.T. and Horlick, G., 1990. An automated direct sample insertion system for inductively coupled plasma-atomic emission spectrometry, Appl. Spectrosc. 44: 380-390.

Chen, Z, Longerich, H.P., and Fryer, B.J., 1992a. Recycling nebulization system with a disposable spray chamber for analysis of sub-milligram samples of geological materials using inductively coupled plasma-mass spectrometry. J. Anal. Atom. Spectrom., 7: 905-913.

Chen, Z., Fryer, B.J., Longerich, H.P., and Jackson, S.E., 1992b. Determination of precious metals in coexisting minerals using recycling solution nebulization ICP-MS and laser ablation microprobe ICP-MS. Abstract with program, GAC/MAC joint annual meeting, Wolfville, N.S.

Chen, Z., Fryer, B.J., Longerich, H.P., and Jackson, S.E., 1993. Determination of precious metals in sulphides and magnetite by inductively coupled plasma-mass spectrometry, after preconcentration using cation exchange. (to be submitted for publication in Chemical Geology)

Chryssoulis, S.L., Cabri, L.J., and Lennard, W., 1989. Calibration of the ion probe for quantitative trace precious metal analyses of ore minerals. Economic Geology, 84: 1684-1689.

Chung, Y.S. and Barnes, R.M., 1988. Determination of gold, platinum, palladium and silver in geological samples by inductively coupled plasma atomic emission spectrometry after poly(dithiocarbamate) resin pre-treatment, J. Anal. Atom. Spectrom., 3: 1079-1082.

Chyi, L.L. and Crocket, J.H., 1976. Partition of platinum. palladium, iridium,

and gold among coexisting minerals from the Deep Ore Zone, Strathcona Mine, Sudbury, Ontario. Econ. Geol., 71: 1196-1205.

Coats, C.J., and Snajdr, P. 1984. Ore deposits of the North Range, Onaping - Lavack area, Sudbury. In E.G. Pye, A.J. Naldrett, and P.E. Giblin eds., The geology and ore deposits of the Sudbury structure.

Cowan, J.C.(1968): The geology of the Strathcona ore deposit. Canadian Mining Metall. Bull. 60 38-54.

Darke, S.A., Long, S.E., Pickford, C.J. and Tyson, J.F., 1989a. Laser ablation system for solid sample analysis by inductively coupled plasma atomic emission spectrometry. J. Anal. Atom. Spectrom., 4: 715-719.

Darke, S.A., Long, S.E., Pickford, C.J. and Tyson, J.F., 1989b. Laser ablation system for solid sample introduction into the inductively coupled plasma. Anal. Proc., 26: 159-160.

Darke, S.A., and Tyson, J.F., 1993. Interaction of laser radiation with solid materials and its significance to analytical spectrometry. J. Anal. Atom. Spectrom., 8: 145-209.

Date, A.R., 1984. ICP-MS applications development at the British Geological Survey. ICP Inf. Newslett., 10: 202-206.

Date, A.R. and Cheung, Y.Y., 1987, Studies in the determination of lead isotope ratios by inductively coupled plasma spectrometry. Analyst 108:159-165.

Date, A.R., Davis, A.E., and Cheung, Y.Y., 1987. The potential of fire assay and ICP-MS for the determination of platinum group elements in geological materials. Analyst, 112: 1217-1222.

Date, A.R. and Gray, A.L., 1983. Development progress in plasma source mass spectrometry. Analyst, 108: 159-165.

Date, A.R. and Gray, A,L., 1985. Determination of trace elements in geological samples by inductively coupled plasma source mass spectrometry. Spectrochim. Acta, 40B: 115-122.

Date, A.R. and Hutchison, D., 1987. Determination of rare earth elements in

geological samples by inductively coupled plasma spectrometry. J. Anal. Atom. Spectrom., 2: 269-276.

Date, A.R. and Jarvis, K.E., 1989. Application of ICP-MS in the earth sciences. In: A.L. Gray and A.R. Date, Inductively coupled plasma mass spectrometry, Glasgow: Blackie, 254pp.

Davis, G.C., 1984. Little Stobie mine: a South Range contact deposit. p.361-369, In E.G. Pye, A.J. Naldrett, and P.E. Giblin eds., Ontario Geological Survey, special volume 1, 604pp.

Dean, J.R., Ebdon, L., Crews, H.M. and Massey, R.C., 1988. Characteristics of flow injection inductively coupled plasma spectrometry for trace metal analysis. J. Anal. Atom. Spectrom., 3: 349-354.

Dietz, R.S., 1964. Sudbury structure as an astrobleme. Journal of Geology, 72: 412-434.

Dickin, A.P., Richardson, J.M., Crocket, J.M., McNutt, R.H., and Peredery, W.V., 1992. Osmium isotope evidence for a crustal origin of platinum group elements in the Sudbury nickel ore, Ontario, Canada. Geochimica et Cosmochimica Acta, 56: 3531-3537.

Ding, T.P. and Schwarcz, H.P., 1984. Oxygen isotropic and chemical compositions of rocks of the Sudbury Basin, Ontario. Canadian Journal of Earth Sciences, 21: 305-318.

Distler, V.V., Malveskiy, A.Yu. and Laputina, I.P., 1977. Distribution of Platinoids between pyrrhotite and pentlandite in crystallization of a sulphide melt. Geochem. Int., 14: 30-40.

Dittrich, K. and Wennrich, R., 1984. Laser vaporization in atomic spectroscopy. Pro. Analyt. Atom. Spectrosc., 7:139-198.

Dittrich, K. and Wennrich, R., 1990. Laser vaporization in atomic spectrometry. in: J. Sneddon (Editor), Sample introduction in atomic spectroscopy.

Doherty, W. and Van der Voet, A., 1985. The application of inductively coupled plasma mass spectrometry to the determination of rare earth elements in geological materials. Can. J. Spectrosc., 30: 135-141.

Doherty, W., 1989. An internal standardization procedure for the determination of yttrium and rare earth elements in geological materials by inductively coupled plasma-mass spectrometry. Spectrochim. Acta, 44B: 263-280.

Faggart, B.E. Jr., Basu A.R., and Tatsumoto, M., 1985. Origin of the Sudbury complex by meteoritic impact: neodymium isotope evidence. Science, 230: 436-439.

Fairbairn, H.W., Faure, G., Pinson, W.H., and Hurley, P.M., 1968. Rb-Sr wholerock age of the Sudbury Lopolith and basin sediments. Canadian Journal of Earth Sciences, 5:707-714.

Farrow, C.E.G., Watkinson, D.H., Hattori, K., and Fouillac, A.-M., 1992. Mineralogical and isotopic characteristics of alteration associated with Ni, Cu and PGE deposition in the North Range of the Sudbury Structure. Abstract volume. GAC/MAC Annual Meeting, Wolfville, 1992.

Fassel, V.A. and Bear, B.R., 1986. Ultrasonic nebulization of liquid samples for analytical inductively coupled plasma-atomic emission spectroscopy: An update. Spectrochim. Acta, 41B: 1089-1113.

Fedorowich, J.S., Richards, J.C., Jain, J.C., Kerrich, R. and Fan J., 1993. A rapid method of REE and trace-element analysis using laser sampling ICP-MS on direct fusion whole-rock glasses. Chemical Geology, 106: 229-249.

Fleet, M.E., Stone W.E., and Crocket, J.H., 1991. Partitioning of palladium, iridium, and platinum between sulphide liquid and basalt melt: Effect of melt composition, concentration, and oxygen fugacity. Geochim. Cosmochim., Acta 55: 2545-2544.

Frarey, M.J., LoverBridge, W.D., and Sullivan, R.W., 1982. A U-Pb zircon age for the Creighton Granite, Ontario; p.129-132. In Rb-Sr and U-Pb Isotopic Age Studies, Report 5, Current Research, Part C, Geological Survey of Canada, Paper 70-40.

Frimpong, A., Fryer, B.J., Longerich, H.P., and Jackson, S.E. 1993. Recovery of the precious metals using NiS fire assay collection: Problem at ng g^{1} concentrations. Analyst (submitted).

Frimpong, A., 1992. Evaluation and improvement of the nickel sulphide fire

assay method with ICP-MS finish, for analysis of rocks for the precious metals. Unpublished Master thesis, Memorial University of Newfoundland.

Fryer, B.J., and Kerrich,R., 1978. Determination of precious metals at ppb levels in rocks by a combined wet chemical and flameless atomic absorption method. Atomic Absorption Newsletter, 17: 4-6.

Fryer, B.J., Jackson, S.E., Longerich, H.P., 1993. Application of laser ablation microprobe-inductively coupled plasma-mass spectrometry (LAM-ICP-MS) to in-situ (U)-Pb geochronology. Chemical Geology, in Press.

Govindaraju, K., 1989. 1989 compilation of working values and sample description for 272 geostandards, Geostandards Newsletter, 13: 1-113.

Grant, R.W. and Bite, A., 1984. Sudbury quartz diorite offset dyke. In E.G. Pye, A.J. Naldrett, and P.E. Giblin eds., Ontario Geological Survey, special volume 1, pp 275-300.

Gray, A.L., 1985. Solid sample introduction by laser ablation for inductively coupled plasma source mass spectrometry. Analyst, 110: 551-556.

Gray, A.L., 1986. Mass spectrometry with an inductively coupled plasma as an ion source: the influence on ultra-trace analysis of background and matrix response. Spectrochim. Acta. 41B: 151-167.

Gregoire, D.C., 1988. Determination of Pt, Pd, Ru and Ir in geological materials by inductively coupled plasma mass spectrometry with sample introduction by electrothermal vaporization. J. Anal. Atom. Spectrom. 3: 309-314.

Greenwood, N.N. and Earnshaw, A., 1984. Chemistry of the elements. Pergamon Press, 1543pp.

Grieve, R.A., Stoffler, D., and Deutsh, A., 1991. The Sudbury structure: controversial or misunderstood? Journal of Geophysical Research, 96:22753-22764.

Hager, J., 1989. Relative elemental responses for laser ablation-inductively coupled plasma mass spectrometry. Anal. Chem., 61: 1243-1248.

Hahn-Weinheimer, P., 1958. Zur Bestimmung von Edelmetallpuren in Gesteinen. Fresenius' Z. Anal. Chem., 162:161-167.

Hawley, J.E., 1962. The Sudbury ores: their mineralogy and their origin. Canadian Mineralogist, 7:1-207.

Hawley, J.E., 1965. Upside-down zoning at Frood, Sudbury, Onatrio. Econ. Geol. 60: 529-575.

Hawley, J.E., and Stanton, R.L., 1962. The fact, the ores, their minerals, metals and distribution. In J.E. Hawley ed., The Sudbury ores: their mineralogy and their origin. Canadian Mineralogist, 7:30-145.

Hermman, A.G., 1972. Yttrium and lanthanides. In Handbook of geochemistry, Vol. 39. Edited by H.K. Wedepohl. pp.56-718, 57-710.

Hoffman, E.L., Naldrett, A.J., Van Loon, J.C., Hancock, R.G.V., and Manson, A., 1978. The determination of all the platinum-group elements and gold in rocks and ore by neutron activation analysis after preconcentration by a nickel sulphide fire-assay technique on large samples. Anal. Chim. Acta, 102: 157-166.

Hoffman, E.L., Naldrett, A.J., Alcock, R.A., and Hancock,R.G.V., 1979. The noble-metal content of ore in the Levack West and Little Stobie mines, Ontario; Canadian Mineralogist, 17:437-451.

Hulmston, P., 1983. A pneumatic recirculating system for small sample volumes, Analyst, 108: 166-170.

Houk, R.S. 1986. Mass Spectrometry of inductively coupled plasmas. Anal. Chem., 58: 97A-105A.

Housh, T. and Bowring, S., 1991. Lead isotopic heterogeneities within alkali feldspars: implications for the determination of initial lead isotopic compositions. Geochimica et Cosmochimica Acta, 55: 2309-2316.

Irvine, T.N., 1975. Crystallization sequences of the Muskox intrusion and other layered intrusions: II. Origin of chromitite layers and similar deposits of other magmatic ores. Geochimica et Cosmochimica Acta 3: 991-1020.

Ishizuka, T. and Uwamino, Y., 1980. Atomic emission spectrometry of solid

samples with laser vaporization-microwave induced plasma system. Anal. Chem., 52: 125-129.

Isoyama, H., Uchida, T., Lida, C. and Nakagawa, G., 1990a. Recycling nebulization system with exchangeable spray chamber for inductively coupled plasma atomic emission spectrometry. J. Anal. At. Spectrom., 6: 365-369.

Isoyama, H., Uchida, T., Lida, C. and Nakagawa, G., 1990b. Determination of trace metals in biological samples by inductively coupled plasma atomic emission spectrometry with discrete nebulization after microwave decomposition. Anal. Sci., 6: 385-388.

Jackson, S.E., Fryer, B.J., Gosse, W., Healey, D.C., Longerich, H.P. and Strong, D.F., 1990. Determination of the precious metals in geological materials by inductively coupled plasma-mass spectrometry (ICP-MS) with nickel sulphide fire-assay collection and tellurium coprecipitation. In: Potts, J., C. Dupuy and J.F.W. Bowles (Guest-Editors), Microanalytical Methods in Mineralogy and Geochemistry. Chemical Geology, 83: 119-132.

Jackson, S.E., Longerich, H.P.,and Fryer, B.J., 1992. Progress in high resolution, in-situ trace analysis of minerals by laser ablation microprobe-inductively coupled plasma-mass spectrometry. V.G. Goldschmidt Conference Abstracts, A53-A54.

Jackson, S.E., Longerich, H.P., Dunning, G.R, and Fryear, B.J., 1993. The application of laser ablation microprobe-inductively coupled plasma-mass spectrometry (LAM-ICP-MS) to in-situ trace element determinations in minerals. Canadian Mineralogist, 30:1049-1064.

Jackson, S.E., Longerich, H.P., Jenner, G.A. and Fryer, B.J., 1993b. Laser ablation microprobe-inductively coupled plasma-mass spectrometry (LAM-ICP-MS). Program with abstract, 1993 European Winter Conference of Plasma Spectrometry, Granada, Spain.

Jarvis, K.E., 1988. Inductively coupled plasma mass spectrometry: a new technique for the rapid or ultra-trace level determination of the rare-earth elements in geological materials. Chem. Geol., 68: 31-39.

Jarvis, K.E., 1989. Determination of rare earth elements in geological samples

by inductively coupled plasma mass spectrometry. J. Anal. Atom. Spectrom., 4: 563-570.

Jarvis, K.E., and Williams, J.H., 1993. Laser ablation inductively coupled plasma mass spectrometry (LA-ICP-MS): a rapid technique for the direct, quantitative determination of major, trace and rare-earth elements in geological samples. Chemical Geology, 106: 251-262.

Jenner, G.A., Longerich, H.P., Jackson, S.E. and Fryer, B.J., 1990. ICP-MS--A powerful tool for high precision trace-element analysis in earth sciences: Evidence from analysis of selected U.S.G.S. reference samples. Chem. Geol., 83: 133-148.

Jiang, S.J. and Houk, R.S.,1986. Arc nebulization for elemental analysis of conducting solid by inductively coupled plasma mass spectrometry. Anal. Chem., 58: 335-344.

Jin, Q., Zhu, C., Brushwyler, K., and Hieftje, G.M., 1990. An efficient and inexpensive ultrasonic nebulizer for atomic spectrometry, Appl. Spectrosc., 44: 183-186.

Kato, K. and Takashima, K., 1989. Recycling nebulization-sample introduction system for inductively coupled plasma atomic emission spectrometry. Anal. Sci., 5: 151-156.

Kerrich, R. and Fryer, B.J., 1979. Archean precious-metal hydrothermal systems, Dome Mine, Abitibi Greenstone Belt. II. REE and Oxygen isotope relations. Canadian Journal of Earth Sciences, 16: 440-458.

Keays, R.R., and Crocket, J.H., 1970. A study of precious metals in the Sudbury Nickel Irruptive ores. Econ. Geol., 65: 438-450.

Kosterin, A.V., 1959. The possible modes of transport of the rare earths by hydrothermal solution. Geochemistry International (U.S.S.R.) (English translation). 1:381-386

Krogh, T.E., Davis, G.L., and Corfu, F., 1984. Precise U-Pb zircon and baddeleyite ages for the Sudbury area. In E.G. Pye, A.J. Naldrett, and P.E. Giblin eds., Ontario Geological Survey, special volume 1, 604pp.

Kuo, H.Y. and Crocket, J.H., 1979. Rare earth elements in the Sudbury Nickel

Irruptive: Comparison with layered gabbros and implications for nickel irruptive petrogenesis. Econ. Geol., 74: 590-605.

Li, C., and Naldrett, A.J., 1993. Platinum-group minerals from the Deep Copper Zone of Strathcona deposit, Sudbury, Ontario. Canadian Mineralogist, 31: 31-44.

Li, C., Naldrett, A.J., Coats, C.J.A., and Johannesses, P., 1992. Platinum, palladium, gold, and copper-rich stringers at the Strathcona Mine, Sudbury: their enrichment by fractionation of a sulphide liquid. Econ. Geol., 87: 1584-1598.

Lichte, F.E., Meier, A.L. and Crock, J.G., 1987. Determination of rare-earth elements in geological materials by inductively coupled plasma mass spectrometry. Anal. Chem., 59: 1150-1157.

Lin, S. and Peng, C., 1990. Studies on the application of laser sampling-Inductively Coupled Plasma Atomic emission spectrometry to the determination of rare earth and refractory elements. J. Anal. Atom. Spectrom., 5: 509-514.

Longerich, H.P., Strong, D.F., and Kantipuly, C.J., 1986. Progress in evaluation of instrumental and other parameters affecting chemical and isotopic analysis by inductively coupled plasma-mass spectrometry (ICP-MS). Can. J. Spectrosc. 31: 111-121.

Longerich, H.P., Fryer, B.J., Strong, D.F. and Kantipuly, C.J., 1987. Effects of operating conditions on the determination of rare earth elements by inductively coupled plasma-mass spectrometry (ICP-MS). Spectrochim. Acta, 42B: 75-92.

Longerich, H.P.,1989. The effect of nitric acid, acetic acid and ethanol on inductively coupled plasma-mass spectrometric ion signals as a function of nebulizer gas flow, with implications on matrix suppression and enhancements, J. Anal. Atom. Spectrom., 4: 665-667.

Longerich, H.P., Jenner, G.A., Fryer,B.J., and Jackson, S.E., 1990. Inductively coupled plasma-mass spectrometric analysis of geological samples: A critical evaluation based on case studies. Chem. Geol., 83: 105-118.

Longerich, H.P., 1993a. Automated two-speed peristaltic pump controller for

reduced sample wash-out time and analysis of small volumes. J. Anal. Atom. Spectrom., 8: 371-374.

Longerich, H.P., 1993b. The analysis of pressed pellets of geological samples using wavelength dispersive X-Ray fluorescence spectrometry. X-Ray spectrometry, in preparation.

Longerich, H.P., Jackson, S.E., Fryer, B.J., and Strong, D.F., 1993a. Machinations: The Laser ablation microprobe-inductively coupled plasma-mass spectrometer (LAM-ICP-MS). Geosciences Canada, 20: 21-27.

Longerich, H.P., Jackson, S.E., Jenner, G.A., Friel, J.K., Chen, Z., Fryer, B.J., and Frimpong, A., 1993b. Progress in the determination of trace elements using solution nebulization ICP-MS. Program with abstract, 1993 European Winter Conference on plasma spectrometry, Granada, Spain.

Lundell, G.E.F, 1933. The chemical analysis of things as they are. Ind. Eng. Chem., Anal. Ed., 5: 221-225.

Maiman, T.H., 1960. Stimulated optical radiation in Ruby. Nature, 187: 493-494.

Makovicky, M., Makovicky, E. and Rose-Hansen, J., 1986. Experimental studies on the solubilities and distribution of platinum group elements in the base-metal sulphides in platinum deposits, in Gallagher, M.J., Ixer, R.A., Neary, C.R., and Pritchard, F.M., eds, Metallogeny of basic and ultrabasic rocks: London, Inst. Mining Metallurgy, F. 415-426.

Malevskiy, A.Yu., Laputina, I.P. and Distler, V.V., 1977. Behaviour of the platinum-group metals during crystallization of pyrrhotite from a sulphide melt. Geochem. Int., 14: 177-184.

Marks, A.G., and Beamish, F.E., 1958. Separation of rhodium and iridium from base metals by ion exchange. Analytical Chemistry, 30:1464-1466.

McLeod, C.W., Routh, M.W., and Tikkanen, M.W., 1992. Introduction of solids into plasmas. In: Montaser, A. and Golightly, D.W., Inductively coupled plasmas in analytical atomic spectrometry, 2nd Edition, 1017pp.

Mitchell, P.G., Sneddon, J., and Radziemski, L.J., 1987. Direct determination

of copper in solid by direct current argon plasma emission spectrometry with sample introduction using laser ablation. Appl. Spectrosc. 41: 141-148.

Moenke-Blankenburg, L., 1989. Laser microanalysis. Chemical Analysis: a series of monographs on analytical chemistry and its applications, Vol. 105, John Wiley & Sons, New York, 288pp.

Montaser, A., 1992. Assessment of the potential and limitations of plasma sources compared to ICP discharges for analytical spectrometry. In: Montaser, A. and Golightly, D.W., Inductively coupled plasmas in analytical atomic spectrometry, 2nd Edition, 1017pp.

Morita, M., Ito, H., Uehiro, T., and Otsuka, K., 1989. High resolution mass spectrometry with inductively coupled argon plasma ionization source. Anal. Sci., 5: 609-610.

Muir, T.L., 1984. The Sudbury structure: considerations and models for an endogenic origin. In E.G. Pye, A.J. Naldrett, and P.E. Giblin eds., Ontario Geological Survey, special volume 1, 604pp.

Nakamura, E., Campbell, I.H., and Sun, S.S., 1985. The influence of subduction processes on the geochemistry of Japanese alkaline basalt. Nature, 36:55-58.

Naldrett, A.J. and Kullerud 1967. A study of Strathcona Mine and its bearing on the origin of the nickel-copper ores of the Sudbury district, Ontario. Jour. Petrology 8: 453-531.

Naldrett, A.J. and Kullerud, G.1968 Emplacement of ore at the Strathcona mine, Sudbury, Canada, as a sulphide-oxide magma in suspension in young noritic intrusion. Internat. Geol. Cong., 23rd, Prague 7: 197-213.

Naldrett, A.J., 1969. A portion of the system Fe-S-O between 900°C and 1080°C and its application to sulphide ore magmas. Journal of Petrology, 10:171-201.

Naldrett, A.J., Bray, J.G., Gasparrini, E.L., Podolsky, T., and Rucklidge, J.C., 1970. Crytic variation and the petrology of the Sudbury Nickel Irruptive. Economic Geology. 65: 122-155.

Naldrett, A.J., Greenman, L., and Hewins, R.H., 1972. The Main Irruptive and the Sublayer at Sudbury, Ontario. Internat. Geol. Cong., 24th, Montreal, sec. 4, pt. 1, 617-628.

Naldrett, A.J., 1981. Nickel sulphide deposits: classification, composition, and genesis. Econ. Geol., 75th Anniversary Volume: 628-685.

Naldrett, A.J., Innes, D.G., Sowa, J. and Gorton, M.P.(1982): Compositional variations within and between five Sudbury ore deposits. Econ. Geol. 77: 1519-1534.

Naldrett, A.J., Hewins, R.H., Dressler, B.O., and Rao, B.V., 1984. The Contact Sublayer of the Sudbury Igneous Complex. In E.G. Pye, A.J. Naldrett, and P.E. Giblin eds., Ontario Geological Survey, special volume 1, 604pp.

Naldrett, A.J. 1984. Mineralogy and composition of the Sudbury ore. In E.G. Pye, A.J. Naldrett, and P.E. Giblin eds., Ontario Geological Survey, special volume 1, 604pp.

Naldrett, A.J. and Hewins, R.H., 1984. The Main Mass of the Sudbury Igneous Complex. In E.G. Pye, A.J. Naldrett, and P.E. Giblin eds., Ontario Geological Survey, special volume 1, 604pp.

Naldrett, A.J., 1984. Ni-Cu ores of the Sudbury Igneous Complex-Introduction. In E.G. Pye, A.J. Naldrett, and P.E. Giblin eds., Ontario Geological Survey, special volume 1, 604pp.

Naldrett, A.J., Rao, B.V., and Evensen, N.M., 1985. Contamination at Sudbury and its role in ore formation. In M.J. Gallagher, R.A. Ixer, C.R. Neary and H.M. Prichard eds., 1985, Metallogeny of basic and ultrabasic rocks: London, Inst. Mining Metallurgy, p75-91.

Novak, J.W., Lillie, Jr., D.E., Boorm, A.W. and Browner, R.F., 1980. Fixed cross-flow nebulizer for use with ICPs and flames, Anal. Chem., 52: 576-579.

Olivares, J.A. and Houk, R.S., 1985. Ion sampling for inductively coupled plasma mass spectrometry. Anal. Chem. 57: 2674-2679.

Park, C.J. and Hall, G.E.M., 1988. Analysis of geological materials by

inductively coupled plasma mass spectrometry with sample introduction by electrothermal vaporization. J. Anal. Atom. Spectrom., 3: 355-362.

Pattison, E.F., 1979. The Sudbury sublayer. Canadian Mineralogist, 17: 257-286.

Peach, C.L., Mathez, E.A., and Keays, R.R., 1990. Sulphide melt-silicate melt distribution coefficients for the noble metals as deduced from MORB: implication for partial melting. Geochimica et Cosmochimica Acta, 54: 3379-3389.

Pearce, N.J.G., Perkins, W.T. and Fuge, R., 1992. Developments in the quantitative and semiquantitative determination of trace elements in carbonate by laser ablation inductively coupled plasma mass spectrometry. J. Anal. Atom. Spectrom., 7: 595-598.

Peredery, W.V. and Morrison, G.G., 1984. Discussion of the origin of the Sudbury Structure. p.491-512. In E.G. Pye, A.J. Naldrett, and P.E. Giblin eds., Ontario Geological Survey, special volume 1, 604pp.

Pettit, W.E. and G. Horlick, 1986. An automated direct sample insertion system for the inductively coupled plasma, Spectrochim. Acta 41B: 699-712.

Plummer, M.E.V., and Beamish, F.E., 1959. Determination of Platinum and Palladium in ores and concentrates, Anal. Chem., 31: 1141-1143.

Pye, E.G.. Naldrett, A.J., and Giblin, P.E., 1984. The geology and ore deposits of Sudbury structure. Ontario Geological Survey Special Volume 1.

Ready, J.F., 1965a. Mechanism of electron emission produced by a giant-pulse laser. Phys. Rev. A, 137: 620-623.

Ready, J.F., 1965b. Effects due to absorption of laser radiation. J. Appl. Phys., 36: 462-468.

Remond, G., Cesbron, F., Traxel, K., Campbell, J.L., and Cabri, L.J., 1987. Electron microprobe analysis and proton induced X-ray spectrometry applied to trace elements analysis in sulfides: problem and prospects. Scan. Microsc. 1: 1017-1037.

Robert, R.V.D., Van Wyk, E. and Palmer, R., 1971. Concentration of the noble

metals by fire-assay technique using NiS as the collector. Nalt. Inst. Metall., Johannesburg, Rep. No. 1371, 15pp.

Robinson, P., Higgins, N. and Jenner, G.A., 1986. Determination of rare-earth elements, yttrium and scandium in rock by an ion exchange-X-ray fluorescence technique, Chem. Geol., 55: 121-137

Rucklidge, J.C., Wilson, G.C., Kilius, L.R., and Cabri, L.J., 1992. Trace element analysis of sulphide concentrations from Sudbury by accelerator mass spectrometry. Canadian Mineralogist, 30: 1023-1032.

Salin, E.D. and Horlick, G., 1979. Direct sample insertion device for inductively coupled plasma emission spectrometry. Anal. Chem. 51: 2284-2286.

Sandell, E.B., 1959. Colorimetric determination of traces of metals. Interscience, New york, N.Y., 3rd ed., 1032pp.

Sant, B.R. and Beamish, F.E., 1961. New fire assay method for Rhodium. Anal. Chem., 33: 304-305.

Sciex, 1986. Elan Model 250 ICP/MS: operators manual, Division of MDS Health Group Ltd.

Scott, R.H., Fassel, V.A., Kniseley, R.N. and Nixon, D.E., 1974. Inductively coupled plasma optical emission analytical spectrometry, a compact facility for trace analysis of solutions, Anal. Chem., 46: 75-80.

Scribbins B., Rae, D.R., and Naldrett, A.J., 1934. Mafic and ultramafic inclusions in the sublayer of the Sudbury Igneous Complex. Canadian Mineralogist, 22: 67-75.

Sen Gupta, J.G., 1989. Determination of trace and ultra-trace amounts of noble metals in geological and related materials by graphite- furnace atomic-absorption spectrometry after separation by ion-exchange or co-precipitation with tellurium, Talanta, 36:651-656.

Shannon, R.D., 1976. Revised effective ionic radii and systematic studies of interatomic distances in halides and chalcogenides. Acta Crystallogr., 32A: 751-767.

Shao, Y. and Horlick, G., 1986. Performance of a direct sample insertion

system for the inductively coupled plasma. Appl. Spectrosc. 40: 368-393.

Sharp, B.L., 1988. Pneumatic nebulisers and spray chambers for inductively coupled plasma spectrometry. J. Anal. Atom. Spectrom., 3: 613-652.

Shen, W.L., Caruso, A., Friche, F.L., and Satzger, R.D., 1990. Electrothermal vaporization interface for samples introduction in inductively coupled plasma spectrometry. J. Anal. At. Spectrom. 5: 451-455.

Shendrikar, A.D. and Berg, E., 1969. Extraction studies of platinum group metals with diantipyrylpropylmethane. Anal Chim. Acta, 47:299-304.

Souch, B.E., Podolsky, T., and Geological Staff, 1969. The sulphide ores of Sudbury: their particular relationship to a distinctive in clusion-bearing species of the Nickel Irruptive. In H.D.B.Wilson ed., Magmatic ore deposits, Economic Geology Monograph 4.

Steele, T.W., Levin, J., and Copelowitz, T. 1975. Preparation and certification of a reference sample of a precious metal ore. Nat. Institute for Metallurgy (South Africa) Report No. 1696.

Stone W.E., Crocket J.H., and Fleet M.E., 1990. Partitioning of palladium, iridium, platinum, and gold between sulphide liquid and basalt melt at 1200°C. Geochim. Cosmochim. Acta, 54: 2341-2344.

Su, G. and Lin, S., 1988. Studies on the complete laser vaporization of powdered solid samples into an inductively coupled plasma for atomic emission spectrometry. J. Anal. Atom. Spectrom., 3: 841-847.

Suvic, M.V., 1957. Bull. Inst. Nucl. Sci. "Boris Kidrich". 7:39-41.

Strong, D.F. and Longerich, H.P., 1985. The inductively coupled plasma/mass spectrometer (ICP-MS). Geoscience Canada, 12: 72-75.

Taylor, S.R. and McLennan, S.M., 1985. The continental crust: its composition and evolution. Blackwell, London, 312 pp.

Tertipis, G.G., and Beamish, F.E., 1960. Ibid, 32: 486. Cf. Sant, B.R. and Beamish, F.E., 1961. New fire assay method for Rhodium. Anal. Chem., 33: 304-305.

Thompson, J.J. and Houk, R.S., 1986. Inductively coupled plasma mass spectrometric detection for multielement flow injection analysis and elemental speciation by reversed phase liquid chromatography. Anal. Chem., 58: 2541-2548.

Thompson, M., Goulter, J.E. and Sieper, F., 1981. Laser ablation for the introduction of solid samples into an inductively coupled plasma for atomic-emission spectrometry. Analyst, 106: 32-39.

Thompson, M., Chenery, S. and Brett, L., 1989. Calibration studies in laser ablation microprobe-inductively coupled plasma atomic emission spectrometry. J. Anal. Atom. Spectrom., 4: 11-16.

Thompson, M., Chenery, S. and Brett, L., 1990. Nature of particulate matter produced by laser ablation-implications for tandem analytical systems. J. Anal. Atom. Spectrom., 5: 49-55.

Viczian, M., Lasztity, A., Wang, X., and Barnes, R.M., 1990. On-line isotope dilution and sample dilution by flow injection and inductively coupled plasma mass spectrometry. J. Anal. At. Spectrom. 5: 125-133.

Vieira, P.A., Zhuang, H.Z. Chan, S. and Montaser, A., 1986. Evaluation of recycling cyclone spray chambers for ICP-AES. Appl. Spectrosc., 38: 405-412.

Walder, A.J. and Freedmen, P.A., 1992. Isotope ratio measurement using a double focusing magnetic sector mass analyzer with an inductively coupled plasma as an ion source. J. Anal. Atom. Spectrom., 7: 571-575.

Walker, R.J., Morgan, J.W., Naldrett, A.J., and Li, C., 1991. Re-Os isotopic systematics of Ni-Cu sulphide ores, Sudbury Igneous Complex, Ontario: Evidence for a major crustal component. Earth Planet. Sci. Lett., 105: 416-429

Wemyss, R.B. and Scott, R.H., 1978. Simultaneous determination of platinum-group metals and gold in ore and related plant materials by inductively coupled plasma-optical emission spectrometry. Anal. Chem., 50: 1694-1697.

Williams, J.G., Gray, A.L. Norman, P. and Ebdon, L. 1987. Feasibility of solid sample introduction by slurry nebulization for inductively coupled plasma

mass spectrometry. J. Anal. Atom. Spectrom., 2: 469-472.

Williams, J.G. and Jarvis, K.E., 1993. Preliminary assessment of laser ablation inductively coupled plasma mass spectrometry for quantitative multi-element determination in silicates. J. Anal. Atom. Spectrom., 8: 25-34.

Wilson, G.C., Kilius, L.R., and Rucklidge, J.C., 1991. In situ analysis of precious metals in polished mineral samples and sulphide "standard" by accelerator mass spectrometry at concentrations of parts-per-billion. Geochimica et Cosmochimica Acta, 55: 2241-2251.

Yates, A.B., 1948. Properties of International Nickel Company of Canada; In Structural geology of Canadian ore deposits, Jubilee Volume, Canadian Institute of Mining and Metallurgy, p.596-617.

Zachariasen, H., and Beamish, F.E., 1962. Separation of ruthenium from base metals by cation exchange, Anal. Chem., 34: 964-966.

Zhuang, H.Z. and Barnes, R.M., 1985. Recycling nebulizer system for millilitre-volume samples with inductively coupled plasma spectrometry. Spectrochim. Acta, 40B: 1141-1146.

Zicai, C. and Barnes, R.M., 1986. Characterization of a recycling nebulization system for inductively coupled plasma spectrometry: 1. stability and humidified argon carrier gas. Spectrochimica Acta, 41B: 979-989.

APPENDIX I: PROCEDURES OF NICKEL SULPHIDE FIRE-ASSAY COLLECTION AND TELLURIUM COPRECIPITATION FOR THE DETERMINATION OF PRECIOUS METALS BY ICP-MS

REAGENTS

All reagents are certified American Chemical Society (ACS) grade except where indicated.

Nickel powder	Carbonyl nickel powder, 99.8% Ni (INCO powder T-123)
Sulphur	precipitated sulphur powder [United State Pharmicopia (U.S.P.) B.D.H. B30317)
Sodium carbonate	anhydrous granular (B.D.H. ACS 777)
Borax	di-sodium tetraborate (B.D.H. ACS 861)
Silica	silicon dioxide floated powder, 240 mesh (Anachemica AC-8130)
Concentrated HCl (12 M)	(E.M. Science)
Concentrated HNO_3 (16 M)	(B.D.H. ACS 579-43)
Aqua regia	A mixture of 75% distilled concentrated HCl and 25% distilled concentrated HNO_3 by volume
HCl (6 M and 0.2 M)	Diluted from distilled concentrated HCl
Te solution	2000 ppm in 10% HCl. Prepared by dissolving Te metal (99.999%, SPEX Industry, Metuchen, New Jersey, USA) in 15 ml aqua regia followed by two evaporation with concentrated HCl; made up to volume with 10% HCl.
$SnCl_2$ solution	110 g of Stannous chloride ($SnCl_2.2H_2O$) (Fisher) dissolved in 150 ml concentrated HCl and diluted to 500 ml with deionized water

A COLLECTION PROCEDURE (Jackson *et al.*, 1990)

1) All sulphide- or chromite-bearing samples were pre-analyzed by X-ray florescence Spectrometry (XRF) for S, Cr, Ni, Cu and Zn.

2) Into a clay crucible were weighed: 15.0 g samples, 5.0 g Ni, 3.0 g S, 10 g sodium carbonate, 20.0 g borax and 3.0 g silica (5.0 g for

ultramafics). For other sample sizes weights were varied proportionally.

3) The mixture was fused in a preheated oven at 1000°C for 1.25 hr. and allowed to cool.

4) The crucible was broken open and the NiS button, which had formed in the bottom of the crucible, was retrieved.

5) The button was weighted, crushed to small chips and transferred to a tall-form 1000-ml beaker. The NiS transferred was weighed to allow correction for loss on crushing.

6) 600 ml of concentrated HCl were added. The beaker was covered with a watchglass, transferred to a hotplate at 350°C. A black, precious-metals- bearing sulphide residue was sometimes evident.

7) When the NiS had dissolved completely, the solution was allowed to cool until warm. Te solution (3.5 ml) was added. The solution was diluted with an equal volume of water and 12 ml of $SnCl_2$ solution were added. A black Te precipitate formed. The solution was brought slowly to boiling over a period of 30 min. to coagulate the precipitate.

8) The solution was allowed to cool until warm and was filter through a Millipore®, filter system (Whatman® 0.45-μm cellulose nitrate membrane filter paper) and washed with 10% HCl.

9) The filter paper was placed in a 30-ml refluxing test tube. 5 ml of concentrated HNO_3 were added, a reflux condenser attached, and the filter paper allowed to dissolve (no heat was applied if Os recovery was required). Concentrated HCl (5 ml) was added through the top of the condenser and the solution was warmed (<100°C) for 20-30 min. to dissolve completely the precipitate (the reflux condenser was used to minimize loss of volatile Os).

10) The solution was allowed to cool for 10 min. The flux condenser was washed down with deionized water, the solution transferred to a 125-ml polypropylene bottle and diluted to 100 g with deionized water.

A MODIFIED PROCEDURE FOR SULPHIDE ORE SAMPLES

The collection procedure described here is modified from Jackson *et al.* as follows:

(1) The major constituents of the samples were determined by X-ray fluorescence Spectrometry (XRF).

(2) 10 g of sample, 6.70 g of Na_2CO_3, and 13.30 g $Na_2B_4O_7$ were weighted into clay crucibles. Silica was added until the SiO_2 content of the sample is equal to 9.50 g. Sulphur was added until the S content in the sample is equal to 4.22 g. Nickel was added until Ni and Cu contents in the sample are equal to 7.00 g. The sample was mixed thoroughly with a spatula.

(3) The mixture was fused in a preheated oven at 1050°C for 1.5 hours. The crucible was removed and allowed to cool.

(4) The crucible was broken open and the NiS button bead retrieved, weighed and transferred to a tall-form 1000 ml pyrex beaker.

(5) 300 to 600 ml distilled 6 N HCl was added. The beaker was covered with a watch glass, transferred to a hotplate at 350°C, and the bead dissolved.

(6) The solution was allowed to cool until warm. 3.5 ml of Te solution (2000 ppm) was added. The solution was diluted with an equal volume of water and 12 ml of $SnCl_2$ solution were added to precipitated the Te. The solution was brought slowly to boiling over a period of 30 minutes to coagulated the black Te precipitate formed.

(7) The solution was cooled until warm and then filtered through a millipore filter system (Whatman 0.45 μm cellulose nitrate membrane filter paper) and washed with deionized water.

(8) The filter paper and its content was placed in a 15 ml teflon jar. 5 ml of concentrated HNO_3 were added, and the filter paper was allowed to dissolve. Concentrated HCl (5 ml) was added and the solution was warmed for 20-30 min. to dissolved completely the precipitate.

(9) The solution was allowed to cool for 10 min. The jar was washed down

with deionized water, the solution transferred to a 125-ml polypropylene bottle and diluted to 100 g with deionized water.

APPENDIX II: SAMPLE LOCATION AND DESCRIPTION OF THE SUDBURY IGNEOUS COMPLEX (SIC)

Sample	Location	Rock type
91-ZC-01	Highway 69N 3.7 km north of LaSalle Blvd.-Notre Dame intersection	South Range border norite
91-ZC-02	Highway 69N 4.5 km north of LaSalle Blvd.-Notre Dame intersection	South Range quartz-rich norite
91-ZC-03	Highway 69N 5.45 km north of LaSalle Blvd.-Notre Dame intersection	Uppermost South Range norite
91-ZC-04	Highway 69N 5.85 km north of LaSalle Blvd.-Notre Dame intersection	South Range quartz gabbro
91-ZC-05	Highway 69N 8.05 km north of LaSalle Blvd.-Notre Dame intersection	South Range quartz diorite
91-ZC-06	Highway 144, discovery site	South Range border norite
91-ZC-07	Intersection of Highway 144 at Elk's Club road, 1.3 km north of Levack turnoff	North Range mafic norite
91-ZC-08	Highway 144 0.5 km south of 91-ZC-07 opposite Tamarack Avenue	North Range felsic norite
91-ZC-09	Intersection of Highway 144N at Levack turnoff	North Range quartz gabbro

91-ZC-10	Highway 144N 0.3 km south of Levack turnoff	North Range granophyre
91-ZC-11	Highway 144N 1.0 km south of Levack turnoff	North Range coarse-grained granophyre
91-ZC-12	Highway 144N 3.7 km south of Levack turnoff	North Range fine-grained granophyre
91-ZC-13	Highway 144N 3.7 km south of Levack turnoff	North Range coarse-grained granophyre
91-ZC-14	Highway 144N 5.8 km south of Levack turnoff	Onaping formation

APPENDIX III: THE ANALYSIS OF PRESSED PELLETS OF GEOLOGICAL SAMPLES USING WAVELENGTH DISPERSIVE X-RAY FLUORESCENCE SPECTROMETRY (Longerich, 1993b)

INSTRUMENT

A FISONS/ARL (Mississauga, Ontario) 8420 + sequential wavelength dispersive X-Ray spectrometer.

SAMPLE PREPARATION

Into a 100 ml glass jar was placed 5.00 g of rock powder and 0.70 g of BRP-5933 Bakelite phenolic resin (Bakelite Thermosets Ltd., Brampton, Ontario). Two 0.5 inch diameter stainless steel ball bearings were added, and the plastic lid was attached. The jar was placed on a roller mixer and rolled for 10 min in order to thoroughly mix the rock powder with the resin. The mixed powder was placed into a Herzog (Germany) pellet press (29 mm diameter mould) and pressed for 5 s at a pressure of 20 tonnes. The pellet was then heated in a 200°C oven for 15 min to set the resin.

DATA ACQUISITION

Data acquisition parameters are described by Longerich (1993b, *c.f.* Table 1). Data was acquired for 30 analyte elements, the Rh Kα compton peak, and 27 background intensities. The sequence of samples was as follows: 6 reference materials (DTS-1, BHVO)-1, SY-2, SY-3, SiO_2, and PACS-1), 8 samples, 6 reference materials (as above), 8 samples, and 6 reference materials (as above). Data acquisition times, which vary from 4 to 100 s, are selected depending on the sensitivity of the analyte emission and the typical geological abundance of the various elements.

PRECISION

The precision for the determination of an element is functionally related to the concentration, the relative uncertainty in the concentration decreasing with increasing concentration. The least squares procedure, in which the standard deviation between samples vs. the concentration is fit to a linear equation, not only provides a measure of the limit of detection but gives the uncertainty as a function of the concentration. The result of these calculations are shown in

Table A1.1.

Table A1.1 Accuracy expressed as a bias [the determined (Mean)-literature value]

Element	Intercept = std dev (c = 0)	Slope = rsd (C > > LD)	High Concentration	Std dev (high concentration
SiO_2		0.26%	100%	0.3%
Al_2O_3	0.005%	0.09%	20%	0.022%
TiO_2	0.003%	0.3%	3%	0.013%
Fe_2O_3	0.0019%	0.16%	15%	0.03%
MnO	0.0003%	0.9%	0.5%	0.005%
MgO	0.009%	0.014%	50%	0.016%
CaO	0.003%	0.23%	15%	0.04%
Na_2O	0.005%	0.17%	10%	0.021%
K_2O	0.004%	0.24%	15%	0.04%
P_2O_5	0.0010%	0.6%	0.5%	0.004%
Cr	3 ppm	0.4%	4000 ppm	20 ppm
Ni	1.5 ppm	0.8%	2500 ppm	22 ppm
Cu	1.1 ppm	0.5%	400 ppm	3 ppm
Zn	0.5 ppm	0.6%	700 ppm	3 ppm
V	2.1 ppm	0.9 %	0.5 %	0.005%

ACCURACY

Accuracy expressed as a bias [the determined (Mean)-literature value] is given in Table A1.1

Table A1.1 Accuracy expressed as a bias [the determined (Mean)-literature value]

Element	Concentration Range	Bias (Mean-Literature)
SiO_2	36 to 100%	-4.1% to 4.4%
Al_2O_3	0 to 18%	+1% to -1%
TiO_2	0 to 3%	-0.1% to +0.05%
FeO	0 to 15%	-0.5% to +0.5%
MnO	0 to 0.3%	+0.01% to -0.01%
MgO	0 to 50%	+1% to -1%
CaO	0 to 13%	-0.2 to +0.2%
Na_2O	0 to 9%	-0.2% to +1.0%
K_2O	0 to 15%	-0.2 to +0.05%
P_2O_5	0 to 0.5%	-0.05% to +0.02%
Cr	0 to 4000 ppm	-50 ppm to +50 ppm
Ni	0 to 2400 ppm	-14 ppm to + 14 ppm
Cu	0 to 400 ppm	-9 ppm to +3 ppm
Zn	0 to 800 ppm	-2 ppm to +23 ppm
V	0 to 640 ppm	-11 to +6 ppm

APPENDIX IV: DETERMINATION OF TRACE- AND RARE EARTH-ELEMENTS USING A Na_2O_2 SINTER (Longerich *et al.*, 1993)

Na_2O_2 SINTER DATA ACQUISITION

A run consists of up to 56 samples, including reference materials, SiO_2 blanks, and duplicates. Data is acquired in cycles of 12 solutions using the autosampler. The standards are supplied in 250 ml bottles, while 10 ml of samples and blanks are contained in 12 ml test tubes. Up to 8 cycles (56 samples, 96 acquisitions) are in each unattended run.

Each cycle of 12 solutions consists of 4 standards, 1 calibration blank (0.2 M HNO_3), and 7 samples.

Standard A contains Sr, Y, Zr, Ba, La, Ce, Pr, Nd, Ho, Er, Tm, Yb and Th.

Standard B contains Sm, Eu, Lu, and Hf.

Standard C contains Gd.

Standard D contains Tb and Dy.

An internal standard solution containing Rb, Cs, Tl, and U is pumped, on line, into a "Y" junction at 1 part spike to 2 parts sample for a total flow rate of 1 g/min.

Data is acquired at each mass for 10 seconds, using a dwell time of 50 ms. The ions measured are ^{85}Rb, ^{86}Sr, ^{89}Y, ^{93}Nb, ^{133}Cs, ^{137}Ba, ^{139}La, ^{140}Ce, ^{141}Pr, ^{145}Nd, ^{147}Sm, ^{151}Eu, ^{157}Gd, ^{159}Tb, ^{160}Gd, ^{163}Dy, ^{165}Ho, ^{167}Er, ^{169}Tm, ^{173}Yb, ^{175}Lu, ^{177}Hf, ^{181}Ta, ^{203}Tl, ^{232}Th, ^{238}U, and $^{238}U^{16}O$.

Na_2O_2 SINTER DATA REDUCTION

All samples and standards are background corrected using the mean of all calibration blanks in a run.

Corrections are applied for the interference of the oxides of Ba, Pr, Nd, Sm, Eu, Gd, Tb, Dy, and Ho on the analytes Eu, Gd, Tb, Dy, Ho, Er, Tm, Yb, Lu, and Hf. Each interference correction is normalized to the UO/U ratio in the

sample relative to the UO/O ratio in the standards. For ^{160}Gd a correction is also applied for the interference from ^{160}Dy. This correction factor is determined from standard D, in order not to included mass discrimination variation in the correction. Calibration is from the 4 external standards for most elements, except for Nb and Ta which are calibrated using Zr and Hf, respectively, as surrogates.

The matrix is corrected using a mass interpolated ratio of the intensity of the internal standards in the samples and the previous standards.

The analysis of Gd is superior using mass 157 for light rare earth element depleted samples. However, for the light rare earth element enriched samples in this study, the use of mass 160 results in less interference.

APPENDIX V: A PUBLICATION RELATED TO THIS THESIS

Recycling Nebulization System With a Disposable Spray Chamber for Analysis of Sub-milligram Samples of Geological Materials Using Inductively Coupled Plasma Mass Spectrometry*

Zhongxing Chen, Henry P. Longerich† and Brian J. Fryer
Department of Earth Sciences and Centre for Earth Resources Research, Memorial University of Newfoundland, St. John's, Newfoundland, Canada A1B 3X5

A recycling nebulization system with a disposable spray chamber was developed and evaluated for inductively coupled plasma mass spectrometry (ICP-MS). With the recycling nebulization system, 0.5 g of sample solution is sufficient for 8 min of data acquisition. The sensitivity of the recycling nebulization system was similar to a conventional Scott spray chamber system. Twenty-six trace elements were determined by ICP-MS using four internal standards (Ge, In, Re and Bi) to correct for matrix effects, instrumental drift and enrichment of the sample solution by evaporation. The ability to analyse mineral separates weighing less than 0.1 mg is demonstrated with detection limits similar to conventional procedures. Analyses of selected geological reference materials: Canada Centre for Energy and Mineral Technology (CANMET) SY-2 Syenite Rock, United States Geological Survey (USGS) reference material BCR-1 and W-1 and Centre de Recherches Petrographiques et Geochimiques (CRPG) reference material BR indicate good limits of detection, good accuracy and precision, a very low memory effect and low consumption of sample solution. Results compare well with data reported using conventional ICP-MS analysis. Analysis of the USGS geological reference material, PCC-1, for 14 rare earth elements, at ultra-trace concentration levels using cation-exchange preconcentration, is demonstrated, with limits of detection for solids of from 0.01 to 1 ng g^{-1} and relative standard deviations of less than 15%.

Keywords: *Inductively coupled plasma mass spectrometry; recycling nebulization system; disposable spray chamber; sub-milligram sample mass; geological applications*

The usual method for sample introduction in inductively coupled plasma mass spectrometry (ICP-MS) is solution nebulization, *via* a Meinhard concentric nebulizer with a Scott spray chamber. However, with this technique, the efficiency of transport of sample into the plasma is low with more than 95% of the sample discarded to waste.[1] Although efficient sample transfer to the plasma is not generally important, there are analyses where the sample volume is limited by the mass of sample available or by the difficulty of dissolving large masses of sample. Also, in some geological materials such as zoned minerals or fine-grained intergrowths, separation of large amounts of specific homogeneous phases can be very difficult or even impossible. In these cases, painstaking manual separation is required to minimize the inclusion of minor phases.

Several designs of recycling nebulization systems have been reported that recycle the waste solution to the nebulizer.[2-7] These systems demonstrate continuous nebulization with small volumes for long periods and the measurement of multiple elements with atomic emission spectrometers. However, these systems have two major problems, namely, enrichment of the concentration of the sample solution by evaporation and memory effects (difficulty in washing a previous sample solution from the nebulizer–spray chamber system). Evaporation of the sample solution can be reduced by humidifying the nebulizer gas,[8] but the memory effect is a more severe problem.[1] The dilution and contamination of samples by the liquid remaining in the spray chamber from previous samples and wash solutions has not been addressed by previous workers. Recently, Isoyama *et al.*[9] reported a recycling configuration that used a replaceable spray chamber for ICP atomic emission spectrometry. These workers discussed the problem of concentration of the sample by evaporation, however, they did not apply the method of standard additions to correct for sample evaporation.

There are several introduction techniques for small samples applicable to the ICP, *i.e.*, electrothermal volatilization, flow injection, laser ablation and the direct insertion nebulizer. However, a recycling nebulization system has several advantages compared with these methods: a homogeneous solution; long data acquisition time (5 min) with a 'stable' signal; and reduced sample mass without the complications of transient signal acquisition and data reduction.

Experimental

Instrumentation

The ICP-MS instrument used in these studies was a modified SCIEX (now Perkin-Elmer SCIEX) Elan Model 250.[8-10] The sampler and skimmer were slightly modified and made in-house.[11] The instrument has been upgraded to a Model 5000 computer system using Perkin-Elmer supplied hardware and software. All of the old printed circuit boards in the computer rack were removed and replaced with two new boards. One of these boards is connected to an IBM PS/2 Model 70, 386/387 computer using IEEE-488 interface hardware. New Elan 5000 software, from Perkin-Elmer, version 1.04-ICPS (a modification of version 1.04 which incorporates an ICP shut-off enhancement) was used. For analyses, in which the recycling system was not used, a Gilson 212B autosampler was employed which replaced the ISCO ISIS autosampler. The Gilson supplied sipper was replaced by a piece of quartz tubing (3 mm o.d. and 1 mm i.d.) installed in a poly(tetrafluoroethylene) (PTFE) holder which was fabricated in-house.

No on-line concentration calculations were made, only count rates were collected using the Elan software. The Elan software was used to create 'report' files, which contain the count rate data in an ASCII format. These files are translated using a Basic program, compiled and written in-house, which translates the data into a Lotus-formatted spread sheet file and saves the file on a floppy disk. This translate program is executed under the SCIEX rec-

*Presented in part at the 1992 Winter Conference on Plasma Spectrochemistry, San Diego, CA, USA, January 6–11, 1992.
†To whom correspondence should be addressed

Table 1 ICP-MS operating conditions

Inductively coupled plasma—	
Plasma gas	Argon
Forward power/W	1200
Reflected power/W	< 5
Gas flow—	
Plasma (outer) gas flow rate/dm^3 min^{-1}	13.0
Auxiliary (intermediate) gas flow rate/dm^3 min^{-1}	1.0
Nebulizer (inner) gas flow rate	See text
Interface—	
Sampling distance (load coil to sample aperture)/mm	21
Sampling aperture	Nickel, 1.1 mm diameter
Skimmer aperture	Nickel, 0.9 mm diameter
Ion lens settings—	
B lens/V	7.0
P lens/V	9.0
E-1 lens/V	19.8
S-2 lens/V	0
Data acquisition parameters—	
Measurement mode	Multichannel
Replicate time/s	10
Dwell time/ms	50
Sweeps per replicate	200
Number of replicates	1
Points across peak	1
Resolution	Normal

ommended DOS shell, vpix. All subsequent data manipulation was performed off-line using commercial spread sheet software on personal computers. For each analytical run (4–12 h), the nebulizer gas flow was adjusted to 0.9–1.1 dm^3 min^{-1}, using a solution containing 100 ng g^{-1} of Cs and Th,[12] so that: ThO^+:Th^+ was <0.1; the sensitivity of Cs was >1000 counts s^{-1} ng^{-1} g; and the sensitivity of Bi was >500 counts s^{-1} ng^{-1} g. These conditions represent a compromise between maximum sensitivity and minimum polyatomic-ion formation. Other operating conditions are given in Table 1.

Recycling Nebulization System

Two recycling nebulization systems, referred to here as 'cyclone' and 'parallel', (Fig. 1) were evaluated. It is recognized that the dimensions of the cyclone spray chamber are not large enough for true cyclone gas flow dynamics, the term cyclone being used only to describe the configuration. Both systems consisted of a nebulizer, disposable spray chamber, glass transport tube and holder. A concentric nebulizer (either Meinhard, Model SB-30-C1 or TR-30-C1) was used with PTFE capillary tubing for sample recycling (25 mm long, 0.3 or 0.5 mm i.d.). The disposable spray chamber was a screw-top plastic centrifuge tube (25 mm o.d., 107 mm high, 30 cm^3 capacity, Sarstedt). The 8 mm o.d. Pyrex transport tube, with the end expanded to 12 mm o.d. to reduce blockage, was connected to the ICP torch with 0.75 m of 8 mm o.d. Tygon tubing. The holder was constructed of PTFE and used O-ring seals for the nebulizer and the glass transport tube and a press fit for the PTFE solution-transport tubing. In the parallel recycling nebulization system, the concentric nebulizer was positioned vertically and parallel to the transport tube [Fig. 1(*a*)], while in the cyclone system [Fig. 1(*b*)], the nebulizer was positioned perpendicular to the transport tube. Initial experiments demonstrated that the parallel recycling system yielded sensitivies higher than the cyclone recycling system. Further investigations were restricted to the parallel recycling system.

Sample Preparation and Reagents

Certified American Chemical Society acids were distilled in non-boiling quartz or PTFE stills and diluted with Barnstead nano-pure distilled, de-ionized water. Powdered samples were dissolved in screw-top 15, 5 or 2 cm^3 perfluoroalkoxy (PFA) resin jars (Savillex) using HF and HNO_3.[12] Silicon was removed as SiF_4 by three repeated evaporations with 8 mol dm^{-3} HNO_3. The samples were diluted by mass to a final concentration of approximately 0.2 mol dm^{-3} HNO_3 in 125 cm^3 polyethylene bottles (Nalgene) or in spray chambers for small samples.

Standard and spike solutions for each element were prepared by dissolving ultra-pure metals (AMES Laboratory, Ames, IA, USA) or plasma-grade powders (SPEX Industries, Metuchen, NJ, USA) using HNO_3 and distilled, de-ionized water. A 0.05% solution of the surfactant, Triton X-100, in water was used in all experiments. All solutions were prepared and dispensed by mass.

Sample Changing Procedure

While Isoyama *et al.*[1] used a stop valve on the tubing which led to the ICP torch for sample exchange, it was observed in our laboratory that the argon back pressure of the plasma gas is sufficient to flush the spray chamber, and further, that the torch will not be extinguished when the nebulizer line to the torch is opened to the atmosphere. If the spray chamber is slowly attached, argon from the torch will flush air from the spray chamber, and the need for a valve, which may contribute to some extent as an obstruction and, hence, as a cause of memory, is removed.

Samples were changed, without extinguishing the plasma, using the following procedure. (*i*) The r.f. power trip was disabled. (*ii*) The capillary tubing was withdrawn from the solution. After the solution remaining in the tubing was completely aspirated, the nebulizer gas was turned off. (*iii*) The spray chamber was removed. (*iv*) Liquid which remained on the inside surface of the chamber holder, the

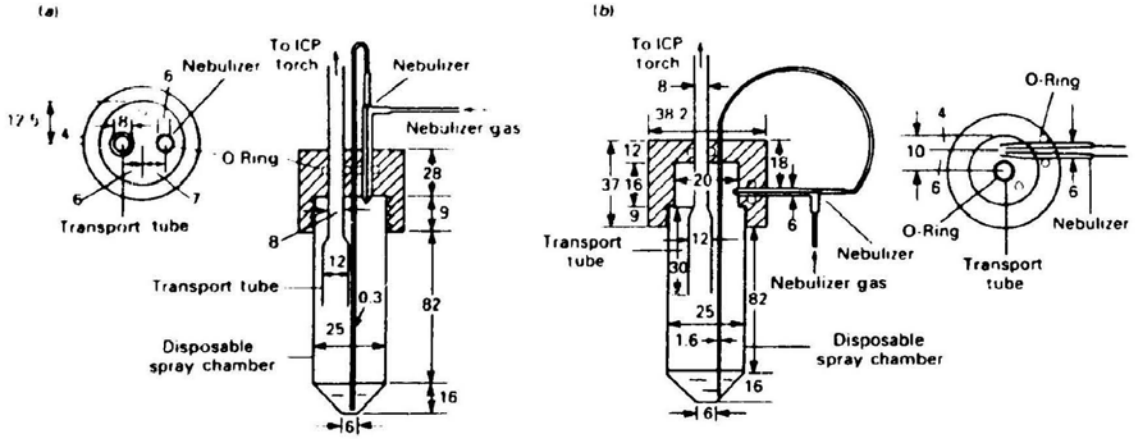

Fig. 1 Two recycling nebulization systems (*a*) 'parallel' and (*b*) 'cyclone', consist of a holder, concentric nebulizer, PTFE capillary tubing for sample recycling, a disposable screw top spray chamber and a Pyrex transport tube

nebulizer and the transport tube was removed with a Kimwipe tissue paper. (*v*) The inside surfaces of the holder, nebulizer and transport tube were rinsed using 0.2 mol dm^{-3} HNO_3 from a wash bottle. (*vi*) As in step (*iv*) adhering liquid was removed. (*vii*) A new spray chamber containing 10 g of 1 mol dm^{-3} HNO_3 wash solution was slowly attached. (*viii*) The nebulizer gas flow rate was slowly increased to approximately 1 dm^3 min^{-1}, while maintaining the r.f. reflected power at < 50 W. The capillary tubing was then inserted into the solution. (*ix*) The wash solution was nebulized for 1 min in order to wash the nebulizer and capillary tubing. (*x*) Steps (*ii*), (*iii*), (*iv*), (*v*) and (*vi*) were repeated. (*xi*) A new spray chamber, containing the next sample, was attached as in steps (*vii*) and (*viii*). (*xii*) The r.f. power trip was enabled. Total time per tube was approximately 15 min, including wash and sample changing.

Data Acquisition and Calibration

Mass selection and interferences are as described by Jenner *et al.*[12] The sensitivities of all but two of the analyte elements were measured in one of the two external standard solutions (STDA or STDB, Table 2). The sensitivities of Nb and Ta were determined by surrogate calibration because of potential solution instability and memory effects.[12] The sensitivity ratios used were $^{93}Nb:^{90}Zr = 1.504$ and $^{181}Ta:^{177}Hf$ 4.81.[12] The elements Ge, In, Re and Bi (Table 2) were used as internal standards. A weighed aliquot of approximately 20 mg of spike was added to each 2 g of solution. In order to reduce the amount of liquid adhering to the inside surfaces of the system, 1 drop of Triton X-100 surfactant solution was added.[1] For samples that were low in Th, 0.05 g of a 3 μg g^{-1} solution of Th was added to monitor oxide formation, precluding the determination of Th in these samples. Samples were run in the following sequence: acid calibration blank (0.2 mol dm^{-3} HNO_3), STDA, flush (1 mol dm^{-3} HNO_3), STDB, flush, acid calibration blank, sample 1, flush, . . . , sample 4, flush, acid calibration blank, STDA, *etc.* After the data were collected, the background was calculated as the mean of six determinations of the acid blank. The most significant interferences in the suite of elements determined in this study are those of Ba and the light rare earth element (REE) oxides on the heavy REE, Hf and Ta.[12,13] For each sample, all oxide interference factors were normalized to the measured $^{232}ThO^+:^{232}Th^+$ ratio.[12] After correction for instrument drift and matrix effects, sample solution concentrations were calculated by external calibration using the mean sensitivity of the two closest calibration standards. Solid sample concentrations were then calculated from the sample and solution masses.

Table 2 Elements and concentrations for STDA, STDB and an internal standard

Element	STDA/ng g^{-1}	STDB/ng g^{-1}	Internal standard/ ng g^{-1}
Ge	—	—	46180
Rb	157.9	198.7	—
Sr	658.9	—	—
Y	104.2	—	—
Zr	205.5	—	—
In	—	—	3930
Cs	112.2	99.5	—
Ba	993.9	—	—
La	110.7	—	—
Ce	88.9	107.4	—
Pr	106.2	—	—
Nd	—	204.5	—
Sm	—	194.3	—
Eu	—	206.6	—
Gd	—	197.9	—
Tb	94.5	—	—
Dy	243.0	—	—
Ho	105.5	—	—
Er	196.8	—	—
Tm	92.9	—	—
Yb	109.9	—	—
Lu	—	108.3	—
Hf	—	79.1	—
Re	—	—	9690
Bi	—	—	3450
Pb	251.7	—	—
Th	89.0	107.7	—
U	93.5	—	—

Results and Discussion

Comparison Between the Recycling Nebulization Spray Chamber and the Scott Spray Chamber System

In order to compare the sensitivity of the recycling nebulizer spray chamber system with that of the Scott system under similar circumstances, the Scott spray chamber was mounted outside the match box and connected to the ICP

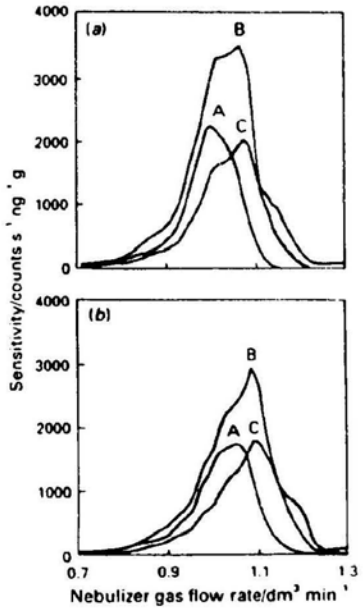

Fig. 2 Sensitivity as a function of nebulizer gas flow rate for a solution containing 100 ng g^{-1} of: A, Y; B, Tm; and C, Bi. (*a*) The Scott spray chamber system and (*b*) the recycling nebulization system

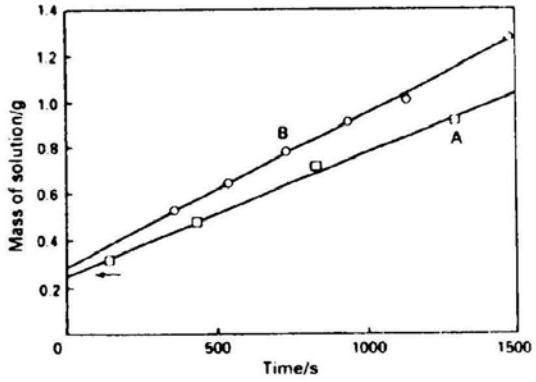

Fig. 3 Mass of sample solution *versus* total nebulization time. Total nebulization time is taken as the time when the count rate reaches a maximum, as observed in Fig. 4. Using A, the Meinhard SB-30-C1 nebulizer, 0.5 g of solution is sufficient for 8 min of data acquisition (dead volume = 0.25 g), while B, the TR-30-C1 nebulizer provides 5.4 min of data acquisition (dead volume = 0.29 g); dead volume is indicated by the arrow

torch using approximately 0.75 m of 8 mm i.d. Tygon tubing. This allowed the acquisition of comparable data for both systems without extinguishing the plasma or realigning of the torch. Solutions containing 100 ng g^{-1} of Y, Tm and Bi were nebulized using nebulizer gas flow rates of 0.7–1.3 dm^3 min^{-1} for both systems. Data were collected alternatively using the two systems to correct for instrument drift. The analytical sensitivity of the recycling nebulization system is similar to that obtained with the Scott spray chamber system in this configuration (Fig. 2).

Minimum Sample Solution Required for Data Acquisition

The aim of this study was the reduction of solution consumption, to allow the determination of small amounts or concentrations of analyte in geological materials. Note that in all work reported in this study, all solutions were prepared and dispensed by mass and hence are reported in mass units. The use of mass rather than volume allows accurate measurements to be made quickly over a large dynamic range, thus the 'volumes' reported in this section are measured in grams of solution. In initial work, a standard concentric nebulizer (Meinhard Model TR-30-C1) with PTFE capillary tubing for sample recycling (25 cm length, 0.5 mm i.d.) was used and the dead volume was found to be 0.29 g (Fig. 3). Using this configuration, 0.5 g of solution was sufficient for 5.4 min of data acquisition. In order to reduce further the minimum volume, a 'small bore', SB-30-C1 Meinhard nebulizer was used, with smaller i.d. (0.3 mm) PTFE capillary tubing. A 'TR' nebulizer has a glass solution input tube which is 4 mm o.d. with an i.d. of 2 mm. An 'SB' nebulizer is identical with a 'TR' nebulizer, except for a smaller solution input tube, which has an o.d. of 3 mm and an i.d. of 1 mm. The 'SB' nebulizer was connected to the tubing using a two-way connector (Omnifit, Atlantic Beach, NY, USA). These modifications reduced the dead volume from 0.29 to 0.25 g and increased the maximum data acquisition time for a 0.5 g sample from 5.4 to 8 min.

In order to determine the portion of the dead volume contained in the nebulizer and capillary tubing, water was nebulized for 2 min and the nebulizer and capillary tubing were weighed. Then the nebulizer and capillary tubing were dried in an oven at 60 °C for 1 h and their dry masses recorded. Of the total 0.25 g dead volume, 0.08 g was contained in the nebulizer and capillary tubing, while 0.17 g was in the spray chamber, holder and transport tube.

Drift and Matrix Effects

Drift and matrix effects cannot be separated chemometrically and in this study both are corrected using internal standards. In any ICP-MS run there is some drift in sensitivity. In addition, when analyses are carried out using a recycling nebulization system, there is a gradual enrichment of samples with time until the sipper is not continuously immersed in solution (Fig. 4). This enrichment is due to evaporation and is a significant cause of signal change.[5,6,7] Matrix effects also cause signal enhancement or depression in sample solutions relative to calibration standards. Matrix effects are mass dependent, with the light

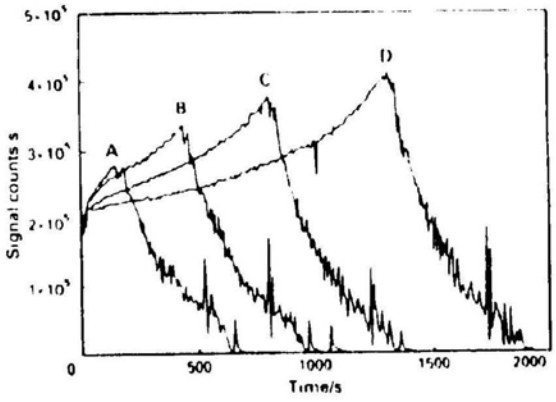

Fig. 4 Signal *versus* time for various masses of sample solution: A, 0.3; B, 0.5; C, 0.7; and D, 0.9 g. Each solution initially contained 100 ng g^{-1} of Cs. Following the maximum count rate, the sipper is not continuously immersed in the solution causing the sharp decrease in signal, and gas bubbles are periodically aspirated causing the large spikes in the intensity data

Table 3 Concentrations ($\mu g\ g^{-1}$) obtained in this work (recycling nebulizer), by the method of Longerich *et al.*[15] and literature values for geological reference materials SY-2, BCR-1 and W-1. LODs for solids calculated for samples prepared using 0.5 g of solid per kg of solution

	Recycling nebulizer			ICP-MS standard additions procedure					
						Literature value			
Element	SY-2 (n = 1)	BCR-1 (n = 2)	W-1 (n = 2)	SY-2 (n = 5)	BCR-1 (n = 5)	SY-2*	BCR-1†	W-1†	Solid LOD
Rb	226	49.7	19.9	221	47.1	226	47.2	21.4	0.028
Sr	286	358	198	275	338	270	330	186	0.06
Y	128	35.5	20.6	120	33.1	129	38	26	0.009
Zr	300	199	90.9	294	186	306	190	99	0.06
Nb	36.1	13.2	8.50	33.6	13.8	30	14	9.9	0.0007
Cs	2.70	0.97	0.89	2.59	0.87	2.7	0.96	0.96	0.015
Ba	452	684	155	459	696	445	681	162	0.19
La	73.1	26.1	11.1	70.7	25.8	67	24.9	11	0.008
Ce	168	54.9	23.4	167	55.2	159	53.7	23.5	0.015
Pr	20.0	6.82	2.93	20.3	6.95	19.5	6.8	3.2	0.008
Nd	76.3	28.3	12.6	77.7	29.1	73.7	28.8	14.6	0.013
Sm	15.8	6.54	3.17	15.3	6.65	15.7	6.59	3.68	0.016
Eu	2.40	1.92	1.06	2.55	1.98	2.5	1.95	1.12	0.016
Gd	17.5	7.05	3.69	17.9	7.45	16.8	6.68	4.01	0.016
Tb	2.89	1.02	0.59	2.97	1.05	3.1	1.05	0.63	0.008
Dy	19.9	6.19	3.65	20.5	6.41	21.3	6.34	3.39	0.019
Ho	4.57	1.24	0.74	4.67	1.28	5.1	1.26	0.81	0.007
Er	15.1	3.55	2.12	15.3	3.68	15.2	3.63	2.3	0.015
Tm	2.41	0.50	0.32	2.51	0.53	2.4	0.56	0.34	0.009
Yb	17.2	3.28	1.94	18.1	3.39	18.1	3.38	2.03	0.005
Lu	2.91	0.50	0.31	2.99	0.51	2.9	0.51	0.317	0.009
Hf	8.07	4.96	2.38	8.69	5.00	8.4	4.95	2.5	0.010
Ta	1.77	0.63	0.54	1.82	0.77	1.9	0.81	0.48	0.0011
Pb	82.1	23.4	6.34	95.5	14.0	96	13.6	7.5	0.08
Th	392	6.20	2.31	385	5.94	389	5.98	2.4	0.05
U	275	1.73	0.61	298	1.74	297	1.75	0.57	0.004

*Ref. 15.
†Ref. 16.

elements more significantly affected by the matrix than the heavy elements.[14,15] In this study, the drift-matrix corrections were made using a mass interpolation of the correction factor determined from the intensities of the internal standards (Ge, In, Re and Bi) in the calibration standards and samples. Note that a short dwell time of 50 ms is used with a total data acquisition time of 10 s, thus the data for each element in an analysis are averaged over the entire data acquisition time.

Memory Effects

Signal enhancement can also be caused by the previous sample remaining in the tubing, nebulizer, spray chamber and torch or deposited on the ICP-MS sampler and skimmer interface cones.[15] A major difficulty in the use of poorly designed spray chambers is memory effect caused by inadequate washing of the previous sample from the chamber, in part owing to poor gas flow dynamics. Systems such as those used in this study, which use replaceable spray chambers and manual washing, reduce spray chamber memory effects to insignificant levels.

Limits of Detection

The limits of detection (LODs) are a measure of instrument performance, defined here as three times the standard deviation of the difference between the count rate of a sample and n replicate determinations of the count rate of the calibration blank. The LOD is calculated as $[3\sigma\sqrt{(1/n+1)}]$, where σ is expressed in concentration units. Solid LODs, for a 100 mg sample dissolved in 200 g of solution (0.5 kg of solid per kg of solution), and with 6 determinations of the calibration blank (n=6), are given in Table 3. For samples prepared at lower concentrations, the solid LODs increase proportionally.

Precision and Accuracy

Elemental abundances for three geological reference materials, SY-2 [Canada Centre for Energy and Mineral Technology (CANMET), BCR-1 and W-1 [United States Geological Survey (USSG)] are presented in Table 3 and Figs. 5–7; values shown were obtained using the recycling nebulizer system, a modified standard additions procedure using conventional nebulization and Scott spray chamber, and from the literature. Relative standard deviations (RSDs) for most elements are less than 5% (Figs. 5–7). Accuracy, calculated as the relative difference between this work and literature values, is given in Fig. 7. The relative difference for most of the elements is less than 15% and is less than 10% for more abundant elements.

Geological Applications

Trace element analyses of sub-milligram samples

In geological studies, there are growing requirements to analyse very small samples. In order to demonstrate the capability of a recycling nebulizer system, small samples of the reference material BR [Centre de Recherches Petrographiques et Geochimiques (CRPG)] were prepared for analysis. Sample masses varying from 0.01 to 1 mg were dissolved in triplicate in screw-top PFA jars (Savillex) using HF and HNO_3. Each sample was diluted to a final mass of 2 g in a disposable spray chamber. Results of these analyses are presented in Tables 4, 5 and 6. Accuracy for samples larger than 0.1 mg are shown in Fig. 8. The agreement is

Table 4 Concentrations determined in this work (μg g⁻¹) and literature values for the geological reference material, BR, using various masses of sample

	Concentration/μg g⁻¹							
Element	1.00 mg (n = 3)	0.50 mg (n = 3)	0.20 mg (n = 3)	0.10 mg (n = 3)	0.01 mg (n = 3)	100 mg (diluted to 0.01 mg level)	Standard additions	Literature value*
Rb	47.8	48.3	46.1	47.9	44.3	47.3	49.8	47
Sr	1424	1412	1328	1340	1070	1365	1368	1320
Y	27.8	27.8	27.2	27.5	26.8	29.1	25.3	30
Zr	276	271	254	269	347	288	270	280
Nb	115	105	80.4	89.6	116	117	134	98
Cs	0.79	0.91	0.79	0.92	2.06	0.76	0.81	1
Ba	1068	1115	1068	1071	867	1095	1062	1080
La	81.6	82.7	80.9	81.6	68.7	88.4	82.6	82
Ce	152	153	150	156	336	161	158	151
Pr	17.3	17.4	17.0	17.5	15.8	17.1	17.4	
Nd	65.3	65.0	63.7	65.7	57.6	66.0	65.3	63
Sm	11.9	11.9	11.8	12.6	11.8	12.4	11.8	12
Eu	3.60	3.67	3.65	3.69	4.02	3.72	3.78	3.7
Gd	10.2	10.6	10.4	10.9	12.2	8.57	12.0	9.8
Tb	1.26	1.31	1.31	1.32	1.44	1.08	1.28	1.25
Dy	6.18	6.24	6.38	6.62	5.66	6.02	6.48	6.2
Ho	1.04	1.07	1.07	1.12	1.08	1.09	1.01	0.2
Er	2.53	2.55	2.51	3.04	3.05	2.08	2.53	3.4
Tm	0.30	0.35	0.31	0.43	0.46	0.31	0.33	
Yb	1.67	1.69	1.76	1.76	1.77	0.32	1.79	1.9
Lu	0.23	0.29	0.25	0.27	0.70	0.19	0.28	0.28
Hf	5.62	5.56	5.31	5.69	8.33	7.19	5.76	5.4
Ta	4.30	4.71	4.56	4.52	10.8	4.64	5.24	6.2
Pb	5.74	7.83	11.6	12.4	67.7	9.62	8.28	8
Th	9.75	9.44	7.96	7.88	7.94	10.5	11.1	11
U	2.40	2.17	1.92	2.03	1.65	0	2.42	2.5

*Ref. 16.

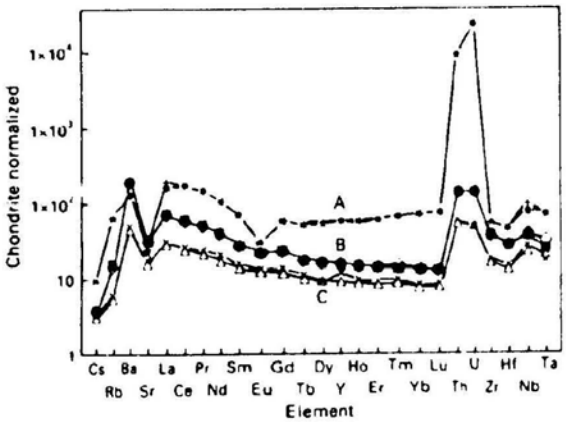

Fig. 5 Mean chondrite-normalized data for geological reference materials for: A, SY-2 [+, this work (n = 1), •, ref. 15]. B, BCR-1 [■, this work (n = 2); ◇, ref. 16], and C, W-1 [△, this work (n = 2), ×, ref. 16]. Solutions were prepared using 100 mg dissolved in 200 g of solution

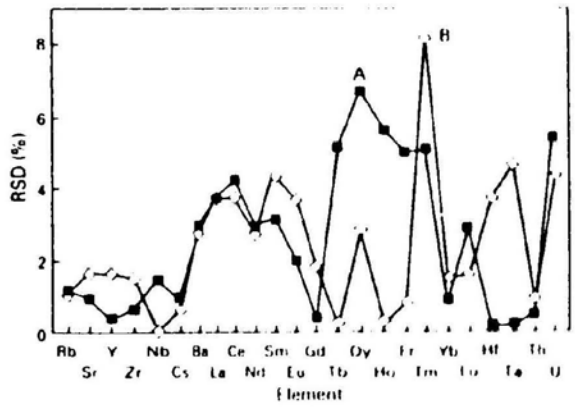

Fig. 6 Precision obtained in the analysis of A, BCR-1 and B, W-1 using the recycling nebulizer system

good, except for Ho, for which the literature values are suspect because Ho is difficult to determine accurately using neutron activation or isotope dilution methods.[12] The anomaly in the chondrite-normalized diagram for Ho (Fig. 8) further suggests that the literature value is in error. For the 0.01 mg sample, there is also a significant disagreement for Ce, which strongly suggests sample heterogeneity. This heterogeneity might be due to the differential partitioning of Ce^{3+} and Ce^{4+} into different minerals relative to the other lanthanide 3+ ions, in the sample. There is also a significant error for Lu, whose value is near the LOD. For comparison LODs are presented in Fig. 9 for various sample masses.

Relative standard deviations for replicates (n = 3) of samples weighing more than 0.10 mg are less than 10% for most elements (Fig. 10). The RSDs for samples weighing 0.01 mg are from 30 to 60% (Fig. 11), suggesting that the large SD of the data for the smallest sample is due to sample heterogeneity. In order to demonstrate that the analytical error of the procedure for this size of sample is also generally less than 10%, a 100 mg sample was prepared and diluted to contain the same amount of sample as the 0.01 mg sample preparations. The result of these analyses, which measure analytical reproducibility, is shown in Fig. 11, where the RSDs are typically less than 10%. These results (Fig. 11) show that the higher error for the determination of most elements in a 0.01 mg sample can indeed be attributed to sampling heterogeneity.

Table 5 Relative standard deviations (%) for geological reference standard, BR, using various masses of sample

	RSD (%)					
Element	1.00 mg (n = 3)	0.50 mg (n = 3)	0.20 mg (n = 3)	0.10 mg (n = 3)	0.01 mg (n = 3)	100 mg diluted to 0.01 mg level (n = 4)
Rb	1.5	1.7	2.7	8	41	2.1
Sr	2.1	0.9	2.9	4	48	0.38
Y	2.1	1.1	2.8	7	34	3
Zr	2.4	0.8	2.8	6	34	1.6
Nb	11	6	17	15	79	2.4
Cs	2.7	14	8	11	51	52
Ba	3	2.4	5	1.2	46	1.2
La	4	1.3	2.3	6	57	2.1
Ce	4	1.7	2.3	1.9	44	2.4
Pr	3	1.3	2.4	7	43	0.9
Nd	4	2.5	4	5	45	2.4
Sm	5	4	4	11	38	4
Eu	4	5	3	6	40	7
Gd	1.9	6	6	14	35	23
Tb	1.4	4	4	11	33	13
Dy	1.8	1.7	4	8	44	6
Ho	1.3	2.8	2.8	8	36	11
Er	4	3.3	1.5	22	38	22
Tm	1.4	19	11	37	31	37
Yb	4	5	9	13	41	236
Lu	4	20	12	20	110	93
Hf	2.3	2.3	2.4	5	16	26
Ta	20	13	56	25	43	4
Pb	1.3	14	32	40	28	114
Th	4	4	8	4	61	53
U	9	6	2.5	38	38	22

Table 6 Relative difference (%) compared with literature values for geological reference material, BR, for various masses of sample

	Relative difference (%)					
Element	1.00 mg	0.50 mg	0.20 mg	0.10 mg	0.01 mg	100 mg (diluted)
Rb	1.8	2.8	−2.0	1.9	−6	0.7
Sr	8	7	0.6	1.5	−19	3
Y	−7	−7	−9	−8	−11	−3
Zr	10	8	1.6	8	39	15
Nb	17	7	−18	−9	18	19
Cs	21	−9	−21	−8	106	−24
Ba	1.7	6	1.7	2.0	−18	4
La	0.4	0.8	−1.3	−0.5	−16	8
Ce	0.8	1.2	−0.5	3	122	6
Nd	0.4	0.05	−1.9	1.1	−11	1.5
Sm	0.8	−0.6	−1.4	5	−1.9	4
Eu	2.6	−0.7	−1.3	−0.04	9	−0.7
Gd	8	11	10	14	29	−10
Tb	0.8	5	5	6	15	−13
Dy	0.22	0.7	3	7	−9	−3
Ho	422	437	433	464	438	445
Er	5	6	5	27	27	−14
Yb	12	−11	−8	−7	−7	−83
Lu	−6	14	0.11	8	181	−22
Hf	4	2.9	−1.7	6	54	33
Ta	31	−24	−26	−27	74	−25
Pb	28	−2.1	46	54	746	20
Th	−11	−14	−28	−28	−28	−5
U	4	−13	−23	−19	−34	−119

Determination of the REE at ultra-trace concentration levels after preconcentration

There are samples in which the REE concentrations are below the LODs (0.01–0.1 $\mu g\ g^{-1}$) obtained using whole rock procedures[14] in which samples are prepared at 0.5 g of rock per kg of solution (0.1 g per 200 g of solution). A procedure, such as ion exchange, which increases the concentration of the REE while maintaining the total dissolved solids at less than 0.1% is required. The experimental difficulties of dissolving and carrying out ion-exchange separations on large sample masses are eliminated when the recycling nebulization system is used for the final instrumental measurements.

In this study, the recycling nebulization system was used to analyse reference material PCC-1 (USGS) after preconcentrating the REE from a 100 mg sample using cation exchange. Samples were dissolved as previously described and separation of the REE was achieved using 10 cm^3 of

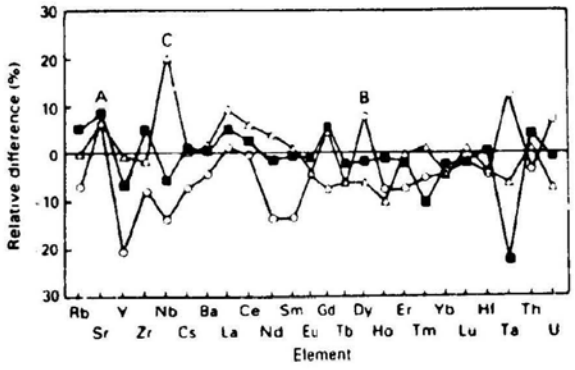

Fig. 7 Accuracy expressed as relative difference between results obtained in this work, using the recycling nebulization system, and literature values for A, BCR-1 ($n = 2$); B, W-1 ($n = 2$); and C, SY-2 ($n = 1$)

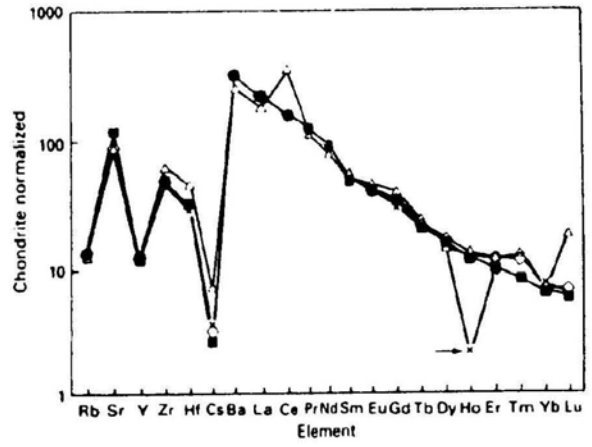

Fig. 8 Mean chondrite-normalized data for the geological reference material, BR, for different masses of sample: ■, 1.00 mg level ($n = 3$), ◇, 0.10 mg level ($n = 3$), △, 0.01 mg level ($n = 3$), and ×, data from ref. 16. The literature value for Ho, indicated by an arrow is suspect. The value for Ce at the 0.01 mg level may indicate homogeneity

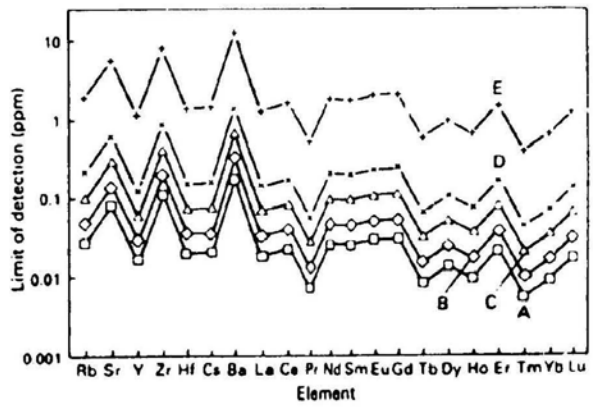

Fig. 9 Solid LODs for sample masses of: A, 1; B, 0.5; C, 0.2; D, 0.1; and E, 0.01 mg dissolved in 2 g of solution

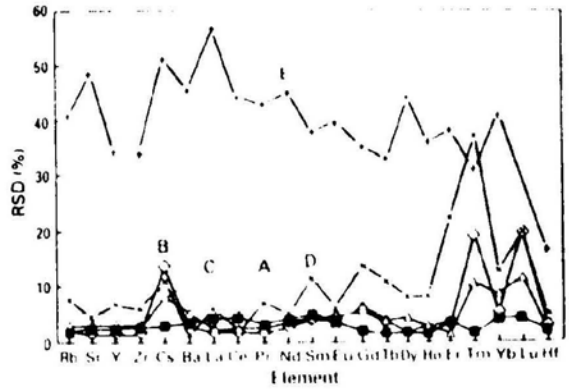

Fig. 10 Relative standard deviation for different masses of the geological reference material, BR: A, 1.00; B, 0.50; C, 0.2; D, 0.10; and E, 0.01 mg, $n = 3$ in each instance

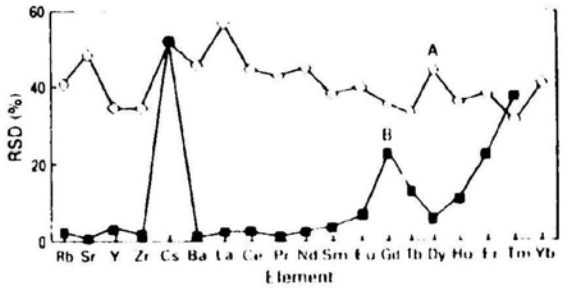

Fig. 11 Relative standard deviation for analysis of the geological reference material, BR. Results are given for A, the analysis of three separate digestions of 0.01 mg in 2 g of solution, and B, the analysis ($n = 4$) of a single digestion of 100 mg diluted to the same concentration (equivalent to a dilution in 20 kg of solution)

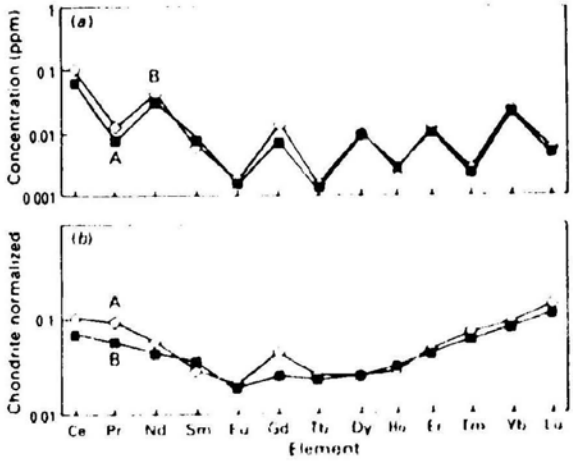

Fig. 12 (*a*) Concentrations (ppm) and (*b*) mean chondrite-normalized data for the reference material, PCC-1 in A, this work and B, ref. 16. The REE in 100 mg samples were separated using ion exchange and taken to a final solution mass of 2 g

cation-exchange resin in a quartz column. Major elements were eluted using 60 ml of a 1.13 mol dm^{-3} HNO_3–0.63 mol dm^{-3} HCl solution. The REE were collected using 25 ml of an 8 mol dm^{-3} HNO_3. The solution containing the REE was evaporated to dryness, the residue dissolved in HNO_3 and the resulting solution diluted to a final mass of 2 g using 0.2 mol dm^{-3} HNO_3. Results for the determination

Table 7 US Geological Survey reference sample PCC-1 ($n = 2$)

Element	Recycling nebulizer/ $\mu g\ g^{-1}$	Literature value*/ $\mu g\ g^{-1}$	LOD/ $\mu g\ g^{-1}$	RSD (%)	Relative difference (%)
Ce	0.069	0.1	0.00006	6	−31
Pr	0.0081	0.013	0.00015	9	38
Nd	0.032	0.042	0.0008	6	24
Sm	0.0082	0.0066	0.0007	16	25
Eu	0.0016	0.0018	0.0008	13	−10
Gd	0.0076	0.014	0.0007	10	−45
Tb	0.0013	0.0015	0.000009	8	11
Dy	0.0096	0.01	0.0005	8	−4
Ho	0.0028	0.0025	0.00012	11	13
Er	0.011	0.012	0.0006	2	−11
Tm	0.0023	0.0027	0.00014	8	16
Yb	0.022	0.024	0.0005	7	10
Lu	0.0046	0.0057	0.0004	4	19
Y	0.080	0.1	0.00011	6	20

*Ref. 16

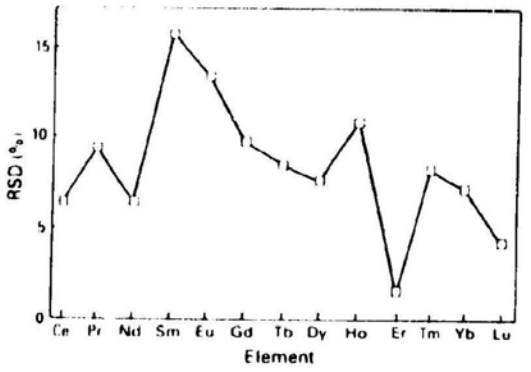

Fig. 13 Relative standard deviation for analysis ($n = 2$) of the geological reference material, PCC-1, following ion-exchange concentration of the REE

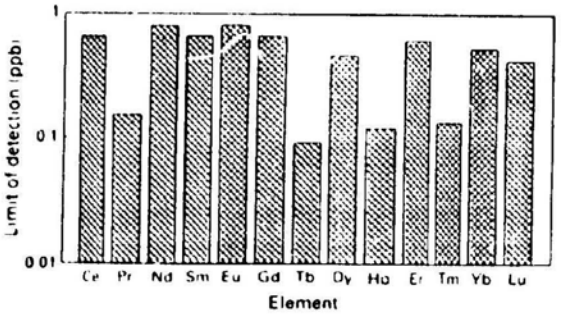

Fig. 14 Limits of detection for a solid sample mass of 100 mg taken to a final volume of 2 g. An REE ion-exchange separation procedure is required

of 14 REE are presented in Table 7 and Fig. 12. The agreement between these data and literature values for most elements, except Gd, is good. The anomaly for Gd in the chondrite-normalized diagram indicates that the literature value is suspect. Limits of detection for solids are 0.01–1 ng g^{-1} (Fig. 13) and RSDs are less than 15% (Fig. 14).

Conclusions

A recycling nebulization system with a disposable spray chamber is demonstrated for ICP-MS. The system described operated successfully for 8 min of data acquisition time using 0.5 cm^3 of sample solution. The memory of preceding samples was reduced to insignificant levels by the use of a removable, disposable spray chamber with manual washing. The performance of the system, in terms of precision, accuracy and sensitivity, is similar to that of the conventional Scott spray chamber system using 10 cm^3 sample volumes. Quantification of trace-element concentrations in sub-milligram amounts of geological samples and the determination of REE at ultra-trace concentration levels in geological materials after preconcentration using cation exchange is demonstrated.

This research was supported by the Natural Sciences and Engineering Research Council (NSERC) of Canada through operating grants to H. P. L. and B. J. F. The SCIEX Elan ICP-MS was purchased through an NSERC major installation grant and is operated with the assistance of an NSERC infrastructure grant. The authors acknowledge the assistance of B. Gosse in sample preparation and B. Chapman and S. E. Jackson in instrument operation. The spray chamber system was constructed by T. Perks and D. Bolger of the Department of Technical Services, whose contribution is gratefully acknowledged. The continuing support of Memorial University is also acknowledged.

References

1 Isoyama, H., Uchida, T., Lida, C., and Nakagawa, G., *J. Anal. At. Spectrom.*, 1990, **6**, 365.
2 Novak, J. W., Jr., Lillie, D. E., Boorn, A. W., and Browner, R. F., *Anal. Chem.*, 1980, **52**, 576.
3 Hulmston, P., *Analyst*, 1983, **108**, 166.
4 Zhuang, H. Z., and Barnes, R. M., *Spectrochim. Acta, Part B*, 1985, **40**, 1141.
5 Vieira, P. A., Zhuang, H. Z., Chan, S., and Montaser, A., *Appl. Spectrosc.*, 1986, **38**, 405.
6 Zical, C., and Barnes, R. M., *Spectrochim. Acta, Part B*, 1986, **41**, 979.
7 Kato, K., and Takashima, K., *Anal. Sci.*, 1989, **5**, 151.
8 Longerich, H. P., Strong, D. F., and Kantipuly, C. J., *Can. J. Spectrosc.*, 1986, **31**, 111.
9 Longerich, H. P., Fryer, B. J., Strong, D. F., and Kantipuly, C. J., *Spectrochim. Acta, Part B*, 1987, **42**, 75.

10 Longerich, H. P., *J. Anal. At. Spectrom.*, 1989, **4**, 665.
11 Jackson, S. E., Fryer, B. J., Gosse, W., Healey, D. C., Longerich, H. P., and Strong, D. F., *Chem. Geol.*, 1990, **83**, 119.
12 Jenner, G. A., Longerich, H. P., Jackson, S. E., and Fryer, B. J., *Chem. Geol.*, 1990, **83**, 133.
13 Jarvis, K. E., *J. Anal. At. Spectrom.*, 1989, **4**, 563.
14 Doherty, W., *Spectrochim. Acta, Part B*, 1989, **44**, 263.
15 Longerich, H. P., Jenner, G. A., Fryer, B. J., and Jackson, S. E., *Chem. Geol.*, 1990, **83**, 105.
16 Govindaraju, K., *Geostand. Newsl.*, 1989, **13**, 1.

Paper 2/00181A
Received January 14, 1992
Accepted June 1, 1992